UTS UNIVERSITY OF TECHNOLOGY SYDNEY

Therapeutic targeting of mitochondrial dysfunction in chronic obstructive pulmonary disease (COPD)

by Shatarupa Das

Thesis submitted in fulfilment of the requirements for the degree of

Doctor of Philosophy

under the supervision of
Prof Phil Hansbro
A/Prof Andy Philp
Dr Matt Johansen
Dr Nicole Hansbro

University of Technology Sydney
Faculty of Science

December 2022

Certificate of Original Authorship

I, ***Shatarupa Das***, declare that this thesis is submitted in fulfilment of the requirements for the award of ***Doctor of Philosophy***, in the ***School of Life Sciences*** at the University of Technology Sydney.

This thesis is wholly my own work unless otherwise referenced or acknowledged. In addition, I certify that all information sources and literature used are indicated in the thesis.

This document has not been submitted for qualifications at any other academic institution.

This research is supported by the Australian Government Research Training Program.

Signature: Production Note:
Signature removed prior to publication.

Date: 23.12.2022

Acknowledgement

This thesis was a new and memorable experience for me. Words cannot express my gratitude to my supervisor and the director of Centenary UTS Centre for Inflammation, Prof. Philip Hansbro for giving me this opportunity as a PhD candidate. My gratitude extends to the Faculty of Science, for the IRS and president's scholarships to undertake my studies at the School of Life Sciences, UTS.

I also could not have undertaken this journey without my co-supervisor A/Prof. Andy Philp, who generously provided his knowledge and expertise. Additionally, this endeavour would not have been possible without the support of our Centre manager, Dr Nicole Hansbro.

I would like to express my profound gratitude to my co-supervisor Dr Matt Johansen, for his invaluable supervision, advice, continuous support, and patience during these last three years. His immense knowledge and plentiful experience have encouraged me and kept me motivated in academic research as well as in my daily life. He has been a wonderful mentor and my best friend throughout the most challenging phase of my life. His influence in shaping my experiment methods and critiquing my results has immensely helped to develop my critical thinking as a scientist. Thank you, for your kind words of encouragement that have made it possible to chase my dreams.

I would like to extend my gratitude to our past and current technical staff, Carol Devine, Simon Gao, Nimmy, and Bob Lu, for their immense hard work in the smoking facility. Special thanks to Solomon Odgers, who has put in a huge amount of work as a technical officer and now as a research assistant. In addition, I would also like to thank our other

research assistants, Dr Duc Nguyen, Dr Christina Nalkurthi, Nisha Panth, Linda Tong, and Caroline Wilson for their constant support.

My wholehearted thanks to all my peers at the Mitochondria metabolism and Ageing lab, Dr Ashleigh Philp, Dr Dean Campelj, and James Sligar with who I have greatly benefited and enjoyed working.

I am also grateful to my friends and colleagues, for being my family in Australia, thank you for all the extreme endpoint days, late-night feedback sessions and moral support. It is their kind help and support that have made my study and life in Sydney a wonderful time. Thank you, Dr Vrushali Chimankar, Dr Annalicia Vaughan, Dr Vyoma Patel, Dr Izabela Galvo, Jacqueline Marshall, Stefan Miemczyk, Hamidreza Sadegh, Tayyaba Sadaf, Angelica Katsifis, Karl Hegarty, and Vamshikrishna Malyla for all the cherished time spent together in the lab and social settings.

I would be remiss in not mentioning my family, especially my mom, and my siblings. Their belief in me has kept my spirits and motivation high during this process. Unforgotten, thank you to my late dad, whom I miss dearly. A special feeling of gratitude for my grandparents and lastly, I would also like to thank my cats for all the entertainment and emotional support.

Summary

Chronic obstructive pulmonary disease (COPD) is characterised by airway inflammation resulting in irreversible damage to the lung, which leads to airway remodelling, alveolar destruction or emphysema, and impaired lung function. Currently, there are no available treatments that inhibit the progression or reverse the disease. Cigarette smoking (CS) is a primary cause of COPD and is an instigator of airway inflammation which is driven by oxidative stress. This further induces the over-activation of nuclear enzyme poly (ADP-ribose) polymerase-1 (PARP-1). PARP-1 is a major consumer of nicotinamide adenine dinucleotide (NAD^+), a critical energy intermediate for the maintenance of all metabolic interactions.

Currently, there is limited knowledge as to how NAD^+ metabolism is altered in COPD and whether targeting NAD^+ pathways can have therapeutic benefits in COPD. Therefore, in Chapter 3, we examined the efficacy of NAD^+ targeted therapeutics, Nicotinamide Riboside (NR) and Pterostilbene (PT) in a prophylactic COPD model. Using our experimental CS-induced COPD mouse model, we found reduced NAD^+ levels associated with PARP hyperactivity in the lung. We also observed an increase in the gene expression of oxidative stress markers like NADPH-oxidase 2 (NOX2) and inflammatory markers like TNFα and CXCL1. Based on these findings, we hypothesised that reduced NAD^+ levels may instigate oxidative stress and inflammation in COPD. Thus, in Chapter 4 we investigated the therapeutic effect of NR and PT in halting the progression and reversing the disease features in COPD. Following daily dietary administration of NR and PT both prophylactically and therapeutically, we found significant reductions in inflammatory cell infiltration into the lung and reduced gene expression of inflammatory markers like TNFα and CXCL1. Further, NR and PT reduced airway remodelling,

emphysema, and improved lung function. NR and PT also restored NAD^+ levels and PARP activity in COPD. This resulted in the protection of mitochondrial structure and function via reduced oxidative stress. In conclusion, NR and PT reduced inflammation, and COPD features via increased mitochondrial function and reduced oxidative stress. Thus, NR and PT have significant potential as therapeutics for COPD.

NAD^+ is essential for cell survival and is tightly regulated by enzymes such as Nicotinamide mononucleotide adenyl transferases (NMNATs). NMNATs are involved in the final step of NAD^+ synthesis. Based on our findings from Chapter 3, imbalances in NAD^+ levels in COPD might be due to imbalances in NAD^+ synthesis. Furthermore, we determined that the administration of NR and PT in COPD increased gene expression of NMNAT1, NMNAT2 and NMNAT3. Therefore, in Chapter 5, we investigated the role of NMNATs in modulating NAD^+ levels in comparison to the treatment of NR and PT in COPD using transgenic NMNAT1 and NMNAT3 overexpressing mice. Additionally, we also administered NR and PT to the overexpressing NMNAT1 and NMNAT3 mice to elucidate if an additional increase in NAD^+ levels can potentially exhibit enhanced benefits in reducing COPD features. We found significant reductions in airway inflammation via reduced cellular infiltrates in the lung as well as a reduction in the gene expression of TNFα and CXCL1 with both the NMNAT1 and NMNAT3 overexpression as well as upon treatment of these mice with NR and PT. Additionally, we observed a reduction in airway remodelling and emphysema for both the NMNAT1 and NMNAT3 overexpression as well as upon treatment with NR and PT. However, there was no improvement in lung function with the overexpression of NMNAT1 and NMNAT3 mice. Additionally, treatment with NR and PT in overexpressed NMNAT1 and NMNAT3 mice further increased impaired lung function in COPD. Moreover, NMNAT1 overexpressing mice did not show an increase in the NAD^+/NADH levels in COPD which did not change

with the administration of NR and PT. On the other hand, NMNAT3 overexpressing mice exhibited an increase in the NAD^+ levels in COPD which did not change further upon NR and PT treatment. We further observed a reduction in PARP hyperactivity with both the NMNAT1 and NMNAT3 overexpression as well as upon treatment with NR and PT, and this further showed a reduction in oxidative stress and an increase in mitochondrial membrane potential. In conclusion, we hypothesise that NMNAT3 might potentially be driving NAD^+ modulation to protect from COPD features. Critically, NAD^+ levels might potentially be rate-limiting and thus treatment of NR and PT in overexpressing NMNAT1 and NMNAT3 mice did not show a further increase in NAD^+ levels in COPD.

The development and progression of COPD is largely driven by chronic inflammation, however, there is limited knowledge about the exact molecular and metabolic interactions in the immune cells involved during the progression of the disease. Therefore, the objective of the Chapter 6 study was to determine if chronic CS exposure alters immunometabolism in COPD and whether pharmacological interventions can restore imbalances and exert therapeutic benefit. Using our CS-induced COPD mouse model, we determined that chronic exposure to CS reduced gene expression of pyruvate kinase markers 2 (PKM2) and Hypoxia-inducible factor 1α (HIF1α) indicating reduced metabolism in the lung, while we also observed an increase in oxidative stress and inflammatory markers. Based on these findings, we hypothesised that the reduction in PKM2 may be an important driver of immunometabolism in COPD. Therefore, we next examined whether immunomodulator TEPP46, which is importantly a PKM2 activator, was able to therapeutically improve COPD disease features. Following administration of TEPP46 three times per week throughout the duration of the model, we observed a significant reduction in airway inflammation followed by reduced airway remodelling, emphysema, and improved partial lung function in COPD. TEPP46 also protected PKM2

and HIF1α protein content and promoted metabolic function, resulting in reduced oxidative stress and protection of mitochondrial structure and function. In conclusion, TEPP46 has significant preclinical potential as a therapeutic for the treatment of COPD.

.

List of publications and conferences

Conference proceedings:

1. Das S., Johansen M. D., Marshall J, Sadega H., Sadaf T., Hansbro N., Thomas C., O'Neil L., Philp A., Hansbro P. M. (2022) **Investigating the therapeutic efficacy of immunomodulator TEPP46 in Chronic Obstructive Pulmonary Disease (COPD).** In: 50th Annual Scientific Meeting of Australia and New Zealand Society for Immunology, Melbourne, Australia: 29th November-2nd December 2022.

2. Das S., Johansen M. D., Marshall J, Sadega H., Sadaf T., Hansbro N, Thomas C., O'Neil L., Philp A., Hansbro P. M. (2022) **Mitochondrial dysfunction and its modulation in Chronic Obstructive Pulmonary Disease (COPD).** In: Australian Inflammation Centres 2022 Symposium-Virtual, Melbourne, Australia: 24th-25th November 2022.

3. Das S., Johansen M. D., Marshall J, Sadega H., Sadaf T., Hansbro N, Thomas C., O'Neil L., Philp A., Hansbro P. M. (2022) **Investigating mitochondrial dysfunction as a potential therapeutic target for Chronic Obstructive Pulmonary Disease (COPD).** In: 16th Annual New South Wales Asthma Meeting (NAMe), Sydney, Australia: 17th-18th of November 2022.

4. Das S., Johansen M. D., Marshall J, Sadega H., Sadaf T., Hansbro N, Thomas C., O'Neil L., Philp A., Hansbro P. M. (2022) **Targeting impaired immunometabolism to prevent the development of Chronic Obstructive Pulmonary Disease (COPD).**

In: 7th biennial Australian conference for mitochondrial research AussieMit 2022, Sydney, Australia: 16th-18th of November 2022.

5. Das S., Johansen M. D., Marshall J, Sadega H., Sadaf T., Hansbro N, Thomas C., O'Neil L., Philp A., Hansbro P. M. (2022) **Investigating the therapeutic efficacy of immunomodulator TEPP46 in Chronic Obstructive Pulmonary Disease (COPD).** In: 9th EMBL Australia Postgraduate Symposium, Melbourne, Australia: 9th-11th of November 2022.

Table of contents

List of Figures

List of tables

Abbreviations

°C	Degrees Celsius
β-HAD	β-hydroxyacyl CoA
ΔΨm	Mitochondria membrane potential
µg	Microgram
µl	Microlitre
µm	Micrometre
4-HNE	4-hydroxy-2-nonenal
3-NT	3-nitrotyrosine
A	estimation of IC
AATD	α-1-antitrypsin deficiency
AAt	α-1-antitrypsin
Acetyl-CoA	Acetyl coenzyme A
ADP	Adenosine diphosphate
ALS	amyotrophic lateral sclerosis
ARC	Animal Resources Centre
ATP	Adenosine triphosphate
BAL	Bronchoalveolar lavage
BSA	Bovine serum albumin

CO_2	Carbon dioxide
COPD	Chronic obstructive pulmonary disease
CRS	Respiratory system compliance
CS	Cigarette smoke
Cst	Static compliance
CXCL1	Chemokine ligand 1
DBQ	Decyl ubiquinone
DC	Detergent Compatible
DMSO	Dimethyl sulfoxide
DPBS	Dulbecco's Phosphate-Buffered Saline
DTNB	5,5-dithio-bis-(2-nitrobenzoic acid)
EC	Endothelial cells
ETC	Electron transport chain
FADH2	Flavin adenine dinucleotide
FEV	Forced expiratory volume
FRC	Functional residual capacity
FVC	Forced vital capacity
FITC	Fluorescein Isothiocyanate
G	Tissue damping
GCN5	Gene control non-derepressible 5

GOLD	Global Initiative on Chronic Obstructive Lung Disease
GLUT1	Glucose transporter 1
H	Tissue elastance
H_2O_2	Hydrogen peroxide
HCL	Hydrochloric acid
HDAC2	Histone deacetylase 2
HIF1α	Hypoxia inducing factor-1α
HK1	Hexokinase-1
HO1	Heme oxygenase 1
HPRT	Hypoxanthine-guanine phosphoribosyl transferase
IC	Inspiratory capacity
IL-1β	Interleukin-1β
ICAM1	Intermolecular adhesion molecule
iNOS	Inducible nitric oxide synthase
KCN	Potassium cyanide
Kpi	Potassium phosphate
LDHA	Lactate dehydrogenase A
LPS	Lipopolysaccharide
LTB4	Leukotriene B4
MMP-12	matrix metalloproteinase-12

MLI	Mean linear intercepts
mtROS	Mitochondrial reactive oxygen species
mtRNS	Mitochondrial reactive nitrogen species
NA	Nicotinic acid
NaCl	Sodium chloride
NAD^+	Nicotinamide adenine dinucleotide
NAAD	Nicotinic acid adenine dinucleotide
NADK1/2	NAD^+ kinase 1/2
NADH	Nicotinamide adenine dinucleotide
NADSYN	NAD^+ synthase
NAFLD	Non-alcoholic fatty liver disease
NAM	Nicotinamide
NAMN	Nicotinic acid mononucleotide
NAMPT	Nicotinamide phosphoribosyl transferase
NAPRT	Nicotinate phosphoribosyl transferase
NF-κβ	Nuclear factor-κβ
NHMRC	National Health and Medical Research Council of Australia
NMN	Nicotinamide mononucleotide
NMNT	Nicotinamide mononucleotide transferase

NMNATs	Nicotinamide mononucleotide adenylyl transferase
NK	Natural killer cells
NOX2	NADHP oxidase
Nrf2	Nuclear factor erythroid 2-related factor-2
NR	Nicotinamide riboside
NRKs	Nicotinamide ribose kinases
NTHi	Non-typeable Haemophilus influenzae
O^-	Superoxide
Oct-4	Octamer binding transcription factor-4
Oxphos	Oxidative phosphorylation
Oxstress	Oxidative stress
PARPs	Poly (ADP-ribose) polymerases
PBS	Phosphate buffer saline with tween
PDK1	3-Phosphoinositide-dependent kinase 1
PDH	Pyruvate dehydrogenase
PEP	Phosphoenol pyruvate
PGC1α	Peroxisome proliferator-activated receptor-gamma co-activator 1α
PK	Pyruvate Kinase
PKF	Phosphofructokinase

PNP	Purine Nucleoside Phosphorylase
qPCR	Quantitative PCR
RBC	Red blood cell
ROS	Reactive oxygen species
Rn	central airway resistance
RNS	Reactive nitrogen species
Rrs	Transpulmonary resistance
RV	Residual volume
SARS-CoV-2	Severe Acute Respiratory Syndrome Coronavirus 2
SEM	Standard error mean
SIRTs	Sirtuins
SLHD	Sydney Local Health District
STAT3	Signal transducer and activator of transcription 3
TBST	Tris buffer saline with tween
TCA	Tricarboxylic acid
TEM	Transmission emission microscopy
TMPRSS2	Transmembrane serine protease 2
TNFα	Tumour necrosis factor α
TLC	Total lung capacity
TRP	Tryptophan

UNSW	University of New South Wales
UPRmt	Mitochondrial unfolded protein responses
VC	Vital capacity
YM1	chitinase-like protein 3

Chapter 1. Literature review

1.1 COPD

1.1.1 Epidemiology

Chronic obstructive pulmonary disease (COPD) is a disease that is characterised by the limitation of airflow in the lungs (1), which leads to shortness of breath (2), wheezing (3), chest tightness (4) and ongoing chronic cough (5). Chronic exposure to cigarette smoke (CS) is one of the predominant causes of COPD (6) however, other causes include long-term exposure to lung irritants—such as air pollution (7), chemical fumes (8), or dust (9, 10). The clinical symptoms of COPD are shortness of breath, wheezing, chest tightness, and ongoing chronic cough. COPD is a heterogeneous progressive disease characterised by common pathologies of chronic airway inflammation (bronchitis) (11), airway remodelling (12) (collagen deposition (13), fibrosis (14), and mucus hypersecretion (15)) and/or emphysema (16) (where alveoli or air sacs are damaged) and impaired lung function and gas exchange leading to severe breathlessness (17).

COPD is the third most common cause of death globally and fifth in Australia (18, 19). Current available treatments include the use of bronchodilators (20), oxygen therapy (21), lung transplantation (22), or lung reduction surgeries that alleviate the disease symptoms (23, 24). However, there are no current available treatments that inhibit the progression or reverse the disease and hence, there is an urgent need to identify effective therapies for the treatment of COPD (25, 26).

COPD is difficult to diagnose in the early stages and can progress for years without any noticeable symptoms (27). COPD stages are classified utilising the criteria stated in the Global Initiative on Chronic Obstructive Lung Disease (GOLD) (28). The GOLD guidelines group the patient according to the symptoms and forced expiratory volume

(FEV) score as mentioned below in table 1.1 (29). The stages are divided into the induction and progression phases (30). The induction phase consists of GOLD stage I-II, where patients are characterised by mild to moderate symptoms, accompanied by shortness of breath, exertion cough and sputum production (31). The progression phase consists of stages III-IV, where patients are characterised by severe disease symptoms, such as extreme shortness of breath, reduced exercise capacity, fatigue, and repeated exacerbations which have a moderate to severe impact on quality of life (32-34).

Table 1.1: GOLD classification of COPD

The severity of COPD stages (based on FEV Score)		
Classification	**Severity**	**FEV1**
GOLD 1	Mild	FEV1 ≥ 80%
GOLD 2	Moderate	FEV1 ≤ 50-79%
GOLD 3	Severe	FEV1 ≤ 30-49%
GOLD 4	Very severe	FEV1 ≤ 30%

1.1.2 COPD pathophysiology

COPD is an umbrella term for a range of chronic lung diseases, such as bronchitis and emphysema in addition to declining lung function (35). Chronic bronchitis and emphysema can occur together or individually and vary in severity among COPD patients (36). Chronic bronchitis is characterised by inflammation in the lining of the airways often accompanied by daily cough and mucus production (37). Emphysema is referred to the damage of the lung parenchyma as a result of chronic exposure to CS and/or other lung irritants (38). Emphysema is characterised by irreversible enlargement of alveoli

accompanied by destruction of the alveolar walls leading to the trapping of air in the alveoli and loss of elasticity of the lung tissue that increases pulmonary compliance and reduces lung function (39, 40). These conditions often lead to structural remodelling of the airways that results in the formation of scar tissue (41), collagen deposition (42) and mucus hypersecretion (43) causing a reduction in lung function (44) by reduced lung elasticity (45) and decreasing hysteresis (46). In combination, these events lead to airway obstruction and further loss of lung function typically observed in moderate to severe COPD patients (47, 48). These structural impairments in the lung are resultant of chronic inflammation in COPD (49).

Chronic exposure to CS or other risk factors leads to increased infiltration of total leukocytes in the lungs, comprising macrophages, neutrophils, eosinophils, and lymphocytes in the airways (50, 51). These events lead to the release of various inflammatory mediators such as leukotriene B4 (LTB4)- produced by macrophages (52), interleukin (IL)-1β (53), and tumour necrosis factor (TNF)-α (54, 55). Followed by the release of inflammatory mediators, activation of epithelial cells and endothelial cells occur, which then serves as a source for chemoattractant cytokines facilitating a further increased infiltration of leukocytes in the airways (56-58). These substantial cellular changes are often associated with a shift in the metabolic state of inflammatory cells leading to the production of reactive oxygen species (ROS) (59) or reactive nitrogen species (RNS) (60) which promote further inflammation to develop a feedback-loop inducing chronic inflammation (61).

1.1.3 Risk factors for COPD

Multiple risk factors play an important role in the development and progression of COPD (62). Cigarette smoking is the most significant risk factor for COPD (63). Other than tobacco, smoking marijuana as well as exposure to passive exposure to cigarette smoking possess a high risk of developing COPD (64). Additionally, chronic exposure to environmental pollutants (65), chemical irritants (23) and the smoke inhaled from indoor cooking are also well-known risk factors for COPD in developing countries (66, 67). A rare genetic mutation causing α -1-antitrypsin deficiency (AATD) is a notable genetic risk factor for COPD (68, 69). About 1-3% of COPD patients are diagnosed with AATD, characterised by a low level of α-1-antitrypsin (AAt) protein (70). AAt is synthesised in the liver and circulated to the lung, which protects the lungs from damage (71). AATD can cause both lung and liver disease (72). Further, people with asthma possess a high risk of developing COPD which further increases with smoking (73). COPD patients are at constant risk of other respiratory infections such as cold, flu or pneumonia (74). COPD can increase the risk of heart disease and heart attacks (75). People with COPD have a higher risk of developing lung cancer and pulmonary hypertension (76).

1.1.4 COPD exacerbations

Exacerbations of COPD is referred to the worsening of the disease symptoms like increased airway and systemic inflammation and structural changes such as hyperinflation of the lung which leads to substantial morbidity and mortality (77). Acute exacerbations are a characteristic of COPD and determine the poor clinical course of the patient (78). Exacerbations are associated with greater disease progression, an increase in chronic airway inflammation, and impaired lung function (79). Most exacerbations are

caused by bacterial and viral respiratory tract infections such as non-typeable Haemophilus influenzae (NTHi), Streptococcus pneumoniae and Severe Acute Respiratory Syndrome Coronavirus 2 (SARS-CoV-2) etc. (80-82). The susceptibility of smokers with COPD to respiratory infections is greater than that of non-smokers (83). This is largely due to the inherent properties of CS exposure causing several disruptions to the innate lung defence mechanisms (84), such as impairment of mucus clearance (85), reductions in ciliary beat frequency and the number of ciliated cells due to squamous metaplasia (86), and impairment of phagocytosis by alveolar macrophages (87). As such COPD patients have higher expression of intermolecular adhesion molecule 1 (ICAM1) which is the receptor for Influenza, and transmembrane serine protease 2 (TMPRSS2), the main protease involved in SARS-CoV-2 infection (88).

The administration of corticosteroids has long been a mainstay therapy for acute COPD exacerbations (89); however, the use of chronic corticosteroids is associated with many adverse events like an increased risk of pneumonia, possibly due to their immunosuppressive action (90). Corticosteroids suppress inflammation by recruiting histone deacetylase 2 (HDAC2) to drive pro-inflammatory gene promoters like nuclear factor-κβ (NF-κβ) (91, 92). Several studies exploring the usage of specific antibiotics in COPD exacerbations have been conducted, and it is known that antibiotic therapy can reduce sputum purulence, which is referred to as a rapid change in the colour of the sputum (93).

1.1.5 Management of COPD exacerbations

COPD has been a significant cause of morbidity and mortality across the globe for over a decade. It is estimated that 328 million people suffer from COPD worldwide (94, 95). Management of COPD depends on the severity of the disease, however, cessation of

smoking is highly recommended for patients at all stages of COPD (96). Several kinds of medications are used to treat the symptoms and complications of COPD such as the use of bronchodilators which can be either short-acting or long-acting (97). Bronchodilators usually come in form of inhalers and help to relax the muscles around the airways (98). This provides relief from chronic cough and shortness of breath (99). Commonly prescribed short-acting bronchodilators include albuterol, ipratropium, and levalbuterol (100, 101) etc. and long-acting bronchodilators include aclidinium, arformoterol, formoterol etc (102-104). For moderate or severe COPD patients, the inhalation of corticosteroids is known to mitigate COPD symptom persistence, reduce airway inflammation, and help to prevent the occurrence of exacerbations (105, 106). Commonly used corticosteroids are fluticasone, and budesonide (107). Based on the severity of the disease, treatments may include a combination of bronchodilators and corticosteroids for example fluticasone and vilanterol, fluticasone, umeclidinium and vilanterol (108). Furthermore, the use of phosphodiesterase-4 inhibitors is known to reduce airway inflammation and relax the airways (109, 110). Therapies such as oxygen therapy (111)**,** a pulmonary rehabilitation program (112)**,** and in-home non-invasive ventilation therapy (113) are recommended for moderate or severe COPD patients. Moreover, **l**ung volume reduction surgery is also an option for treatment whereby lung sections are removed (114) from moderate or severe COPD patients. Other surgery options include bullectomy, where damaged sections of the lungs are removed and lung transplantation (24, 115)**.** All these treatment options alleviate symptoms and exacerbations but currently, there is no cure for COPD, therefore, there is a need for new therapies that can prevent the induction or inhibit the progression of COPD.

1.1.6 Animal models of COPD

Animal models are crucial in studying the pathological process of diseases (116). To study the pathogenesis of COPD and explore potential therapeutic approaches, we need a reliable animal model to mimic the hallmark features of COPD (117). As COPD is a heterogeneous disease (118), it is nearly impossible to replicate all pathological features and the complexity of COPD in a single model (119). Previous studies have been performed on numerous models that can recapitulate the disease features in animals including rodents (120), guinea pigs (121), sheep (122), dogs (123), and non-human primates (124). However, the use of mice offers several advantages over other species that include the feasibility of breeding and maintenance, ease of genetic modification and the heterogeneity within different mouse strains (125, 126).

Several experimental models of COPD are available where the disease can be induced via elastase instillation (127), genetic manipulation (128), CS exposure (129), bleomycin administration (130), lipopolysaccharide (LPS) exposure (131), fluorescein isothiocyanate (FITC) (132) and silica administration (133). Primitive studies were performed assuming COPD as a disease of emphysema in elderly patients deficient in α-1-antitrypsin, leading to a build-up of elastase (134). Therefore, elastase instillation was one of the first COPD models adapted using a single dosage of elastase resulting in immediate loss of the alveolar wall (135). The major drawback of this model was a reduction of the immune cell environment which forms a vital aspect in the pathogenesis of COPD (136). Several studies have investigated the role of genetic factors in COPD utilising transgenic mutant mouse models such as matrix metalloproteinase-12 (MMP-12) knockouts to validate the protective role of MMP-12 against smoke induced-emphysema (137). Given that CS is the leading risk factor for the induction and

progression of COPD (138), exposure to CS is an appropriate method to induce hallmark pathological features of COPD in animal models (117). Several studies have adopted mouse smoke exposure protocols that vary with delivery route, frequency, length and number of cigarettes being used (139). In addition, the process of smoke exposure is a critical factor that varies between mainstream smoke introduced via inhalation or sidestream smoke generated passively via the burning of cigarettes (140). Moreover, the disease features in CS exposure models also vary between whole-body smoke exposure typically accompanied by less severe features (141) and nose-only smoke exposure which causes more prominent disease features (142). Another most widely used model for fibrotic lung damage is generated via bleomycin administration, a compound known to induce lung fibrosis (143). Commonly used bleomycin models only require one intranasal dosage of bleomycin to induce fibrotic changes in the lung accompanied by localised inflammation within 3-4months (144). Similar to bleomycin, FITC and silica models are widely used where mice are treated with FITC or silica particles and these induce localised inflammation and lung damage which is sustained for up to 5 months (132, 145).

Our group has developed a mouse model that recapitulates the main pathological features of COPD in a short timeframe of 8 weeks using CS exposure (146). The custom-designed nose-only inhalation system enables us to deliver CS directly into the airways of the mouse to develop critical features of COPD. These features include infiltration of cells in the lungs, alveolar enlargement and remodelling, damage in the lung parenchyma and reduced lung function (146). Cessation of smoke after 8 weeks in this experimental COPD model did not improve airway inflammation, alveolar enlargement, or impaired lung functions. This is consistent with the progressive and irreversible nature of COPD pathogenesis observed in patients even after cessation of smoking, making this a useful

model to better understand the pathogenesis of COPD during CS exposure and following CS cessation.

1.2 Inflammation and COPD

Chronic inflammation in COPD involves the infiltration of inflammatory cells in the lungs such as macrophages, neutrophils, lymphocytes, mast cells and innate lymphoid cells (147). This infiltration of inflammatory cells often contributes to detrimental effects in the residential cells of the lungs such as airway epithelial cells, parenchyma cells and stromal cells which leads to tissue destruction and airway remodelling in COPD (148, 149). The inflammatory response in COPD requires a combined activation of innate immune cells (eg, macrophages and neutrophils) and adaptive immune cells including T-lymphocytes and vascular cells (eg, endothelial cells and vascular smooth muscle cells) (148). The classical inflammatory response progresses through two distinct phases: initiation and resolution (150). The initiation phase is characterised by the recognition of damage by the resident immune cells, and the activation of endothelial cells (ECs) (151), followed by clonal expansion, proliferation, and recruitment of additional immune cells to the site of the injury (152). The resolution phase includes the removal of the activated immune cells, the formation of memory immune cells and the restoration of homeostasis (153). Macrophages release chemokines like CXCL1 to recruit neutrophils (154). Additionally, macrophages and neutrophils add to the continuous inflammatory response by releasing ROS, which induces apoptosis in epithelial cells (155). Further, activated macrophages release MMPs, enzymes that can disintegrate various matrix components, including collagen and elastin as a normal immune response (156).

Sustained inflammation in COPD leads to continuous tissue injury and repair in the lungs, causing irreversible damage to the lung tissues and worsening lung function. However, to date, there is a lack of understanding of how inflammatory mediators affect this process of airway remodelling and damage in lung parenchyma and how that contributes to reduced lung function in COPD. Recent studies have highlighted that immune cells in COPD are highly active with their proliferation, and effector functions, which require extensive anabolic processes such as secretion of lipid and protein mediators like saturated or unsaturated fatty acids and nucleic acid content as well as catabolic processes like digestion of phagocytosed materials. To drive these processes, immune cells require an immediate influx of glucose to meet the high demands for adenosine triphosphate (ATP). Henceforth, these cells undergo a metabolic shift whereby they favour glycolysis over oxidative phosphorylation (oxphos). Glucose metabolism by glycolysis generates ~2 ATP molecules as compared to one complete cycle of respiration including glycolysis, the tricarboxylic acid (TCA) cycle or the Krebs cycle, and electron transport chain (ETC) followed by oxphos which generates ~34-36 molecules of ATP (Figure 1.1). This shift of immune cells from oxphos to aerobic glycolysis is referred to as the Warburg effect (Figure 1.1) (157).

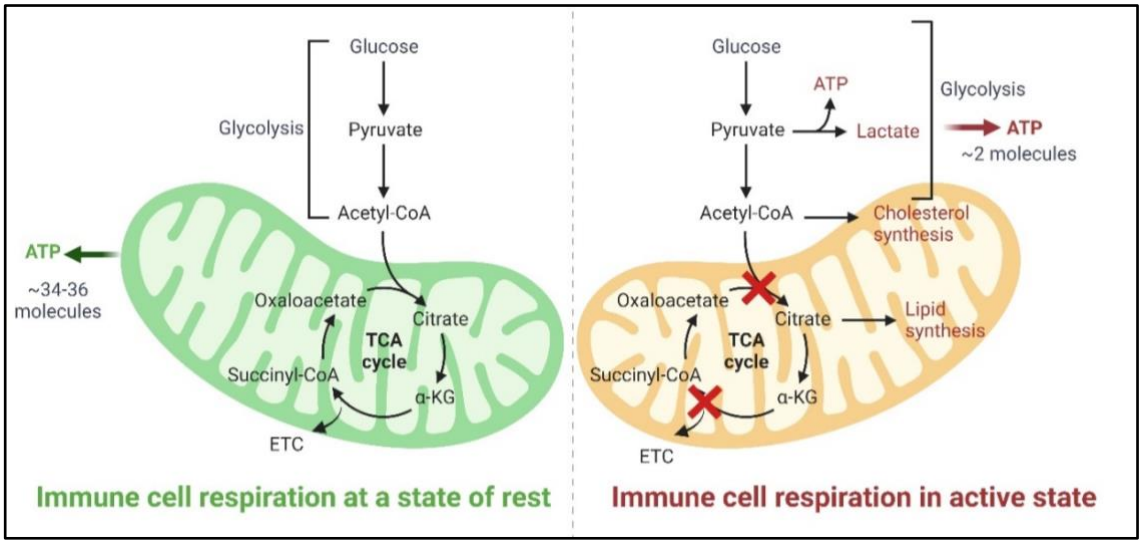

Figure 1.1: The Warburg effect

Immune cells during a state of rest undergo a full respiration cycle that includes glycolysis, TCA cycle, ETC and oxphos producing ~34-36 molecules of ATP. Upon activation, immune cells prefer glycolysis over oxphos for an instant source of energy, producing 2 molecules of ATP.

The switch of metabolic flux in immune cells from oxphos to aerobic glycolysis is a potential mechanism driving sustained inflammation (158). The final rate-limiting step of aerobic glycolysis is modulated by the pyruvate kinase (PK) marker 2 (PKM2) enzyme and plays an important role in modulating cellular immunometabolism (159). PKM2 catalyses the transfer of a phosphate group from phosphoenolpyruvate (PEP) to adenosine diphosphate (ADP) generating pyruvate and ATP (160). PK exists in four isoforms including PKM1, PKM2, PK-L and PK-R. PKM2 oligomer can either exist in a dimer or a tetramer form (161). The tetramer form of PKM2 has higher enzymatic activity and has a high level of affinity for PEP, and can quickly catalyse PEP to form pyruvate (162). On the other hand, the PKM2 dimer has a lower catalytic activity and cannot produce

pyruvate at a normal rate, resulting in the accumulation of upstream glycolysis intermediates (160). As a result of this blockade, the composition of the intracellular environment becomes disordered, including the accumulation of large amounts of acidic glycolysis intermediates leading to imbalances in the acid-base equilibrium of the cell and resulting in oxidative stress (163).

Further, PKM2 has unique nuclear functions and binds to and activates the transcription factors Hypoxia Inducing Factor (HIF)-1α, signal transducer and activator of transcription-3 (STAT3) and octamer binding transcription factor-4 (Oct-4), thus promoting the activation of the related signalling pathways and inflammation (164, 165). HIF1α plays an important role in metabolic reprogramming in inflammatory cells by promoting the expression of genes such as glucose transporter 1 (GLUT1), lactate dehydrogenase A (LDHA), phosphofructokinase 1 (PKF1) and hexokinase 1 (HK1) (165). PKM2 and HIF1α are involved in a positive feedback loop in which HIF1α activates gene transcription of PKM2, whereas PKM2 interacts with HIF1α to promote the transactivation of HIF1α target genes (166). Moreover, the expression of PKM2 plays a protective role against oxidative stress by exerting an antioxidant effect during inflammation, therefore, is a potential target for controlling inflammatory responses in COPD (167).

1.3 Oxidative stress in COPD

Oxidative stress is a well-known instigator of inflammation in COPD, produced due to oxidant-antioxidant imbalance in cells (168). Mitochondria are one of the major sources of reactive oxygen and nitrogen species (mtROS/mtRNS) (169). High levels of ROS cause the oxidation of proteins, lipids and DNA resulting in tissue injury and triggering

inflammatory responses (170). COPD patients have increased oxidative stress markers such as 4-hydroxy-2-nonenal (4HNE), 3-nitrotyrosine (3-NT), inducible nitric oxide synthase (iNOS) (171, 172), decreased mitochondrial biogenesis (172), impaired mitochondrial activity (173), and coupling of mitochondrial respiratory chain complexes (174), leading to cellular apoptosis (175). Recent studies show that mtROS is an important driver of inflammation (176), and is known to modify protein thiols (177) through peroxisome proliferator-activated receptor-gamma coactivator 1α (PGC1α) (178), and is required to produce pro-inflammatory cytokines (179) and chemokines (180) such as TNFα (181), chemokine ligand 1 (CXCL1) (177) and IL-1β (182) (Figure 1.2). Oxidative stress levels remain elevated in COPD patients after smoke cessation, suggesting that damaged mitochondria and impaired metabolism lead to endogenous ROS and are likely involved in the disease progression (183). Studies have shown that mtROS play important pathogenic roles in the development of COPD, through the induction of inflammation and damage of pulmonary cells and tissues and represents an important therapeutic avenue (184).

1.4 Mitochondrial dysfunction in COPD

Mitochondrial dysfunction in COPD is characterised by lower mitochondria membrane potential (ΔΨm), reduction in ETC complex activities, low ATP levels, and increased ROS production which contributes to the release of apoptotic factors (185, 186). Mitochondria are double membrane-bound organelles that serve as energy producers in a cell (187). Mitochondria are often referred to as the powerhouse of the cell, as these organelles catalyse the oxidation of metabolites to drive ATP production via the process of oxphos (188). Oxphos involves the transfer of high-energy electrons derived from

nicotinamide adenine dinucleotide (NADH) and flavin adenine dinucleotide (FADH2) generated by the Krebs cycle through the ETC complexes that donate electrons to molecular oxygen (189, 190). During this process, protons are pumped across the inner mitochondrial membrane resulting in a proton-motive force also known as ΔΨm that is utilized to produce ATP (191, 192). Mitochondria are commonly between 0.75 to 3 µm in diameter but vary considerably in size and structure (193). Mitochondria are composed of several compartments including the outer membrane, the intermembrane space, the inner membrane, the cristae, and the matrix (194). The production of ATP relies on many proteins, including NADH dehydrogenase, cytochrome c reductase, and cytochrome c oxidase, located in the inner membrane (195). These proteins oxidize pyruvate, glucose, and NADH in the cytosol and perform the energy transfer (196). This type of cellular respiration relies on oxygen and is known as aerobic respiration. In addition to supplying ATP, mitochondria are also involved in cell signalling, cellular differentiation, cell cycle regulation and cell growth (197). Although the process of ATP production is very efficient, it often contributes to electron leaks from the respiratory chain and can form ROS (198). Therefore, mitochondrial dysfunction has been implicated in a wide range of chronic diseases such as Alzheimer's, Parkinson's, cardiac dysfunction, diabetes, and COPD etc (199) and is an important therapeutic target.

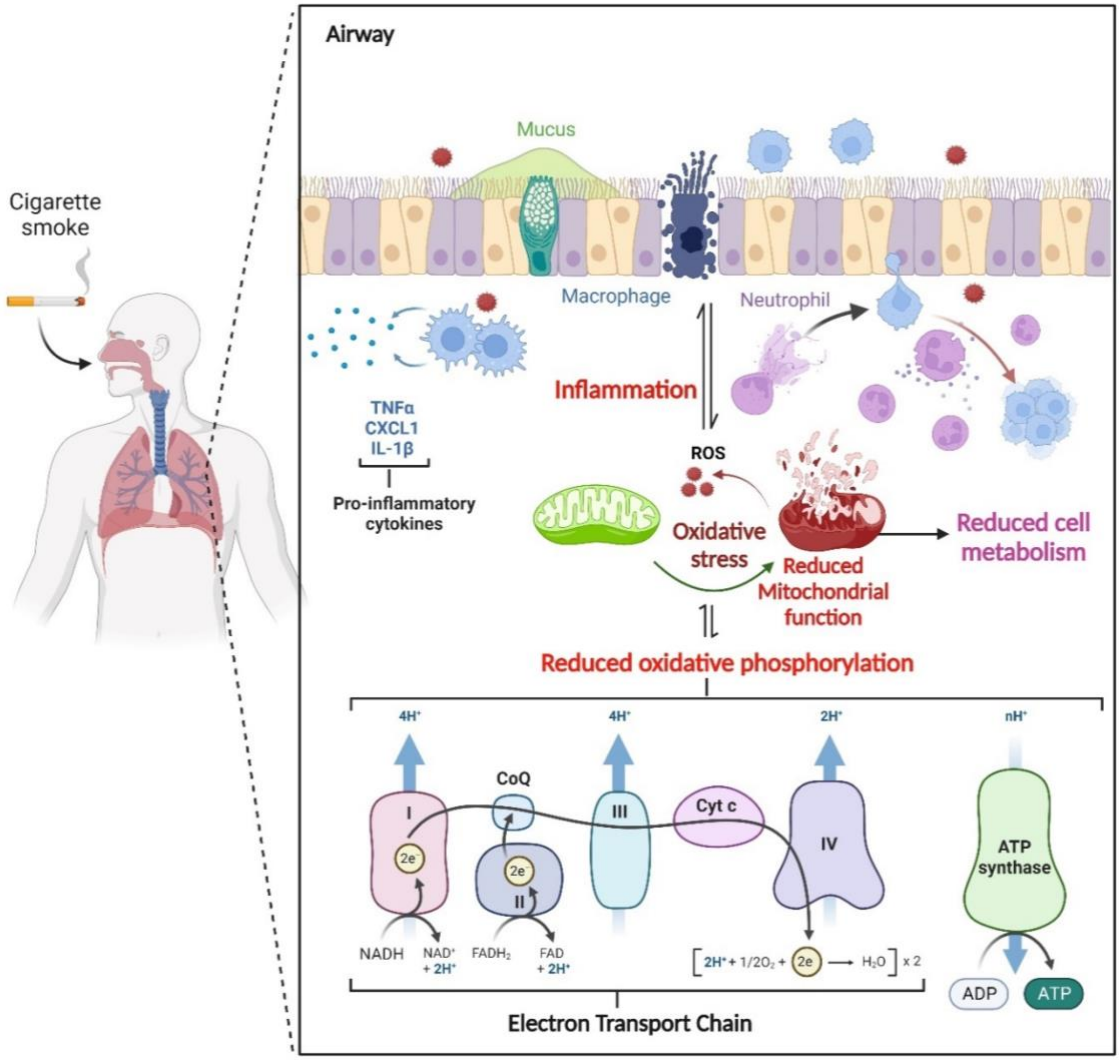

Figure 1.2:CS exposure in COPD

Chronic exposure to CS is a form of exogenous ROS in COPD and can initiate oxidative stress, inducing inflammatory responses. This further leads to the release of endogenous ROS from inflammatory cells such as macrophages and neutrophils as well as mtROS via disruption in the electron transport chain (ETC) during oxidative phosphorylation (oxphos). This further leads to altered cellular metabolism and cell death via apoptosis causing increased COPD exacerbations.

1.5 Glycolysis

Glycolysis is a process where glucose is broken down to produce energy (200). The process occurs in the cytoplasm of a cell and does not require oxygen. Glycolysis can produce two molecules of pyruvate, ATP, NADH and water (201) (Figure 1.3). Glycolysis is the primary step of cellular respiration and occurs in two distinct phases energy-requiring phase and the energy-releasing phase (202). The energy-requiring phase is completed over five different steps followed by the energy-releasing phase over the next five steps where glucose is converted into two molecules of pyruvate (203). In the presence of oxygen, pyruvate is circulated to the Krebs cycle or is reduced to lactate in absence of oxygen (204).

Recent studies have highlighted the importance of glycolysis in COPD as glycolysis generates pyruvate and the availability of pyruvate determines the rate of lactate production which contributes to disruption in metabolism. Multiple studies have shown a higher rate of glycolysis in COPD patients which contributes to the imbalance of production and oxidation of pyruvate leading to a reduction in acetyl coenzyme-A (acetyl-CoA) levels. Furthermore, these imbalances contribute to oxidative stress and impaired metabolism in the immune cells and therefore, are an important therapeutic target in COPD.

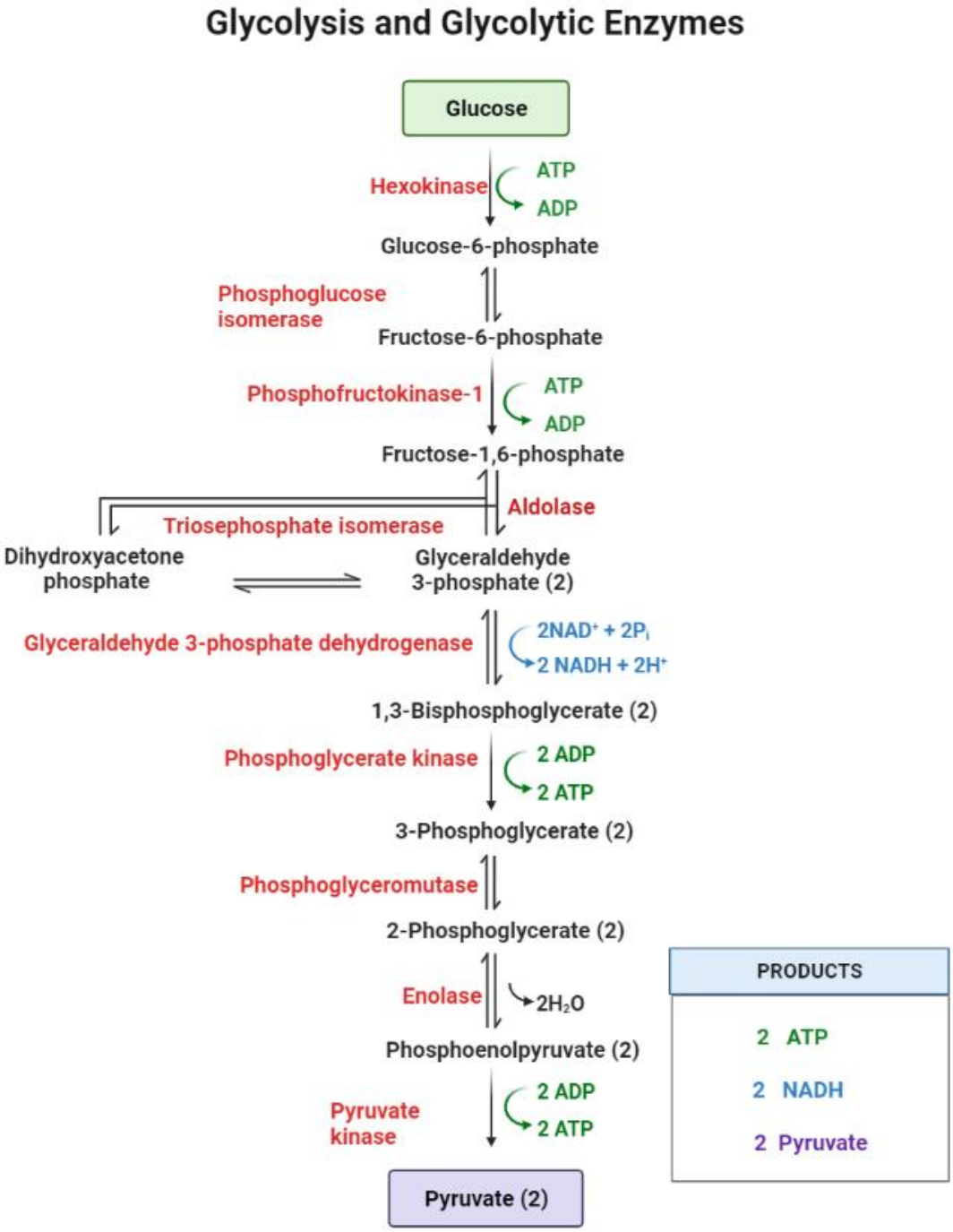

Figure 1.3: Glycolysis:

Glycolysis is the primary step in glucose metabolism, harnessing the breakdown of glucose for the generation of ATP, NADH and biosynthetic intermediates. The pathway produces pyruvate under aerobic conditions, and lactate under anaerobic conditions. Pyruvate is used as a resource to initiate the Krebs cycle.

1.6 Krebs cycle

Cellular metabolism comprises the utilization of carbohydrates, fats, and proteins, to synthesize energy (205). The Krebs cycle, also known as the TCA cycle, or citric acid cycle is an important part of aerobic respiration (Figure 1.4) (206). The Krebs cycle plays a major role in glucose metabolism whereby glucose is catalysed to form pyruvate, which is then oxidised to enter the cycle as acetyl coenzyme-A (207). This cycle harnesses the available chemical energy of acetyl-CoA into reducing NADH to nicotinamide adenine dinucleotide (NAD^+) (208). The Krebs cycle is dependent on multiple pathways for the constant supply of its various intermediates comprising fatty acids, amino acids, or porphyrins (209). Impaired metabolism leads to a diversion in these intermediates thus compromising the integrity of the Krebs cycle and failure to generate ATP (210). The Krebs cycle generates 2 molecules of ATP, 8 molecules of NADH, 2 molecules of $FADH_2$ and 6 molecules of carbon dioxide (CO_2) which is then passed onto the ETC to generate ATP (211).

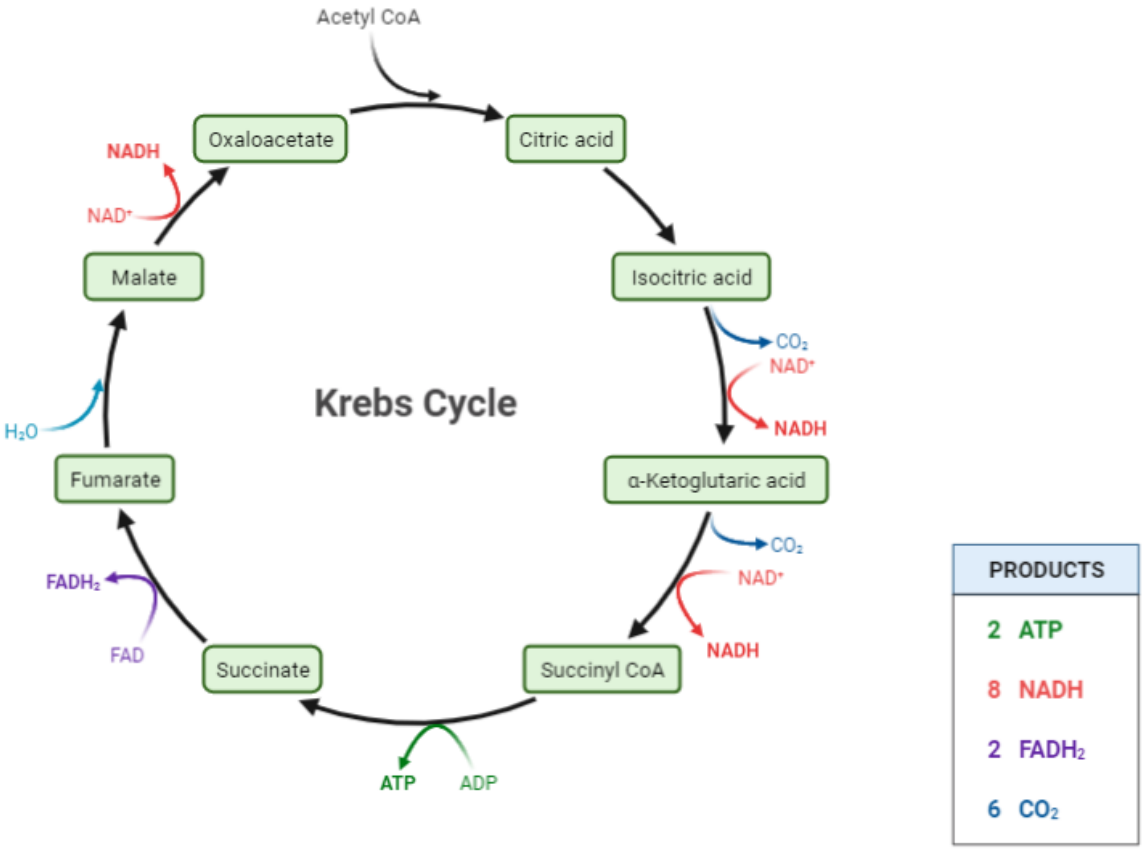

Figure 1.4: Krebs cycle

The Krebs cycle plays an important role to generate energy in aerobic cell metabolism. The intermediates of the Krebs cycle also plays important role in other biochemical pathways. Pyruvate, the end product of glycolysis is converted into acetyl-CoA which then enters the Krebs cycle. The metabolites undergo a series of chemical reactions catalysed by the Krebs cycle enzymes to generate 2 molecules of ATP, 8 molecules of NADH, 2 molecules of FADH2 and 6 molecules of CO_2.

1.7 Oxidative phosphorylation and electron transport chain

Oxidative phosphorylation or oxphos is a cellular process that harnesses the reduction of oxygen to generate ATP (212). It comprises a series of oxidation-reduction reactions that

involve the transfer of electrons from NADH and FADH2 to oxygen across several proteins, and lipid complexes in the mitochondria known as the ETC. The ETC utilises NADH and FADH2 generated from the Krebs cycle (213). There are four protein complexes involved in electron transfer that function as enzymes in the ETC (Figure 1.5) (214). These ETC complexes carry out oxidation and reduction reactions, using the transfer of electrons from one complex to the next in series (215). The complexes are named: Complex I, II, III, and IV. Of the four complexes, complexes I, III, and IV are responsible for pumping 4 protons into the intermembrane space, which is then carried to the next complex and eventually to complex V by cytochrome C or coenzyme Q10 (216). Complex V is also known as ATP synthase, and is functionally different from the other complexes, as it is not involved in the transfer of electrons but facilitates the generation of ATP (217). The transfer of electrons via all the complexes to complex V for ATP synthesis is referred to as oxphos and can generate 36~38 ATP molecules in one complete cycle (218).

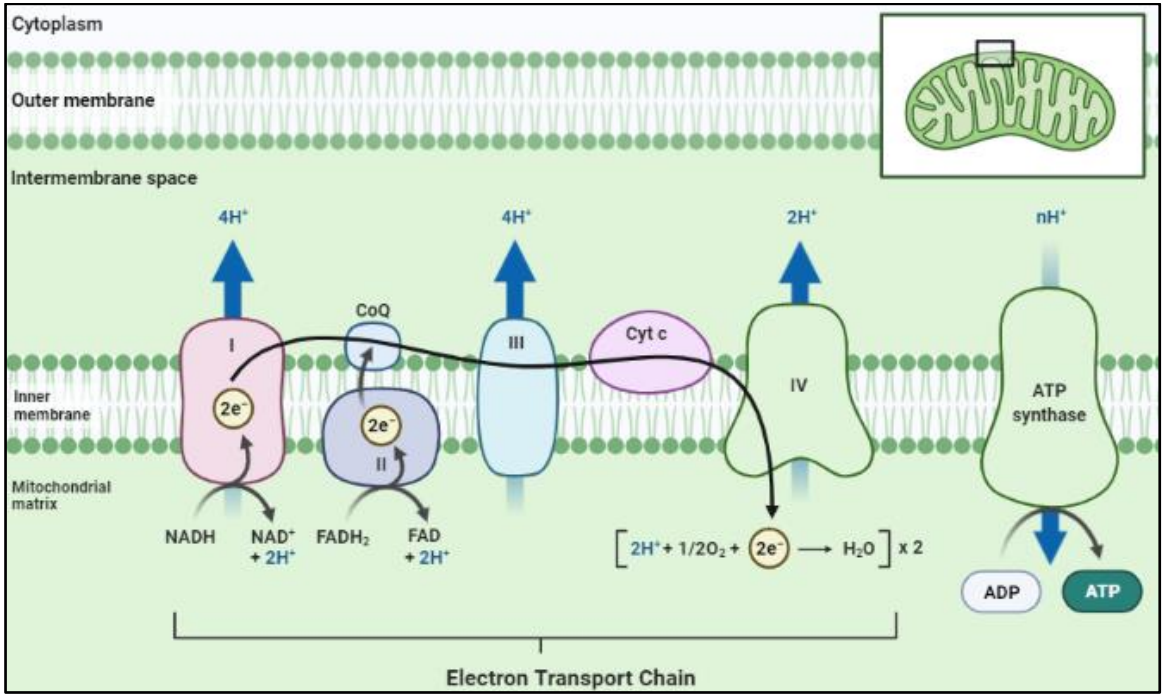

Figure 1.5: The electron transport chain

ETC consists series of complexes that transfer electrons in the membrane to create a gradient of protons in the mitochondrial inner membrane. Electron donors, NADH and $FADH_2$ generated from the Krebs cycle release electrons that are accepted by electron acceptors (redox reactions) creating a proton gradient driving ATP production through ATP synthase, a process known as oxphos.

1.8 NAD^+, a potential therapeutic target for COPD

NAD^+ is both a crucial coenzyme and a co-substrate for all metabolic reactions in living organisms (219). Maintenance of NAD^+ levels is essential for cellular energy, homeostasis, survival, and proliferation (220). NAD^+ and its reduced form, NADH, play an important role in maintaining cell survival and metabolism via regulating numerous biosynthetic pathways including redox protective roles (220, 221). NAD^+ serves as an electron acceptor and transfers energy between different metabolic pathways such as glycolysis and the Krebs cycle (220, 222). Depletion of NAD^+ levels leads to disruption in the mitochondrial metabolism and results in an imbalance in cellular redox homeostasis (223). NADH on the other hand is an electron donor that is oxidised during oxphos leading to ATP production (222). NAD^+ can regulate multiple signalling pathways including immune and inflammatory responses (221, 222). NAD^+ availability is determined by the rate of NAD^+ biosynthesis or consumption (Figure 1.6) (222). There are several NAD^+ precursors like tryptophan (TRP), Nicotinamide riboside (NR), Nicotinamide mononucleotide (NMN), Nicotinamide (NAM) and Nicotinic acid (NA) which synthesise NAD^+ via different pathways such as *de novo* biosynthesis pathway, Preiss-handler pathway, and Salvage pathway (Figure 1.6) (221). Mammalian cells can generate NAD^+ from dietary TRP using the *de novo* synthesis pathway via the intermediate ACMS which can spontaneously cyclize to quinolinic acid (QA) (Figure 1.6) (224). Additionally, the Preiss-Handler pathway can convert dietary NA to NMN by nicotinate phosphoribosyl transferase (NAPRT) (Figure 1.6) (225). Further, NAM, NA, NR and NMN can be catalysed to generate NAD^+ via the salvage pathway (Figure 1.6) (226).

Poly (ADP-ribose) polymerases (PARPs) (227), CD38 (228), and Sirtuins (SIRTs) (229) are the major consumers of NAD^+. PARPs are the most abundant and highly expressed nuclear enzymes and are widely involved in DNA damage responses, apoptosis, and epigenetic modifications (230). Chronic exposure to CS leads to DNA damage in COPD patients, and this is further elevated with an increase in oxidative stress. As a consequence, activation of PARPs is initiated to facilitate DNA repair, however, the constant DNA damage in COPD instigates the overactivation of PARPs leading to NAD^+ depletion and ultimately apoptosis (231). CD38 is a transmembrane glycoprotein (232) and plays an important role in cell adhesion (233), migration (234) and signal transduction (235). Additionally, CD38 is involved in the regulation of pro-inflammatory cytokines in monocytes, natural killer (NK) cells, and activated B and T lymphocytes (236). CD38 has been postulated to be the major NAD^+ consumer in cells and defective CD38 signalling exhibits impaired innate immunity and immune responses (237). Aside from playing a key role in various cellular enzymatic reactions and signalling pathways, NAD^+ also dictates the host's innate and adaptive immune responses (238). NAD^+ regulates TNFα expression in macrophages via regulating the expression of CD38, indicating a link between the metabolic/redox state of the cell and its inflammatory responses (239). This results in the induction of CD38 which can further scavenge the cellular NAD^+ pool (181, 240). Several studies have demonstrated elevated TNFα levels in COPD patients suggesting an increase in the CD38 expression, however, to date the role of CD38 in COPD is less clear. SIRTs depend entirely on NAD^+ and are involved in the chemical reversal of acetyllysine modifications of cellular proteins (222, 229). SIRTs are class III histone deacetylases that play a crucial role in restoring cellular homeostasis during stress responses (241). Recent studies have highlighted the protective mechanisms of SIRTs in aging-related diseases (242), such as cancer (243),

cardiovascular (244) and neurodegenerative diseases (245), osteoporosis (246), and COPD (247). Previous studies have shown the protective role of SIRT1 and SIRT6 against COPD (248), however, currently, there is no evidence of the effect of NAD^+ depletion on SIRTs during the development or progression of COPD. NAD^+ also inhibits T-cell proliferation and cytotoxic activity which are implicated during the pathogenesis of COPD (249). However, to date, the role of NAD^+ in COPD remains unclear and further studies are required to unveil the contributions of NAD^+ in COPD and potential therapeutic targets for the treatment of COPD.

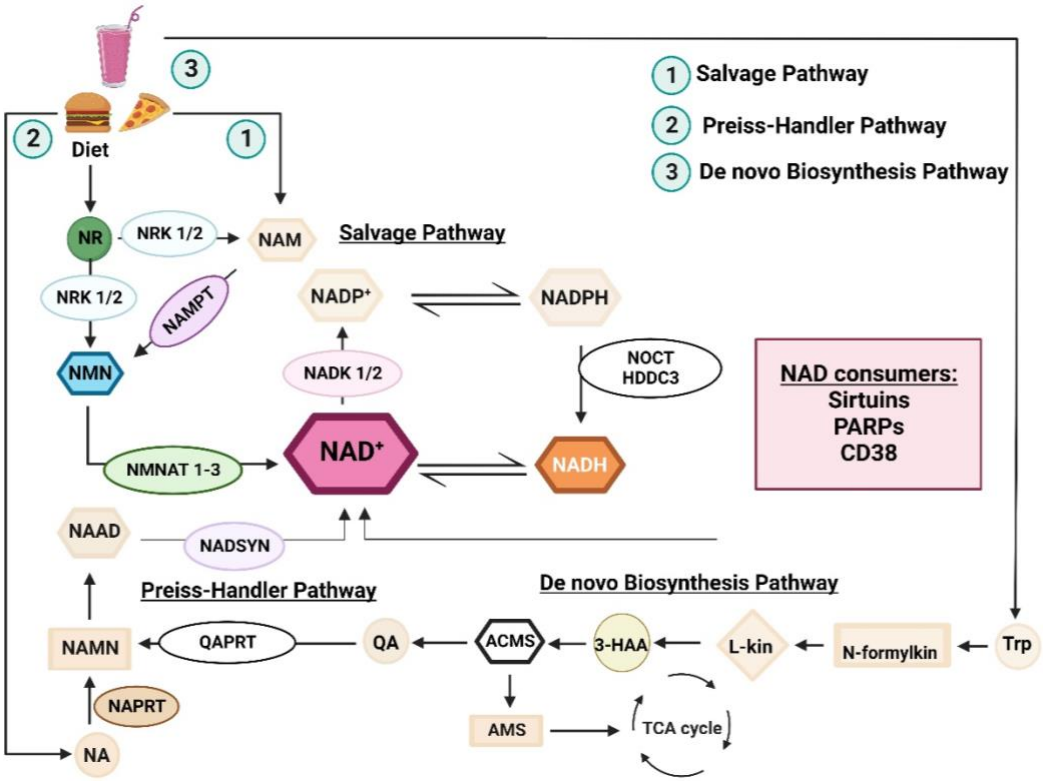

Figure 1.6: NAD biosynthesis and consumption

NAD biosynthesis occurs through three different pathways- Salvage pathway, Preiss-Handler's pathway, and de novo synthesis pathway. The salvage pathway converts NMN, NR, NAM and NA to NAD^+ in various cellular compartments including the nucleus and mitochondria. SIRTs, PARPs and CD38 are the major scavengers of NAD^+. The de

novo pathway of NAD^+ synthesis converts tryptophan to NAD^+ via intermediate components, this further links to the Preiss-Handlers pathway, which is a three-step pathway using dietary NA to generate Nicotinic acid mononucleotide (NAMN) and nicotinic acid adenine dinucleotide (NAAD) and is then converted to NAD^+.

1.9 NAD^+ modulators

The synthesis of NAD^+ is usually met by either the internal regeneration of NAD^+ by using endogenous metabolite such as QA or via dietary intake of NAD^+ precursors, globally termed as Vitamin B3. Vitamin B3 precursors of NAD^+ comprise NA, NAM, NMN, and NR. These modulators have been largely used in the research areas of neurodegenerative diseases, aging and diabetes (250).

1.9.1 Nicotinamide Riboside (NR)

NR, the precursor molecule of NAD^+, is derived from vitamin B3 and is known to be the most efficient way of restoring NAD^+ through the salvage pathway (Figure 1.8) (251). NR can synthesise NAD^+ through the salvage pathway either via generating NAM or by undergoing phosphorylation via nicotinamide ribose kinases (NRKs) to generate NMN (Figure 1.8). Further, NMN is then transformed into NAD^+ by NMN adenylyltransferase (NMNATs) (Figure 1.8). There are three different isoforms, NMNAT1 is localised in the nucleus, NMNAT2 is expressed in the cytoplasm and NMNAT3 is localised in the mitochondria (Figure 1.8). NR has been extensively used in aging research and has been demonstrated to restore NAD^+ levels in aged patients (252). Restoration of NAD^+ levels has also been shown in different studies to be beneficial in preventing cognitive decline (253), and loss of vision (254) and hearing in aged patients (255), as well as also improving motor dysfunction (256), immunodeficiency (257), cardiovascular diseases

(258), hepatic steatosis (259, 260), diabetes (253), infertility (261), kidney injury (262), obesity (263), cancer (264), sarcopenia (265), and inflammation (266).

1.10 Pterostilbene

PT is a naturally occurring analogue of resveratrol with increased bioavailability (267). The unique structure of PT has been attributed to its antioxidant, anti-inflammatory, and chemopreventative effects (268). PT upregulates SIRT1, NRF2, and NF-κB exhibiting anti-inflammatory benefits in various diseases such as neurological disorders, vascular diseases, diabetes and cancer. Further, PT is also known to upregulate AMPK displaying anti-oxidant properties which further leads to the upregulation of fatty acid oxidation and increases mitochondrial function (269). Additionally, the chemopreventative effects of PT revolve around its ability to target pleiotropic signalling pathways including mitogenesis, cell cycle regulation, and apoptosis (268, 269).

Based on the properties of both NR and PT it is hypothesised to synergistically support metabolic regulation through NR increasing NAD^+ levels which then acts as a substrate for PARPs, SIRTs and CD38. Furthermore, PT activates SIRT1 for enhanced NAD^+ consumption (Figure 1.7). NR and PT together have been widely used in studies targeting the restoration of NAD^+ in aging, mitochondrial function and metabolism, redox reactions, circadian cycle, DNA repair, cell division, signalling and inflammation (270).

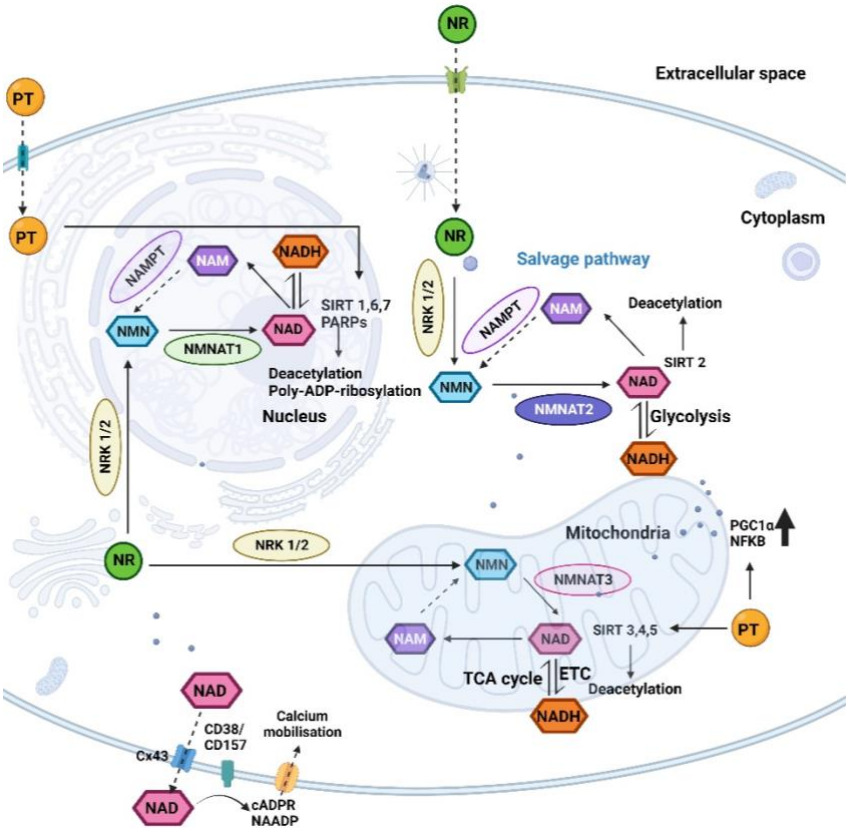

Figure 1.7: NR and PT regulating NAD$^+$ pool: NR is a precursor of NAD$^+$ and can synthesise NAD$^+$ via the salvage pathway providing NAD$^+$ for all the seven SIRTs. Whereas PT activates SIRT1 for enhanced consumption of NAD$^+$ and this further regulates the NAD$^+$ pool which is essential for maintaining cellular energy, homeostasis, survival, and proliferation.

1.11 TEPP46

TEPP46 is a chemically synthesised small molecule activator of PKM2 (271). It binds specifically to PKM2, inducing tetramerisation of PKM2 dimer to tetramer formation that further stimulates pyruvate production and activation of oxphos (271) (Figure 1.8). The imbalances in the production of pyruvate and reduction in oxphos can in turn reduce pro-inflammatory responses and promote anti-inflammatory responses in the cells (272). The

tetramerisation of PKM2 is crucial in determining the fate of glycolysis in the immune cells (273). Studies have shown that TEPP46 alleviates oxidative stress and suppresses apoptosis in cardiomyocytes (274) as well as inhibits glycolysis in T-cells (275). However, the role of PKM2 in the development and pathogenesis of COPD remains unknown and might potentially be an important therapeutic target.

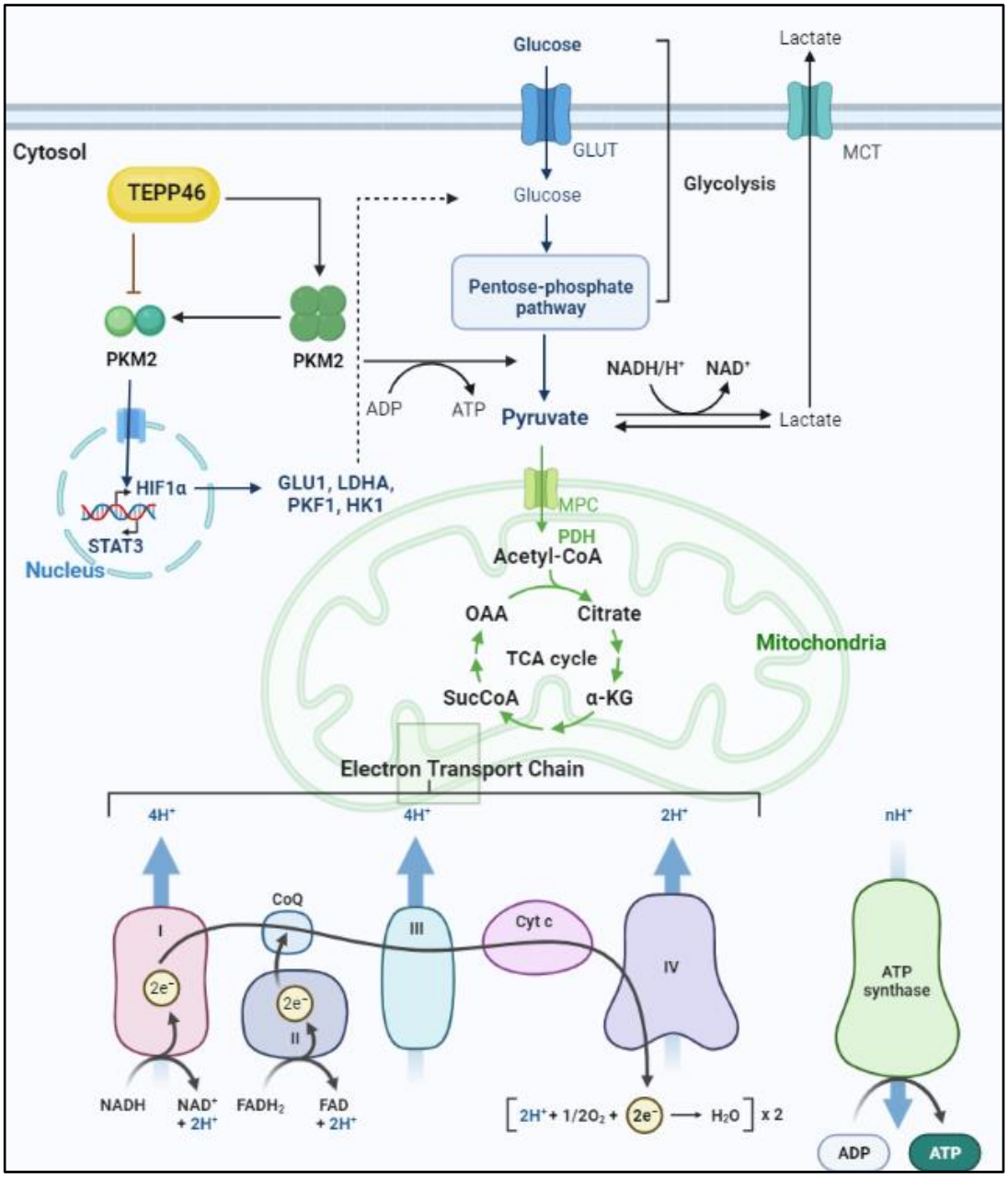

Figure 1.7: Tetramerisation of PKM2 by TEPP46

TEPP46 binds to PKM2 dimers inducing the formation of PKM2 tetramer and promoting the rate-limiting step of glycolysis and pyruvate production. Pyruvate enters the TCA cycle and stimulates the cell to begin oxphos.

1.12 Study rationale

Chronic exposure to CS is the predominant cause of COPD (276). The mechanisms that drive the development and progression of chronic inflammation in COPD are not well understood, and this has hampered the development of effective treatments for the disease (277). Current therapeutic approaches are limited and aim to manage symptoms and reduce exacerbations (277). Thus, there is a need for new therapies that inhibit the induction and progression of COPD (278). Recent studies have highlighted the importance of mitochondrial dysfunction (279) in COPD leading to decreased mitochondrial density and biogenesis (280), followed by impaired mitochondrial activity and apoptosis (281) during the pathogenesis of the disease. This decline in mitochondrial function causes oxidative stress further causing alterations in immune cell metabolism (282, 283). NAD^+ directly influences immune cell function via regulating energy metabolic pathways such as glycolysis, Krebs cycle, oxphos etc (284), subsequently leading to the production of ATP. Additionally, recent findings have also stated that metabolic marker PKM2, involved in catalysing the last step of glycolysis might potentially be involved in the metabolic reprogramming of immune cells further driving the sustained inflammation in COPD (160).

Currently, there is no evidence of the contribution of NAD^+ in impaired immunometabolism driving COPD (238). The objective of this thesis was to understand the role of NAD^+ and impaired immunometabolism involved in the induction, progression, and development of COPD. The study investigates the role of NR, PT, and TEPP46 as a therapeutic intervention in both prophylactic and therapeutic studies in a clinically relevant CS-induced experimental COPD murine model.

Chapter 2. General materials and methods

2.1 General reagents

2.1.1 Nuclease-free water

Nuclease-free water- UltraPure™ DNase/RNase-free distilled water (#10977023, Thermo Fischer Scientific, United States) was commercially obtained for all the experiments.

2.1.2 MilliQ water

MilliQ water was obtained from Milli-Q® Benchtop Lab Water Purification Systems (Merck, United States). Water purification was performed using the recommended specifications of resistivity > 10 MΩ at 25°C, total organic carbon < 500 ppb, bacteria <10 CFU/mL, and filtration of particles > 0.22 μm.

2.1.3 Ethanol (70% v/v)

Ethanol, absolute (#EL043, Chem supply, Australia)	70 mL
Milli-Q water	30 mL

2.1.4 Phosphate buffered saline (PBS) (1X)

1X Dulbecco's Phosphate-Buffered Saline (DPBS) powder (# 21600010, Thermo Fisher Scientific, United States)

Milli-Q water	1000 mL

2.1.5 Phosphate buffered saline – Tween-20 (PBST) (1X) (0.5%)

1X Dulbecco's Phosphate-Buffered Saline (DPBS) powder (# 21600010, Thermo Fisher Scientific, United States)	
Milli-Q water	1000 mL
Tween-20 (#P7949, Sigma Aldrich, United States)	0.5 mL

2.1.6 Sodium Chloride (NaCl) (0.9%)

Sodium Chloride (#S9888, Sigma Aldrich, United States)	9 g
MilliQ water	1000 mL

2.2 Animal models

2.2.1 Ethics statement

This thesis was performed following the Australian Code of Practice recommendations for the care and use of animals for scientific purposes issued by the National Health and Medical Research Council of Australia (NHMRC). All experiments were approved by the Sydney Local Health District (SLHD) Animal welfare committee of the Centenary Institute of Cancer Medicine and Cell Biology and covered by protocol 2019/003A and 2019/037A. All treated mice were weighed daily from the beginning of the exposure periods and monitored daily according to ethical criteria.

2.2.2 Experimental mice model

Female BALB/c mice, aged 6-8 weeks were obtained from the Animal Resources Centre (ARC), Western Australia used unless otherwise stated. Mice were maintained at 20 ±

2°C on a 12:12 hours day-night cycle and fed a standard sterile diet of mouse chow with water allowed *ad libitum* during an acclimatisation period of 7 days before experimental procedures.

2.2.3 Smoke inhalation system

Mice were subjected to either Room Air or CS exposure from 12 research-grade 3R4F cigarettes (University of Kentucky, USA) twice a day, five days a week for up to12 weeks using a custom-designed nose-only inhalation system (Scireq, Montreal, Canada) (Figure 2.1) (146).

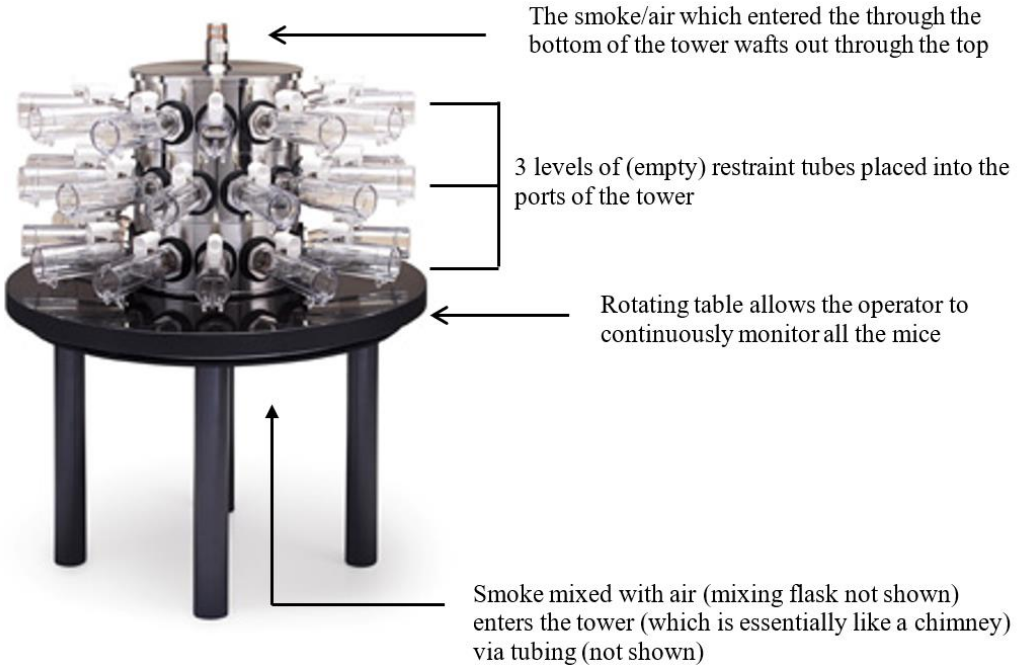

Figure 2.1: Smoke inhalation system:

Custom-built nose-only smoke exposure system to induce COPD via CS inhalation (146).

2.2.4 Preparation and exposure of mice to cigarette smoke

Research cigarettes were stored at -80°C and were removed from the freezer a day before the experimental procedure. Cigarettes were placed in an air-lock container along with a

petri dish of saturated 35% sodium bromide (# 746401, Sigma Aldrich, Australia) solution to ensure appropriate moisture content.

Mice were gently placed into custom-designed restraint tubes, with a plunger against the rear of the mouse. The tubes enable the mice to rest in a comfortable position for the whole smoke exposure session (Figure 2.2). The tubes were further connected to the ports in the smoke tower for exposure as shown in Figure 2.1.

The smoke machine is operated within a class II biological safety cabinet. The machine is connected to a compressed air inlet to ensure the dilution of the smoke extracts from every puff of the cigarette. The machine is set up by turning on the power for all the attached devices to the smoke machine and ensuring that the compressed air flow is set at 2.4 L/min. The machine is operated with an attached computer using custom-designed software, Human Profil Pump Interface. The script; CIR55_30sec_12puffs, was then executed which automatically lights the cigarette attached to the piston. Each puff volume is 55.19 cc/min and takes a total of 333 secs to complete the whole process with an interval of 10 secs between each puff for each cigarette. One round of smoke exposure consists of 12 cigarettes and takes up to 75 mins to complete. This was completed twice daily.

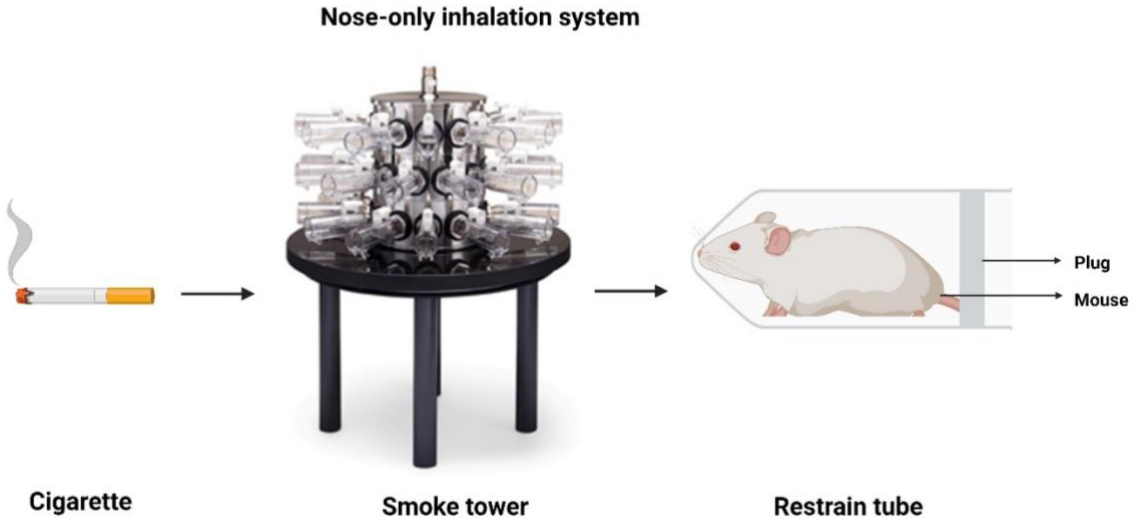

Figure 2.2: CS exposure of mice

Mouse restrain tubes for custom-built nose-only smoke exposure are inserted into the smoke tower which is then connected to the cigarette through a computer-operated system.

2.2.5 Euthanasia

Mice were euthanised via intraperitoneal administration of sodium pentobarbital for all the 2 weeks of acute studies. All the mice used in the 8 weeks or 12 weeks of COPD studies were subjected to surgical anesthesia using a mixture of ketamine and xylazine administered intraperitoneally for a terminal procedure of lung function measurements.

2.2.6 Blood and Serum

A cardiac bleed was performed on anaesthetised mice using a 26G needle. Collected blood was centrifuged at 8000 x *g* for 10 mins at 4°C, after which the serum fraction was collected and stored at -80°C for downstream analysis.

2.2.7 BAL

Bronchoalveolar lavage (BAL) was performed on the left lung lobe using Hank's media (# H9394, Sigma Aldrich, United States) (285). The BAL samples were centrifuged at 300 x *g* for 5 mins at 4°C, after which the supernatant was collected and stored at -80°C for downstream analysis. The cell pellet was then resuspended in 200 µL of homemade red blood cell (RBC) lysis buffer (Table 2.1) and was incubated for 3 mins at room temperature. Following incubation, 700 µL of Hank's media was added to neutralise the reaction and then centrifuged at 300 x *g* for 5 mins at 4°C. The supernatant was then discarded, and the pellet was resuspended in 160 µL of Hank's media. Total leukocyte counts were enumerated by mixing 10 µL of cell suspension with a 1:1 dilution of trypan blue (#15250061, Life Technologies) and then loaded onto a hemocytometer for counting. To perform differential counts to determine the major cell populations in the BAL, the remaining cell suspension was deposited onto microscope slides using a cytocentrifuge (Cytospin 4, Thermo Scientific, United States) at 300 RPM for 7 mins.

Table 2.1: RBC lysis buffer formulation

RBC lysis buffer (pH 7.35)	
Ammonium chloride (#A9434, Sigma Aldrich, United States)	4.15 g
Sodium bicarbonate (#8805, Sigma Aldrich, United States)	0.5 g
Ethylenediaminetetraacetic acid (EDTA) (#E1644, Sigma Aldrich, United States)	0.0185 g
Milli-Q water	500 mL

2.2.8 Differential counts on BAL

The cytospin slides were stained using the May Grunwald-Giemsa staining protocol for morphological analysis of leukocytes (286). The slides were incubated with May Grunwald (#MG1L, Point of Care Diagnostics, Australia) primary stain for 5 mins and rinsed in three changes of water for 5 mins each. The slides were further counterstained with Giemsa stain (#GIEM1L, Point of Care Diagnostics, Australia) for 20 mins. The slides were rinsed under running tap water for 5 mins, air-dried overnight, and then mounted with mounting media (#IM0225, ProSciTech, Australia) and coverslips (#CS24X50, Living Stone, Australia) and were subjected to drying overnight (146, 287). Differential leukocyte counts were analysed at 40X magnification using a bright-field microscope Axio Imager microscope (Zeiss, Oberkochen, Germany) accompanied by a camera (Zeiss Axiocam ICm1, Carl Zeiss AG, Germany). For each cytospin sample, morphological criteria for white blood cells (WBC) were enumerated for a total of 200 cells to identify major populations including monocytes/macrophages, neutrophils, eosinophils, and lymphocytes.

2.2.9 Processing of lung samples for histopathological analysis

The left lung lobe was perfused with 0.9% sodium chloride (NaCl) (#S7653, Sigma Aldrich, United States) to remove excess accumulated blood from the lung tissue. Following perfusion, the left lung lobe was gently inflated with 0.5 mL 10% neutral buffer formalin (#HT501320 Sigma Aldrich, United States) through the trachea and was submerged in 10% neutral buffer formalin for 24-48 hrs. After initial fixation, formalin was replaced with 70% ethanol (#E7023, Sigma Aldrich, United States) and 30% PBS (# 21600010, Life Technologies, United States) and tissue samples were processed in an

automatic tissue processor (Histocore PEARL, Leica, Wetzlar, Germany) through a series of dehydration steps of 1 hr each using ethanol 50%, 70%, 80%, 90%, 95%, 100% (thrice), Xylene (#VWRC28975.325, Bio-strategy, Australia) (thrice) and paraplast (#39601006, Leica, Wetzlar, Germany) at 60°C (288). Tissues were then embedded in paraplast using moulds to prepare paraffin blocks. All the blocks were sectioned longitudinally at 3.5 µm thickness using a microtome (# RM 2245 Leica, Wetzlar, Germany). Sections were then used for staining purposes.

2.2.10 Hematoxylin and Eosin stain

The lung sections were dewaxed before staining via immersing into xylene twice for 10 mins, followed by ethanol of 100%, 90%, 80%, 70%, and 50% for 5 mins each, and were then rehydrated in PBS. Lung sections were incubated in hematoxylin nuclear stain (#H3136, Sigma Aldrich, United States) for 10 mins followed by rinsing in water thrice for 5 mins each. The samples were counterstained with eosin (#861006, Sigma Aldrich, United States) followed by three water rinses for 5 mins each (289). The slides were then mounted with mounting media (#IM0225, ProSciTech, Australia) and coverslips (#CS24X50, Living Stone, Australia) and air-dried overnight (289). Slides were imaged under 40X magnification using a bright-field microscope Axio Imager microscope (Zeiss, Germany) embedded with a camera (Zeiss Axiocam ICm1, Carl Zeiss AG, Germany) and analysed using Zen Imaging Software (Zen 3.0 blue edition, Carl Zeiss Microscopy). The mean linear intercept was calculated using MLI/DI plugin in ImageJ (National Institute of Health, United States).

2.2.11 Sirius red and fast green stain

Sections were dewaxed and rehydrated as mentioned previously and were stained using Fast-green (#F7252-5G, Sigma Aldrich, United States) for 8 mins followed by a water rinse for 10 mins. The sections were counterstained using Picro-Sirius (Direct RED-80 #365548, Sigma Aldrich, US) stain for 1 hr. The slides were rinsed twice in acidified water, blot dried, then mounted with mounting media (#IM0225, ProSciTech, Australia) and coverslips (#CS24X50, Living Stone, Australia), and left to air-dry overnight (290). Slides were imaged under 40X magnification using a bright-field microscope Axio Imager microscope (Zeiss, Germany) embedded with a camera (Zeiss Axiocam ICm1, Carl Zeiss AG, Oberkochen, Germany) and analysed using Zen Imaging Software (Zen 3.0 blue edition, Carl Zeiss Microscopy). The mean alveolar diameter of the collagen deposition around the basement membrane of small airways was calculated using the colour deconvolution plugin for Sirius red and fast green in ImageJ (National Institute of Health, United States).

2.2.12 Lung function

Forced manoeuvre and forced oscillation techniques were used to assess lung function parameters. Mice were anesthetised with three different doses of anaesthetics to achieve surgical anaesthesia with regular breathing. The first dose of anaesthetics ensured the withdrawal of reflexes which was observed by toe pinch, whisker movements and palpebral reflex elicited by a gentle touch and was achieved by intraperitoneal administration of 13 mg/mL of ketamine and 1.6 mg/mL of xylazine at a volume of 200 µL for a 20 gm mouse. Along with the withdrawal of reflexes, the respiratory rate and pattern were also closely monitored by observing the thoracic movement. Once the

cessation of reflexes was achieved, the second anaesthetic dose of 40 mg/mL of ketamine and 2 mg/mL of xylazine was administered to the mice via intraperitoneal administration at a volume of 100 μL for a 20 gm mouse. Upon accomplishment of surgical anaesthesia, a tracheostomy was performed on the mice by making an incision on the skin above the trachea and excising the submaxillary gland by removing the muscle layer covering the trachea. The trachea was then gently lifted using a pair of forceps and a suture was passed underneath the trachea. A 19-gauge needle was used to create a small incision above the largest cartilage ring, followed by the insertion of a custom-fit 18-gauge cannula (Scireq, Canada), after which the cannula was secured with a suture enabling an airtight seal between the trachea and cannula. A third anesthetic dose of 2 mg/mL xylazine was then administered to the mice as a muscle relaxant to ensure respiratory compliance throughout the lung function procedure. Mice were then placed onto the FlexiVent apparatus (291) (FX2 System; Scireq, Montreal, Canada) and mice were ventilated with a baseline tidal volume of 8 mL/Kg at a respiratory rate of 450 breaths/min. Following compliance of the mouse once ventilation was commenced, the forced pulmonary manoeuvre script was commenced using the FlexiWare 7 software (292). Lung parameters measured included forced vital capacity (FVC), inspiratory capacity (IC), total lung capacity (TLC), and area (hysteresis). A "snapshot perturbation" manoeuvre was imposed to measure resistance (Rrs), compliance (Crs), and elastance (Ers) of the whole respiratory system (airways, lungs, and chest wall). Forced oscillation perturbation ("Quick prime-3") was consequently applied and resulted in the measurement of the transpulmonary resistance (Rn), tissue damping (G), and tissue elastance (H). The maximal PV loops (PVs-V = PV-stepwise-volume regulated; PVr-V = PV-ramp-volume regulated; PVr-P = PV-ramp pressure regulated) were generated to obtain maximal TLC, IC, the form of deflating PV loop, and hysteresis (area between inflating and deflating part of the loop). All the

manoeuvres and perturbations were performed until three correct measurements were achieved.

2.2.13 Lung function analysis

FlexiWare7 software was employed to automatically calculate and display lung parameters associated with each perturbation (292). FlexiWare7 provides a coefficient of determination (COD) that reflects the fit of the mathematical model to the data. Each data set with an insufficient COD is excluded by the software. The datasets having a sufficient COD were exported through the *Review & Reporting* module of the software for the parameters such as pressure-volume curves, raw dataset signals and subject information to a spreadsheet application. A mean of baseline measurements was calculated for each parameter with the exclusion of the first value and used for further analysis in GraphPad Prism version 9.0 for Windows (GraphPad Prism software, San Diego, California, United States).

2.2.14 Immunofluorescence staining

Sections were dewaxed and rehydrated as mentioned previously under section 2.7 and then incubated in the citrate-EDTA buffer as mentioned below in table 2.2 at 80°C for 30 mins. The slides were allowed to cool for 20 mins at 4°C and were immersed in PBS to wash off the citrate buffer for 5 mins. The sections were then blocked in 5% bovine serum albumin (BSA) (#A7030, Sigma Aldrich, United States) for 1 hr at room temperature. Samples were further incubated with 1:300 dilutions of primary antibody specific to different targets as listed below in table 2.3 for 1 hr at room temperature for each antibody staining. Slides were rinsed thrice with PBS with 0.5% tween (PBST) for 5 mins each

prior to incubation with 1:600 dilution cross-adsorbed secondary antibody as listed in table 2.3, for 1 hr at room temperature in the dark. Slides were then rinsed thrice with PBST, mounted with coverslips using Gold-antifade conjugated with DAPI nuclei stain (#P36935, Thermo Scientific, United States) and air-dried in the dark overnight (293). Fluorescence signals were detected at random locations of the sample using an Axio Imager microscope (Zeiss, Germany) embedded with a camera (Zeiss Axiocam ICm1, Carl Zeiss AG, Germany). A total of ten images were obtained per sample and analysed using Zen Imaging Software (Zen 3.0 blue edition, Carl Zeiss Microscopy).

Table 2.2: Citrate EDTA Buffer (pH 6.2)

Citrate-EDTA Buffer (pH 6.2)	
Citric Acid monohydrate (10mM) (#C1909 Sigma Aldrich, United States)	2.1014g
EDTA (2mM)	0.74g
Milli-Q	up to 1000 mL
Tween 20 (0.05%) (#P7949, Sigma Aldrich, United States)	0.5 mL

Table 2.3: List of primary antibodies used in immunofluorescence staining

Primary antibodies	**Dilutions**	**Secondary antibodies**	**Dilutions**
Anti-4-hydroxynenal antibody (ab46545, Abcam, United States)	1: 300	goat anti-rabbit IgG (H+L) Alexa Fluor 555 (#A32732, Thermo Scientific, United States)	1: 600

PKM2 antibody (# PA528700, Thermo Fisher, United States)	1:300	goat anti-mouse IgG (H+L) Alexa fluor (#A21422, Thermo Scientific, United States)	1:600
HIF1α antibody (# MA1-516, Thermo Fisher, United States)	1:300		
Anti-3-Nitrotyrosine antibody (#ab110282, Abcam, United States)	1:300		
F4/80 antibody (#MCA497G, Biorad, United States)	1:100		
EPCAM antibody (#ab213502, Abcam, United States)	1:100		

2.2.15 Transmission Electron microscopy

The post-caval lung lobe was perfused with 0.9% NaCl as previously described in section 2.6. The lobe was then excised and diced into approximately 1 mm^3 cube and dispensed into the 2.5% glutaraldehyde working solution listed below in table 2.6. The tissue samples were processed in a BioWave Pro$^+$ Microwave Tissue Processing System (TED Pella Inc., United States) following the manufacturer's protocol. The samples were stained with 1% osmium tetroxide and counterstained with 2% uranyl acetate prepared

according to the table below 2.7 and 2.8 (294). Samples were then dehydrated using ethanol 50%, 60%, 70%, 80%, 90%, 95%, and 100% (thrice) and were subjected to resin infiltration with procure of 25%, 50%, 75%, and 100% (thrice). Tissue samples were embedded in resin (#C045, ProSciTech, Australia) and allowed to dry at 60°C in a hot air oven for 2 days. Resin blocks were polished using a glass knife (# 8030 TED Pella, United States) in ultramicrotome (#UC7, Leica, Wetzlar, Germany) and were sectioned using a Diatome 45° diamond knife (#DU4530, EMgrid, Australia) at a thickness of 60 nm. Sections were collected on a copper grid (EMSHC200-AU-100, ProSciTech, Australia) and imaged using JEOL 1400 (JEM, United States) transmission electron microscopy (TEM). A total of 10 images were obtained per sample and analysed using Image J (National Institute of Health, United States). Mitochondria with an intact double membrane with visible cristae and dense matrix were counted as healthy or normal mitochondria, whilst unhealthy or abnormal mitochondria had distorted membranes with swollen cristae and sparse matrix (295).

Table 2.4: Recipe for 0.4M sodium cacodylate buffer

Sodium cacodylate buffer (0.4M)	
Sodium cacodylate trihydrate (#C0250, Sigma Aldrich, United States)	10.7g
Milli-Q water	125 mL

Table 2.5: Recipe for 0.2M sodium cacodylate buffer

Sodium cacodylate buffer (0.2M) (pH-7.2)	
0.4M Cacodylate buffer	50 mL

0.2M Hydrochloric Acid (HCL)	8 mL
Milli-Q water	Top up to 100 mL

Table 2.6: Recipe for 0.1M sodium cacodylate buffer

Sodium cacodylate buffer (0.1M) (pH-7.2)	
0.2M Cacodylate buffer	50 mL
Milli-Q water	Top up to 100 mL

Table 2.7: Recipe for 2.5% glutaraldehyde working solution

Glutaraldehyde (2.5% working solution)	
Glutaraldehyde (25% v/v) (#G5882, Sigma Aldrich, United States)	8 mL
0.2M Cacodylate buffer	50 mL
Milli-Q water	Top up to 100 mL

Table 2.8: Recipe for 1% osmium tetroxide

Osmium tetroxide (1% working solution)	
Osmium tetroxide (#75632, Sigma Aldrich, United States)	1g
Milli-Q water	100 mL

Table 2.9: Recipe for 2% uranyl acetate

Uranyl acetate (2% working solution)

Uranyl acetate (#541-09-3, ProSciTech, Australia)	2g
Milli-Q water	100 mL

2.2.16 RNA extraction

Mouse lungs were excised and snap-frozen in liquid nitrogen before being stored at -80°C until required. At the time of analysis, samples were thawed gently on ice, and then RNA was extracted using the Trizol-chloroform method (296) (TRI reagent, Chloroform, Sigma Aldrich, USA) according to the manufacturer's instructions. Briefly, lung tissues were homogenised in 1 mL of trizol using stainless steel beads (Qiagen, USA) using a bead homogeniser (Qiagen, USA). The homogenate was transferred into a fresh 1.5 mL tube and centrifuged at 12,000 x *g* for 10 mins at 4°C, after which the clarified supernatant was transferred into a fresh 1.5 mL tube. To the supernatant, 250 µL of chloroform (#C2432, Sigma Aldrich, USA) was added to each sample and vortexed until a homogenous solution was achieved. The samples were then incubated at room temperature for 10 mins, followed by centrifugation at 12,000 x *g* for 15 mins at 4°C. After centrifugation, the aqueous phase was transferred carefully into a fresh 1.5 mL tube and then 500 µL of ice-cold Isopropyl alcohol (#I9516, Sigma Aldrich, USA) was added to each tube. The samples were vortexed and incubated at room temperature for 10 mins, followed by centrifugation at 4°C, 12000 x *g* for 10 mins. Following centrifugation, the supernatant was discarded, and the RNA pellet was carefully washed with 1 mL of 75% Ethanol followed by vortexing and centrifugation at 8,000 x *g* for 5 mins at 4°C. This step was repeated. The supernatant was then discarded, and the RNA pellet was subjected to air drying for 15 mins on ice. Further, the RNA pellet was resuspended in 30 µL of

nuclease-free water (#10977023, ThermoFisher Scientific, USA). The concentration and quality of RNA were measured using a Nanodrop (Thermo Scientific, USA).

2.2.17 cDNA preparation

RNA was reverse transcribed into cDNA using Bioscript (# BIO-21118, Bioline, Australia) and random hexamer primers (# BIO-38028, Bioline, Australia) (297). An equivalence of 1000 ng of RNA was used for cDNA preparation and the volume was made up to a total volume of 8 µL, to which 2 µL of DNase I mix was added, consisting of 10X DNase reaction buffer and DNase I and incubated at room temperature for 15 mins. To ensure the chemical inactivation of DNase I, 1 µL of DNase I STOP solution was added and mixed gently. The samples were transferred to a T100-Thermal Cycler (Bio-Rad) and incubated at 65°C for 10 mins. A cocktail of 2 µL of 50 ng/µL random primers and 10mM dNTP mix was added to the samples and incubated at 65°C for 5 mins. Following the incubation, 7 µL of MMLV master mix was added to each reaction, comprising of 5X MMLV (1^{st} strand) reaction buffer, 100 mM DTT and 1 µL of nuclease-free water and incubated at 37°C for 2 mins. After the incubation, 1 µL of MMLV reverse transcriptase was added to each reaction and incubated at 25°C for 10 mins, followed by 37°C for 50 mins and 70°C for 15 mins. After the completion of the final reaction, cDNA samples were diluted by the addition of 79 µL of nuclease-free water and the final volume was brought up to 100 µL. The samples were stored at -20°C until further required.

2.2.18 Quantitative PCR

Quantitative PCR (qPCR) reactions were completed as previously described (297) using real-time PCR systems (Biorad, United States) Each reaction consisted of 2 µL of 1/100

dilution of cDNA, 500 nM of both forward and reverse primers, 6.25 µL of iTaq Universal SYBR green supermix (#172-5124, BioRad) with the final reaction volume brought up to a total of 12.5 ul with nuclease-free water. Cycling conditions consisted of the following program: 50°C for 2 mins, 95°C for 2 mins, 95°C for 15 secs and 60°C for 30 secs for a total of 40 cycles, and the reaction terminated at 95°C for 10 secs followed by 60°C for 5 secs. The fluorescent acquisition was obtained through the SYBR channel. Samples were run in duplicate with reaction specificity confirmed based on the post-amplification dissociation curve.

2.2.19 Gene expression

The relative mRNA expression was determined in comparison to the housekeeping gene hypoxanthine-guanine phosphoribosyl transferase (*Hprt*) by qPCR using a CFX384 Touch Real-Time PCR Detection System (Bio-Rad, United States). Custom-designed primers (Integrated DNA Technologies, United States) were used as represented below in table 2.9.

Table 2.10: Primer sequences

Gene	**Primer Sequence (5'-3')**
Cxcl-1	GCTGGGATTCACCTCAAGAA CTTGGGGACACCTTTTAGCA
Gene control non-derepressible 5 (*Gcn5*)	GGGCTTCTCCAAAGACATCAA GATTCAGCTCACACTCCATCAG
Hif1α	KiCQSTART PRIMER_KSPQ12012G Species: Mouse Primer Pair ID: M_Hif1a_1

Heme Oxygenase (*Ho*)1	CACTCTGGAGATGACACCTGAG GTGTTCCTCTGTCAGCATCACC
Il-1β	TGGGATCCTCTCCAGCCAAGC AGCCCTTCATCTTTTGGGGTCCG
iNos	AGCGAGGAGCAGGTGGAAGACT CCATAGGAAAAGACTGCACCGAA
NAD^+ kinase (*Nadk*)*1*	GTGTTTCTGGAGATGGCTAGG CCCTGTTGTGTGAGGAATGT
Nadk2	CTTCTGGCTGCGAGTAAAGT CAGGGAAGGAATGCGTGTAT
NAD^+ synthase (*Nadsyn*)*1*	CTCCATGAACAGGCACAAGA CAGAAAGGGTCTCAGGTCAAA
Nicotinamide phosphoribosyl transferase (*Nampt*)	AATCCAGGAGGCCAAAGAAG CCTTTACTTCAATCGGGAGATGA
Nfκb	CTGCTCAGGTCCACTGTCTG TTGCGGAAGGATGTCTCCAC
Nicotinamide mononucleotide transferase (*Nmnt*)	CCACCATCTATCAGCTTCTCTC GGTTCCTTCTTCAGCCATTTC
Nmnat1	GTGGAGACTGTGAAGGTGCTC GTGAGCTTTGTGGGTAACTGC
Nmnat2	TGGAGCGCTTCACTTTTGTA CGATCTCCTCATACCGCATC

Nmnat3	CACCAAACAGGAAGGTACCA AAGCCACCAGGTCTTTCTTC
Nrk1	GGATGGAACAAGGTCTGAAGAG CACTCCATCTGTGTGGTGTTAT
Nrk2	TGGGTAAGGAGAAACAACATCTAC CTAGCTGGACACACCAACTTAC
NADHP oxidase (*Nox*) -2	AACTGG GCTGTGAATGAAGG CAGCAGGATCAGCATACAGTTG
Parp1	ACAAGGAGAGCAGGTACTGGA GGAGGGCATCTGCTCAAGTT
3-Phosphoinositide-dependent kinase 1 (*Pdk1*)	GGACTTCGGGTCAGTGAATGC TCCTGAGAAGATTGTCGGGGA
Pgc1α	GTTGAAAAAGCTTGACTGGCGTC AGTTCAGGAAGATCTGGGCAAAG
Pkm1	GTCTGGAGAAACAGCCAAGG TCTTCAAACAGCAGACGGTG
Pkm2	GTCTGGAGAAACAGCCAAGG CGGAGTTCCTCGAATAGCTG
Purine Nucleoside Phosphorylase (*Pnp*)	GTTGGTTCACACTCCTTCTCT CCCTCAGTTATGCCCTCTATTT
Sirt1	CAGCCGTCTCTGTGTCACAAA GCACCGAGGAACTACCTGAT

Sirt2	GCAGTGTCAGAGCGTGGTAA CTAGTGGTGCCTTGCTGATG
Sirt3	CTGACTTCGCTTTGGCAGAT GTCCACCAGCCTTTCCACAC
Sirt4	CGCTGCTCAAGATCCCTAAG GCGACACAGCTACTCCATCA
Sirt5	AGCCAGAGACTCAAGACGCCA AGGGCGAGCTCTCTGTCCACC
Sirt6	TCGGGCCTGTAGAGGGGAGC CGGCGCTTAGTGGCAAGGGG
Sirt7	GGCACTTGGTTGTCTACACG AGGTCGGCAGCACTCACAGG
Tnf-α	TCTGTCTACTGAACTTCGGGGTGA TTGTCTTTGAGATCCATGCCGTT
chitinase-like protein 3 (*Ym-1*)	CCCCAGGAAGTACCCTATGCCT AACCACTGAAGTCATCCATGTCC
Hprt (housekeeping)	AGGCCAGACTTTGTTGGATTTGAA CAACTTGCGCTCATCTTAGGCTTT

2.2.20 Analysis of qPCR experiments

Using the software (Biorad) threshold cycle values were automatically generated for each sample and analysed using the △△Cq method relative to the internal control gene (HPRT) (146). The data were expressed as the relative expression for each target gene, normalised to the average of the control group (air).

2.2.21 Protein isolation and quantitation

Lung tissues were crushed into powder on dry ice using a tissue grinder (#D8938, Sigma Aldrich, United States). To 150 mg of powdered tissue, 150 µL of sucrose homogenisation buffer was added and supplemented with PhoSTOP phosphatase and Complete ULTRA protease inhibitors cocktails (Roche Diagnostics, Manheim, Germany). The samples were processed in a high-speed benchtop FastPrep-24 5G instrument and centrifuged at 10,000 x *g* for 10 mins at 4°C. The supernatant was then transferred to a new 1.5 mL tube for protein quantification using.

2.2.22 Detergent Compatible (DC) assay

The detection of protein is based on Lowry's principle in which the reaction of protein with an alkaline copper tartrate solution (Reagent A) and Folin reagent (Reagent B) develops colour. The reaction reaches 90% of its maximum colour development within 15 mins. The protein concentrations were further determined from the standard curve.

The Bio-Rad DC Protein Assay (#5000116, Bio-Rad, USA) is a colorimetric assay for protein concentration following detergent solubilization (298). A working reaction of reagent A was prepared as per the manufacturer's instructions by adding 20 µL of reagent S to each mL of reagent A. Further, protein standard was prepared from a range of 0.1 mg/mL to 5.5 mg/mL of BSA. Tissue lysates obtained from lung homogenates as previously mentioned (2.18) were serially diluted 10-fold and were added to a 96-well microplate along with the reaction mix (table 2.6). The plate was incubated for 15 mins at room temperature and OD was measured at 750 nm using a plate reader (FluoSTAR Omega microplate reader, BMG-Labtech, Australia).

Table 2.11: Reaction mix for protein quantitation using DC assay

Reaction mix	Volume
Samples/standards	5 µL
Reagent (A+S)	25 µL
Reagent B	200 µL

2.2.23 Western blotting

Lung tissue homogenates were prepared and quantitated as previously mentioned (section 2.19). A sample volume of 15 µL was prepared to adjust the concentrations to 20 µg of protein, to that 4X loading dye (table 2.11). The samples were then heat denatured at 95°C for 5 mins. Further, the samples along with standards (Precision Plus Protein Dual Color Standards, # 161-0374, Biorad, USA) were subjected to SDS-PAGE electrophoresis using 4-15% Mini-PROTEAN™ TGX Stain-Free gels (#4568086, Biorad, USA). The run was performed at 100 V for 1.5 rs using 1X SDS running buffer as listed below (table 2.12) (299). Upon completion of the run, the protein was transferred onto a PVDF membrane (Immun-Blot, #1620177, Biorad, USA) following a wet transfer protocol at 100V for 1 hr using a transfer buffer prepared as listed (table 2.13) (300).

Following the transfer, the membrane was subjected to blocking for 1 hr at room temperature using a blocking buffer (table 2.14). Further, the membrane was incubated using 1:1000 dilutions of primary antibodies specific to different targets (table 2.16), overnight at 4°C. The membrane was washed thrice for 5 mins each using tris buffer saline with 1% tween 1X TBST (table 2.13). The membrane was then incubated with 1:5000 dilution of anti-mouse/rabbit secondary IgG-HRP conjugated antibody for 1 hr at

room temperature. Followed by three washes in 1X TBST the membrane was subjected to imaging using ChemiDoc (ChemiDoc MP system, Bio-Rad, USA) (301).

The membrane was then stripped twice using the stripping buffer (table 2.15) for 10 mins each at room temperature. Followed by three washes in 1X TBST, the process of blocking and incubation in the antibody was repeated for the loading control (301).

Table 2.12: Recipe for loading buffer (4X)

4X Laemmli sample buffer (#1610747, Biorad, United States)	900 µL
2-Mercapethanol (#21985023, Thermo Fischer Scientific, United States)	100 µL

Table 2.13: Recipe for SDS running buffer (1X)

25 mM Tris (#BIO3094T, Astral Scientific, Australia)	3.03g
192 mM Glycine (#G8898, Sigma Aldrich, United States)	14.41g
SDS (0.1% v/v) (#L3771, Sigma Aldrich, United States)	1g
Milli-Q water	Top up to 1000 mL

Table 2.14: Recipe for Transfer buffer (1X) (pH-8.3)

25 mM Tris	3.03g
192 mM Glycine	14.41g
Methanol (20% v/v) (#34885, Sigma Aldrich, United States)	200 mL
Milli-Q water	Top up to 1000 mL

Table 2.15: Recipe for blocking buffer

BSA (5%)	5g
Milli-Q water	100 mL

Table 2.16: Recipe for TBST wash buffer (1X) (pH-7.6)

10 mM Tris	12.1g
120 mM NaCl	70.1g
Tween-20 (0.5% v/v)	0.5 mL
Milli-Q water	Top up to 1000 mL

Table 2.17: Recipe for Stripping buffer (1X) (pH-2.34)

Glycine	3.75g
SDS	0.25g
Tween-20	2.5 mL
Milli-Q water	Top up to 250mL

Table 2.18: List of primary antibodies

Anti-NMNAT1 antibody (#SANTSC-271557, Santa Cruz Biotechnology Inc., United States)
Anti-NMNAT2 antibody (#SANTSC-515206, Santa Cruz Biotechnology Inc., United States)
Anti-NMNAT3 antibody (#SANTSC-390433, Santa Cruz Biotechnology Inc., United States)

Sirtuin Antibody Sampler Kit (#9787, Cell Signalling Technology, United States)
PARP1 antibody (#9542S, Cell Signalling Technology, United States)
CD38 antibody (#14637S, Cell Signalling Technology, United States)
Total oxphos Rodent WB Antibody Cocktail (#ab110413, Abcam, United States)
Anti-beta Actin antibody Loading Control (#ab8226, Abcam, United States)

2.2.24 PK activity

The PK assay detects the catalysis of PEP and ADP by PK to generate pyruvate and ATP. The generated pyruvate is oxidized by pyruvate oxidase to produce colour (λ = 570 nm). The increase in colour is proportional to the increase in pyruvate amount.

PK activity was measured using a kit-based protocol as per the manufacturer's instructions (#K709-100, Biovision, USA) (302). Lung tissues were homogenised using a bead homogeniser at 50 O/S for 3 mins in the assay buffer provided in the kit and were quantitated as mentioned previously under 2.19. A sample volume of 50 µL/well was added adjusting the concentrations to 20 µg of protein to standardise each reaction. The following reaction mix was added to each sample as mentioned below in table 2.17. Initial OD was measured using a microplate reader (FluoSTAR Omega microplate reader, BMG-Labtech, Australia) at 570 nm followed by an incubation of 30 mins at 25°C in the dark. Final readings were measured after the 30 mins incubation.

Table 2.19: Reaction mix for measuring PK activity

	Pyruvate Kinase measurement	**Background control**
Assay Buffer	44 µL	46 µL
Substrate Mix	2 µL	-
Enzyme Mix	2 µL	2 µL

OxiRed™ Probe	2 µL	2 µL

2.2.25 Pyruvate Dehydrogenase (PDH) activity

PDH activity was measured using a kit-based protocol as per the manufacturer's instructions (#K679-100, Biovision, USA) (303). Lung tissues were homogenised using a bead homogeniser at 50 O/S for 3 mins using ice-cold assay buffer (provided in the kit) and were quantitated as mentioned previously (section 2.19). A sample volume of 50 µL/well was added adjusting the concentrations to 20 µg of protein to standardise each reaction. The following reaction mix was added to each sample (table 2.18). The OD was measured immediately at 450 nm in a kinetic mode for 10 to 60 mins at 37°C using a microplate reader.

Table 2.20: Reaction mix for measurement of PDH activity

	Reaction mix	Background control
PDH assay buffer	46 µL	48 µL
PDH developer	2 µL	2 µL
PDH substrate	2 µL	-

2.2.26 NAD^+/NADH measurement

NAD^+/NADH was measured using a kit-based protocol as per the manufacturer's instructions (#ab65348, Abcam, USA) (304). Lung tissues were rinsed in ice-cold PBS and homogenised using a bead homogeniser at 50 O/S for 3 mins using the NAD^+/NADH extraction buffer at room temperature (provided in the kit) and were quantitated as mentioned (section 2.19). Tissue homogenates were subjected to heat decomposition at 60°C for 30 mins for NADH measurements. A sample volume of 50 µL/well was added

adjusting the concentrations to 20 µg of protein to standardise each reaction for NAD^+/NADH measurement. The following reaction mix was added to each sample as mentioned below in table 2.19. The OD was measured at 450nm after 30 mins and 60 mins at 37°C using a microplate reader.

Table 2.21: Reaction mix for NAD^+/NADH measurement

	Reaction mix	Background control
NAD^+ cycling buffer	98 µL	10 µL
NAD^+ cycling enzyme	2 µL	2 µL
NAD^+ developer	10 µL	10 µL

2.2.27 PARP activity measurement

PARP activity was measured using a colorimetric assay kit using the manufacturer's protocol (#RDS4677096K, In Vitro technologies, USA) (305). Lung homogenates were prepared as previously mentioned (sections 2.18 and 2.19). PARP standards were prepared from a range of 0, 0.25, 0.5, 1, 1.5, and 2.0 units. Strip wells coated with histones (provided in the kit) were rehydrated using 1X I-PAR assay buffer (provided in the kit) and incubated at room temperature for 30 mins. Further, the buffer was removed from the wells by tapping the strip wells. Samples were added to the wells at a volume of 25 µL followed by the addition of 25 µL of the PARP substrate cocktail which was prepared as mentioned in tables 2.20 and 2.21. The reaction was then incubated for 30 mins. Further, the strip wells were washed twice with 1X PBS + 0.1% Triton X-100 (200 µL/well) followed by two washes with 1X PBS. To that 50 µL of Strep-HRP solution was added and incubated for 60 mins at room temperature. Followed by two washes with 1X PBS + 0.1% Triton X-100 (200 µL/well) and drying, 50 µL of pre-warmed TACS-Sapphire

colorimetric substrate was added and incubated in dark for 15 mins. The reaction was stopped by the addition of 0.2 M HCl, and the absorbance was measured at 450 nm using a microplate reader.

Table 2.22: Sample preparation for PARP activity measurements

Reaction component	**Volume**	**Order of Addition**
Samples/Standards	X µL	1
Diluted PARP-HAS Enzyme (0.5 unit)	Y µL	2
1X PARP cocktail	25 µL	3
Total volume	50 µL	
Where X+Y=25 µL		

Table 2.23: Recipe for PARP cocktail

Reaction component	Volume
10X PARP Cocktail	2.5 µL /well
10X Activated DNA	2.5 µL /well
1XPARP Buffer	20 µL/well

2.2.28 Mitochondrial respiratory chain activity assay

The investigation of mitochondrial function was performed by the assessment of mitochondrial respiratory chain enzymatic activities. Tissue lysates were obtained as mentioned previously (sections 2.18 and 2.19). All reagents were prepared as mentioned (table 2.22). For each sample, 20 µg of protein were used for the activity measurements of ETC (306) complex I (NADH: ubiquinone oxidoreductase) (Table 2.23), complex II (Succinate dehydrogenase) (Table 2.24), complex III (decylubiquinol cytochrome C

oxidoreductase) (Table 2.25), complex IV (cytochrome C oxidase) (Table 2.26), complex I+III (NADH cytochrome C oxidoreductase) (Table 2.27), complex II+III (succinate cytochrome C reductase) (Table 2.28), citrate synthase (Table 2.29) and β-hydroxyacyl CoA (β-HAD) (Table 2.30). The enzyme activity for each mitochondrial enzyme was calculated as nmol min^{-1} mg^{-1} of protein according to the equation below:

Enzyme activity (nmol min^{-1} mg^{-1}) = (Δ Absorbance/min × 1,000)/ [(extinction coefficient × volume of sample used in mL) × (sample protein concentration in mg mL^{-1})]

Table 2.24: Stock reagent recipe for Mitochondrial respiratory chain activity assay

Stock preparation	
Acetyl CoA (#A2181, Sigma Aldrich, all USA?)	12.5 mM (mmol/L)
Acetoacetyl CoA (#21219, Sigma Aldrich)	5mM (mmol/L)
Antimycin A (#A8674, Sigma Aldrich)	0.5 mM (mmol/L)
Cytochrome C (#C2506, Sigma Aldrich)	1 mM (mmol/L)
Decyl ubiquinone (DBQ) (#D7911, Sigma Aldrich)	10 mM (mmol/L)
5,5-dithio-bis-(2-nitrobenzoic acid) (DTNB) (#D218200, Sigma Aldrich)	1 mM (mmol/L)
EDTA	200 mM (mmol/L)
FA-Free Bovine Serum Albumin (#A6003, Sigma Aldrich)	10 % (g/100 mL)
β-nicotinamide adenine (NADH) (# N4505, Sigma Aldrich)	2 mM (mmol/L)
Oxaloacetic acid (#O4126, Sigma Aldrich)	5 mM (mmol/L)
Potassium cyanide (KCN) (# 60178, Sigma Aldrich)	50 mM (mmol/L)
Potassium phosphate (Kpi) Buffer (pH 7.4) Monopotassium Phosphate (# P8709, Sigma Aldrich)	0.5 M (mol/L)

Dipotassium Phosphate (#P2222, Sigma Aldrich)	0.5 M (mol/L)
Rotenone (#R8875, Sigma Aldrich)	0.125 mM (mmol/L)
Sodium Succinate (#S2378, Sigma Aldrich)	100 mM (mmol/L)
Triton X-100 (#X100, Sigma Aldrich)	10% (g/100 mL)
Ubiquinone-1 (#C7956, Sigma Aldrich,)	5 mM (mmol/L)

Table 2.25: Protocol for measurement of mitochondrial ETC complex I activity

Complex I (NADH: ubiquinone oxidoreductase) activity		
[Stock]		Amount/well
0.5 M	Kpi	25 µL
2 mM	NADH	25 µL
25 mM	KCN	3 µL
1 mg/mL	Antimycin A	2.5 µL
100 mg/mL	BSA	7.5 µL
20 µg/mL	Sample	30 µL
	Water	137 µL
All the reagents except the sample were premixed and pre-heated at 30°C		
Samples/blanks were pipetted into appropriate wells		
200 µL of the above reagent mix was added to each well		
2.5 µL of 5 mM Ubiquinone-1 was added to each well		
Baseline absorbance was measured every 15 seconds for 3 mins at 340 nm		
10 µM of Rotenone was added to each well		
Final absorbance was measured every 15 seconds for 3 mins at 340 nm		

Table 2.26: Protocol for measurement of mitochondrial ETC complex II activity

Complex II (Succinate dehydrogenase) activity		
[Stock]		Amount/ well
0.5 M	Kpi	12.5 µL
25 mM	KCN	3 µL
1 mM	DCPIP	20 µL
0.1 M	Succinate	50 µL
20 µg/mL	Sample	10 µL
	Water	149.5 µL
All the reagents except the sample were premixed and pre-heated at 30°C		
Samples/blanks were pipetted into appropriate wells		
235 µL of the above reagent mix were added to each well and incubated for 10 mins		
Baseline readings were measured every 15 seconds for 1 min at 600 nm		
5 µL of 5 mM DBQ was added to each well		
Absorbance was measured every 15 seconds for 3 mins at 600 nm		
12.5 µL of 100 mM Malonate was added to each well		
Final absorbance was measured every 15 seconds for 1 min at 600 nm		

Table 2.27: Protocol for measurement of mitochondrial ETC complex III activity

Complex III (Decylubiquinol-Cytochrome C oxidoreductase) activity		
[Stock]		Amount/ well
0.5 M	Kpi	12.5 µL
25 mM	KCN	5 µL

5 %	Tween-20	1.25 µL
1.25 mM	Oxidised cytochrome C	15 µL
20 µg/mL	Sample	4 µL
	Water	207.3 µL
All the reagents except the sample were premixed and pre-heated at 30°C		
Samples/blanks were pipetted into appropriate wells		
241 µL of the above reagent mix were added to each well		
2.5 µL of 1 mg/mL of Antimycin A was added to each well		
Absorbance was measured every 15 seconds for 5 mins at 550 nm		

Table 2.28: Protocol for measurement of mitochondrial ETC complex IV activity

Complex IV (Cytochrome C oxidase) activity		
[Stock]		Amount/ well
0.5 M	Kpi	25 µL
	Water	197 µL
20 µg/mL	Sample	10 µL
All the reagents except the sample were premixed and pre-heated at 30°C		
Samples/blanks were pipetted into appropriate wells		
222 µL of the above reagent mix were added to each well		
15 µL of 1 mM of Cytochrome C was added to each well		
Absorbance was measured every 10 seconds for 3 mins at 550 nm		
3 µL of 25 mM KCN was added to each well		
Absorbance was measured every 15 seconds for 1 min at 550 nm		

Table 2.29: Protocol for measurement of mitochondrial ETC complex I + III activity

Complex I+III (NADH cytochrome C oxidoreductase) activity		
[Stock]		Amount/ well
0.5 M	Kpi	25 µL
25 mM	KCN	3 µL
100 mM	Malonate	12.5 µL
1 mM	Oxidised cytochrome C	12.5 µL
100 mg/mL	BSA	2.5 µL
20 µg/mL	Sample	5 µL
	Water	164.5 µL
All the reagents except the sample were premixed and pre-heated at 30°C		
Samples/blanks were pipetted into appropriate wells		
220 µL of the above reagent mix were added to each well		
Baseline absorbance was measured every 15 seconds for 1 min at 550 nm		
25 µL of 2mM NADH was added to each well		
Absorbance was measured every 15 seconds for 3 mins at 550 nm		
20 µL of 0.125 mM Rotenone was added to each well		
Final absorbance was measured every 15 seconds for 1 min at 550 nm		

Table 2.30: Protocol for measurement of mitochondrial ETC complex II+ III activity

Complex II+III (Succinate-cytochrome C oxidoreductase) activity		
[Stock]		Amount/ well
0.5 M	Kpi	10 µL

25 mM	KCN	3 µL
0.1 M	Succinate	25 µL
20 µg/mL	Sample	20 µL
	Water	179.5 µL
All the reagents except the sample were premixed		
Samples/blanks were pipetted into appropriate wells		
217.5 µL of the above reagent mix was added to each well and incubated at 30°C for 10 mins in a plate reader		
Baseline absorbance was measured every 15 seconds for 1 min at 550 nm		
12.5 µL of 1 mM Oxidised Cytochrome C was added to each well		
Absorbance was measured every 15 seconds for 3 mins at 550 nm		
12.5 µL of 100 mM Malonate was added to each well		
Final absorbance was measured every 15 seconds for 1 min at 550 nm		

Table 2.31: Protocol for measurement of mitochondrial citrate synthase activity

Citrate Synthase activity		
[Stock]		Amount/ well
1 M	Tris (pH 8.0)	12.5 µL
1 mM	DTNB	25 µL
12.5 mM	Acetyl CoA	2 µL
20 µg/mL	Sample	10 µL
	Water	195.5 µL
All the reagents except the sample were premixed and preheated at 30°C		
Samples/blanks were pipetted into appropriate wells		

235 µL of the above reagent mix was added to each well
Baseline absorbance was measured every 15 seconds for 1 min at 412 nm
5 µL of 5 mM Oxaloacetic acid was added to each well
Absorbance was measured every 15 seconds for 3 mins at 412 nm

Table 2.32: Protocol for measurement of β-HAD activity

β-HAD activity		
[Stock]		Amount/ well
1 M	Tris (pH 7.0)	12.5 µL
2 mM	NADH	25 µL
200 mM	EDTA	2.5 µL
10%	Triton X-100	5 µL
20 µg/mL	Sample	15 µL
	Water	185 µL
All the reagents except the sample were premixed and preheated at 30°C		
Samples/blanks were pipetted into appropriate wells		
230 µL of the above reagent mix was added to each well		
Baseline absorbance was measured every 11 seconds for 1 min at 340 nm		
5 µL of 5 mM Acetoaceyl CoA was added to each well		
Absorbance was measured every 11 seconds for 3 mins at 340 nm		

2.2.29 Measurement of Mitochondria membrane potential (ΔΨm)

ΔΨm was measured using JC1 dye as per the manufacturer's instructions (#m34152, Life Technologies, USA) (307). JC1 accumulates in healthy mitochondria to form J-

aggregates exhibiting red fluorescence with an emission of ~590 nm whereas, it remains as J-monomers upon depolarisation in unhealthy mitochondria showing green fluorescence emission at ~529 nm. For this purpose, sections were dewaxed and rehydrated as mentioned previously under section 2.7 and were subjected to antigen retrieval followed by blocking in 5% BSA as mentioned previously under section 2.11. The samples were further incubated with 2 µg/mL of JC1 conjugate for 1 hr at room temperature for each antibody staining. The slides were rinsed thrice with PBS and 0.5% Tween (#P7959, Sigma Aldrich, USA) for 5 mins each. The slides were mounted with coverslips using Gold-antifade conjugated with DAPI nuclei stain and air dried as mentioned previously in 2.11. Fluorescence signals were detected with an Axio Imager microscope and analysed using Zen Imaging Software as mentioned previously in 2.11. Further, the mean fluorescence intensity (MFI) was calculated for J-monomers and J-aggregates for each sample.

2.2.30 Statistical analysis

All the data are presented as ± standard error mean (SEM) with 6-8 mice in each experimental group unless otherwise stated. Statistical significance between two groups was determined using an unpaired students t-test, whereas multiple comparisons using One-way ANOVA were used for analyses of more than two groups followed by Tukey's multiple comparisons using GraphPad Prism version 9.0 for Windows (GraphPad Prism software, San Diego, California United States, www.graphpad.com). Statistical significance was confirmed with P-values ≤ 0.05.

Chapter 3. Elucidating the therapeutic implications of NR and/or PT in preventing the progression of COPD in vivo

3.1 Introduction

COPD is characterised by chronic airway inflammation that results in progressive and irreversible damage to the lung (23). Oxstress is an important driver of inflammation and tissue damage in COPD and occurs when the levels of ROS overwhelm endogenous antioxidants (168, 308). Mitochondria are the ultimate producer of energy in a cell and are also known to be one of the major sources of mtROS (180). High levels of ROS cause the oxidation of proteins, lipids and DNA resulting in tissue injury and triggering inflammatory responses in COPD (183). ROS is produced both via exogenous factors such as environmental pollutants, radiation, cigarette smoking etc. (180, 183), whereas, endogenous ROS are released from inflammatory cells such as macrophages and neutrophils, as well as epithelial and endothelial cells (309). Additionally, mtROS are generated via CS-induced ROS as by-products of the ETC, located on the inner mitochondrial membrane during oxphos (310). Electrons leaking from complex I and complex III of the ETC lead to a partial reduction of oxygen to form superoxide(O^-) (311). The sequential reduction of oxygen through the addition of electrons leads to the formation of several types of ROS including superoxide, hydrogen peroxide (H_2O_2), hydroxyl radical (OH), hydroxyl ion (OH^-), and NO (312). Cells can protect themselves from ROS using natural defence mechanisms including apoptosis, mitochondrial biogenesis, mitophagy, mitochondrial homeostasis, and mitochondrial antioxidants (313, 314). However, in diseased conditions, impaired mechanisms result in the damage of cell membranes, DNA, and proteins that attenuate cellular survival (314). Excessive DNA

repair depletes levels of NAD^+ within the cell and reduces the production of ATP via oxphos leading to reduced cellular metabolism (238). Restoration of NAD^+ is important to restore impaired mitochondrial function and thereby reduce oxidative stress and inflammation in COPD (238, 315).

CS is the leading cause of COPD (139). The mechanisms that drive the inception and progression of chronic inflammation and disease are not well understood, and this has hampered the development of effective treatments for COPD (316). Current therapeutic approaches are limited and aim to manage symptoms and reduce exacerbations (317). Thus, there is a need for new therapies that inhibit the induction and progression of COPD. Oxidative stress is a known cause of inflammation in COPD and is produced as a consequence of mitochondrial dysfunction (311), decreased mitochondrial density and biogenesis (177), impaired mitochondrial activity and apoptosis (317). NAD^+ is responsible for carrying out several important reactions for ATP production in mitochondria which provides the ultimate source of energy in a cell (318). Currently, there is no evidence of the contribution of NAD^+ depletion to COPD (277). The objective of the current study was to investigate the role of NAD^+ in the pathogenesis of COPD, with the overall objective to identify a novel therapeutic approach to halt or reverse the disease progression. The study delineates the therapeutic implications of NR and/or PT in the induction, progression/suppression of COPD using our previously established CS-induced COPD murine model.

3.2 Methodology

3.2.1 Experimental COPD model

Female BALB/c mice aged 6-8 weeks were obtained from the ARC and maintained at 20 ± 2°C on a 12:12 hours day-night cycle and fed a standard sterile diet as previously mentioned under section 2.2.1.

3.2.2 Experimental procedure

Mice were subjected to CS/Air exposure from up to 12 research-grade 3R4F cigarettes (University of Kentucky) twice a day, five days a week for 2 or 8 weeks using a custom-designed nose-only inhalation system as mentioned previously (146).

3.2.3 Experimental designs

This study involved a 2-week and an 8-week smoke model subjected to an administration of 400 mg/kg of NR in drinking water, and 80 mg/kg of PT in mushy chow provided *ad libitum* followed by smoke exposure as described in 4.2.2. The 2-week study was a pilot experiment performed to determine the efficacy of NR and PT in ameliorating lung inflammation (Figure 3.1A) and was followed by the 8-week study to elucidate the effects of NR and PT during the development and progression of COPD (Figure 3.2B).

Each day, mice were weighed before exposure to smoke and were closely monitored after smoking each day. Any mice losing between 10-15% of their body weight were subjected to smoke cessation for 24 hours with intensive monitoring.

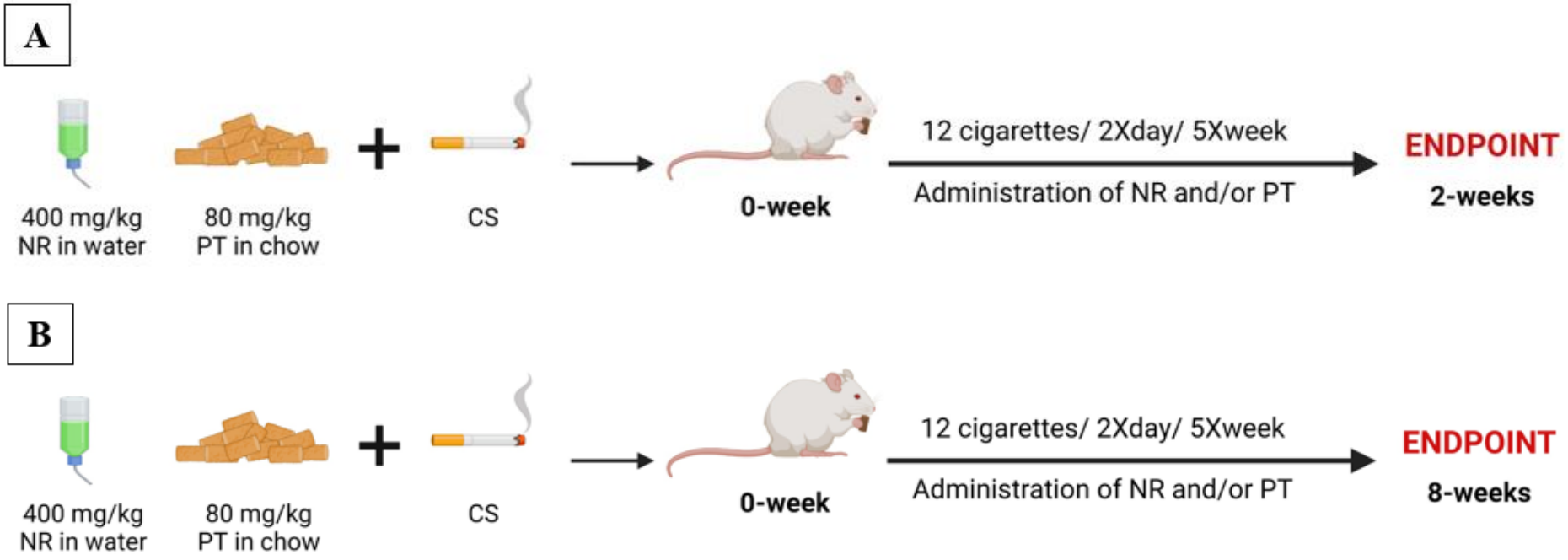

Figure 3.1: Experimental design

Mice were subjected to nose-only CS exposure to 12 cigarettes, twice a day, five days a week and were treated with 400 mg/kg of NR added to drinking water and 80 mg/kg of PT added to mushy chow for (A) 2-week acute CS-exposed model and (B) 8-week experimental COPD study.

3.2.4 Experimental groups

The different experimental groups in the 2-week study are listed below in Table 3.1. Both the control groups of air and smoke were fed with untreated water and chow. The treatment groups for both air and smoke were subjected to 400 mg/kg of NR in drinking water and/or 80 mg/kg of PT in mushy chow both individually as well as in combination as mentioned below.

Table 3.1: Experimental groups of the 2-week COPD study

Experimental groups	Smoke exposure	Treatments
Air	-	-
Air NR	-	400 mg/kg of NR in drinking water
Air PT	-	80 mg/kg of PT in mushy chow
Air NRPT	-	400 mg/kg of NR in drinking water and 80 mg/kg of PT in mushy chow
Smoke	12 cigarettes, 2X day, 5X week	-
Smoke NR	12 cigarettes, 2X day, 5X week	400 mg/kg of NR in drinking water
Smoke PT	12 cigarettes, 2X day, 5X week	80 mg/kg of PT in mushy chow
Smoke NRPT	12 cigarettes, 2X day, 5X week	400 mg/kg of NR in drinking water and 80 mg/kg of PT in mushy chow

The different experimental groups used in the 8-week COPD study are listed below in Table 3.2. Both the control groups of air and smoke were fed with untreated water and chow for 8 weeks. Followed by the treatment groups for NR and/or PT which were subjected to 400 mg/kg of NR in drinking water and/or 80 mg/kg of PT in mushy chow both individually as well as in combination as mentioned below.

Table 3.2: Experimental groups of the 8-week COPD study

Experimental groups	Smoke exposure	Treatments
Air	-	-
Smoke	12 cigarettes, 2X day, 5X week	-
Smoke NR	12 cigarettes, 2X day, 5X week	400 mg/kg of NR in drinking water
Smoke PT	12 cigarettes, 2X day, 5X week	80 mg/kg of PT in mushy chow
Smoke NRPT	12 cigarettes, 2X day, 5X week	400 mg/kg of NR in drinking water and 80 mg/kg of PT in mushy chow

3.3 Results

3.3.1 Imbalance in NAD^+ homeostasis during the development of COPD

Lung homogenates from mice at 2, 4, 6, 8 and 12-week CS exposure in our COPD murine model were used for the measurement of total NAD^+ and NADH levels. The total NAD^+ levels in the smoke group were significantly lower than that of the air group for all the time points (P<0.0001) (Figure 3.2A). The NADH levels were significantly higher in the smoke group than in the air group at all time points (P<0.0001) (Figure 3.2B). The ratio of total NAD^+ and NADH was observed to be significantly reduced in the smoke group in comparison with the air group at each time point (P<0.0001) (Figure 3.2C).

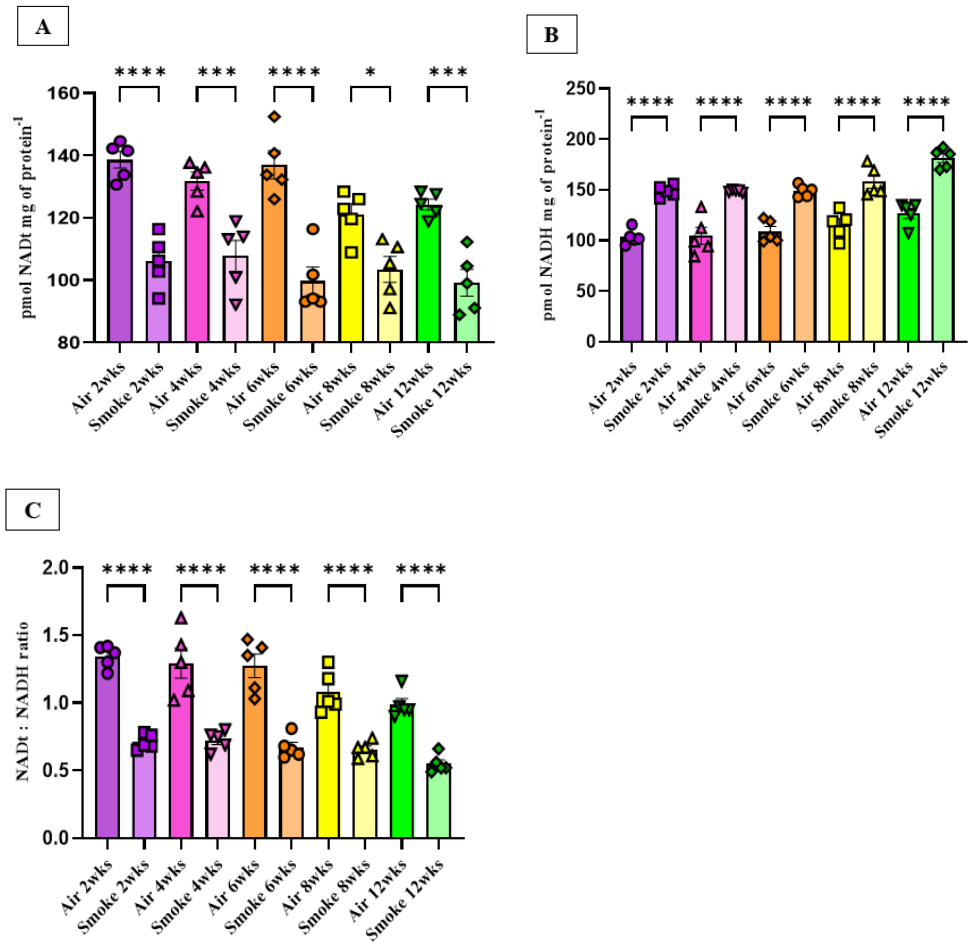

Figure 3.2: Imbalance in NAD^+ homeostasis during the development of COPD:

*(A) Total NAD^+ level in mouse lung homogenates, (B) NADH level in mouse lung homogenates, (C) Ratio of total NAD^+/NADH in mouse lung homogenates. Data represented are means ± SEM of 5 mice/group, * P<0.05, ** P<0.01, *** P<0.001, **** P<0.0001.*

3.3.2 Administration of NR and/or PT reduced inflammation in acute CS exposure

Administration of NR and/or PT in the 2-week acute CS-induced inflammatory model reduced cellular infiltration in BAL. Cell counts for the total leukocytes (Figure 3.3A), macrophages (Figure 3.3B), and neutrophils (Figure 3.3C) increased in the smoke group as compared to the air group (P<0.0001). Inflammation was significantly reduced in both the smoke PT group and the smoke NRPT group in comparison to the smoke group (P<0.0001).

Further, the body weight of all the experimental groups was monitored daily as mentioned previously in 3.2.3. There was no significant weight loss observed between the air group and the experimental groups at any of the time points examined (Figure 3.3D).

The gene expression of TNFα increased in the smoke group in comparison to the air group (P<0.001). Furthermore, the expression of TNFα did not change in the smoke NR, smoke PT and smoke NRPT groups with respect to the smoke group (Figure 3.3E), however, there was a significant increase in the gene expression of TNFα in the smoke PT group in comparison to the air group (P<0.01). We also observed an increase in the expression of CXCL1 in the smoke group as compared to the air group (P<0.0001) which was significantly reduced in the smoke NR (P<0.01), smoke PT (P<0.01) and smoke NRPT group (P<0.001) (Figure 3.3F). Further, a significant increase in the expression of YM1 was observed in the smoke group in comparison to the air group (P<0.001) and did not

show any significant reduction in the smoke NR, smoke PT and smoke NRPT group (Figure 3.3G).

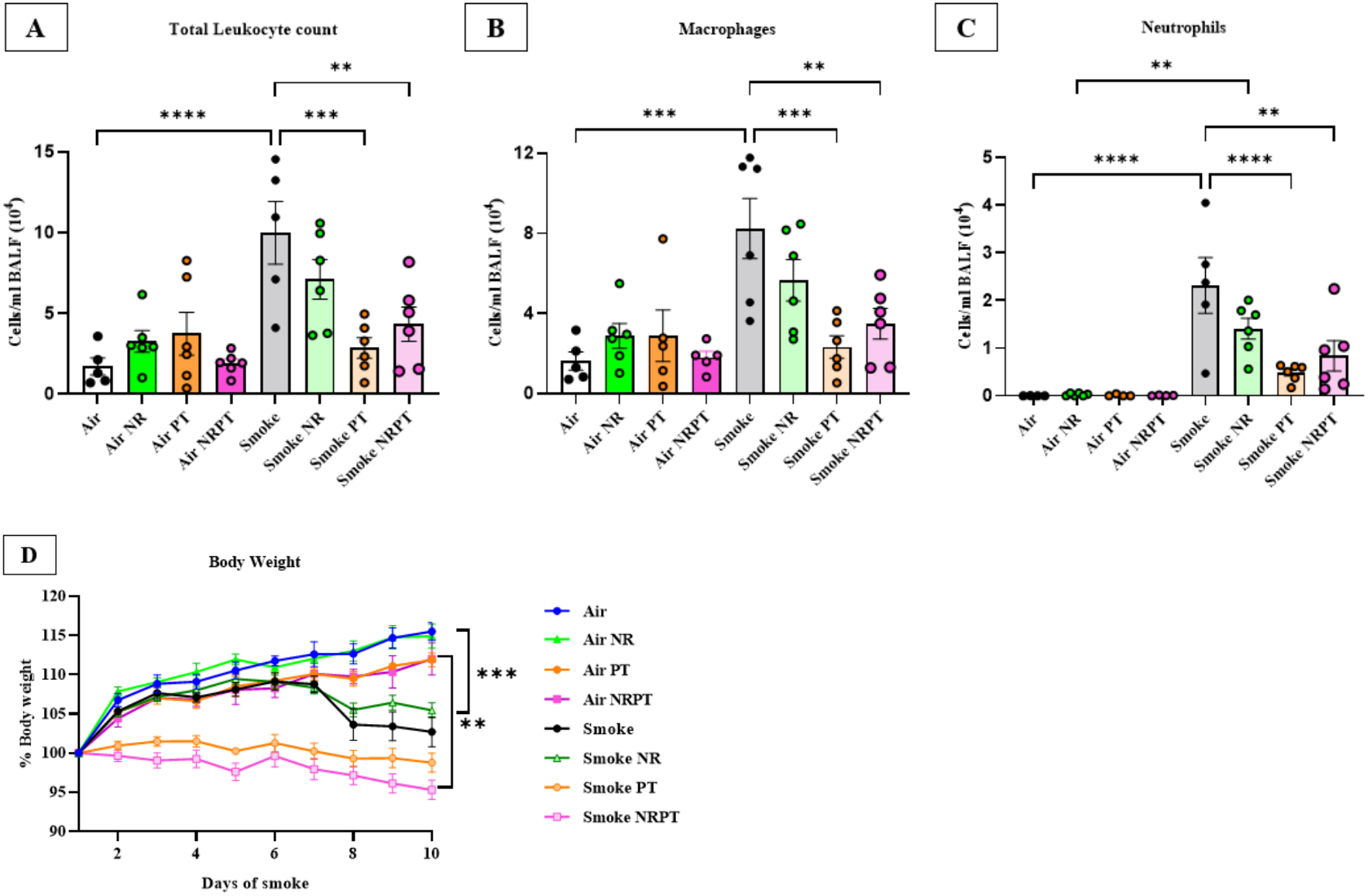
A
Total Leukocyte count
Cells/ml BALF (10^4)
15
10
5
0
****
***
**
Air
Air NR
Air PT
Air NRPT
Smoke
Smoke NR
Smoke PT
Smoke NRPT
B
Macrophages
Cells/ml BALF (10^4)
12
8
4
0
***
***
**
C
Neutrophils
Cells/ml BALF (10^4)
5
4
3
2
1
0
**
****
****
**
D
Body Weight
% Body weight
120
115
110
105
100
95
90
2
4
6
8
10
Days of smoke
***
**
Air
Air NR
Air PT
Air NRPT
Smoke
Smoke NR
Smoke PT
Smoke NRPT

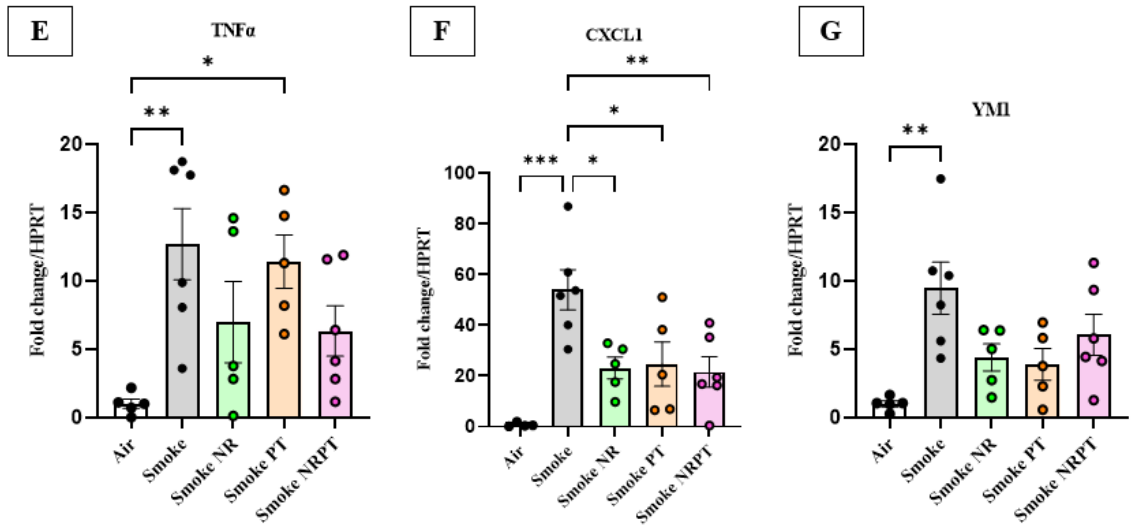

Figure 3.3: Administration of NR and/or PT reduced inflammation in acute CS exposure:

*Graphical representation of (A) cellular infiltrates in the parenchyma, (B) macrophages, (C) neutrophils; (D) Changes in body weight across different experimental groups in acute CS exposed study; (E) Gene expression levels of TNFα, (F) CXCL1, and (G) YM1. Data represented are means ± SEM of 6 mice/group, * P<0.05, ** P<0.01, *** P<0.001, **** P<0.0001.*

3.3.3 Administration of NR and PT restores NAD^+/NADH balance in acute CS exposure

Lung homogenates from the 2-week CS-induced inflammatory model were used for the measurement of total NAD^+ and NADH levels. The total NAD^+ levels in the smoke group were significantly reduced compared to that of the air group (P<0.0001), followed by the smoke NR group (P<0.0001), smoke PT group (P<0.0001) and smoke NRPT group (P<0.001), however an increase in the total NAD^+ levels were observed in the smoke NRPT in comparison to the smoke group (P<0.01) (Figure 3.4A). The NADH levels were significantly higher in the smoke group than in the air group (P<0.0001) and were

significantly reduced in all the treatment groups of smoke NR, smoke PT and smoke NRPT as compared to the smoke group (P<0.0001) (Figure 3.4B). The ratio of total NAD^+ and NADH was observed to be significantly reduced in the smoke group in comparison with the air group (P<0.0001). However, smoke NR, smoke PT and smoke NRPT treatments showed a significant increase in the ratio of total NAD^+ and NADH with respect to the smoke group (P<0.0001) (Figure 3.4C).

Further, the gene expression for various NAD^+ regulators was measured whereby we observed no changes in the expression of NADSYN (Figure 3.4D), NADK2 (Figure 3.4F), NMNT (Figure 3.4H), NRK1 (Figure 3.4I), NRK2 (Figure 3.4J) PGC1α (Figure 3.4K) and NFκB (Figure 3.4L) in all the experimental groups. A significant increase in NADK1 was observed in the smoke group (P<0.05) and smoke NRPT group (P<0.05) in comparison to the air group (Figure 3.4E). Further, reduced expression of NAMPT was observed both in the smoke group (P<0.01) and the smoke NRPT group (P<0.0001) in comparison to the air group (Figure 3.4G). A significant reduction in the gene expression of PNP (Figure 3.4M) and GCN5 (Figure 3.4N) was also observed in groups smoke PT (P<0.001) and smoke NRPT (P<0.01) with respect to the air group.

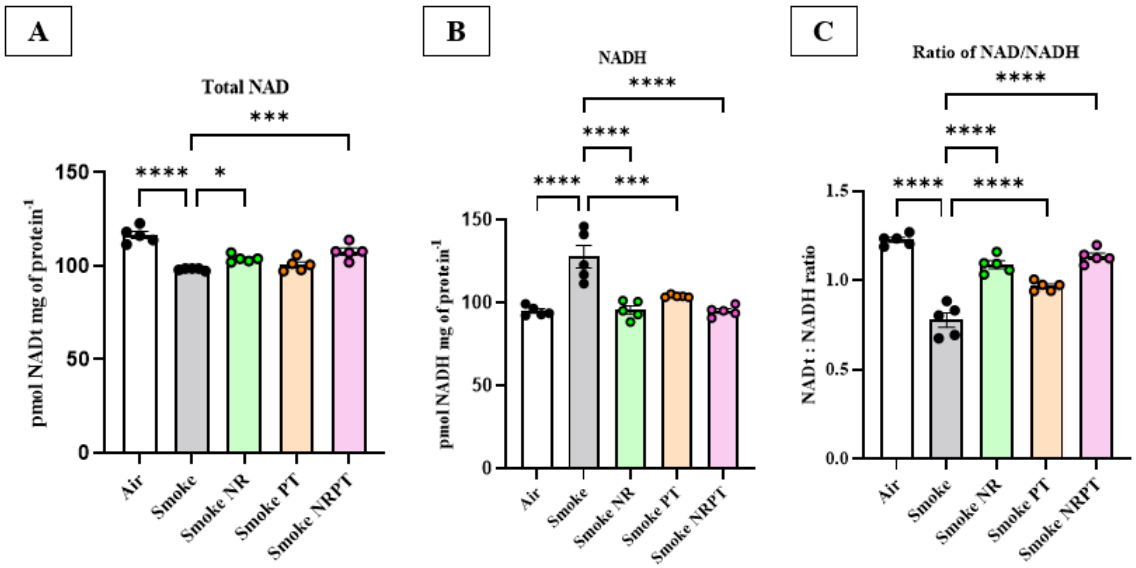

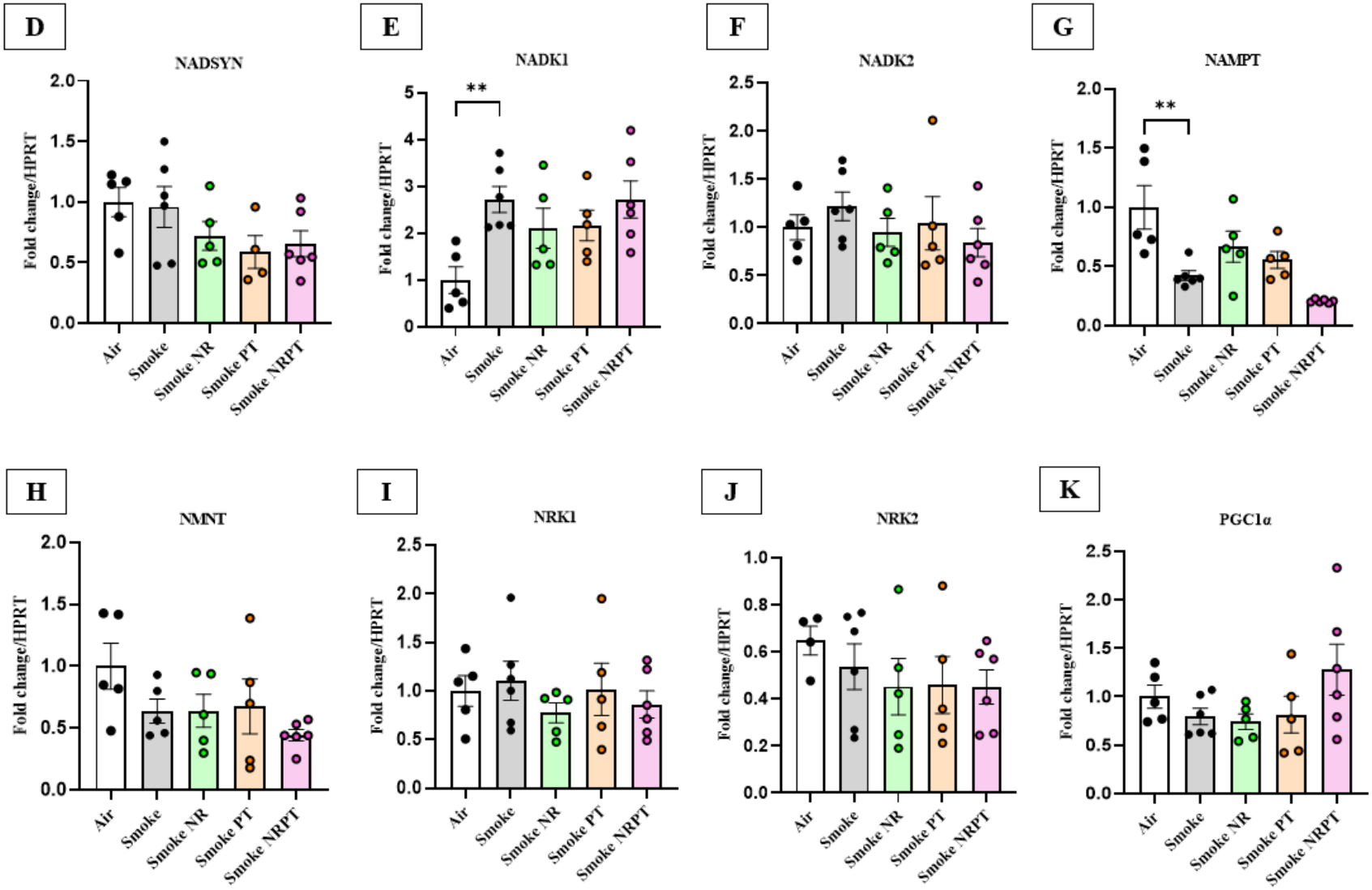
D
NADSYN
Fold change/HPRT
2.0
1.5
1.0
0.5
0.0
Air
Smoke
Smoke NR
Smoke PT
Smoke NRPT
E
NADK1
**
Fold change/HPRT
5
4
3
2
1
0
F
NADK2
Fold change/HPRT
2.5
2.0
1.5
1.0
0.5
0.0
G
NAMPT
**
Fold change/HPRT
H
NMNT
Fold change/HPRT
I
NRK1
Fold change/HPRT
J
NRK2
Fold change/HPRT
1.0
0.8
0.6
0.4
0.2
0.0
K
PGC1α
Fold change/HPRT

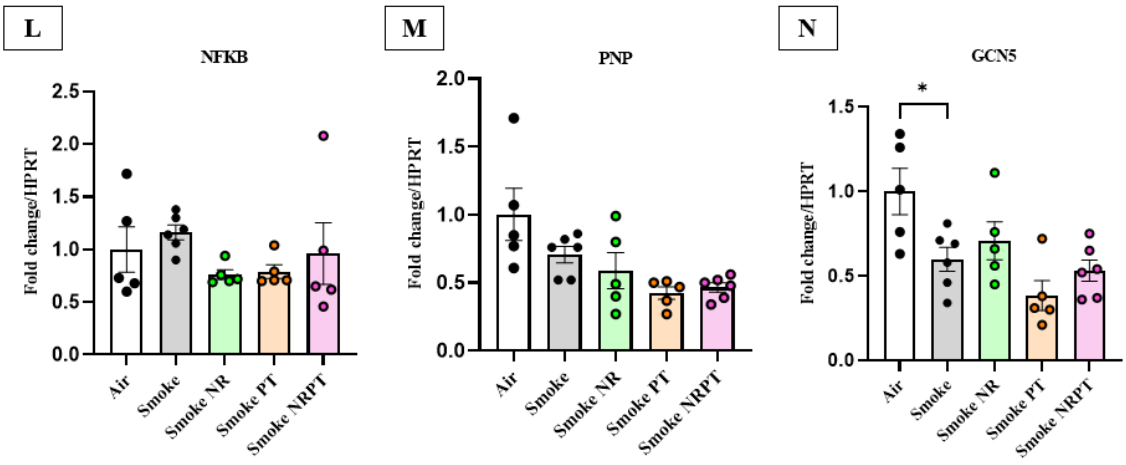

Figure 3.4: Administration of NR and/or PT restored imbalance in NAD+ homeostasis in acute CS exposure:

*(A) total NAD^+ levels in mouse lung homogenates; (B) NADH level in mouse lung homogenates; (C) ratio of total NAD^+/NADH. Gene expression levels of (D) NADSYN, (E) NADK1, (F) NADK2, (G) NAMPT; (H) NMNT, (I) NRK1, (J) NRK2, (K) PGC1α, and (L) NFκB; (M) PNP and (N) GNN5. Data represented are means ± SEM of 6 mice/group, * P<0.05, ** P<0.01, *** P<0.001, **** P<0.0001.*

3.3.4 Administration of NR and/or PT reduced hyperactivity of NAD^+ consumers in acute CS exposure

There were no changes observed in the expression of NAD^+ consumers that encode for PARP1 (Figure 3.5A), SIRT1 (Figure 3.5C), SIRT2 (Figure 3.5D), SIRT3 (Figure 3.5E), SIRT5 (Figure 3.5G), SIRT6 (Figure 3.5H), and SIRT7 (Figure 3.5I). However, we observed an increase in the transcripts that encode for SIRT4 (Figure 3.5F) in the smoke group in comparison to the air group (P<0.01) and was reduced in all the treatment groups of smoke NR, smoke PT and smoke NRPT as compared to the smoke group (P<0.0001). Further, we also observed a significant increase in PARP activity levels (Figure 3.5B) in the smoke group as compared to the air group (P<0.0001) and was reduced in all the

treatment groups of smoke NR, smoke PT and smoke NRPT as compared to the smoke group (P<0.0001).

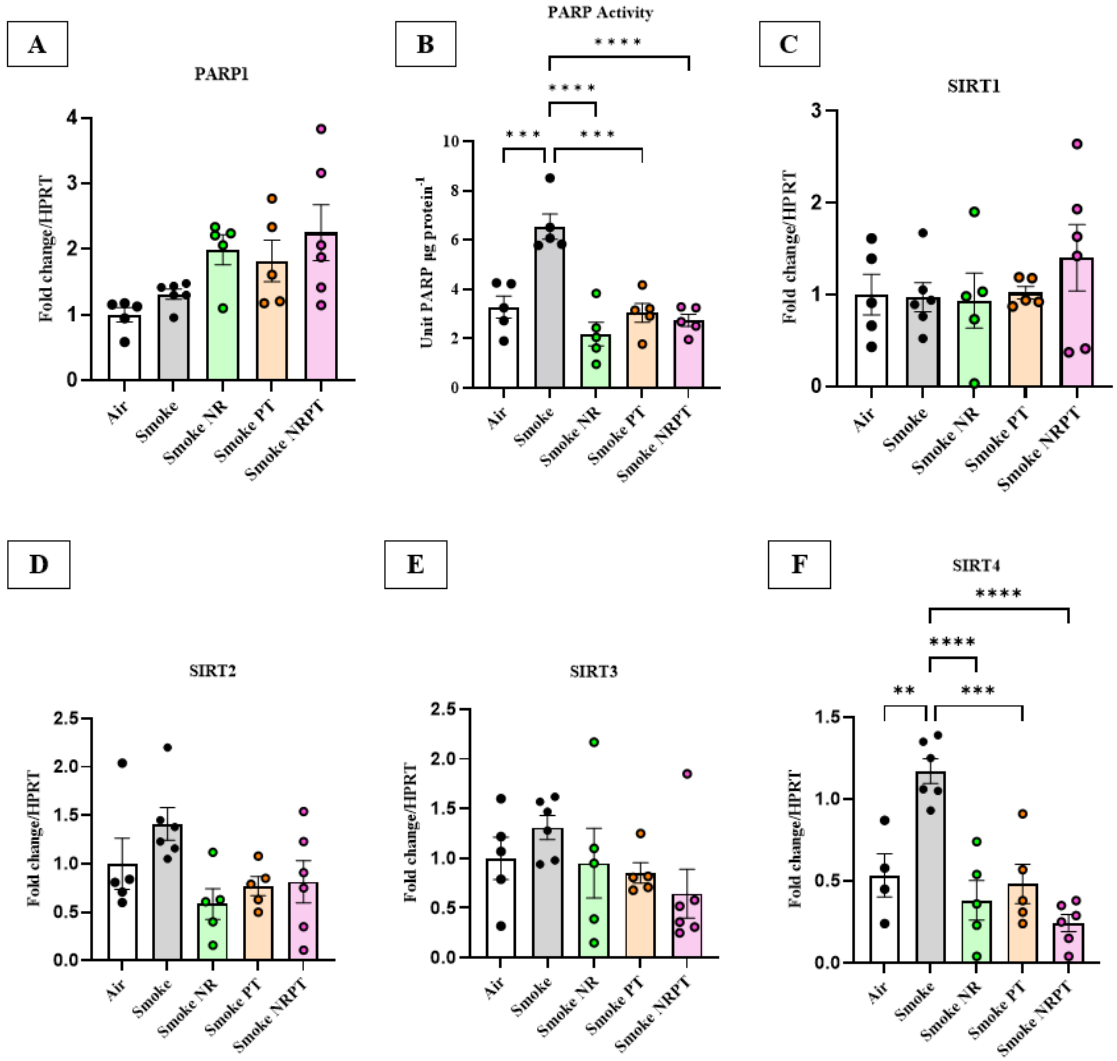

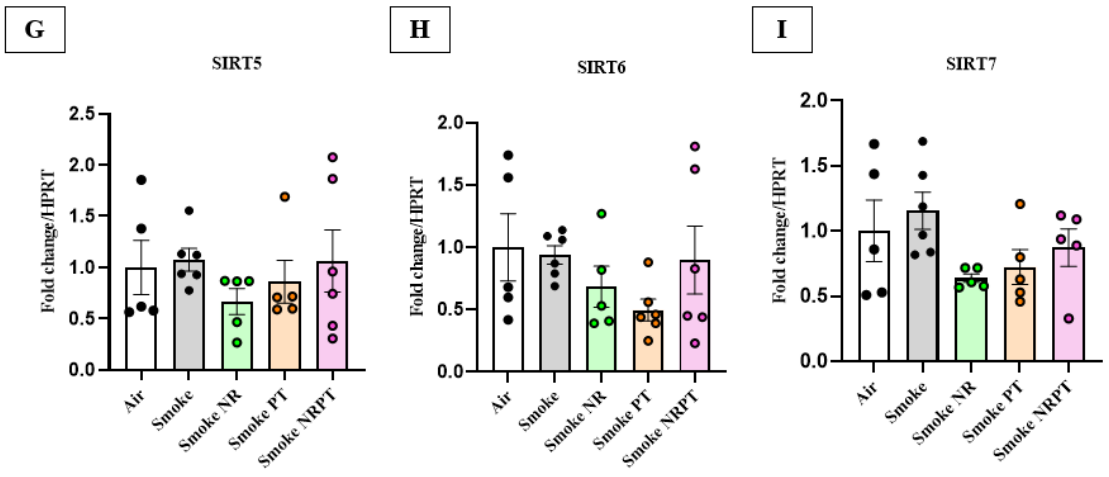

Figure 3.5: : Administration of NR and/or PT reduced hyperactivity of NAD+ consumers in acute CS exposure:

*(A) Gene expression of PARP1, (B) PARP activity level; Gene expression levels of (C) SIRT1, (D) SIRT2, (E) SIRT3, (F) SIRT4, (G) SIRT5, (H) SIRT6, (I) SIRT7. Data represented are means ± SEM of 6 mice/group, * P<0.05, ** P<0.01, *** P<0.001, **** P<0.0001.*

3.3.5 Administration of NR and PT reduced airway inflammation in COPD

The 8 weeks CS-induced COPD murine model with NR and/or PT showed reduced inflammatory cell infiltration in BAL. There was an increase in the total leukocytes (Figure 3.6A), macrophages (Figure 3.6B) and neutrophils (Figure 3.6C) in the smoke group as compared to the air group (P<0.0001), which was significantly reduced in all the treatment groups of smoke NR, smoke PT and smoke NRPT in comparison to the smoke group (P<0.0001).

The body weight of all the experimental groups was monitored daily, where we observed a significant weight loss in the smoke group, smoke NR, smoke PT and smoke NRPT in comparison to the air group (P<0.0001). Further, there was a significant reduction in

weight in the smoke NR group in comparison to the smoke group (P<0.001) (Figure 3.6D).

The gene expression of TNFα (Figure 3.6E), CXCL1 (Figure 3.6F) and YM1 (Figure 3.6G) was significantly increased in the smoke group with respect to the air group (P<0.001). Further, there was a significant reduction observed in the TNFα expression levels of the smoke NR (P<0.01), smoke PT (P<0.0001) and smoke NRPT (P<0.0001) in comparison to the smoke group (Figure 3.6E). Likewise, there was a significant increase in the expression of CXCL1 in the smoke group as compared to the air group (P<0.0001), which was further reduced in all the treatment groups of smoke NR, smoke PT and smoke NRPT in comparison to the smoke group (P<0.0001) (Figure 3.6F). We also observed an increase in the expression levels of YM1 in the smoke group, smoke NR, smoke PT and smoke NRPT in comparison to the air group (P<0.0001) (Figure 3.6G).

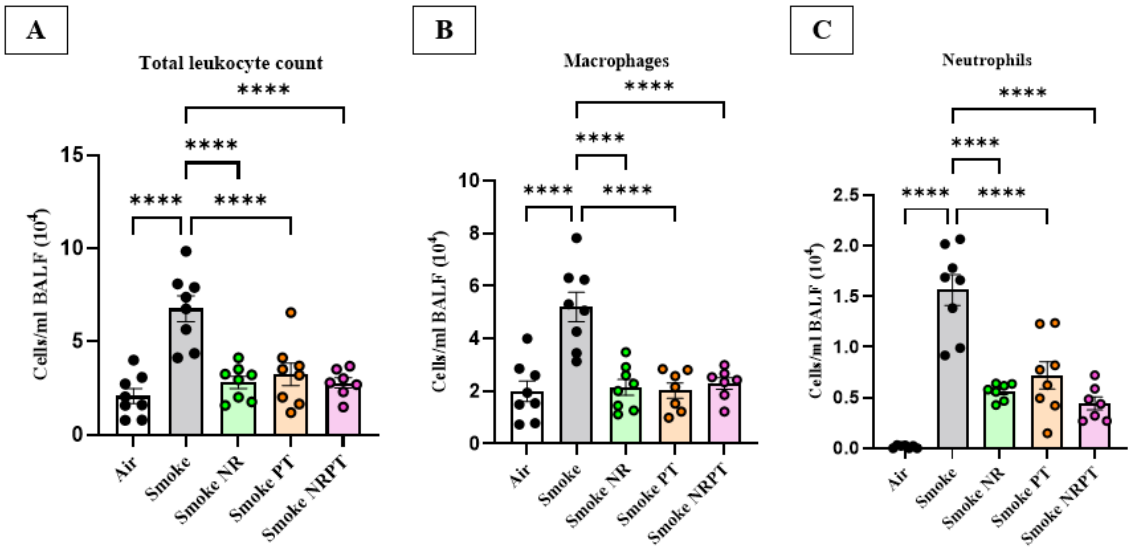

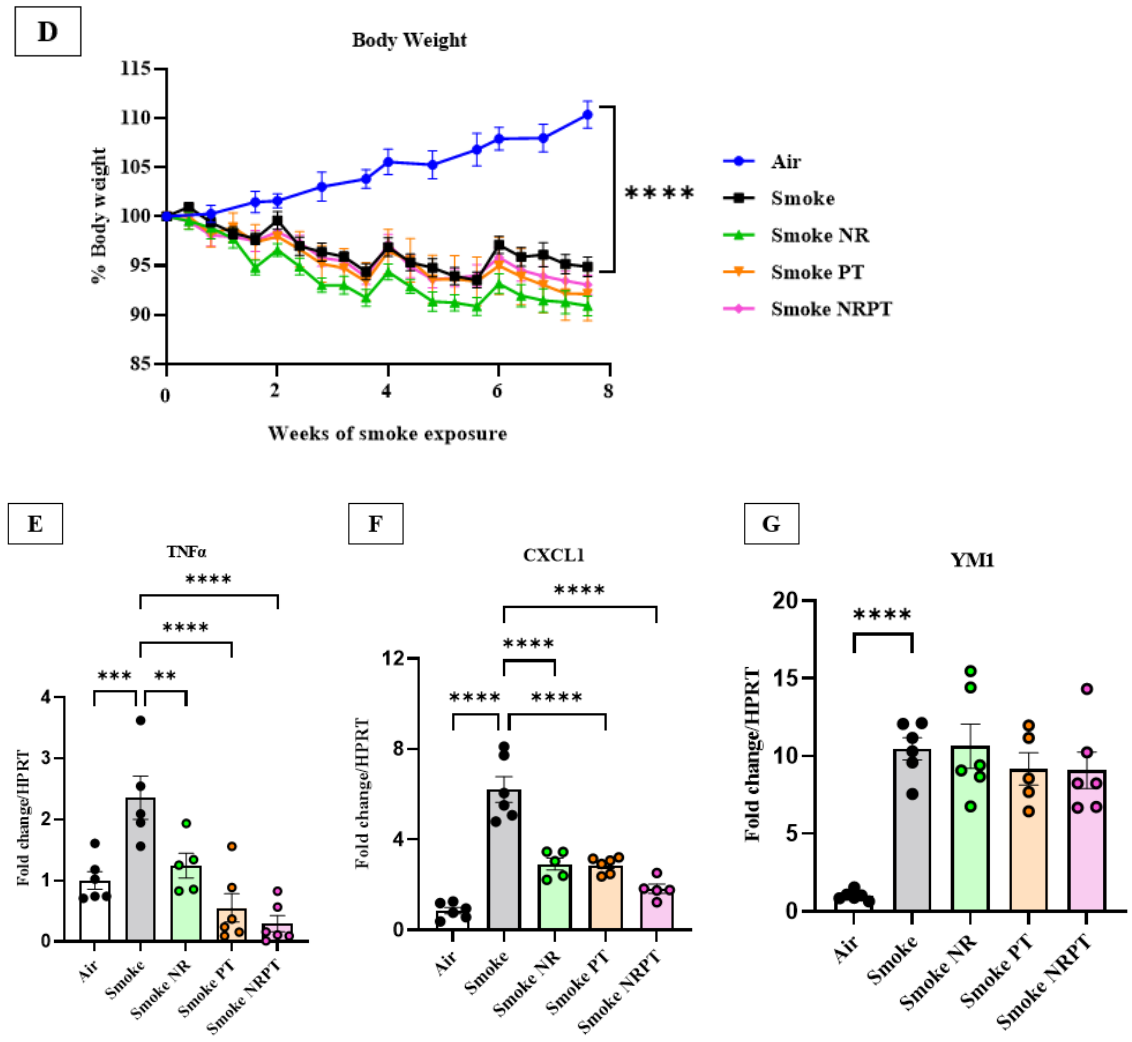

Figure 3.6: Administration of NR and/or PT reduced airway inflammation in COPD:

*Graphical representation of (A) total leukocytes, (B) macrophages and (C) neutrophils obtained in BAL; (D) Changes in body weight in the smoke group; Gene expression of (E) TNFα, (F) CXCL1, and (G) YM1. Data represented are means ± SEM of 6-8 mice/group, * P<0.05, ** P<0.01, *** P<0.001, **** P<0.0001.*

3.3.6 Administration of NR and/or PT attenuated airway remodelling and emphysema in COPD

Lung sections from the 8-week CS-induced COPD model treated with NR and/or PT were used for the measurement of airway remodelling. Chronic exposure to CS resulted in increased collagen deposition around the basement membrane of small airways in the smoke group in comparison to the air group (P<0.0001). However, this was significantly reduced in all the treatment groups of smoke NR and/or PT as compared to the smoke group (P<0.0001) (Figure 3.7A)

Further, MLI counts were performed to determine alveolar destruction where we observed an increase in the MLI counts in the smoke group with respect to air (P<0.0001) and were significantly reduced in all the treatment groups of smoke NR and/or PT (P<0.0001) (Figure 3.7B).

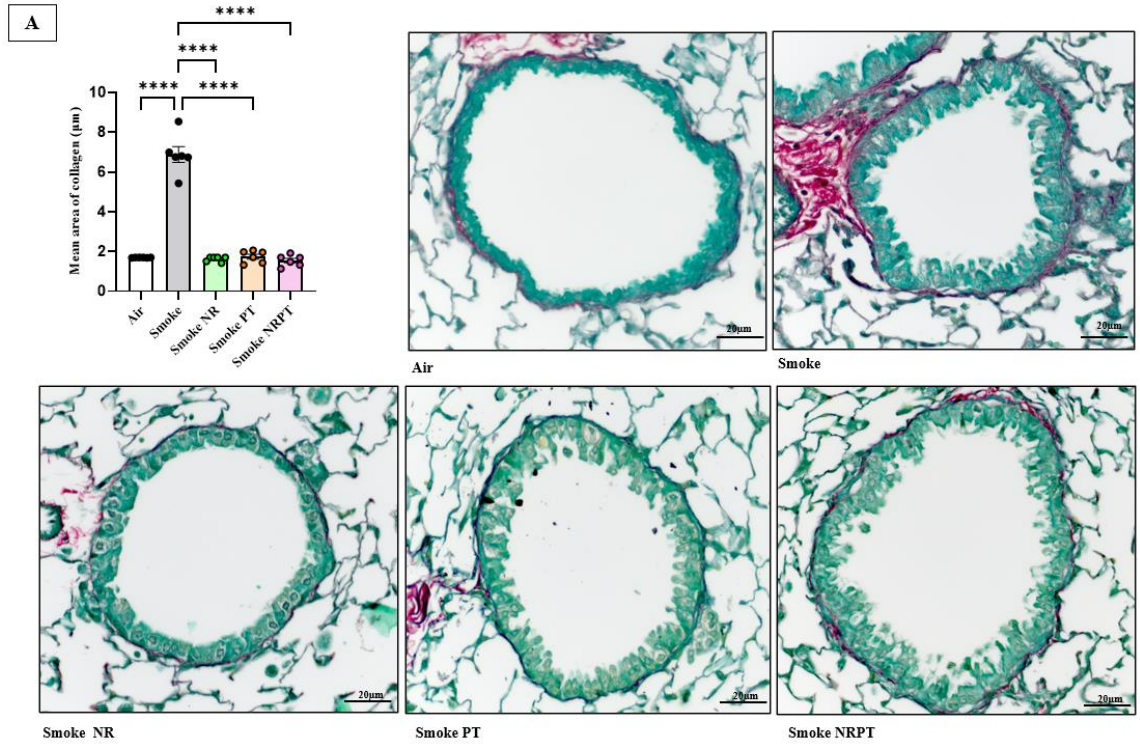

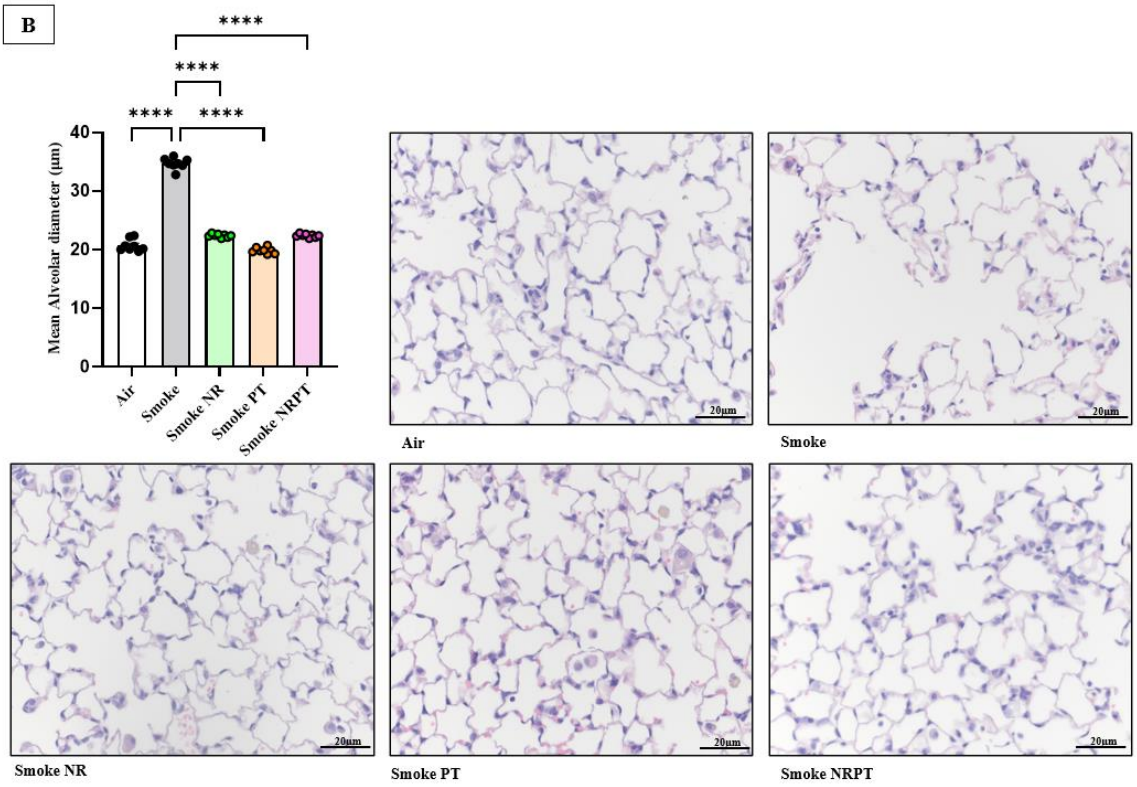

Figure 3.7: Administration of NR and/or PT attenuates airway remodelling and emphysema in COPD:

*(A) Collagen deposition, (B) Emphysema. Data represented are means ± SEM of 8 mice/group, * P<0.05, ** P<0.01, *** P<0.001, **** P<0.0001.*

3.3.7 Administration of NR and/or PT improved lung function in COPD

Mouse lung parameter changes were measured using FlexiVent as mentioned previously. Lung parameters such as inspiratory capacity (IC) (Figure 3.8A), area or hysteresis (Figure 3.8B), and total lung capacity (TLC) (Figure 3.8C) were increased in the smoke group in comparison to the air group (P<0.0001). We observed a reduction in the IC in treatment groups of smoke NR (P<0.0001), smoke PT (P<0.0001) and smoke NRPT (P<0.01) in comparison to the smoke group. Further, we also observed a reduction in the area with the treatment of smoke NR (P<0.0001) and smoke NRPT (P<0.01) in

comparison to the smoke group. Likewise, there was also a significant reduction of TLC observed in the treatment group of smoke NRPT as compared to the smoke group ($P<0.0001$). Additionally, lung compliance curves were analysed for all the experimental groups. We observed an increase in the compliance curve in the smoke group (grey) in comparison to the air group (blue) (Figure 3.8D). Additionally, we observed a reduction in the compliance curve with the individual treatment groups of smoke NR (green) (Figure 3.8E) and smoke PT (orange) (Figure 3.8F) in comparison to the smoke group (grey). Further, the treatment group of smoke NRPT (pink) showed a reduced compliance curve in comparison to the smoke group (grey).

However, other parameters like central airway resistance (Rn) (Figure 3.8H), transpulmonary resistance (Rrs) (Figure 3.8G), respiratory system compliance (CRS) (Figure 3.8I), forced vital capacity (FVC) (Figure 3.8J), tissue damping (G) (Figure 3.8K), and tissue elastance (H) (Figure 3.8L) did not show any changes between any groups in the current study.

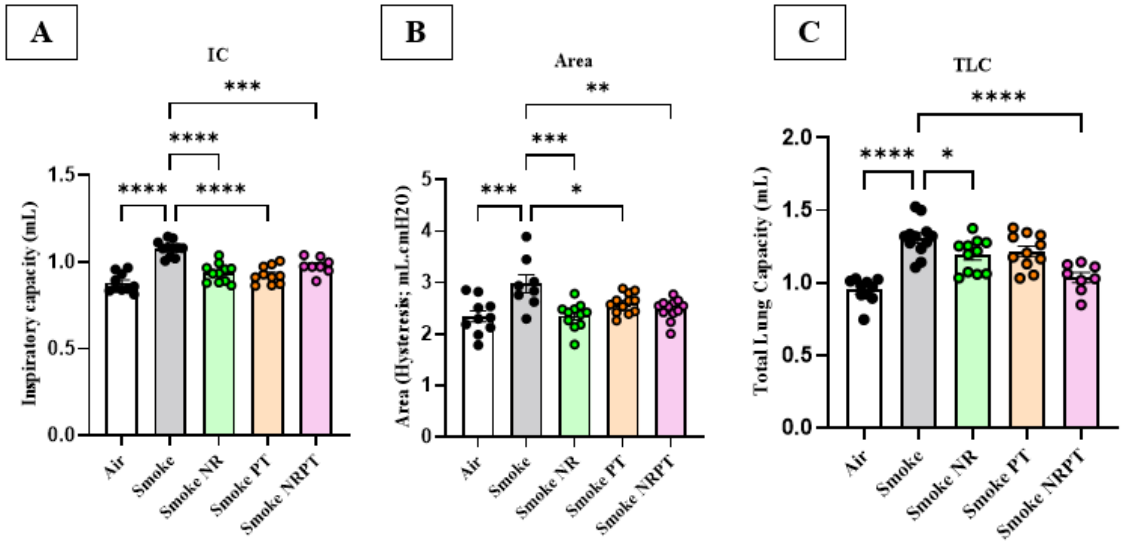

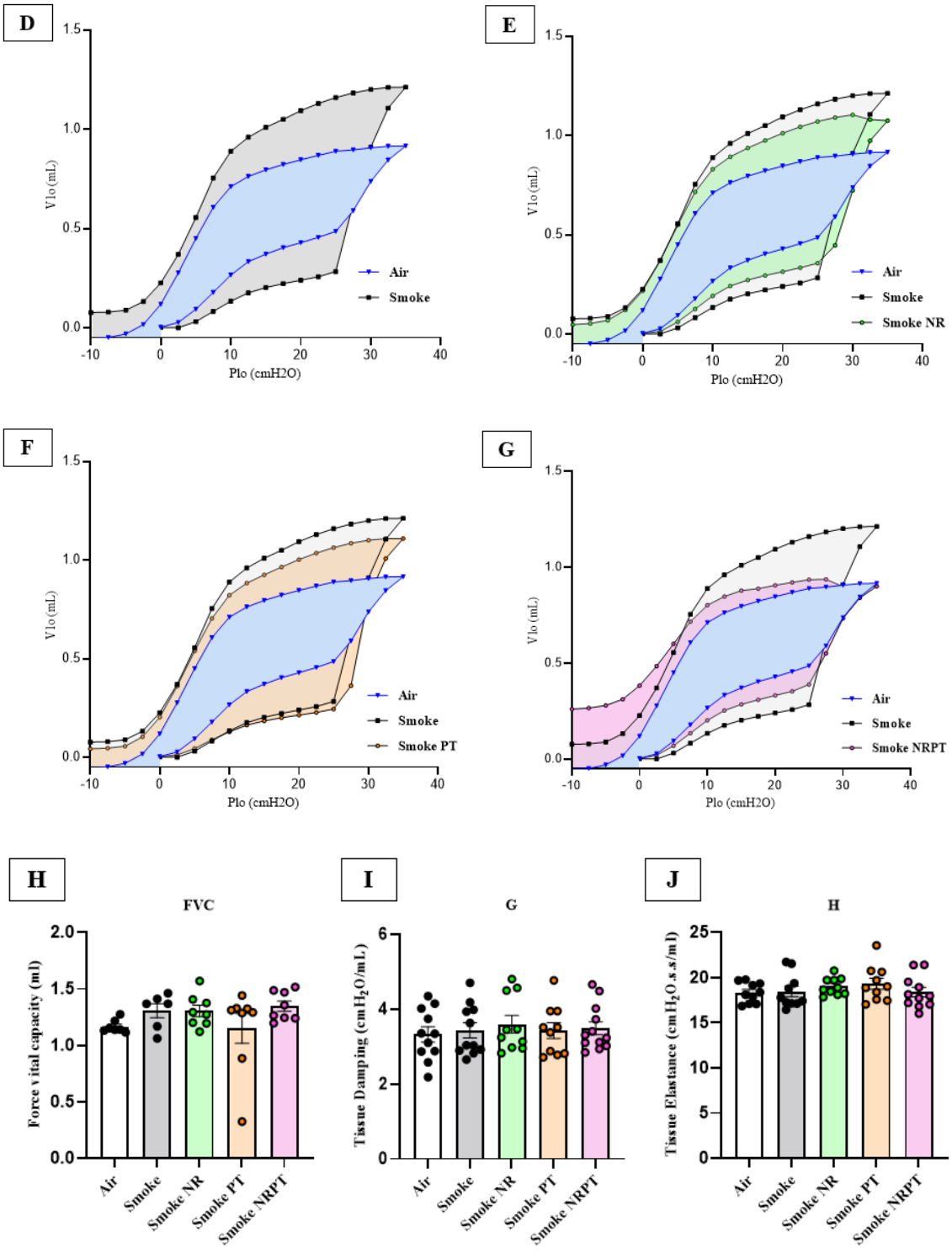
D
E
F
G
H
I
J
Vlo (mL)
Plo (cmH2O)
Air
Smoke
Smoke NR
Smoke PT
Smoke NRPT
FVC
Force vital capacity (ml)
G
Tissue Damping (cmH2O/mL)
H
Tissue Elastance (cmH2O.s.s/ml)

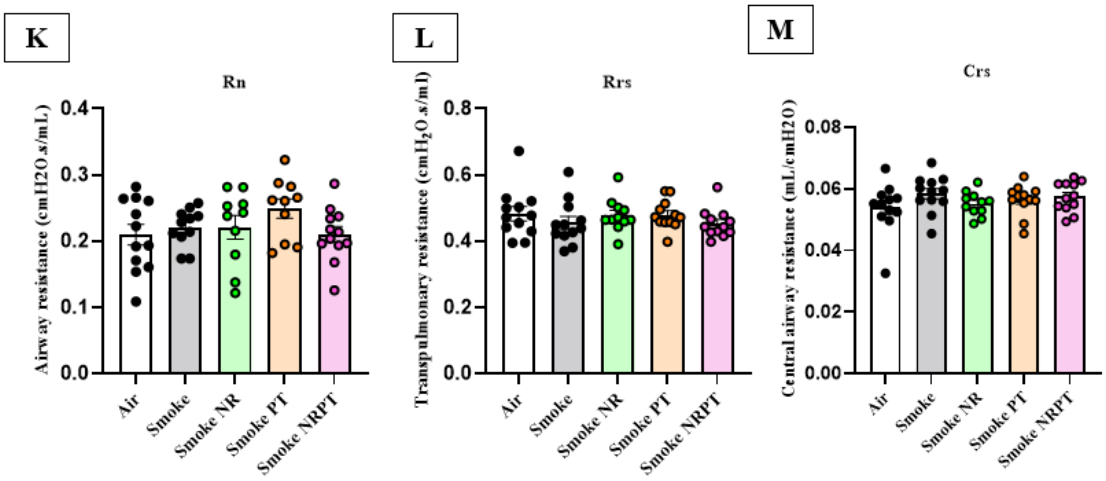

Figure 3.8: Administration of NR and/or PT improved lung function in COPD:

*Graphical representation of lung function parameters (A) IC, (B) area, (C) TLC, (D) lung compliance curves air vs smoke group, (E) lung compliance curves for air, smoke and smoke NR group, (F) lung compliance curves for air, smoke and smoke PT group, (G) lung compliance curves for air, smoke and smoke NRPT group, (H) FVC, (I) G, (J) H, (K) Rn, (L) Rrs, (M) Crs. Data represented are means ± SEM of 12 mice/group, * P<0.05, ** P<0.01, *** P<0.001, **** P<0.0001.*

3.3.8 Administration of NR and/or PT regulated NAD^+/NADH levels in COPD

We observed a reduction in the total NAD^+ levels in the smoke group in comparison to the air group (P<0.05) (Figure 3.9A). Interestingly, there was a significant increase in the total NAD^+ levels of the smoke NR, smoke PT and smoke NRPT group in comparison to the smoke group (P<0.01) (Figure 3.9A). Further, we observed an increase in the NADH levels in the smoke group as compared to the air group (P<0.0001) (Figure 3.9B). Additionally, the ratio of total NAD^+:NADH (Figure 3.9C) was observed to be significantly reduced in the smoke group in comparison to the air group (P<0.0001). The

treatment groups of smoke NR ($P<0.05$) and smoke NRPT ($P<0.001$) showed an increase in the ratio of total NAD^+:NADH in comparison to the smoke group.

Further, we examined the gene expression of NAD^+ adapters and sensors and observed no changes in the expression levels of NADSYN (Figure 3.9D), NADK1 (Figure 3.9E), NADK2 (Figure 3.9F), NAMPT (Figure 3.9G), NMNT (Figure 3.9H), NRK1 (Figure 3.9I), NRK2 (Figure 3.9J), GCN5 (Figure 3.9M), and PNP (Figure 3.9N) in all of the experimental groups. A significant reduction in the gene expression levels of PGC1α (Figure 3.9K) and NFκB (Figure 3.9L) was observed in the smoke group with respect to the air group ($P<0.0001$) and was increased significantly in the smoke NRPT group in comparison to the smoke group ($P<0.0001$).

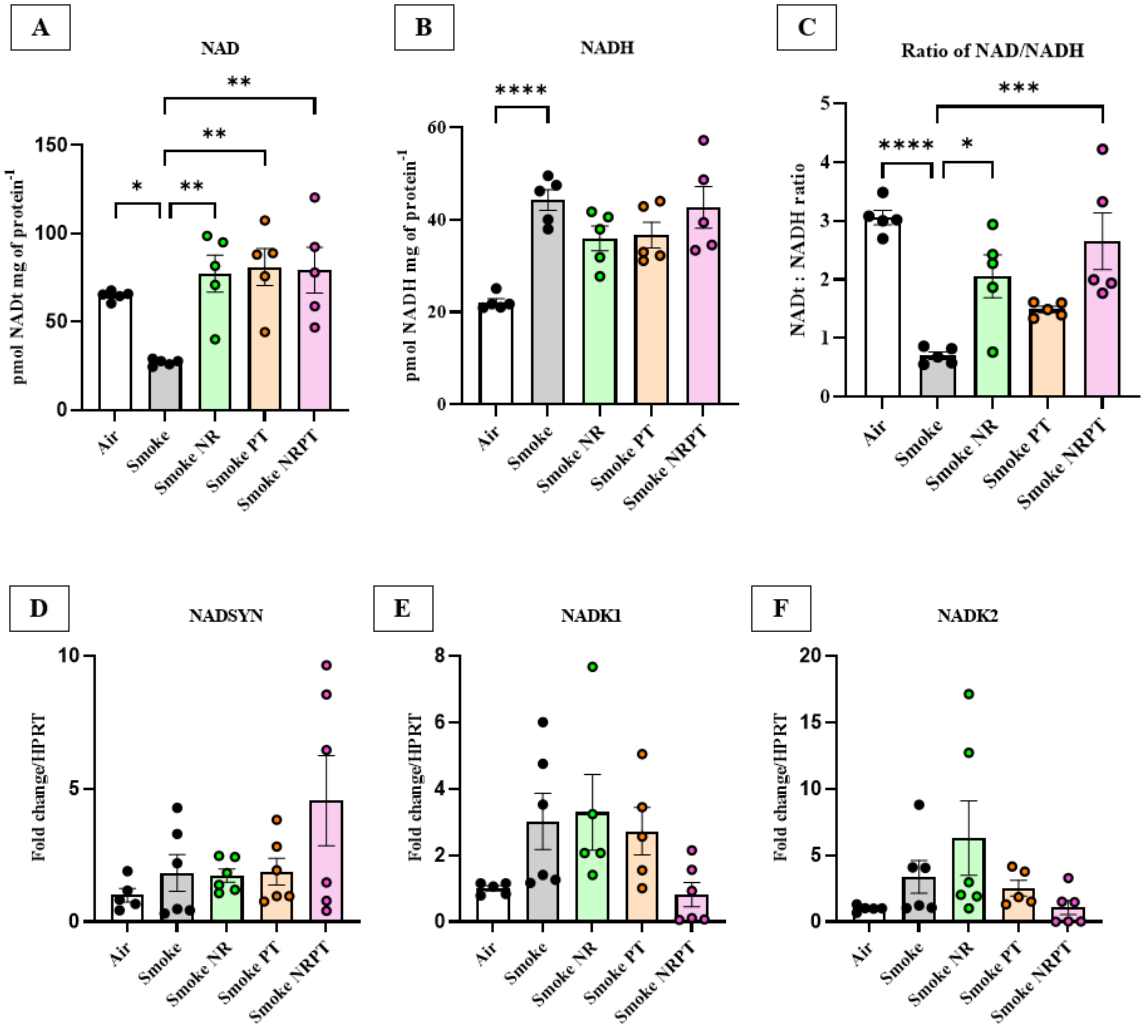

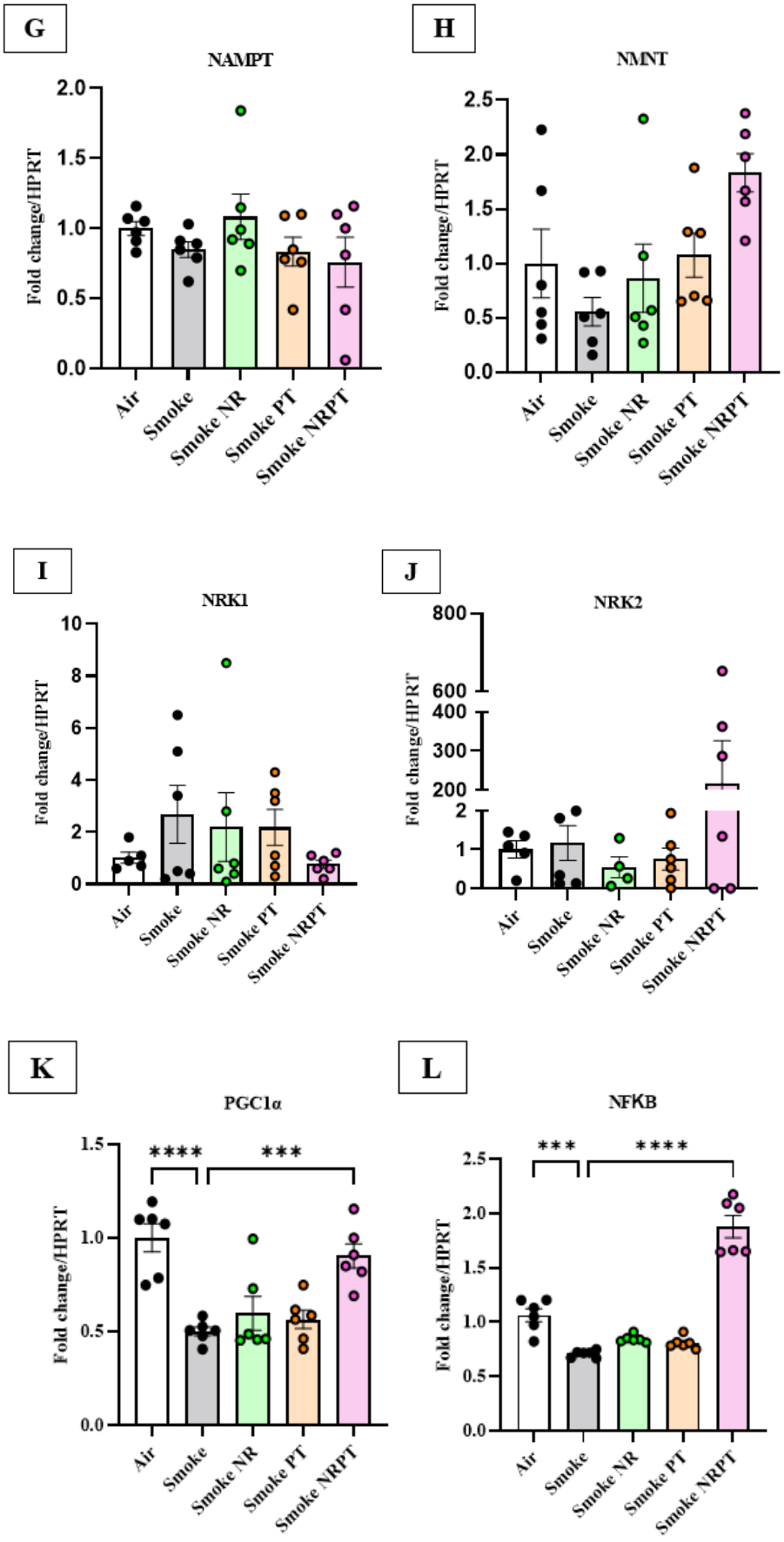
G
NAMPT
Fold change/HPRT
2.0
1.5
1.0
0.5
0.0
Air
Smoke
Smoke NR
Smoke PT
Smoke NRPT
H
NMNT
Fold change/HPRT
2.5
2.0
1.5
1.0
0.5
0.0
Air
Smoke
Smoke NR
Smoke PT
Smoke NRPT
I
NRK1
Fold change/HPRT
10
8
6
4
2
0
Air
Smoke
Smoke NR
Smoke PT
Smoke NRPT
J
NRK2
Fold change/HPRT
800
600
400
300
200
2
1
0
Air
Smoke
Smoke NR
Smoke PT
Smoke NRPT
K
PGC1α
Fold change/HPRT
****
***
1.5
1.0
0.5
0.0
Air
Smoke
Smoke NR
Smoke PT
Smoke NRPT
L
NFKB
Fold change/HPRT
***
****
2.5
2.0
1.5
1.0
0.5
0.0
Air
Smoke
Smoke NR
Smoke PT
Smoke NRPT

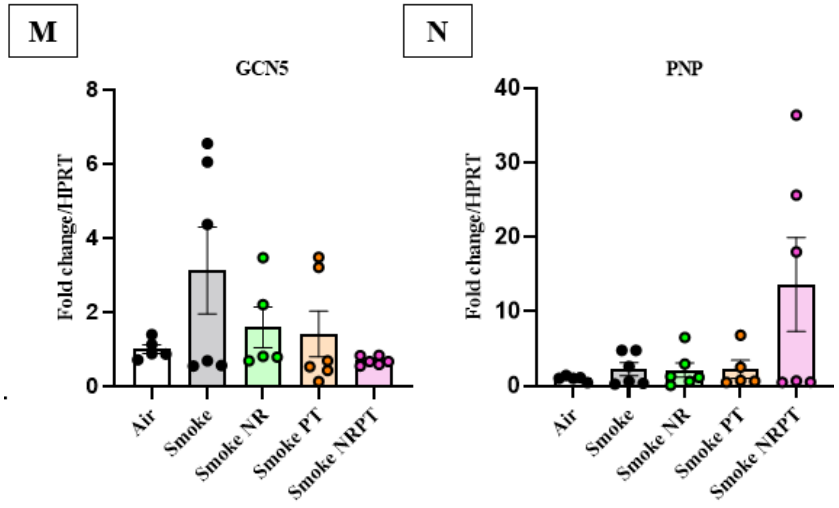

Figure 3.9: Administration of NR and/or PT restored imbalance of NAD^+ homeostasis in COPD:

(*A) total NAD^+ level in mouse lung homogenates, (B) NADH level in mouse lung homogenates, (C) ratio of NAD^+/NADH. Gene expression levels of (D) NADSYN, (E) NADK1, (F) NADK2, (G) NAMPT, (H) NMNT, (I) NRK1, (J) NRK2, (K) PGC1α, (L) NFκB, (M) GCN5 and (N) PNP. Data represented are means ± SEM of 5-6 mice/group, * P<0.05, ** P<0.01, *** P<0.001, **** P<0.0001.*

3.3.9 Administration of NR and/or PT regulated NAD^+ consumers in COPD

PARP1 gene (Figure 3.10A) and protein expression (Figure 3.10B) were measured and a significant reduction in the gene expression of PARP1 was observed in the smoke group in comparison to the air group (P<0.05), which was increased with the smoke NRPT (P<0.0001) as compared to the smoke group (Figure 3.10A). Additionally, we observed a similar reduction in the protein expression of PARP1 in the smoke group in comparison to the air group (P<0.01) which was further increased in the smoke NR (P<0.05), smoke PT (P<0.01) and smoke NRPT (P<0.05) in comparison to the smoke group (Figure 3.10B). Further, the PARP activity levels (Figure 3.10C) were measured and an increase

in the activity level was observed in the smoke group with respect to the air group ($P<0.0001$) and was significantly reduced in all the different treatment groups of smoke NR and/or PT in comparison to the smoke group ($P<0.0001$) (Figure 3.10C).

Additionally, we observed a significant reduction of CD38 protein expression in the smoke group in comparison to the air group ($P<0.05$) which was increased in the smoke NR ($P<0.05$) and smoke PT ($P<0.05$) respectively (Figure 3.10D).

Further, a reduction in the SIRT1 gene expression level was observed in the smoke group ($P<0.001$) in comparison to the air group (Figure 3.10E). Further, no significant changes were observed across all groups in the protein expression of SIRT1 (Figure 3.10L). However, we observed a significant reduction in the protein expression levels of phospho-SIRT1 (pSIRT1) (Figure 3.10M) in the smoke group in comparison to the air group ($P<0.01$) and was significantly increased in all the treatment groups of smoke NR ($P<0.01$), smoke PT ($P<0.01$) and smoke NRPT ($P<0.05$). No significant changes were observed in the gene expression of SIRT2 (Figure 3.10F) between the air and the smoke group, but there was a significant increase in the treatment group of smoke NR when compared to the smoke group ($P<0.01$). In contrast, we observed a reduction in the SIRT2 protein levels (Figure 3.10N) in the smoke group as compared to the air group ($P<0.01$), which was upregulated in all the treatment groups of smoke NR and smoke PT in comparison to the smoke group ($P<0.0001$). Interestingly, a reduction in the gene expression of SIRT3, SIRT5, SIRT6 and SIRT7 (Figure 3.10G, 3.10I, 3.10J & 3.10K) was observed in the smoke group in comparison to the air group ($P<0.05$). The treatment groups of smoke NR and smoke NRPT showed an increase in the gene expression of SIRT6 in comparison to the smoke group ($P<0.05$). However, we did not see any significant changes in the protein expression of SIRT3 (Figure 3.10O) across all the experimental groups, but a reduction in the SIRT5 (Figure 3.10P), SIRT6 (Figure 3.10Q)

and SIRT7 (Figure 3.10R) protein levels were observed in the smoke group as compared to the air group ($P<0.05$) and were upregulated in the treatment groups of smoke NR and/or PT ($P<0.05$). Surprisingly, we observed no changes in the gene expression of SIRT4 (Figure 3.10H) across all the experimental groups.

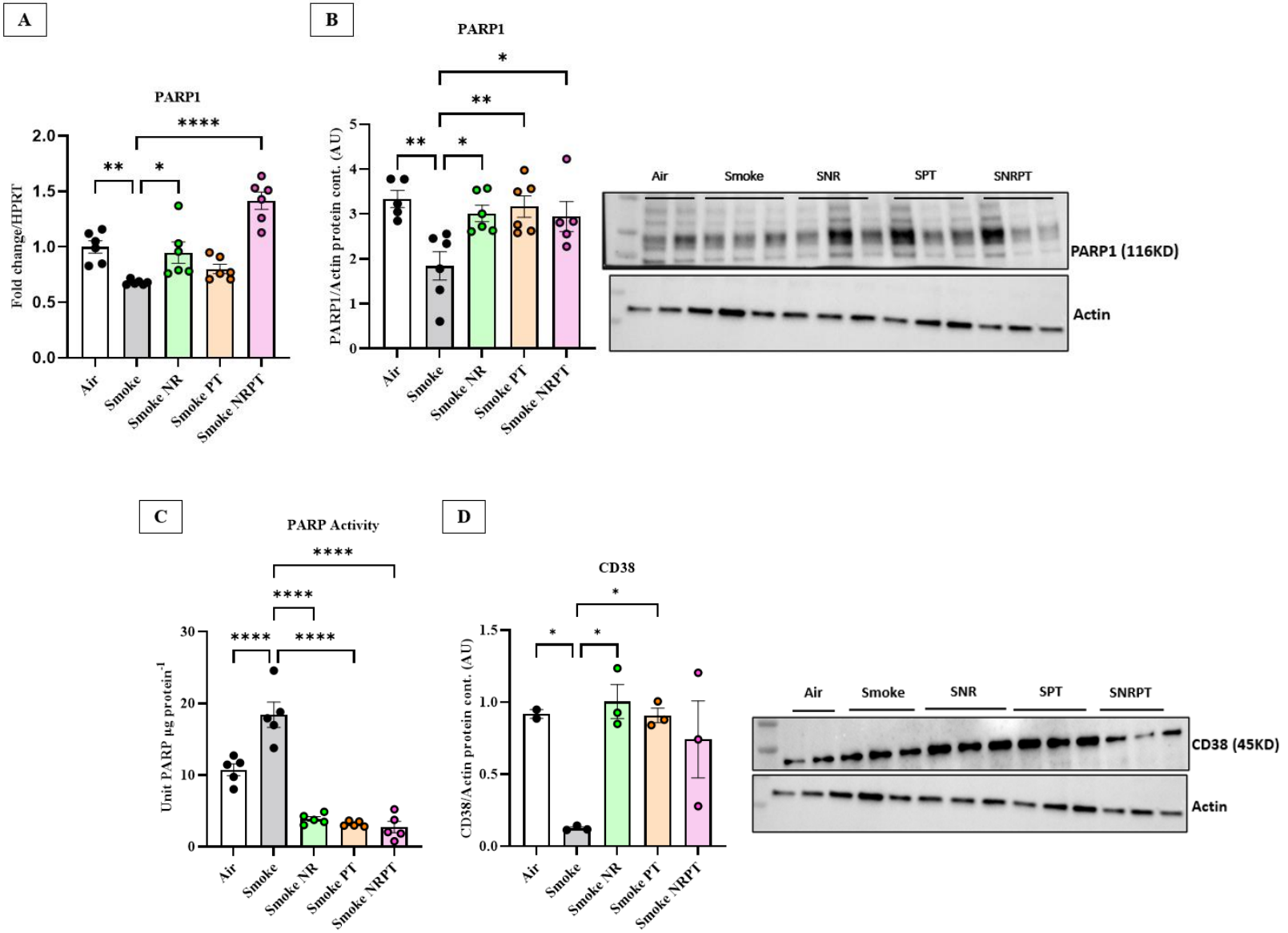
A
PARP1
Fold change/HPRT
2.0
1.5
1.0
0.5
0.0
**
*
****
Air
Smoke
Smoke NR
Smoke PT
Smoke NRPT
B
PARP1
PARP1/Actin protein cont. (AU)
5
4
3
2
1
0
*
**
**
*
Air
Smoke
Smoke NR
Smoke PT
Smoke NRPT
Air
Smoke
SNR
SPT
SNRPT
PARP1 (116KD)
Actin
C
PARP Activity
Unit PARP µg protein-1
30
20
10
0
****
****
****
****
Air
Smoke
Smoke NR
Smoke PT
Smoke NRPT
D
CD38
CD38/Actin protein cont. (AU)
1.5
1.0
0.5
0.0
*
*
*
Air
Smoke
Smoke NR
Smoke PT
Smoke NRPT
Air
Smoke
SNR
SPT
SNRPT
CD38 (45KD)
Actin

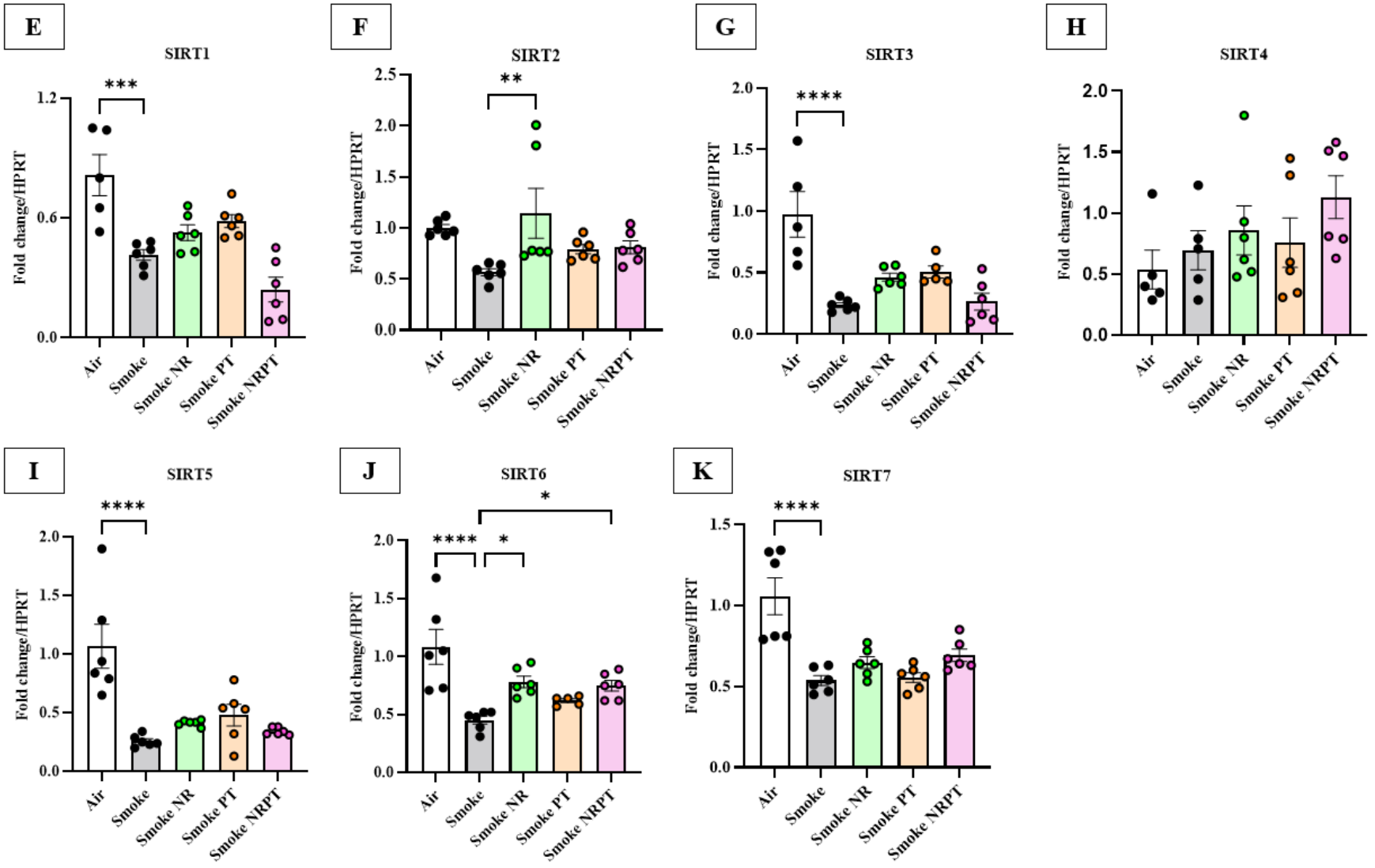
E
SIRT1
***
Fold change/HPRT
1.2
0.6
0.0
Air
Smoke
Smoke NR
Smoke PT
Smoke NRPT
F
SIRT2
**
Fold change/HPRT
2.5
2.0
1.5
1.0
0.5
0.0
Air
Smoke
Smoke NR
Smoke PT
Smoke NRPT
G
SIRT3
****
Fold change/HPRT
2.0
1.5
1.0
0.5
0.0
Air
Smoke
Smoke NR
Smoke PT
Smoke NRPT
H
SIRT4
Fold change/HPRT
2.0
1.5
1.0
0.5
0.0
Air
Smoke
Smoke NR
Smoke PT
Smoke NRPT
I
SIRT5
****
Fold change/HPRT
2.0
1.5
1.0
0.5
0.0
Air
Smoke
Smoke NR
Smoke PT
Smoke NRPT
J
SIRT6
*
****
*
Fold change/HPRT
2.0
1.5
1.0
0.5
0.0
Air
Smoke
Smoke NR
Smoke PT
Smoke NRPT
K
SIRT7
****
Fold change/HPRT
1.5
1.0
0.5
0.0
Air
Smoke
Smoke NR
Smoke PT
Smoke NRPT

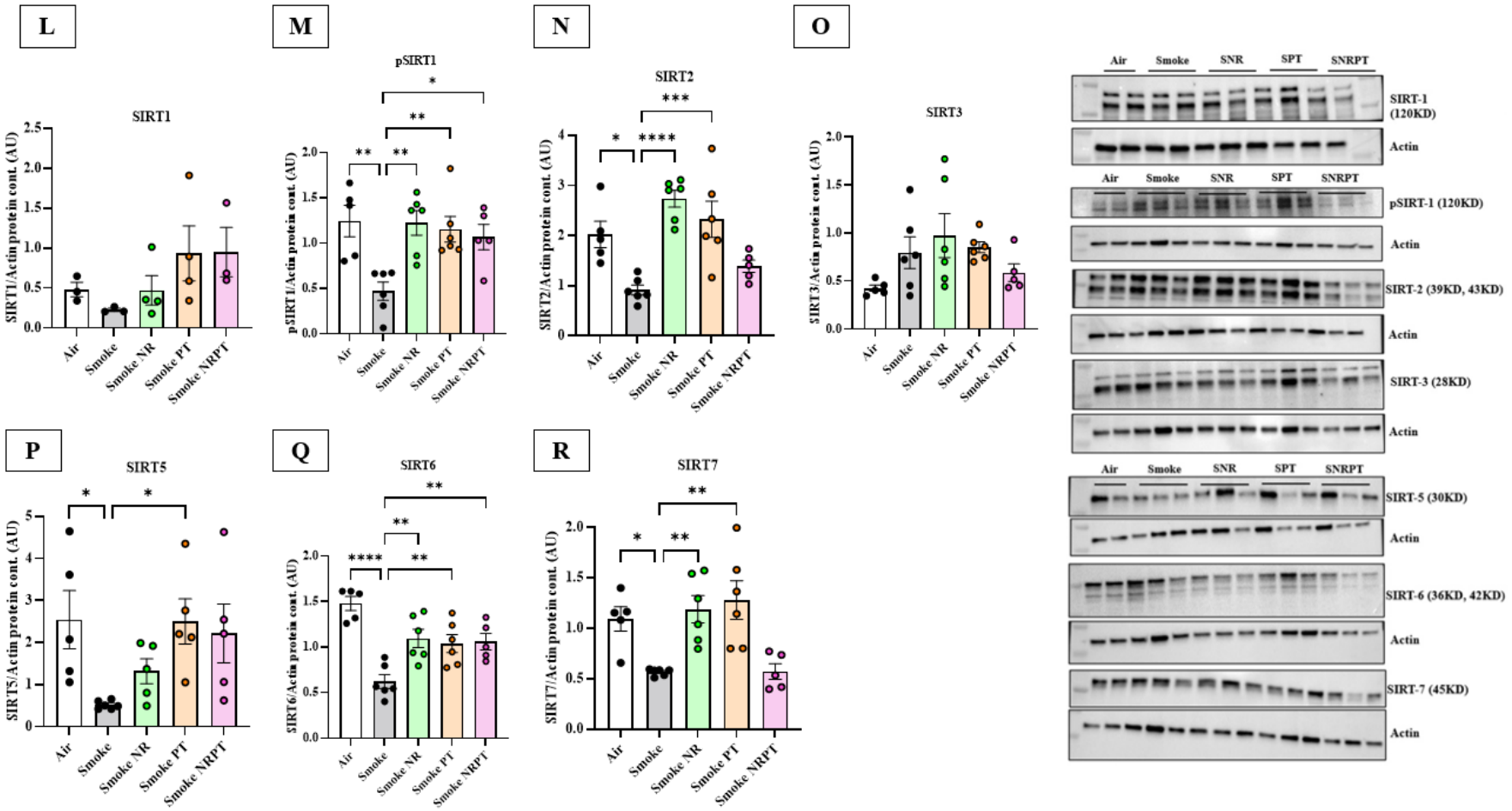

Figure 3.10: Administration of NR and/or PT regulates NAD^+ consumers in COPD:

*(A) Gene expression level of PARP1, (B) protein expression of PARP1, (C) PARP activity levels, (D) CD38 protein expression. Gene expression of (E) SIRT1, (F) SIRT2. (G) SIRT3, (H) SIRT4, (I) SIRT5, (J) SIRT6, (K) SIRT7; Protein levels of (L) SIRT1, (M) SIRT2, (N) SIRT3, (O) SIRT5, (6) SIRT6, (7) SIRT7. Data represented are means ± SEM of 6 mice/group, * P<0.05, ** P<0.01, *** P<0.001, **** P<0.0001.*

3.3.10 Administration of NR and/or PT preserved mitochondrial structure in COPD

Mitochondrial morphology was determined using TEM as mentioned previously. We observed an increase in mitochondrial number or density in the smoke group (Figure 3.11B) as compared to the air group (P<0.001) (Figure 3.11A). However, there was a reduction in mitochondrial density in the treatment groups of smoke NR (P<0.01) (Figure 3.11C) and smoke NRPT (P<0.001) (Figure 3.11E) in comparison to the smoke group, in contrast to smoke PT which was increased with respect to the air group (P<0.01) (Figure 3.11D).

Further, the mitochondrial area was measured for all the experimental groups. A significant increase in the mitochondrial area was observed in the smoke group (Figure 3.11G) in comparison to the air group (P<0.001) (Figure 3.11F). We observed a reduction in mitochondrial area in all the treatment groups of smoke NR (P<0.05) (Figure 3.11H), smoke PT (P<0.05) (Figure 3.11I) and smoke NRPT (P<0.01) (Figure 3.11J) as compared to the smoke group.

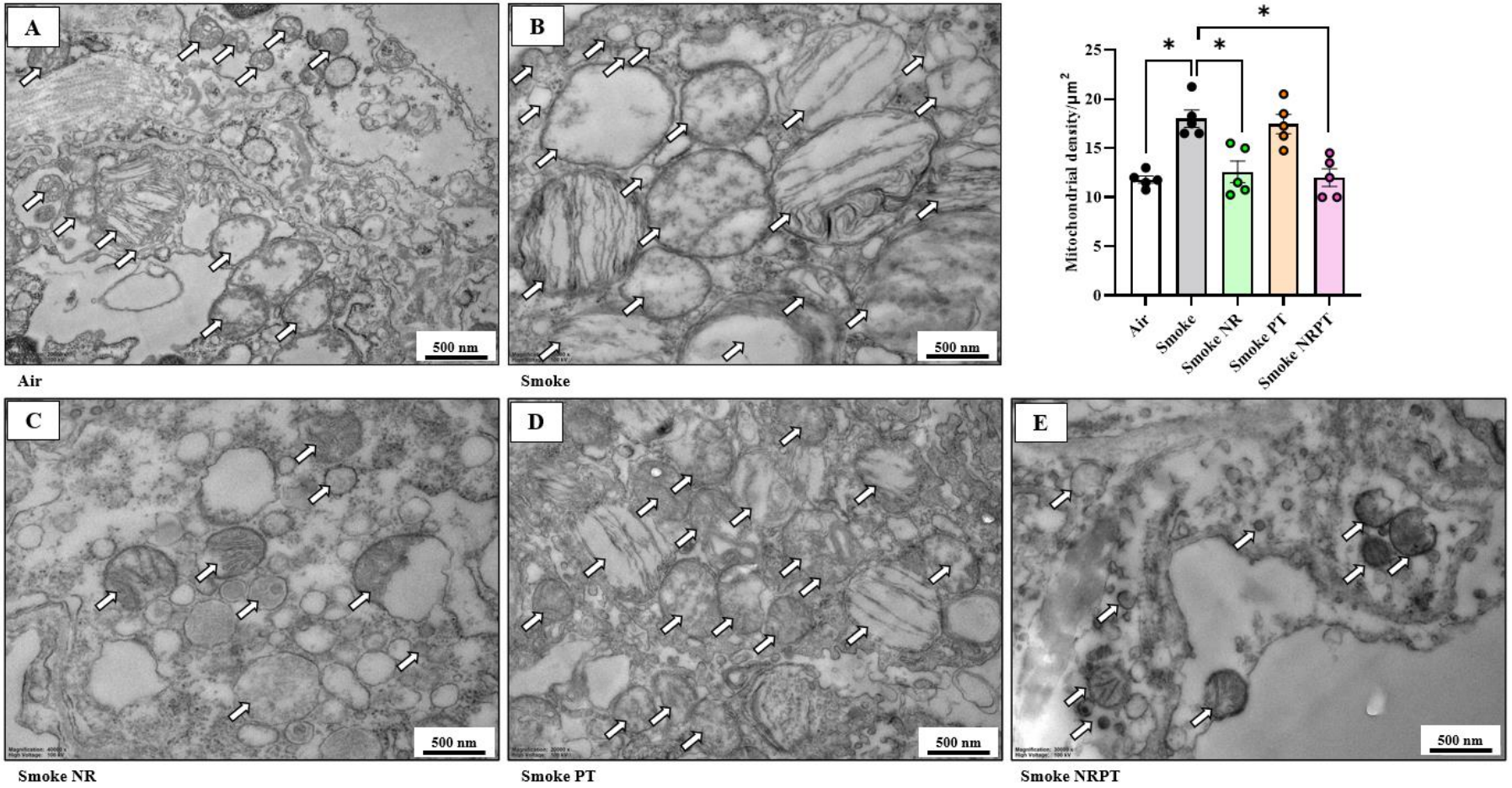
A
500 nm
Air
B
500 nm
Smoke
Mitochondrial density/µm²
25
20
15
10
5
0
*
*
*
Air
Smoke
Smoke NR
Smoke PT
Smoke NRPT
C
500 nm
Smoke NR
D
500 nm
Smoke PT
E
500 nm
Smoke NRPT

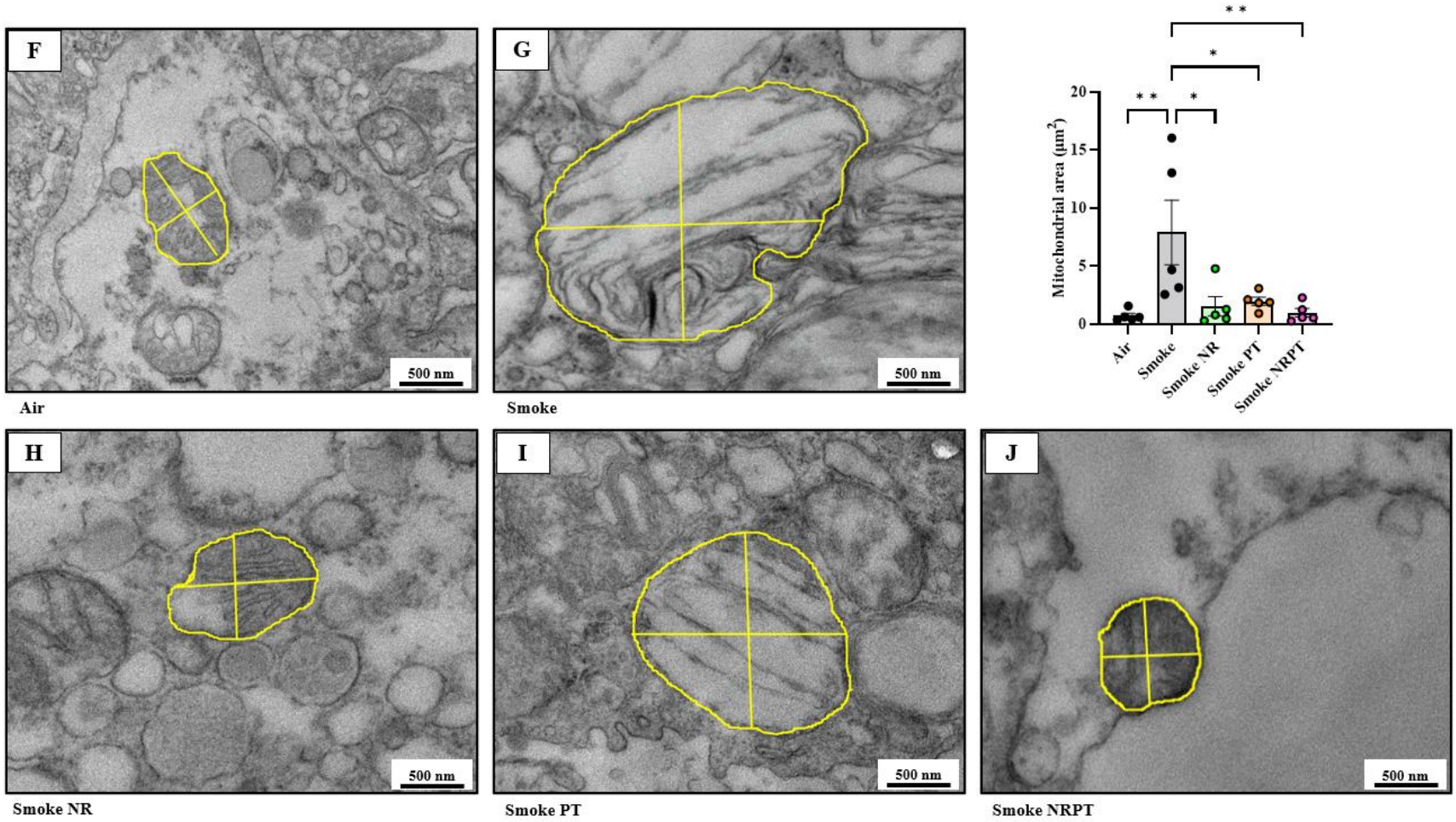

Figure 3.11: Administration of NR and/or PT preserved mitochondrial structure in COPD:

*Mitochondrial density represented with white arrows (A) Air, (B) Smoke, (C) Smoke NR, (D) Smoke PT, (E) Smoke NR and PT; Mitochondrial area represented with yellow outline (F) Air, (G) Smoke, (H) Smoke NR, (I) Smoke PT, (J) Smoke NR and PT; Data represented are means ± SEM of 5 mice/group, * P<0.05, ** P<0.01, *** P<0.001, **** P<0.0001.*

3.3.11 Administration of NR and/or PT preserved mitochondrial cristae structure in COPD

Using TEM we further measured cristae density (Figure 3.12A), cristae volume (Figure 3.12B) and cristae area (Figure 3.12C) in all the experimental groups. There was a significant reduction in cristae density (P<0.01), volume (P<0.0001), and area (P<0.05) in the smoke group (Figure 3.12E) as compared to the air group (Figure 3.12D). This was further increased in the treatment groups of smoke NR (Figure 3.12F), smoke PT (Figure 3.12G) and smoke NRPT (Figure 3.12H) with respect to the smoke group (P<0.05).

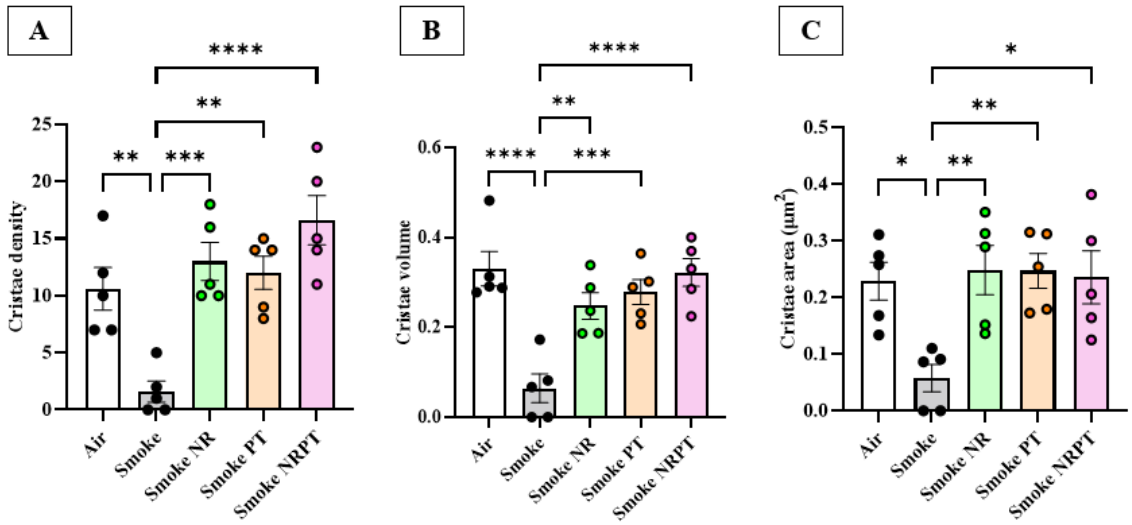

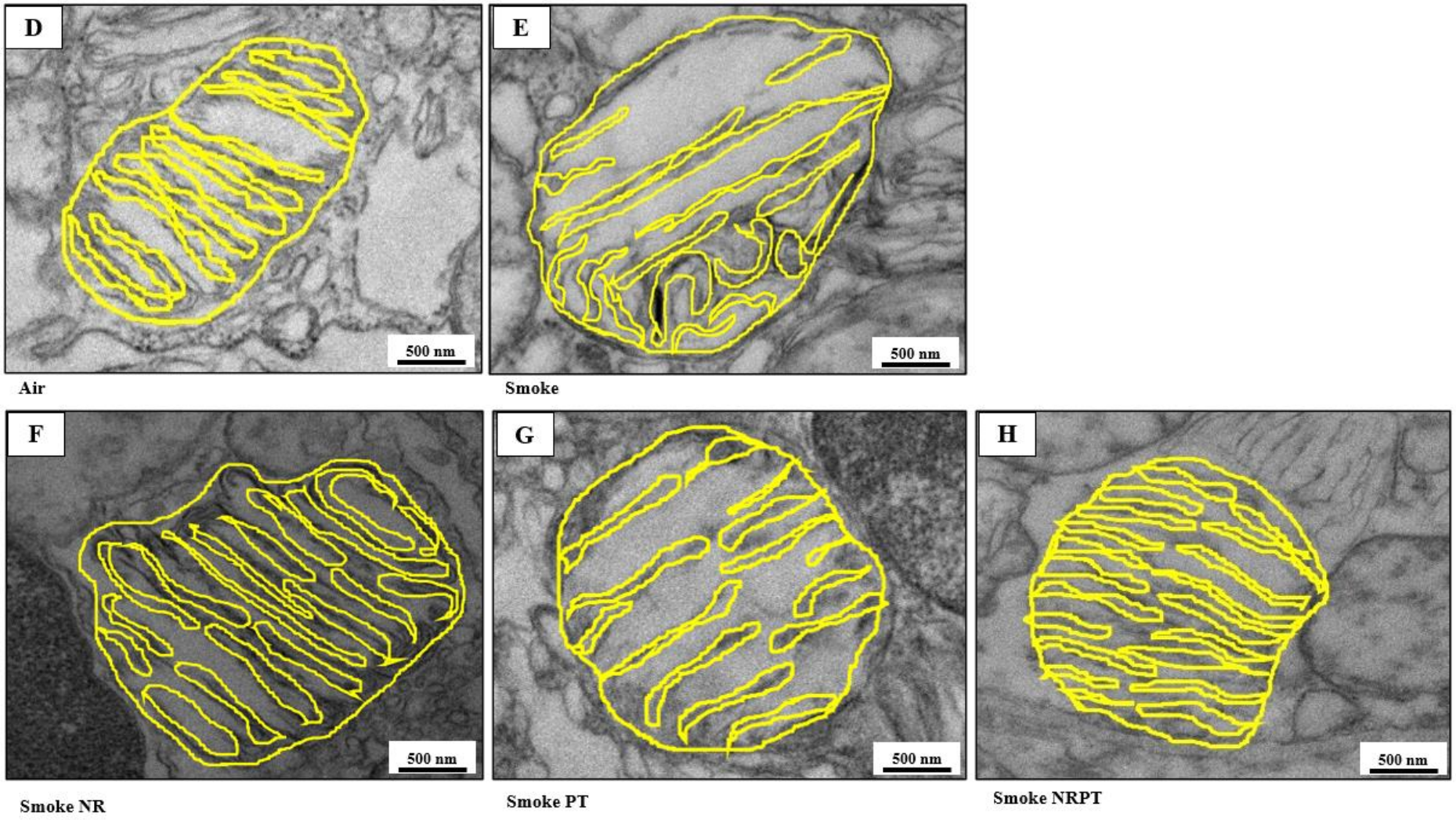

Figure 3.12: Administration of NR and/or PT preserved mitochondrial cristae structure in COPD:

*Graphical representation of (A) cristae density, (B) cristae volume, (C) cristae area; Cristae structure is outlined in yellow for all the experimental groups: (D) Air, (E) Smoke, (F) Smoke NR, (G) Smoke PT, (H) Smoke NR and PT. Data represented are means ± SEM of 5 mice/group, * P<0.05, ** P<0.01, *** P<0.001, **** P<0.0001.*

3.3.12 Administration of NR and/or PT promoted mitochondrial function in COPD

Mitochondrial respiratory chain enzymatic activities were measured in lung homogenates for complex I (Figure 3.13A), complex II (Figure 3.13B), complex III (Figure 3.13C), complex IV (Figure 3.13D), complex I+III (Figure 3.13E), complex II+III (Figure 3.13F), citrate synthase (Figure 3.13G) and β-HAD (Figure 3.13H). We observed a reduction in the activity of complex I, II, III, IV, II+III and β-HAD in the smoke group in comparison to the air group ($P<0.05$) and this was further increased in the treatment groups of smoke NR ($P<0.01$) and/or PT ($P<0.001$) with respect to the smoke group. Moreover, we also observed a significant increase in the activity levels of complex I+III and citrate synthase in the smoke NR ($P<0.001$) and/or PT groups ($P<0.01$) as compared to the smoke group. In contrast, we observed an increase in the citrate synthase activity in the smoke group with respect to the air group ($P<0.01$).

Furthermore, we also measured the protein expression level of complex I-NDUFB8 (Figure 3.13I), complex II-SDHB (Figure 3.13J), complex III-UQCRC2 (Figure 3.13K), complex IV-MTCO1 (Figure 3.13L), and complex V-ATP5A (Figure 3.13M). A significant increase in the protein levels of complex I, III, IV and V were observed in the treatment groups of smoke NR and/or PT in comparison to both the smoke group and air group ($P<0.05$). In contrast, there was no change in the protein expression of complex II other than in the smoke NRPT group which showed a significant increase in comparison to the smoke group ($P<0.001$).

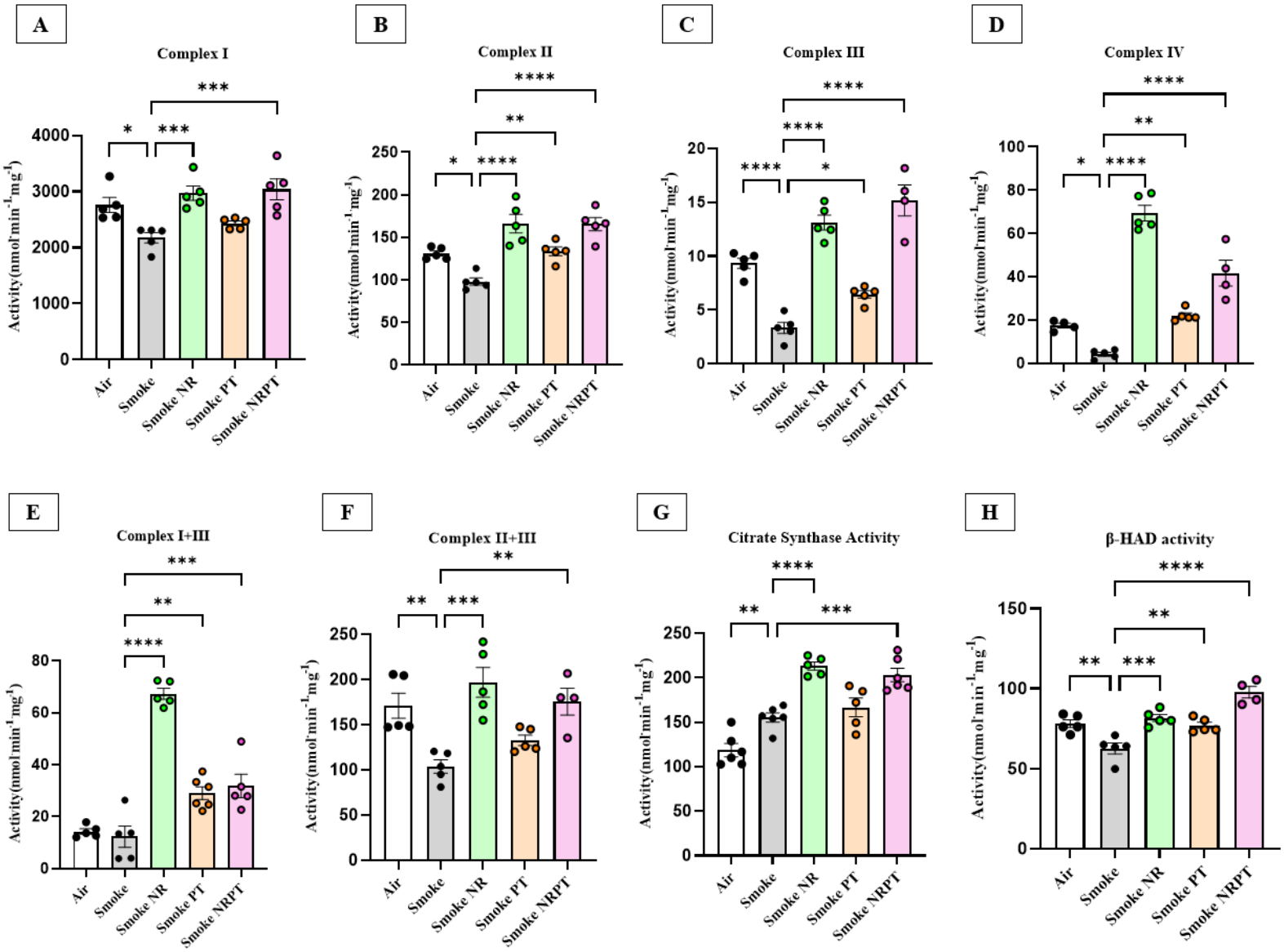
A
Complex I
Activity(nmol min-1 mg-1)
Air
Smoke
Smoke NR
Smoke PT
Smoke NRPT
B
Complex II
C
Complex III
D
Complex IV
E
Complex I+III
F
Complex II+III
G
Citrate Synthase Activity
H
β-HAD activity

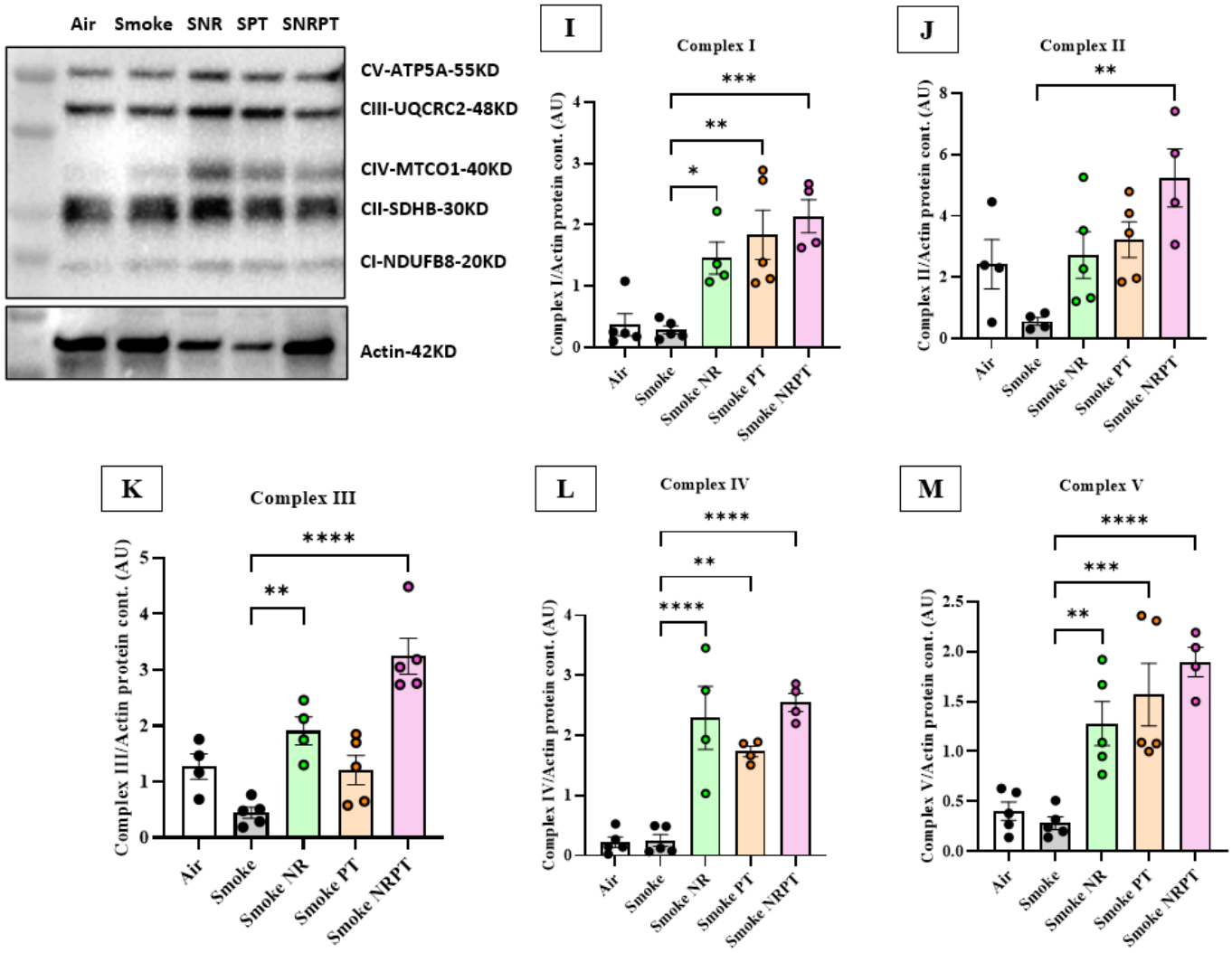

Figure 3.13: Administration of NR and/or PT promotes mitochondrial function in COPD:

*Increase in mitochondrial respiratory chain enzymatic activity of (A) Complex I, (B) Complex II, (C) Complex III, (D) Complex IV, (E) Complex I+III, (F) Complex II+III, (G) Citrate synthase (H) β-HAD in the smoke NR and/or PT group in comparison to the smoke group (P<0.05); Increased protein expression of (I) Complex I-NDUFB8, (J) Complex II-SDHB, (K) Complex III-UQCRC2, (L) Complex IV-MTCO1, (M) Complex V-ATP5A in the smoke NR and/or PT group in comparison to the smoke group (P<0.05); Data represented are means ± SEM of 5 mice/group, * P<0.05, ** P<0.01, *** P<0.001, **** P<0.0001.*

3.3.13 Administration of NR and/or PT promoted mitochondrial membrane potential in COPD

To further explore functional parameters related to mitochondrial dysfunction, we examined ΔΨm using JC1 staining on lung sections. The ratio of J-aggregates (red) in comparison to J-monomers (green) was measured for all the groups. J-aggregates remained unchanged across all the experimental groups (Figure 3.14A). J-monomers increased in the smoke group with respect to the air group (P<0.0001) and were significantly reduced in the smoke NR and/or PT treatments in comparison to the smoke group (P<0.0001) (Figure 3.14B). Further, the ΔΨm was reduced in the smoke group as compared to the air group (P<0.05) and increased in the smoke NR (P<0.01) and/or PT (P<0.001) treatment groups with respect to the smoke group (Figure 3.14C). The representative images below represent J-aggregates in the Texas Red channel (red, excitation at 580-604 nm), J-monomers in the Fluorescin (FIT-C) channel (green, excitation at 400-535 nm) and nuclear stain DAPI (blue, excitation at 359 nm) followed by a merged image of all the channels showing a co-localisation of J-aggregates and J-monomers (orange).

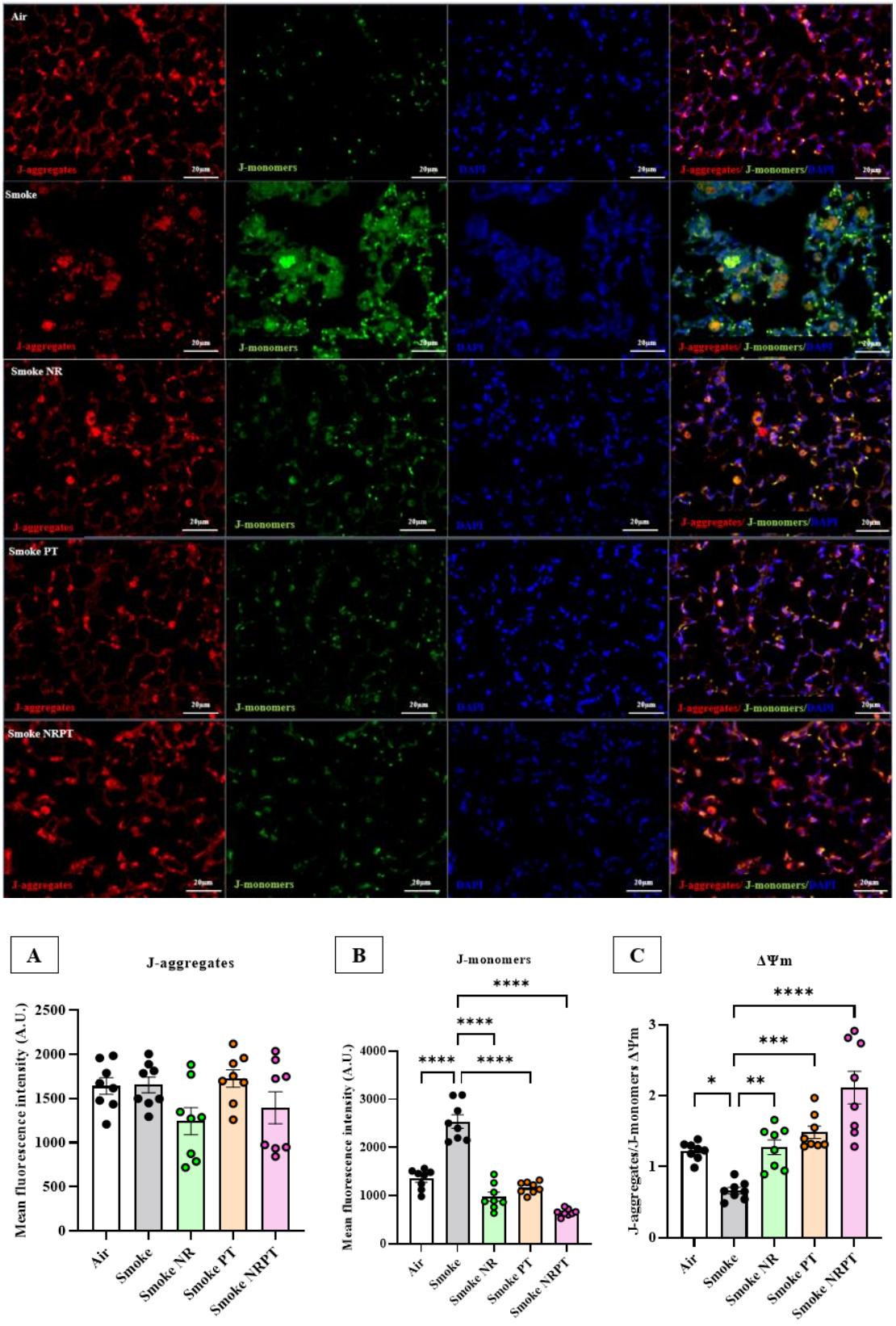

Figure 3.14: Administration of NR and/or PT promoted mitochondrial membrane potential in COPD:

*Measure of mitochondrial membrane potential (A) J-aggregates, (B) Reduced J-monomers (P<0.05), and (C) increased in the ΔΨm in smoke NR and/or PT group as compared to the smoke group (P<0.05). Representative images of J-aggregates are shown in red, J-monomers in green, nuclear stain DAPI in blue, and co-localisation of J-aggregates and J-monomers in orange. Data represented are means ± SEM of 8 mice/group, * P<0.05, ** P<0.01, *** P<0.001, **** P<0.0001.*

3.3.14 Administration of NR and/or PT reduced oxidative stress in COPD

The gene expression for NOX2 was measured, whereby an increase in NOX2 was observed in the smoke group in comparison to the air group (P<0.01) and was significantly reduced in the smoke NRPT treatment group with respect to the smoke group (P<0.001) (Figure 3.15A).

Further, an increase in the MFI was observed for 4-HNE in the smoke group in comparison to the air group (P<0.0001) which was reduced in all the treatment groups of smoke NR and/or PT with respect to the smoke group (P<0.0001). Images below represent 4-HNE (green) co-stained with F4/80 (red) and DAPI (blue) (Figure 3.15B).

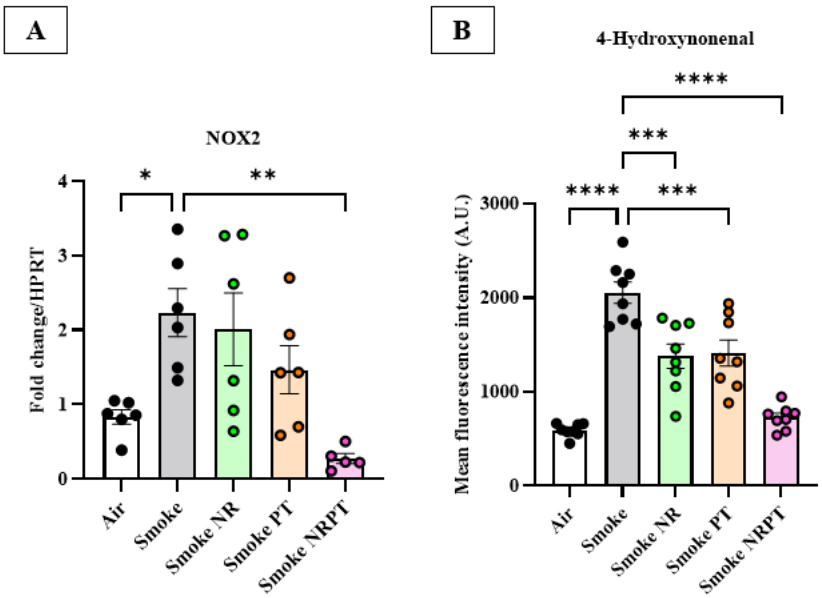

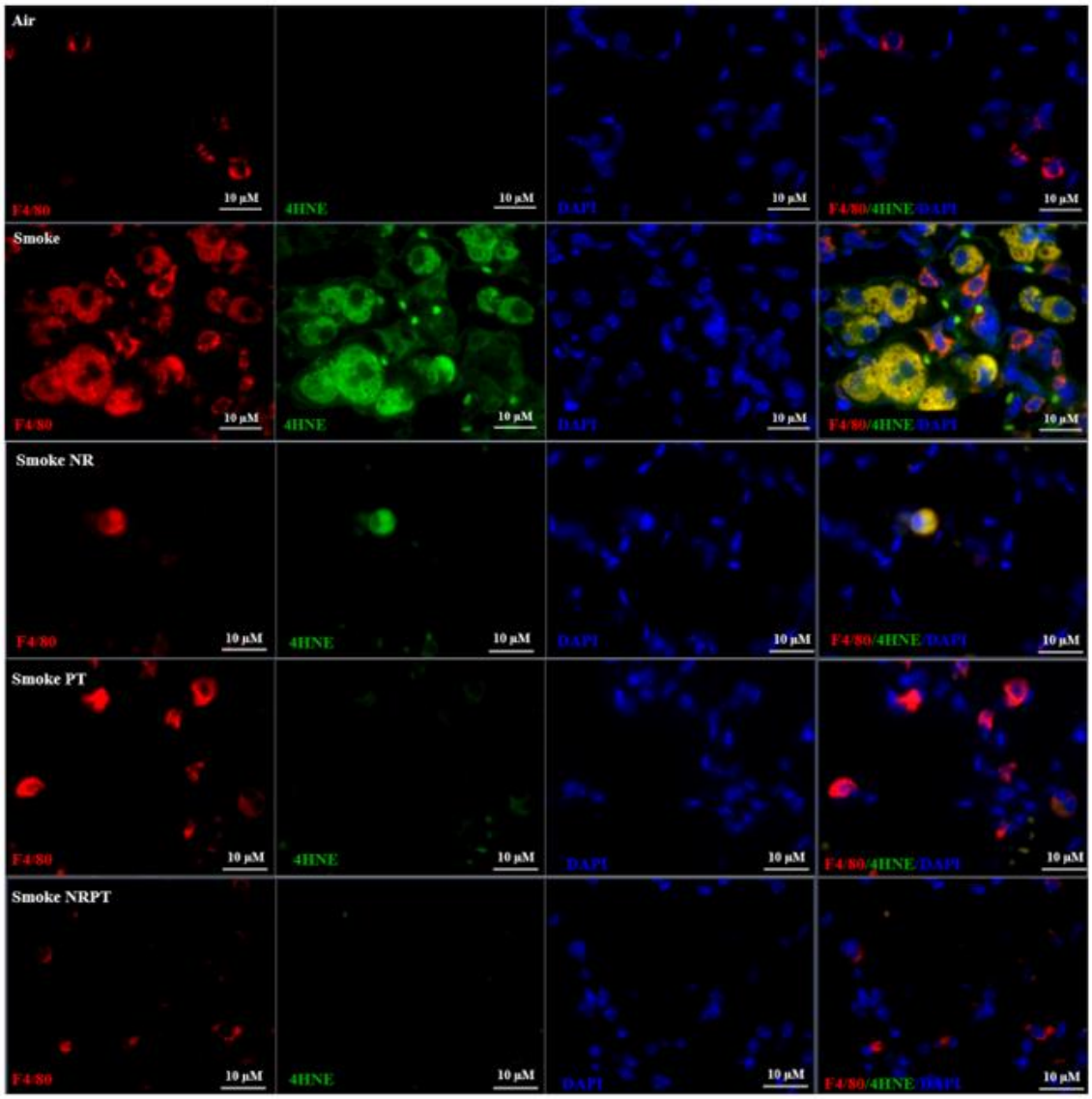

Figure 3.15: Administration of NR and PT reduces oxidative stress in COPD:

*(A) Reduced gene expression of NOX2 in smoke NRPT as compared to the smoke group (P<0.001); (B) Graphical representation of MFI in arbitrary units (A.U.) of reduced 4-HNE levels in smoke NR and/or PT in comparison to smoke group (P<0.0001), images show fluorescence localisation of F4/80 (red), 4-HNE (green), DAPI-nuclei stain (blue). Data represented are means ± SEM of 6-8 mice/group, * P<0.05, ** P<0.01, *** P<0.001, **** P<0.0001.*

3.4 Discussion

The objective of this study was to elucidate the role of NAD^+ metabolism in the development and progression of COPD by deciphering the therapeutic effects of NR and/or PT in our experimental COPD mouse model. Studies have stated that inflammation in COPD is accompanied by tissue destruction and degradation, and other cellular and molecular processes like oxidative stress and apoptosis (319). The imbalance of chemokines and cytokines during inflammation results in disrupted cellular homeostasis and consequently impairs cellular metabolism and function leading to disease progression (320, 321). Altered immunometabolism often results in impaired immune responses (322) and thus, pharmacological manipulation of these metabolic processes has been the focus of recent research to develop novel therapeutic interventions for COPD (323). NAD^+ is an important metabolic intermediate that serves as an enzyme cofactor in the redox reaction and is also used as a co-substrate by adenosine diphosphate ribose transferases (324) and synthases, as well as SIRTs (241). These activities enable NAD^+ metabolism to regulate a broad spectrum of cellular functions such as energy metabolism (315) and DNA repair. Therefore, manipulation of NAD^+ using modulators such as NR and/or PT can have immunomodulatory effects in chronic inflammatory diseases.

Studies have demonstrated that the depletion of NAD^+ levels and alterations of NAD^+ homeostasis are common in aging, cancer, diabetes, metabolic disorders, and cardiovascular and neurodegenerative diseases (primary references). To date, there is limited knowledge about the exact mechanisms of NAD^+ depletion in COPD. As such, this study aimed to unveil the mechanism of alterations of NAD^+ homeostasis during the development and progression of the disease.

The findings from our study show a significant reduction in the ratio of total NAD^+ to NADH levels in 2-weeks, 4-weeks, 6-weeks, 8- and 12-weeks CS-induced COPD model

(Figure 3.2C) suggesting that there is an imbalance of NAD^+/NADH ratios during the development and progression of COPD. Based on the important role of NAD^+ in regulating mitochondrial metabolism, it is therefore plausible that imbalances in NAD^+ homeostasis may be potential drivers of mitochondrial dysfunction in COPD and a contributing factor driving COPD progression.

Further, we investigated the therapeutic efficacy of NR and/or PT using our 2-week acute CS exposure model. We observed an increase in the leukocyte infiltration in the BAL of the smoke group compared to air, which was significantly reduced in all three treatment groups of NR, PT and NRPT (Figure 3.3). We also observed an increase in the transcripts encoding TNFα, CXCL1, and YM1 in the smoke group in comparison to the air group which was further reduced in the treatment groups of NR and/or PT. This further validated the anti-inflammatory properties of NR and/or PT in the 2-week acute CS exposure study (Figure 3.3).

Additionally, our findings from the 2-week acute CS exposure study demonstrated a reduction in the NAD^+/NADH ratio in the smoke group in comparison to the air group. This was further increased with the administration of NR and/or PT in comparison to the smoke group and is indicative of the restoration of NAD^+ levels. We also observed an increase in total PARP activity upon acute CS exposure which was reduced in the treatment groups of NR and/or PT (Figure 3.5B). Similarly, the gene expression of SIRT4 (Figure 3.5F) was upregulated in the smoke group and was reduced in all the treatment groups of NR and/or PT. Collectively these results demonstrate the hyperactivity of the NAD^+ consumer PARPs and gene expression of SIRT4 during acute CS exposure which may result in the depletion of NAD^+ levels. Administration of NR and/or PT reduced the overactivation of PARP and the gene expression of SIRT4, in parallel to a restoration of basal NAD^+ levels. Taken together, this data suggested that NR and/or PT regulated

NAD^+ levels by increasing NAD^+ synthesis as well as by reducing the overactivation of NAD^+ consumers which further led to a reduction in airway inflammation during acute CS exposure.

Our 8-week CS-induced COPD murine model was characterised by increased infiltration of leukocytes in the lung upon exposure to CS in comparison to the air exposure and was significantly reduced with the administration of NR and/or PT (Figure 3.6), suggesting that anti-inflammatory responses of NR and/or PT are beneficial in reducing the influx of inflammatory cells in the lung parenchyma in COPD. The gene expression of TNFα, CXCL1 and YM-1 was upregulated upon exposure to CS as a result of increased airway inflammation. The expression of TNFα was significantly lower in the treatment groups of NR and/or PT as compared to the smoke group (Figure 3.6E). The regulation of TNFα is majorly controlled by the intercellular NAD^+ levels (181). A high level of TNFα leads to inflammation in COPD and hence, controlled production of TNFα is important to maintain healthy conditions (239, 240). Chronic CS exposure leads to increased production of CXCL1 by resident macrophages and epithelial cells for the recruitment of neutrophils, which further leads to increased infiltrates in the airway. Reduced expression of CXCL1 in the treatment groups of smoke NR and/or PT further validated the anti-inflammatory benefits of these modulators in COPD (Figure 3.6F). YM-1 is a marker of M2-macrophage (325), which supports the high expression of YM-1 in all the experimental groups with prolonged exposure to smoke (Figure 3.6G).

Emphysema and chronic bronchitis are two important disease features in COPD driven by inflammation and tissue destruction and are instigated by chronic exposure to CS (278, 326). However, the exact mechanisms that drive these features remain unclear and have led to subsequent delays in the development of effective therapies (327, 328). In our study, we observed increased airway remodelling and emphysema in the smoke group

further validating the disease features. Interestingly, we observed a significant reduction in both these features in the treatment groups of smoke NR and/or PT (Figure 3.7), suggesting that NR and/or PT protected lung structure from the damage induced by chronic exposure to CS in COPD.

Furthermore, we validated impaired lung function in the smoke group exhibiting a reduction in IC (Figure 3.8A), area (Figure 3.8B), and TLC (Figure 3.8C) in comparison to the air group. All the parameters of IC, area and TLC were improved in the treatment groups of smoke NR and/or PT with respect to the smoke group. Additionally, an increase in lung compliance was observed in the smoke group representing the poor recoiling property of the lung due to chronic exposure to CS and was reduced with the treatment group of NRPT suggesting improved expandability of lungs with the treatment (Figure 3.8G). This is surprising given that until recently, the only known effective intervention to restore lung function was a cessation of smoke exposure (25, 316). The current study shows NRPT might potentially restore or delay the reduced lung function in COPD.

The constant cycle of damage and repair during inflammation in COPD requires an abundance of NAD^+, which is known to be in a constant state of synthesis (252), degradation (220), and recycling (318). Chronic exposure to CS resulted in NAD^+ depletion and a reduction in the NAD^+/NADH ratio. Administration of NR and/or PT improved total NAD^+ levels in our COPD study and showed an increase in the NAD^+/NADH ratio (Figure 3.9). We did not observe any differences in the gene expression of NAD^+ biosynthesis markers, however, the expression of PGC1α (Figure 3.9K) and NFκB (Figure 3.9L) was reduced in the smoke group and was increased in the treatment group of NRPT, suggesting that NRPT in combination can potentially increase mitochondrial biogenesis or improve mitochondrial function in COPD. Furthermore, we observed an increase in total PARP activity upon chronic exposure to CS which was

reduced with the treatment of NR and/or PT (Figure 3.10C), however, there were no differences observed in the gene expression of PARP1 (Figure 3.10A). In contrast, PARP1 protein levels were reduced upon smoke exposure and increased in all the treatment groups of smoke NR and/or PT (Figure 3.10B). Collectively, these results validated the previous findings of overactivation of PARPs in COPD (329), interestingly, a reduction of PARP activity was observed with NR and/or PT suggesting the protective features of NAD^+ modulators via restoration of NAD^+ levels in COPD. In contrast, we observed a reduction in CD38 protein levels in the smoke group which was further increased in the treatment groups of NR and/or PT (Figure 3.10D). However, the total protein levels of CD38 in our study were inconclusive and requires further assessment of CD38 activity to unveil its role in COPD.

Additional to PARPs and CD38, SIRTs are also one of the major NAD^+-dependent metabolic and epigenetic regulators (242, 251). Recent evidence suggests that the Sirtuin family (SIRT1-7) protect cellular homeostasis by sensing bioenergy needs and by making alterations in the cell nutrients (229, 330). SIRTs are known to play a critical role in restoring homeostasis during inflammation (251, 331). In our study, the gene and protein expression of SIRTs (1-7) reduced upon chronic exposure to smoke and were increased in the treatment groups of NR and/or PT (Figure 3.10E-R), suggesting that in correspondence to restoring NAD^+/NADH imbalance, SIRTs also exhibit anti-inflammatory properties in COPD. However, we did not see any changes in SIRT3 and SIRT 4 gene expression across all the experimental groups which is potentially due to the prophylactic administration of NR and/or PT along with exposure to CS. Taken together, our study demonstrated that the dietary modulators of NAD^+, NR and PT are capable of restoring or protecting NAD^+ levels by regulating NAD^+ consumers, PARPs and SIRTs which further attenuates airway inflammation in COPD.

Mitochondrial ultrastructural changes have revealed novel pathologies in different studies but there has been no evidence of mitochondrial structural changes in COPD lung morphology (332-334). Impaired mitochondrial structure largely contributes to the loss of mitochondrial function due to the placement of ETC complexes in the inner mitochondrial membrane and cristae. Our study showed an increase in the unhealthy mitochondrial population upon chronic exposure to CS which comprised of abnormal increase in mitochondrial density and area (mitochondrial swelling). Further, these abnormal mitochondrial populations were also characterised by reduced cristae density, cristae volume and cristae area which further validated abnormal mitochondria in COPD. These results suggest that an abnormal increase in the mitochondrial density is potentially due to the cellular defence mechanism against damage instigated by CS.

Comparatively, we observed a reduction in the mitochondrial population in the air and the treatment groups of smoke NR and/or PT. In contrast to the smoke group, the mitochondria in the air and the treatment groups displayed a well-defined structure of cristae and double membrane (Figures 3.11 and 3.12). We did not observe mitochondrial swelling in the air or any of the treatment groups in comparison to the smoke group suggesting that CS might potentially be inducing mitochondrial swelling and further investigation will be required to identify if this is due to mitochondrial fission.

Additionally, these mitochondrial populations possessed dense cristae structure and volume suggesting that NR and/or PT protected mitochondrial ultrastructure in COPD. This is surprising as currently there is no treatment available for COPD exhibiting the protection of the mitochondrial structure. However, one limitation of this analysis is that samples are processed and embedded in resin for ultrastructural sectioning and imaging and ultimately the orientation of tissue is unknown which might lead to crosssections with elongated mitochondria instead of a circular structure. To account for this limitation, the

samples from every experimental group were treated and analysed in the same way without allowing any variation.

Furthermore, recent evidence suggests that COPD patients have reduced mitochondrial function (335, 336). In our study, we observed a reduction in the respiratory chain complex activity for complex I (Figure 3.13A), II (Figure 3.13B), III (Figure 3.13C), IV (Figure 3.13D), I+III (Figure 3.13E), and II+III (Figure 3.13F) in the smoke group which supports the evidence of reduced mitochondrial function in COPD. Interestingly, we observed an increase in the activity levels of all the complexes in the treatment groups of smoke NR and/or PT. This was further reflected in the increased protein levels of oxphos in all the treatment groups of smoke NR and/or PT. Collectively these results demonstrated that NR and/or PT improved mitochondrial function by restoring NAD^+/NADH balance in COPD. Additionally, we also observed an increase in $\Delta\Psi m$ in the treatment groups of NR and/or PT (Figure 3.14) which was reduced in the smoke group further demonstrating that NR and/or PT protected from mitochondrial damage in COPD.

Damage in mitochondrial structure leads to impaired mitochondrial function resulting in oxidative stress in numerous chronic diseases and is one of the most common drivers of inflammation (337). COPD patients show increased oxidative stress in the lungs induced by airway inflammatory and structural cells (168, 313). These changes lead to a reduction in antioxidant defence with the inactivation of several transcription factors and antioxidant enzymes such as NF-κB and nuclear factor erythroid 2-related factor-2 (Nrf2) (313) leading to increased inflammation and subsequent damage in COPD. The current study showed increased levels of oxidative stress marker, 4-HNE in the smoke group in comparison to the air group. The treatments NR and/or PT showed a significant reduction in 4-HNE resulting in reduced oxidative stress in COPD. Moreover, increased expression

of NOX2 in the smoke group was observed which was reduced with the treatment groups of NR and/or PT (Figure 3.15). Collectively, these results suggested that the administration of NR and/or PT protected from oxidative stress in COPD.

In conclusion, this study has demonstrated that chronic exposure to CS leads to an imbalance in the NAD^+/NADH levels induced by hyperactivity of PARPs in COPD, which potentially drives inflammation causing an influx of inflammatory cells in the airways and leading to damage to lung structure and function. The therapeutic interventions NR and PT in the CS-induced COPD murine model reduced inflammatory cell infiltration in the lung, leading to improvements in lung structure and function. Critically, NR and PT also improved the ratio of NAD^+ and NADH levels, reducing the overactivation of PARP and leading to an increase in SIRTs. As a consequence, NR and PT further improved the structure and function of mitochondria and reduced oxidative stress in COPD. Additional studies will be required to decipher the therapeutic potential of NR and PT in reversing the damage in COPD.

Chapter 4. Investigating the role of NR and PT in reversing or delaying the progression of COPD

4.1 Introduction

COPD remains the 3rd leading cause of death globally according to WHO 2022 (338). Chronic exposure to CS is a well-recognised cause of COPD, inducing airway inflammation which leads to the disease progression (339). Henceforth, cessation of smoke and nicotine-replacement therapy is so far the only known therapeutic intervention to prevent the progression of COPD (340, 341). Besides, other available treatments for COPD are largely symptomatic and include the use of bronchodilators (342, 343), inhalation of anticholinergics, (344, 345) and corticosteroids (342, 346), which alleviates the symptoms but do not reduce the inflammatory responses or prevent the progression of the disease (338, 347, 348). In addition, long-term use of corticosteroids leads to the systemic side effects of COPD such as cachexia (349-351). Furthermore, long-term COPD patients suffer from severe hypoxia (352) and are required to undergo oxygen therapy or lung transplantations as treatments fail to improve due to the severity of the disease (353, 354).

On the other hand, pulmonary rehabilitation has been shown to reduce the symptoms of breathlessness and improves physical and psychological conditions which further enhances the quality of life in severe COPD patients (355-357). These treatment options (Figure 4.1) alleviate symptoms and exacerbations but currently, there is no cure for COPD, therefore, there is a need for new therapies that can prevent the induction or inhibit the progression of COPD (358).

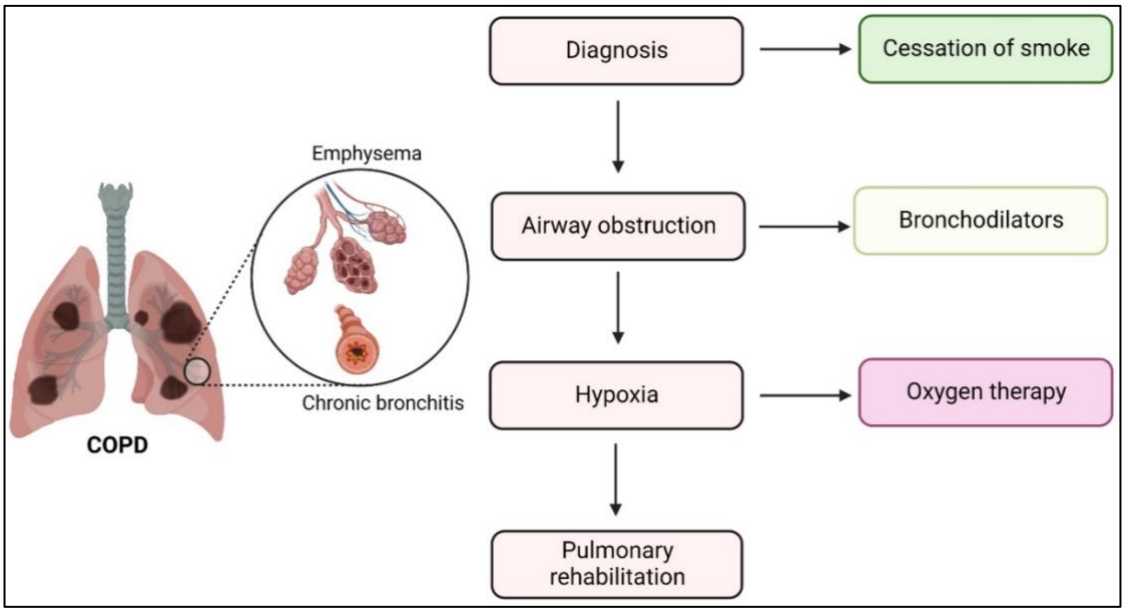

Figure 4.1: Progressive treatment approaches for COPD

In the previous chapter (Chapter 3), we demonstrated that chronic exposure to CS leads to an imbalance in the NAD^+/NADH levels induced by hyperactivity of PARPs in COPD, which potentially drives inflammation causing infiltration of inflammatory cells in the airways leading to damage to lung structure and function. The therapeutic interventions; NR and PT, significantly reduced inflammatory cell infiltration in the lung, leading to improvements in lung structure and function of our prophylactic COPD studies. Additionally, NR and PT also improved the ratio of NAD^+ and NADH levels, reducing PARP activity levels and leading to an increase in NAD^+ consumers such as SIRTs. However, additional investigation is required to elucidate if NR and PT can potentially halt the progression and reverse or restore the damage in COPD.

In the current study, utilising our clinically relevant COPD mouse model, we aimed to decipher the therapeutic potential of NR and PT in delaying the progression of the disease as well as reversing the damage in COPD.

4.2 Methodology

4.2.1 Experimental COPD model

Female BALB/c mice aged 6-8 weeks were obtained from the ARC and were maintained at 20 ± 2°C on a 12:12 hours day-night cycle and fed a standard sterile diet of mouse chow as previously described in chapter 2 under section 2.2.1.

4.2.2 Experimental procedure of smoking:

Mice were subjected to CS/Air exposure for up to 12 research-grade 3R4F cigarettes (University of Kentucky) twice a day, five days a week for up to 12 weeks using a custom-designed nose-only inhalation system as mentioned previously in chapter 2 under section 2.2.2. (146).

4.2.3 Experimental designs

This study involved two 12-week smoke models subjected to administration of 400 mg/kg of NR in drinking water and 80 mg/kg of PT in mushy chow provided *ad* libitum followed by smoke exposure as described in 4.2.2.

The different experimental groups for the 12-week smoke model-1 (Figure 4.2A & B) consisted of five experimental groups which include three control groups comprising of air and smoke and two treatment groups with NR and PT. The control groups include the air group, whereby mice were subjected to air exposure for 12 weeks, the smoke (12 weeks) group whereby mice were subjected to CS for 12 weeks, and the smoke (8wks) rest (4wks) group whereby mice were subjected to CS for 8 weeks followed by a rest period of 4 weeks. Additionally, the treatment groups comprised the smoke NRPT

(12wks) whereby mice were subjected to CS for 12 weeks and were administered with 400 mg/kg of NR in drinking water and 80 mg/kg of PT in mushy chow for 12 weeks, and finally, and smoke (8wks) NRPT (4wks) group whereby mice were subjected to CS for 8 weeks followed by a rest period and administration of 400 mg/kg of NR in drinking water and 80 mg/kg of PT in mushy chow as listed in below in table 4.1.

Table 4.1: Experimental groups in 12-week model-1

Experimental groups	Smoke exposure period	Rest period	Treatments
Air	-	-	-
Smoke (12wks)	12 cigarettes, 2x/day, 5x/week for up to 12 weeks	-	-
Smoke NRPT (12wks)	12 cigarettes, 2x/day, 5x/week for up to 12 weeks	-	400 mg/kg of NR in drinking water and 80 mg/kg of PT in mushy chow for 12 weeks
Smoke (8wks) Rest (4wks)	12 cigarettes, 2x/day, 5x/week for up to 12 weeks	4 weeks	-
Smoke (8wks) NRPT (4wks)	12 cigarettes, 2x/day, 5x/week for up to 12 weeks	4 weeks	400 mg/kg of NR in drinking water and 80 mg/kg of PT in mushy chow for 4 weeks

Further, the 12-week smoke model-2 (Figure 4.2C) consisted of three experimental groups, including the air group, whereby mice were subjected to air exposure for 12 weeks, the smoke (12wks) group whereby mice were subjected to CS for 12 weeks and the smoke NRPT (4wks) group whereby mice were subjected to CS for 12 weeks and were administered with 400 mg/kg of NR in drinking water and 80 mg/kg of PT in mushy chow for the last 4 weeks of the study as listed in below in table 4.2.

Table 4.2: Experimental groups in 12-week model-2

Experimental groups	Smoke exposure period	Treatments
Air	-	-
Smoke (12wks)	12 cigarettes, 2x/day, 5x/week for up to 12 weeks	-
Smoke NRPT (4wks)	12 cigarettes, 2x/day, 5x/week for up to 12 weeks	400 mg/kg of NR in drinking water and 80 mg/kg of PT in mushy chow for 4 weeks

All mice were weighed daily before exposure to smoke, five days a week for 12 weeks and were closely monitored during and after smoke exposure. Any mice losing up to 15% of their body weight were subjected to smoke cessation for 24 hours with intensive monitoring.

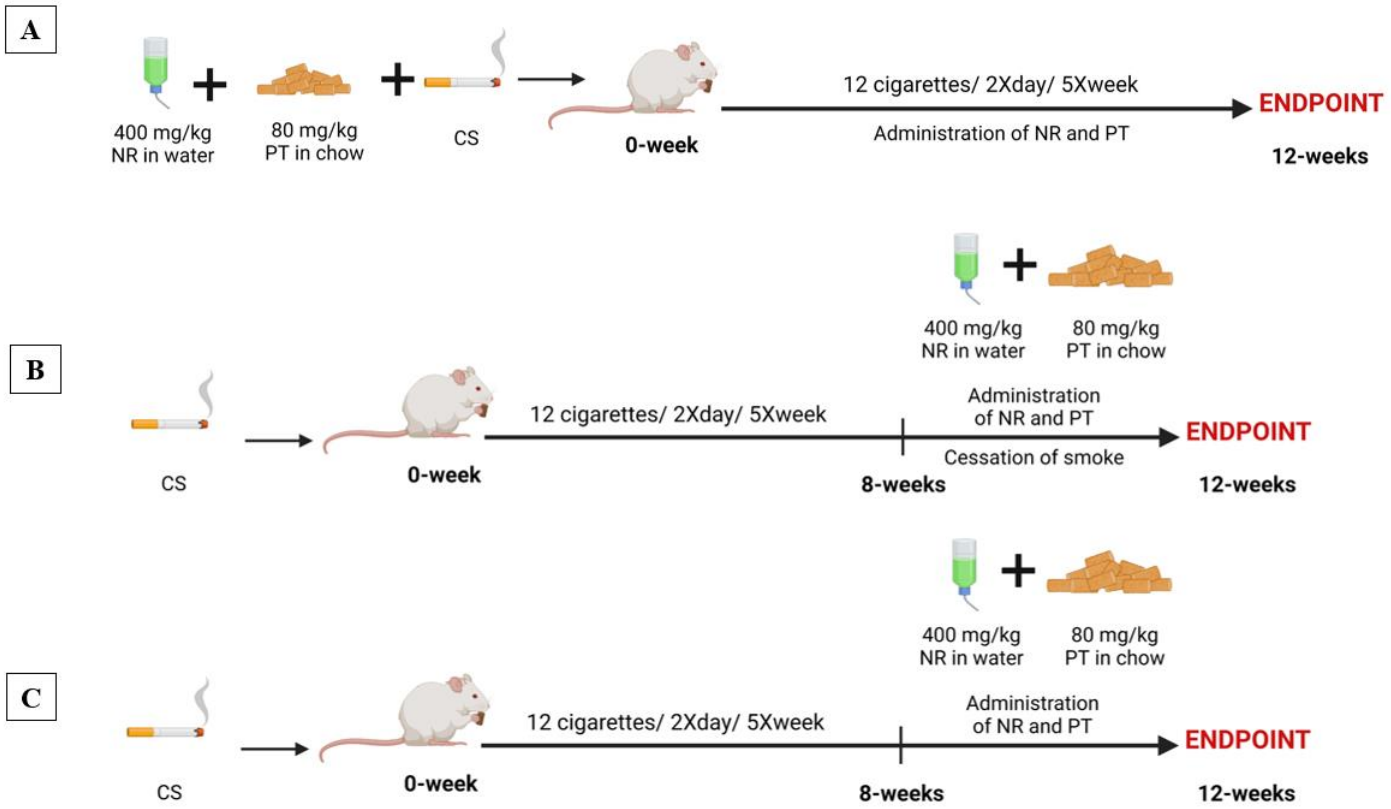

Figure 4.2: Experimental design for 12-week advanced COPD study:

(A) Mice exposed to CS and administered with NR and PT for 12 weeks; (B) Mice exposed to CS for 8 weeks and subjected to rest/administered with NR and PT for 4 weeks; (C) Mice were exposed to CS for 12 weeks and administered with NR and PT for the last 4 weeks of the study.

4.3 Results

4.3.1 Administration of NR and PT reduced inflammation in advanced COPD

Mice exposed to CS for 12 weeks in the smoke (12wks) group exhibited an increase in immune cell infiltration (Figure 4.3A) and comprised of macrophages (Figure 4.3B) and neutrophils (Figure 4.3C) in the BALF in comparison to the air group ($P<0.0001$). Administration of NR and PT in the smoke NRPT (12wks) group resulted in a significant decrease in the total leukocytes, as well as macrophages and neutrophils as compared to the smoke (12wks) group ($P<0.0001$). Further, a decrease in total leukocytes, as well as macrophages and neutrophils was observed both in the smoke (8wks) rest (4wks) as well as smoke (8wks) NRPT (4wks) with respect to the smoke (12wks) group ($P<0.0001$). Additionally, the gene expression of TNFα (Figure 4.3D) and CXCL1 (Figure 4.3E) was measured in the lungs, and observed to be significantly increased in the smoke (12wks) group in comparison to the air group ($P<0.0001$). Besides, we also observed an increase in both these gene expressions in the smoke (8wks) rest (4wks) groups in comparison to the air group ($P<0.05$). However, a reduction in the expression of both TNFα and CXCL1 was observed in smoke NRPT (12wks) ($P<0.0001$), smoke (8wks) rest (4wks) ($P<0.05$) and smoke (8wks) NRPT (4wks) ($P<0.01$) in comparison to the smoke (12wks) group. Furthermore, the body weight of all the experimental groups was measured daily as mentioned previously in 4.3.3. We observed a significant increase in the weight of the mice in the air group in comparison to mice in all the smoke groups ($P<0.0001$) across all weeks following smoke exposure commencement (Figure 4.3F). Further, we also observed an increase in the weight of the mice in the smoke (8wks) rest (4wks) group in comparison to the smoke (12wks) group ($P<0.001$). We also observed an increase in the

body weight of mice in the smoke (8wks) NRPT (4wks) group at 10 weeks post-smoking in comparison to smoke (8wks) rest (4wks) ($P<0.01$) (Figure 4.3E).

.

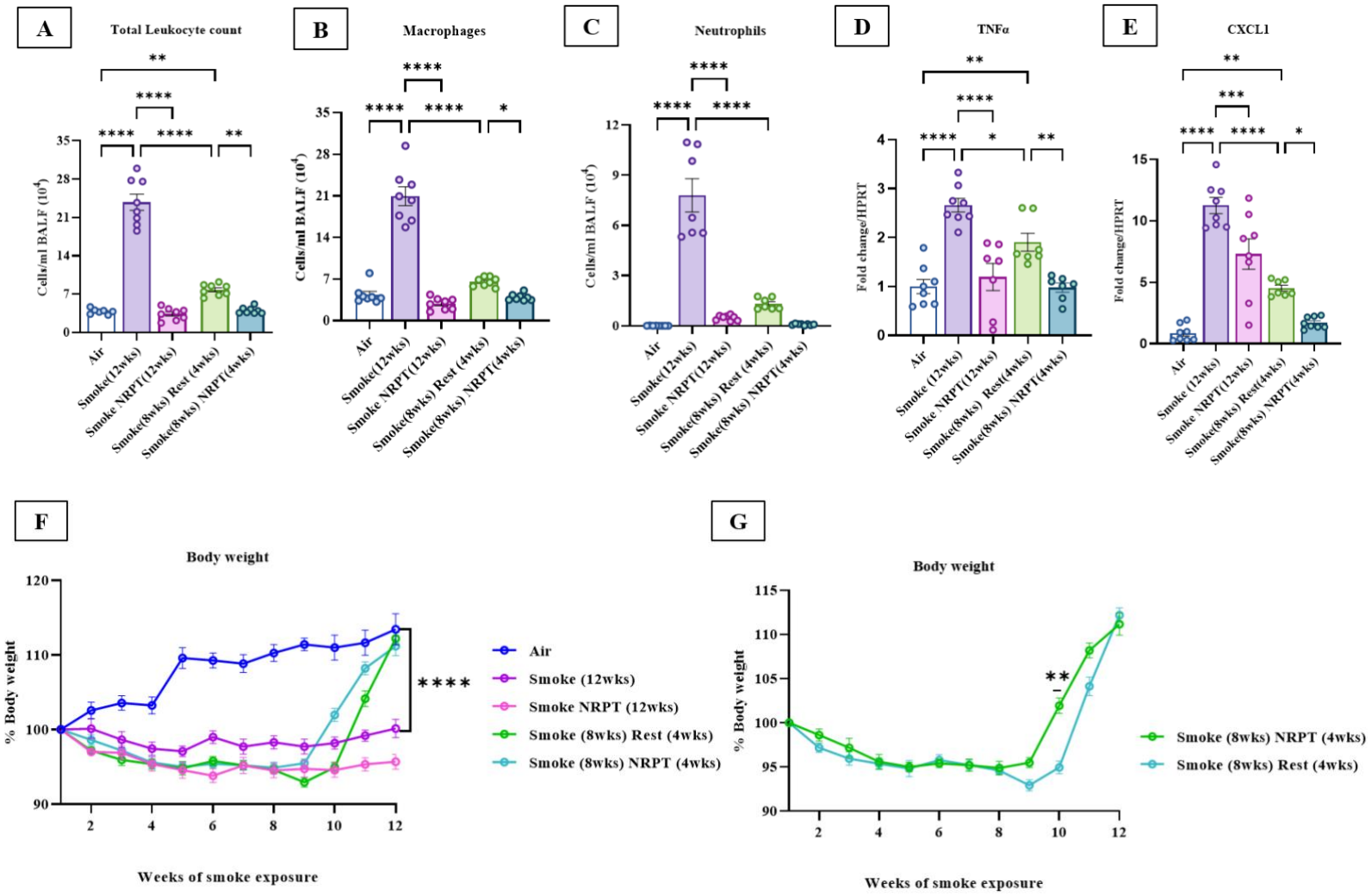

Figure 4.3: Administration of NR and PT restored inflammation in advanced COPD:

*(A) Cellular infiltrates in the BALF, (B) Macrophages, and (C) Neutrophils obtained from BALF; Gene expression for (E) TNFα and (F) CXCL1 in the lung. Changes in body weight: (D) All experimental groups (E) Smoke (8wks) rest (4wks) vs Smoke (8wks) NRPT (4wks); Data represented are means ± SEM of 8 mice/group, * P<0.05, ** P<0.01, *** P<0.001, **** P<0.0001.*

4.3.2 Administration of NR and PT attenuated COPD features in advanced diseases stages

Chronic exposure to CS resulted in collagen deposition around the basement membrane of small airways in the smoke (12wks) group as well as in the smoke (8wks) rest (4wks) group in comparison to the air group (P<0.01). There was a significant reduction observed in the collagen deposition for both the smoke NRPT (12wks) and smoke (8wks) NRPT (4wks) in comparison to the smoke (12wks) group (P<0.0001) (Figure 4.4A)4

In addition, an increase in the MLI counts was observed in the smoke (12wks) group as well as in the smoke (8wks) rest (4wks) group in comparison to the air group (P<0.01). moreover, we observed a significant reduction in both the treatment groups of smoke NRPT (12wks) and smoke (8wks) NRPT (4wks) in comparison to the smoke (12wks) group (P<0.0001) as well as smoke (8wks) rest (4wks) (Figure 4.4B).

Lung function changes were measured using FlexiVent as mentioned previously in chapter 2 under section 2.9. An increase in IC was observed in the smoke (12wks) group (P<0.0001), smoke NRPT (12wks) (P<0.01), and smoke (8wks) rest (4wks) (P<0.0001) in comparison to the air group (Figure 4.4C). We observed reduced IC in the treatment group of smoke (8wks) NRPT (4wks) in comparison to the smoke (8wks) rest (4wks) group (P<0.01). We also observed an increase in Area in both the smoke (12wks) group (P<0.01) and the smoke (8wks) rest (4wks) group (P<0.001) in comparison to the air

group (Figure 4.4D). A reduction in the area was observed in the smoke (8wks) NRPT (4wks) with respect to the smoke (8wks) rest (4wks) group ($P<0.05$). Further, an increase in TLC (Figure 4.4E) was observed in the groups of the smoke (12wks), smoke NRPT (12wks) and smoke (8wks) rest (4wks). Additionally, lung compliance curves shown in figures 4.4F-H were analysed to measure alveolar damage and were observed to have an increased AUC in the smoke (12wks) group, and smoke NRPT (12wks) in comparison to the air group (Figure 4.4F). We also observed an increase in the AUC of the smoke (12wks) group in comparison to the smoke (8wks) rest (4wks) group and the air group (Figure 4.4G). Further, smoke (8wks) NRPT (4wks) did not show any changes in the AUC with respect to the smoke (8wks) rest (4wks) group and the air group (Figure 4.4H).

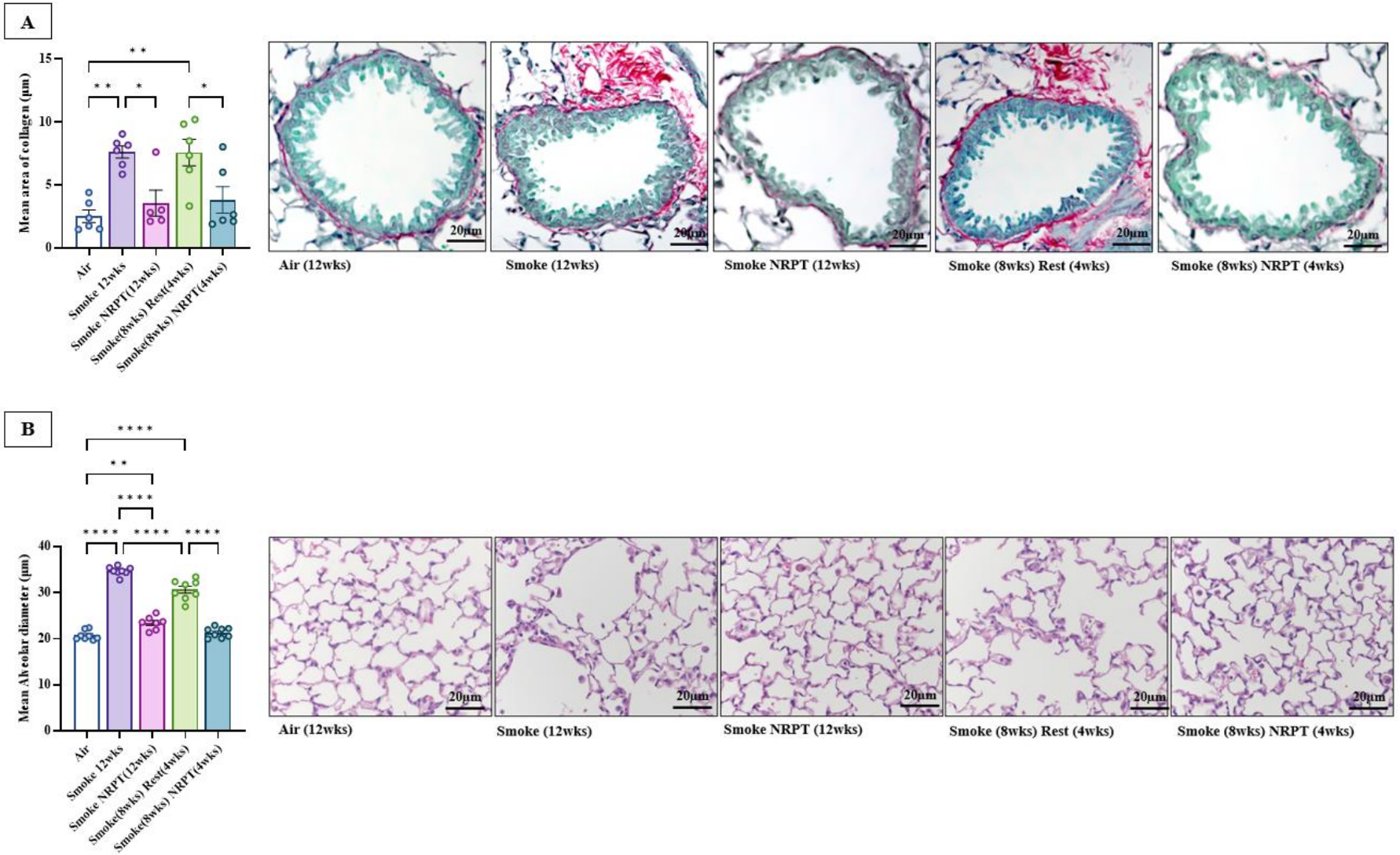
A
Mean area of collagen (µm)
15
10
5
0
**
**
*
*
Air
Smoke 12wks
Smoke NRPT(12wks)
Smoke(8wks) Rest(4wks)
Smoke(8wks) NRPT(4wks)
20µm
Air (12wks)
Smoke (12wks)
Smoke NRPT (12wks)
Smoke (8wks) Rest (4wks)
Smoke (8wks) NRPT (4wks)
B
Mean Alveolar diameter (µm)
40
30
20
10
0
****
**
****
****
****
****
Air
Smoke 12wks
Smoke NRPT(12wks)
Smoke(8wks) Rest(4wks)
Smoke(8wks) NRPT(4wks)
20µm
Air (12wks)
Smoke (12wks)
Smoke NRPT (12wks)
Smoke (8wks) Rest (4wks)
Smoke (8wks) NRPT (4wks)

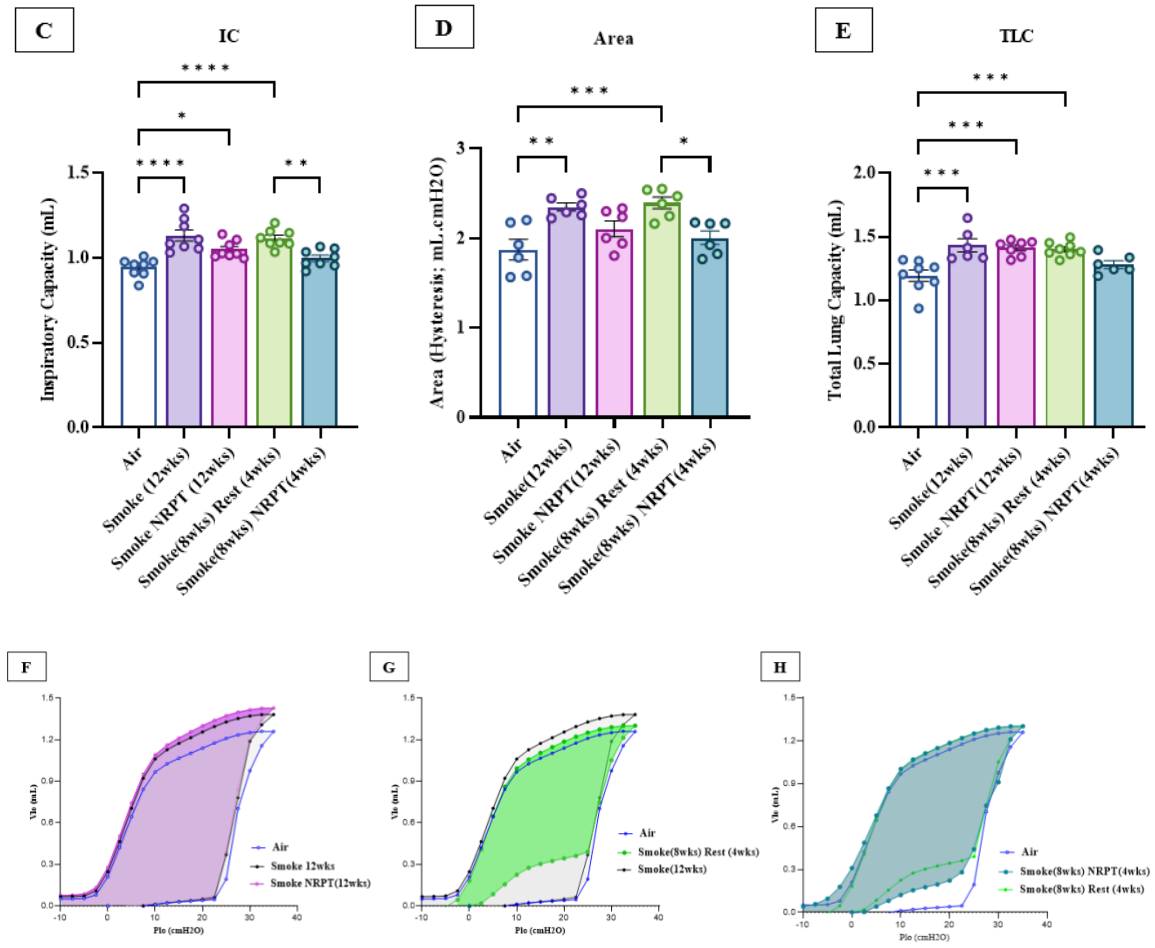

Figure 4.4: Administration of NR and PT attenuated COPD features:

*(A) Collagen deposition, (B) Emphysema, Lung function parameters (C) IC, (D) Area, (E) TLC, (F) lung compliance curves for the air, smoke (12wks) and smoke (8wks) rest (4wks) groups, (G) lung compliance curves for the air, smoke (12wks) and smoke NRPT (12wks) groups, and (H) lung compliance curves for the air, smoke (12wks) and smoke NRPT (12wks) groups. Data represented are means ± SEM of 5-6 mice/group, * P<0.05, ** P<0.01, *** P<0.001, **** P<0.0001.*

4.3.3 Administration of NR and PT increased NAD^+ levels in advanced COPD

Lung homogenates from the 12 weeks advanced COPD study were used for the measurement of total NAD^+ and NADH levels. We observed a significant reduction in

the total NAD^+ levels of the smoke (12wks) group ($P<0.0001$), smoke NRPT (12wks) ($P<0.0001$), and smoke (8wks) rest (4wks) ($P<0.01$) in comparison to the air group (Figure 4.5A). Additionally, there was a significant increase in the total NAD^+ levels of the smoke (8wks) NRPT (4wks) group with respect to the smoke (8wks) rest (4wks) ($P<0.001$) as well as in the smoke (8wks) rest (4wks) in comparison to the smoke (12wks) group ($P<0.01$).

The NADH levels were significantly higher in the smoke (12wks) ($P<0.0001$), smoke NRPT (12wks) ($P<0.0001$), smoke (8wks) rest (4wks) ($P<0.05$) and the smoke (8wks) NRPT (4wks) ($P<0.05$) groups in comparison to the air group. Further, we observed a significant reduction in the NADH levels in the treatment group of smoke NRPT (12wks) ($P<0.01$) in comparison to the smoke (12wks) group, this was also reflected in the smoke (8wks) rest (4wks) group ($P<0.0001$). However, we did not see a difference in the NADH levels in the smoke (8wks) NRPT (4wks) in comparison to the smoke (8wks) rest (4wks) (Figure 4.5B).

The ratio of total NAD^+ and NADH was observed to be significantly reduced in the smoke (12wks) group ($P<0.0001$), smoke NRPT (12wks) ($P<0.0001$), and the smoke (8wks) rest (4wks) group ($P<0.001$) in comparison with the air group. However, there was an increase in the ratio in the smoke (8wks) NRPT (4wks) in comparison to the smoke (8wks) rest (4wks) group which was not significant and showed a non-significant change from the air group (Figure 4.5C).

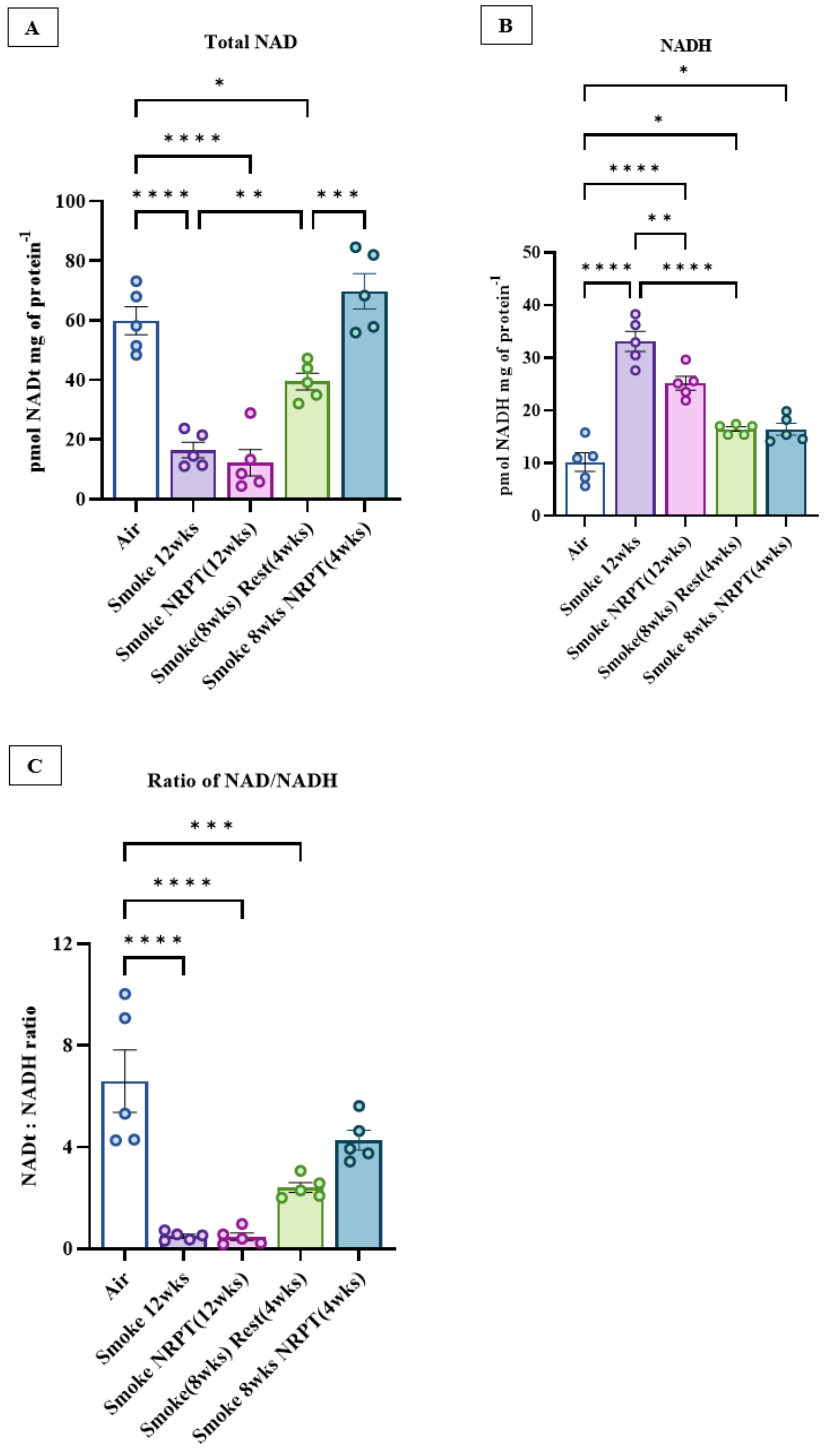

Figure 4.5: Administration of NR and PT increased NAD^+ levels in advanced COPD:

*(A) total NAD^+ level in mouse lung homogenates, (B) NADH level in mouse lung homogenates, (C) ratio of NAD^+/NADH. Data represented are means ± SEM of 5 mice/group, * P<0.05, ** P<0.01, *** P<0.001, **** P<0.0001.*

4.3.4 Administration of NR and PT regulated PARPs and CD38 in COPD

Lung RNA and protein from the 12-week advanced COPD model were used to determine the PARP1 gene (Figure 4.6A) and protein expression (Figure 4.6B). We did not observe any change in the gene expression of PARP1 across all the experimental groups however, we observed a significant increase in PARP1 protein expression in the smoke (8wks) NRPT (4wks) in comparison to both the air group ($P<0.0001$) and the smoke (12wks) group ($P<0.001$). Interestingly, we observed a reduction in the PARP1 protein level in the smoke (8wks) NRPT (4wks) as compared to the smoke (8wks) rest (4wks) ($P<0.0001$). Further, the PARP activity levels were measured in lung homogenates where an increase in the activity level was observed in the smoke (12wks) group with respect to the air group ($P<0.01$). Reduced activity of PARP was observed in the smoke (8wks) rest (4wks) in comparison to the smoke (12wks) group ($P<0.05$) which was further reduced in the smoke (8wks) NRPT (4wks) with respect to the smoke (8wks) rest (4wks) ($P<0.05$) (Figure 4.6C).

Additionally, CD38 protein levels were measured where we observed a significant increase in the CD38 protein expression in the smoke (8wks) rest (4wks) group in comparison to the air group ($P<0.0001$) as well as the smoke (12wks) group ($P<0.0001$). Furthermore, the protein expression of CD38 was reduced in the smoke (8wks) NRPT (4wks) group as compared to the smoke (8wks) rest (4wks) ($P<0.0001$) (Figure 4.6D).

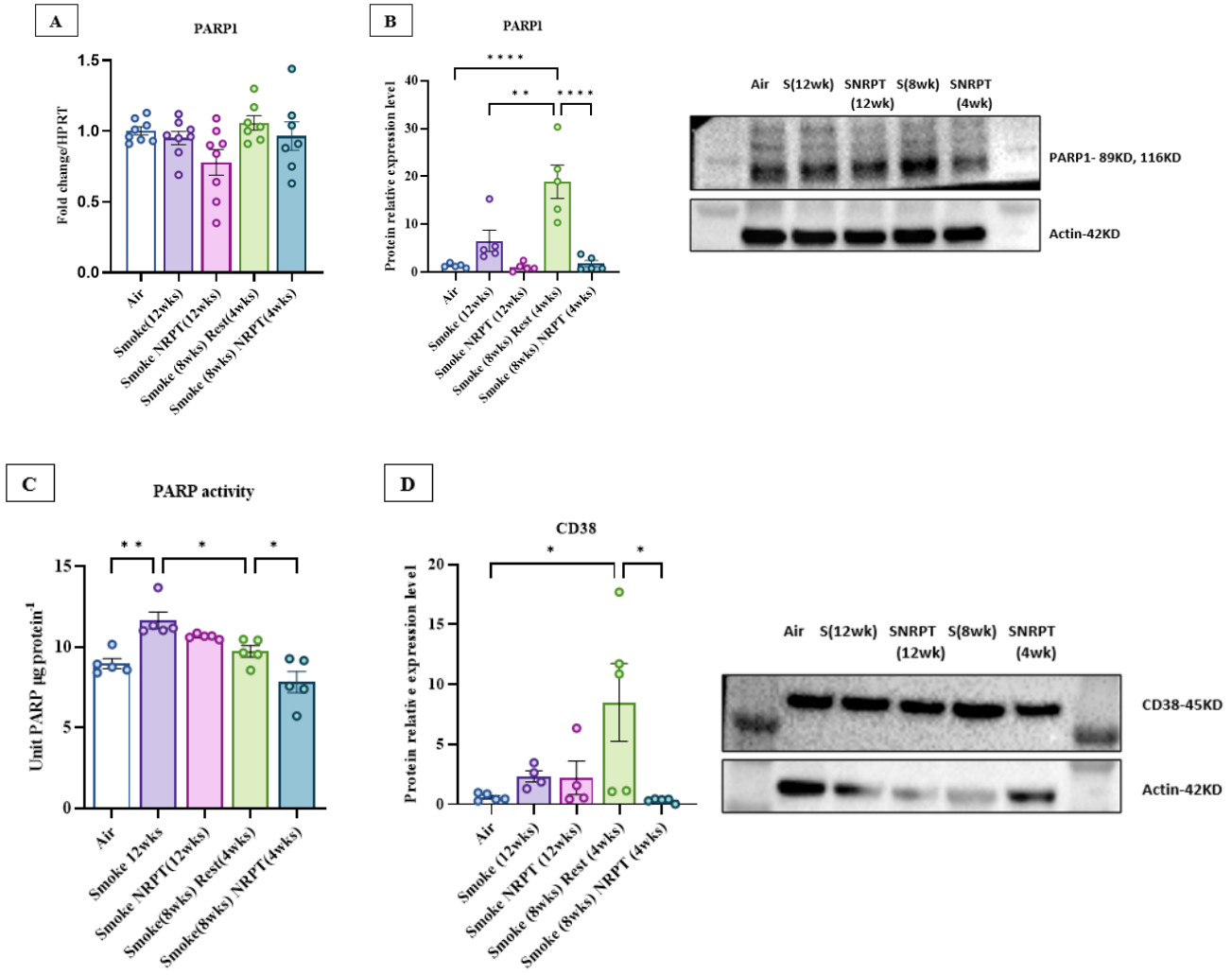

Figure 4.6: Administration of NR and PT restored PARP and CD38 levels in COPD:

*(A) Gene expression of PARP1, (B) Protein expression level of PARP1, (C) PARP activity levels in lung homogenates, (D) Protein expression level of CD38. Data represented are means ± SEM of 5-8 mice/group, * P<0.05, ** P<0.01, *** P<0.001, **** P<0.0001.*

4.3.5 Administration of NR and PT regulated SIRTs in advanced COPD

The expression of SIRTs was measured using both RNA and protein from the lung. Gene expression of SIRT1 showed a reduction in the smoke NRPT (12wks) group in comparison to the air group (P<0.05) as well as the smoke (12wks) group (P<0.01) with no other changes observed in the other experimental groups (Figure 4.7A). The gene expression of SIRT2 was reduced in the smoke (8wks) rest (4wks) group with respect to the smoke (12wks) groups (P<0.01), and in the smoke (8wks) NRPT (4wks) group with respect to the air group (P<0.05) (Figure 4.7B). Further, we did not see any change in the expression of SIRT3 (Figure 4.7C) and SIRT4 (Figure 4.7D) across all the experimental groups. However, the gene expression of SIRT5 was reduced in the smoke (12wks) group with respect to air (P<0.01). We further observed a reduction in the expression of SIRT5 in the smoke NRPT (12wks) group in comparison to the air group (P<0.01), which was increased in the smoke (8wks) rest (4wks) group as compared to the smoke (12wks) group (Figure 4.7E). A reduced gene expression of SIRT6 was observed in the smoke (12wks) group as compared to the air group (P<0.05) (Figure 4.7F). Moreover, the gene expression of SIRT7 was reduced in the smoke (12wks) group (P<0.05) as well as the smoke NRPT (12wks) group (P<0.001) in comparison to the air group and was increased in the smoke (8wks) rest (4wks) group as compared to the smoke (12wks) (P<0.01) (Figure 4.7G).

In contrast, the protein expression of SIRT1 was upregulated in the smoke NRPT (12wks) group in comparison to the smoke (12wks) group (P<0.01). A reduction in the protein expression of SIRT1 in the smoke (8wks) rest (4wks) group was observed in comparison

to the air group ($P<0.05$) which was increased in the smoke (8wks) NRPT (4wks) group with respect to the air group ($P<0.001$) as well as the smoke (8wks) rest (4wks) group ($P<0.0001$) (Figure 4.7H). Additionally, the protein expression for pSIRT1 was reduced in the smoke (8wks) rest (4wks) group in comparison to the air group ($P<0.05$). An increase in the protein expression of pSIRT1 was observed in the treatment group of smoke (8wks) NRPT (4wks) as compared to the smoke (8wks) rest (4wks) (Figure 4.7I). In contrast to the gene expression of SIRT2 the protein expression was upregulated in the smoke (8wks) rest (4wks) in comparison to both the air group ($P<0.01$) as well as the smoke (12wks) group ($P<0.05$) (Figure 4.7J). We observed no change in the protein expression of SIRT3 (Figure 4.7K) across all the experiment groups in this study. Further, the protein expression of SIRT5 was downregulated in the smoke (12wks), smoke NRPT (12wks) and smoke (8wks) rest (4wks) groups with respect to the air group ($P<0.01$) (Figure 4.7L). The protein expression of SIRT6 was reduced in the smoke (12wks) group with respect to the air group ($P<0.01$). Followed by, a reduction of SIRT6 protein was observed in the smoke (8wks) rest (4wks) in comparison to the air group ($P<0.05$) which was increased in the smoke (8wks) NRPT (4wks) as compared to the smoke (8wks) rest (4wks) ($P<0.05$) (Figure 4.7M). Moreover, the protein expression of SIRT7 in the smoke (12wks) group reduced with respect to the air group ($P<0.001$) and increased in the smoke NRPT (12wks) group in comparison to the smoke (12wks) group ($P<0.001$). Followed by upregulation of SIRT7 protein was observed in the smoke (8wks) rest (4wks) group as compared to the smoke (12wks) group ($P<0.0001$) and reduced in the smoke (8wks) NRPT (4wks) in comparison to the smoke (8wks) rest (4wks) ($P<0.05$) (Figure 4.7N).

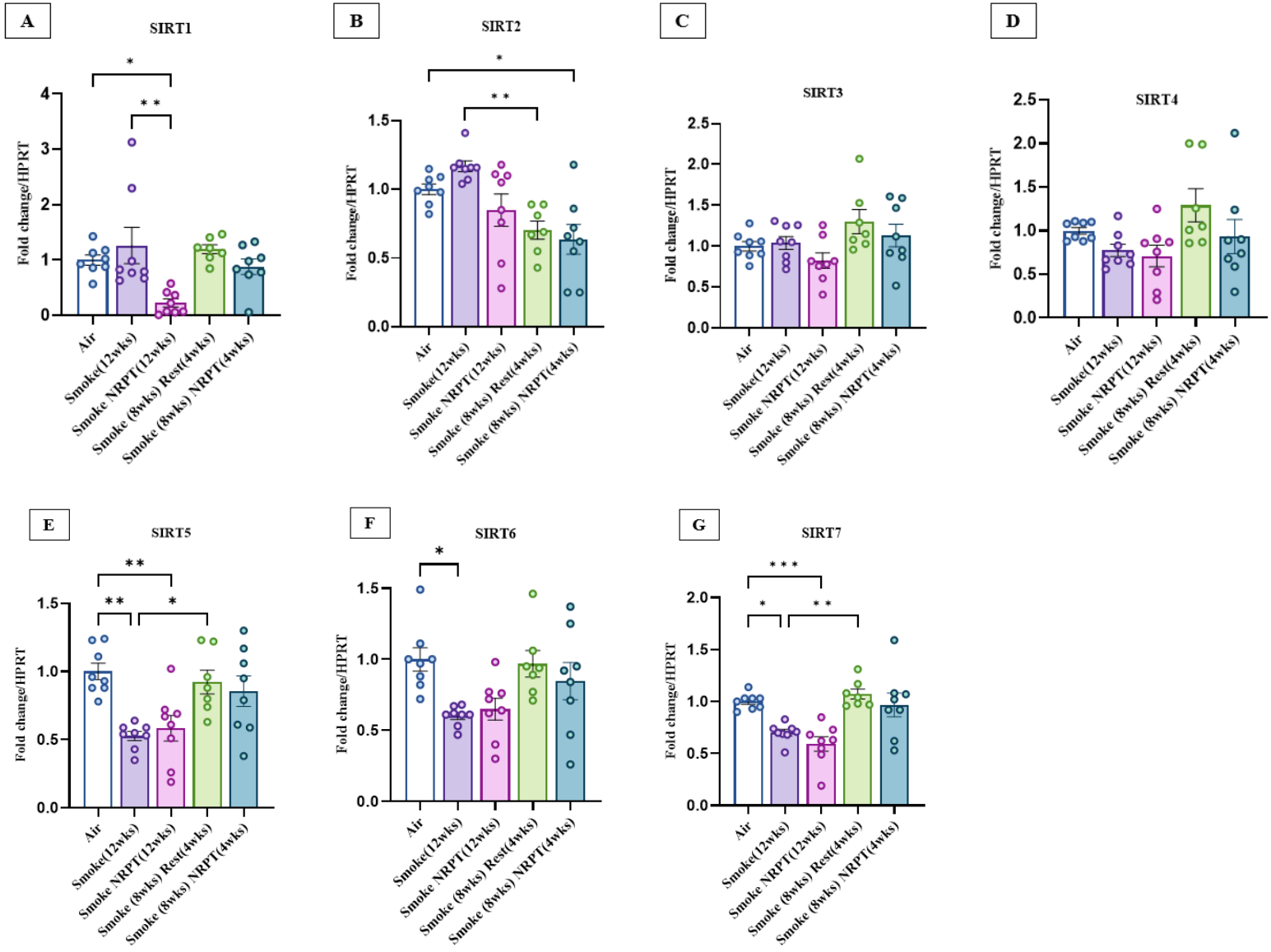
A
SIRT1
Fold change/HPRT
B
SIRT2
Fold change/HPRT
C
SIRT3
Fold change/HPRT
D
SIRT4
Fold change/HPRT
E
SIRT5
Fold change/HPRT
F
SIRT6
Fold change/HPRT
G
SIRT7
Fold change/HPRT
Air
Smoke(12wks)
Smoke NRPT(12wks)
Smoke (8wks) Rest(4wks)
Smoke (8wks) NRPT(4wks)

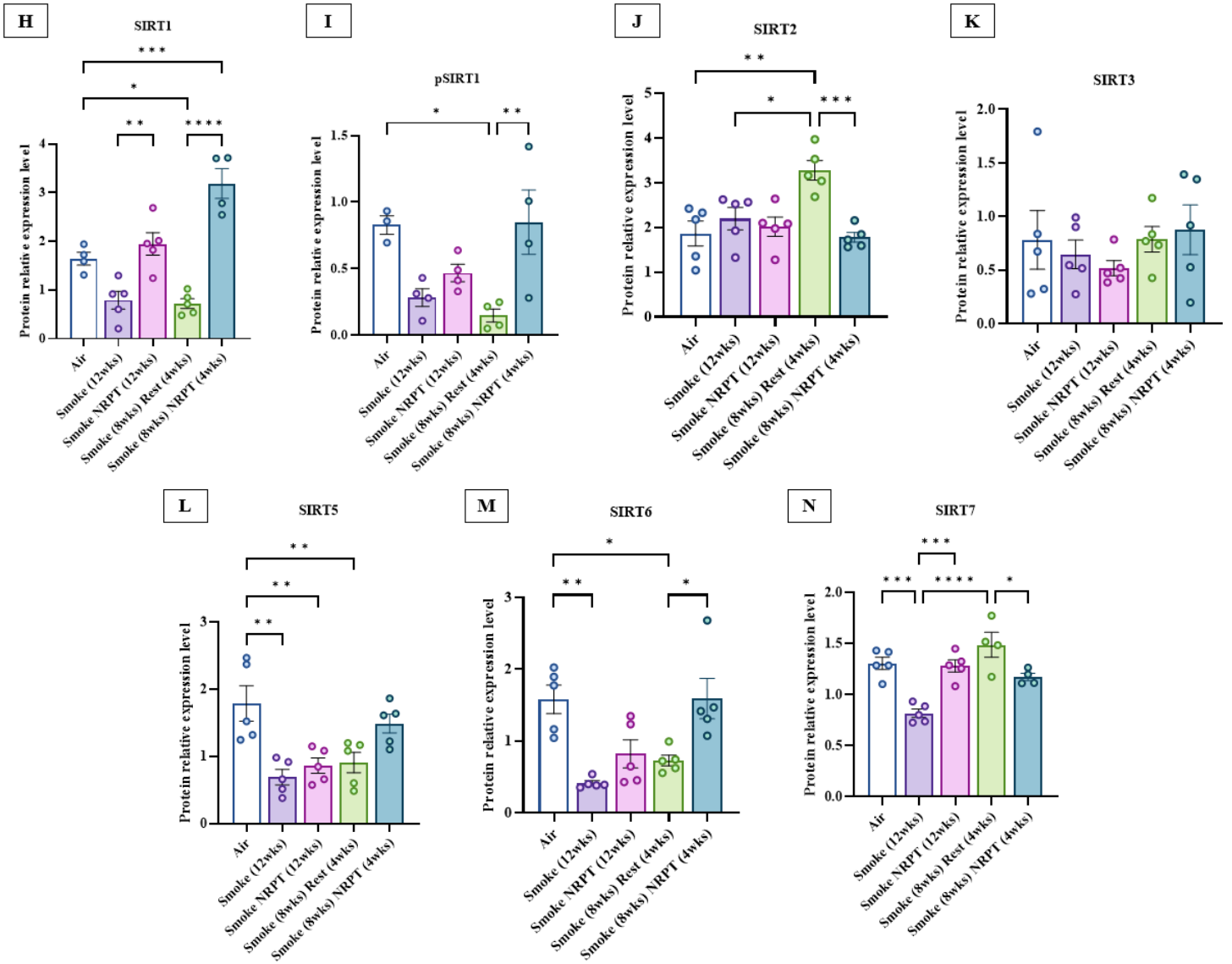
H
SIRT1
Protein relative expression level
I
pSIRT1
Protein relative expression level
J
SIRT2
Protein relative expression level
K
SIRT3
Protein relative expression level
L
SIRT5
Protein relative expression level
M
SIRT6
Protein relative expression level
N
SIRT7
Protein relative expression level
Air
Smoke (12wks)
Smoke NRPT (12wks)
Smoke (8wks) Rest (4wks)
Smoke (8wks) NRPT (4wks)

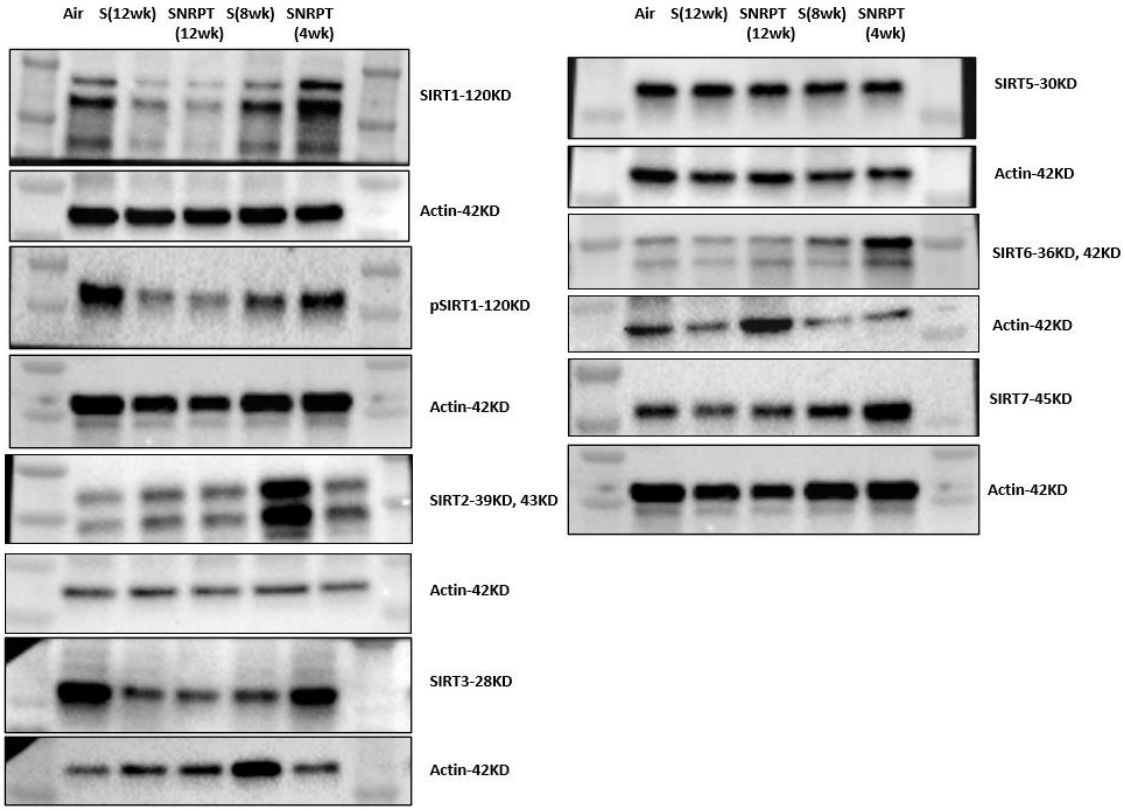

Figure 4.7: Administration of NR and PT regulated SIRTs in advanced COPD:

*(A) gene expression of SIRT1, (B) protein levels SIRT1, (C) protein levels pSIRT1, (D) gene expression of SIRT2, (E) protein levels SIRT2, (F) gene expression of SIRT3, (G) protein levels SIRT3, (H) gene expression of SIRT4, (I) gene expression of SIRT5, (J) protein levels SIRT5, (K) gene expression of SIRT6, (L) protein levels SIRT6, (M) Gene expression of SIRT7, (N) protein levels SIRT7. Data represented are means ± SEM of 5 mice/group, * P<0.05, ** P<0.01, *** P<0.001, **** P<0.0001.*

4.3.6 Administration of NR and PT protected mitochondrial structure in advanced COPD

Lung samples from the 12-week advanced COPD study were processed to assess mitochondrial morphology with TEM as mentioned previously. We observed an increase in mitochondrial density or number in the smoke group (Figure 4.8B) as compared to the

air group ($P<0.0001$) (Figure 4.8A). However, there was a reduction in mitochondrial density in the smoke (12wks) NRPT (4wks) group (Figure 4.8C) as well as smoke (8wks) rest (4wks) (Figure 4.8D) in comparison to the smoke (12wks) group ($P<0.0001$). In contrast, an increase in mitochondrial density was also observed in the smoke (8wks) NRPT (4wks) (Figure 4.8E) with respect to the smoke (8wks) rest (4wks) ($P<0.05$).

Further, the mitochondrial area or swelling was measured for all the experimental groups. A significant increase in the mitochondrial area was observed in the smoke group (Figure 4.8G) in comparison to the air group ($P<0.01$) (Figure 4.8F). We also observed a reduction in mitochondrial area in the treatment group of smoke NRPT (12wks) (Figure 4.8H) in comparison to the smoke (12wks) group ($P<0.01$). We also observed an increase in the mitochondrial area in the smoke (8wks) rest (4wks) which was reduced in the treatment group of smoke (8wks) NRPT (4wks) but was not statistically significant.

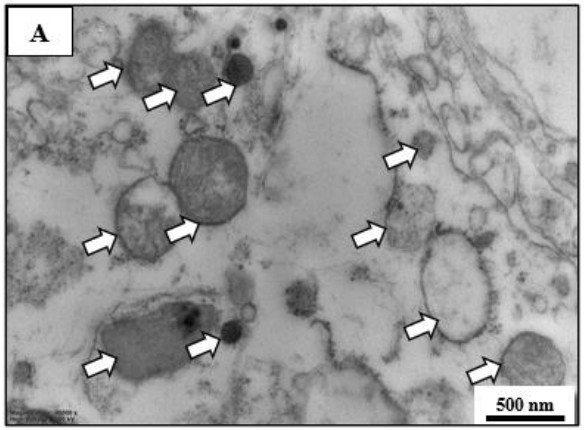

Air

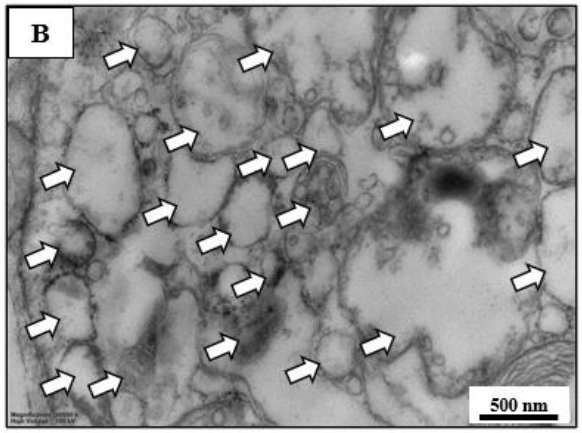

Smoke (12wks)

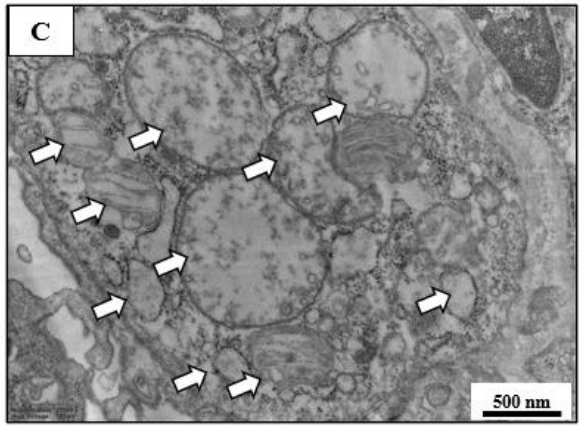

Smoke NRPT (12wks)

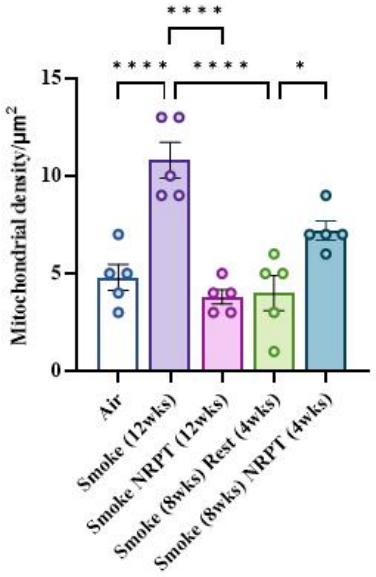

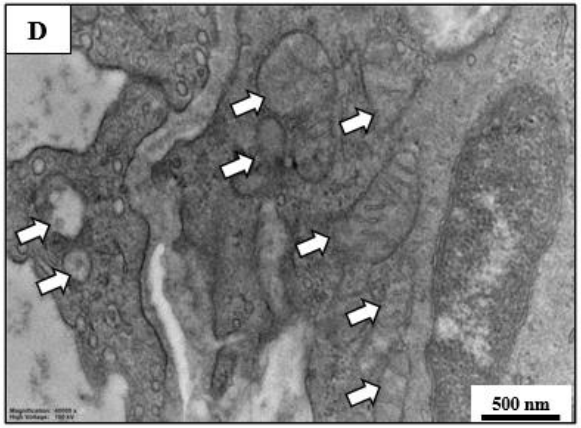

Smoke (8wks) Rest (4wks)

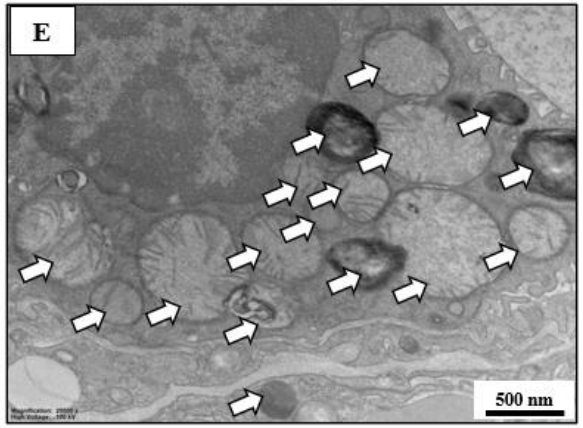

Smoke (8wks) NRPT (4wks)

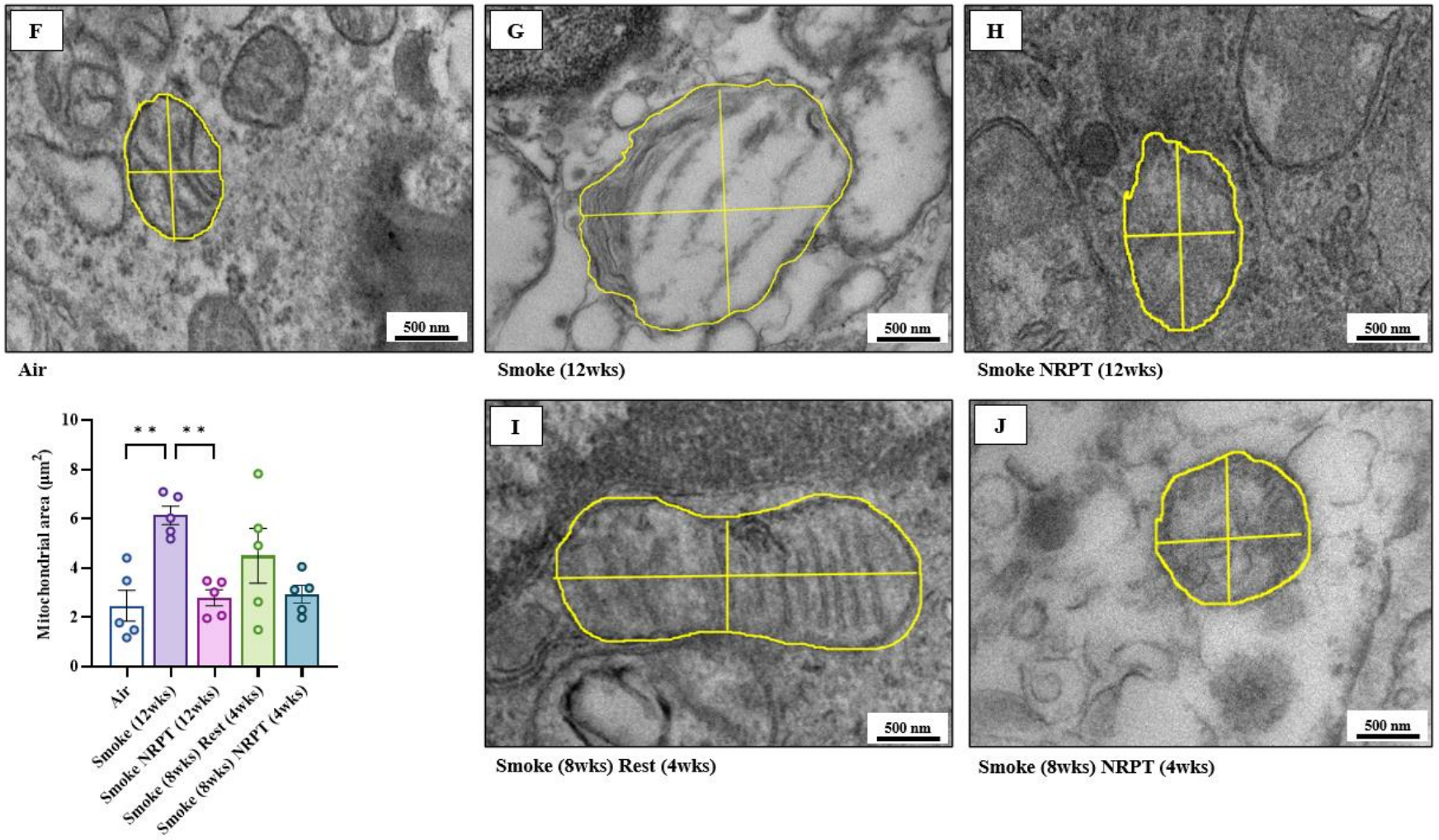

Figure 4.8: Administration of NR and PT protected mitochondrial structure in advanced COPD:

*Mitochondrial density (A) Air (B) Smoke (12wks), (C) Smoke NRPT (12wks), (D) Smoke (8wks) rest (4wks), (E) Smoke (8wks) NRPT (4wks); Mitochondrial area (F) Air (G) Smoke (12wks), (H) Smoke NRPT (12wks), (I) Smoke (8wks) rest (4wks), (J) Smoke (8wks) NRPT (4wks). Data represented are means ± SEM of 5 mice/group, * P<0.05, ** P<0.01, *** P<0.001, **** P<0.0001.*

4.3.7 Administration of NR and PT preserved mitochondrial cristae structure in COPD

We measured cristae density (Figure 4.9F), cristae volume (Figure 4.9G) and cristae area (Figure 4.9H) in all the experimental groups. We observed an increase in cristae density in the smoke NRPT (12wks) (Figure 4.9C) in comparison to the smoke (12wks) group (Figure 4.9B) ($P<0.001$) as well as an increase in the smoke (8wks) NRPT (4wks) (Figure 4.9E) compared to the smoke (8wks) rest (4wks) (Figure 4.9D) ($P<0.05$). Further, we observed an increase in the cristae volume of smoke NRPT (12wks) in comparison to the smoke (12wks) group ($P<0.05$). In contrast, we did not observe any significant changes in the cristae area across all the different experimental groups.

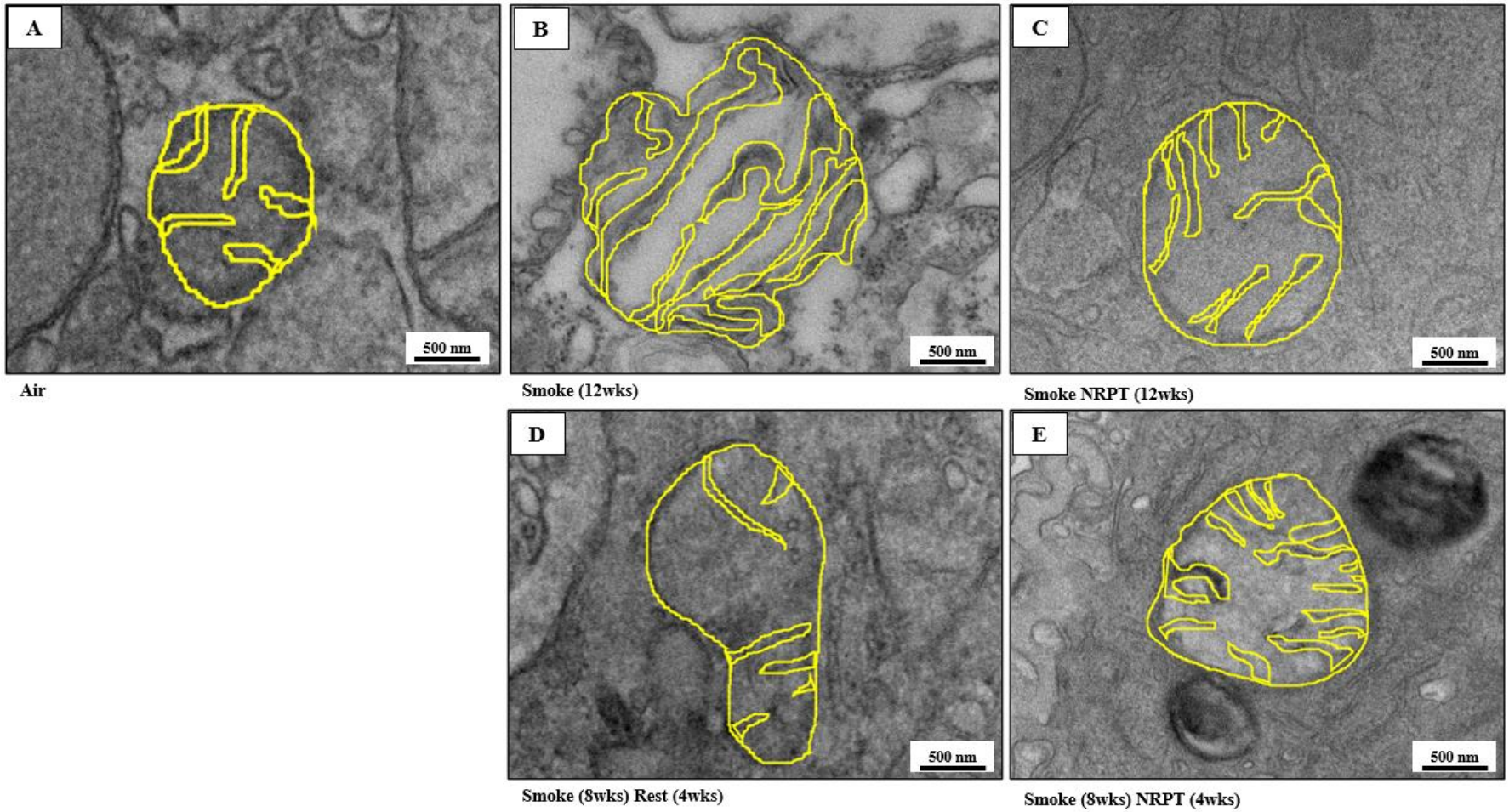
A
500 nm
Air
B
500 nm
Smoke (12wks)
C
500 nm
Smoke NRPT (12wks)
D
500 nm
Smoke (8wks) Rest (4wks)
E
500 nm
Smoke (8wks) NRPT (4wks)

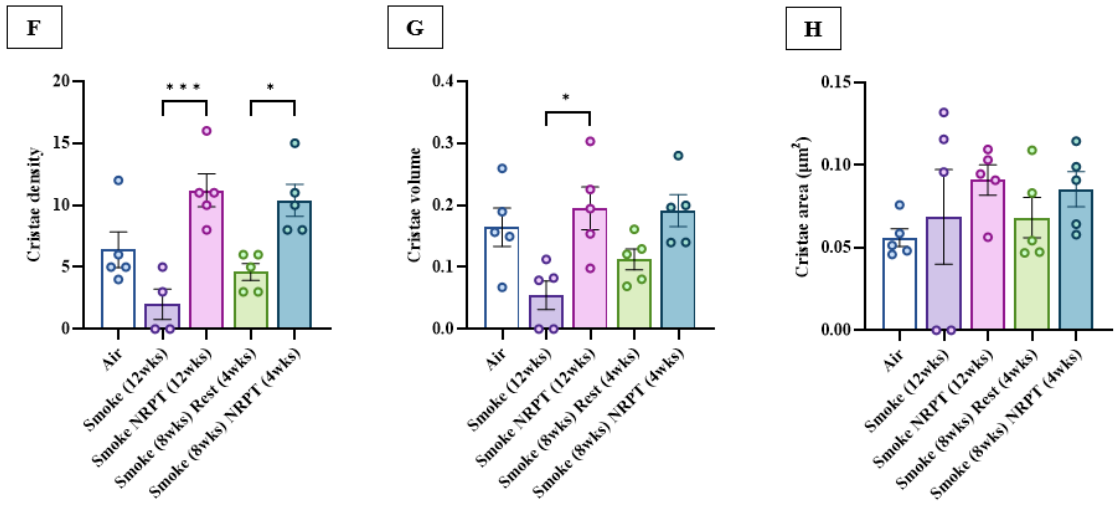

Figure 4.9: Administration of NR and PT protected mitochondrial cristae structure in advanced COPD:

*Representative cristae structure images (A) Air (B) Smoke (12wks), (C) Smoke NRPT (12wks), (D) Smoke (8wks) rest (4wks), (E) Smoke (8wks) NRPT (4wks); Graphical representation of (F) cristae structure, (G) cristae volume, (H) cristae volume. Data represented are means ± SEM of 5 mice/group, * P<0.05, ** P<0.01, *** P<0.001, **** P<0.0001.*

4.3.8 Administration of NR and PT restored mitochondrial function in advanced COPD

We measured the protein expression level of complex I-NDUFB8 (Figure 4.10A), complex II-SDHB (Figure 4.10B), complex III-UQCRC2 (Figure 4.10C), complex IV-MTCO1 (Figure 4.10D), and complex V-ATP5A (Figure 4.10E) in the lung of 12 weeks advanced COPD mice. A reduction was observed in the protein levels of all complexes examined in both the smoke (12wks) group as well as the smoke (8wks) rest (4wks) group in comparison to the air group (P<0.0001). This was further increased in the smoke NRPT

(12wks) group with respect to the smoke (12wks) group (P<0.05) as well as smoke (8wks) NRPT (4wks) as compared to the smoke (8wks) rest (4wks) group (P<0.05).

Mitochondrial respiratory chain enzymatic activities were measured in lung homogenates for complex I (Figure 4.10F), complex IV (Figure 4.10G), citrate synthase (Figure 4.10H) and β-HAD (Figure 4.10I). We observed a reduction in the activity of complex I, IV, citrate synthase, and β-HAD in the smoke (12wks) group as well as the smoke (8wks) rest (4wks) group in comparison to the air group (P<0.05). This was significantly increased in the treatment groups of smoke NRPT (12wks) in comparison to the smoke (12wks) group (P<0.05) as well as smoke (8wks) NRPT (4wks) with respect to the smoke (8wks) rest (4wks) (P<0.05).

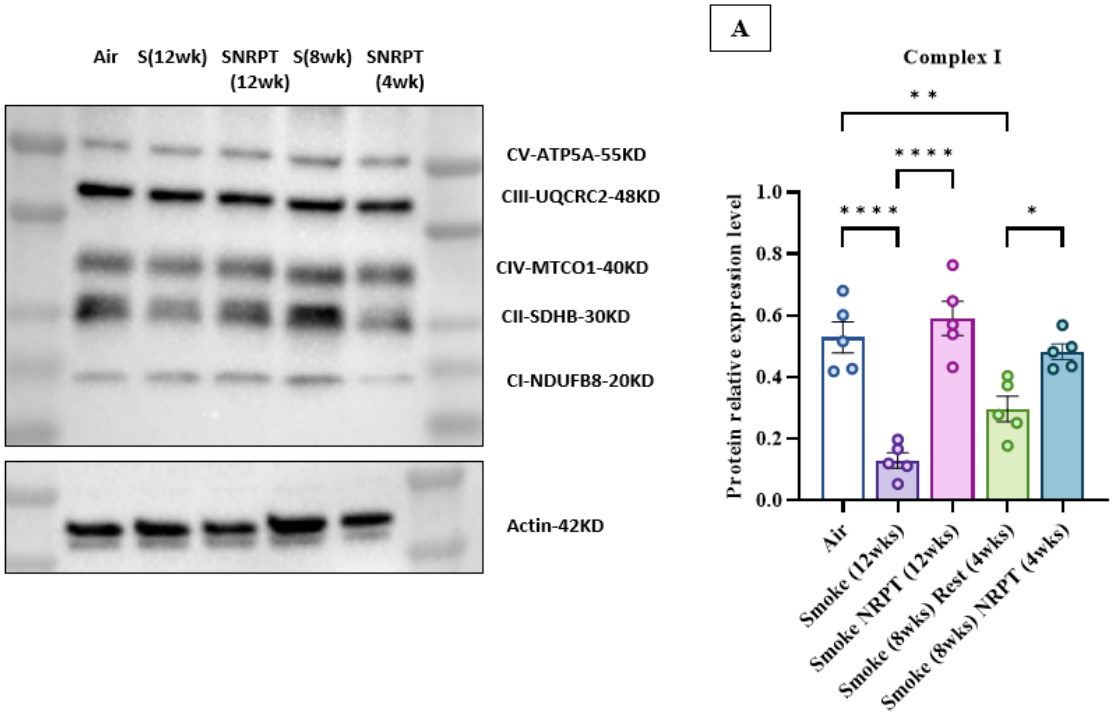

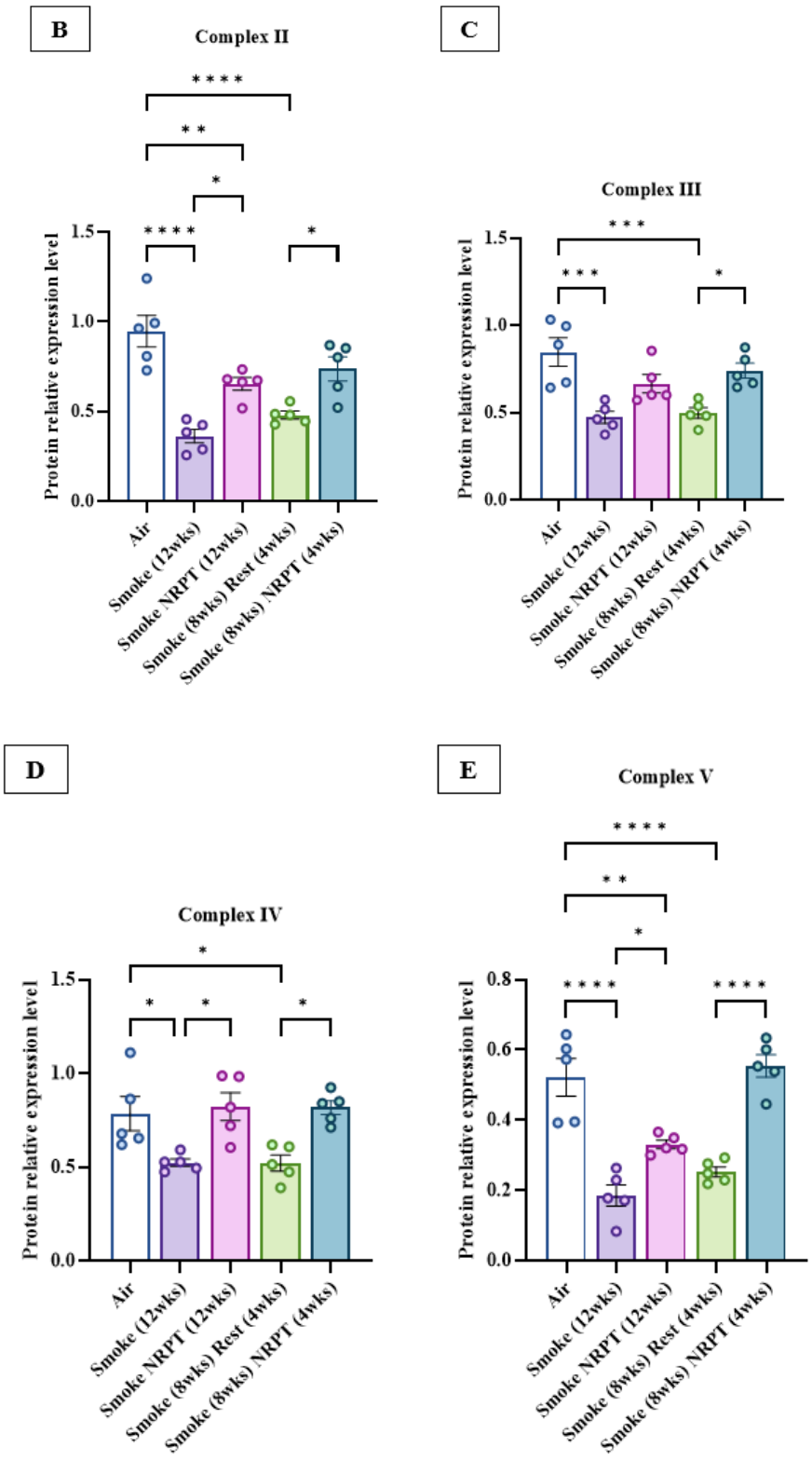
B
Complex II
Protein relative expression level
1.5
1.0
0.5
0.0
****
**
*
****
*
Air
Smoke (12wks)
Smoke NRPT (12wks)
Smoke (8wks) Rest (4wks)
Smoke (8wks) NRPT (4wks)
C
Complex III
Protein relative expression level
1.5
1.0
0.5
0.0
***
***
*
Air
Smoke (12wks)
Smoke NRPT (12wks)
Smoke (8wks) Rest (4wks)
Smoke (8wks) NRPT (4wks)
D
Complex IV
Protein relative expression level
1.5
1.0
0.5
0.0
*
*
*
*
Air
Smoke (12wks)
Smoke NRPT (12wks)
Smoke (8wks) Rest (4wks)
Smoke (8wks) NRPT (4wks)
E
Complex V
Protein relative expression level
0.8
0.6
0.4
0.2
0.0
****
**
*
****
****
Air
Smoke (12wks)
Smoke NRPT (12wks)
Smoke (8wks) Rest (4wks)
Smoke (8wks) NRPT (4wks)

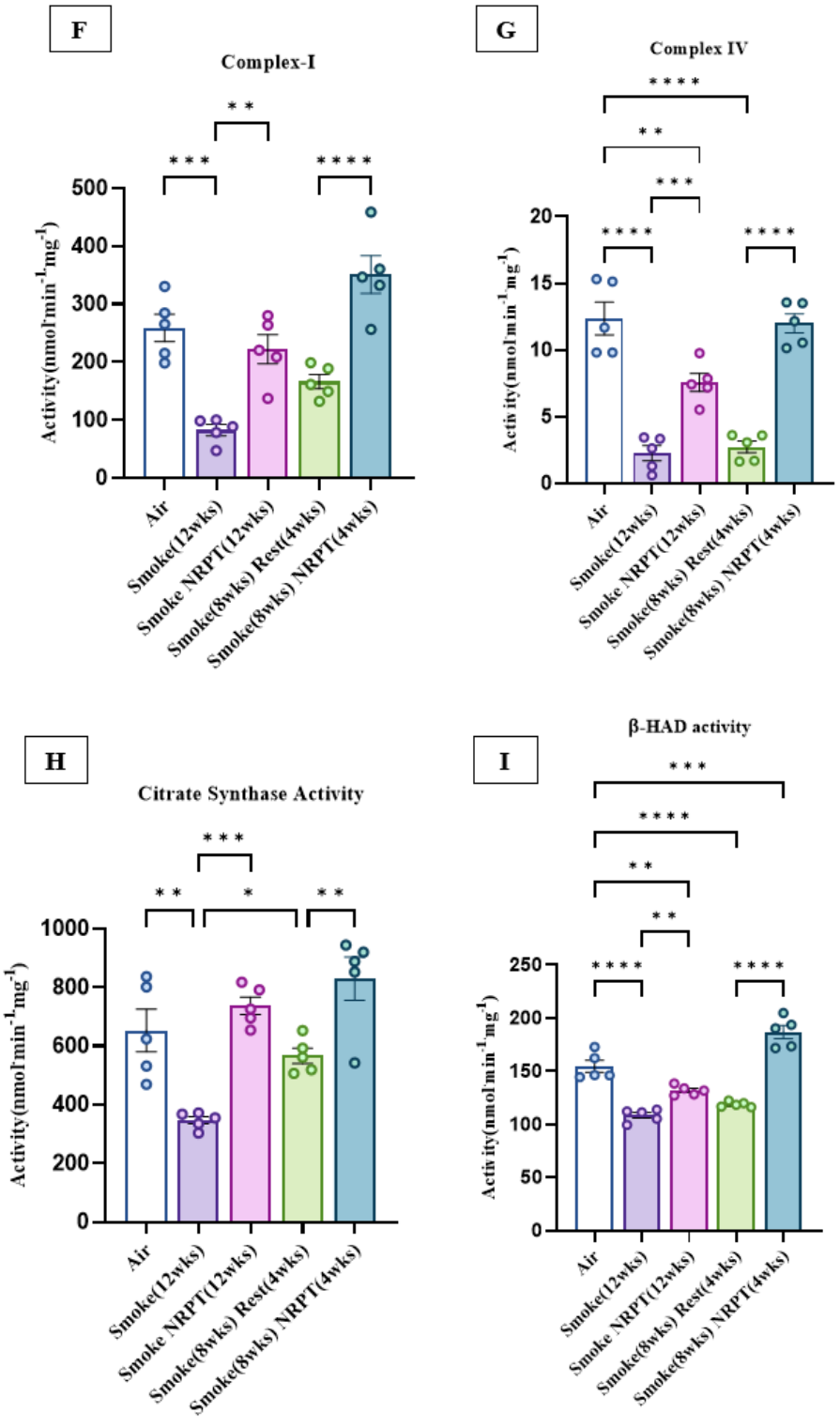

Figure 4.10: Administration of NR and PT promoted mitochondrial function in advanced COPD:

Protein expression of (A) Complex I-NDUFB8, (B) Complex II-SDHB, (C) Complex III-UQCRC2, (D) Complex IV-MTCO1, (E) Complex V-ATP5A. Mitochondrial respiratory

*chain enzymatic activity of (F) Complex I, (G) Complex IV, (H) Citrate synthase (I) β-HAD; Data represented are means ± SEM of 5 mice/group, * P<0.05, ** P<0.01, *** P<0.001, **** P<0.0001.*

4.3.9 Administration of NR and PT restored mitochondrial membrane potential in COPD

ΔΨm was examined on lung sections of 12 weeks advanced COPD mice. The MFI of J-aggregates in the smoke (12wks) (P<0.0001) and smoke (8wks) rest (4wks) groups were significantly reduced in comparison to the air group (P<0.05). We also observed increased J-aggregates in the smoke NRPT (12wks) as compared to the smoke (12wks) (P<0.0001) (Figure 4.11A). Further, J-monomers increased in the smoke (12wks) group as well as smoke (8wks) rest (4wks) with respect to the air group (P<0.0001). A significant reduction of J-monomers was observed in the smoke NRPT (12wks) in comparison to the smoke (12wks) group (P<0.0001) as well as smoke (8wks) NRPT (4wks) as compared to the smoke (8wks) rest (4wks) (P<0.0001) (Figure 4.11B). Further, the ΔΨm was reduced significantly both in the smoke (12wks) and smoke (8wks) rest (4wks) in comparison to the air group (P<0.0001). We also observed a significant increase in ΔΨm in the smoke NRPT (12wks) compared to the smoke (12wks) group (P<0.0001) and in the smoke (8wks) NRPT (4wks) in comparison to the smoke (8wks) rest (4wks) (P<0.01) (Figure 4.11C). The representative images below represent J-aggregates in the Texas Red channel, J-monomers in the FIT-C channel and nuclear stain DAPI followed by a merged image of all the channels showing a co-localisation of J-aggregates and J-monomers (orange).

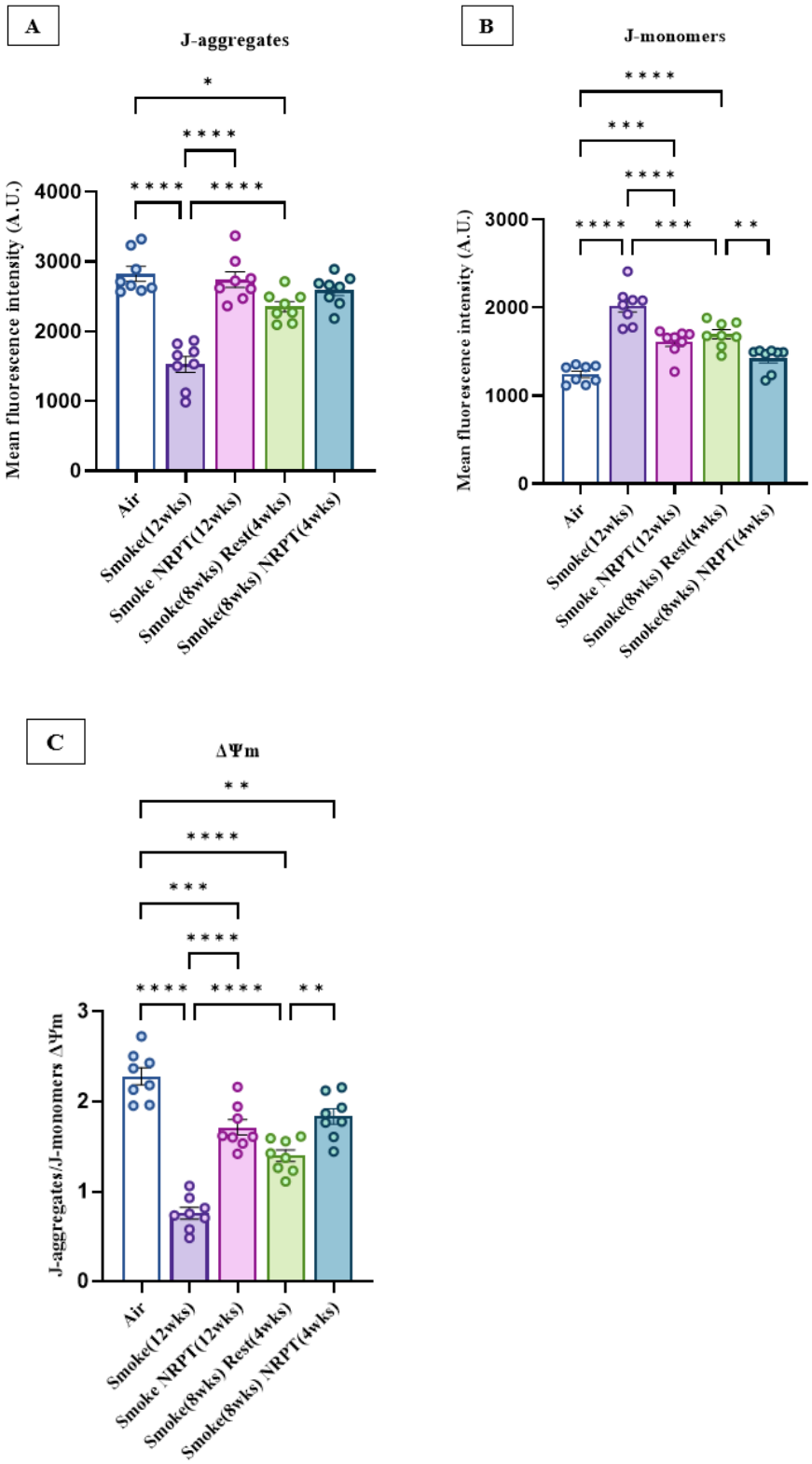
A
J-aggregates
Mean fluorescence intensity (A.U.)
4000
3000
2000
1000
0
*
****
****
****
Air
Smoke(12wks)
Smoke NRPT(12wks)
Smoke(8wks) Rest(4wks)
Smoke(8wks) NRPT(4wks)
B
J-monomers
Mean fluorescence intensity (A.U.)
3000
2000
1000
0
****
***
****
****
***
**
Air
Smoke(12wks)
Smoke NRPT(12wks)
Smoke(8wks) Rest(4wks)
Smoke(8wks) NRPT(4wks)
C
ΔΨm
J-aggregates/J-monomers ΔΨm
3
2
1
0
**
****
***
****
****
****
**
Air
Smoke(12wks)
Smoke NRPT(12wks)
Smoke(8wks) Rest(4wks)
Smoke(8wks) NRPT(4wks)

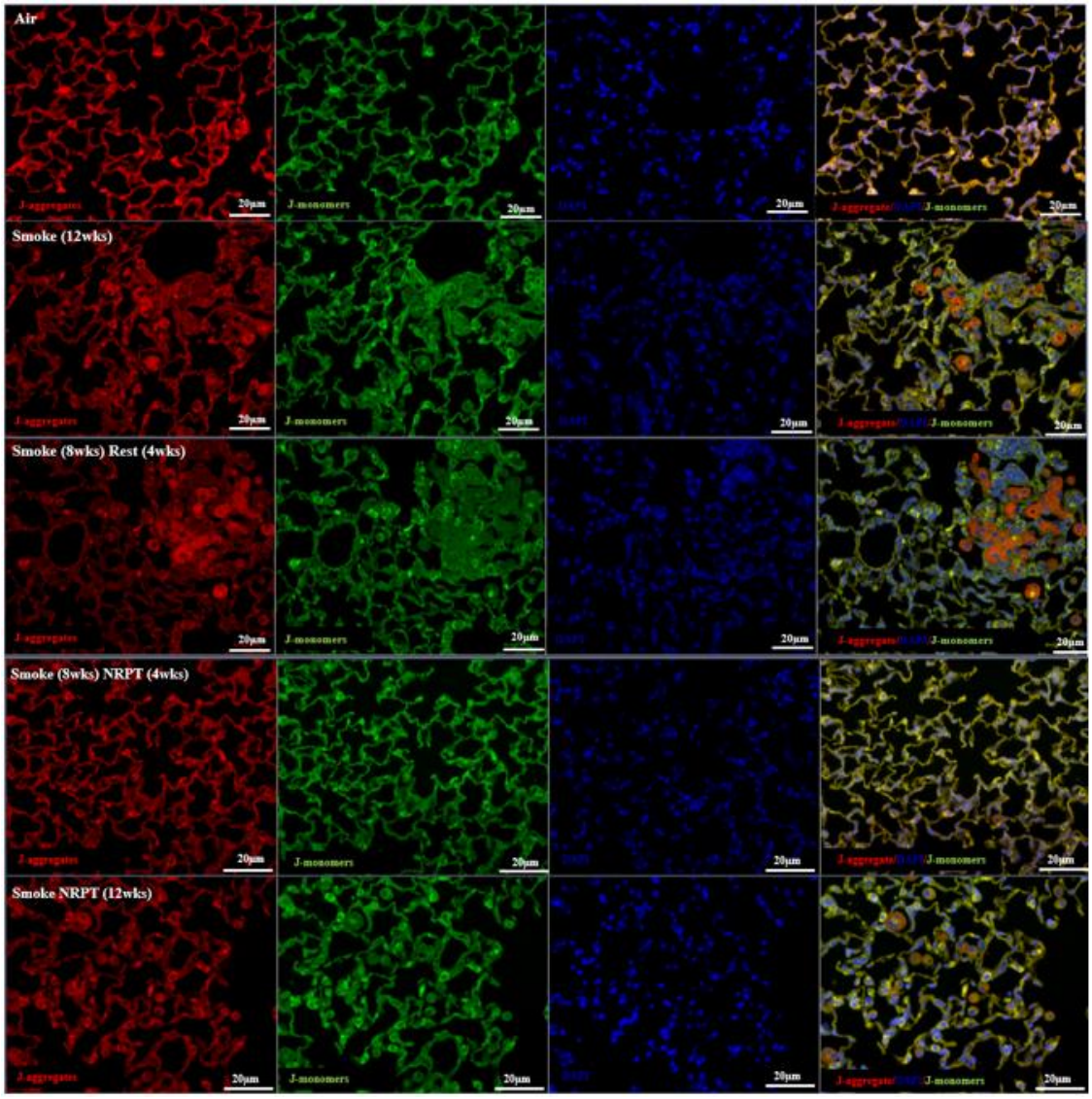

Figure 4.11: Administration of NR and PT restored mitochondria membrane potential in advanced COPD:

*Measure of mitochondrial membrane potential (A) J-aggregates (Red), (B) Reduced J-monomers (green) (P<0.05), and (C) increased in the ΔΨm in smoke NR and/or PT group as compared to the smoke group (P<0.05). Data represented are means ± SEM of 8 mice/group, * P<0.05, ** P<0.01, *** P<0.001, **** P<0.0001.*

4.3.10 Administration of NR and PT reduced oxidative stress in advanced COPD

We observed an increase in the gene expression for NOX2 in the smoke (12wks) group in comparison to the air group (P<0.0001), which was significantly reduced in the smoke NRPT (12wks) treatment group (P<0.001) as well as the smoke (8wks) rest (4wks) (P<0.01) with respect to the smoke (12wks) group (Figure 4.12A). In contrast, the gene expression of HO1 was reduced in the groups of smoke (12wks) (P<0.0001), smoke NRPT (12wks) (P<0.0001), and smoke (8wks) NRPT (4wks) (P<0.001) in comparison to the air group. The gene expression of HO1 was increased in the smoke (8wks) rest (4wks) as compared to the smoke (12wks) group (P<0.01) and was reduced in the smoke (8wks) NRPT (4wks) with respect to the smoke (8wks) rest (4wks) (Figure 4.12B).

Additionally, we observed an increase in the MFI for 4-HNE via IF in the smoke (12wks) and smoke (8wks) rest (4wks) group in comparison to the air group (P<0.0001) which was reduced in the treatment groups of smoke NRPT (12wks) with respect to the smoke (12wks) group (P<0.0001) as well as smoke (8wks) NRPT (4wks) group in comparison to the smoke (8wks) rest (4wks) (P<0.0001) group. Images below represent 4-HNE (green) co-stained with F4/80 (red) and DAPI (Figure 4.12C).

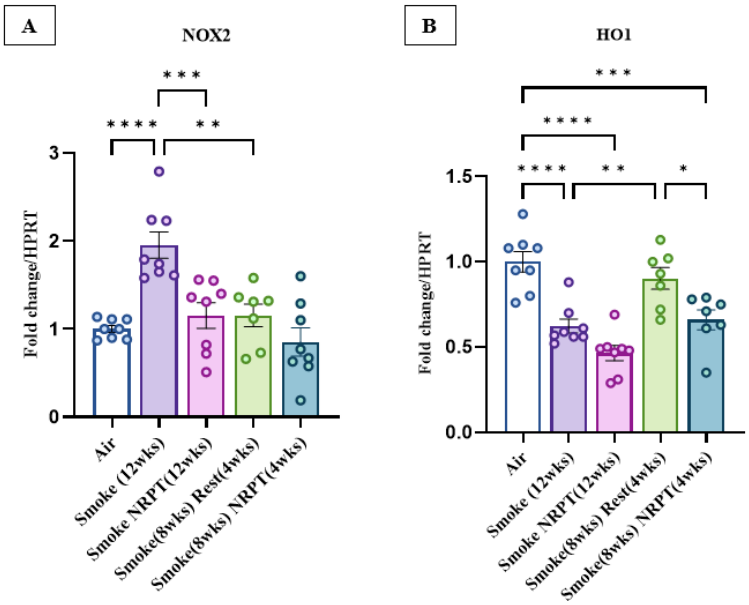

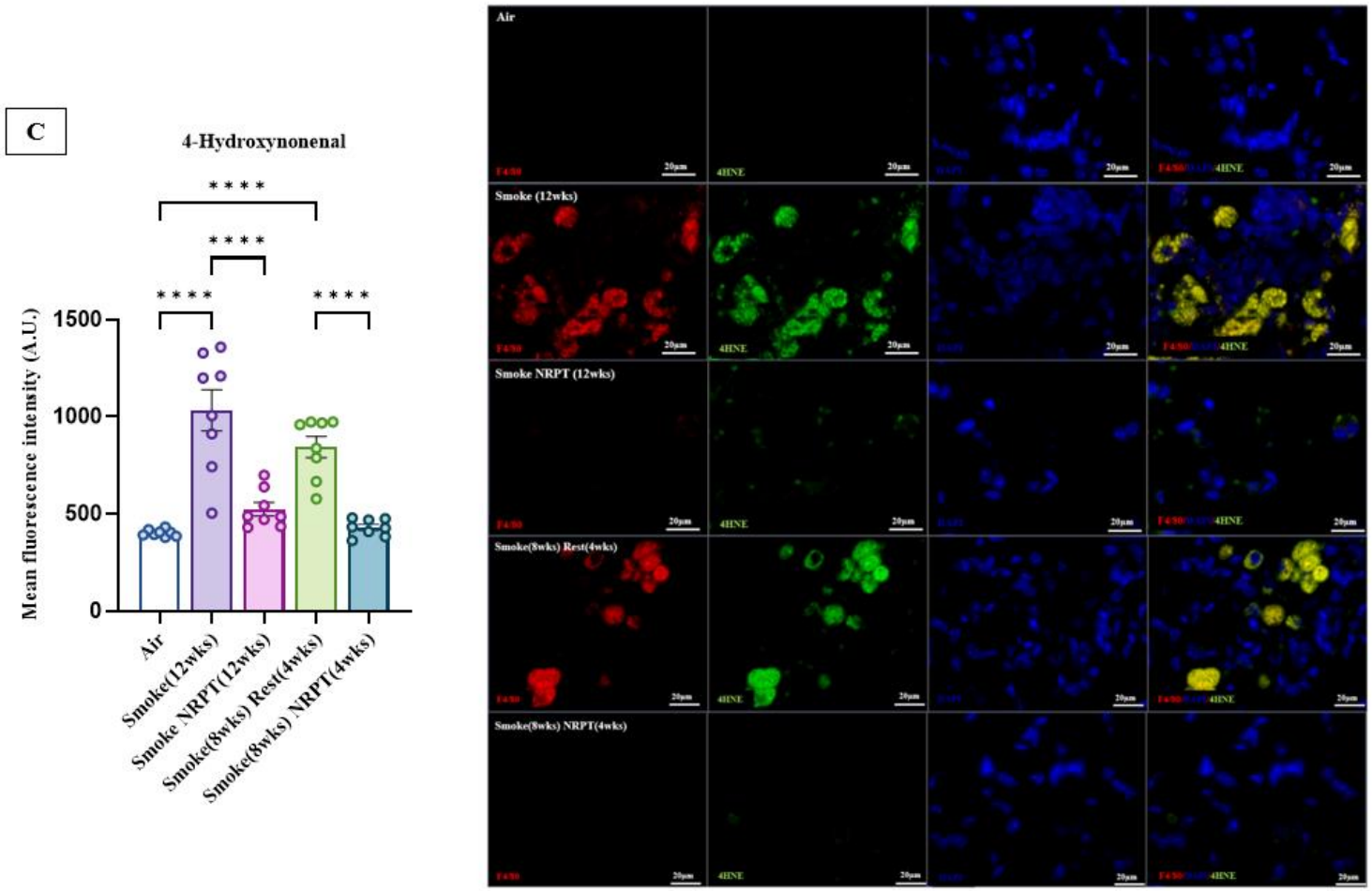

Figure 4.12: Administration of NR and PT reduces oxidative stress in advanced COPD:

*Gene expression of (A) NOX2 and (B) HO1, (C) Graphical representation of MFI in arbitrary units (A.U.) of reduced 4-HNE levels in smoke NR and/or PT in comparison to smoke group (P<0.0001), images show fluorescence localisation of F4/80 (red), 4-HNE (green), DAPI-nuclei stain (blue); Data represented are means ± SEM of 8 mice/group, * P<0.05, ** P<0.01, *** P<0.001, **** P<0.0001.*

4.3.11 Administration of NR and PT reduced inflammation in advanced COPD

Mice exposed to CS for 12 weeks in the smoke (12wks) group displayed an increase in immune cell infiltration (P<0.0001) (Figure 4.13A) comprising macrophages (P<0.001) (Figure 4.13B) and neutrophils (P<0.0001) (Figure 4.13C) in the BALF in comparison to the air group. We observed a reduction in total cell counts (P<0.0001), macrophages (P<0.05) and neutrophils (P<0.0001) in the smoke (12wks) NRPT (4wks) group as compared to the smoke (12wks) group. In addition, the gene expression of TNFα (Figure 4.13D) and CXCL1 (Figure 4.13E) identified a significant increase in the smoke (12wks) group as well as the smoke (12wks) NRPT (4wks) group in comparison to the air group (P<0.0001).

The body weight of all the experimental groups was monitored daily as mentioned previously in 4.2.3. There was a significant weight loss observed in the smoke (12wks) group and smoke (12wks) NRPT (4wks) in comparison to the air group (P<0.0001) (Figure 4.13F).

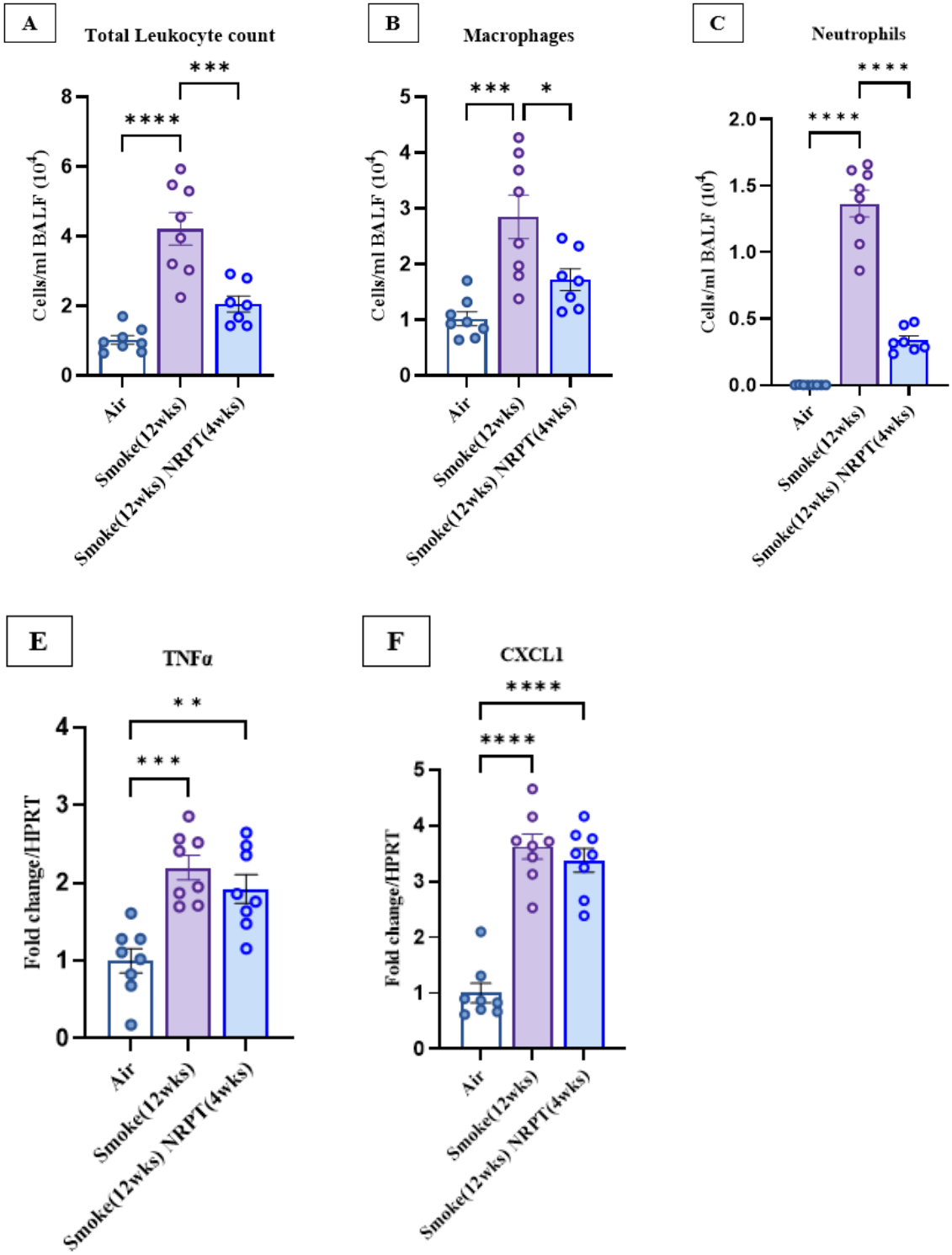
A
Total Leukocyte count
Cells/ml BALF (10^4)
Air
Smoke(12wks)
Smoke(12wks) NRPT(4wks)
B
Macrophages
C
Neutrophils
E
TNFα
Fold change/HPRT
F
CXCL1

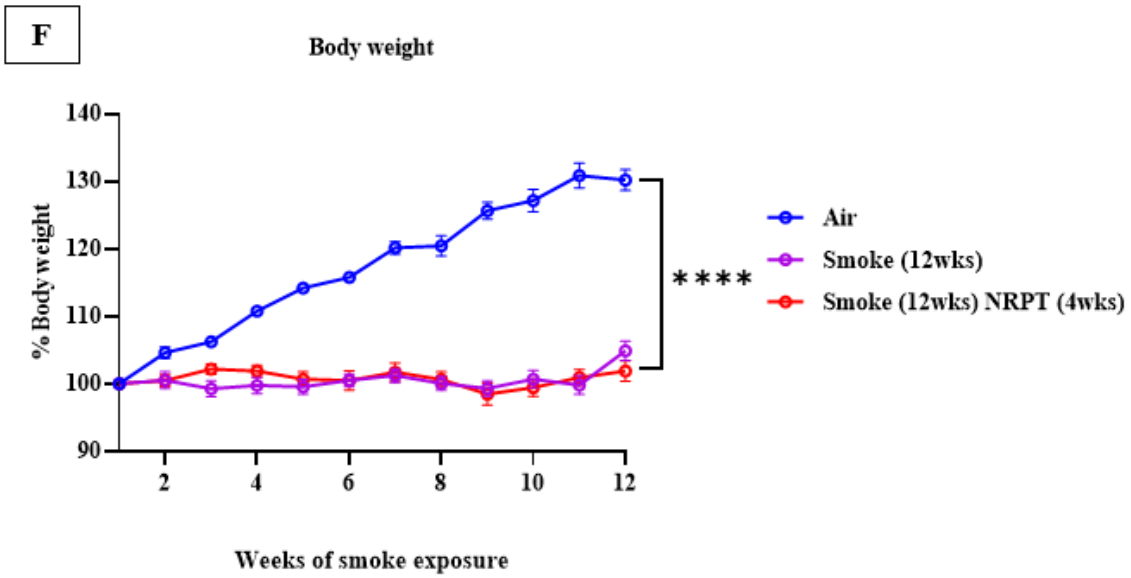

Figure 4.13: Administration of NR and PT restored inflammation in COPD:

(A) Cellular infiltrates in the lung parenchyma, (B) Macrophages, (C) Neutrophils; Gene expression for (D) TNFα and (E) CXCL1; (F) Changes in body weight. Data represented are means ± SEM of 8 mice/group, * P<0.05, ** P<0.01, *** P<0.001, **** P<0.0001.

4.3.12 Administration of NR and PT attenuated COPD features in advanced disease stages

Lung sections from the 12 weeks advanced COPD model treated with NR and PT was used for the measurement of collagen deposition as previously described. Chronic exposure to CS resulted in increased collagen deposition around the basement membrane of small airways in the smoke (12wks) group in comparison to the air group (P<0.0001). Further, there was a significant reduction in the collagen deposition in the treatment group of smoke (12wks) NRPT (4wks) with respect to the smoke (12wks) group (P<0.01) (Figure 4.14A).

To measure emphysema, we performed MLI counts in the lung sections obtained from a 12-week advanced COPD study. We observed an increase in the alveolar diameter in the

smoke (12wks) group ($P<0.0001$) and smoke (12wks) NRPT (4wks) ($P<0.001$) in comparison to the air group ($P<0.0001$). This was significantly reduced in the smoke (12wks) NRPT (4wks) group as compared to the smoke (12wks) group ($P<0.0001$) (Figure 4.14B).

Furthermore, lung function parameter changes were measured using FlexiVent as mentioned previously. An increase in IC was observed in the smoke (12wks) group in comparison to the air group ($P<0.01$) and was reduced in the smoke (12wks) NRPT (4wks) group with respect to the smoke (12wks) ($P<0.05$) (Figure 4.14C). We did not observe any change in the area across all the experimental groups in this study (Figure 4.14D). However, we observed an increase in the TLC in the smoke (12wks) group as compared to the air group ($P<0.01$), and a reduction in the smoke (12wks) NRPT (4wks) group in comparison to the smoke (12wks) group ($P<0.05$) (Figure 4.14E). Additionally, lung compliance curves were analysed for the smoke (12wks) group, the air group and the smoke (12wks) NRPT (4wks) (Figure 4.14F).

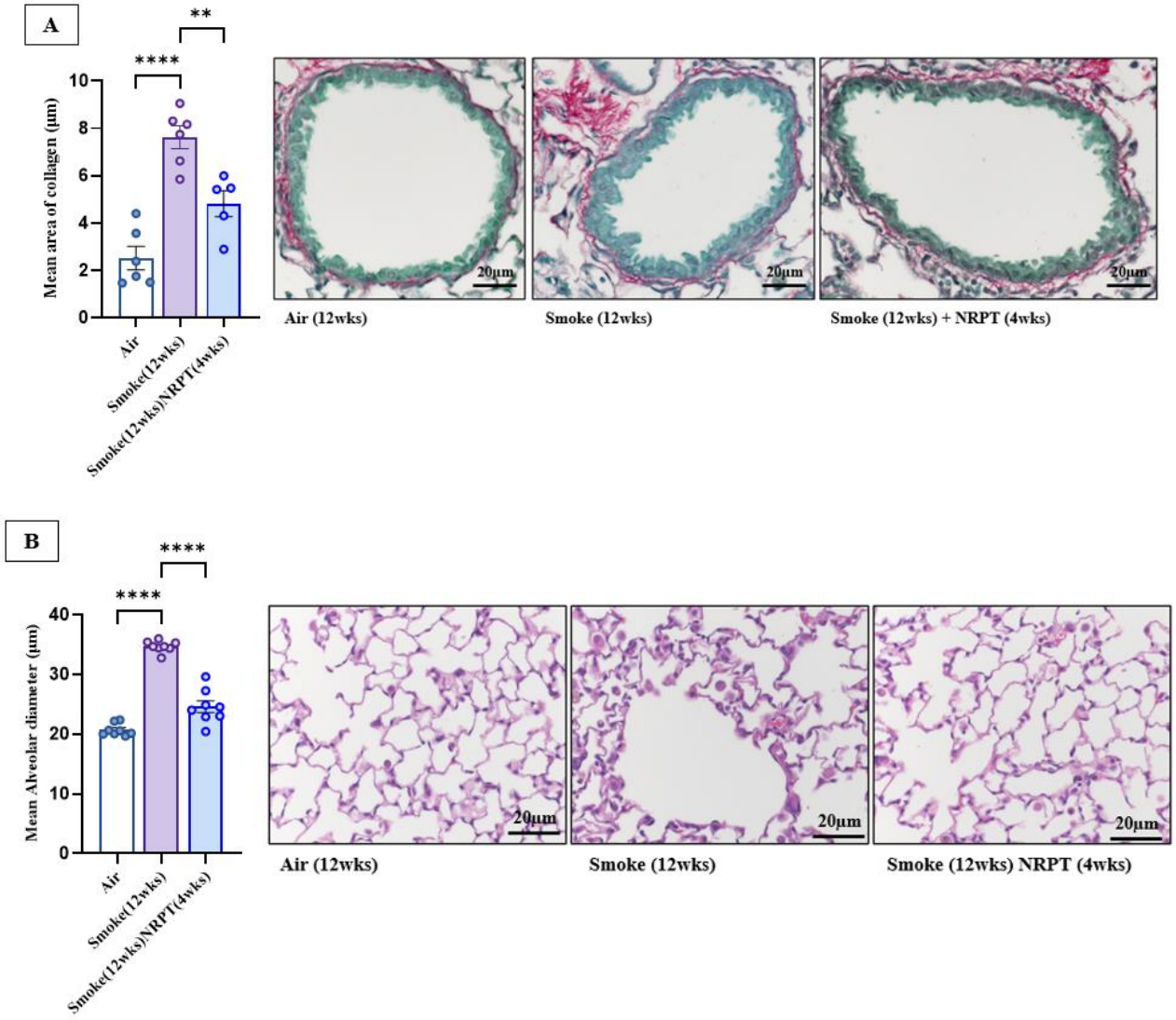
A
**
****
Mean area of collagen (µm)
10
8
6
4
2
0
Air
Smoke(12wks)
Smoke(12wks)NRPT(4wks)
20µm
Air (12wks)
Smoke (12wks)
Smoke (12wks) + NRPT (4wks)
B
****
****
Mean Alveolar diameter (µm)
40
30
20
10
0
Air
Smoke(12wks)
Smoke(12wks)NRPT(4wks)
20µm
Air (12wks)
Smoke (12wks)
Smoke (12wks) NRPT (4wks)

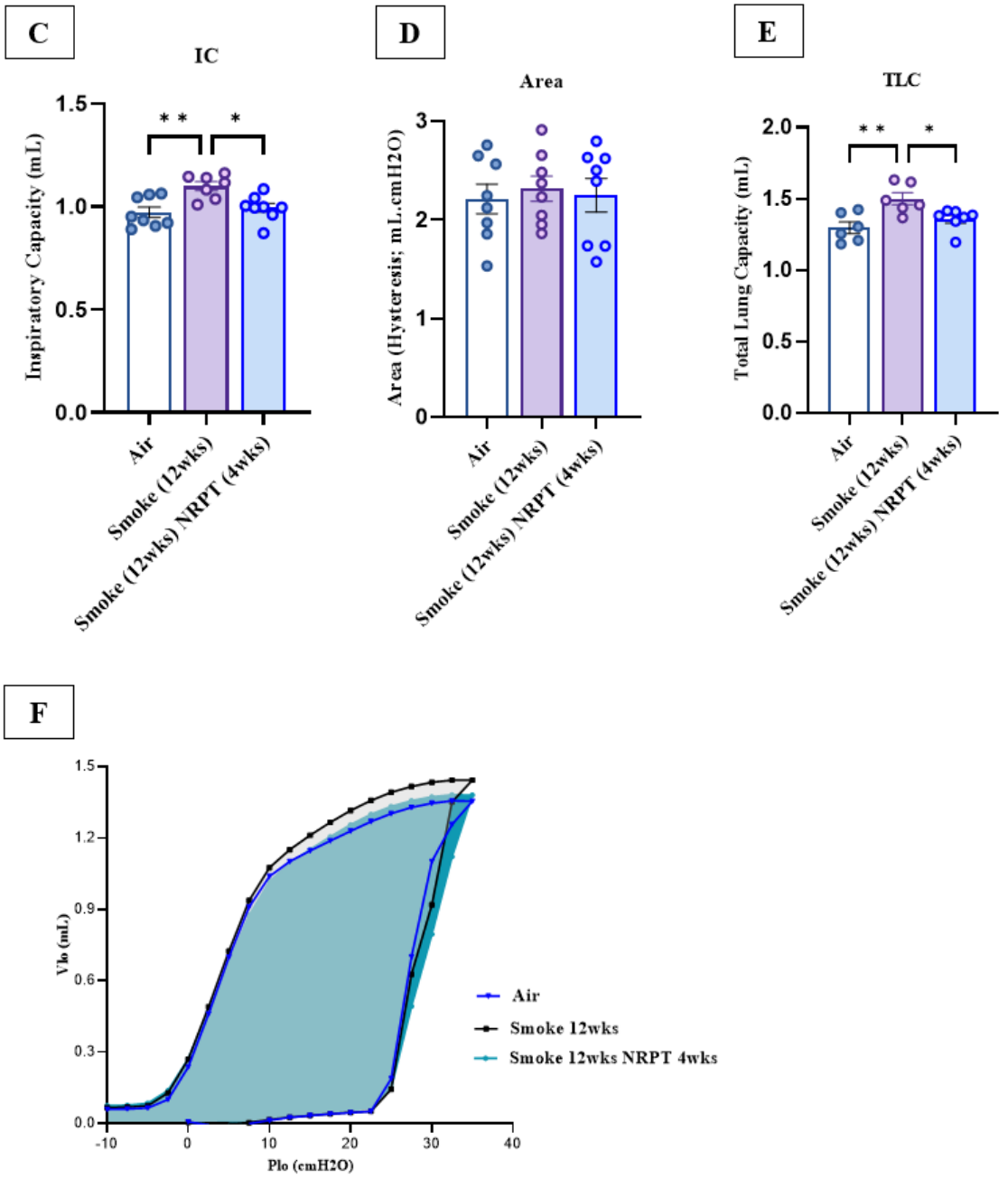

Figure 4.14: Administration of NR and PT restored COPD features in advanced disease stages:

(A) Collagen deposition around airways, (B) Alveolar destruction; (C) IC, (D) Area, (E) TLC, (F) Lung compliance curves. Data represented are means ± SEM of 8 mice/group, * P<0.05, ** P<0.01, *** P<0.001, **** P<0.0001.

4.3.13 Administration of NR and PT restored NAD^+ levels in COPD

Total NAD^+ and NADH levels were assessed in lung homogenates of a 12-week advanced COPD study. There was a significant reduction of total NAD^+ levels in the smoke (12wks) ($P<0.0001$) and smoke (12wks) NRPT (4wks) ($P<0.001$) in comparison to the air group (Figure 4.14A). Total NAD^+ levels were further increased in the smoke (12wks) NRPT (4wks) group in comparison to the smoke (12wks) group ($P<0.05$). NADH levels were increased in the smoke (12wks) group in comparison to the air group ($P<0.0001$), and were significantly reduced in the smoke (12wks) NRPT (4wks) as compared to the smoke (12wks) group ($P<0.0001$) (Figure 4.14B). Further, the ratio of total NAD^+/NADH was reduced in the smoke (12wks) group ($P<0.0001$) and the smoke (12wks) NRPT (4wks) ($P<0.01$) in comparison to the air group, which was increased in the treatment group of smoke (12wks) NRPT (4wks) with respect to the smoke (12wks) group ($P<0.0001$) (Figure 4.14C).

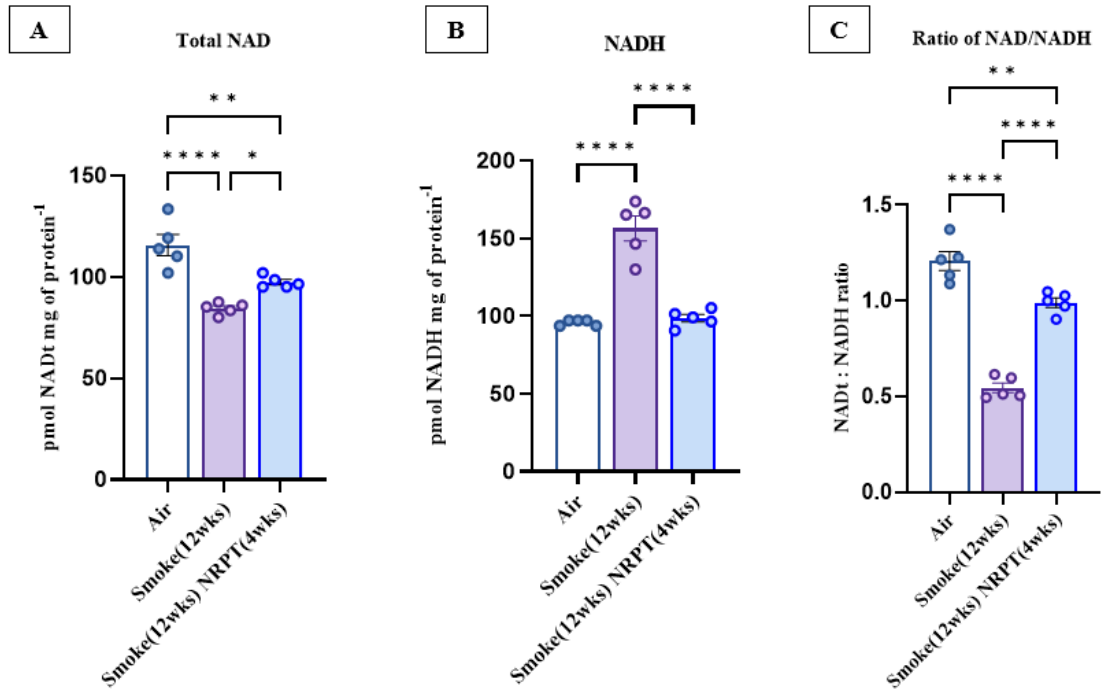

Figure 4.15: Administration of NR and PT restored NAD+ homeostasis in advanced COPD:

*(A) total NAD^+ level in mouse lung homogenates, (B) NADH level in mouse lung homogenates, (C) ratio of NAD^+/NADH. Data represented are means ± SEM of 5 mice/group, * P<0.05, ** P<0.01, *** P<0.001, **** P<0.0001.*

4.3.14 Administration of NR and PT regulated PARP and CD38 in advanced COPD

We did not observe any change in the PARP1 gene expression (Figure 4.16A) in the smoke (12wks) group with respect to the air group, however, we observed a reduction in the gene expression of PARP1 in the smoke (12wks) NRPT (4wks) in comparison to the smoke (12wks) group (P<0.05). We also measured the protein levels of PARP1 and observed a decrease in both smoke (12wks) group (P<0.001) as well as the smoke (12wks) NRPT (4wks) group (P<0.01) with respect to the air group (Figure 4.16B). Further, an increase in the PARP activity was observed in the smoke (12wks) group as compared to

the air group (P<0.001) which was reduced in the smoke (12wks) NRPT (4wks) in comparison to the smoke (12wks) group (P<0.05) (Figure 4.16C).

Additionally, we observed a reduction in CD38 protein expression in the smoke (12wks) group in comparison to the air group (P<0.05) which was significantly upregulated in the smoke (12wks) NRPT (4wks) group as compared to the smoke (12wks) group (P<0.05) (Figure 4.16D).

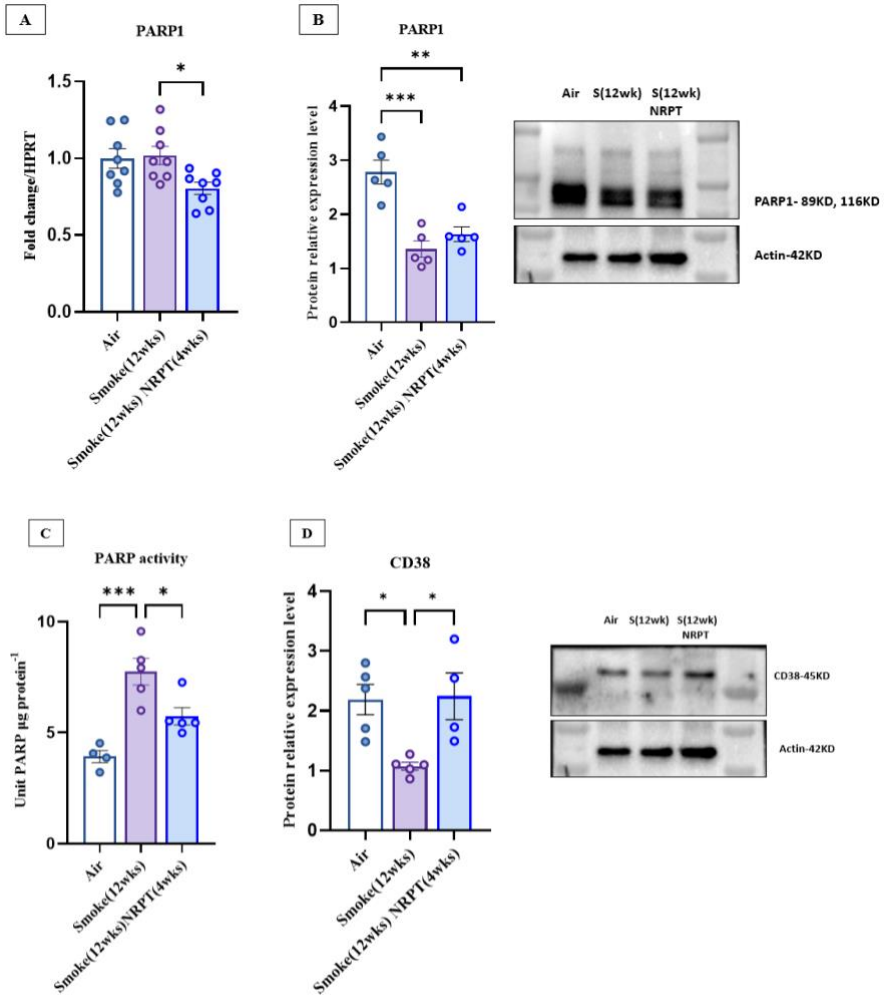

Figure 4.16: Administration of NR and PT regulated PARP and CD38 levels in COPD

*(A) Gene expression of PARP1, (B) Protein expression level of PARP1, (C) PARP activity levels in lung homogenates, (D) Protein expression level of CD38. Data represented are means ± SEM of 5 mice/group, * P<0.05, ** P<0.01, *** P<0.001, **** P<0.0001.*

4.3.15 Administration of NR and PT regulated SIRTs in COPD

Gene expression of SIRT1 showed an increase in the smoke (12wks) NRPT (4wks) group in comparison to the air group ($P<0.01$) (Figure 4.17A). Further, the gene expression of SIRT3 was reduced in the smoke (12wks) NRPT (4wks) group in comparison to both the air group ($P<0.001$) and smoke (12wks) group ($P<0.01$) (Figure (4.17C). We also observed a reduction in the gene expression of SIRT4 in smoke (12wks) NRPT (4wks) in comparison to the air group ($P<0.05$) (Figure 4.17D). In contrast, we did not observe any change in the gene expression of SIRT2 (Figure 4.17B), SIRT5 (Figure 4.17E), SIRT6 (Figure 4.17F) and SIRT7 (Figure 4.17G) across the different experiments groups in the 12-week smoke model-2.

In contrast to the gene expression, we observed a reduction in the protein expression of all SIRTs examined (SIRT1-7) in the smoke (12wks) group as compared to the air group ($P<0.05$) (Figure 4.17H-M). We further observed a reduced protein expression of SIRT3 (Figure 4.17J), SIRT5 (Figure 4.17K) and SIRT6 (Figure 4.17L) in the smoke (12wks) NRPT (4wks) ($P<0.05$) with respect to the air group. Additionally, we observed an increased protein expression of SIRT7 (Figure 4.17M) in the smoke (12wks) NRPT (4wks) as compared to the smoke (12wks) group ($P<0.05$).

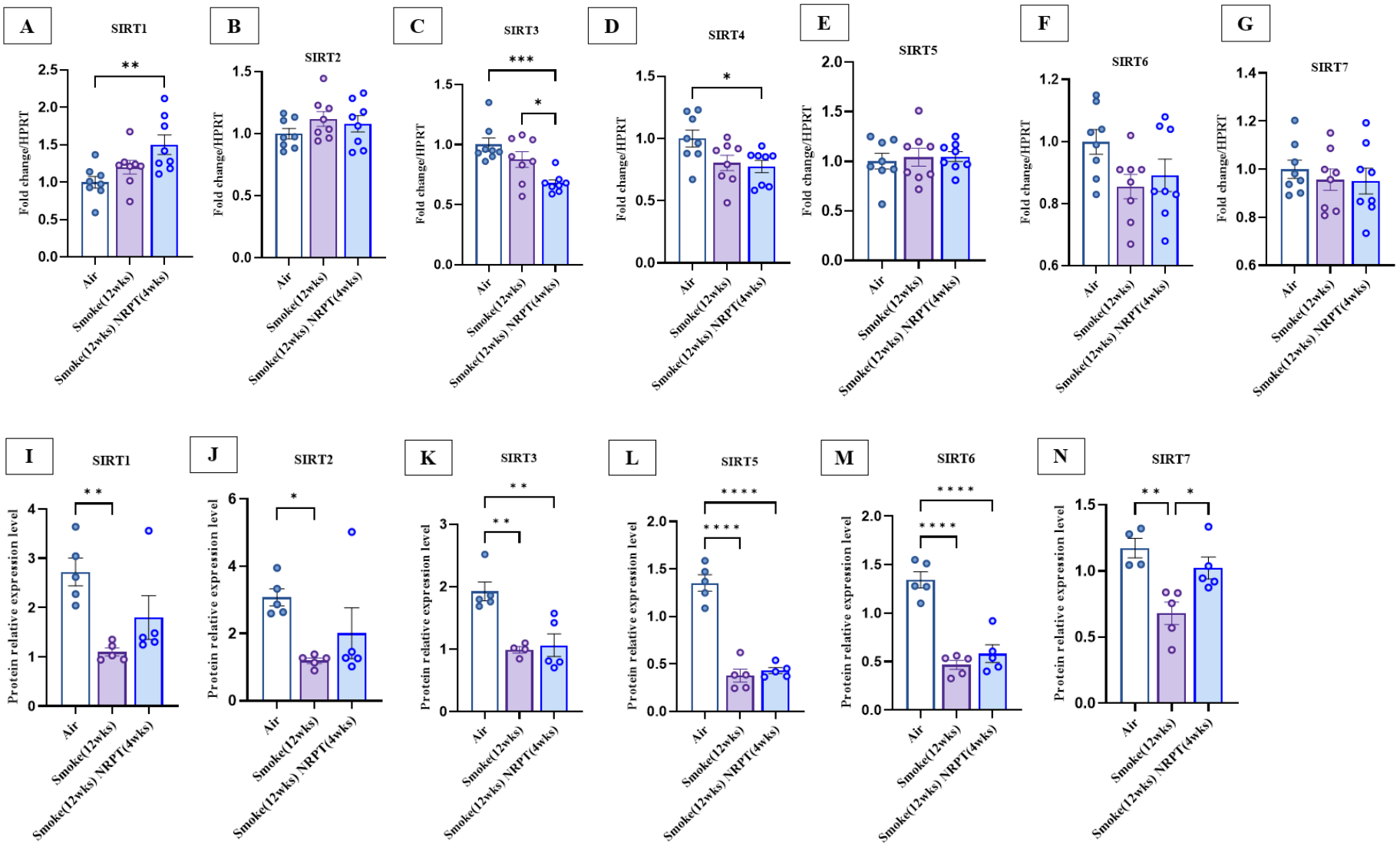
A
SIRT1
Fold change/HPRT
B
SIRT2
Fold change/HPRT
C
SIRT3
Fold change/HPRT
D
SIRT4
Fold change/HPRT
E
SIRT5
Fold change/HPRT
F
SIRT6
Fold change/HPRT
G
SIRT7
Fold change/HPRT
I
SIRT1
Protein relative expression level
J
SIRT2
Protein relative expression level
K
SIRT3
Protein relative expression level
L
SIRT5
Protein relative expression level
M
SIRT6
Protein relative expression level
N
SIRT7
Protein relative expression level
Air
Smoke(12wks)
Smoke(12wks) NRPT(4wks)

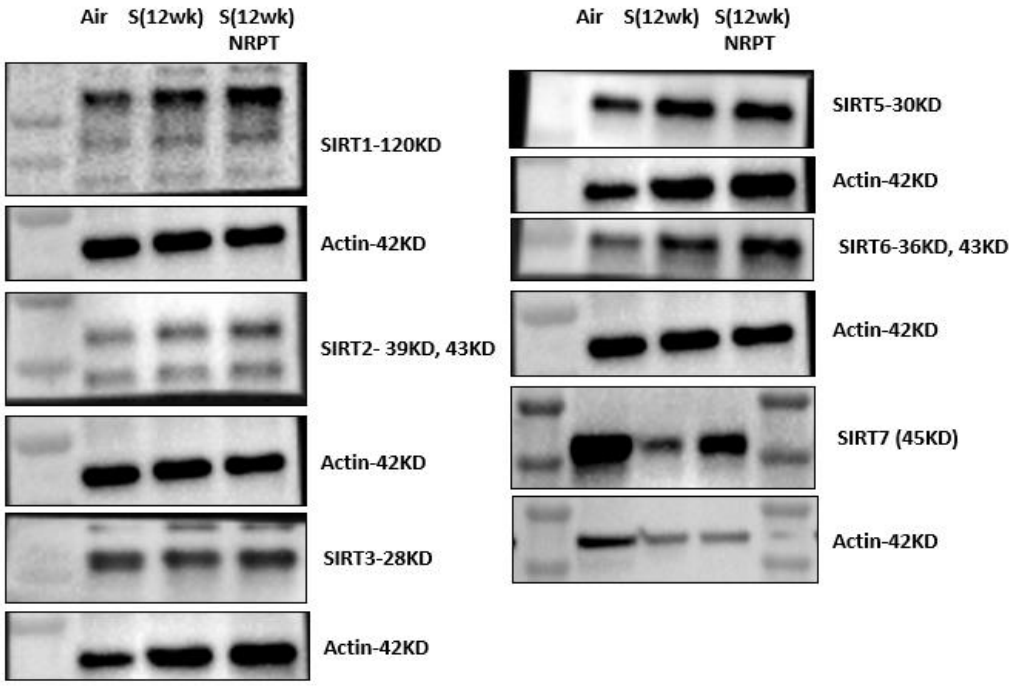

Figure 4.17: Administration of NR and PT regulates SIRTs in advanced COPD studies:

*(A) gene expression of SIRT1, (B) protein levels SIRT1, (C) gene expression of SIRT2, (D) protein levels SIRT2, (E) gene expression of SIRT3, (F) protein levels SIRT3, (G) gene expression of SIRT4, (H) gene expression of SIRT5, (I) protein levels SIRT5, (J) gene expression of SIRT6, (K) protein levels SIRT6, (L) Gene expression of SIRT7, (M) protein levels SIRT7. Data represented are means ± SEM of 5 mice/group, * P<0.05, ** P<0.01, *** P<0.001, **** P<0.0001.*

4.3.16 Administration of NR and PT restored mitochondrial structure in advanced COPD

We observed an increase in mitochondrial density/numbers in the smoke (12wks) group (Figure 4.18B) as compared to the air group (P<0.0001) (Figure 4.18A). However, we

did not observe any difference in the mitochondrial density in the smoke (12wks) NRPT (4wks) (Figure 4.18C) in comparison to either smoke (12wks) group or the air group. Further, we observed a significant increase in mitochondrial area in the smoke (12wks) group (Figure 4.18E) in comparison to the air group (Figure 4.18D) ($P<0.001$) which was reduced in the smoke (12wks) NRPT (4wks) group (Figure 4.18F) with respect to the smoke (12wks) group ($P<0.0001$).

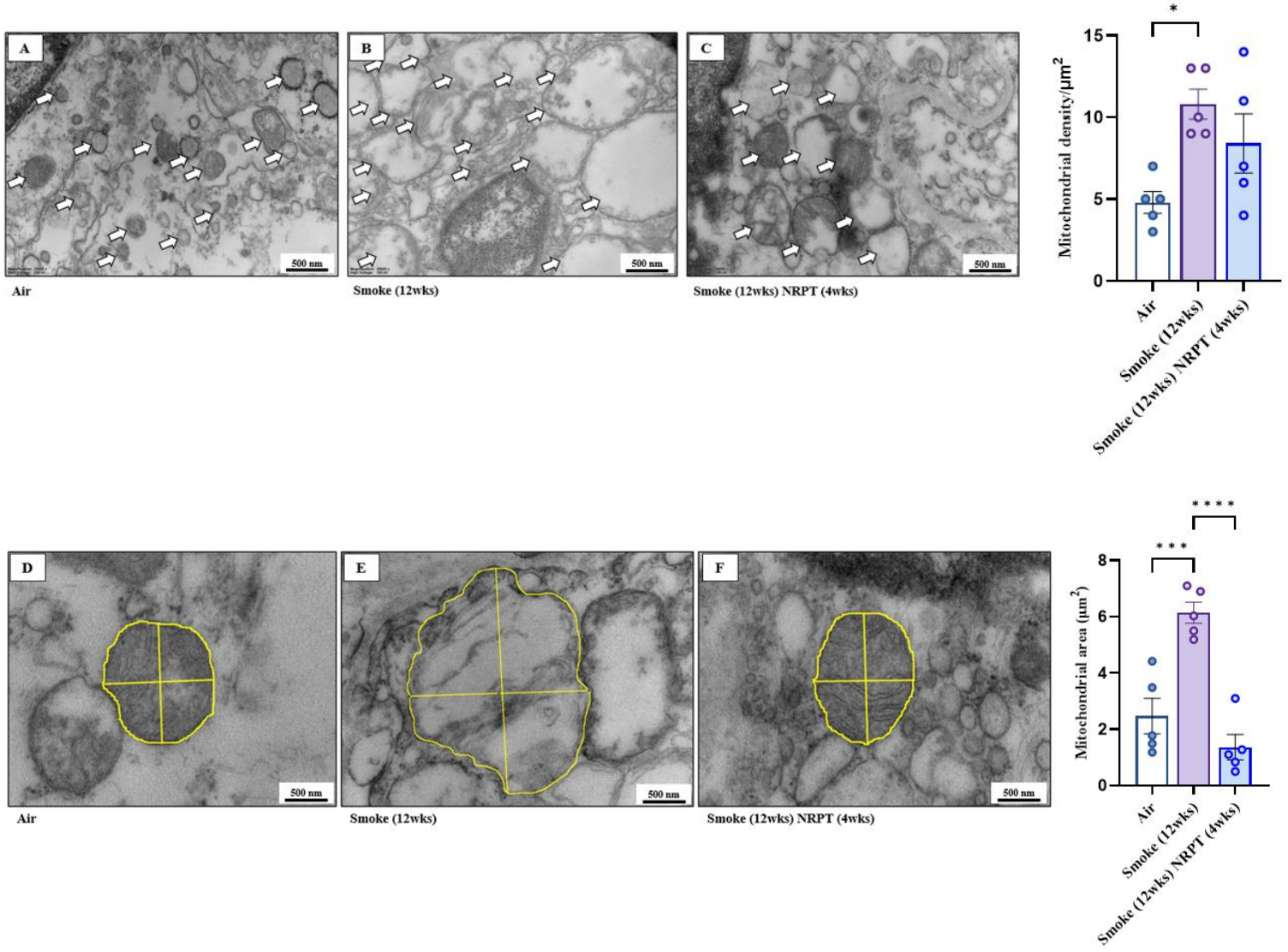

Figure 4.18: Administration of NR and PT restored mitochondrial structure in advanced COPD:

*Mitochondrial density (A) Air (B) Smoke (12wks), (C) Smoke (12wks) NRPT (4wks); Mitochondrial area (D) Air (E) Smoke (12wks), (F) Smoke (12wks) NRPT (4wks). Data represented are means ± SEM of 5 mice/group, * P<0.05, ** P<0.01, *** P<0.001, **** P<0.0001.*

4.3.17 Administration of NR and PT preserved mitochondrial cristae structure in advanced COPD

We measured cristae density (Figure 4.19D), cristae volume (Figure 4.19E) and cristae area (Figure 4.19F) in all the experimental groups from our 12-week smoke model-2. We observed a reduction in the cristae density and cristae volume (P<0.05) in the smoke (12wks) group (Figure 4.19B) in comparison to the air group (Figure 4.19A).

Both the cristae density (P<0.01) and cristae area (P<0.001) were increased in the treatment group of smoke (12wks) NRPT (4wks) (Figure 4.19C) with respect to the smoke (12wks) group. In contrast, we did not observe any significant difference in the cristae volume across all the experimental groups in the 12-week smoke model-2.

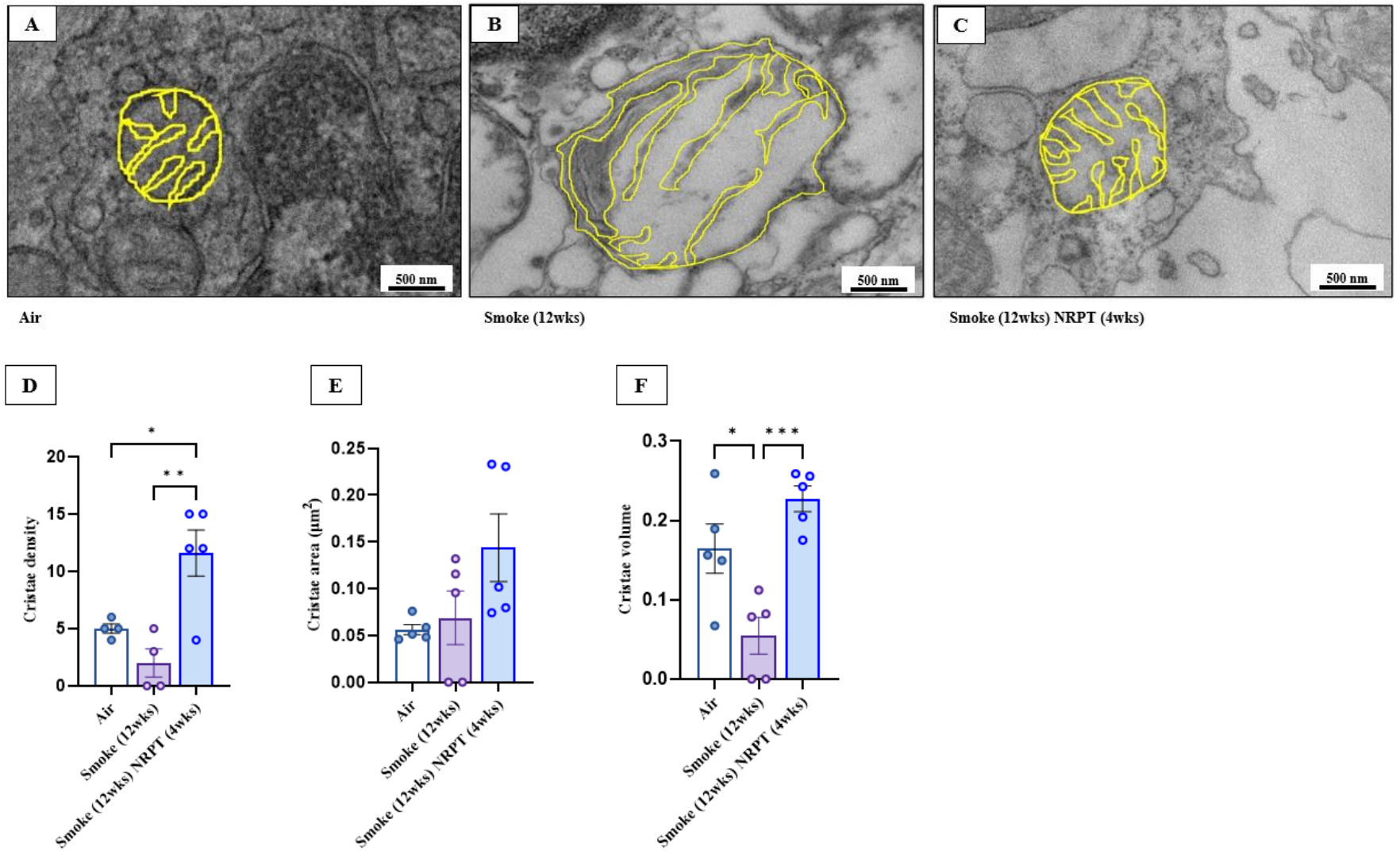

Figure 4.19: Administration of NR and PT restored mitochondrial cristae structure in advanced COPD:

*Representative cristae structure images (A) Air (B) Smoke (12wks), (C) Smoke (12wks) NRPT (4wks); Graphical representation of (D) cristae structure, (E) cristae volume, (F) cristae volume. Data represented are means ± SEM of 5 mice/group, * P<0.05, ** P<0.01, *** P<0.001, **** P<0.0001.*

4.3.18 Administration of NR and PT restored mitochondrial function in advanced COPD

We measured the protein expression level of complex I-NDUFB8 (Figure 4.20A), complex II-SDHB (Figure 4.20B), complex III-UQCRC2 (Figure 4.20C), complex IV-MTCO1 (Figure 4.20D), and complex V-ATP5A (Figure 4.20E) using the lung samples from 12-week smoke model-2. A reduction was observed in the protein levels of complex I, II, III, IV and V both in the smoke (12wks) group in comparison to the air group (P<0.05) and was further increased in the treatment group of smoke (12wks) NRPT (4wks) as compared to the smoke (12wks) group (P<0.05).

Furthermore, we measured mitochondrial respiratory chain enzymatic activities in lung homogenates for complex I (Figure 4.20F), complex IV (Figure 4.20G), citrate synthase (Figure 4.20H) and β-HAD (Figure 4.20I). We observed a reduction in the activity of complex I, IV, citrate synthase, and β-HAD in the smoke (12wks) group as well as the smoke (8wks) rest (4wks) group in comparison to the air group (P<0.05). We observed an increase in the activity of complex I, IV and citrate synthase in the treatment group of smoke (12wks) NRPT (4wks) in comparison to the smoke (12wks) group (P<0.05), however, there was no change in the β-HAD activity in the smoke (12wks) NRPT (4wks) group and remained reduced with respect to the air group (P<0.05).

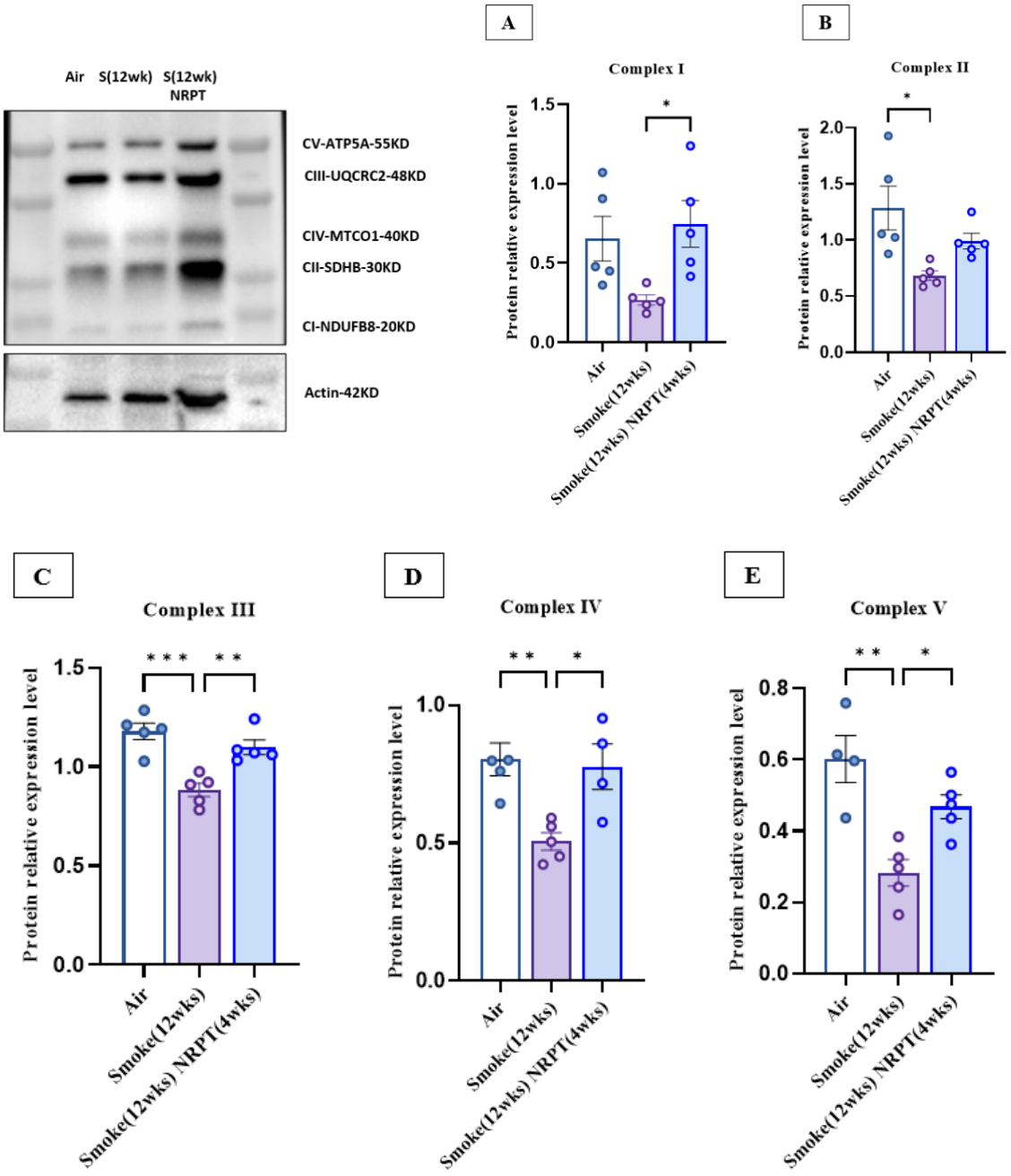
A
B
C
D
E
Air
S(12wk)
S(12wk) NRPT
CV-ATP5A-55KD
CIII-UQCRC2-48KD
CIV-MTCO1-40KD
CII-SDHB-30KD
CI-NDUFB8-20KD
Actin-42KD
Complex I
Complex II
Complex III
Complex IV
Complex V
Protein relative expression level
Air
Smoke(12wks)
Smoke(12wks) NRPT(4wks)

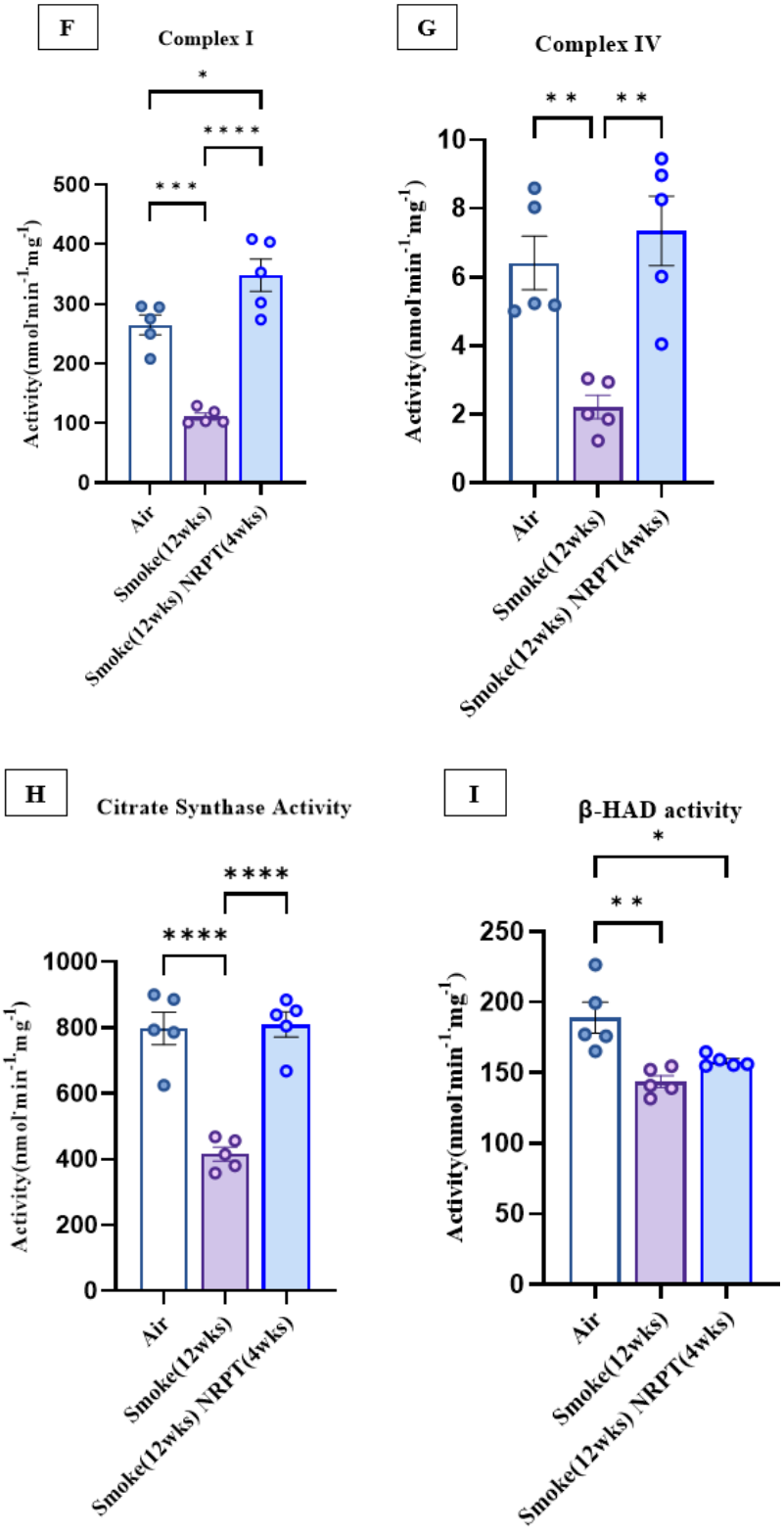

Figure 4.20: Administration of NR and PT promoted mitochondrial function in advanced COPD:

*Mitochondrial respiratory chain enzymatic activity of (A) Complex I, (B) Complex II, (C) Complex III, (D) Complex IV, (E) Complex I+III, (F) Complex II+III, (G) Citrate synthase (H) β-HAD; Protein expression of (I) Complex I-NDUFB8, (J) Complex II-SDHB, (K) Complex III-UQCRC2, (L) Complex IV-MTCO1, (M) Complex V-ATP5A; Data represented are means ± SEM of 5 mice/group, * P<0.05, ** P<0.01, *** P<0.001, **** P<0.0001.*

4.3.19 Administration of NR and PT restored mitochondrial membrane potential in advanced COPD

ΔΨm was determined with JC1 staining on lung sections as mentioned previously. The MFI of J-aggregates were reduced in the smoke (12wks) group in comparison to the air group (P<0.05) and was increased in the smoke (12wks) NRPT (4wks) group with respect to the smoke (12wks) group (P<0.001) (Figure 4.21A). Further, J-monomers increased in the smoke (12wks) group (P<0.0001) as well as smoke (12wks) NRPT (4wks) (P<0.001) with respect to the air group. This was significantly reduced in the smoke (12wks) NRPT (4wks) group in comparison to the smoke (12wks) group (P<0.0001) (Figure 4.21B). Moreover, the ΔΨm was reduced significantly in the smoke (12wks) in comparison to the air group (P<0.0001) which was increased in the smoke (12wks) NRPT (4wks) group with respect to the smoke (12wks) group (P<0.0001) (Figure 4.21C).

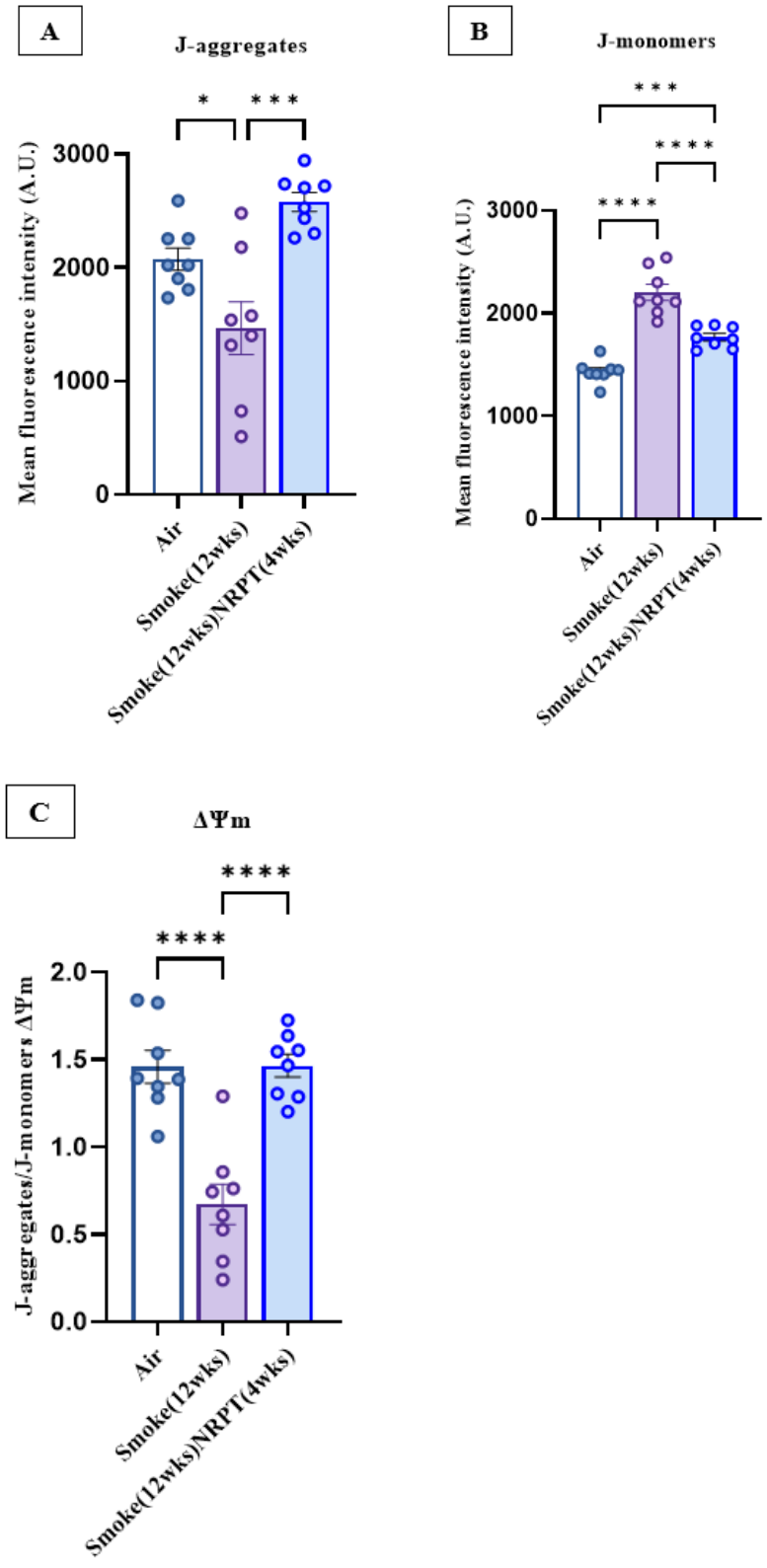
A
J-aggregates
Mean fluorescence intensity (A.U.)
3000
2000
1000
0
*
***
Air
Smoke(12wks)
Smoke(12wks)NRPT(4wks)
B
J-monomers
***
****
****
Mean fluorescence intensity (A.U.)
3000
2000
1000
0
Air
Smoke(12wks)
Smoke(12wks)NRPT(4wks)
C
ΔΨm
****
****
J-aggregates/J-monomers ΔΨm
2.0
1.5
1.0
0.5
0.0
Air
Smoke(12wks)
Smoke(12wks)NRPT(4wks)

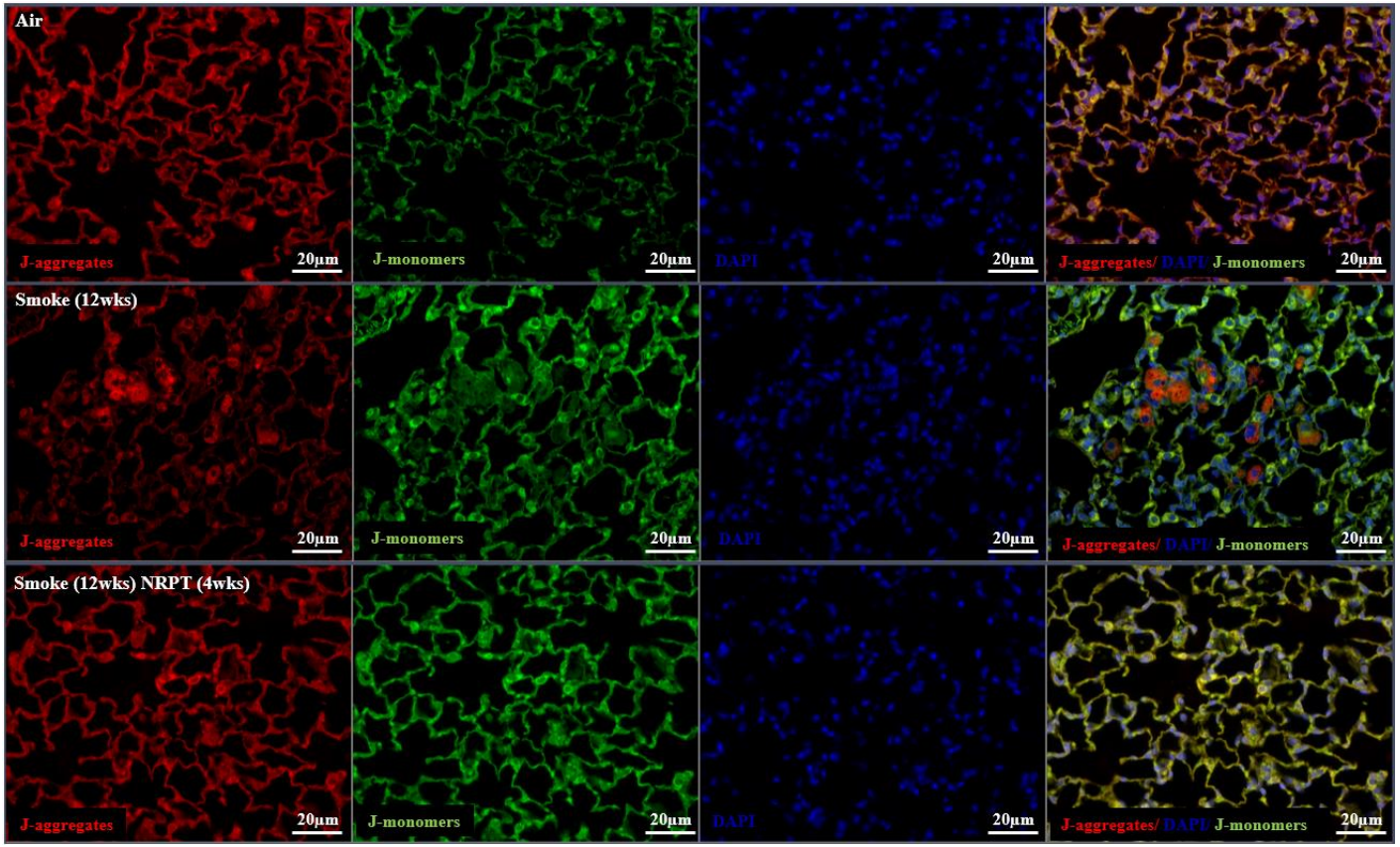

Figure 4.21: Administration of NR and PT restored mitochondria membrane potential in advanced COPD:

Measure of mitochondrial membrane potential (A) J-aggregates, (B) Reduced J-monomers (P<0.05), and (C) increased in the ΔΨm in smoke NR and PT group as compared to the smoke group (P<0.05). Data represented are means ± SEM of 8 mice/group, * *P*<0.05, ** *P*<0.01, *** *P*<0.001, **** *P*<0.0001.

4.3.20 Administration of NR and PT reduced oxidative stress in advanced COPD

We observed an increase in the gene expression of NOX2 in the smoke (12wks) group as well as the smoke (12wks) NRPT (4wks) group in comparison to the air group ($P<0.0001$) (Figure 4.22A). In addition, the gene expression for HO1 was reduced in the smoke (12wks) NRPT (4wks) group with respect to the air group ($P<0.01$) (Figure 4.22B). Additionally, we observed an increase in the MFI for 4-HNE via IF in the smoke (12wks) group in comparison to the air group ($P<0.0001$) which was reduced in the treatment groups of smoke (12wks) NRPT (4wks) with respect to the smoke (12wks) group ($P<0.0001$). Images below represent 4-HNE (FITC) co-stained with F4/80 (Texas red) and DAPI (Figure 4.22C).

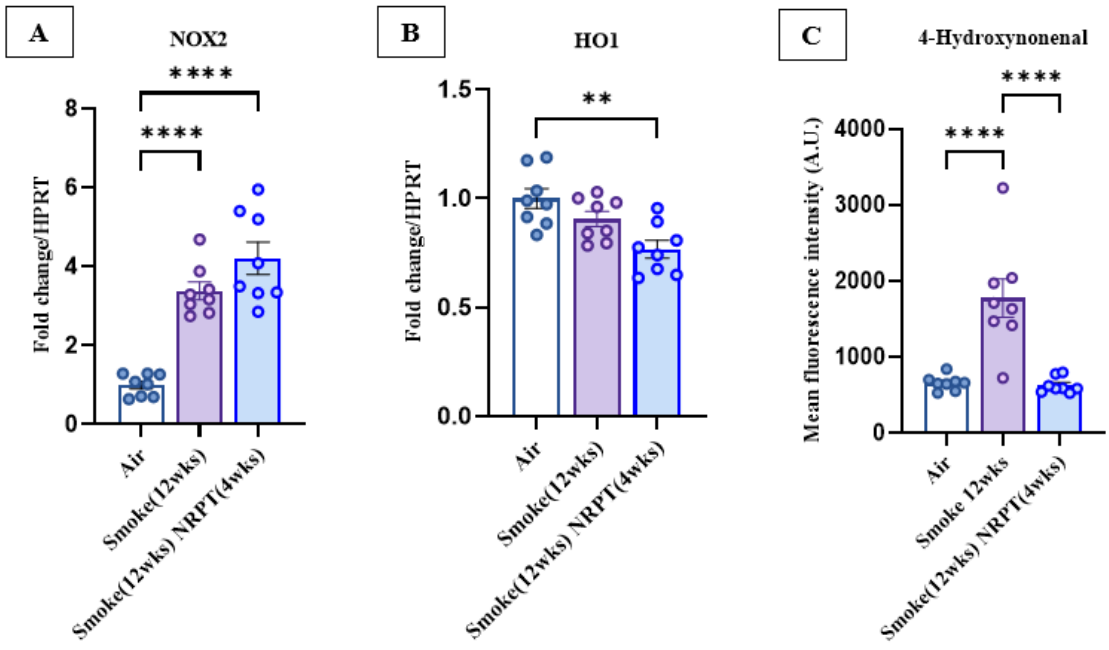

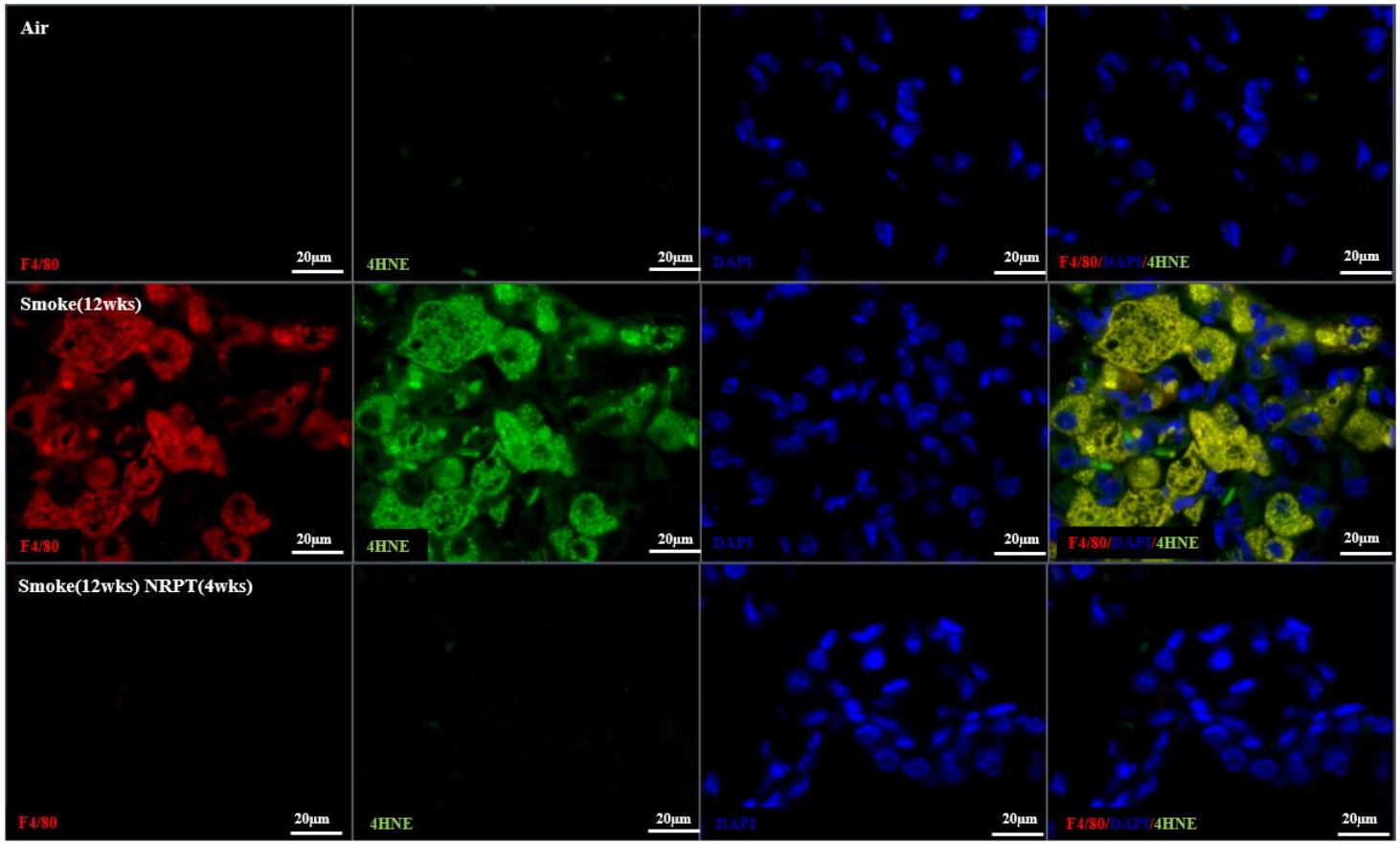

Figure 4.22: Administration of NR and PT reduces oxidative stress in COPD:

*Gene expression of (A) NOX2 and (B) HO1, (C) Graphical representation of MFI in arbitrary units (A.U.) of reduced 4-HNE levels in smoke NR and/or PT in comparison to smoke group (P<0.0001), images show fluorescence localisation of F4/80 (red), 4-HNE (green), DAPI-nuclei stain (blue); Data represented are means ± SEM of 8 mice/group, * P<0.05, ** P<0.01, *** P<0.001, **** P<0.0001.*

4.4 Discussion

The objective of the current study was to delineate the therapeutic effects of NR and PT in delaying the progression of COPD, as well as reversing COPD upon cessation of smoking in combination with NR and PT administration. Our previous study (Chapter 3) demonstrated improvements in COPD features in an 8-week prophylactic study following treatment with NR and/or PT. which is reflective of the early stages of the disease. Consequently, we aimed to investigate the therapeutic benefits of NR and PT in the advanced stages of the disease using a 12-week prophylactic COPD model, whereby NR and PT were administered throughout the whole 12 weeks of CS exposure. Simultaneously, we also used a therapeutic COPD model whereby NR and PT were administered in a completely developed disease state with and without cessation of smoke.

Our findings from this study showed increased airway inflammation in a 12-week CS-induced COPD murine model which was characterised by an increased number of cellular infiltrates in the lung. We observed a significant reduction of cellular infiltration upon the administration of NR and PT in all the different treatment conditions (Figures 4.3 & 4.13). Furthermore, we observed an increase in the gene expression of TNFα and CXCL1 during the advanced stages of the disease as reflected in our 12-week smoke exposure. A reduced gene expression for both TNFα and CXCL1 was observed in all the different treatment groups of NR and PT with respect to the smoke-exposed groups. Together, these results validated the anti-inflammatory response of NR and PT in reducing airway inflammation in COPD which was previously demonstrated in chapter 3. Corticosteroids have been commonly used as anti-inflammatories in COPD (359), however, they are limited in their efficacy during the early stages of the disease (360) with the cessation of smoke (361), and fail to protect from inflammation during the advanced stages of the disease (362).

Our data suggested that NR and PT reduced airway inflammation in advanced stages of COPD with or without cessation of smoke. NR and PT have been known to ameliorate TNFα levels *in vitro* ALS (amyotrophic lateral sclerosis) model (363) but currently, there is no such evidence in COPD. Henceforth, it is interesting that the administration of dietary modulators NR and PT reduced airway inflammation during the advanced stages of COPD.

In addition, we validated COPD features such as collagen deposition leading to airway remodelling, alveolar destruction or emphysema, and lung function changes in this study. We observed an increase in collagen deposition and emphysema upon chronic CS exposure for both 8 and 12 weeks which did not reduce upon cessation of smoke in the smoke (8wks) rest (4wks) group. This was not surprising as it has been known that the cessation of smoke may terminate the progression of structural damages in COPD, however, does not revert the existing damages in the lung (364, 365). Interestingly, both features of airway remodelling and emphysema were reduced in all the treatment groups of smoke NRPT (12wks), smoke (8wks) NRPT (4wks), and smoke (12wks) NRPT (4wks) (Figure 4.4 & 4.14). Furthermore, we observed an increase in the lung function parameters of IC, area, and TLC in both the smoke (12wks) group as well as smoke (8wks) rest (4wks) reflecting the impaired lung function in COPD. Interestingly, we observed a reduction in the parameters of IC and area in the smoke (8wks) NRPT (4wks) in comparison to the smoke (8wks) rest (4wks), which reflected that administration of NR and PT along with the cessation of smoke is protective of impaired lung function in COPD. Additionally, we observed a reduction in IC and TLC in the smoke (12wks) NRPT (4wks) in comparison to the smoke (12wks) group indicating that treatment with NR and PT even without the cessation of smoke restored impairment of lung function in COPD. However, lung function parameters did not improve in the smoke NRPT (12wks), this

was an interesting observation and may reflect a limitation due to the prolonged administration of NR and PT in COPD. Collectively, these results suggested that 4 weeks of administration of NR and PT is beneficial in reducing and reversing COPD features during advanced disease stages with or without cessation of smoke. This is surprising as until recently, cessation of smoke was the only known intervention in delaying the progression of the disease (366-368) but did not protect from lung function impairment (369-371). Recent studies have also shown that smoke cessation does not improve bronchoconstriction and spirometry in COPD patients (372, 373). Our data demonstrated that administration of NR and PT with or without cessation of smoke reversed damage in the lung structure and protected from impaired lung function during advanced COPD stages.

Previously in chapter 3, we demonstrated that the constant cycle of damage and repair during inflammation in COPD is dependent on the balance of NAD^+ and NADH. Chronic CS exposure resulted in NAD^+ depletion and a reduction in the ratio of NAD^+/NADH in the smoke (12wks) groups as well as in smoke (8wks) rest (4wks) (Figure 4.5). Moreover, we observed an improvement in the ratio of NAD^+/NADH due to the cessation of smoke in the smoke (8wks) rest (4wks) group and was further improved when subjected to NRPT treatment in the smoke (8wks) NRPT (4wks) as well as the in the smoke (12wks) NRPT (4wks) group (Figure 4.15). However, prolonged administration of NR and PT for 12 weeks did not show an increase in the NAD^+/NADH balance in COPD. These results further suggested limited benefits of NR and PT over prolonged administration as previously also observed in the measure of lung function parameters. In addition, these findings also suggested that the 4 weeks administration of NR and PT with or without cessation of smoke is beneficial in protecting and restoring the NAD^+/NADH balance in COPD. This could be a potential adverse effect of high levels of NR and PT, as currently

there is a lack of understanding of the possible disadvantages of prolonged use of NR and PT and future studies will be required to understand the underlying mechanisms contributing to these effects.

The bioavailability of NAD^+ is important for the regulation of NAD consumers such as PARPs, CD38, and SIRTs. We have previously shown the hyperactivity of PARPs in our 8-week experimental COPD studies as a contributing factor in the depletion of NAD^+ during the progression of the disease in chapter 3. To substantiate our previous findings, we investigated the role of PARPs in 12-week COPD studies (Figure 4.6 & 4.16); the gene expression of PARP1 remained unchanged in all our experimental groups except for the smoke (12wks) NRPT (4wks) group which was reduced and is also reflected in the protein expression of PARP1. However, we observed an upregulation of PARP1 protein in the smoke (8wks) rest (4wks) group which was reduced upon the treatment in the smoke (8wks) NRPT (4wks) group. However, the gene and protein expression of PARP1 was inconclusive and hence we measured total PARP activity. We observed an increase in the PARP activity in smoke (12wks) which was further reduced in the smoke (8wks) rest (4wks) as well as the treatment groups of smoke (8wks) NRPT (4wks) and smoke (12wks) NRPT (4wks) but remained unchanged in the smoke NRPT (12wks). Taken together, these results suggested that there is an increased activity of PARPs in COPD which is reduced with the cessation of smoke, as well as in the short-term treatment of NRPT with or without cessation of smoke. PARPs are known to play an important role in regulating immune responses and cell survival (374, 375). As such, the hyperactivity of PARPs in COPD is likely due to increased DNA methylation and histone acetylation (376-378). Additionally, recent research evidence suggests that the inhibition of PARPs represents a promising therapeutic intervention for lung inflammatory diseases including acute lung injury (ALI), asthma, and COPD as well as cancer (329, 379).

Furthermore, we measured CD38 protein levels (Figures 4.6 & 4.16) and observed an upregulation in the smoke (12wks) and smoke(8wks) rest (4wks) which was reduced in all the NR and PT treatment groups. CD38 is highly expressed in macrophages resulting in increased NAD^+ consumption during inflammation (380). This further supports our findings suggesting the administration of NR and PT reduces inflammation which leads to the downregulation of CD38. However, future studies will be required to validate the CD38 enzyme activity levels in our study.

Moreover, we determined the role of SIRTs in our study as the third major NAD^+-dependent metabolic regulator of cellular stress (Figure 4.7 & 4.17). SIRT1 and SIRT7 are expressed in the nucleus and have been observed to downregulate in our smoke (12wks) group, in contrast, we observed an upregulation of SIRT1 and SIRT7 in the smoke (8wks) rest (4wks) group. Studies have previously shown that chronic exposure to smoke leads to damage in the nucleus causing apoptotic changes (381) which is potentially the cause of decreased nucleus-expressed SIRT1 and SIRT7. On the other hand, we observed an increase in the SIRT1, and SIRT7 upon administration of NR and PT both in the smoke NRPT (12wks) as well as smoke (12wks) NRPT (4wks), suggesting the important role of NR and PT in protecting the lung from damage caused during chronic exposure to CS. We also observed a decrease in the SIRT1 and 7 in the smoke (8wks) rest (4wks) which suggested a reduced immune response due to the cessation of smoke. This trend of expression is also followed by SIRT2 which is largely cytosolic but is capable of locating in the nucleus during cell division (mitosis) (382). Another nuclear-expressed member of this family is SIRT6 (383), in contrast to the above, we observed a downregulation in SIRT6 in both smoke (12wks) as well as smoke (8wks) rest (4wks), which did not improve with NR and PT administration in the smoke NRPT (12wks) and smoke (12wks) NRPT (4wks) but increased in the smoke (8wks) NRPT (4wks),

suggesting the anti-inflammatory roles of SIRT6 in our study. Furthermore, SIRT3, 4, and 5 are mitochondria-expressed members of this family (384), and we observed no change or decrease in their expression in all our smoke-exposed groups. SIRT3, 4 and 5 are involved in metabolic pathways in mitochondria and regulate enzymatic activities promoting ATP production and consumption (385-387). Hence no change or reduced expression of SIRT3, 4 and 5 is unsurprising as chronic exposure to CS potentially leads to increased ATP consumption. Taken together, these results suggest that an increase in PARPs in COPD, leads to a depletion in the NAD^+ pool, reducing the protective effects of SIRTs and CD38. The administration of NR and PT increases the availability of NAD^+, which leads to an increase in cellular defence mechanisms via increased SIRTs and CD38. Additionally, cessation of smoke promoted the protective role of PARPs, SIRTs and CD38 which was further improved with NR and PT treatment showing increased recovery in COPD features.

Previously, in our 8-week COPD study in chapter 3, we have shown that chronic exposure to CS leads to damage in the mitochondrial ultra-structure which was protected in our treatment groups of NR and/or PT. We further validated these changes in mitochondrial ultra-structure in our current study and observed a similar outcome, whereby chronic CS exposure induced damage in mitochondrial structure (Figures 4.8 & 4.18), and reduced cristae density, area and volume (Figures 4.9 & 4.19). Additionally, we also observed an increase in mitochondrial area or swelling in the smoke (12wks) group which is an indication of damage and a potential compensation during oxidative stress. Interestingly, our treatment groups of smoke NRPT (12wks), smoke (8wks) NRPT (4wks) and smoke (12wks) NRPT (4wks) protected mitochondrial ultrastructure from acquiring damage induced due to chronic CS exposure via exhibiting reduced mitochondrial area, increased cristae density, area and volume. This is interesting, as mitochondrial dysfunction

associated with COPD is largely contributed by oxstress (175, 388), production of ROS (389, 390), autophagy (347, 391) and apoptosis (392, 393) which leads to the structural as well functional deterioration of the mitochondria. Administration of NR and PT could be of potential benefit in the restoration of mitochondrial structure and function in COPD. Furthermore, recent evidence suggested that reduced mitochondrial function has been observed in COPD patients (336, 394, 395). This is also reflected in our previous 8-week COPD studies, and in our current 12-week study where we observed reduced mitochondrial complex proteins as well as reduced complex activity in the smoke (12wks) group. In addition, the mitochondrial complex protein levels did not increase after the cessation of smoke in the smoke (8wks) rest (4wks) group, suggesting reduced mitochondrial function. Administration of NR and PT in all our groups of smoke NRPT (12wks), smoke (12wks) NRPT (4wks) and smoke (8wks) NRPT (4wks) increased both the activity levels as well as the total protein levels of mitochondrial complex proteins (Figure 5.10 & 5.20). Previous studies have shown PT in combination with various mitochondrial cofactors has the potential to improve mitochondrial function *in vitro (396)*. NR can boost NAD^+ levels which improves mitochondrial function (263). This evidence further supported our findings of increased mitochondrial function with NR and PT treatment in COPD. To further validate mitochondrial health, we measured mitochondrial membrane potential. We observed a reduced membrane potential in the smoke (12wks) group which was improved with the cessation of smoke in the smoke (8wks) rest (4wks) and was further increased with the NR and PT treatments in all the groups of smoke NRPT (12wks), smoke (8wks) NRPT (4wks), and smoke (12wks) NRPT (4wks) (Figure 4.11 & 4.21). These findings further validate the efficacy of NR and PT in promoting mitochondrial function. This is interesting, as there are currently no known

treatments for COPD which is capable of protecting the mitochondrial structure and promoting mitochondrial function.

Oxstress has been associated with COPD as the driver of inflammation (312, 397, 398) and we have previously shown that NR and PT reduced oxidative stress in our 8-week COPD studies. To further validate this, we measured NOX2, HO1 and 4-HNE in our 12-week study (Figure 4.12 & 4.22). We observed an increase in oxidative stress following chronic CS exposure which was reflected in our smoke (12wks) group and interestingly was not reduced with the cessation of smoke in the smoke (8wks) rest (4wks) group. However, the administration of NR and PT in all the different treatment groups exhibited a reduction in oxidative stress which is supportive of our previous findings of increased mitochondrial function.

In conclusion, this study has demonstrated the therapeutic efficacy of NR and PT in the advanced stages of COPD both in halting the disease progression as well as reversing the disease features. Using our 12-week prophylactic COPD study with NR and PT, we have highlighted the benefits of reducing airway inflammation, and improvements in lung structure. Additionally, we have shown a reduction in oxidative stress which further improved the mitochondrial structure and function. However, prophylactic treatment with NR and PT for 12 weeks did not show improvements in impaired lung function as well as failed to increase total NAD^+ levels. As a consequence, we did not observe a reduction in PARP hyperactivity levels or an increase in SIRTs, suggesting that prolonged treatment with NR and PT might potentially have adverse effects on the progression of the disease. Furthermore, using our 12-week therapeutic COPD study with NR and PT with or without cessation of smoke, we have demonstrated that only 4 weeks of treatment reduced all the COPD features. In addition, we observed increased availability of NAD^+ to SIRTs and CD38, which further reduced PARP activity levels in 4 weeks of treatment using NR and

PT. This further improved the structure and function of mitochondria and reduced oxidative stress, suggesting prospective therapeutic interventions that may promote COPD resolution.

We have also exhibited the benefit of cessation of smoke in reducing airway inflammation and oxidative stress as well as increasing citrate synthase activity and mitochondria membrane potential. However, damage to the lung structure and impaired lung function persisted with the cessation of smoke. In addition, we did not observe mitochondrial structure and function with cessation of smoke, suggesting that additional treatments are required upon smoke cessation to reverse the damage in COPD. Our findings with NR and PT treatment will be further validated in future studies using human COPD clinical specimens such as broncho epithelial cells as well as macrophages obtained from bronchoalveolar lavage of COPD patients prior to implementation in pre-clinical human trials.

Chapter 5. Therapeutic targeting of NAD^+ modulation in COPD using overexpressed NMNAT1 and NMNAT3 *in vivo*

5.1 Nicotinamide mononucleotide adenyl transferases (NMNATs) isoforms

NAD^+ metabolism encompasses various cellular energetic pathways involved in inflammation and metabolism that are essential for cell survival (399, 400). NAD^+ is tightly regulated by various enzymes such as NMNATs (401), NAM (400, 402), and NAMPT (403) which are involved in the NAD^+ biosynthesis and consumption pathways (225, 404). The NAD^+ biosynthesis pathway initiates with the uptake of the essential amino acid L-tryptophan from dietary sources following the *de novo* biosynthesis pathway (405, 406). Alternatively, NAM and NR, also obtained from dietary sources can synthesise NAD^+ via the salvage and the Preiss-Handlers pathway (406, 407). NMNATs are essential enzymes involved in catalysing the key reaction in the conversion of NMN to NAD^+ (401, 408, 409). NMNATs have three different isoforms with distinct molecular and catalytic properties (410, 411) (Figure 5.1). Each isoform is essential for cell survival and plays a critical role in modulating NAD^+ levels in a compartment-specific manner (412-414). NMNAT1 is localised to the nucleus (415, 416), NMNAT2 in the cytosol (417, 418) and NMNAT3 is localised to the mitochondria (419, 420) (Figure 5.1). Additionally, each NMNAT isoform is responsible for supplying NAD^+ to specific NAD^+-dependent enzymes such as PARPs (421), SIRTs (422, 423), and/or CD38 (422, 424), thus regulating their activity with an impact on several biological processes such as DNA repair (425), proteostasis (426), cellular differentiation (425) as well as neuronal maintenance (427). Importantly, NMNATs can replenish NAD^+ levels during the inflammatory activation of immune cells, thereby reducing inflammation. Studies have

shown that deletion of individual genes for NMNAT1-3 in mice is neonatal lethal (428-430), highlighting that the three isoforms are unable to compensate for each other (430, 431). To date, there is limited evidence available on NAD^+ biosynthesis for each NMNAT isoform. However, recent studies have largely focused on targeting NMNAT activity to understand the pathogenesis of various chronic diseases (432) such as cancer (408), diabetes (433) as well as aging (434).

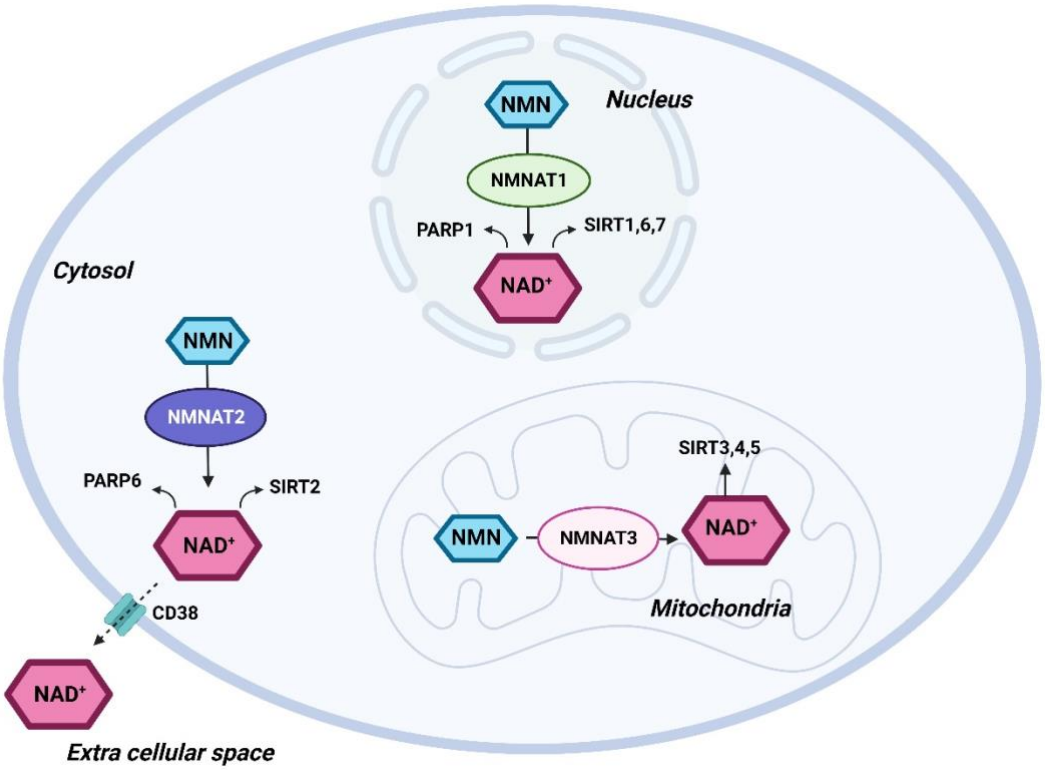

Figure 5.1: NMNAT isoforms

The schematic diagram shows the subcellular compartmentalisation of the three different isoforms of NMNAT highlighting their functional interaction with NAD^+-consuming enzymes. NMNAT1 is localised in the nucleus and provides NAD^+ to PARP1, SIRT1, SIRT6 and SIRT7. NMNAT2 is in the cytosol and functionally interacts with PARP6, SIRT2 and CD38. NMNAT3 is localised in the mitochondria and provides NAD^+ to SIRT3, SIRT4 and SIRT5.

5.1.1 Generation of transgenic NMNAT1 and NMNAT3 overexpressed mice

NMNAT1 and NMNAT3 overexpressing transgenic mouse lines were obtained from Professor Nigel Turner (University of New South Wales, Sydney, Australia). The generation of NMNAT1 and NMNAT3 transgenic mice was previously described by Naoki *et.al* 2009 (435).

5.1.2 Study rationale

In the previous study (Chapter 3), we demonstrated that chronic exposure to CS for 8 weeks leads to an imbalance in NAD^+/NADH levels. This imbalance in NAD^+ level is likely induced by the overactivation of PARPs and reduction in SIRTs. As a consequence, there is an increase in immune cell infiltration in the lung causing further damage to the lung structure and function in our CS-induced COPD mouse model.

The dietary modulators NR and PT in the CS-induced COPD murine model reduced airway inflammation, leading to improvements in lung structure and function in the prophylactic COPD study. Additionally, we have also demonstrated the therapeutic efficacy of NR and PT in the advanced stages of COPD both in halting the disease progression as well as reversing the disease features (Chapter 4). Currently, there is no evidence of the mechanisms involved in the restoration of NAD^+ imbalances in the COPD model following NR and PT administration. As NMNATs are involved in the final catalysis of NMN to NAD^+, therefore, we investigated the benefits of NMNAT1 and NMNAT3 in COPD using transgenically overexpressed mice in comparison to the treatment with NR and PT. Critically, we also investigated if the administration of NR

and PT in overexpressed NMNAT1 and NMNAT3 mice had additional benefits from the development of COPD.

5.2 Methodology

5.2.1 Experimental COPD model

Female NMNAT1 and NMNAT3 overexpressing mice along with WT littermate controls, aged 6-8 weeks were provided by Prof Nigel Turner at the University of New South Wales (UNSW), Australia. Mice were maintained at 20 ± 2°C on a 12:12 hours day-night cycle and fed a standard sterile diet of mouse chow with water allowed *ad libitum* during an acclimatisation period of 7 days before experimental procedures as previously described (Section 2.2.1).

5.2.2 Experimental procedure

Following our previously mentioned protocol, mice were subjected to CS/Air exposure from up to 12 research-grade 3R4F cigarettes (University of Kentucky) twice a day, five days a week for 8 weeks using a custom-designed nose-only inhalation system as mentioned previously described (Section 2.2.2)(146).

5.2.3 Experimental designs

This current study involved two 8-week smoke models using NMNAT1 and NMNAT3 overexpressing mice, subjected to an administration of 400 mg/kg of NR in drinking water, and 80 mg/kg of PT in mushy chow provided *ad libitum* followed by smoke exposure as described in 5.2.2 (Figure 5.2A & B).

Figure 5.2: Experimental design of NMNAT1/3 overexpressed mice:

Mice were subjected to nose-only CS exposure to 12 cigarettes, twice a day, five days a week and were treated with 400 mg/kg of NR added to drinking water and 80 mg/kg of PT added to mushy chow for (A) WT/ NMNAT1 8-week COPD study and (B) WT/ NMNAT3 8-week experimental COPD study.

5.2.4 Experimental groups

The different experimental groups in the WT/NMNAT1 and WT/NMNAT3 8-week COPD study are listed below in Tables 5.1 and 5.2. All control groups for WT/NMNAT1 and WT/NMNAT3 air and smoke were fed with untreated water and standard chow. The treatment groups for both WT/NMNAT1 and WT/NMNAT3 air and smoke were subjected to 400 mg/kg of NR in drinking water and 80 mg/kg of PT in mushy chow in combination as mentioned below.

Table 5.1: Experimental groups of the WT/NMNAT1 8-week COPD study

Experimental groups	Smoke exposure	Treatments
WT Air	-	-
WT Smoke	12 cigarettes, 2x/day, 5x/week for up to 8 weeks	-
WT Smoke NRPT	12 cigarettes, 2x/day, 5x/week for up to 8 weeks	400 mg/kg of NR in drinking water and 80 mg/kg of PT in mushy chow
NMNAT1 Air	-	-
NMNAT1 Smoke	12 cigarettes, 2x/day, 5x/week for up to 8 weeks	-
NMNAT1 Smoke NRPT	12 cigarettes, 2x/day, 5x/week for up to 8 weeks	400 mg/kg of NR in drinking water and 80 mg/kg of PT in mushy chow

Table 5.2: Experimental groups of the WT/NMNAT3 8-week COPD study

Experimental groups	Smoke exposure	Treatments
WT Air	-	-
WT Smoke	12 cigarettes, 2x/day, 5x/week for up to 8 weeks	-
WT Smoke NRPT	12 cigarettes, 2x/day, 5x/week for up to 8 weeks	400 mg/kg of NR in drinking water and 80 mg/kg of PT in mushy chow
NMNAT3 Air	-	-
NMNAT3 Smoke	12 cigarettes, 2x/day, 5x/week for up to 8 weeks	-
NMNAT3 Smoke NRPT	12 cigarettes, 2x/day, 5x/week for up to 8 weeks	400 mg/kg of NR in drinking water and 80 mg/kg of PT in mushy chow

5.3 Results

5.3.1 Administration of NR and PT in COPD promoted increased expression of NMNAT1 and NMNAT3

The gene expression of NMNAT1/2/3 was measured using lung RNA of WT BALB/C mice from previous studies of chapters 3 and 4. We observed a reduction in the gene expression of NMNAT1/2/3 in the smoke group (Figure 5.3A-C) in comparison to the air group ($P<0.05$). A significant increase in the gene expression of NMNAT1/2/3 in the smoke NRPT group was observed as compared to the smoke group ($P<0.0001$). The gene expression of NMNAT1 and NMNAT3 was reduced in the smoke (12wks) group in comparison to the air group ($P<0.05$) (Figure 5.3D-I). Further, we observed an increase in NMNAT1/3 gene expression in the smoke (8wks) rest (4wks) ($P<0.001$), smoke (8wks) NRPT (4wks) ($P<0.0001$) and smoke (12wks) NRPT (4wks) ($P<0.01$) as compared to the smoke (12wks). Additionally, there was an increase in the gene expression of NMNAT3 in the smoke NRPT (12wks) in comparison to the smoke (12wks) group ($P<0.05$).

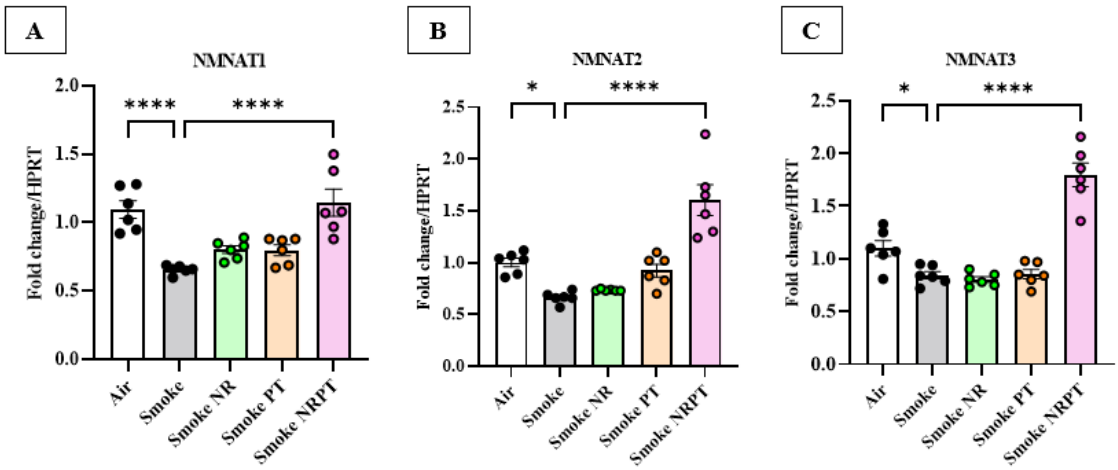

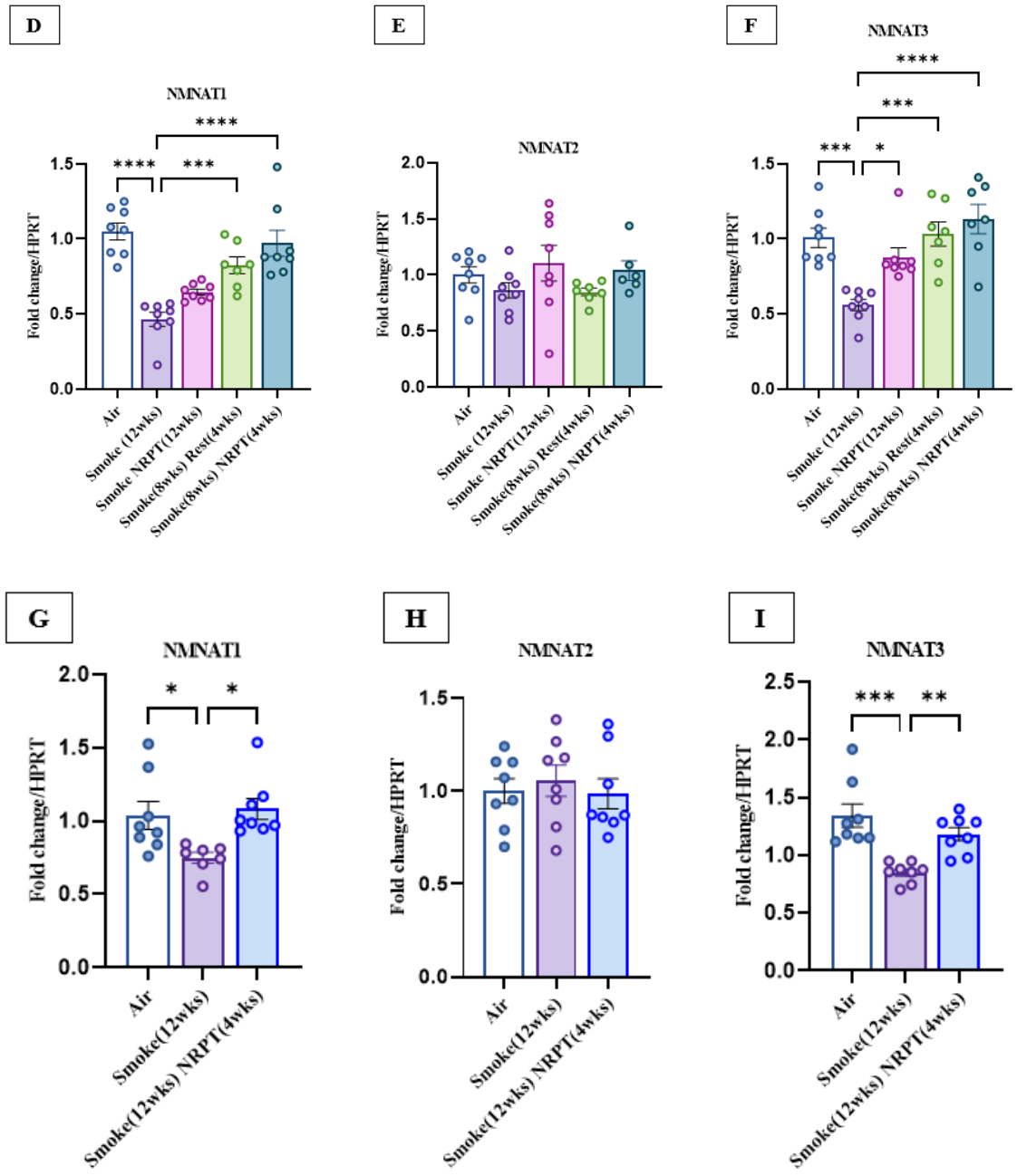

Figure 5.3: Administration of NR and PT increased the gene expression of NMNAT1 and NMNAT3:

The gene expression in 8-week COPD study with NR and/or PT (A) NMNAT1, (B) NMNAT2, (C) NMNAT3; The gene expression in 12-week advanced COPD study with NR and PT (D) NMNAT1, (E) NMNAT2, (F) NMNAT3; The gene expression in 12-week advanced COPD study without cessation of smoke (G) NMNAT1, (H) NMNAT2, (I)

*NMNAT3. Data represented are means ± SEM of 6-8 mice/group, * P<0.05, ** P<0.01, *** P<0.001, **** P<0.0001.*

5.3.2 Overexpression of NMNAT1 reduced inflammation in COPD

There were an increase in the number of total leukocytes (Figure 5.4A), macrophages (Figure 5.4B) and neutrophils (Figure 5.4C) in the BAL from the WT smoke group as compared to the WT air group (P<0.0001). Further, there was a reduced number of total leukocytes, macrophages and neutrophils in the WT smoke NRPT group and NMNAT1 smoke group in comparison to the WT smoke group (P<0.0001).

The body weight of all the experimental groups in the NMNAT1 study was monitored daily as mentioned previously in 5.2.3. There was a significant difference in weight observed between the WT air group and the WT smoke group as well as the NMNAT1 air group and the NMNAT1 smoke group (P<0.05) (Figure 5.4D).

Additionally, we observed an increase in the gene transcripts for TNFα (Figure 5.4D) in the WT smoke group in comparison to the WT air group (P<0.0001). A reduction in the expression of TNFα was observed in the WT smoke NRPT group and the NMNAT1 smoke group in comparison to the WT smoke group (P<0.0001). However, we also observed an increase in the gene expression of TNFα in the NMNAT1 smoke group as compared to the NMNAT1 air group (P<0.001). Similarly, the gene expression of CXCL1 (Figure 5.4E) increased in the WT smoke group in comparison to the WT air group (P<0.0001). Further, a reduction in the gene expression of CXCL1 was observed in the WT smoke NRPT group as well as the NMNAT1 smoke group in comparison to the WT smoke group (P<0.0001).

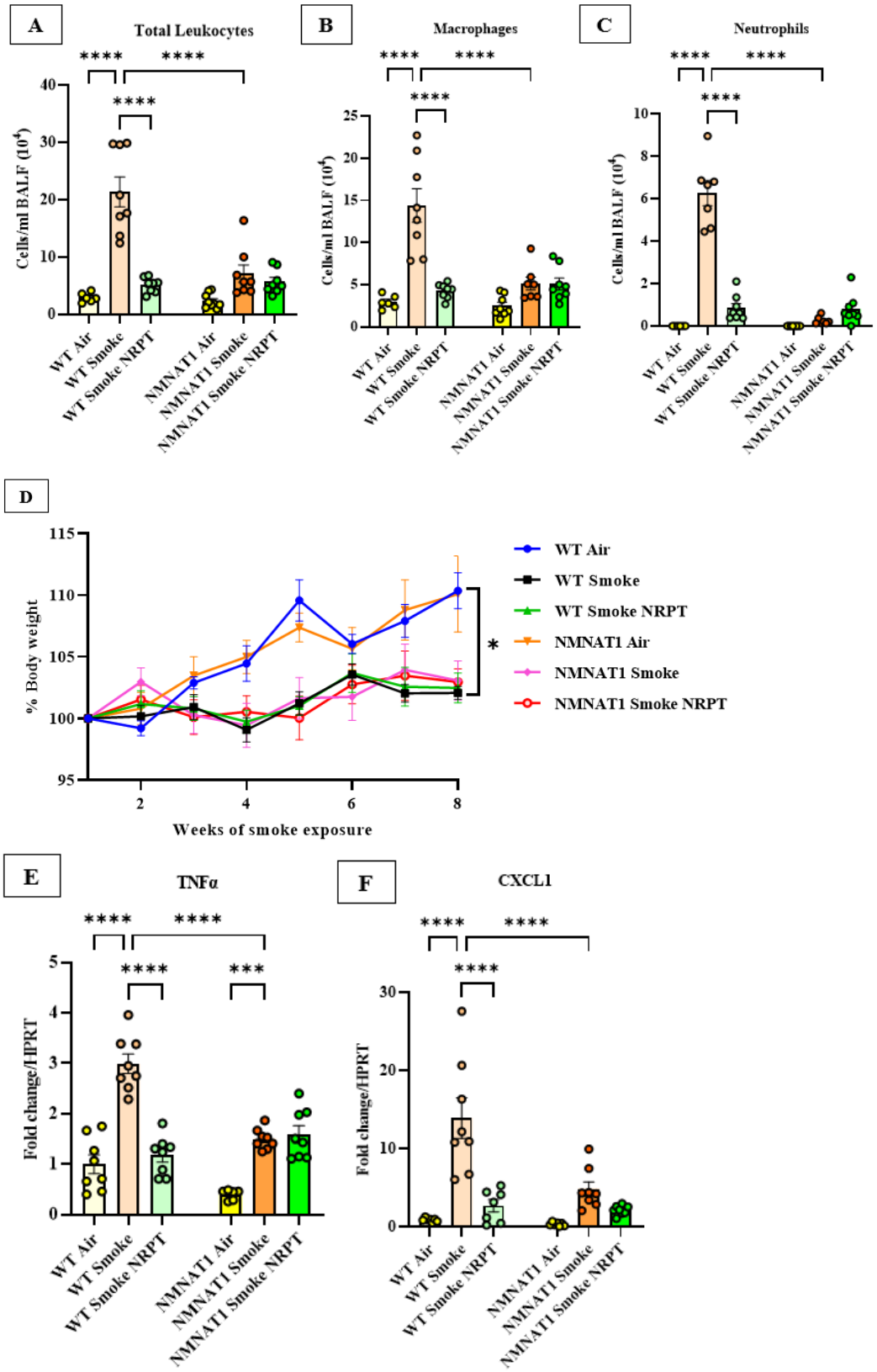

Figure 5.4: NMNAT1 overexpression reduced airway inflammation in COPD:

Graphical representation of (A) total cellular infiltrates in the BAL, (B) macrophages, (C) neutrophils; (D) Graphical representation of body weight; Gene expression of (E)

*TNFα and (F) CXCL1 in the lung. Data represented are means ± SEM of 6-8 mice/group, * P<0.05, ** P<0.01, *** P<0.001, **** P<0.0001.*

5.3.3 Overexpression of NMNAT1 protected from airway remodelling and emphysema in COPD

We observed an increase in the thickness of collagen deposition in the WT smoke group in comparison to the WT air group (P<0.0001). Additionally, we observed a reduction in the collagen deposition in the WT smoke NRPT group and NMNAT1 smoke group in comparison to the WT smoke group (P<0.0001) (Figure 5.5A).

We observed an increase in alveolar diameter with increased MLI counts for the WT smoke group in comparison to the WT air group (P<0.0001). The counts obtained from MLI analysis for the WT smoke NRPT group and the NMNAT1 smoke group were reduced in comparison to the WT smoke group (P<0.0001) (Figure 5.5B). Representative images of the alveolar diameter of each experimental group are displayed below in Figure 5.5B.

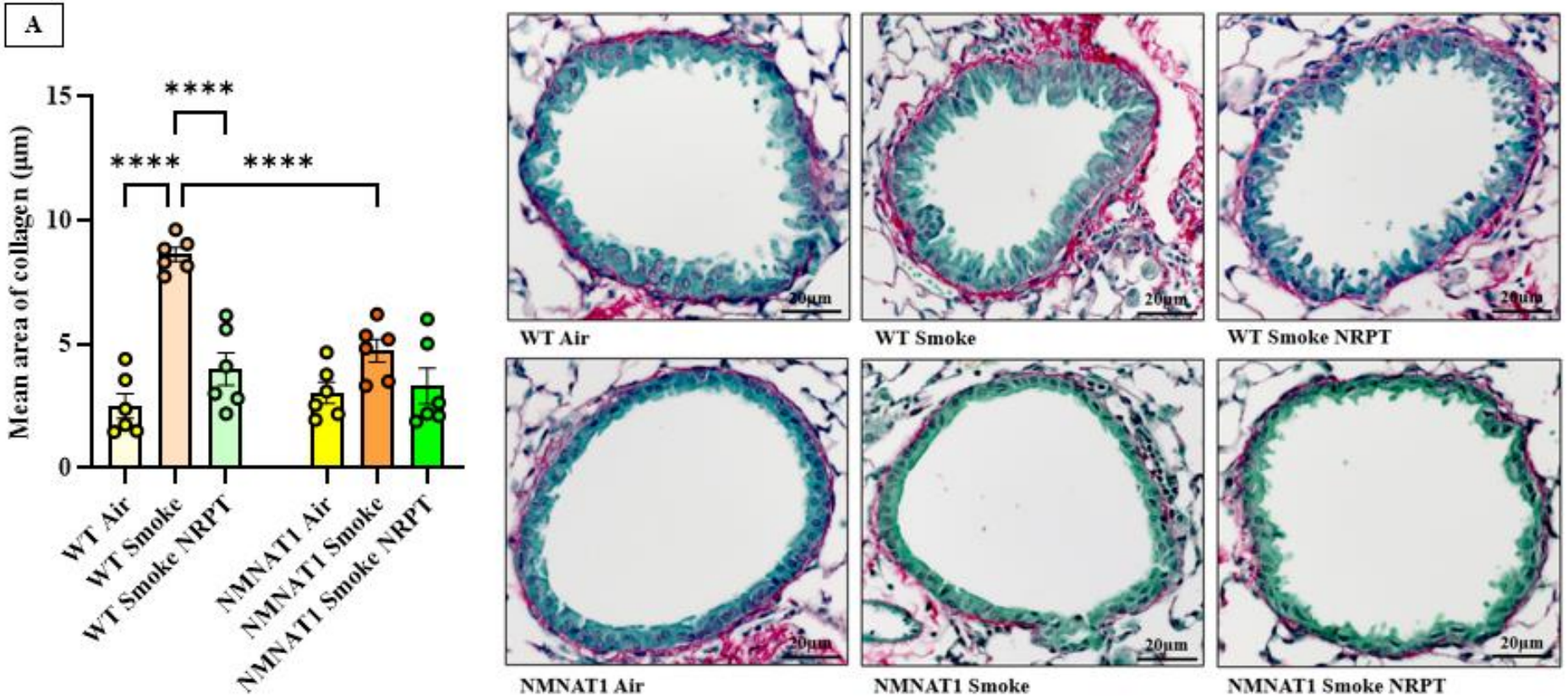
A
Mean area of collagen (µm)
15
10
5
0
****
****
****
WT Air
WT Smoke
WT Smoke NRPT
NMNAT1 Air
NMNAT1 Smoke
NMNAT1 Smoke NRPT
20µm
WT Air
WT Smoke
WT Smoke NRPT
NMNAT1 Air
NMNAT1 Smoke
NMNAT1 Smoke NRPT

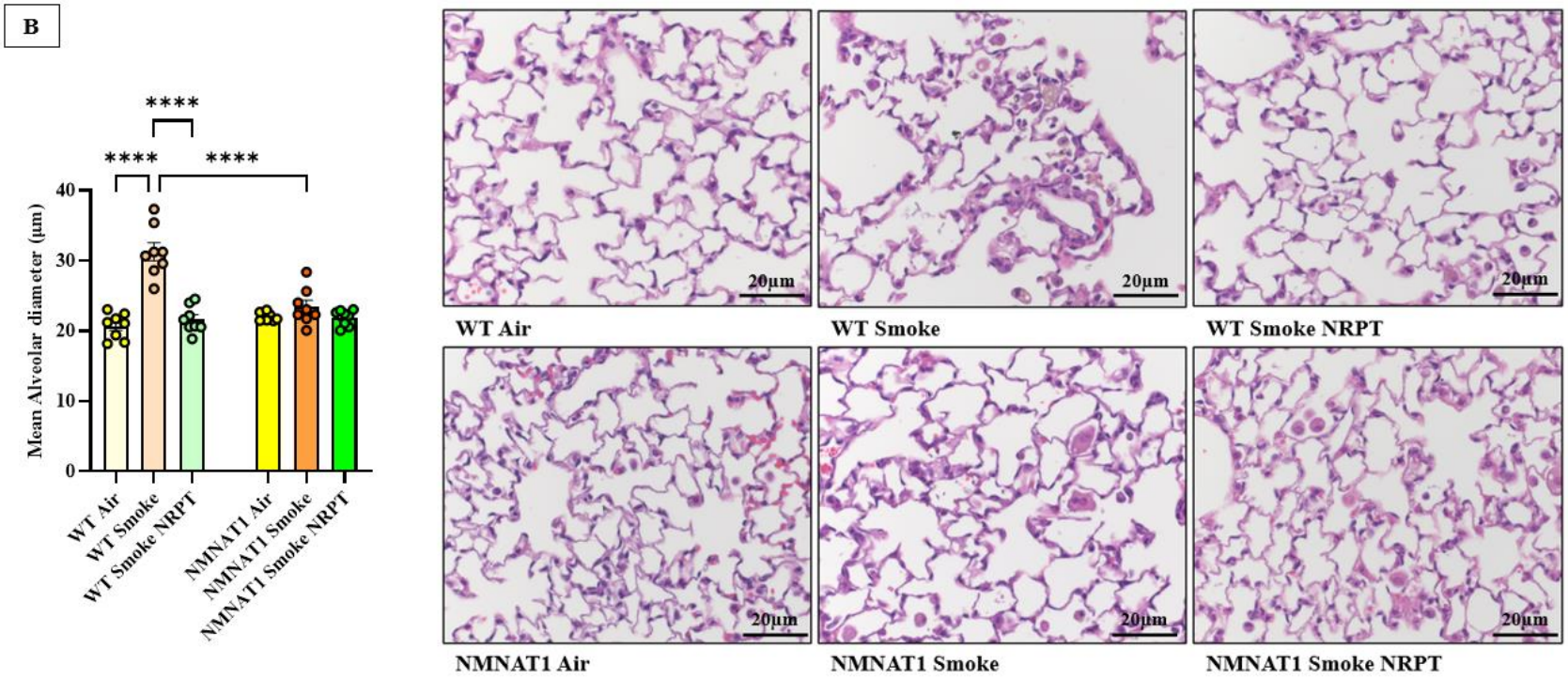

Figure 5.5: NMNAT1 overexpression protected from airway remodelling and emphysema in COPD:

*(A) Graphical representation of the mean area of collagen and representative images of airway remodelling (B) Graphical representation of MLI counts and representative images of emphysema. Data represented are means ± SEM of 6-8 mice/group, * P<0.05, ** P<0.01, *** P<0.001, **** P<0.0001.*

5.3.4 Overexpression of NMNAT1 protects from impaired lung function in COPD

Lung function parameters were measured for NMNAT1 overexpressed mice as mentioned previously. An increase in IC (Figure 5.6A) was observed in the WT smoke group in comparison to the WT air group ($P<0.05$). Similarly, an increase in IC was also observed in NMNAT1 smoke in comparison to the NMNAT1 air ($P<0.05$). In contrast, we observed an increase in IC in the NMNAT1 smoke NRPT group in comparison to the WT smoke NRPT ($P<0.05$). Additionally, the estimation of IC (A) (Figure 5.6B) increased in the WT smoke group in comparison to the WT air group ($P<0.0001$). A reduced level of A was observed in the WT smoke NRPT group in comparison to the WT smoke group ($P<0.05$). In contrast, we observed an increase in parameter A for the NMNAT1 smoke NRPT group in comparison to the WT smoke NRPT ($P<0.01$). We observed an increase in the parameter Area and FEV (Figure 5.6C-D) in the WT smoke group in comparison to the WT air ($P<0.001$), and this was also reflected in the NMNAT1 smoke group with respect to the NMNAT1 air group ($P<0.01$). Further, we observed an increase in FVC (Figure 5.6E) in the WT smoke group in comparison to the WT air group ($P<0.0001$). We also observed an increase in FVC in the NMNAT1 smoke group as compared to the NMNAT1 air group ($P<0.0001$). In contrast, there was an increase in FVC in the NMNAT1 smoke NRPT group in comparison to the WT smoke NRPT group ($P<0.01$). There was an increase in the parameter vital capacity (VC) (Figure 5.6F) in the WT smoke group in comparison to the WT air group ($P<0.001$) and this was also reflected between the NMNAT1 smoke group and NMNAT1 air group ($P<0.001$). In contrast, there was an increase in VC in the NMNAT1 smoke NRPT in comparison to the WT smoke NRPT ($P<0.01$). We observed an increase in static compliance (Cst) (Figure 5.6J) in the WT smoke group as compared to the WT air group ($P<0.01$). Followed by an increase in functional residue capacity (FRC) (Figure 5.6M) in the WT smoke group in

comparison to the WT air group ($P<0.01$) which was also reflected in between NMNAT1 smoke and NMNAT1 air group ($P<0.0001$). We also observed an increase in FRC in the NMNAT1 smoke NRPT in comparison to the WT smoke NRPT ($P<0.001$). Interestingly, we observed a reduction in residual volume (RV) (Figure 5.6N) in the WT smoke NRPT ($P<0.001$) group as well as the NMNAT1 smoke ($P<0.01$) group in comparison to the WT smoke group. Additionally, we observed an increase in TLC (Figure 5.6O) in the WT smoke group in comparison to the air group ($P<0.05$). Furthermore, we did not observe any changes in the parameters of Rn (Figure 5.6G), G (Figure 5.6H), H (Figure 5.6I), Rrs (Figure 5.6K), and Crs (Figure 5.6L). Additionally, the lung compliance curves between the WT air, WT smoke and WT smoke NRPT are represented in Figure 5.6P. Followed by the compliance curves between NMNAT1 air, NMNAT1 smoke and NMNAT1 smoke NRPT are represented below in Figure 5.6Q. Further, the compliance curves between NMNAT1 smoke and WT smoke are represented in Figure 5.6R.

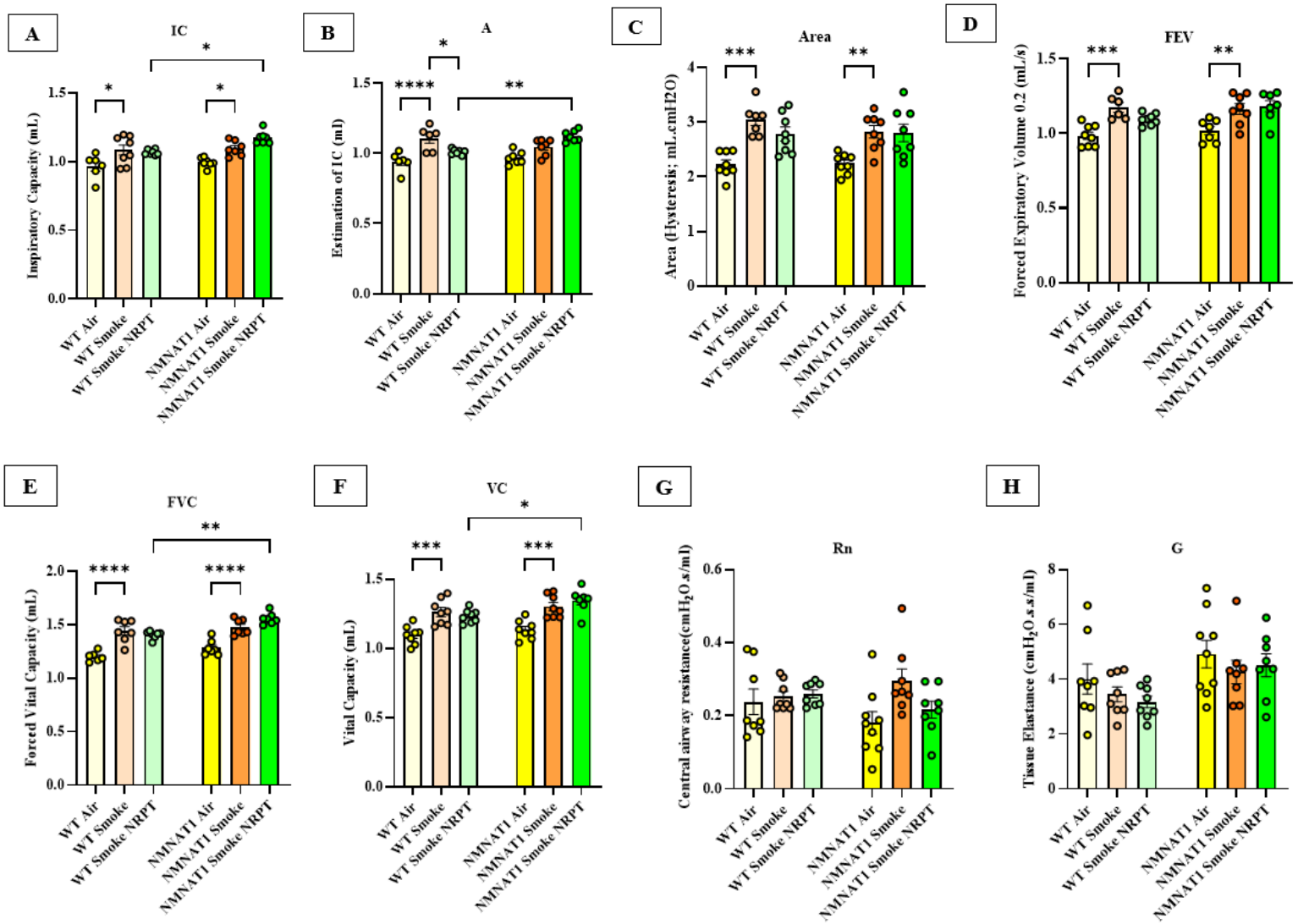
A
IC
Inspiratory Capacity (mL)
B
A
Estimation of IC (ml)
C
Area
Area (Hysteresis; mL.cmH2O)
D
FEV
Forced Expiratory Volume 0.2 (mL/s)
E
FVC
Forced Vital Capacity (mL)
F
VC
Vital Capacity (mL)
G
Rn
Central airway resistance(cmH2O.s/ml)
H
G
Tissue Elastance (cmH2O.s/ml)
WT Air
WT Smoke
WT Smoke NRPT
NMNAT1 Air
NMNAT1 Smoke
NMNAT1 Smoke NRPT

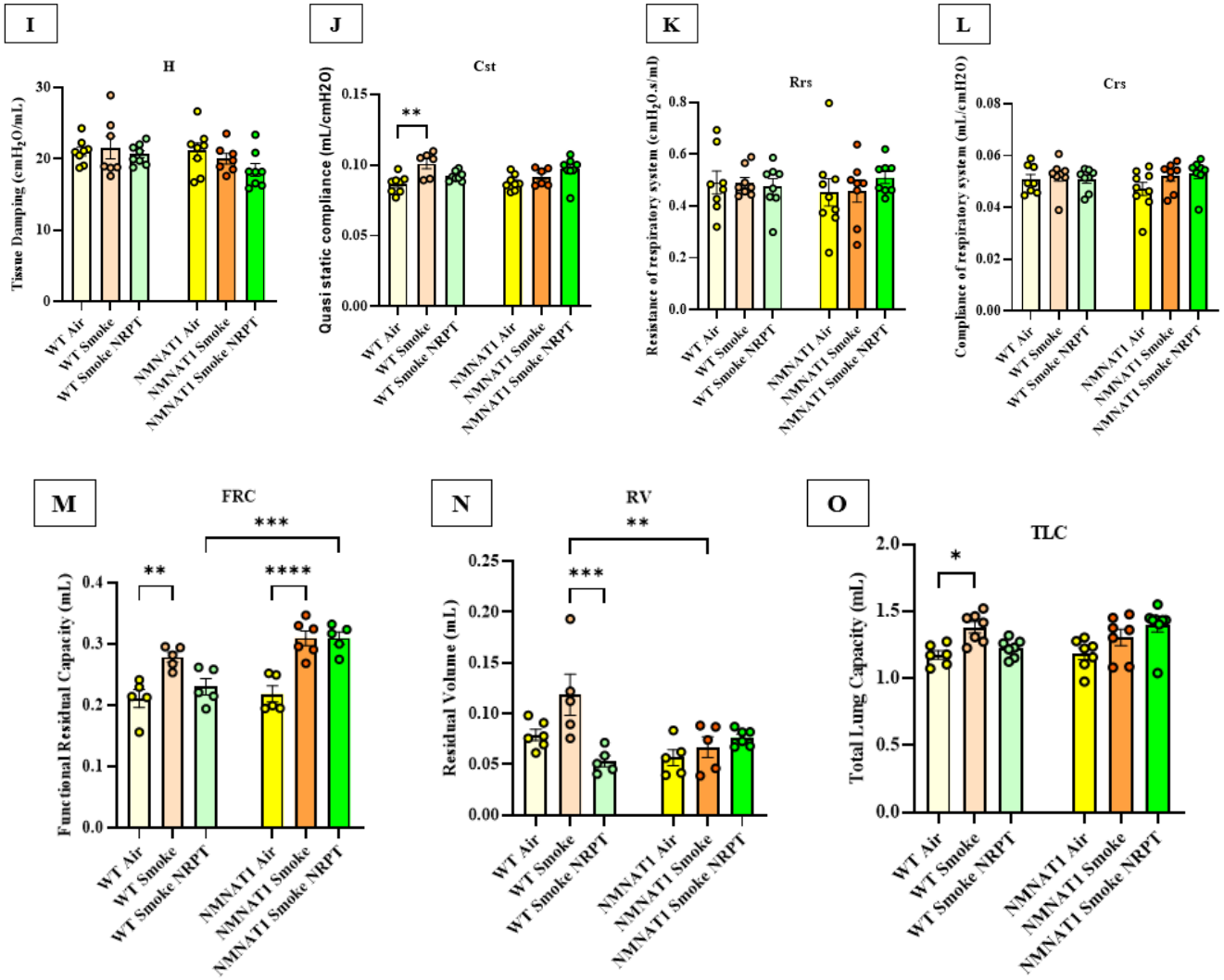
I
H
Tissue Damping (cmH2O/mL)
J
Cst
Quasi static compliance (mL/cmH2O)
**
K
Rrs
Resistance of respiratory system (cmH2O.s/ml)
L
Crs
Compliance of respiratory system (mL/cmH2O)
WT Air
WT Smoke
WT Smoke NRPT
NMNAT1 Air
NMNAT1 Smoke
NMNAT1 Smoke NRPT
M
FRC
Functional Residual Capacity (mL)
**
***
****
N
RV
Residual Volume (mL)
**
***
O
TLC
Total Lung Capacity (mL)
*

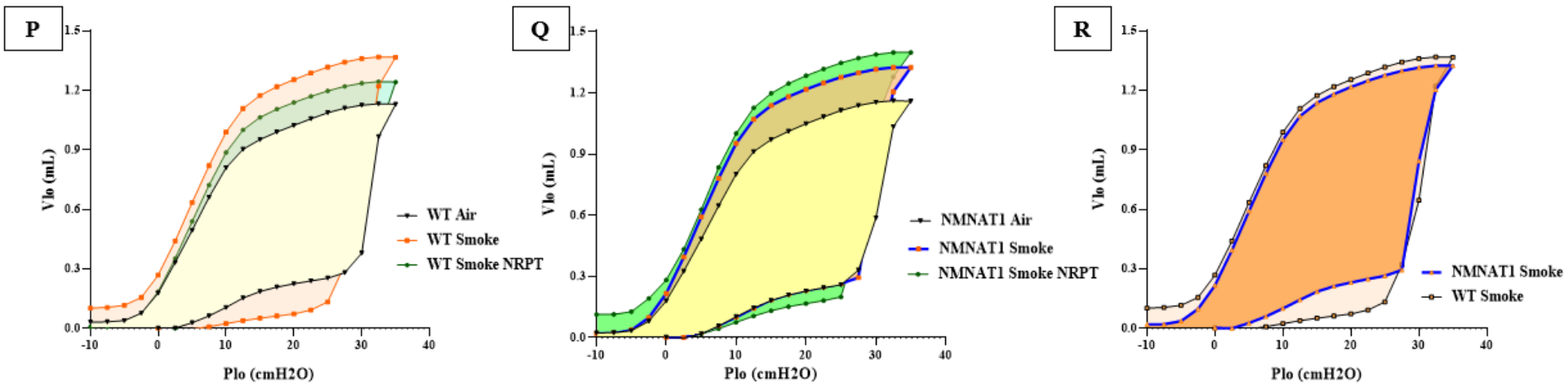

Figure 5.6: NMNAT1 overexpression protected from impaired lung function in COPD:

*Graphical representation of lung function parameters: (A) IC, (B) Estimation of IC (A), (C) Area, (D) Forced expiratory volume (FEV), (E) Forced vital capacity (FVC), (F) Vital capacity (VC), (G) Central airway resistance (Rn), (H) Tissue elastance (G), (I) Tissue damping (H), (J) Quasi-static compliance (Cst), (K) Resistance of respiratory system (Rrs), (L) Compliance of respiratory system (Crs), (M) Functional residual capacity (FRC), (N) Residual volume (RV), (O) Total lung capacity (TLC); Lung compliance curves for (P) WT air, WT smoke and WT smoke NRPT, (Q) NMNAT1 air, NMNAT1 smoke, and NMNAT1 smoke NRPT, (R) NMNAT1 smoke and WT smoke. Data represented are means ± SEM of 6-8 mice/group, * P<0.05, ** P<0.01, *** P<0.001, **** P<0.0001.*

5.3.5 Effect of NMNAT1 overexpression on NAD^+ biosynthesis in COPD

We observed a significant increase in the gene expression of NMNAT1 between the WT air and NMNAT1 air ($P<0.0001$), WT smoke and NMNAT1 smoke ($P<0.001$) as well as WT smoke NRPT and NMNAT1 smoke NRPT ($P<0.0001$) (Figure 5.7A). Further, we observed a reduction in the gene expression of NMNAT2 in the WT smoke group in comparison to the air group ($P<0.0001$). An increase in the gene expression of the NMNAT2 was observed in the WT smoke NRPT group as compared to the WT smoke group ($P<0.0001$) (Figure 5.7B). Similarly, we also observed a reduction in the gene expression of NMNAT3 in the WT smoke group in comparison to the WT air group ($P<0.01$). Furthermore, we observed an increase in NMNAT3 in the WT smoke NRPT group in comparison to the WT smoke group ($P<0.0001$). In contrast, we observed a reduction in the gene expression of NMNAT3 in the NMNAT1 smoke NRPT group in comparison to the WT smoke NRPT group ($P<0.0001$) (Figure 5.7C).

Furthermore, we observed an increase in the ratio of total NAD/NADH levels in the WT smoke NRPT group in comparison to the WT smoke group ($P<0.0001$). However, we observed a reduction in the ratio of total NAD/NADH levels in the NMNAT1 smoke NRPT group in comparison to the WT smoke NRPT group ($P<0.001$) (Figure 5.7D). Similarly, the total NAD^+ levels increased in the WT smoke NRPT group in comparison to the WT smoke group ($P<0.01$). We observed a reduction in the total NAD^+ levels in the NMNAT1 smoke NRPT group as compared to the WT smoke NRPT group ($P<0.01$) (Figure 5.7E). Moreover, there was an increase in the NADH levels in the WT smoke group in comparison to the WT air group ($P<0.01$). We observed a reduction in the NADH levels in the WT smoke NRPT group as compared to the WT smoke group ($P<0.01$).

Additionally, we observed a reduction in the NADH levels in the NMNAT1 smoke group in comparison to the WT smoke group (P<0.05) (Figure 5.7F).

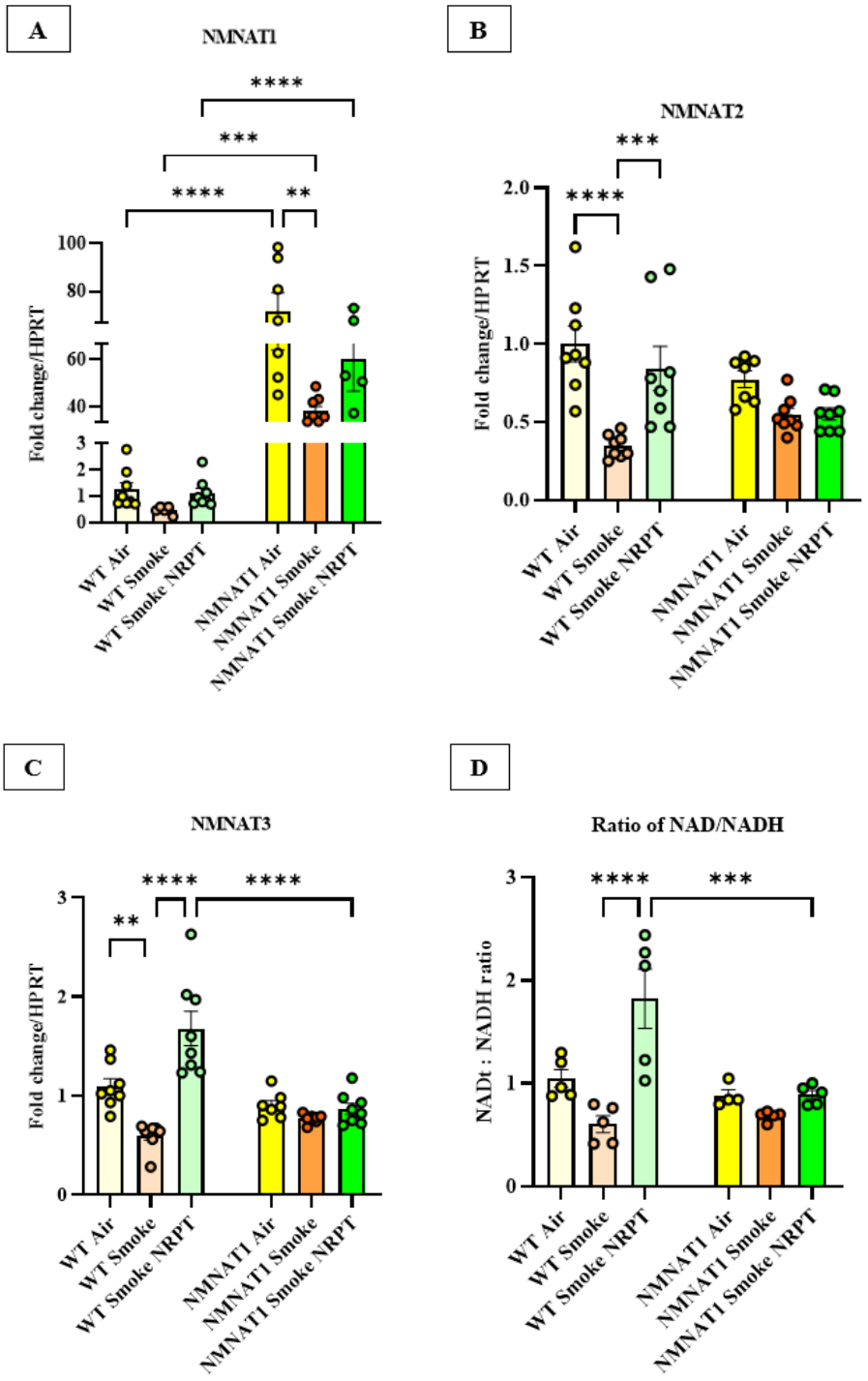

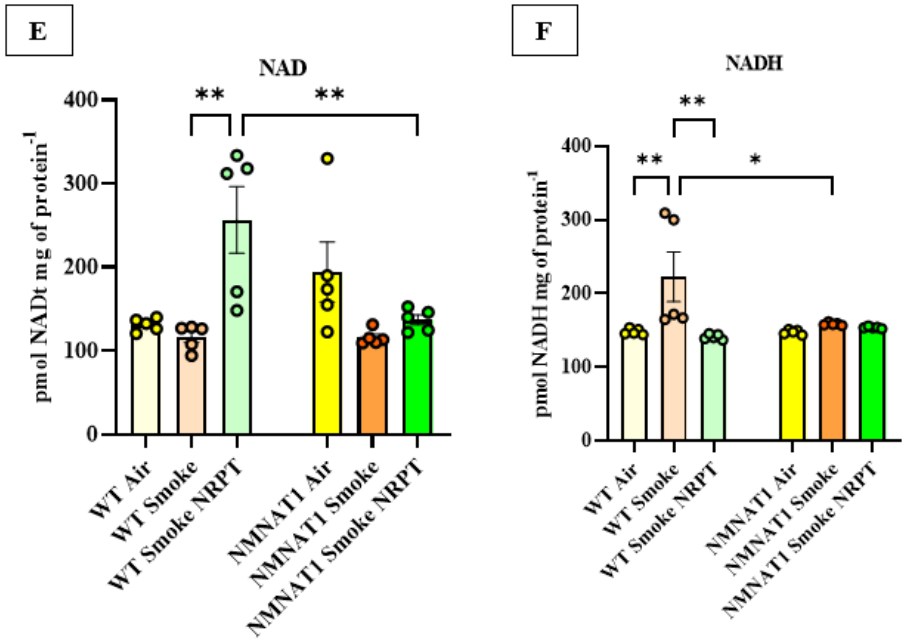

Figure 5.7: Effect of NMNAT1 overexpression on NAD^+ biosynthesis in COPD:

*Gene expression of (A) NMNAT1, (B) NMNAT2, and (C) NMNAT3; (D) ratio of NAD^+/NADH, (E) total NAD^+ levels, (F) NADH levels. Data represented are means ± SEM of 6-8 mice/group, * P<0.05, ** P<0.01, *** P<0.001, **** P<0.0001.*

5.3.6 NMNAT1 overexpression regulated NAD^+ consumers in COPD

We observed an increase in PARP activity (Figure 5.8A) in the WT smoke group in comparison to the WT air group (P<0.0001). Furthermore, a reduction in the PARP activity was observed both in the WT smoke NRPT and NMNAT1 smoke group in comparison to the WT smoke group (P<0.0001). In contrast, we observed a reduction in the gene expression of PARP1 (Figure 5.8B) in the WT smoke group as compared to the WT air group (P<0.05). Additionally, we observed an increase in the gene expression of PARP1 in the WT smoke NRPT group in comparison to the WT smoke group (P<0.0001). In contrast, there was a reduction in the gene expression of PARP1 in the NMNAT1 smoke NRPT group with respect to the WT smoke NRPT group (P<0.05).

A reduction in the gene expression of SIRT1 ($P<0.05$) (Figure 5.8C), SIRT4 ($P<0.001$) (Figure 5.8F) and SIRT5 ($P<0.0001$) (Figure 5.8G) was observed in the WT smoke group in comparison to the WT air group. We observed an increase in the gene expression of SIRT1 ($P<0.01$), SIRT5 ($P<0.05$) and SIRT7 ($P<0.01$) (Figure 5.8I) in the WT smoke NRPT group as compared to the WT smoke group. A reduction in the gene expression of SIRT1, SIRT5 and SIRT7 was observed in the NMNAT1 smoke NRPT in comparison to the WT smoke NRPT ($P<0.01$). We also observed a reduction in the gene expression of SIRT3 (Figure 5.8E) in the NMNAT1 smoke with respect to the WT smoke group ($P<0.01$). We observed a reduced gene expression of SIRT3 ($P<0.001$), SIRT4 ($P<0.05$) and SIRT5 ($P<0.01$) in the NMNAT1 smoke group in comparison to the NMNAT1 air group. SIRT3 and SIRT4 gene expression were increased in the NMNAT1 smoke NRPT group as compared to the NMNAT1 smoke group ($P<0.01$). We also observed a reduction in the gene expression of SIRT1, SIRT5 and SIRT7 in the NMNAT1 smoke NRPT group in comparison to the WT smoke NRPT group ($P<0.01$). We did not observe any change in the gene expression of SIRT2 (Figure 5.8D) and SIRT6 (Figure 5.8H) across any experimental groups in this study.

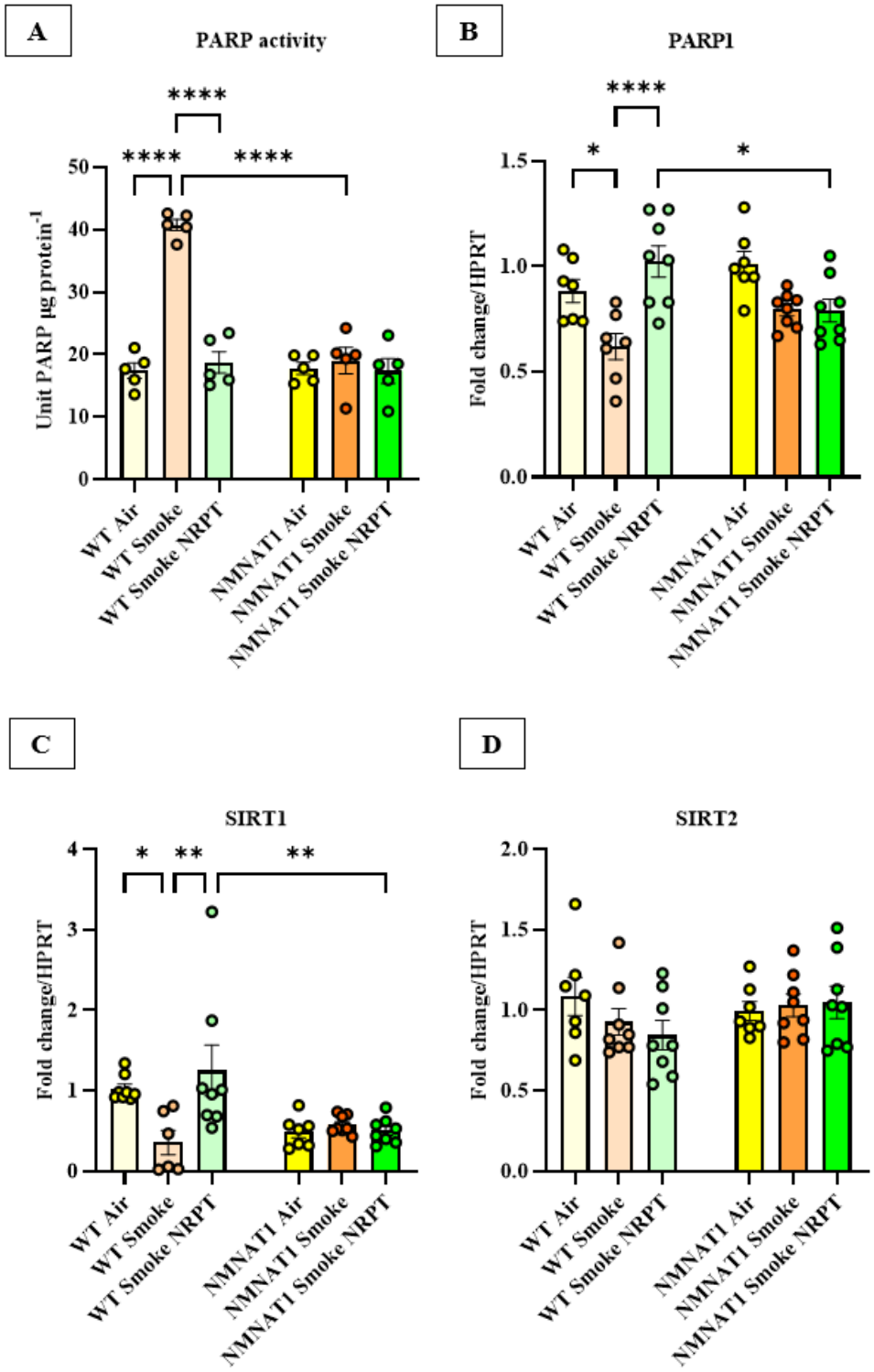
A
PARP activity
Unit PARP µg protein-1
****
****
****
50
40
30
20
10
0
WT Air
WT Smoke
WT Smoke NRPT
NMNAT1 Air
NMNAT1 Smoke
NMNAT1 Smoke NRPT
B
PARP1
Fold change/HPRT
****
*
*
1.5
1.0
0.5
0.0
C
SIRT1
Fold change/HPRT
*
**
**
4
3
2
1
0
D
SIRT2
Fold change/HPRT
2.0
1.5
1.0
0.5
0.0

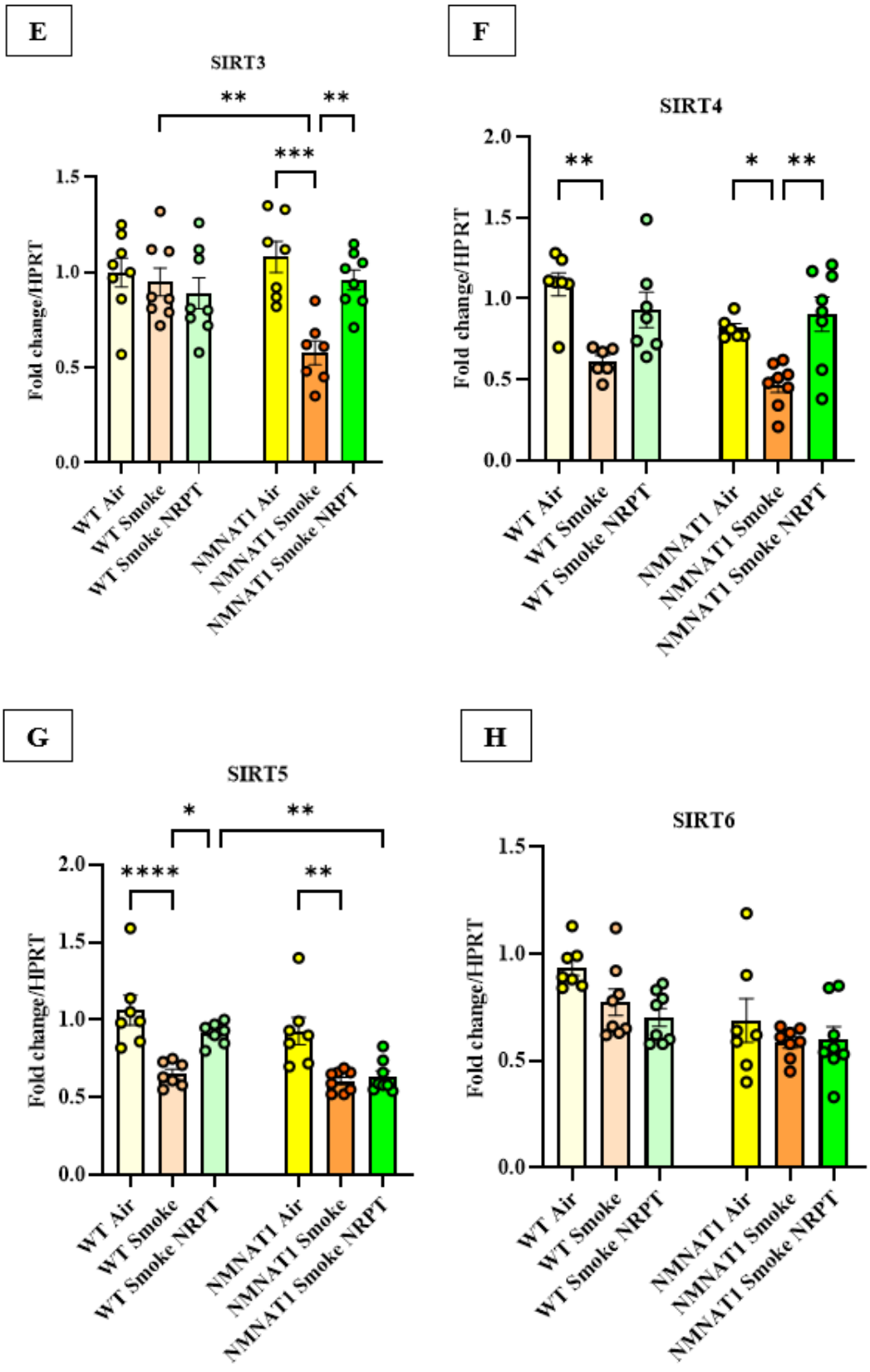
E
SIRT3
**
**
***
Fold change/HPRT
1.5
1.0
0.5
0.0
WT Air
WT Smoke
WT Smoke NRPT
NMNAT1 Air
NMNAT1 Smoke
NMNAT1 Smoke NRPT
F
SIRT4
**
*
**
Fold change/HPRT
2.0
1.5
1.0
0.5
0.0
WT Air
WT Smoke
WT Smoke NRPT
NMNAT1 Air
NMNAT1 Smoke
NMNAT1 Smoke NRPT
G
SIRT5
*
**
****
**
Fold change/HPRT
2.0
1.5
1.0
0.5
0.0
WT Air
WT Smoke
WT Smoke NRPT
NMNAT1 Air
NMNAT1 Smoke
NMNAT1 Smoke NRPT
H
SIRT6
Fold change/HPRT
1.5
1.0
0.5
0.0
WT Air
WT Smoke
WT Smoke NRPT
NMNAT1 Air
NMNAT1 Smoke
NMNAT1 Smoke NRPT

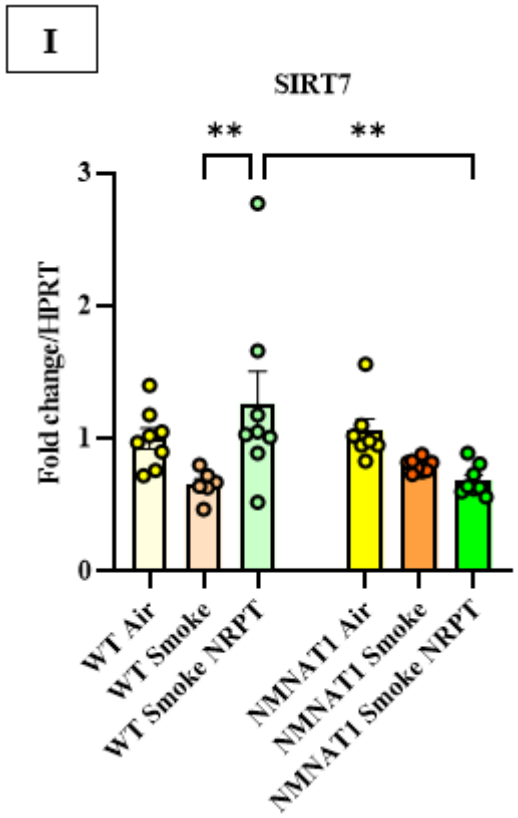

Figure 5.8: NMNAT1 overexpression regulated NAD^+ consumers in COPD:

*(A) PARP activity; Gene expression for (B) PARP1, (C) SIRT1, (D) SIRT2, (E) SIRT3, (F) SIRT4, (G) SIRT5, (H) SIRT6, (I) SIRT7. Data represented are means ± SEM of 6-8 mice/group, * P<0.05, ** P<0.01, *** P<0.001, **** P<0.0001.*

5.3.7 NMNAT1 overexpression increased mitochondria membrane potential in COPD

Mitochondria membrane potential was measured in this study as mentioned described (Section 2.2.29). We observed a decrease in the MFI of J-aggregates (red) (Figure 5.9A) in the WT smoke group in comparison to the WT air group (P<0.0001). There was an increase in the MFI of J-aggregates in the WT smoke NRPT as compared to the WT smoke group (P<0.01). In contrast, we observed an increase in the MFI of J-aggregates in the NMNAT1 smoke group in comparison to the NMNAT1 air group, NMNAT1

smoke NRPT group as well as the WT smoke group ($P<0.0001$). Furthermore, a reduction in the MFI of J-aggregates was observed in the NMNAT1 air group in comparison to the WT air group ($P<0.0001$).

Simultaneously, we also measured the MFI of J-monomers (green) (Figure 5.9B) and observed an increase in the WT smoke group with respect to the WT air, WT smoke NRPT as well as NMNAT1 smoke group ($P<0.0001$). Additionally, we observed an increase in the MFI of J-monomers in the NMNAT1 smoke group as compared to the NMNAT1 air group ($P<0.05$). We also observed a reduction in the MFI of J-monomers obtained for the NMNAT1 air group in comparison to the WT air group ($P<0.0001$).

Furthermore, the ratio of J-aggregates/J-monomers was analysed to obtain the measure of $\Delta\Psi m$ (Figure 5.9C). We observed a reduction of $\Delta\Psi m$ in the WT smoke group in comparison to the WT air group, WT smokeNRPT group, and the NMNAT1 smoke group ($P<0.0001$). In contrast, we also observed an increase in the $\Delta\Psi m$ in the NMNAT1 air group with respect to the WT air group ($P<0.05$).

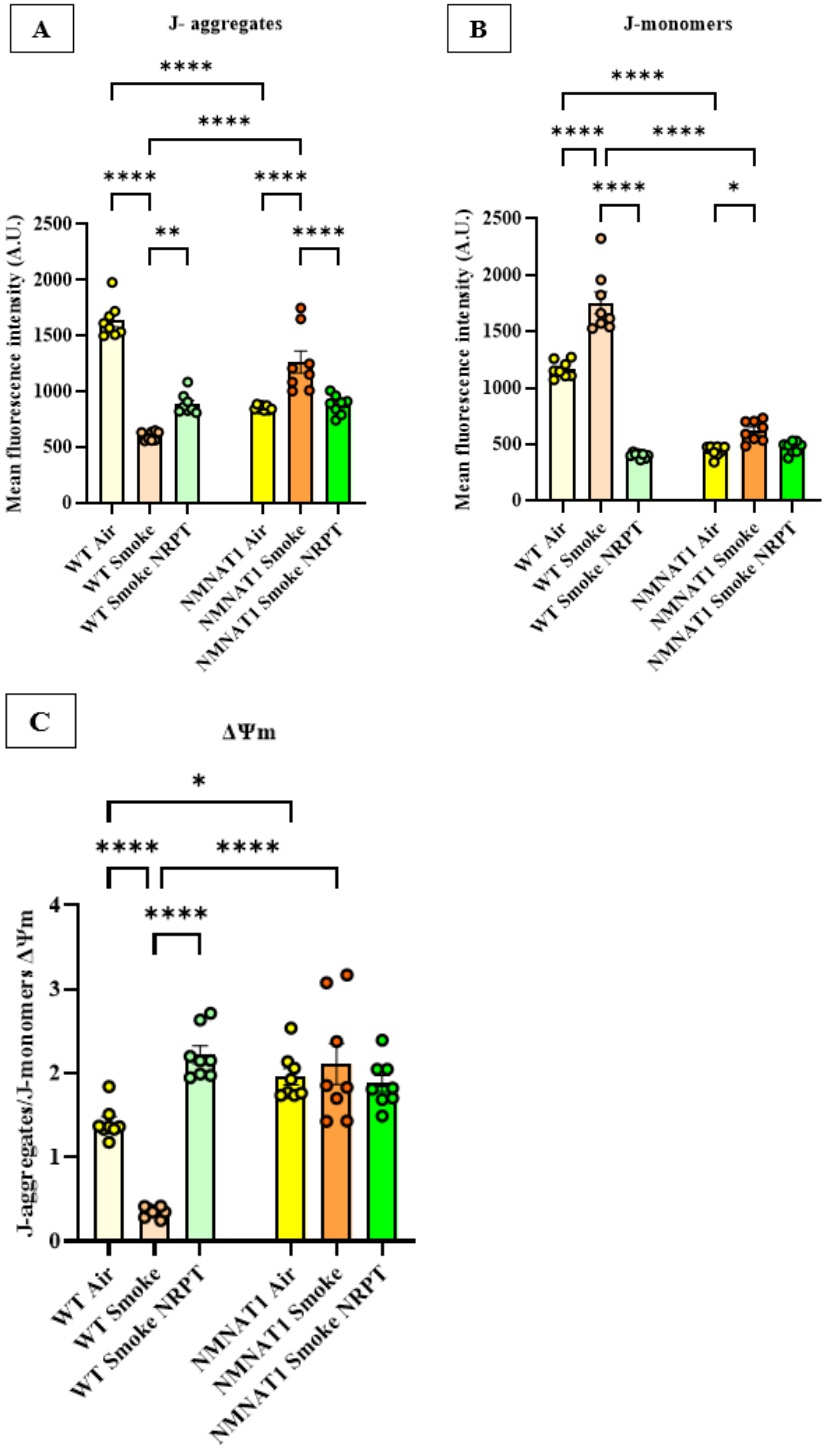
A
J- aggregates
Mean fluorescence intensity (A.U.)
2500
2000
1500
1000
500
0
****
****
****
****
**
****
WT Air
WT Smoke
WT Smoke NRPT
NMNAT1 Air
NMNAT1 Smoke
NMNAT1 Smoke NRPT
B
J-monomers
Mean fluorescence intensity (A.U.)
2500
2000
1500
1000
500
0
****
****
****
****
*
WT Air
WT Smoke
WT Smoke NRPT
NMNAT1 Air
NMNAT1 Smoke
NMNAT1 Smoke NRPT
C
ΔΨm
J-aggregates/J-monomers ΔΨm
4
3
2
1
0
*
****
****
****
WT Air
WT Smoke
WT Smoke NRPT
NMNAT1 Air
NMNAT1 Smoke
NMNAT1 Smoke NRPT

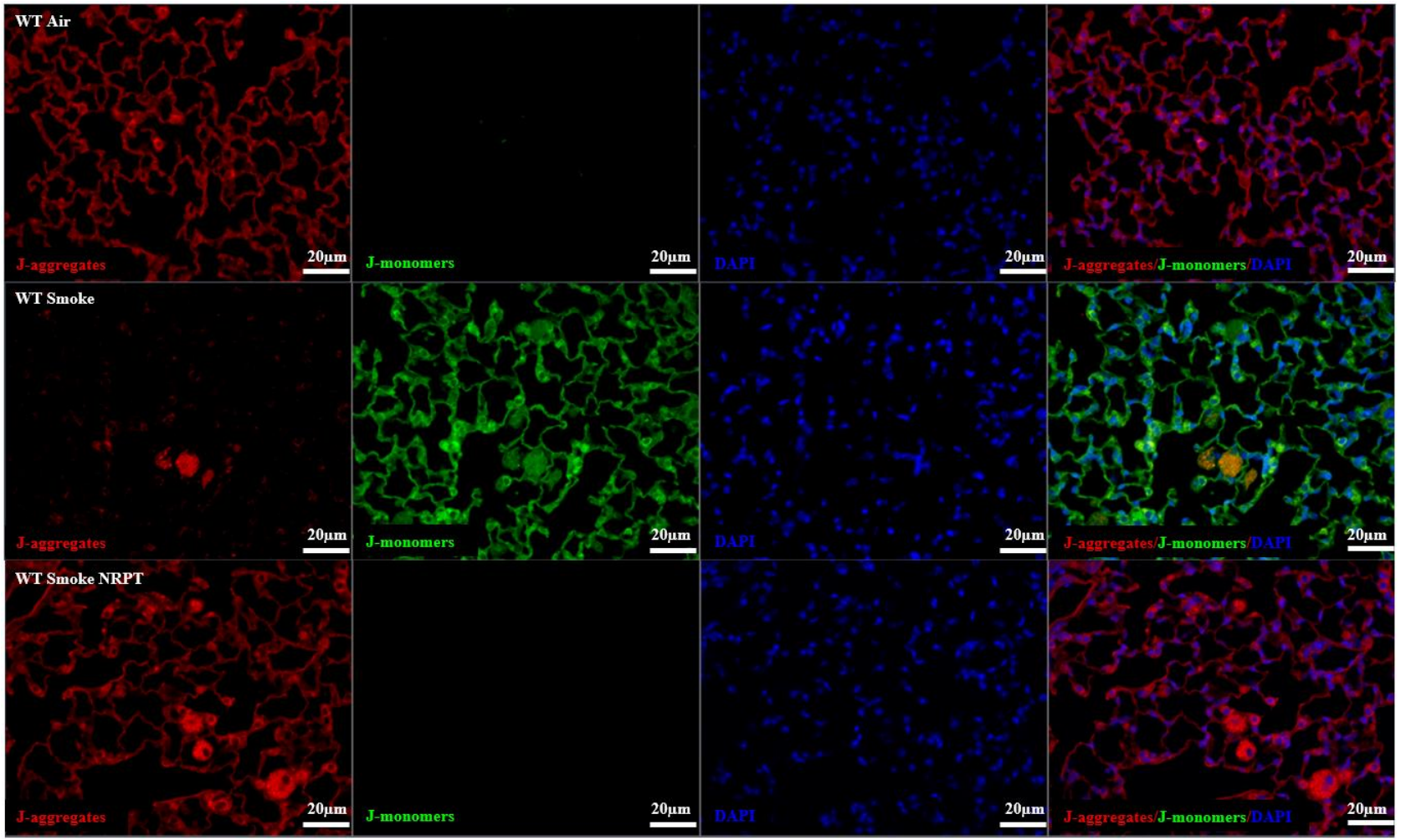
WT Air
J-aggregates
20μm
J-monomers
20μm
DAPI
20μm
J-aggregates/J-monomers/DAPI
20μm
WT Smoke
J-aggregates
20μm
J-monomers
20μm
DAPI
20μm
J-aggregates/J-monomers/DAPI
20μm
WT Smoke NRPT
J-aggregates
20μm
J-monomers
20μm
DAPI
20μm
J-aggregates/J-monomers/DAPI
20μm

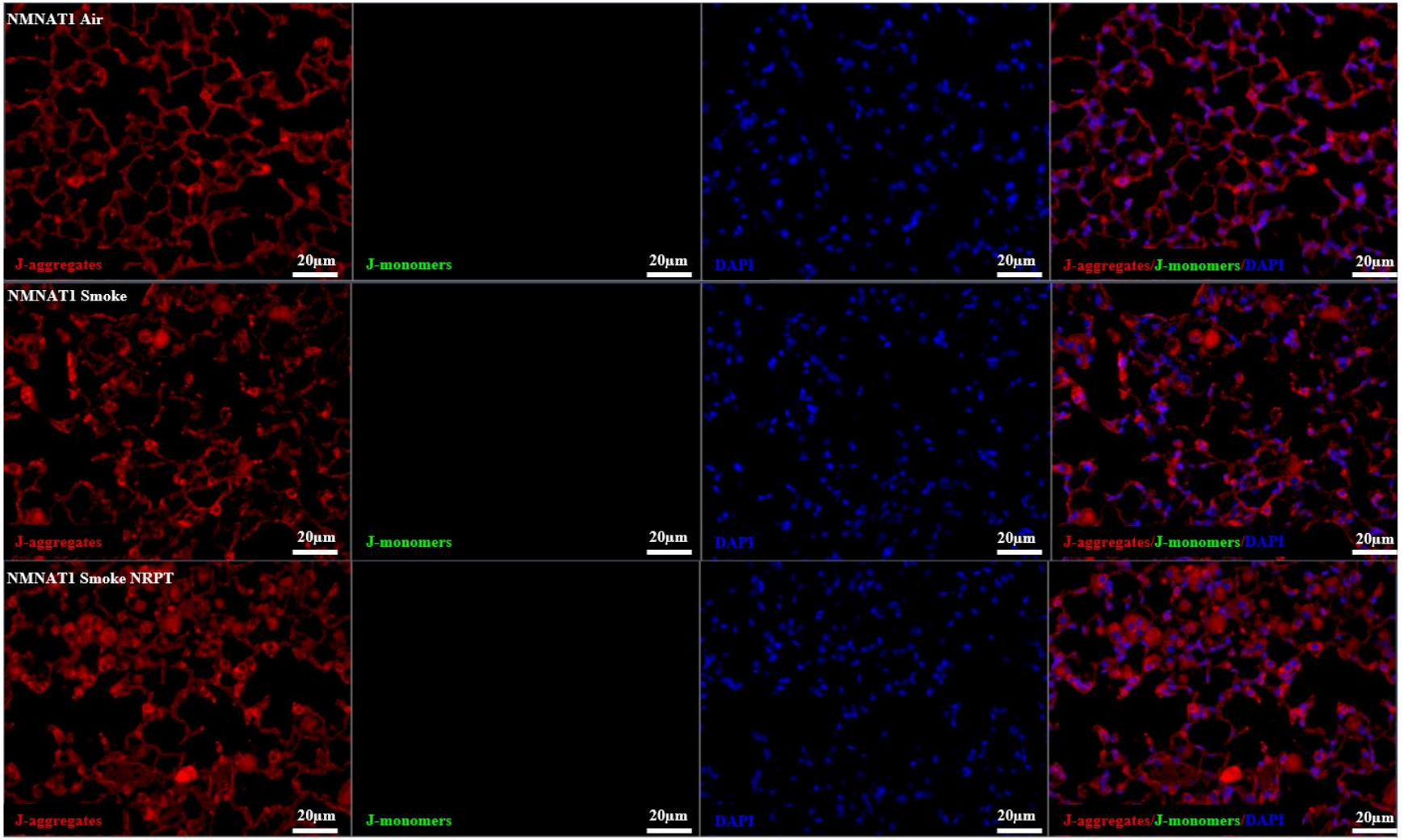

Figure 5.9: NMNAT1 overexpression increase ΔΨm in COPD:

Graphical representation of MFI obtained for (A) J-aggregates (red), (B) J-monomers (green), (C) Ratio of J-aggregates/J-monomers (ΔΨm). Representative images from all the experimental groups under different channels: J-aggregates in red, J-monomers in green, and nuclear stain DAPI in blue followed by a merged image of all the channels.

5.3.8 NMNAT1 overexpression protected from oxidative stress in COPD

We observed an increase in gene expression of NOX2 (Figure 5.10A) in the WT smoke group in comparison to the WT air group ($P<0.0001$), WT smoke NRPT group ($P<0.0001$) and NMNAT1 smoke group ($P<0.0001$). Similarly, we observed an increase in the gene expression of HO1 (Figure 5.10B) in the WT smoke group in comparison to the WT air group ($P<0.05$), WT smoke NRPT group ($P<0.01$) and NMNAT1 smoke group ($P<0.01$).

In addition, we observed an increase in the MFI obtained from 4-HNE in the WT smoke group in comparison to the WT air group ($P<0.0001$), WT smoke NRPT group ($P<0.0001$) and NMNAT1 smoke group ($P<0.0001$). We also observed an increase in the MFI of 4-HNE in the NMNAT1 air group as compared to the WT air group ($P<0.001$). Images below represent 4-HNE (green) co-stained with F4/80 (red) and DAPI (blue) (Figure 5.10C).

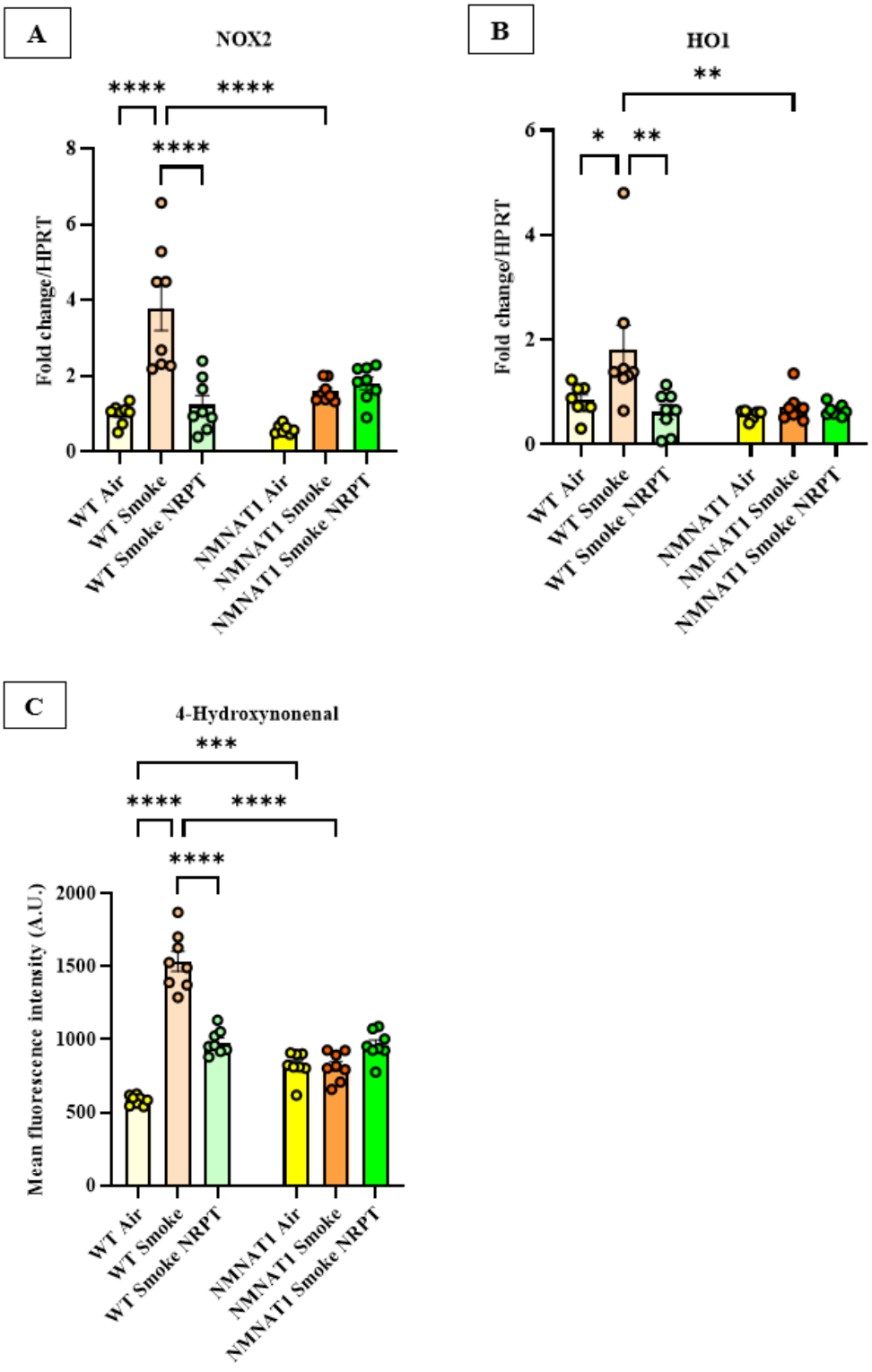
A
NOX2
****
****
****
Fold change/HPRT
0
2
4
6
8
WT Air
WT Smoke
WT Smoke NRPT
NMNAT1 Air
NMNAT1 Smoke
NMNAT1 Smoke NRPT
B
HO1
**
*
**
Fold change/HPRT
0
2
4
6
WT Air
WT Smoke
WT Smoke NRPT
NMNAT1 Air
NMNAT1 Smoke
NMNAT1 Smoke NRPT
C
4-Hydroxynonenal
***
****
****
Mean fluorescence intensity (A.U.)
0
500
1000
1500
2000
WT Air
WT Smoke
WT Smoke NRPT
NMNAT1 Air
NMNAT1 Smoke
NMNAT1 Smoke NRPT

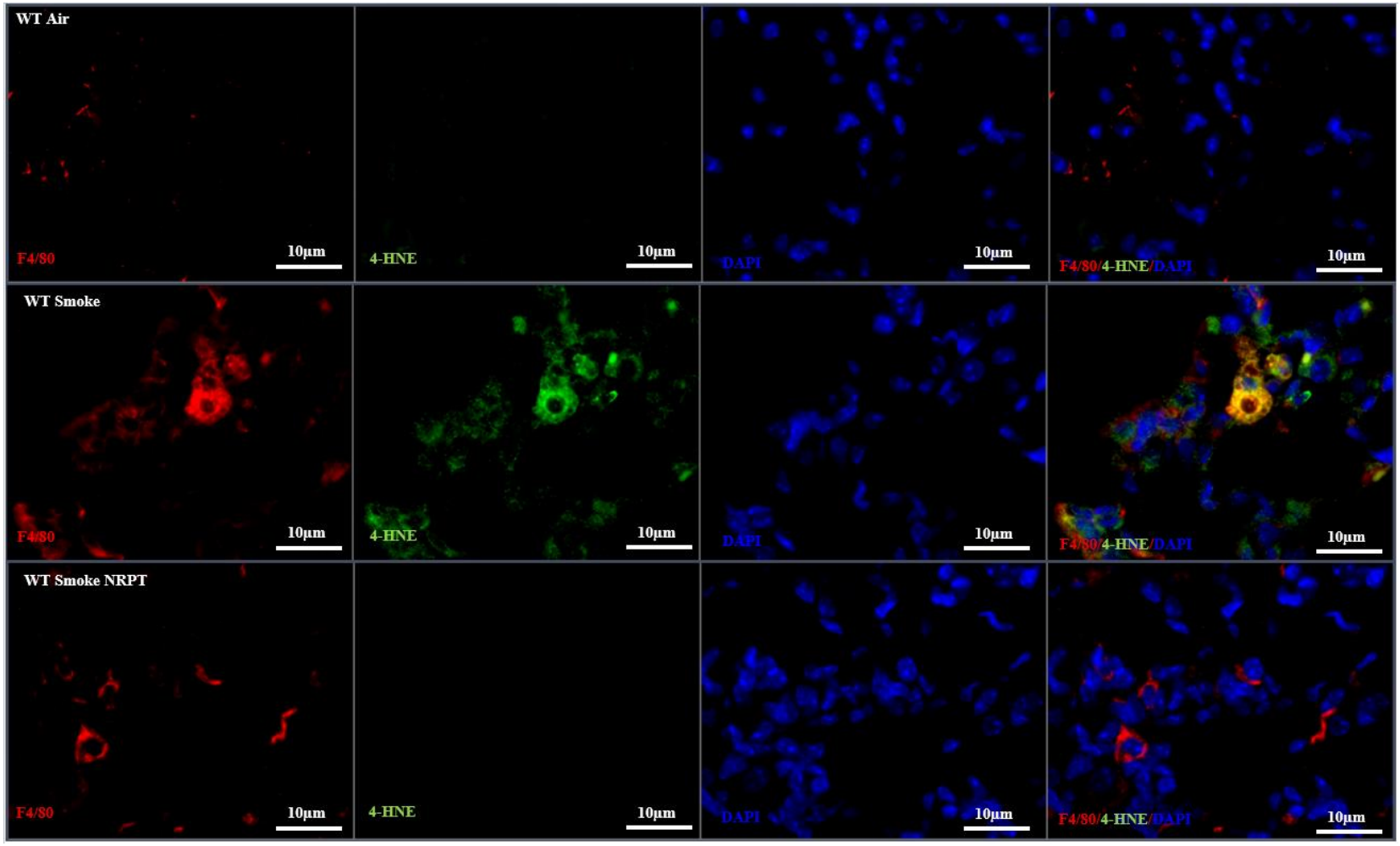
WT Air
F4/80
10μm
4-HNE
10μm
DAPI
10μm
F4/80/4-HNE/DAPI
10μm
WT Smoke
F4/80
10μm
4-HNE
10μm
DAPI
10μm
F4/80/4-HNE/DAPI
10μm
WT Smoke NRPT
F4/80
10μm
4-HNE
10μm
DAPI
10μm
F4/80/4-HNE/DAPI
10μm

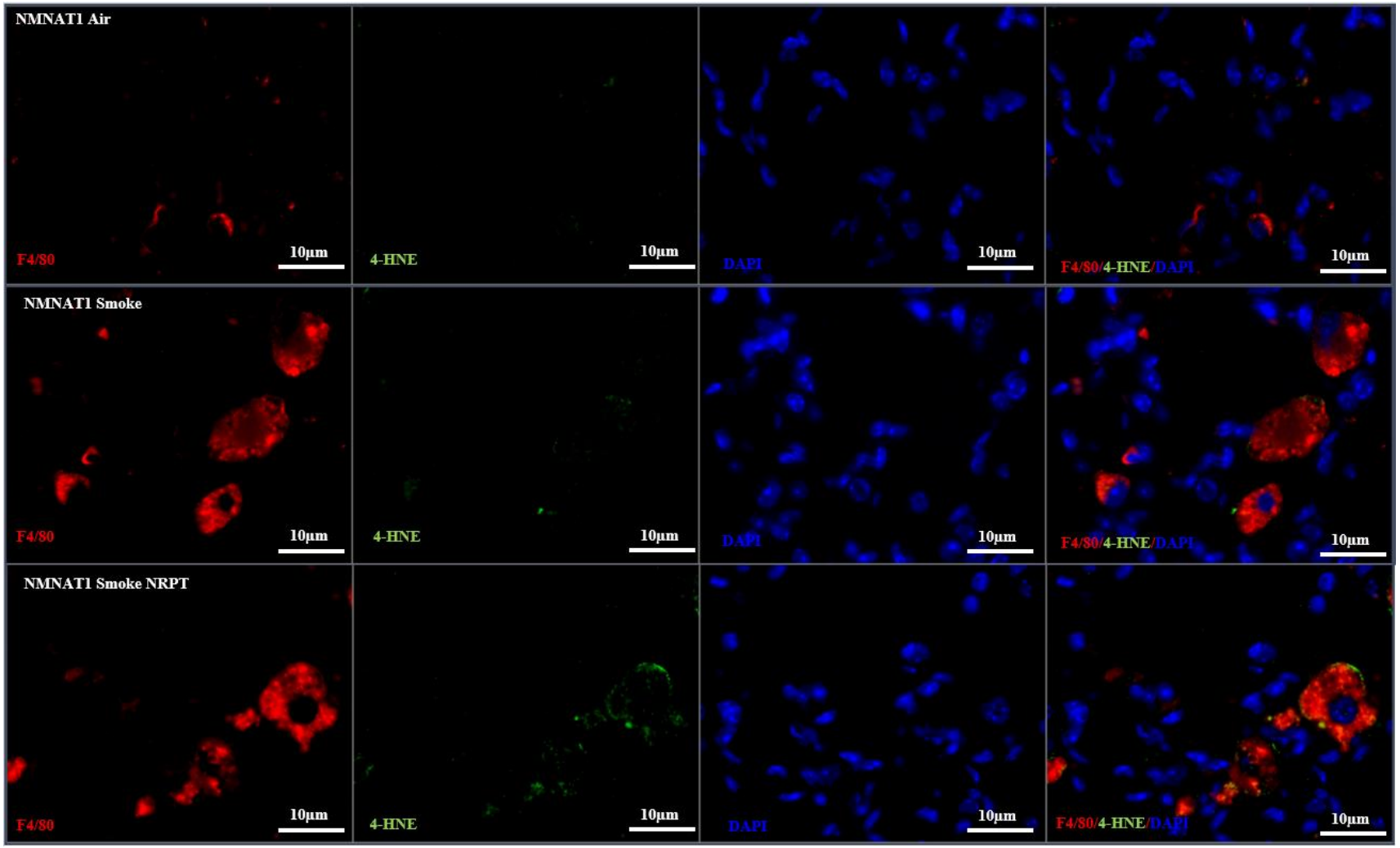

Figure 5.10:NMNAT1 overexpression reduced oxidative stress in COPD:

*Gene expression of (A) NOX2, (B) HO1; (C) Graphical representation of MFI in arbitrary units (A.U.) of 4-HNE images show fluorescence localisation of F4/80 (red), 4-HNE (green), DAPI-nuclei stain (blue). Data represented are means ± SEM of 6-8 mice/group, * P<0.05, ** P<0.01, *** P<0.001, **** P<0.0001.*

5.3.9 NMNAT3 overexpression reduced inflammation in COPD

There was an increase in the number of total leukocytes in the BAL (Figure 5.11A), as well as an increase in the total number of macrophages (Figure 5.11B) and neutrophils (Figure 5.11C) in the WT smoke group as compared to the WT air group (P<0.0001). Importantly, there was a reduced number of total leukocytes, macrophages and neutrophils in the WT smoke NRPT group and NMNAT3 smoke group in comparison to the WT smoke group (P<0.0001). Further, an increase in the counts of total leukocytes (P<0.0001) and macrophages (P<0.001) were observed in the NMNAT3 smoke NRPT as compared to the WT smoke NRPT group. Additionally, we also observed an increase in the total leukocyte counts (P<0.0001), macrophages (P<0.001) and neutrophils (P<0.0001) in the NMNAT3 smoke group in comparison to the NMNAT3 air group.

The body weight of all the experimental groups in the NMNAT3 study was monitored daily as mentioned previously in 5.2.3. There was a significant difference in weight observed between the WT air group and the WT smoke group as well as the NMNAT3 air group and the NMNAT3 smoke group (P<0.05) (Figure 5.11D).

Furthermore, we observed an increase in the gene transcripts for TNFα (Figure 5.11E) in the WT smoke group in comparison to the WT air group (P<0.0001). A reduction in the expression of TNFα was observed in the WT smoke NRPT group and the NMNAT3 smoke group in comparison to the WT smoke group (P<0.0001). Moreover, we also

observed an increase in the gene expression of TNFα in the NMNAT3 smoke group as compared to the NMNAT3 air group (P<0.01). Similarly, we also observed an increase in the gene expression of CXCL1 (Figure 5.11F) in the WT smoke group in comparison to the WT air group (P<0.0001). A reduction in the gene expression of CXCL1 was observed in the WT smoke NRPT group as well as the NMNAT1 smoke group in comparison to the WT smoke group (P<0.0001). However, we observed an increase in the gene expression of CXCL1 in the NMNAT3 smoke group in comparison to the NMNAT3 air group (P<0.0001).

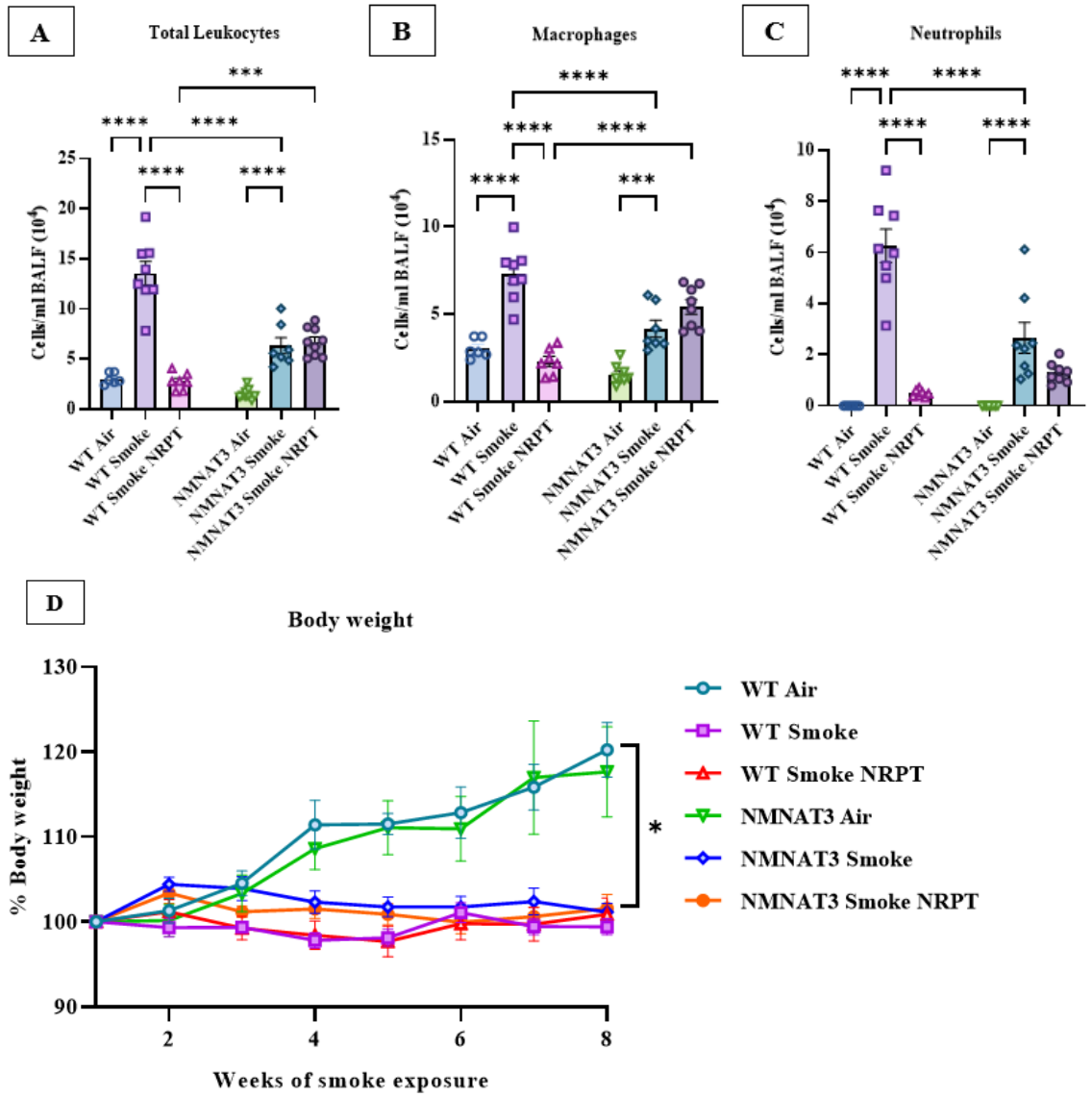

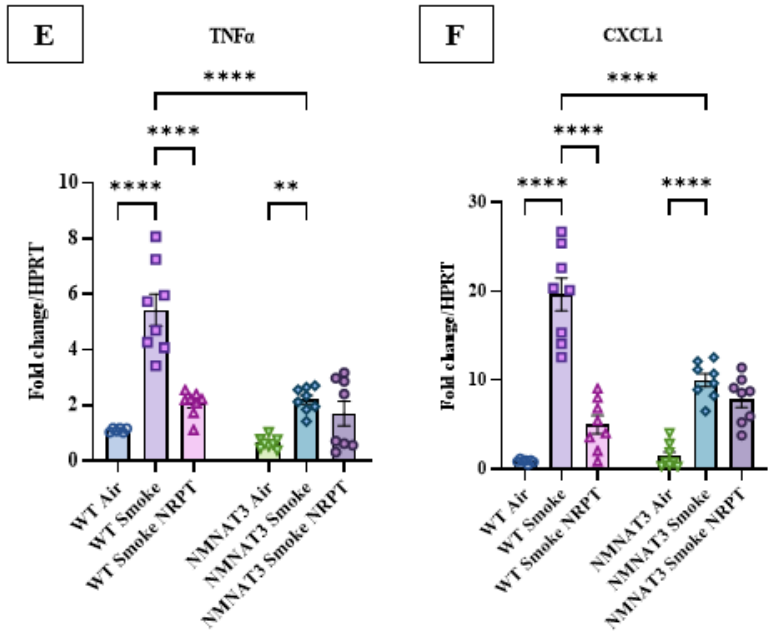

Figure 5.11: NMNAT3 overexpression reduced airway inflammation in COPD:

*Graphical representation of (A) total cellular infiltrates in the BAL, (B) macrophages, (C) neutrophils; (D) Body weight; Gene expression of (E) TNFα and (F) CXCL1 in the lung. Data represented are means ± SEM of 6-8 mice/group, * P<0.05, ** P<0.01, *** P<0.001, **** P<0.0001.*

5.3.10 NMNAT3 overexpression protected from airway remodelling and emphysema in COPD

We observed an increase in the area of collagen deposition in the WT smoke group in comparison to the WT air group (P<0.0001). Additionally, we observed a reduction in the collagen deposition in the WT smoke NRPT group and NMNAT1 smoke group in comparison to the WT smoke group (P<0.0001) (Figure 5.12A).

We observed an increase in alveolar diameter with increased MLI counts for the WT smoke group in comparison to the WT air group (P<0.0001). The counts obtained from MLI analysis for the WT smoke NRPT group and the NMNAT3 smoke group were

reduced in comparison to the WT smoke group ($P<0.0001$) (Figure 5.12B). Furthermore, we observed an increase in MLI counts for the NMNAT3 air group in comparison to the WT air group ($P<0.01$). Additionally, a reduction in the MLI counts was observed in the NMNAT3 smoke group in comparison to the NMNAT3 air group ($P<0.05$). Representative images of the alveolar diameter of each experimental group are displayed below in Figure 5.12B.

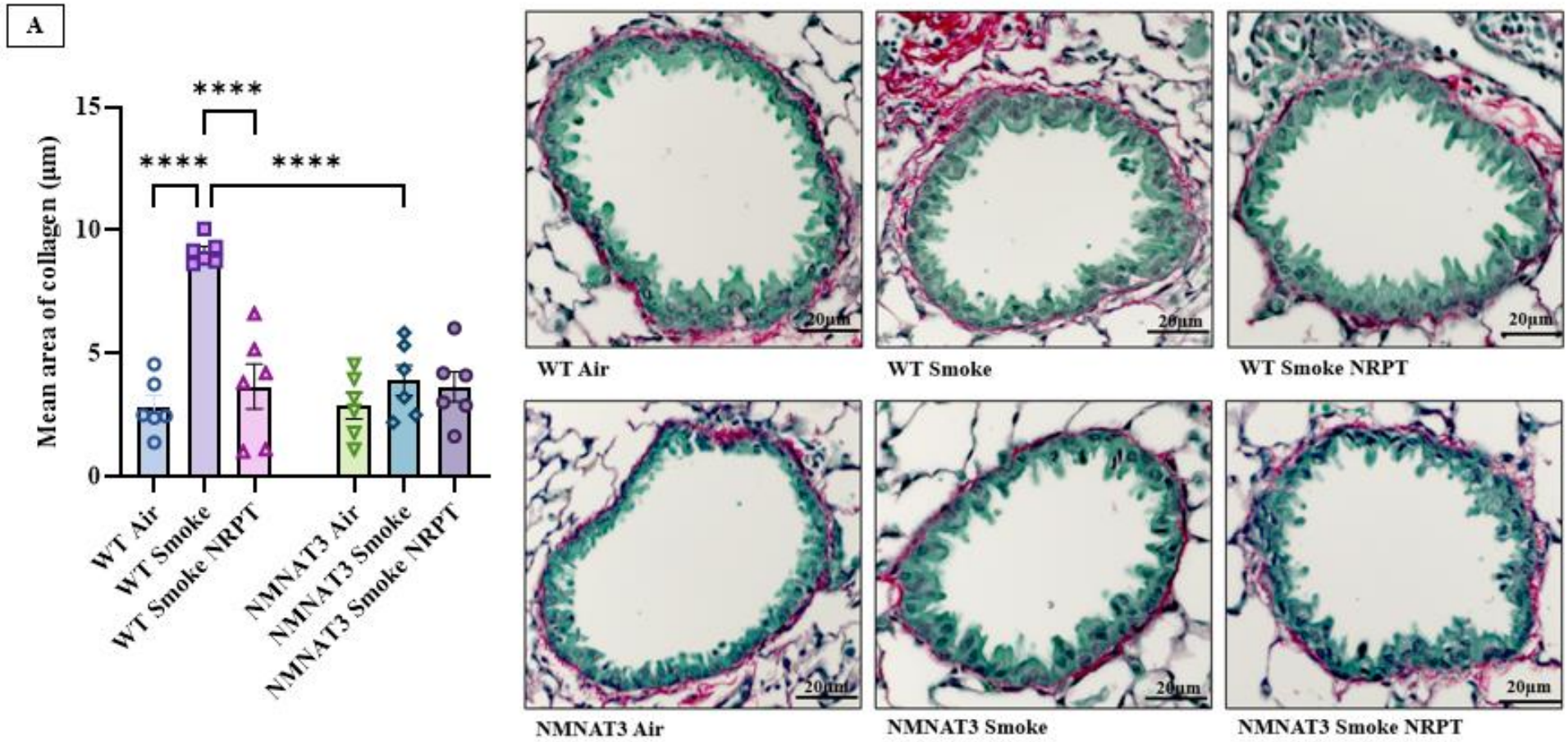
A
Mean area of collagen (µm)
15
10
5
0
****
****
****
WT Air
WT Smoke
WT Smoke NRPT
NMNAT3 Air
NMNAT3 Smoke
NMNAT3 Smoke NRPT
20µm
WT Air
WT Smoke
WT Smoke NRPT
NMNAT3 Air
NMNAT3 Smoke
NMNAT3 Smoke NRPT

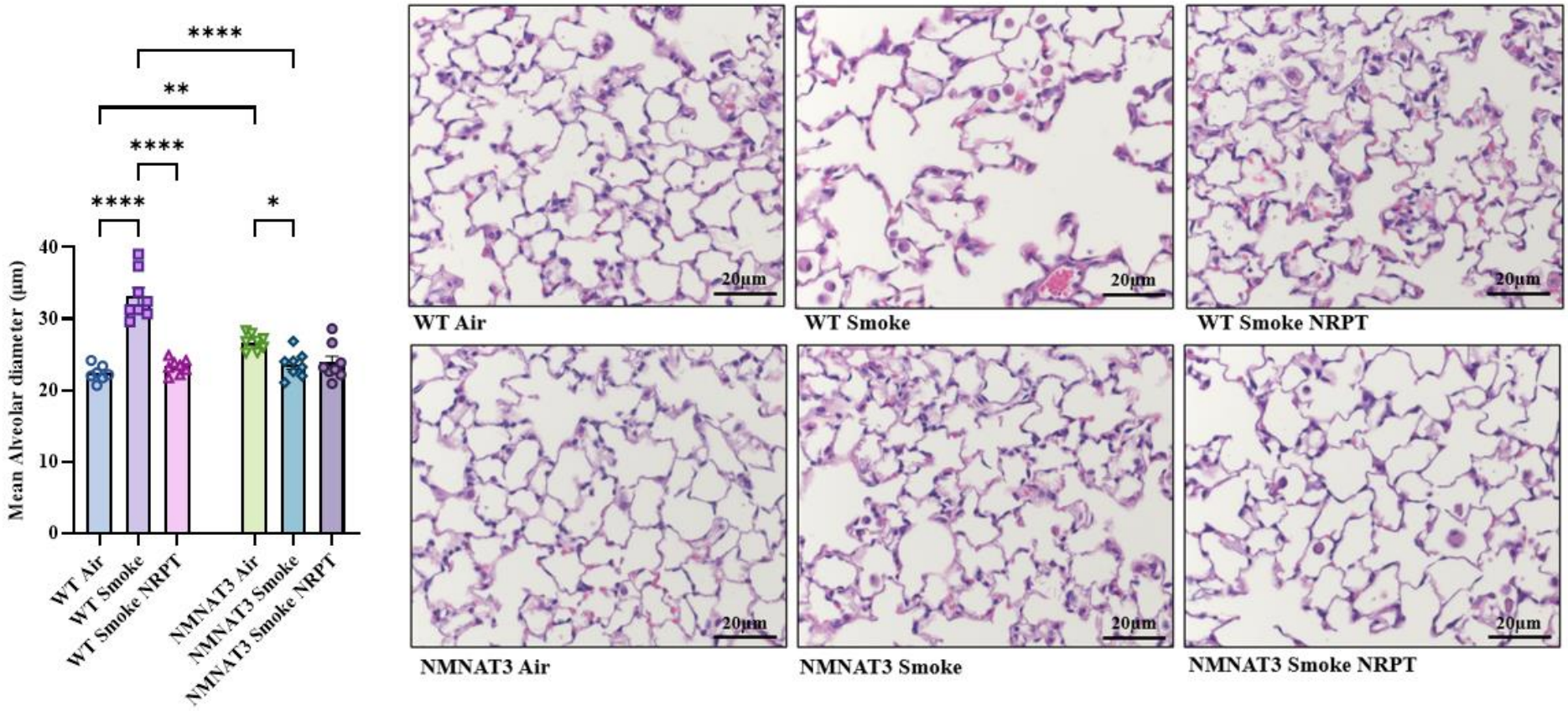

Figure 5.12: NMNAT3 overexpression protected from airway remodelling and emphysema in COPD:

*(A) Graphical representation of the mean area of collagen and representative images of airway remodelling (B) Graphical representation of MLI counts and representative images of emphysema. Data represented are means ± SEM of 6-8 mice/group, * P<0.05, ** P<0.01, *** P<0.001, **** P<0.0001.*

5.3.11 Overexpression of NMNAT3 protects from impaired lung function in COPD

Lung function parameters were measured for NMNAT3 overexpressing mice as mentioned previously under section 2.2.12. An increase in IC (Figure 5.13A) was observed in the WT smoke group in comparison to the WT air group (P<0.001). Similarly, an increase in IC was also observed in NMNAT3 smoke in comparison to the NMNAT3 air (P<0.01). Further, the estimation of IC (A) (Figure 5.13B) increased in the WT smoke group in comparison to the WT air group (P<0.001). We also observed an increase in parameter A for the NMNAT3 smoke group in comparison to the NMNAT3 air group (P<0.01). We observed an increase in the parameter Area (Figure 5.13C) in the WT smoke group in comparison to the WT air group (P<0.001). Similarly, an increase in the Area was also observed in the NMNAT3 smoke as compared to the NMNAT3 air group (P<0.05). An increase in FEV (Figure 5.13D) was observed in the WT smoke group in comparison to the WT air (P<0.0001). We observed an increase in FVC (Figure 5.1E) in the WT smoke group in comparison to the WT air group (P<0.0001). Besides, there was an increase in the parameter VC (Figure 5.13F) in the WT smoke group in comparison to the WT air group (P<0.0001) and this was also reflected between the NMNAT3 smoke group and NMNAT3 air group (P<0.05). In contrast, there was a reduction in VC in the NMNAT3 smoke group in comparison to the WT smoke group(P<0.05). We observed an increase in the parameter Rn (Figure 5.13G) in the NMNAT3 smoke NRPT group in comparison to the WT smoke NRPT group (P<0.01). We also observed an increase in Cst

(Figure 5.13J) in the WT smoke group as compared to the WT air group ($P<0.001$). An increase in the parameter Rrs (Figure 5.13K) was observed in the NMNAT3 smoke NRPT in comparison to the WT smoke NRPT. Followed by an increase in FRC (Figure 5.13M) in the WT smoke group in comparison to the WT air group ($P<0.0001$) and this was further reduced in the NMNAT3 smoke group as compared to the WT smoke group ($P<0.05$). We observed an increase in TLC (Figure 5.13O) in the WT smoke group in comparison to the air group ($P<0.0001$). In contrast, we did not observe any changes in the parameters of G (Figure 5.13H), H (Figure 5.13I), and RV (Figure 5.13N). The lung compliance curves between the WT air, WT smoke and WT smoke NRPT are represented in Figure 5.13P. Followed by the compliance curves between NMNAT3 air, NMNAT3 smoke and NMNAT3 smoke NRPT are represented below in Figure 5.13Q. Further, the compliance curves between NMNAT3 smoke and WT smoke are represented in Figure 5.13R.

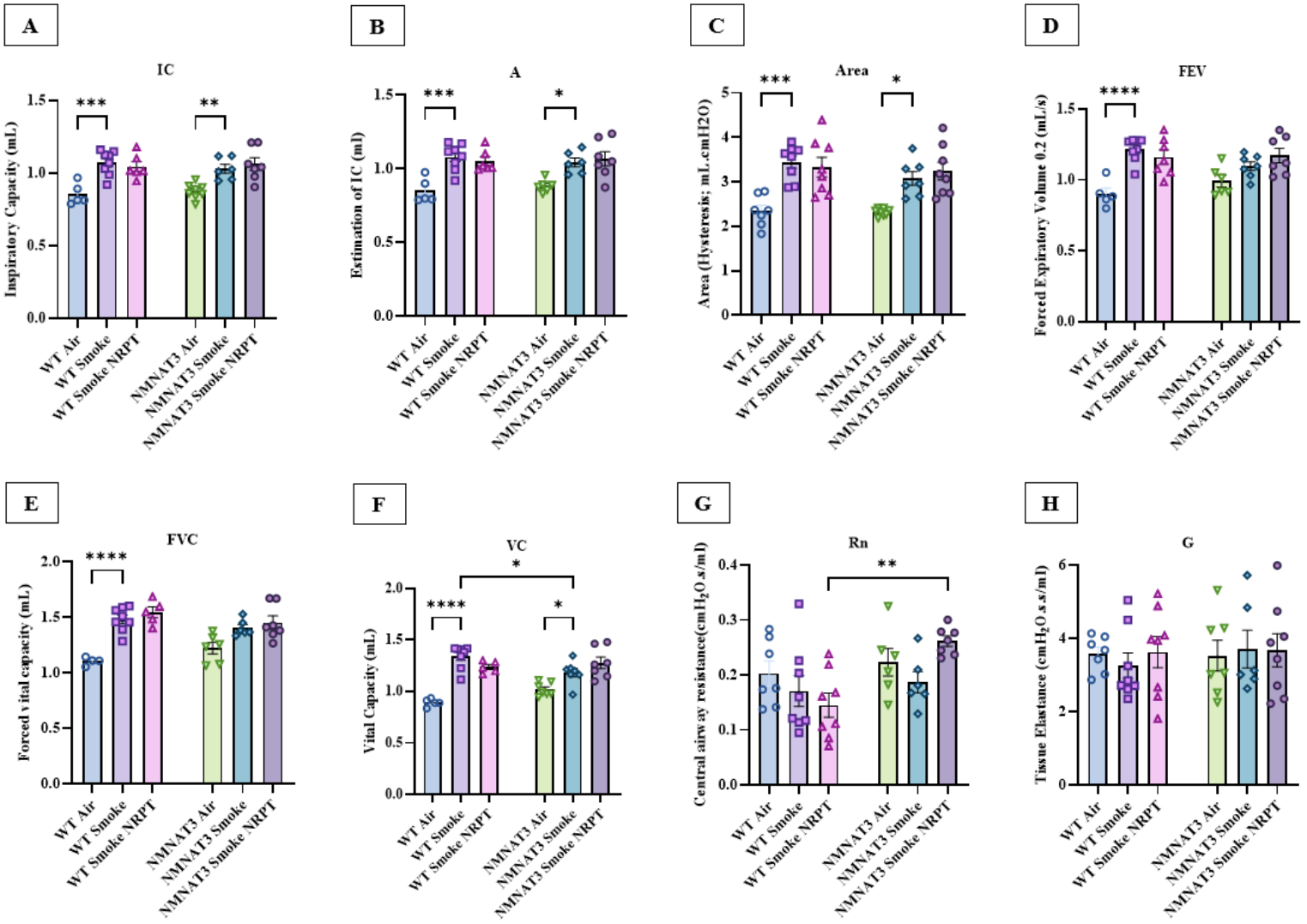
A
IC
Inspiratory Capacity (mL)
***
**
B
A
Estimation of IC (ml)
***
*
C
Area
Area (Hysteresis; mL.cmH2O)
***
*
D
FEV
Forced Expiratory Volume 0.2 (mL/s)
****
E
FVC
Forced vital capacity (mL)
****
F
VC
Vital Capacity (mL)
*
****
*
G
Rn
Central airway resistance(cmH2O.s/ml)
**
H
G
Tissue Elastance (cmH2O.s.s/ml)
WT Air
WT Smoke
WT Smoke NRPT
NMNAT3 Air
NMNAT3 Smoke
NMNAT3 Smoke NRPT

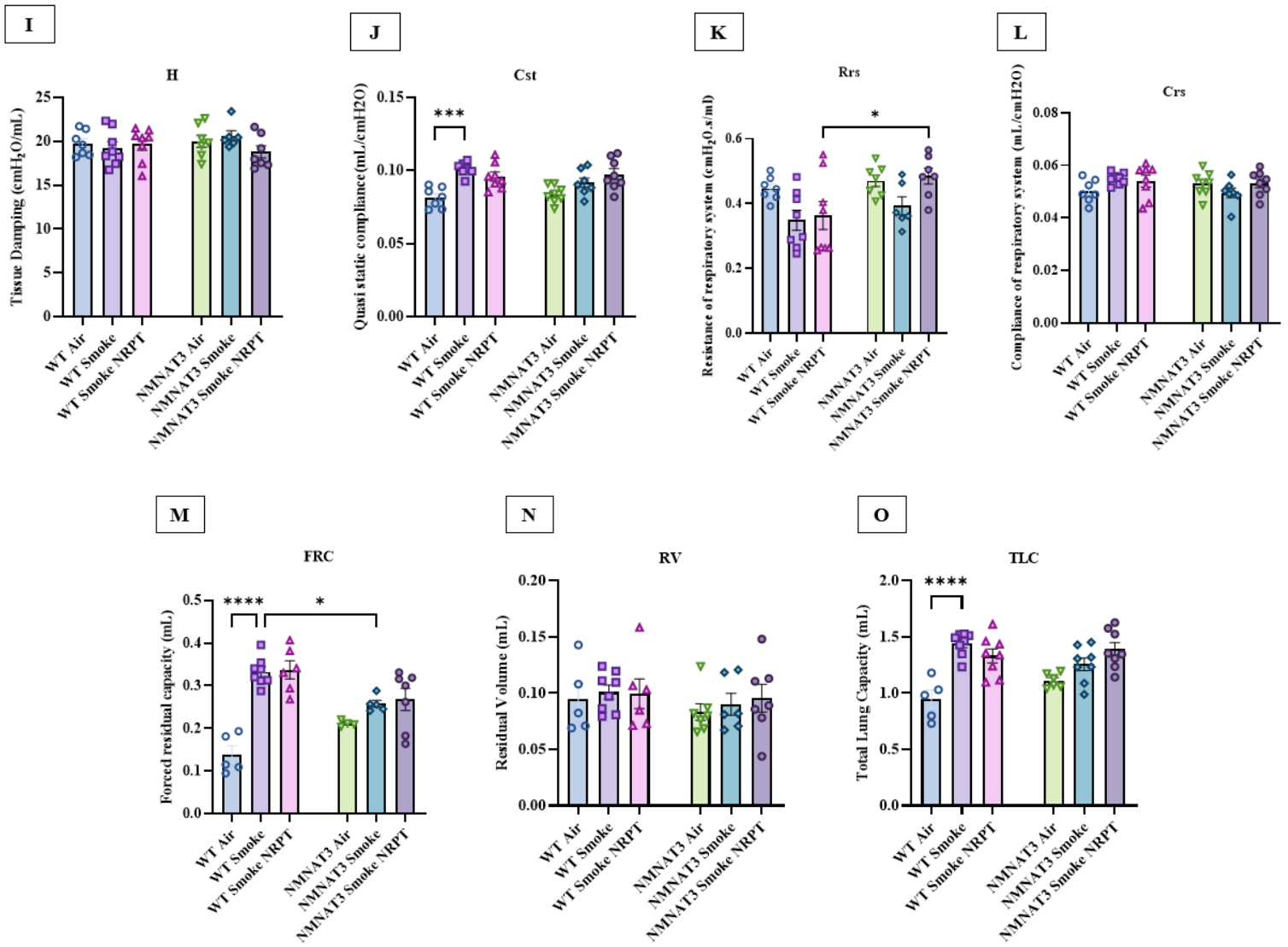
I
H
Tissue Damping (cmH2O/mL)
J
Cst
Quasi static compliance (mL/cmH2O)
***
K
Rrs
Resistance of respiratory system (cmH2O.s/ml)
*
L
Crs
Compliance of respiratory system (mL/cmH2O)
M
FRC
Forced residual capacity (mL)
****
*
N
RV
Residual Volume (mL)
O
TLC
Total Lung Capacity (mL)
****
WT Air
WT Smoke
WT Smoke NRPT
NMNAT3 Air
NMNAT3 Smoke
NMNAT3 Smoke NRPT

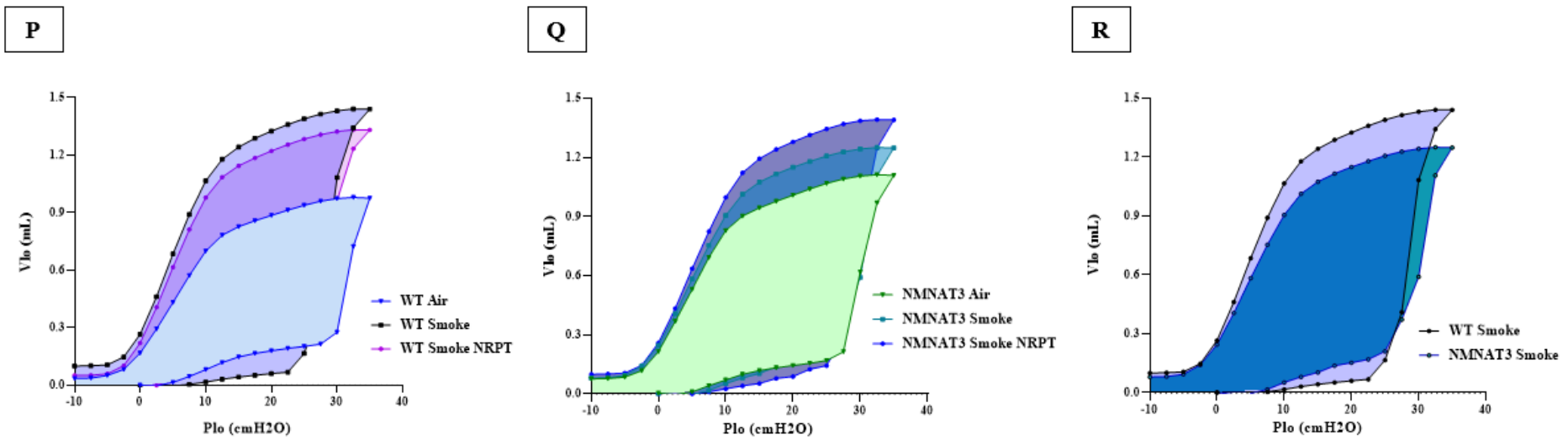

Figure 5.13: NMNAT3 overexpression protected from impaired lung function in COPD:

*Graphical representation of lung function parameters: (A) IC, (B) Estimation of IC (A), (C) Area, (D) Forced expiratory volume (FEV), (E) Forced vital capacity (FVC), (F) Vital capacity (VC), (G) Central airway resistance (Rn), (H) Tissue elastance (G), (I) Tissue damping (H), (J) Quasi-static compliance (Cst), (K) Resistance of respiratory system (Rrs), (L) Compliance of respiratory system (Crs), (M) Functional residual capacity (FRC), (N) Residual volume (RV), (O) Total lung capacity (TLC); Lung compliance curves for (P) WT air, WT smoke and WT smoke NRPT, (Q) NMNAT1 air, NMNAT1 smoke, and NMNAT1 smoke NRPT, (R) NMNAT1 smoke and WT smoke. Data represented are means ± SEM of 6-8 mice/group, * P<0.05, ** P<0.01, *** P<0.001, **** P<0.0001.*

5.3.12 NMNAT3 overexpression regulated NAD^+ biosynthesis in COPD

We observed a significant increase in the gene expression of NMNAT1 (Figure 5.14A) between the WT air and NMNAT3 air ($P<0.001$). A reduction in the gene expression of NMNAT1 was observed both in the NMNAT3 smoke group ($P<0.001$) and the NMNAT3 smoke NRPT group ($P<0.01$) with respect to the NMNAT3 air group. We did not observe any change in the gene expression of NMNAT2 (Figure 5.14B) across all the experimental groups. Additionally, we observed an increase in the gene expression of NMNAT3 (Figure 5.14C) in the NMNAT air group in comparison to the WT air group ($P<0.0001$). In contrast, a reduction in the gene expression of NMNAT3 was observed in the NMNAT3 smoke NRPT group in comparison to the NMNAT3 air group. Furthermore, we observed an increase in the ratio of total NAD/NADH levels in the WT smoke group in comparison to the WT smoke NRPT group as well as the WT air group ($P<0.0001$). An increase in the ratio of total NAD/NADH levels was observed in the NMNAT3 smoke group in comparison to the NMNAT air group ($P<0.0001$). Further, we also observed an increase in the ratio of total NAD/NADH levels in the NMNAT3 smoke NRPT group in comparison to the WT smoke NRPT group ($P<0.0001$) (Figure 5.14D). Similarly, the total NAD^+ levels increased in the WT smoke NRPT group in comparison to the WT smoke group ($P<0.01$). We observed an increase in the total NAD^+ levels in the NMNAT3 smoke group as compared to the WT smoke group ($P<0.05$) (Figure 5.14E). Moreover, there was a decrease in the NADH levels in the WT smoke group in comparison to the WT air group as well as the WT smoke NRPT group ($P<0.0001$). We observed a reduction in the NADH levels in the NMNAT3 smoke NRPT group as compared to the WT smoke NRPT group ($P<0.0001$). Additionally, we observed a reduction in the NADH levels in the NMNAT3 smoke group in comparison to the NMNAT3 air group ($P<0.0001$) (Figure 5.14F).

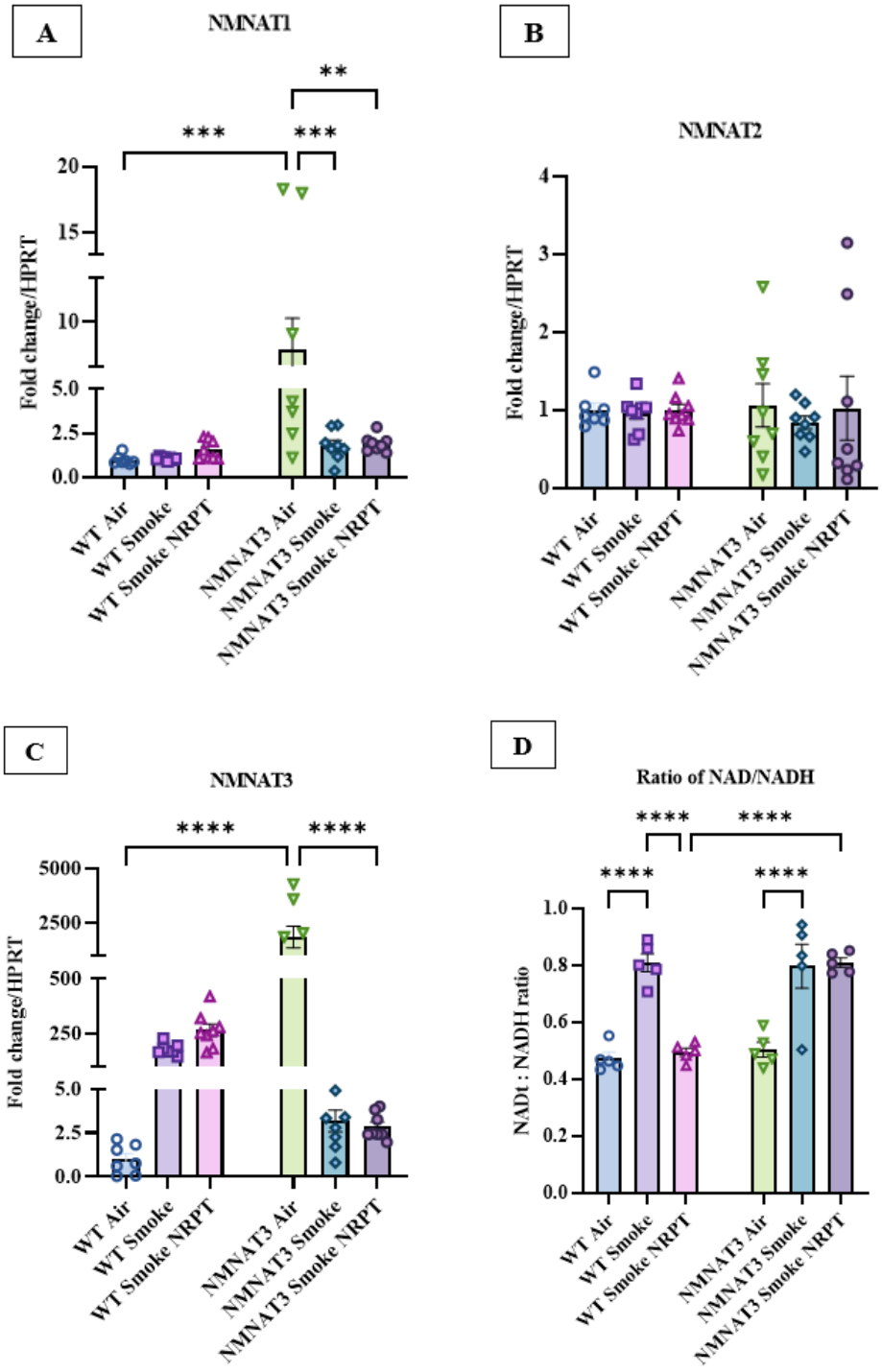
A
NMNAT1
**
***
***
Fold change/HPRT
20
15
10
5.0
2.5
0.0
WT Air
WT Smoke
WT Smoke NRPT
NMNAT3 Air
NMNAT3 Smoke
NMNAT3 Smoke NRPT
B
NMNAT2
Fold change/HPRT
4
3
2
1
0
WT Air
WT Smoke
WT Smoke NRPT
NMNAT3 Air
NMNAT3 Smoke
NMNAT3 Smoke NRPT
C
NMNAT3
****
****
Fold change/HPRT
5000
2500
500
250
5.0
2.5
0.0
WT Air
WT Smoke
WT Smoke NRPT
NMNAT3 Air
NMNAT3 Smoke
NMNAT3 Smoke NRPT
D
Ratio of NAD/NADH
****
****
****
****
NADt : NADH ratio
1.0
0.8
0.6
0.4
0.2
0.0
WT Air
WT Smoke
WT Smoke NRPT
NMNAT3 Air
NMNAT3 Smoke
NMNAT3 Smoke NRPT

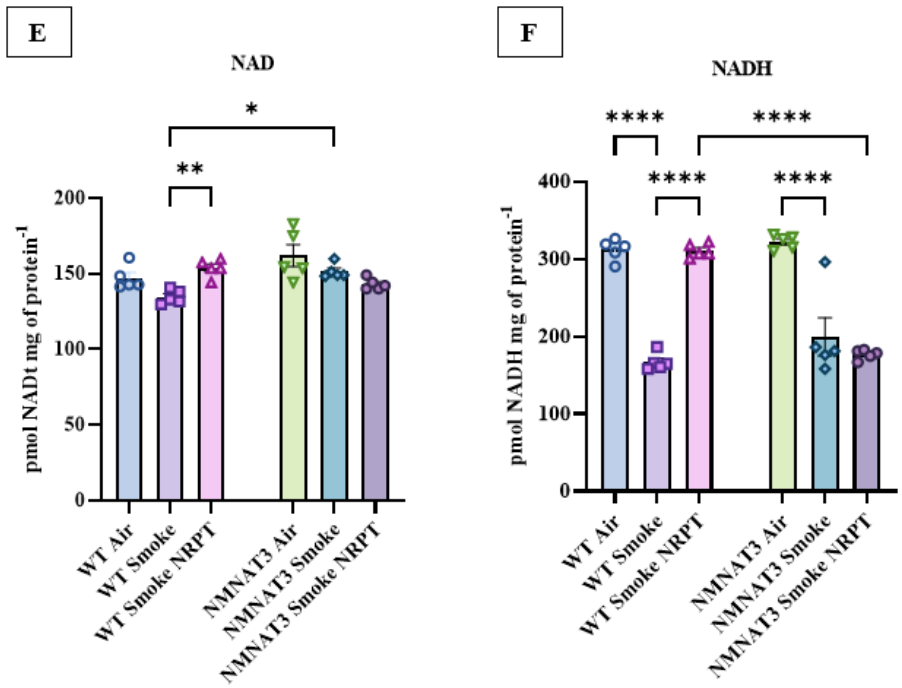

Figure 5.14: Effect of NMNAT3 overexpression on NAD^+ biosynthesis in COPD:

*Gene expression of (A) NMNAT3, (B) NMNAT2, and (C) NMNAT3; (D) ratio of NAD^+/NADH, (E) total NAD^+ levels, (F) NADH levels. Data represented are means ± SEM of 6-8 mice/group, * P<0.05, ** P<0.01, *** P<0.001, **** P<0.0001.*

5.3.13 NMNAT3 overexpression regulated NAD^+ consumers in COPD

We observed an increase in PARP activity levels (Figure 5.15A) in the WTsmoke group in comparison to the WT air group (P<0.0001). Furthermore, a reduction in the PARP activity was observed both in the WT smoke NRPT and NMNAT3 smoke group in comparison to the WT smoke group (P<0.0001). In contrast, we did not observe any changes in the gene expression of PARP1 (Figure 5.15B) across all the experimental groups.

Further, we observed a reduction in the gene expression of SIRT2 (Figure 5.15D) in the NMNAT3 smoke NRPT group in comparison to the WT smoke NRPT group (P<0.01).

We observed an increase in the gene expression of SIRT3 in the NMNAT3 smoke group in comparison to the NMNAT3 air group and this expression was further increased in the NMNAT3 smoke NRPT group as compared to the NMNAT3 smoke group ($P<0.05$). An increase in the gene expression of NMNAT3 was observed in the NMNAT3 smoke NRPT group as compared to the WT smoke NRPT group ($P<0.0001$). In contrast, we did not observe any change in the gene expression of SIRT1 (Figure 5.15C), SIRT4 (Figure 5.15F), and SIRT5-7 (Figure 5.15G-I).

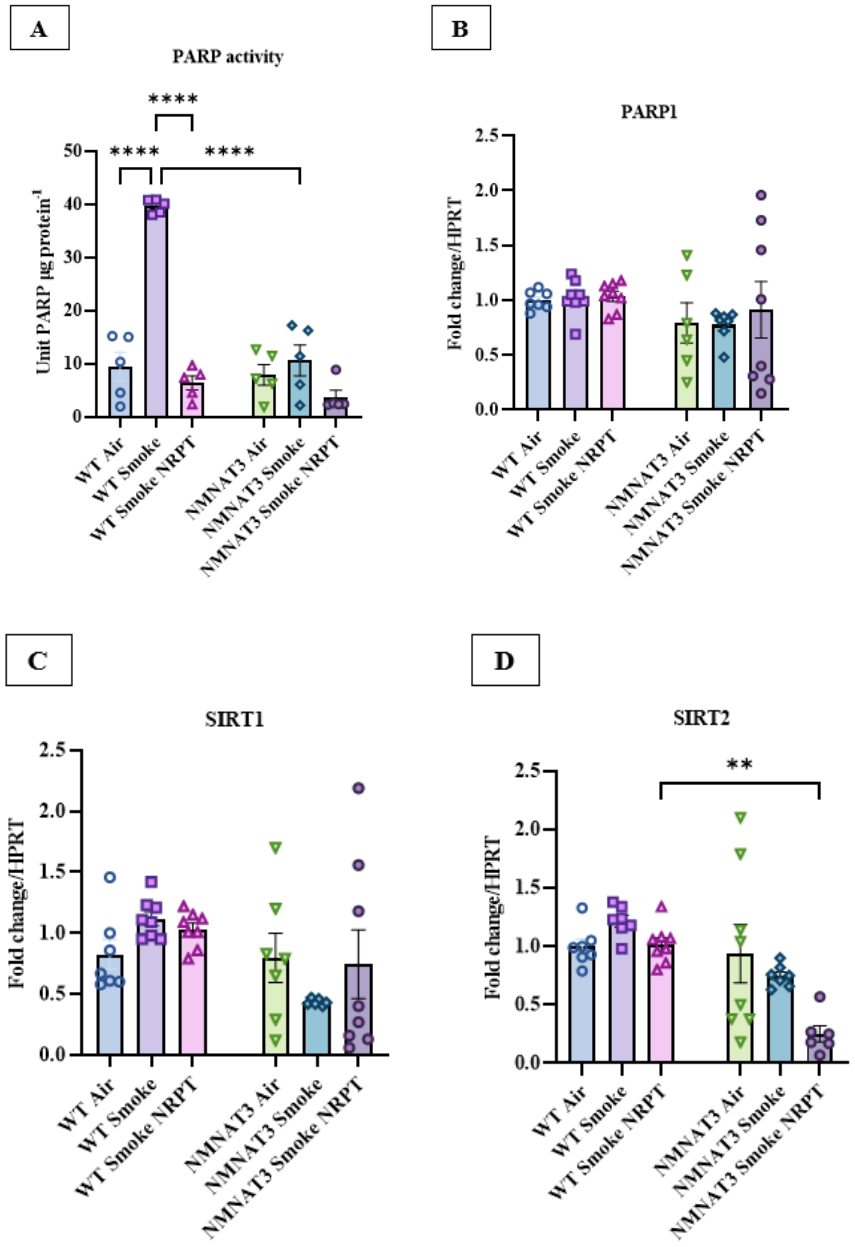

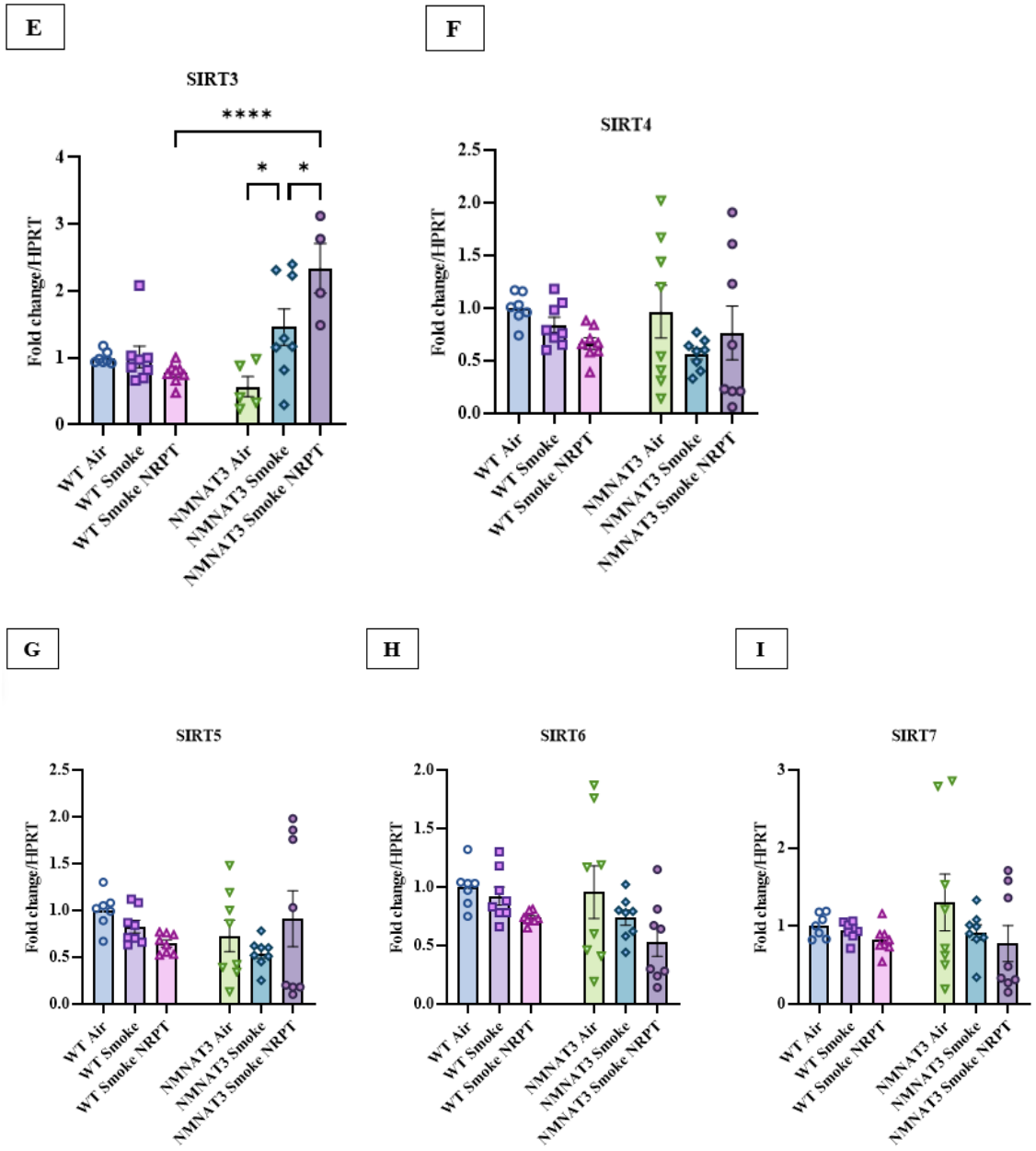

Figure 5.15: NMNAT3 overexpression regulated NAD$^+$ consumers in COPD:

*(A) PARP activity; Gene expression for (B) PARP1, (C) SIRT1, (D) SIRT2, (E) SIRT3, (F) SIRT4, (G) SIRT5, (H) SIRT6, (I) SIRT7. Data represented are means ± SEM of 6-8 mice/group, * P<0.05, ** P<0.01, *** P<0.001, **** P<0.0001.*

5.3.14 NMNAT3 overexpression increased mitochondria membrane potential

We observed a decrease in the MFI of J-aggregates (Figure 5.16A) in the WT smoke group ($P<0.001$) and NMNAT3 air group ($P<0.0001$) in comparison to the WT air group. We observed an increase in the J-aggregates in the NMNAT3 smoke group in comparison to the NMNAT3 air group ($P<0.01$) as well as the NMNAT3 smoke NRPT group ($P<0.01$). We also observed a reduction in the J-aggregates in the NMNAT3 smoke NRPT group in comparison to the WT smoke NRPT group ($P<0.0001$). Simultaneously, we also measured the MFI of J-monomers (Figure 5.16B) and observed an increase in the WT smoke group with respect to the WT air, WT smoke NRPT as well as NMNAT3 smoke group ($P<0.0001$). Furthermore, we observed a reduction in the MFI of J-monomers in the NMNAT3 smoke NRPT group as compared to the WT smoke NRPT group ($P<0.05$). We observed a reduction of $\Delta\Psi m$ (Figure 5.16C) in the WT smoke group in comparison to the WT air group, WT smoke NRPT group, and the NMNAT3 smoke group ($P<0.0001$). An increase in the $\Delta\Psi m$ was observed in the NMNAT3 smoke group in comparison to the NMNAT3 air group ($P<0.001$). We observed an increase in the $\Delta\Psi m$ in the NMNAT3 smoke NRPT in comparison to the WT smoke NRPT group ($P<0.0001$). In contrast, we observed a reduction in the $\Delta\Psi m$ in the NMNAT3 air group with respect to the WT air group ($P<0.05$).

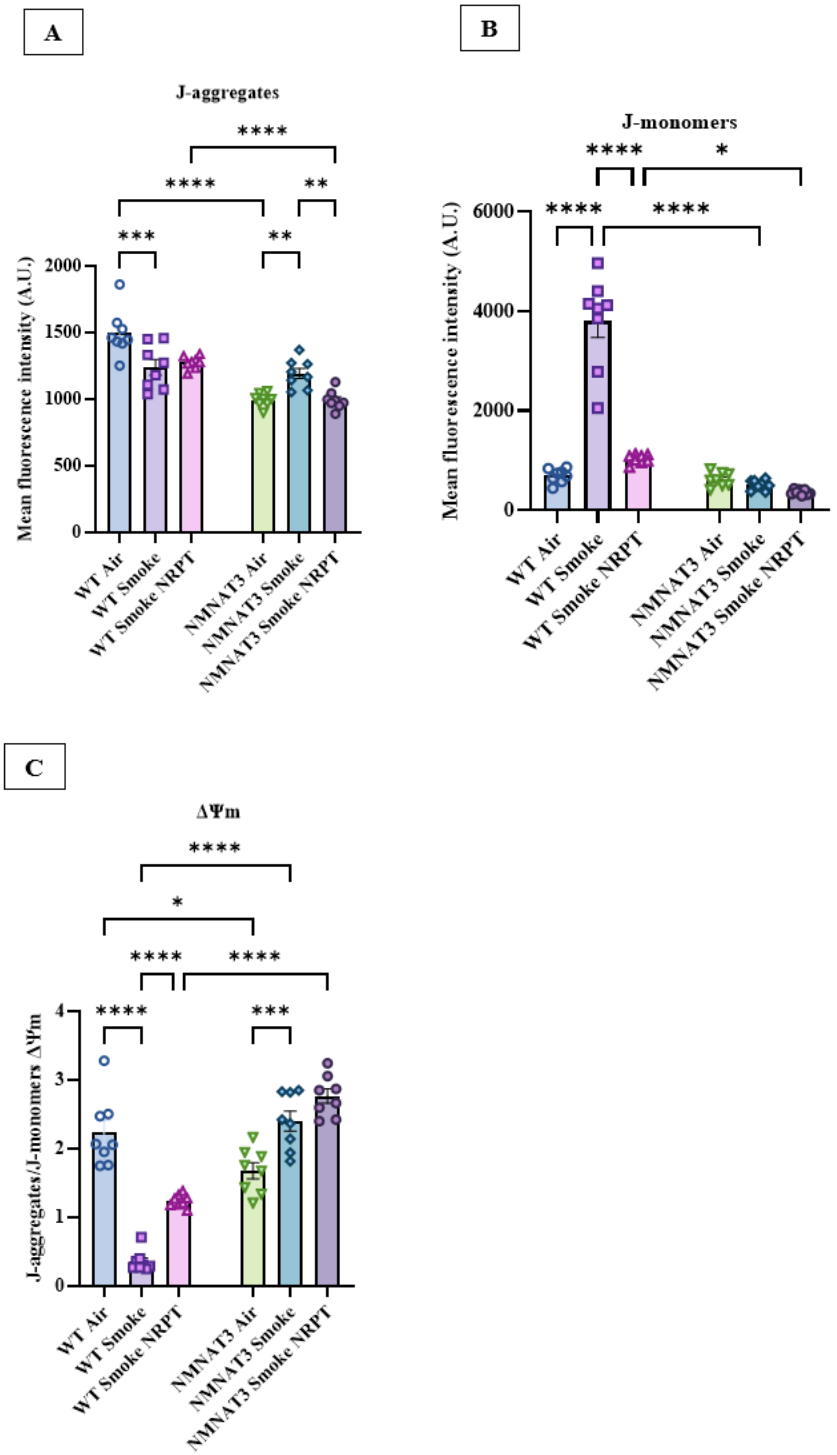
A
J-aggregates
Mean fluorescence intensity (A.U.)
2000
1500
1000
500
0
****
****
**
***
**
WT Air
WT Smoke
WT Smoke NRPT
NMNAT3 Air
NMNAT3 Smoke
NMNAT3 Smoke NRPT
B
J-monomers
Mean fluorescence intensity (A.U.)
6000
4000
2000
0
****
****
*
WT Air
WT Smoke
WT Smoke NRPT
NMNAT3 Air
NMNAT3 Smoke
NMNAT3 Smoke NRPT
C
ΔΨm
J-aggregates/J-monomers ΔΨm
4
3
2
1
0
****
*
****
****
****
***
WT Air
WT Smoke
WT Smoke NRPT
NMNAT3 Air
NMNAT3 Smoke
NMNAT3 Smoke NRPT

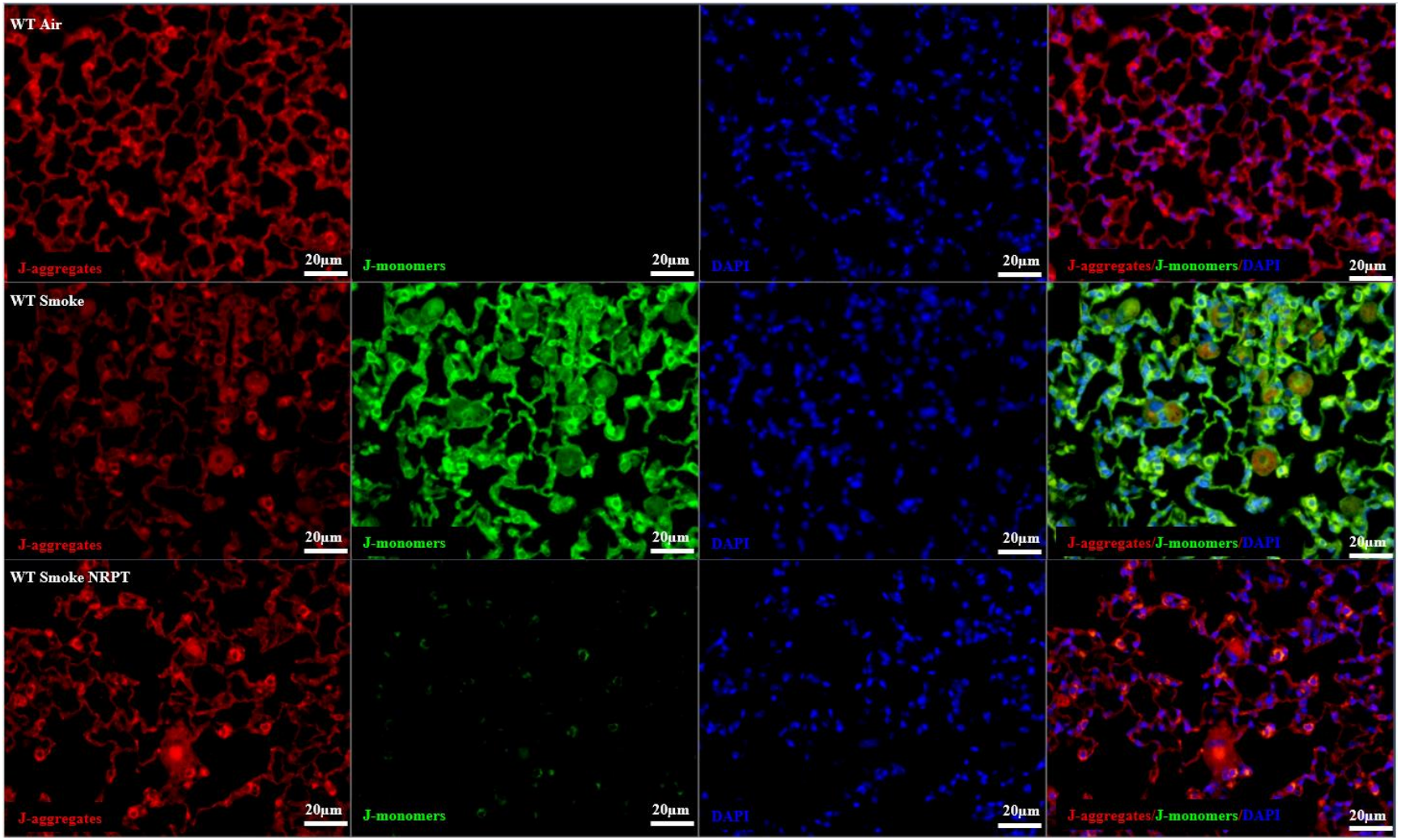
WT Air
J-aggregates
20μm
J-monomers
20μm
DAPI
20μm
J-aggregates/J-monomers/DAPI
20μm
WT Smoke
J-aggregates
20μm
J-monomers
20μm
DAPI
20μm
J-aggregates/J-monomers/DAPI
20μm
WT Smoke NRPT
J-aggregates
20μm
J-monomers
20μm
DAPI
20μm
J-aggregates/J-monomers/DAPI
20μm

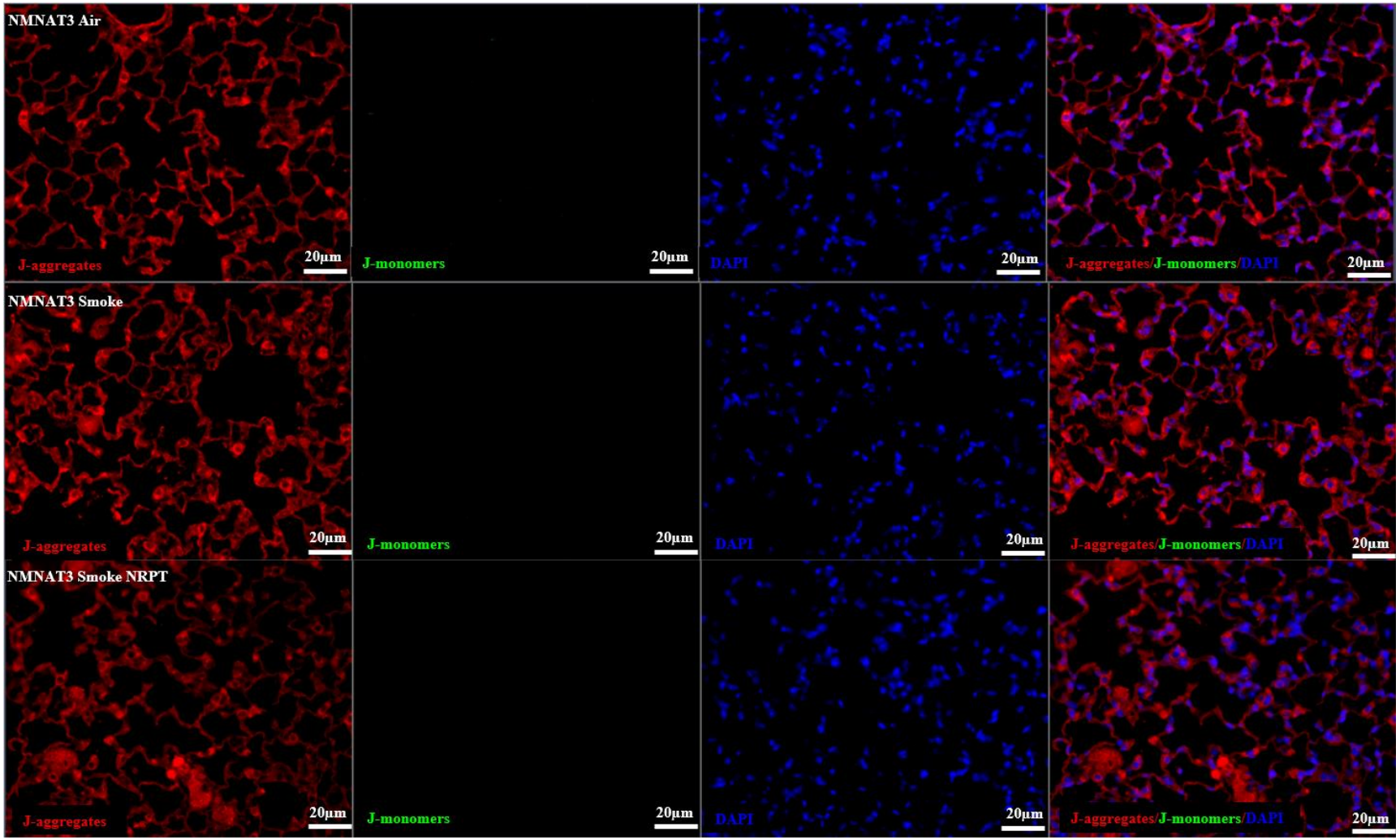

Figure 5.16: NMNAT3 overexpression increased mitochondria membrane potential in COPD:

Graphical representation of MFI obtained for (A) J-aggregates (red), (B) J-monomers (green), (C) Ratio of J-aggregates/J-monomers (ΔΨm). Representative images from all the experimental groups under different channels: J-aggregates in red, J-monomers in green, and nuclear stain DAPI in blue followed by a merged image of all the channels.

5.3.15 NMNAT3 overexpression reduced oxidative stress in COPD

We observed an increase in gene expression of NOX2 (Figure 5.17A) in the WT smoke group in comparison to the WT air group ($P<0.0001$). Further, we also observed an increase in the gene expression of NOX2 in the NMNAT3 group in comparison to the NMNAT3 air group ($P<0.0001$) as well as the NMNAT3 smoke NRPT group ($P<0.05$). In contrast, there was no change observed in the gene expression of HO1 (Figure 5.17B) across all the experimental groups in this study.

In addition, we observed an increase in the MFI obtained from 4-HNE in the WT smoke group in comparison to the WT air group ($P<0.0001$), WT smoke NRPT group ($P<0.0001$) and NMNAT3 smoke group ($P<0.0001$). Images below represent 4-HNE co-stained with F4/80 and DAPI (Figure 5.17C).

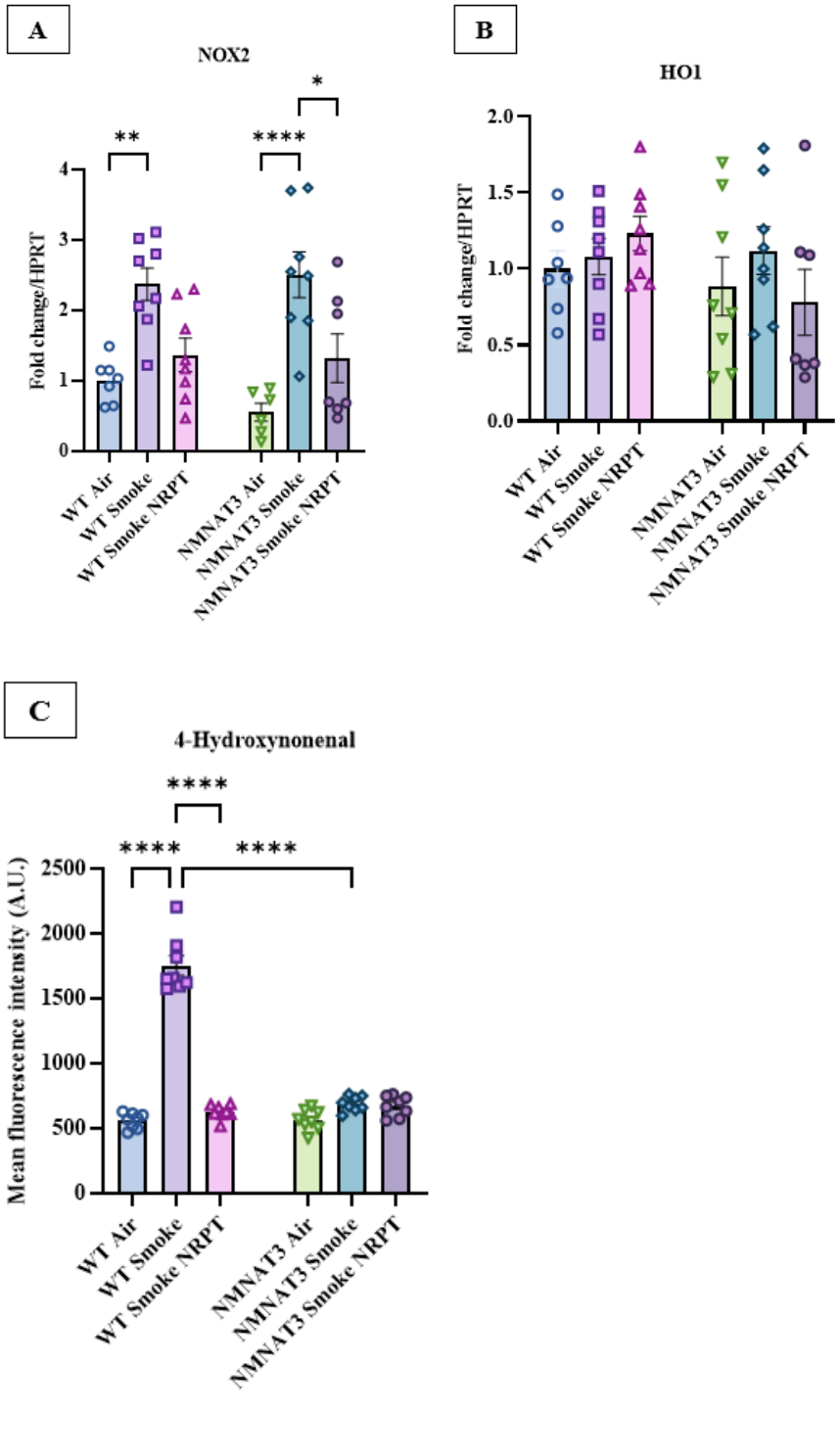
A
NOX2
Fold change/HPRT
**
****
*
WT Air
WT Smoke
WT Smoke NRPT
NMNAT3 Air
NMNAT3 Smoke
NMNAT3 Smoke NRPT
B
HO1
Fold change/HPRT
C
4-Hydroxynonenal
Mean fluorescence intensity (A.U.)

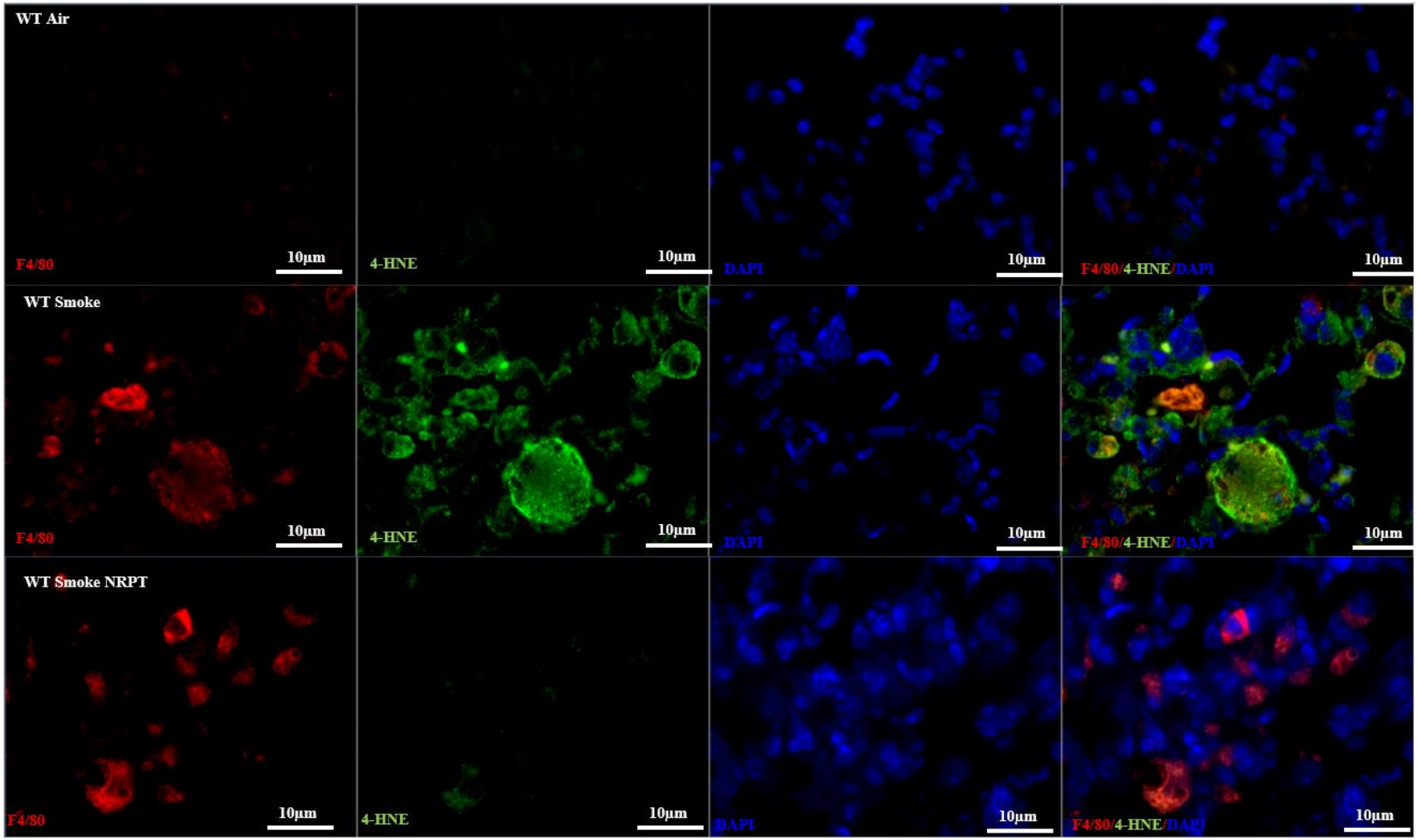
WT Air
F4/80
10μm
4-HNE
10μm
DAPI
10μm
F4/80/4-HNE/DAPI
10μm
WT Smoke
F4/80
10μm
4-HNE
10μm
DAPI
10μm
F4/80/4-HNE/DAPI
10μm
WT Smoke NRPT
F4/80
10μm
4-HNE
10μm
DAPI
10μm
F4/80/4-HNE/DAPI
10μm

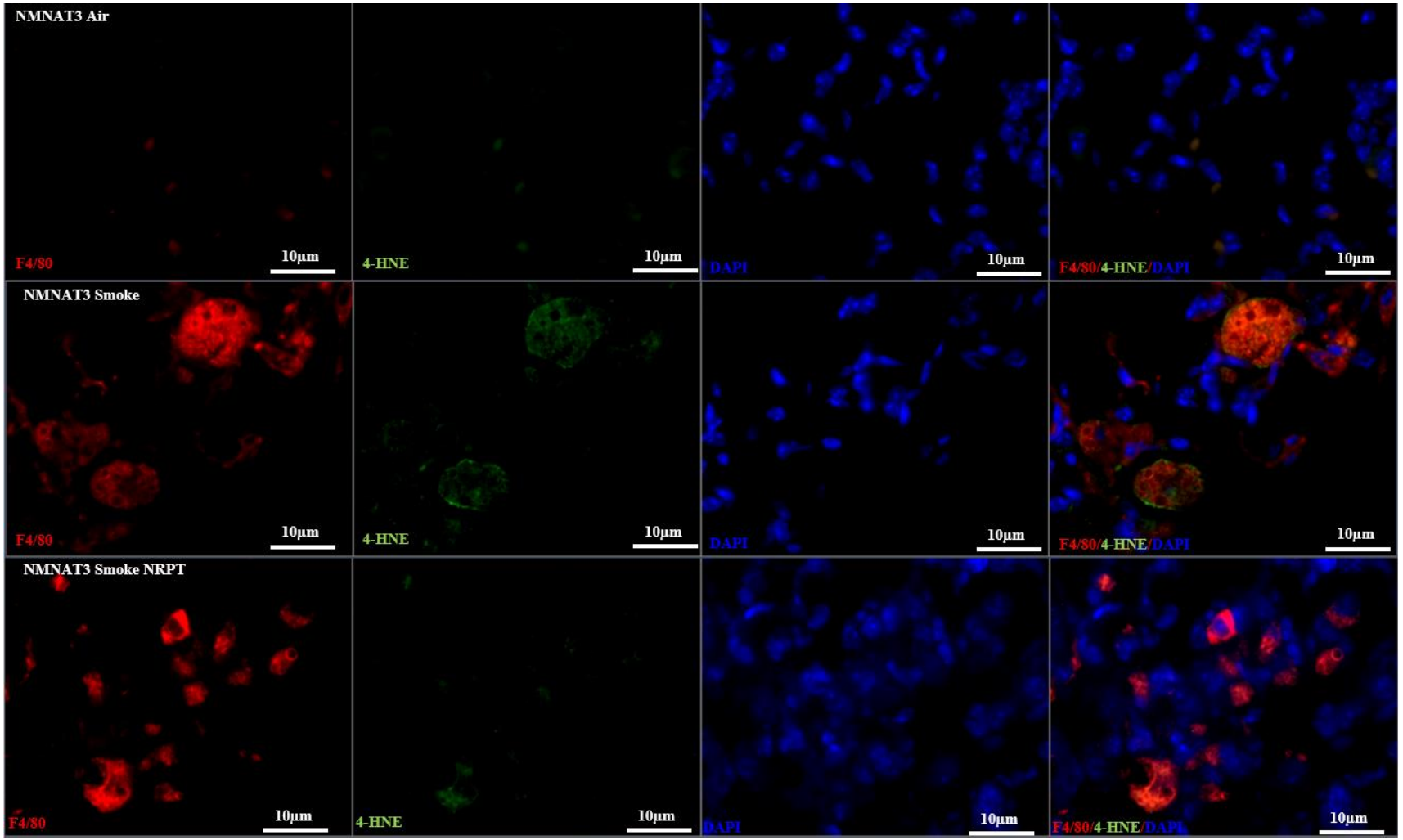

Figure 5.17: NMNAT3 overexpression reduced oxidative stress in COPD:

*Gene expression of (A) NOX2, (B) HO1; (C) Graphical representation of MFI in arbitrary units (A.U.) of 4-HNE images show fluorescence localisation of F4/80 (red), 4-HNE (green), DAPI-nuclei stain (blue). Data represented are means ± SEM of 6-8 mice/group, * P<0.05, ** P<0.01, *** P<0.001, **** P<0.0001.*

5.4 Discussion

In the previous studies (chapters 3 & 4), we demonstrated that imbalances in the NAD^+ level play an important role in the development and progression of COPD. Additionally, modulation of NAD^+ synthesis and consumption using NR and PT exhibited benefits from COPD features in both prophylactic and therapeutic studies. However, the key pathway responsible for the regulation of NAD^+ via NR and PT treatment in COPD remains unknown. In our current study, we investigated the role of NMNATs in modulating NAD^+ levels in comparison to the treatment of NR and PT in COPD. To further unveil the protective mechanisms of NR and PT in COPD, we utilised overexpressing NMNAT1 and NMNAT3 transgenic mice to exert the benefits of elevated NAD^+ levels in COPD in the absence of treatment with NR and PT. Additionally, we also administered NR and PT to the overexpressing NMNAT1 and NMNAT3 transgenic mice to further elucidate if inordinate NAD^+ levels can potentially exert additional benefits from COPD.

Utilising previously obtained lung samples from our 8-week (Chapter 3) and 12-week (Chapter 4) COPD study with NR and PT, we measured the gene expression of various candidates of the NAD^+ biosynthesis pathways and found NMNAT1, NMNAT2 and NMNAT3 to be promising targets to be further explored our study. We observed a reduction in the gene expression of NMNAT1/2/3 in the smoke group after 8 weeks of CS exposure in comparison with the air groups (Figure 5.3A-C), suggesting that the decreased expression of NMNAT1/2/3 is likely involved in the reduced synthesis of NAD^+, in addition to the hyperactivity of NAD^+ consumer, PARPs leading to an imbalance of NAD^+ levels in COPD. This was further reflected in our 12-week study,

where we observed a reduction in the gene expression of NMNAT1 and NMNAT3 in the smoke group after 12 weeks of CS exposure (Figures 5.3D & F, 5.3G & H).

Interestingly, we observed an increase in the gene expression of NMNAT1/2/3 in the NR and PT treatment groups after 8 weeks (Figure 5.3 A-C), suggesting that NR and PT in combination are driving increased NMNAT1-3 expression in COPD, potentially increasing NAD^+ levels and reducing the overactivation of PARPs and increasing sirtuin activity. In addition, we observed an increase in the gene expression of NMNAT1 in the short-term administration of NR and PT with/without cessation of CS in the 12-week COPD study but this did not improve with the long-term treatment of NR and PT (Figures 5.3D & 5.3G). This is not surprising as we previously observed an increase in the NAD^+ levels with the short-term administration of NR and PT but not with the prolonged treatment (Chapter 4). As NMNAT1 is localised in the nucleus, therefore it is plausible that the nuclear-synthesised NAD^+ via NMNAT1 is rapidly degraded due to the overactivation of nuclear-localised PARPs such as PARP1. In addition, we also observed an increase in the gene expression of NMNAT3 both in the prophylactic and therapeutic administration of NR and PT with or without the cessation of CS in the 12-week study (Figures 5.3F & 5.3I). These findings further support the increase in NMNATs leading to an increase in NAD^+ levels. We have also demonstrated that prolonged treatment of NR and PT increased the gene expression of NMNAT3, which potentially drives the benefits of improvement in mitochondrial structure and function as highlighted previously (Chapter 4). Henceforth, NR and PT contribute to NAD^+ synthesis and consumption pathways via NMNAT1/2/3 in COPD. There are limited effects of NMNAT1 in advanced stages of the disease when treated with NR and PT for a longer duration, due to the rapid degradation of NAD^+ via hyperactivity of PARPs and this exerts limited benefits of prolonged NR and PT treatment. Critically, both short and prolonged treatment with NR

and PT increased NMNAT3 expression indicating that mitochondria localised NMNAT3 is protective against damage caused in COPD.

In contrast, we did not observe any changes in the gene expression of NMNAT2 in the 12-week study (Figure 5.3E & 5.3H), which isn't surprising as cytosolic NAD^+ consumers like SIRT2 and CD38 levels remain unchanged in the study as well. This suggested that cytosolic NAD^+ level isn't crucial in COPD, however, we will measure additional cytosolic NAD^+ consumers like PARP6 and SARM1 to validate if there is a rapid degradation of NAD^+ level in the cytosol which potentially contributes to this. Taken together, these findings suggested that NR and PT administration in COPD increased NAD^+ levels via increasing NMNAT1 and NMNAT3 further contributing to improvements in COPD features.

To further validate our above findings, we used overexpressing NMNAT1 and NMNAT3 transgenic mice and induced a COPD phenotype with or without the administration of NR and PT. We observed an increase in the infiltration of leukocytes in the BALF upon exposure to CS in the WT smoke mice in comparison to WT air-exposed mice (Figure 5.4 &5.14). As shown in previous chapters (Chapters 3 and 4), there was a significant reduction in cellular infiltrates in the BALF with the administration of NR and PT in the WT mice supporting our previous observations of anti-inflammatory responses of NR and PT in reducing airway inflammation in COPD. Additionally, NMNAT1 and NMNAT3 overexpressing mice demonstrated reduced cellular infiltrates in the BALF with 8 weeks of CS exposure. We observed a reduction in cellular infiltrates with the administration of NR and PT both in NMNAT1 and NMNAT3 overexpressed mice. These results further suggested that elevated NMNAT1 and NMNAT3 with or without the treatment of NR and PT have anti-inflammatory potential in COPD. Furthermore, TNFα (Figures 5.4E & 5.11E) and CXCL1 (Figures 5.4F & 5.11F) expression was upregulated in the lungs of

WT mice upon exposure to CS as a result of increased airway inflammation in COPD. We observed a reduction in the gene expression of TNFα and CXCL1 in both the NMNAT1 and NMNAT3 overexpressed mice with or without the administration of NR and PT. These findings further supported the anti-inflammatory potential of elevated NMNAT1 and NMNAT3 in COPD. This was interesting as NMNAT1 and NMNAT3 drive NAD^+ levels with or without NR and PT which might potentially reduce the overactivation of PARPs and promote the activation of SIRTs as a consequence, further reducing inflammation in COPD. Previous studies have stated the potential involvement of impaired NAD^+ metabolism in increasing inflammation (436, 437) via an increase in ROS (438), however, to date, there is limited knowledge about the exact underlying mechanisms involved in this process.

Additionally, we observed a significant difference in body weight between WT air mice and WT smoke mice (Figures 5.4D & 5.11D). This was further observed in between NMNAT1 air and NMNAT1 smoke as well as NMNAT3 air and NMNAT3 smoke. This could be due to systemic inflammation which plays an important role during the progression of COPD and further studies will be required to understand the underlying mechanisms for the restoration of body weight.

We further validated different features of COPD in our study including airway remodelling, emphysema and impaired lung function. We observed an increase in airway remodelling and emphysema in the smoke group of WT mice which further validated the disease features (Figures 5.5 & 5.12). Interestingly, we observed a significant reduction in the features of airway remodelling and emphysema in the smoke groups of NMNAT1 and NMNAT3 overexpressing mice. Additionally, we also observed a reduction in airway remodelling and emphysema with the administration of NR and PT in both WT as well as NMNAT1 and NMNAT3 overexpressed mice. These findings further suggested that

NMNAT1 and NMNAT3 overexpression protected lung structure from the damage induced by chronic exposure to CS in COPD with or without NR and PT. These findings indicate that NMNAT1 and NMNAT3 with or without NR and PT are capable of regulating NAD^+ synthesis and consumption, which reduces the damage caused due to the overactivation of PARPs resulting in reduced inflammation in COPD. This further contributes to reduced tissue damage, henceforth protecting from airway remodelling and emphysema. This was interesting as currently there is no evidence on the protective aspects of NMNAT1 and NMNAT3 in COPD. However, both NMNAT1 (428, 439) and NMNAT3 (440, 441) have been previously shown to protect axon degeneration in neuronal diseases.

Furthermore, we validated impaired lung function in our COPD study with WT mice as well as NMNAT1 and NMNAT3 overexpressed mice (Figures 5.6 & 5.13). We observed an increase in the lung parameters of IC, A, Area, FEV, FVC, VC and FRC in the WT mice after 8 weeks of CS exposure in comparison to the air-exposed mice. An increase in the lung parameters of WT smoke mice suggested the development of the disease as previously observed in our earlier studies (Chapters 3 & 4). However, following the administration of NR and PT for 8 weeks in WT CS-exposed mice, we observed a reduction in parameters A and RV. However, there was no significant reduction in the parameters of IC, area and TLC as shown in our previous chapter, hence NR and PT treatment in the WT littermates only partially protected from impaired lung function in COPD. This could be potentially due to variation in the strain of mice as the mice in our current study is on C57BL6 background. Studies have shown that C57BL6 mice have a higher airway reactivity in asthma and fibrosis models. This, therefore, contributes to severe disease features, and we have previously observed limited benefits of prophylactic treatment with NR and PT in severe disease stages mentioned previously (Chapter 4). CS-

exposed NMNAT1 overexpressed mice showed a reduction in the parameter RV in comparison to the WT smoke mice suggesting NMNAT1 overexpression partially protected from impaired lung function in COPD. The reduction of RV suggested a decrease in the volume of trapped air in the lung indicating reduced emphysema in the NMNAT1 overexpressed mice and this was also depicted in our histology data. Furthermore, CS-exposed NMNAT3 mice showed a reduction in the parameters VC and FRC in comparison to the WT smoke mice suggesting NMNAT3 overexpression also partially protected from impaired lung function in COPD. Moreover, an increase in the lung compliance curves was observed in the WT smoke group in comparison to the WT air group with an upward shift, representing the poor recoiling property of the lung due to chronic exposure to CS. We also observed a reduced lung compliance curve supported by the downward shift in the curve in the NMNAT3 smoke group in comparison to the WT smoke group suggesting improved expandability of lungs with NMNAT3 overexpression. In conclusion, we have demonstrated that the overexpression of NMNAT1 and NMNAT3 exhibited partial protection from impaired lung function in COPD.

In addition to our above findings, upon administration of NR and PT in the overexpressing NMNAT1 mice not only failed to protect from impaired lung function but also worsened the severity of several lung parameters such as IC, A, FVC, VC, and FRC in comparison to the WT mice. We also observed a similar effect in NMNAT3 overexpressed mice with a further increase in the parameters of Rn and Rrs with the treatment of NR and PT in comparison to the WT mice. These results further suggested that NR and PT exert limited benefits on overexpressed NMNAT1 and NMNAT3 mice in COPD with potential off-target effects or a consequence of NAD^+ toxicity which further worsened the disease features. Previous studies have stated that inordinate levels of NAD^+ would have a global

impact on cellular proteins and homeostasis which will further lead to the development of cancer (442).

Further, we analysed the gene expression of NMNAT1/2/3 in the lungs of both WT as well as NMNAT1 and NMNAT3 overexpressed mice after 8 weeks of CS exposure. An increase in the gene expression of NMNAT1 was observed in all the NMNAT1 overexpressed groups with respect to the WT groups validating the NMNAT1 overexpression in COPD. We observed a decrease in the gene expression of NMNAT2 and NMNAT3 in the WT smoke group in comparison to the WT air group which was increased in the WT smoke NRPT group. These results further validated our previous findings of an increase in NMNAT1/2/3 (Figure 5.7A-C) with the administration of NR and PT in WT mice. However, we did not observe any changes in the expression of NMNAT2 in the NMNAT1 overexpressing mice. In contrast, we observed a reduction in the gene expression of NMNAT3 in the NMNAT1 overexpressing mice upon treatment with NRPT in comparison to the WT mice, further validating our above findings of limited benefits of NR and PT treatment in NMNAT1 overexpressed mice. This is important, as NMNAT1 overexpression did not induce an increase in the NMNAT2 and NMNAT3 expression showing no off-target effects of the overexpression.

Moreover, chronic exposure to CS resulted in NAD^+ depletion and a reduction in the ratio of NAD^+ to NADH ratio in both WT and NMNAT1 overexpressed mice (Figure 5.7D). Administration of NR and PT improved the total NAD^+ levels (Figure 5.7E) in our COPD study using WT mice and showed an increase in the ratio of NAD^+ to NADH. However, we did not see a difference in the total NAD^+ levels in the NMNAT1 overexpressing mice, resulting in no difference in the ratio of NAD^+ to NADH when compared to the WT smoke. In contrast, there was a decrease in the ratio of NAD^+ to NADH in the NMNAT1 overexpressing mice upon administration of NR and PT as compared to WT smoke

NRPT. To conclude, we did not observe an increase in NAD^+ levels with NMNAT1 overexpression and this is further supported by recent evidence suggesting that overexpression of NMNAT1 does not increase NAD^+ levels (428, 443). Therefore, NMNAT1 overexpression exerted limited benefits in reducing COPD features.

We observed a decrease in the gene expression of NMNAT1 (Figure 5.14A) and NMNAT3 (Figure 5.14C) in the overexpressing NMNAT3 mice upon exposure to CS. A decrease in the expression of these genes was surprising and future studies will be performed to measure the NMNAT3 protein levels in isolated mitochondrial samples to further conclude these findings. Furthermore, we observed an increase in the NAD^+ levels (Figure 5.14E) in the NMNAT3 overexpressed mice with or without NR and PT administration suggesting that elevated NMNAT3 regulates NAD^+ levels in COPD. Interestingly, we also observed a reduction in the NADH levels in the NMNAT3 overexpressed mice with or without NR and PT in comparison to the WT mice, further supporting our above results. However, we observed an increase in the ratio of NAD^+/NADH (Figure 5.14D) in the WT smoke mice, which is contradictory to the total NAD^+ levels and NADH levels (Figure 5.14F) measured in this study. To conclude, NMNAT3 overexpression with or without NR and PT increased the total NAD^+ in the lung which further contributed to the additional benefits of reducing COPD features. Studies have shown that overexpression of NMNAT3 drives an increase in NAD^+ levels in aging studies (444, 445) and supports our above findings of increased NAD^+ levels in COPD.

NMNATs have been suggested to functionally interact with PARPs (446, 447), SIRTs (448, 449) and CD38 (450, 451). However, there is no evidence of the mechanisms that elucidate the regulation of NAD^+ consumers by NMNAT1 and NMNAT3 in COPD. To address this, we measured the PARP activity (Figures 5.8A & 5.15A) in our COPD study

using transgenically overexpressing NMNAT1 and NMNAT3 mice. We observed an overactivation of PARPs in the WT smoke mice which were reduced in both the overexpressing NMNAT1 and NMNAT3 smoke mice. This shows that overexpression of NMNAT1 and NMNAT3 reduced PARP hyperactivity in COPD. Therefore suggesting that NMNAT1 and NMNAT3 overactivation can inhibit the overactivation of PARPs in COPD potentially contributing to additional therapeutic benefits. Upon the administration of NR and PT both in the WT mice as well as NMNAT1 and NMNAT3 overexpressing mice, there was a reduction in the PARP activity. These results further supported our previous findings of reduced PARP activity with the administration of NR and PT in COPD. Studies have stated both NMNAT1 and PARP1 (452, 453), key regulators of NAD^+ metabolic pathways (454, 455), are localised in the nucleus and functionally interact to control a variety of nuclear processes such as PARP1-dependent PARylation (456, 457). Currently, there is no evidence of interaction between NMNAT3 and the PARP family. However, studies have shown that NMNAT3 is dispensable in mitochondrial NAD^+ maintenance (458, 459), suggesting that in the absence of NMNAT3, translocation of nuclear NMNAT1 (455) or cytosolic NMNAT2 (460) into the mitochondria maintains NAD^+ metabolism.

SIRTs are NAD^+-dependent deacylases and play important roles in the maintenance of cellular metabolism, health, and aging (400, 461, 462). We observed a reduction in the gene expression of SIRT1 (Figures 5.8C and 5.15C) and SIRT5 (Figures 5.8G & 5.15G) in the WT smoke group which was increased in the treatment of NR and PT. We also observed an increase in SIRT7 (Figure 5.8I and 5.15I) gene expression with the administration of NR and PT in WT mice. This evidence supports our previous findings in Chapter 3. However, we observed a reduction in the gene expression of SIRT3-5 in the NMNAT1 smoke group in comparison to the NMNAT1 air group. An increase in the

gene expression of SIRT3 (Figures 5.8E) and SIRT4 (Figures 5.8F) was observed in the NMNAT1 smoke NRPT group in comparison to the NMNAT1 smoke group. These results suggested that NMNAT1 overexpression interacts with mitochondrially expressed SIRT3, SIRT4, and SIRT5. However, the reduction in gene expression of SIRT3-5 in NMNAT1 overexpressing mice exhibited limited protection in COPD. Interestingly, the administration of NR and PT displayed protective effects of mitochondrially expressed SIRT3 and SIRT4 genes in NMNAT1 overexpressed mice in COPD. SIRT3 and SIRT4 can regulate metabolic interaction(463) by regulation post-translational modification via protein deacetylation (464) through NAD^+-dependent ADP-ribosylation (465). This further inhibits mitochondrial oxstress in the airway epithelium by increasing anti-oxidant defence via manganese superoxide dismutase (MnSOD), thereby declining the pathogenesis of COPD (466). Furthermore, we observed an increase in the gene expression of SIRT3 (Figure 5.15E) in the overexpressing NMNAT3 smoke mice which was further increased with the NR and PT administration, suggesting that NMNAT3 interacts with SIRT3 which might potentially protect from mitochondrial damage in COPD. Collectively, these results suggested the overexpression of NMNAT1 and NMNAT3 regulated sirtuin expression, potentially explaining the reduced disease features in COPD. Additionally, NR and PT administration in NMNAT1 and NMNAT3 overexpressed mice further protected the expression of SIRTs in COPD. Previous studies have shown that the overexpression of NMNAT3 improves mitochondrial function via regulation of the NAD^+-SIRT3 pathway (467-469) and further supports our findings on the protective role of NMNAT1 and NMNAT3 overexpression in COPD. Future studies will be performed to measure SIRT3 protein expression and activity levels in both NMNAT1 and NMNAT3 overexpressed mice to further validate the NAD^+-SIRT3 pathway in COPD.

Additionally, we also observed an increase in ΔΨm (Figures 5.9 & 5.16) in the WT mice treated with NR and PT which was reduced in the WT smoke group further demonstrating our previous findings (Chapters 3 & 4) of increased ΔΨm with the treatment of NR and PT in COPD. Similarly, we observed an increase in ΔΨm in the NMNAT1 and NMNAT3 overexpressing mice in COPD with or without the treatment of NR and PT. These findings further suggest that NMNAT1 and NMNAT3 protected mitochondria membrane potential in COPD. Currently, there is no evidence of NMNAT1 and NMNAT3 increasing mitochondria membrane potential, however, studies on neurons have shown that elevation of NMNAT1 and NMNAT3 results in increased mitochondrial respiration (419, 470, 471). Therefore, indicating that overexpression of NMNAT1 and NMNAT3 is capable of protecting mitochondrial function in COPD. Future studies will be performed in frozen lung samples to measure mitochondrial oxygen consumption rate using a seahorse analyser to further conclude these results.

The current study showed increased levels of oxidative stress marker (Figures 5.10 & 5.17), 4-HNE in the smoke group of WT mice which was reduced in the smoke group of NMNAT1 and NMNAT3 overexpressed mice. 4-HNE is released as a by-product of lipid peroxidation and is an important mediator of oxidant-induced cell signalling and apoptosis (472, 473). Studies have previously shown high levels of 4-HNE in the lungs of COPD patients (474, 475). Both NR and PT in WT mice as well as NMNAT1 and NMNAT3 overexpressing mice, showed a significant reduction in 4-HNE resulting in reduced oxstress in COPD. Therefore, suggesting that NMNAT1 and NMNAT3 overexpression with or without NR and PT treatment can protect from the release of 4-HNE, hence reducing oxidative stress resulting in reduced inflammation and additional benefits in COPD. Moreover, increased expression of NOX2 in the smoke group of WT mice was observed which was reduced with the treatment groups of NR and PT as well

as with the overexpression of NMNAT1 and NMNAT3 mice. Collectively, these results suggested that the overexpression of NMNAT1 and NMNAT3 with or without the administration of NR and PT exhibited protection from oxidative stress by reducing 4-HNE in COPD and hence NR and PT are dispensable for oxstress reductions in NMNAT1 and NMNAT3 overexpressed mice. Previous studies have shown that NMNAT1 modulates mitochondrial oxidative stress via inhibiting caspase-3 signalling in Alzheimer's disease (476, 477). Additionally, NMNAT3 is also known to inhibit caspase-3 signalling in neurons (478, 479) but there is limited evidence available of the reduction of oxidative stress.

In conclusion, we have demonstrated that NMNATs are functionally involved in increasing NAD^+ levels upon the treatment of NR and PT in COPD. Using transgenically overexpressing NMNAT1 and NMNAT3 mice we have shown protection from the development of COPD features. In addition, we have also demonstrated that overexpression of NMNAT1 and NMNAT3 exhibited a reduction in PARP hyperactivity and regulation of SIRTs. As a consequence, there was a reduction in oxidative stress and an increase in mitochondria membrane potential. Although, upon administration of NR and PT to the overexpressing NMNAT1 and NMNAT3 mice exhibited important benefits in COPD such as reducing inflammation, protection from airway remodelling and emphysema, reducing PARP hyperactivity and oxidative stress followed by increasing mitochondria membrane potential. Critically, we found that NR and PT are dispensable for NMNAT1 and NMNAT3 overexpressing mice as the treatment did not show any additional benefits in protecting against COPD features. Importantly, NMNAT1 and NMNAT3 regulate NAD^+ imbalances in COPD, thereby reducing the hyperactivity of PARPs and promoting SIRTs, which further reduced oxidative stress and inflammation subsequently protecting against structural and functional damage to the lung in COPD.

Chapter 6. Investigating the therapeutic efficacy of immunomodulator TEPP46 in Chronic Obstructive Pulmonary Disease (COPD)

6.1 Introduction

COPD is a condition that is characterised by the limitation of airflow in the lungs, which leads to shortness of breath, wheezing, chest tightness and ongoing chronic cough (297). Chronic exposure to CS is one of the predominant causes of COPD however, other causes include long-term exposure to lung irritants—such as air pollution, chemical fumes, or dust (117). COPD pathologies are associated with chronic airway inflammation such as bronchitis, airway remodelling, collagen deposition, fibrosis, mucus hypersecretion and emphysema which worsens as the disease progresses (326). COPD is difficult to diagnose in the early stages and can progress for years without any noticeable symptoms (146). COPD is the third most common cause of death globally and current available treatments include the use of bronchodilators, oxygen therapy, lung transplantation, or reduction surgeries that alleviate the disease symptoms (23). However, there are no current available treatments that inhibit the progression or reverse the disease and hence, there is an urgent need to identify effective therapies for the treatment of COPD (25).

The mechanisms that drive the inception and progression of chronic inflammation in COPD are not well understood, and this has hampered the development of effective treatments for the disease (277). Current therapeutic approaches are limited and aim to manage symptoms and reduce exacerbations (277). Thus, there is a need for new therapies that inhibit the induction and progression of COPD (278).

Altered metabolism in immune cells leads to oxidative stress resulting in sustained inflammation in COPD (282), accompanied by impaired metabolism (283), mitochondrial dysfunction (279), decreased mitochondrial density and biogenesis (280),

and impaired mitochondrial activity and apoptosis (281). Metabolic marker PKM2 plays an important role in catalysing the last step in the glycolysis pathway which subsequently leads to the production of ATP via oxphos in mitochondria and provides the ultimate source of energy in the cell (160).

The objective of the current study was to investigate the role of impaired immunometabolism and pharmaceutical targeting of this process using the immunomodulator TEPP46 in the induction, progression, and development of COPD in a clinically relevant CS-induced experimental COPD murine model.

6.2 Methods

6.2.1 Experimental designs and groups

This study involved a 2-week (Figure 6.1A) and an 8-week (Figure 6.1B) CS-exposed mouse model treated with intranasal administration of TEPP46. Mice were subjected to nose-only CS exposure of 12 cigarettes, twice a day, five days a week for a period of 2 and 8 weeks.

TEPP46 was dissolved in a cocktail of 4% dimethyl sulfoxide (DMSO) (Sigma Aldrich #D8418) and 20% β-cyclodextrin (Sigma Aldrich # H107-5G) in phosphate buffer saline (PBS) (Life technologies #21600010), which was further also used as a vehicle for the control groups. All mice were weighed daily before intranasal administration of TEPP46/vehicle. The different experimental groups in this study were comprised of the air vehicle group, the smoke vehicle group, and the smoke TEPP46 treatment group as mentioned below in tables 6.1 and 6.2.

The 2-week model was a pilot study performed to determine the optimum dosage of TEPP46 required for the 8-week study. The 2-week study consisted of three different doses of TEPP46; 4 mg/kg, 2 mg/kg, and 1 mg/kg which were selected based on the available literature (Figure 6.1A). For our 8-week study, a dosage of 1mg/kg TEPP46 was intranasally administered every alternate day up to three times a week (Figure 6.1B).

The treated mice were subjected to rest for 2 hrs prior to smoke exposure and were closely monitored after each smoke run. Any mice that lost up to 10-15% of their body weight were rested from treatment and smoke exposure for 24 hrs with intensive monitoring. Once mice were below 10% body weight loss, they were able to recommence treatment and smoke exposure.

Table 6.1: Experimental groups of 2-week TEPP46 study

Experimental groups	Smoke exposure	Treatments
Air vehicle	-	Vehicle (4% DMSO+20% β-cyclodextrin in PBS)
Smoke vehicle	12 cigarettes, 2X day, 5X week	Vehicle (4% DMSO+20% β-cyclodextrin in PBS)
Smoke TEPP46 – 4 mg/kg	12 cigarettes, 2X day, 5X week	TEPP46 – 4 mg/kg (4% DMSO+20% β-cyclodextrin in PBS)
Smoke TEPP46 – 2 mg/kg	12 cigarettes, 2X day, 5X week	TEPP46 – 2 mg/kg (4% DMSO+20% β-cyclodextrin in PBS)
Smoke TEPP46 – 1 mg/kg	12 cigarettes, 2X day, 5X week	TEPP46 – 1 mg/kg (4% DMSO+20% β-cyclodextrin in PBS)

Table 6.2: Experimental groups of 8-week TEPP46 study

Experimental groups	Smoke exposure	Treatments
Air vehicle	-	Vehicle (4% DMSO+20% β-cyclodextrin in PBS)
Smoke vehicle	12 cigarettes, 2X day, 5X week	Vehicle (4% DMSO+20% β-cyclodextrin in PBS)

Smoke TEPP46 – 1 mg/kg	12 cigarettes, 2X day, 5X week	TEPP46 – 1 mg/kg (4% DMSO+20% β-cyclodextrin in PBS)

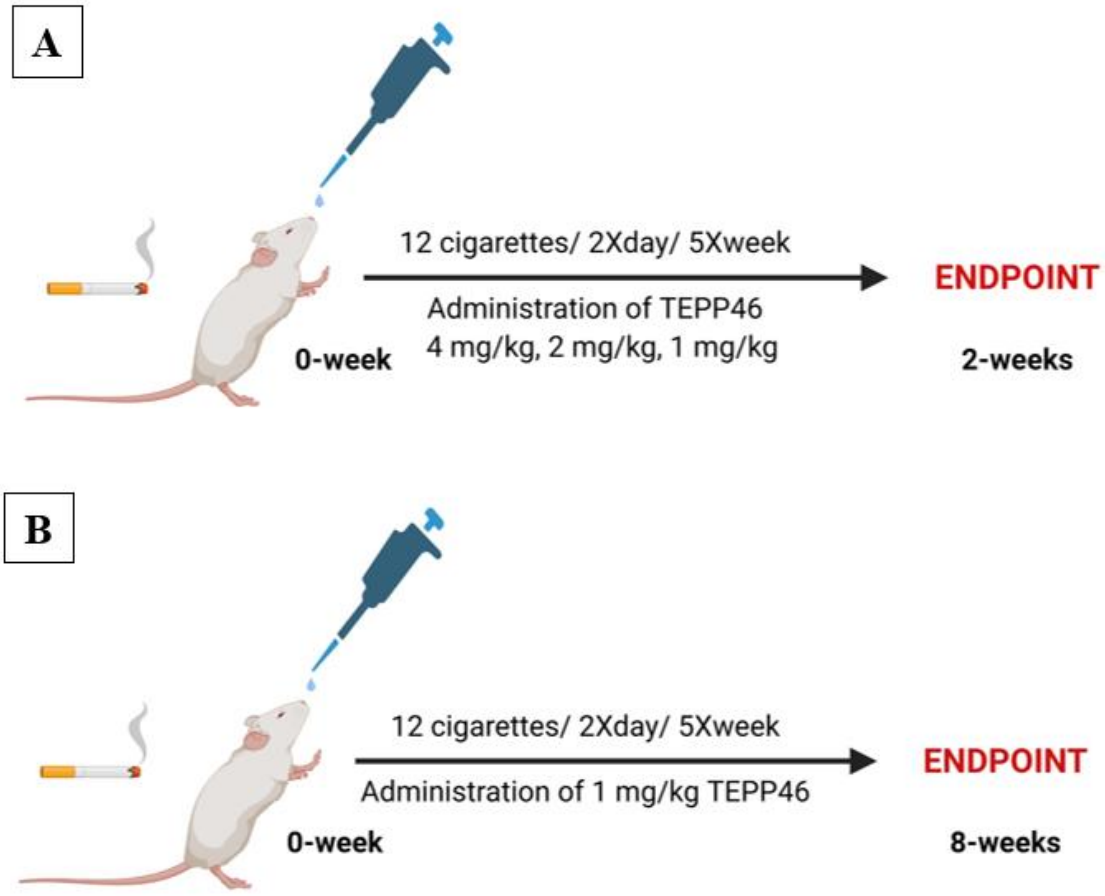

Figure 6.1: Experimental design:

(A) Mice were subjected to nose-only CS exposure to 12 cigarettes, twice a day, five days a week and were treated daily with an intranasal administration of TEPP46 at different doses of 4 mg/kg, 2 mg/kg, and 1 mg/kg; (B) Mice were exposed to CS for up to 12 cigarettes, twice a day, five days a week and were subjected to intranasal administration of 1 mg/kg TEPP46 for up to three times a week.

6.3 Results

6.3.1 Oxidative stress and mitochondrial dysfunction drive impaired metabolism in experimental COPD model

Lung sections from the 8-week CS-induced COPD model were sectioned and stained with 4-HNE to determine the level of oxidative stress in experimental COPD. The fluorescent intensity measured in the smoke group was significantly higher than in the air group ($P<0.05$) (Figure 6.2A). Further, mRNA levels of transcripts that encode HO1 (Figure 6.2B) and NOX2 (Figure 6.2C) were observed to be significantly higher in the smoke group as compared to the air group ($P<0.01$).

JC1 staining was also performed on lung sections from the 8-week CS-induced COPD model to measure $\Delta\Psi m$. The MFI of J-aggregates was significantly lower in the smoke group as compared to the air group ($P<0.0001$) (Figure 6.2D), while the MFI of J-monomers was significantly higher in the smoke group in comparison to the air group ($P<0.0001$) (Figure 3.6E). Furthermore, the ratio of J-aggregates/J-monomers showed a significant decrease in the smoke group as compared to the air group ($P<0.0001$) (Figure 6.2F).

Further, the gene expression profiles of TNFα (Figure 6.2 G), CXCL1 (Figure 6.2H), YM1 (Figure 6.2I) and PARP1 (Figure 6.2J) was upregulated in the smoke group as compared to the air group ($P<0.05$); whereas the expression of iNOS (Figure 6.2K), PGC1α (Figure 6.2L), PKM1 (Figure 6.2M), PKM2 (Figure 6.2N), and HIF1α (Figure 6.2O) was downregulated in the smoke group ($P<0.05$).

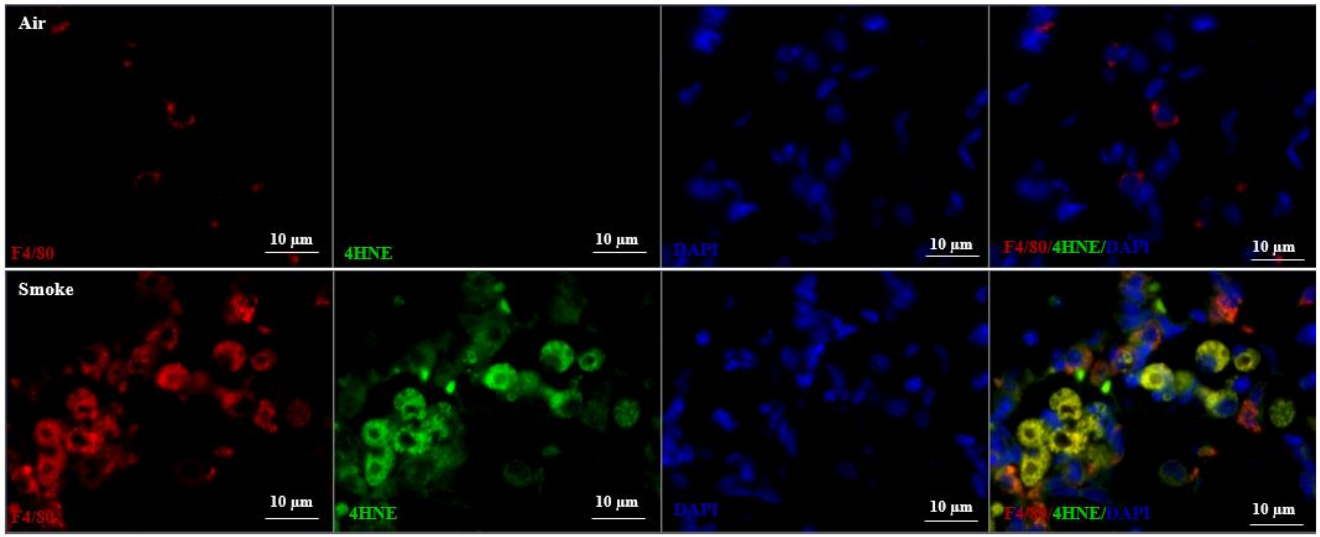
Air
F4/80
10 µm
4HNE
10 µm
DAPI
10 µm
F4/80/4HNE/DAPI
10 µm
Smoke
F4/80
10 µm
4HNE
10 µm
DAPI
10 µm
F4/80/4HNE/DAPI
10 µm

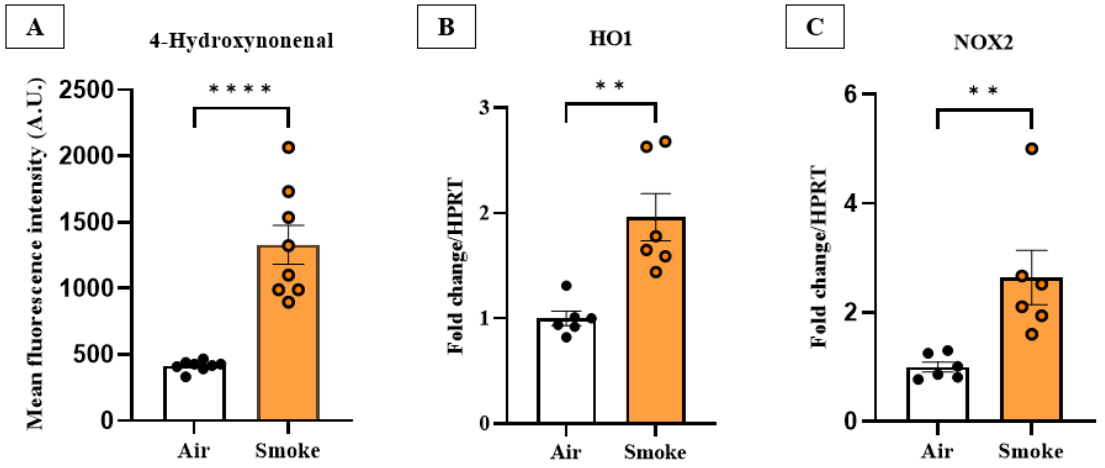
A
4-Hydroxynonenal
Mean fluorescence intensity (A.U.)
2500
2000
1500
1000
500
0
* * * *
Air
Smoke
B
HO1
Fold change/HPRT
3
2
1
0
* *
Air
Smoke
C
NOX2
Fold change/HPRT
6
4
2
0
* *
Air
Smoke

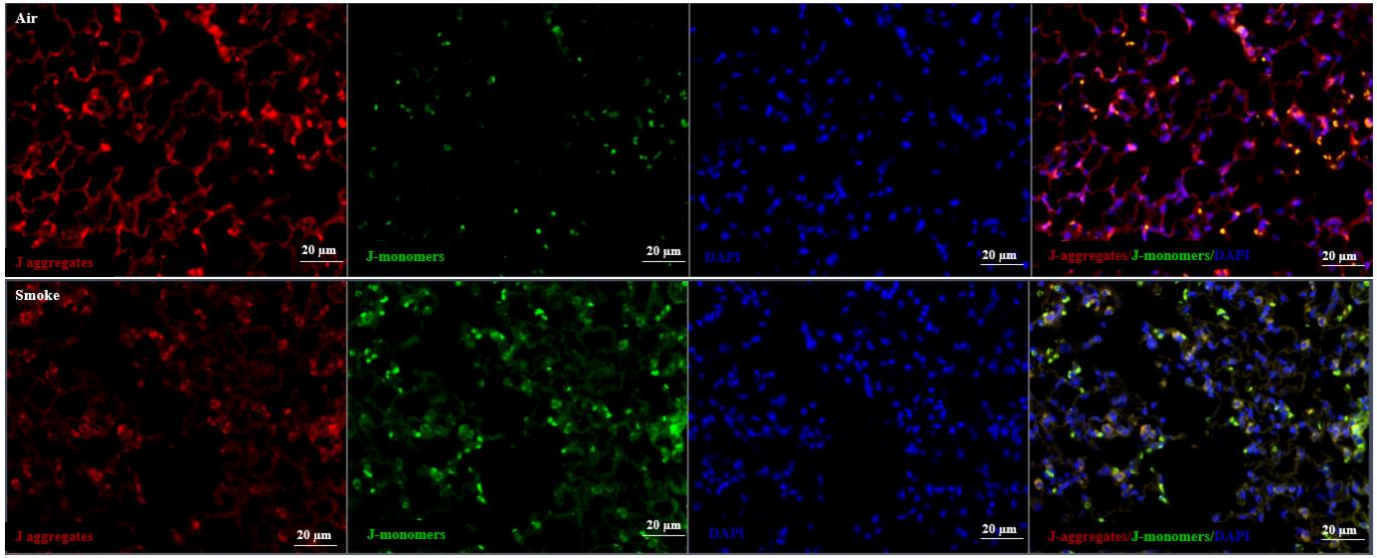
Air
J aggregates
20 µm
J-monomers
20 µm
DAPI
20 µm
J-aggregates/J-monomers/DAPI
20 µm
Smoke
J aggregates
20 µm
J-monomers
20 µm
DAPI
20 µm
J-aggregates/J-monomers/DAPI
20 µm

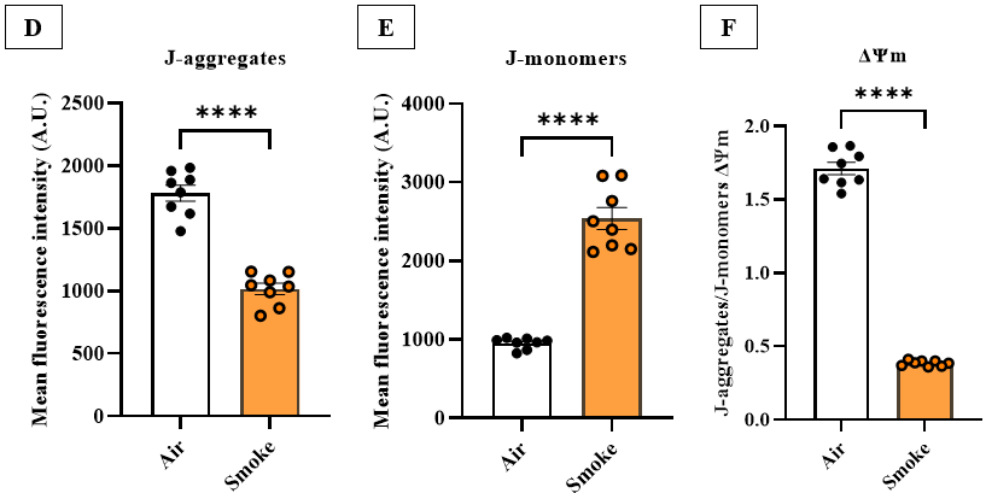
D
J-aggregates
Mean fluorescence intensity (A.U.)
2500
2000
1500
1000
500
0
****
Air
Smoke
E
J-monomers
Mean fluorescence intensity (A.U.)
4000
3000
2000
1000
0
****
Air
Smoke
F
ΔΨm
J-aggregates/J-monomers ΔΨm
2.0
1.5
1.0
0.5
0.0
****
Air
Smoke

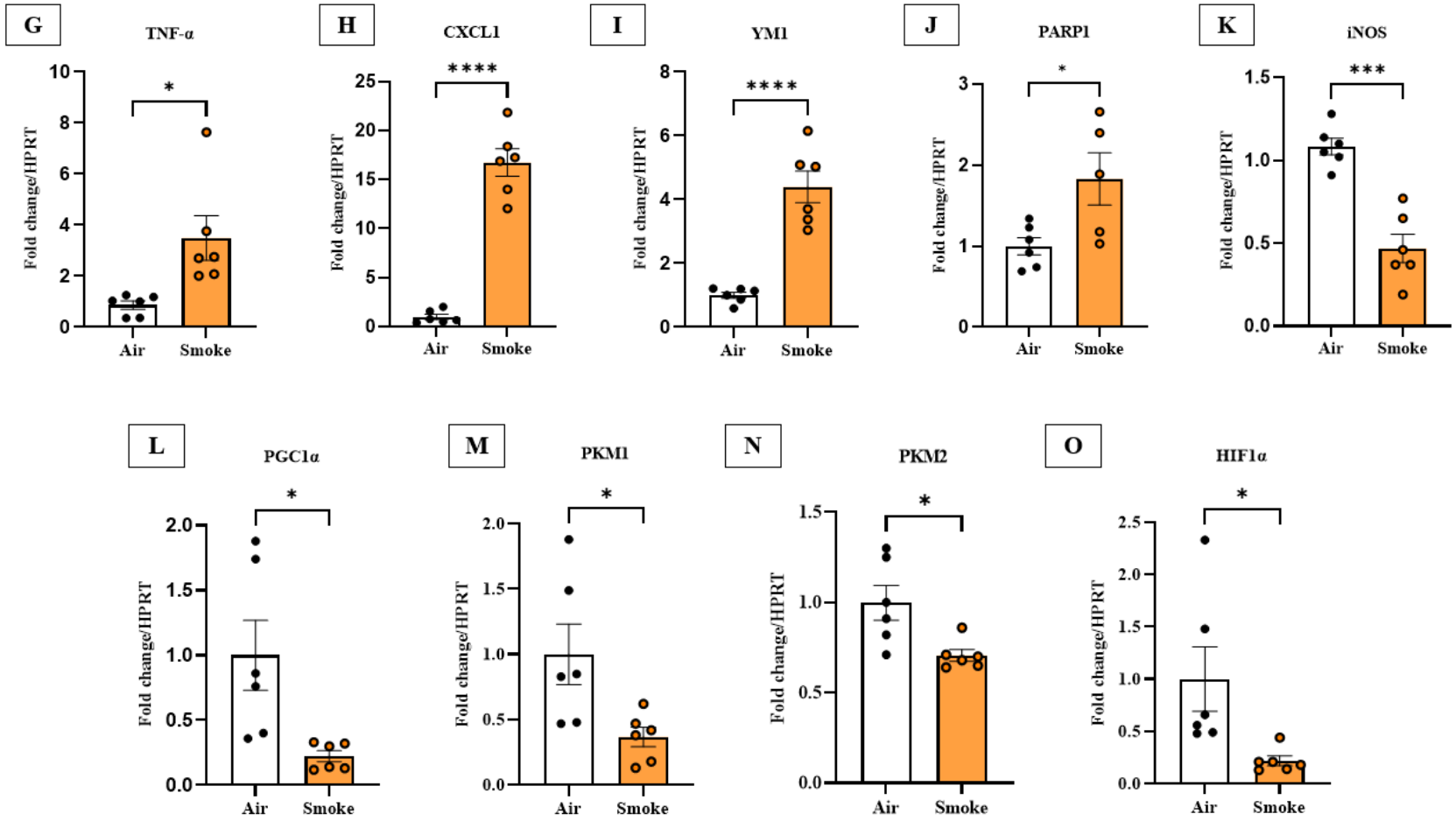

Figure 6.2: Oxidative stress is the potential driver of inflammation in experimental COPD:

*(A) 4HNE staining in lung sections of air and 8-week smoke-exposed mice (n=6); Increase in gene expression for oxidative stress markers, (B) HO1, (C) NOX2; Mitochondrial membrane potential staining shows an increase in the accumulation of (D) J aggregates in the air group and (E) J monomers in the smoke group, (F) reduced ΔΨm in the smoke group; Graphical representation of gene expression of inflammatory and metabolic markers: Increased expression in the smoke group for (G) TNFα, (H) CXCL1, (I) YM1, (J) PARP1; Reduced gene expression for (K) iNOS, (L) PGC1α, (M) PKM1, (N) PKM2, (O) HIF1α. Data represented are means ± SEM of 6 mice/group, * P<0.05,** P<0.01, *** P<0.001, **** P<0.0001.*

6.3.2 Administration of TEPP46 reduced inflammatory cell influx in acute CS exposure

Administration of TEPP46 at 4 mg/kg, 2 mg/kg and 1 mg/kg in the 2-week acute CS model showed significantly reduced total leukocyte counts in BAL as compared to the smoke vehicle group (P<0.0001) (Figure 6.3A). Differential counts for macrophages and neutrophils also showed significant reductions associated with TEPP46 administration for all the doses of 4 mg/kg, 2 mg/kg, and 1 mg/kg as compared to the smoke vehicle group (P<0.0001) (Figure 6.3B-C).

The body weight of all experimental groups was monitored daily throughout the 2-week model. We observed a ~10-12% total body weight loss in the mice treated with higher doses of TEPP46 i.e., 4 mg/kg and 2mg/kg as compared to all the other groups of the air vehicle, smoke vehicle and smoke TEPP46-1 mg/kg (Figure 6.3D). Mice from these groups were also observed to have hunched posture, ruffled fur, shaking after smoke exposure and were inactive when compared to the other experimental groups of smoke TEPP46 1 mg/kg, smoke vehicle and air vehicle

The gene expression of TNF-α (Figure 6.3E), CXCL1 (Figure 6.3F), IL-1β (Figure 6.3G), and YM1 (Figure 6.3H) increased ($P<0.05$) in the smoke vehicle group with respect to the air vehicle group, which was reduced in the smoke TEPP46-1 mg/kg. However, the expression of iNOS was reduced in both the smoke vehicle and smoke TEPP46-1 mg/kg as compared to the air vehicle group (Figure 6.3E).

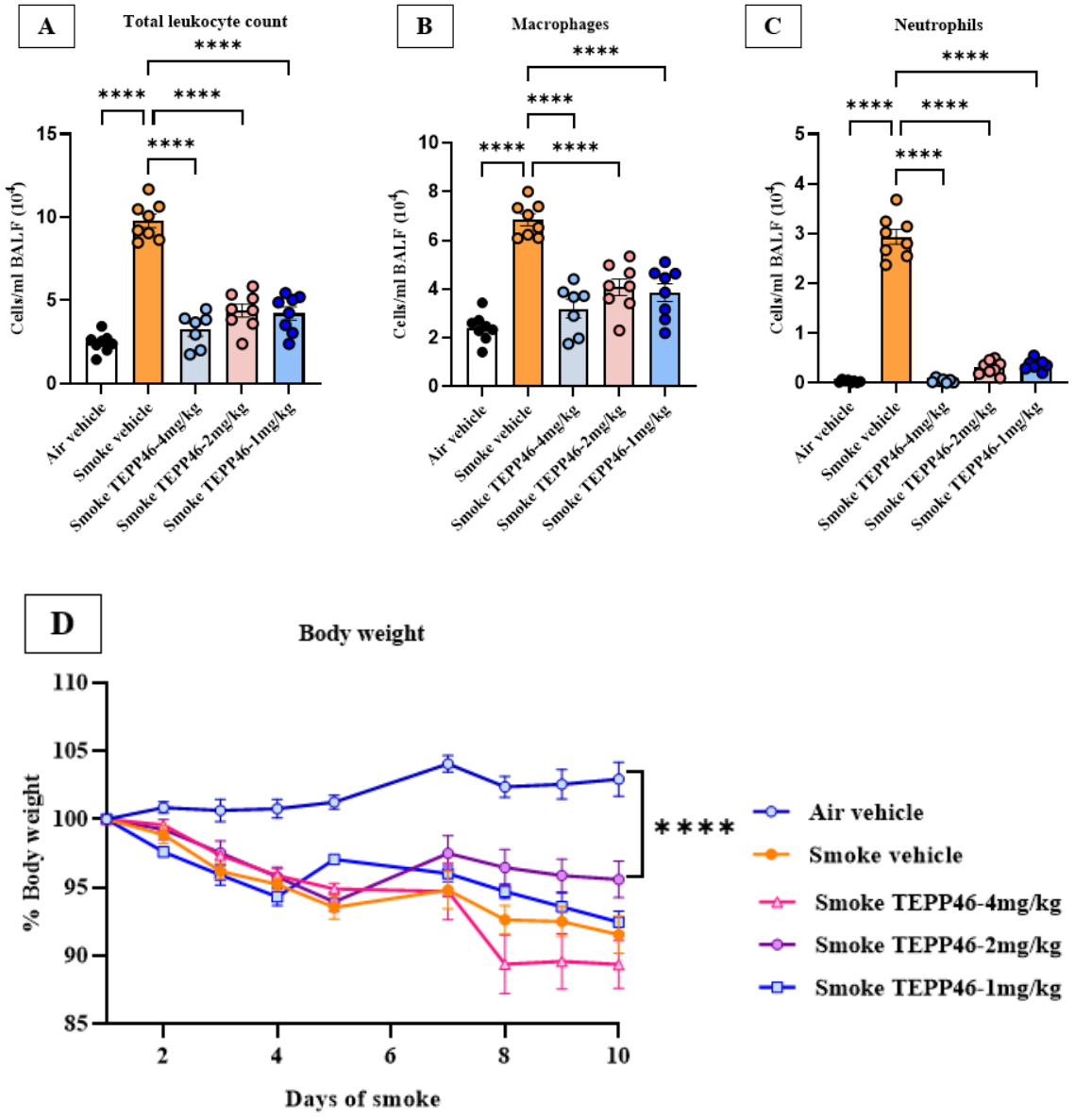

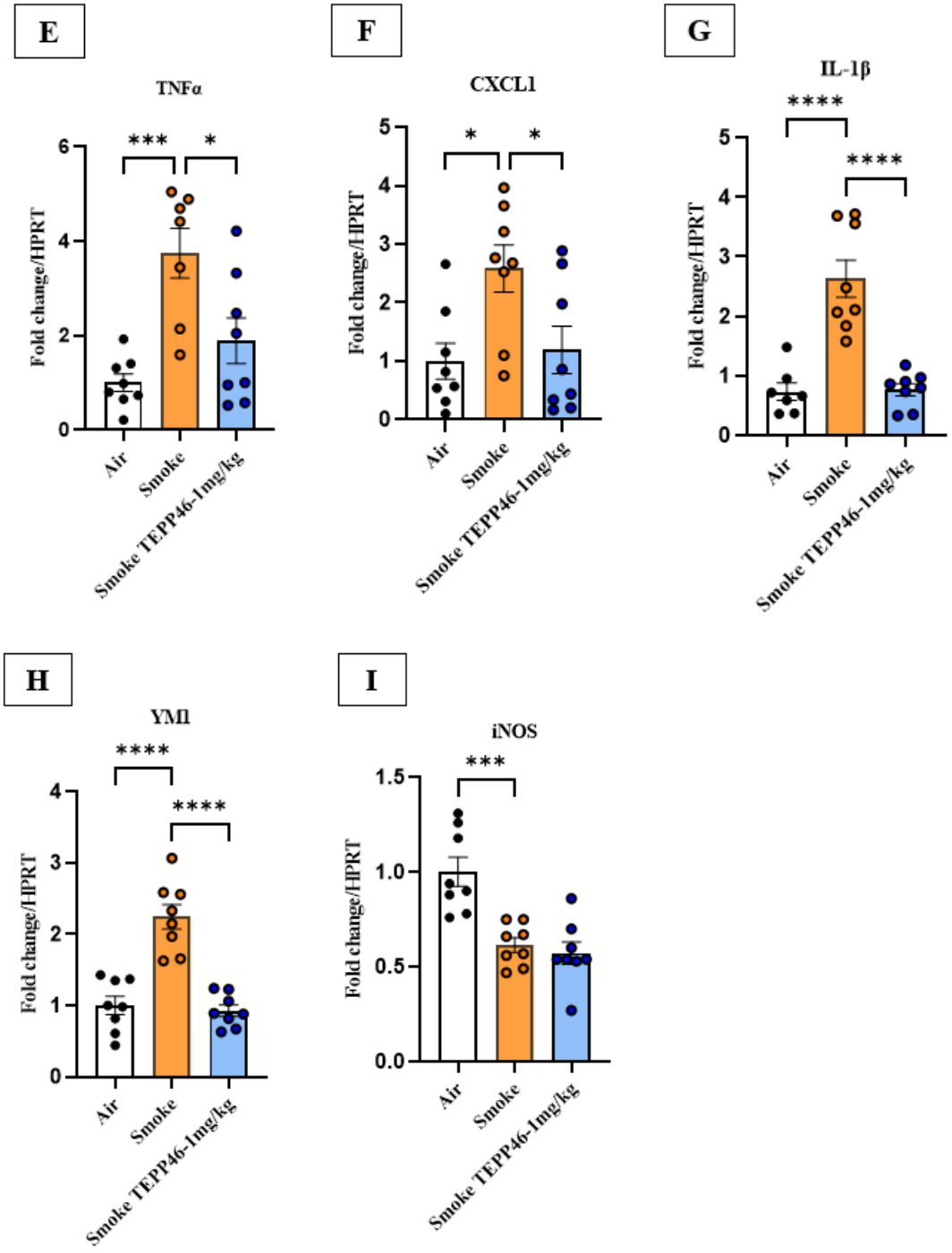

Figure 6.3: Administration of TEPP46 reduced inflammation in acute CS exposed model:

Graphical representation of (A) reduced cellular infiltrates in the parenchyma, (B) reduced macrophages and (C) neutrophils obtained in BAL; (D) Changes in body weight upon administration of the different dosages of TEPP46; Reduced levels of transcripts

*upon TEPP46 treatment that encode (E) TNFα, (F) CXCL1, (G) IL-1β, (H) YM1, and (I) iNOS. Data represented are means ± SEM of 6-8 mice/group, * P<0.05, ** P<0.01, *** P<0.001, **** P<0.0001.*

6.3.3 Administration of TEPP46 protected from alveolar damage during acute CS exposure

An increase in the MLI was observed in the smoke vehicle group in comparison to the air vehicle group and was protected in the smoke TEPP46-1 mg/kg (P<0.0001) (Figure 6.4).

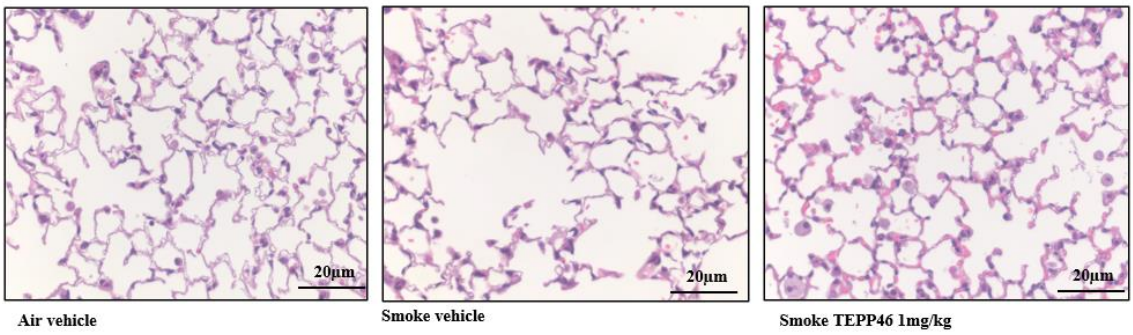

Air vehicle | Smoke vehicle | Smoke TEPP46 1mg/kg

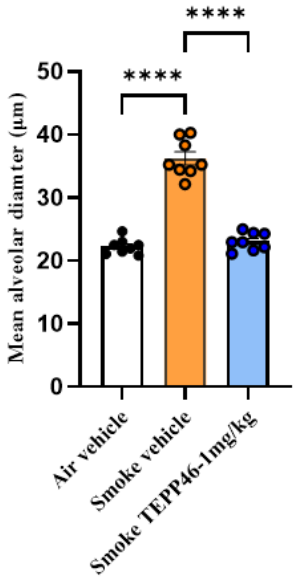

Figure 6.4: Administration of TEPP46 protected from alveolar damage during acute CS exposure:

*Reduced mean alveolar diameter in the smoke TEPP46-1mg/kg group (P<0.05). Data represented are means ± SEM of 6-8 mice/group, * P<0.05, ** P<0.01, *** P<0.001, **** P<0.0001.*

6.3.4 TEPP46 promoted tetramerisation of PKM2 in acute CS exposure

Reduced PK activity levels were measured in the smoke vehicle group as compared to the air vehicle group(P<0.0001) and were found to be significantly increased in the smoke TEPP46-1 mg/kg as compared to the smoke vehicle group (P<0.0001) (Figure 6.5A). Further, the gene expression profile for PKM2 was found to be similar between air vehicle, smoke vehicle and smoke TEPP46-1 mg/kg (Figure 6.5B). However, protein levels of PKM2 were measured by immunofluorescence in which the MFI of PKM2 was found to be significantly increased in the smoke TEPP46-1 mg/Kg as compared to both the air vehicle (P<0.01) and smoke vehicle groups (P<0.0001).

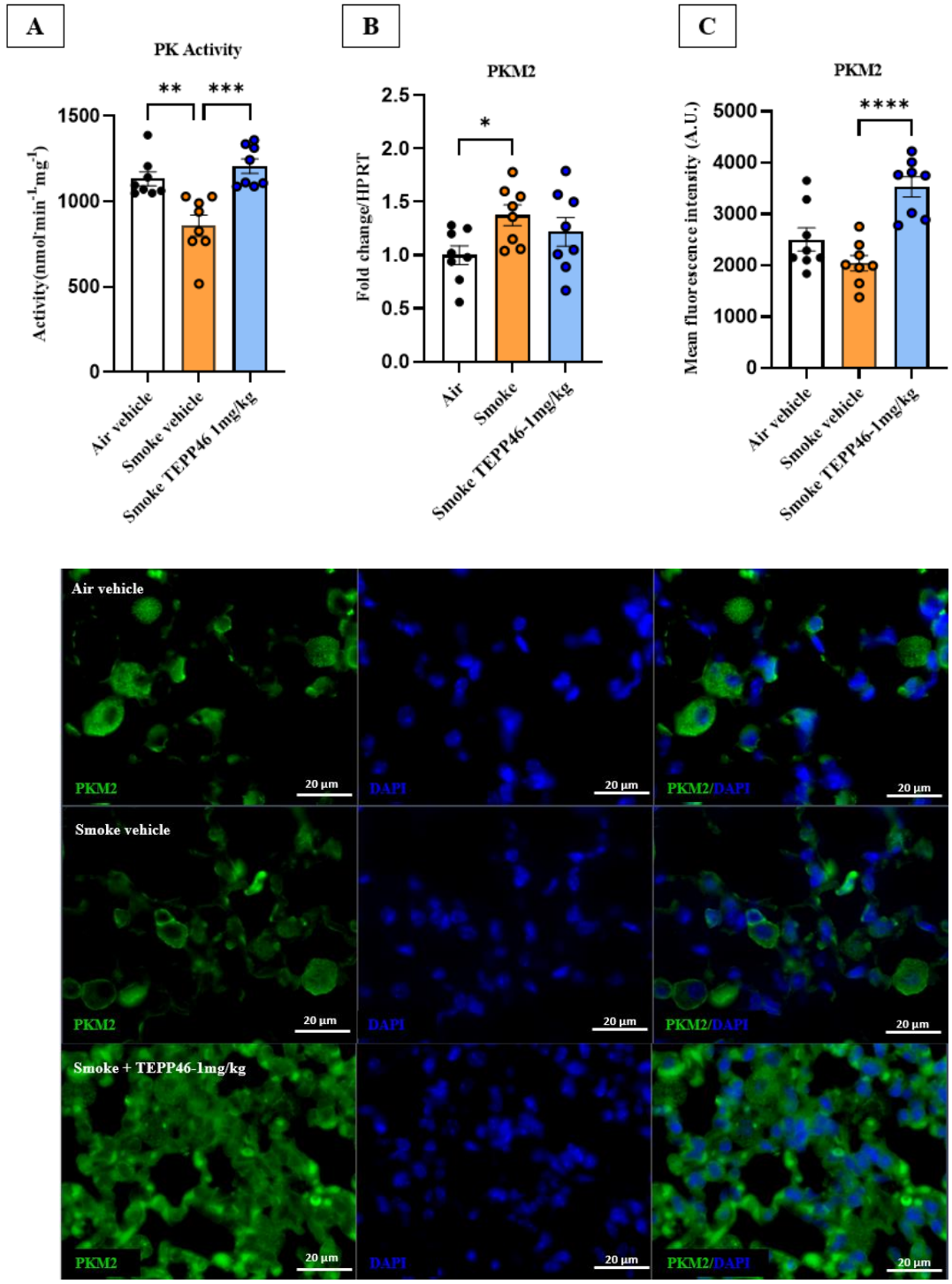

Figure 6.5: TEPP46 promoted tetramerisation of PKM2 in acute CS exposed inflammation:

*(A) Increase in the PK activity; (B) Gene expression of PKM2 in lung tissues (C) Increase in the protein levels of PKM2. Data represented are means ± SEM of 6-8 mice/group, * P<0.05, ** P<0.01, *** P<0.001, **** P<0.0001.*

6.3.5 Administration of TEPP46 promoted the metabolic role of PKM2

PDH activity was observed to be significantly reduced in the smoke vehicle group as compared to the air vehicle group ($P<0.05$) as shown below and was restored to baseline levels in the smoke TEPP46-1 mg/kg, which was significantly different to the smoke vehicle group ($P<0.0001$) (Figure 6.6A).

An increase in the gene expression of HIF1α in the smoke vehicle group was observed as compared to the air vehicle group ($P<0.0001$) and was significantly reduced in the smoke TEPP46-1 mg/kg ($P<0.0001$) (Figure 6.6B). However, the protein level of HIF1α was reduced in the smoke vehicle group as compared to the air vehicle group ($P<0.05$) and was significantly increased in the smoke TEPP46-1 mg/kg ($P<0.05$) (Figure 6.6C).

Further, the gene expression of metabolic markers was measured such as PDK1 (Figure 6.6D) which remains unchanged in all the groups; PGC1α, which was reduced in the smoke vehicle group in comparison to the air vehicle group ($P<0.001$), and was protected in the smoke TEPP46-1 mg/kg ($P<0.05$) (Figure 6.6E); PARP1 remained unchanged in all the experimental groups (Figure 6.6F), and PKM1 which was reduced in the smoke TEPP46-1 mg/kg with respect to the smoke vehicle group ($P<0.05$) (Figure 6.6G).

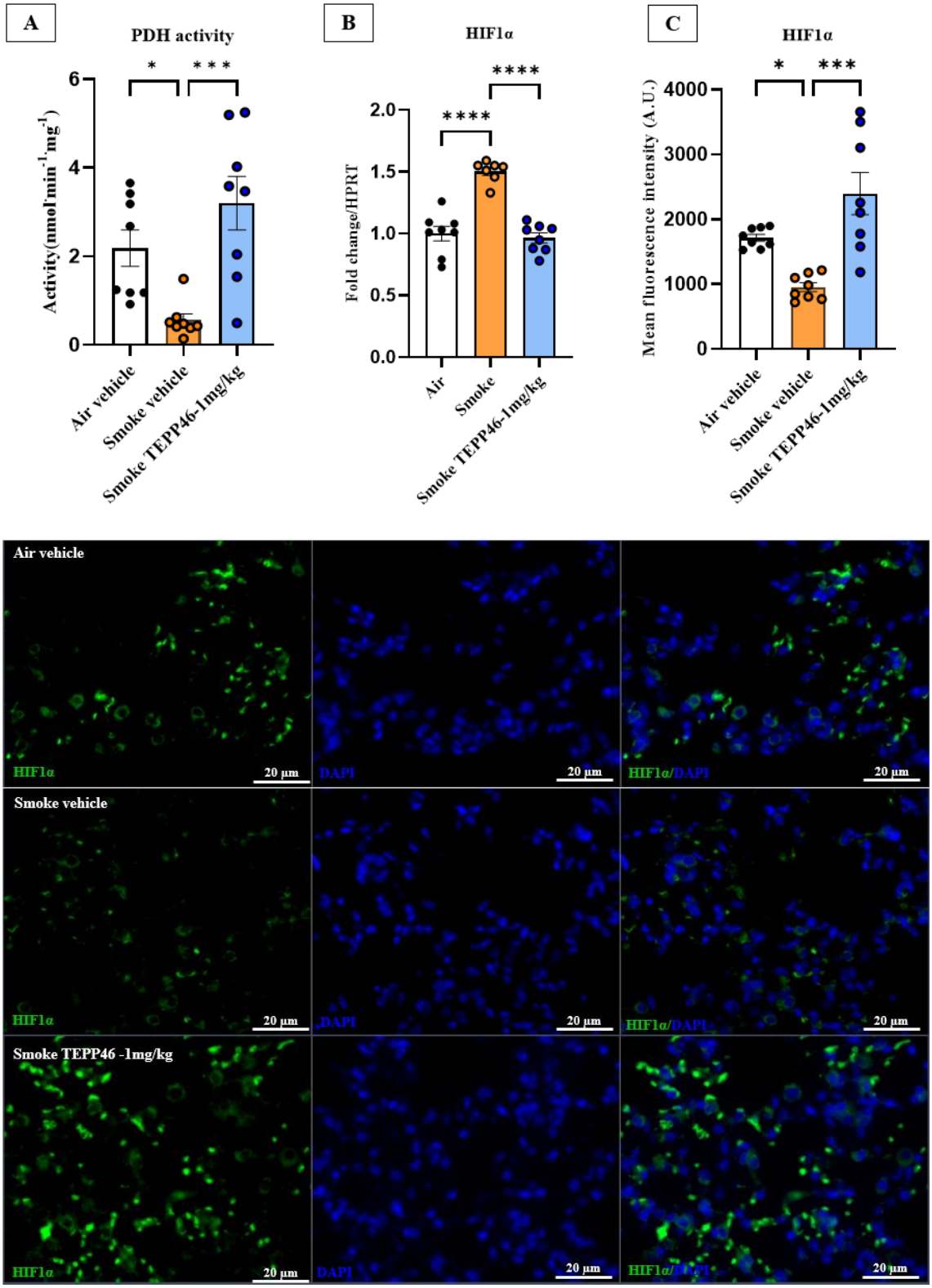
A
PDH activity
Activity(nmol'min-1'mg-1)
Air vehicle
Smoke vehicle
Smoke TEPP46-1mg/kg
B
HIF1α
Fold change/HPRT
Air
Smoke
Smoke TEPP46-1mg/kg
C
HIF1α
Mean fluorescence intensity (A.U.)
Air vehicle
Smoke vehicle
Smoke TEPP46-1mg/kg
Air vehicle
Smoke vehicle
Smoke TEPP46 -1mg/kg
HIF1α
DAPI
HIF1α/DAPI
20 μm

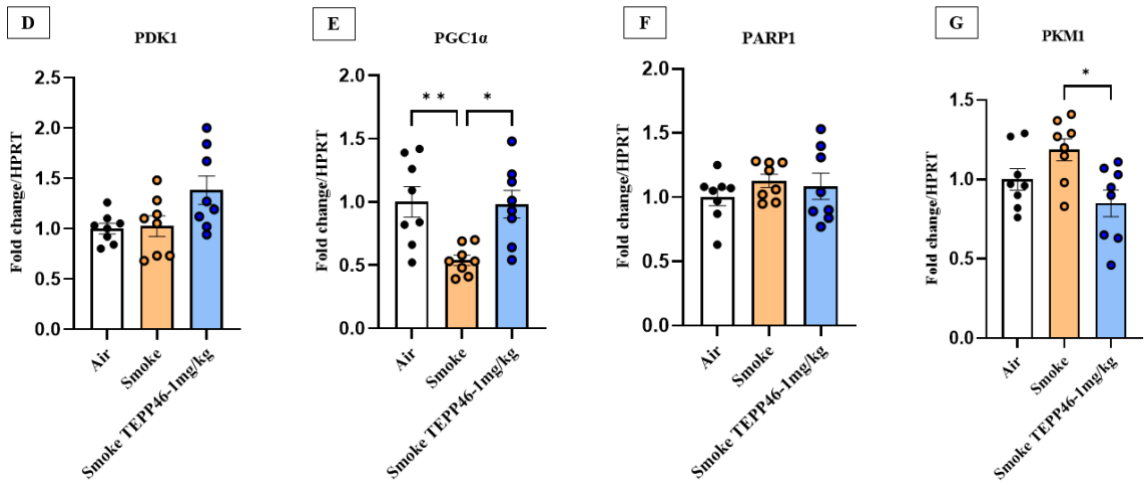

Figure 6.6Administration of TEPP46 promoted the metabolic role of PKM2 in COPD:

*(A)TEPP46 increased PDH activity levels, (B) TEPP46 reduced gene expression of HIf1α, (C) TEPP46 increased protein levels of HIf1α; Gene expression levels of (D) PDK1 was unchanged, (E) PGC1α was reduced with TEPP46 treatment, (F) PARP1was unchanged and (G) PKM1was reduced with TEPP46 treatment. Data represented are means ± SEM of 6-8 mice/group, * P<0.05, ** P<0.01, *** P<0.001, **** P<0.0001.*

6.3.6 TEPP46 promoted mitochondria membrane potential (ΔΨm) during acute CS exposure

ΔΨm was measured for all groups in which J-aggregates remained unchanged in the air vehicle, smoke vehicle and smoke TEPP46-1 mg/kg (Figure 6.7A). J-monomers increased in the smoke vehicle group with respect to the air vehicle group (P<0.0001) and were significantly reduced in the smoke TEPP46-1 mg/kg (P<0.0001) (Figure 6.7B). Importantly, ΔΨm, which is the ratio of J-aggregates to J-monomers was reduced in the smoke vehicle group as compared to the air vehicle group (P<0.0001), which was protected in the smoke TEPP46-1 mg/kg (P<0.0001) (Figure 6.7C).

NOX2 gene expression was increased in the smoke vehicle group in comparison to the air vehicle group (P<0.0001) and was significantly reduced in the smoke TEPP46-1 mg/kg (P<0.01) (Figure 6.7D). There was no change in the expression of HO1 in any of the experimental groups examined (Figure 6.7E).

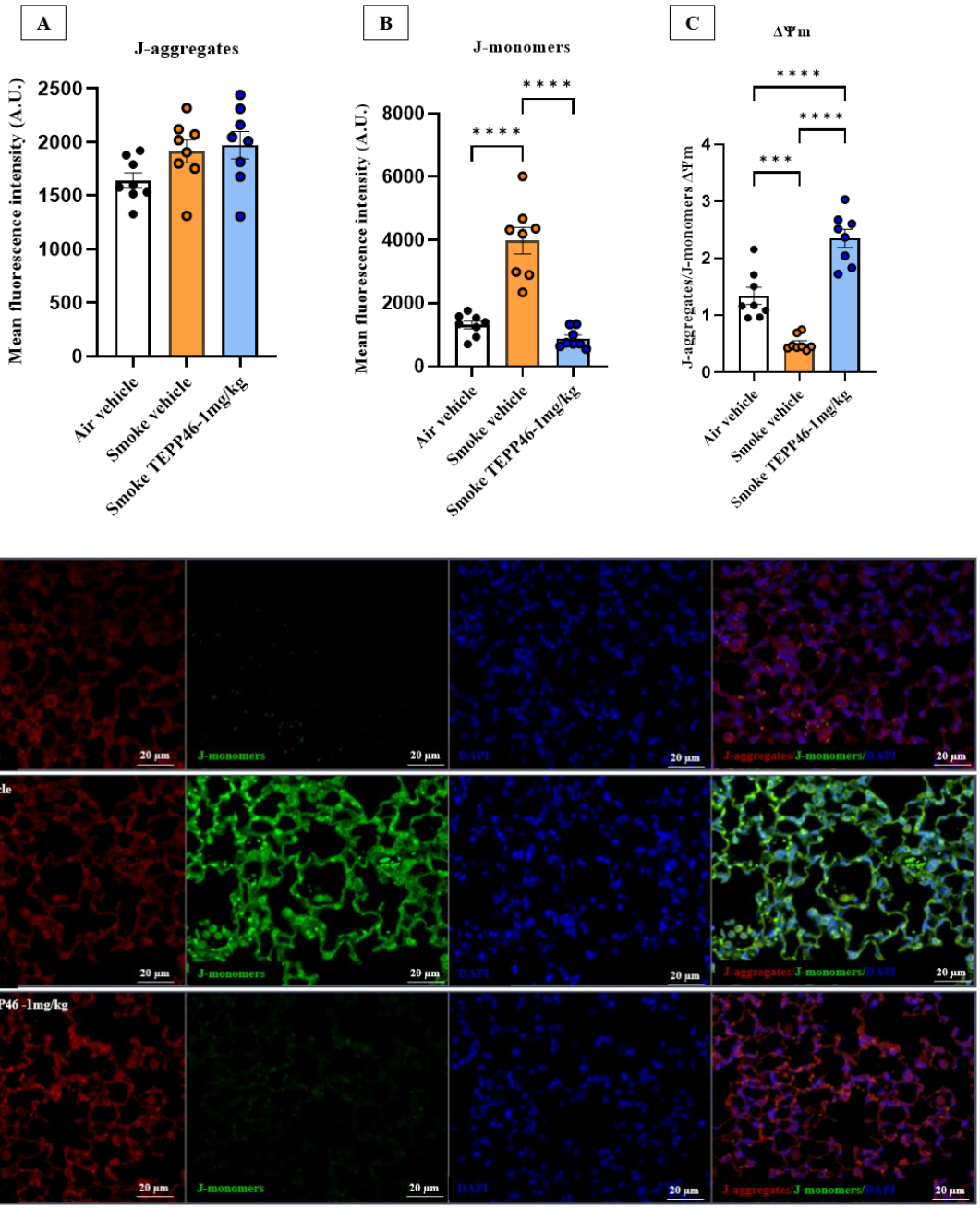

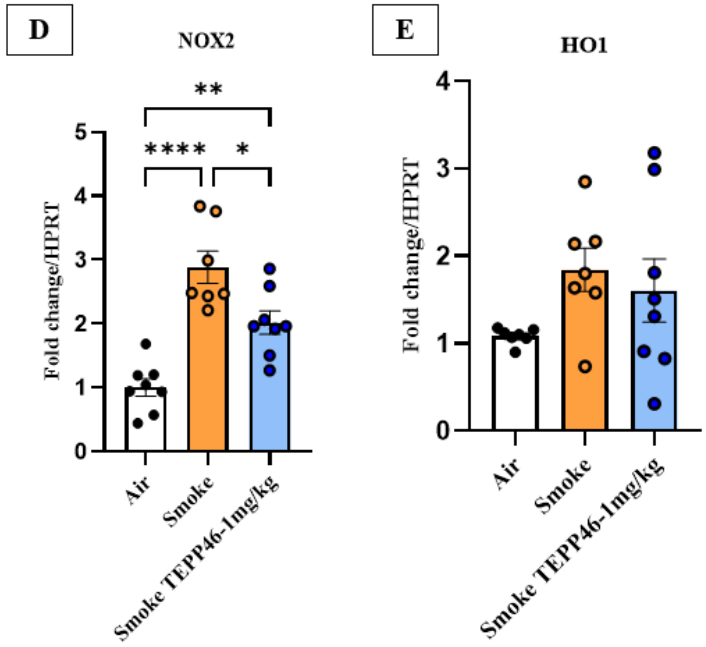

Figure 6.7: Administration of TEPP46 promoted mitochondrial function during acute CS exposure:

*TEPP46 administration showed (A) no change in J-aggregates (B) reduced J-monomers (C) increased ΔΨm; Gene expression of oxidative stress markers in TEPP46 treatment (D) reduced NOX2 and (E) exhibited no change in HO1. Data represented are means ± SEM of 6-8 mice/group, * P<0.05, ** P<0.01, *** P<0.001, **** P<0.0001.*

6.3.7 Administration of TEPP46 reduced inflammation in experimental COPD model

The 8-week CS-induced experimental COPD mouse model was performed as outlined previously in the section 6.2. An increase in total leukocytes (Figure 6.8A), macrophages (Figure 6.8B) and neutrophils (Figure 6.8C) were significantly elevated in the smoke vehicle group as compared to the air vehicle group (P<0.0001) and was significantly reduced in the TEPP46 smoke group (P<0.0001).

Body weight was measured daily for the duration of the 8-week model. There was a significant weight loss observed in the smoke vehicle group in comparison to the air vehicle group (P<0.0001) however, there was no change observed in the smoke TEPP46-1 mg/kg group in comparison to the smoke vehicle group (Figure 6.8D).

The expression of TNFα (Figure 6.8 E) and CXCL1 (Figure 6.8F) increased significantly in the smoke vehicle group as compared to the air vehicle group (P<0.0001). This was significantly reduced in the smoke TEPP46-1 mg/kg group as compared to the smoke vehicle group (P<0.0001). The expression of iNOS (Figure 6.8G) was significantly reduced in the smoke TEPP46-1 mg/kg as compared to the air vehicle group (P<0.001), however, there was no significant difference between the smoke TEPP46-1 mg/kg and the smoke vehicle group. Furthermore, the expression of YM1 (Figure 6.8H) increased significantly in the smoke vehicle group in comparison to the air vehicle group (P<0.0001) and remained unchanged in the smoke TEPP46-1 mg/kg group.

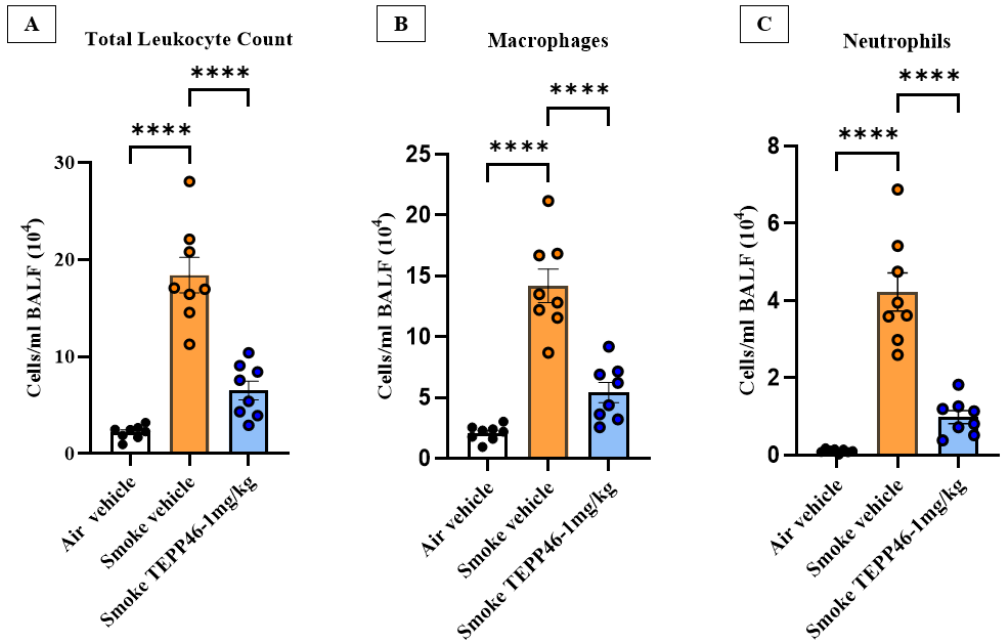

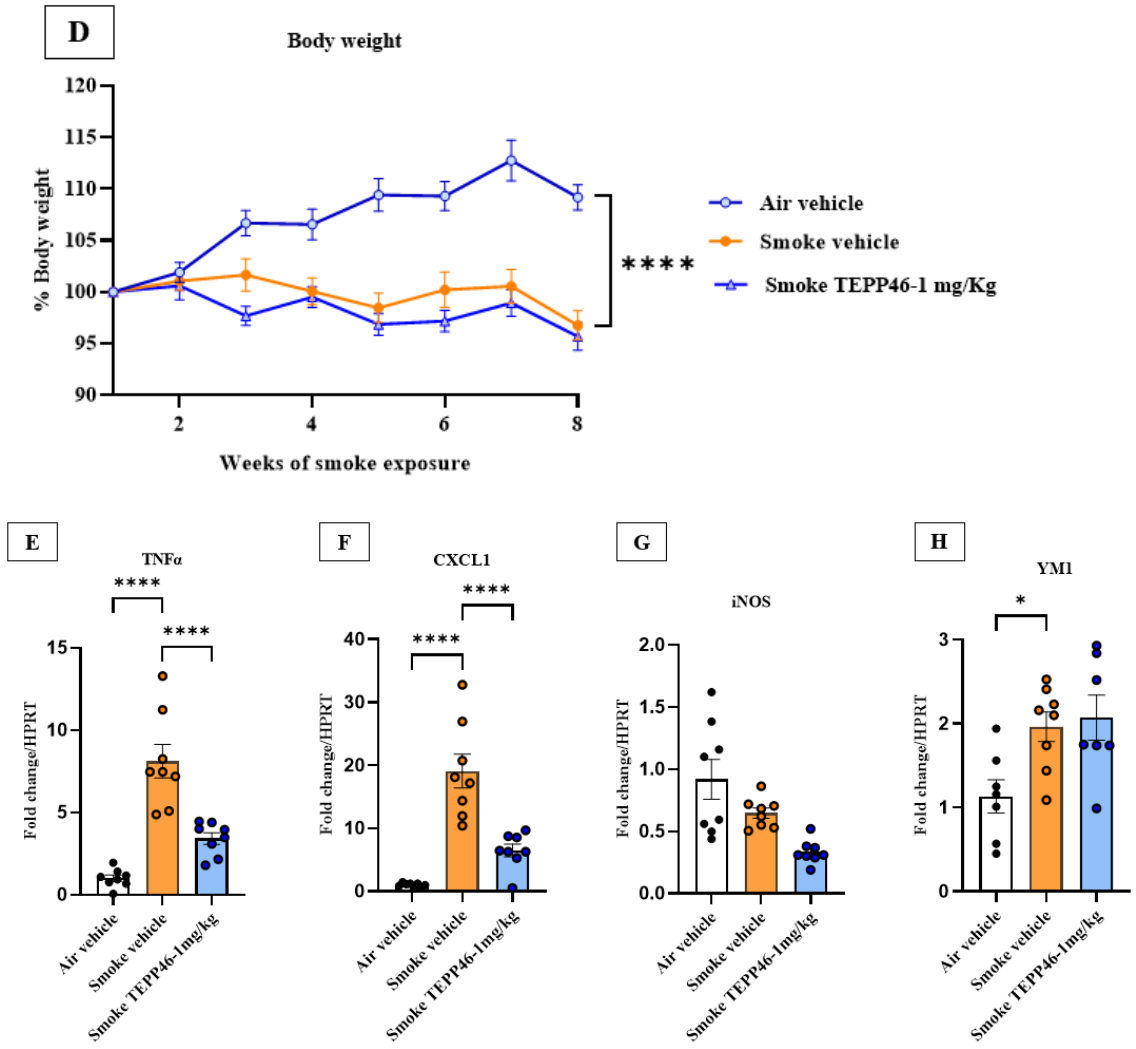

Figure 6.8: Administration of TEPP46 reduced inflammation in experimental COPD model:

*TEPP46 treatment reduced (A) cellular infiltrates in the parenchyma, (B) macrophages and (C) neutrophils obtained in BAL; (D) Changes in body weight. TEPP46 administration (E) reduced the gene expression for TNFα, (F) CXCL1, (G) iNOS and (H) increased the expression levels of YM1. Data represented are means ± SEM of 6-8 mice/group, * P<0.05, ** P<0.01, *** P<0.001, **** P<0.0001.*

6.3.8 Administration of TEPP46 protected from COPD features in experimental COPD studies

Measurement of collagen deposition around airways in the lung leading to airway remodelling was performed. Figure 6.9A below represents collagen deposition around the airways which was significantly increased in the smoke vehicle group as compared to the air vehicle group ($P<0.0001$) and was protected in the smoke TEPP46-1 mg/kg group ($P<0.0001$).

Further, a significant increase in the MLI counts was observed in the smoke vehicle group as compared to the air vehicle group ($P<0.05$) and was protected in the smoke TEPP46-1 mg/kg group ($P<0.0001$) as represented below in Figure 6.9B).

Mouse lung parameter changes were measured using FlexiVent as mentioned previously under 2.2.9. We observed an increase in IC ($P<0.001$) (Figure 6.9C); area ($P<0.001$) (Figure 6.9D), FVC ($P<0.001$) (Figure 6.9E), FEV ($P<0.001$) (Figure 6.9F), Cst ($P<0.01$) (Figure 6.9G), A ($P<0.01$) (Figure 6.9H), and TLC ($P<0.01$) (Figure 6.9I) in the smoke vehicle group as compared to the air vehicle group which did not reduce in the treatment group of smoke TEPP46-1 mg/kg. Further, we observed an increase in the lung compliance curves in the smoke vehicle group as compared to the air-vehicle group, which were reduced in the smoke TEPP46-1 mg/kg group (Figure 6.9J).

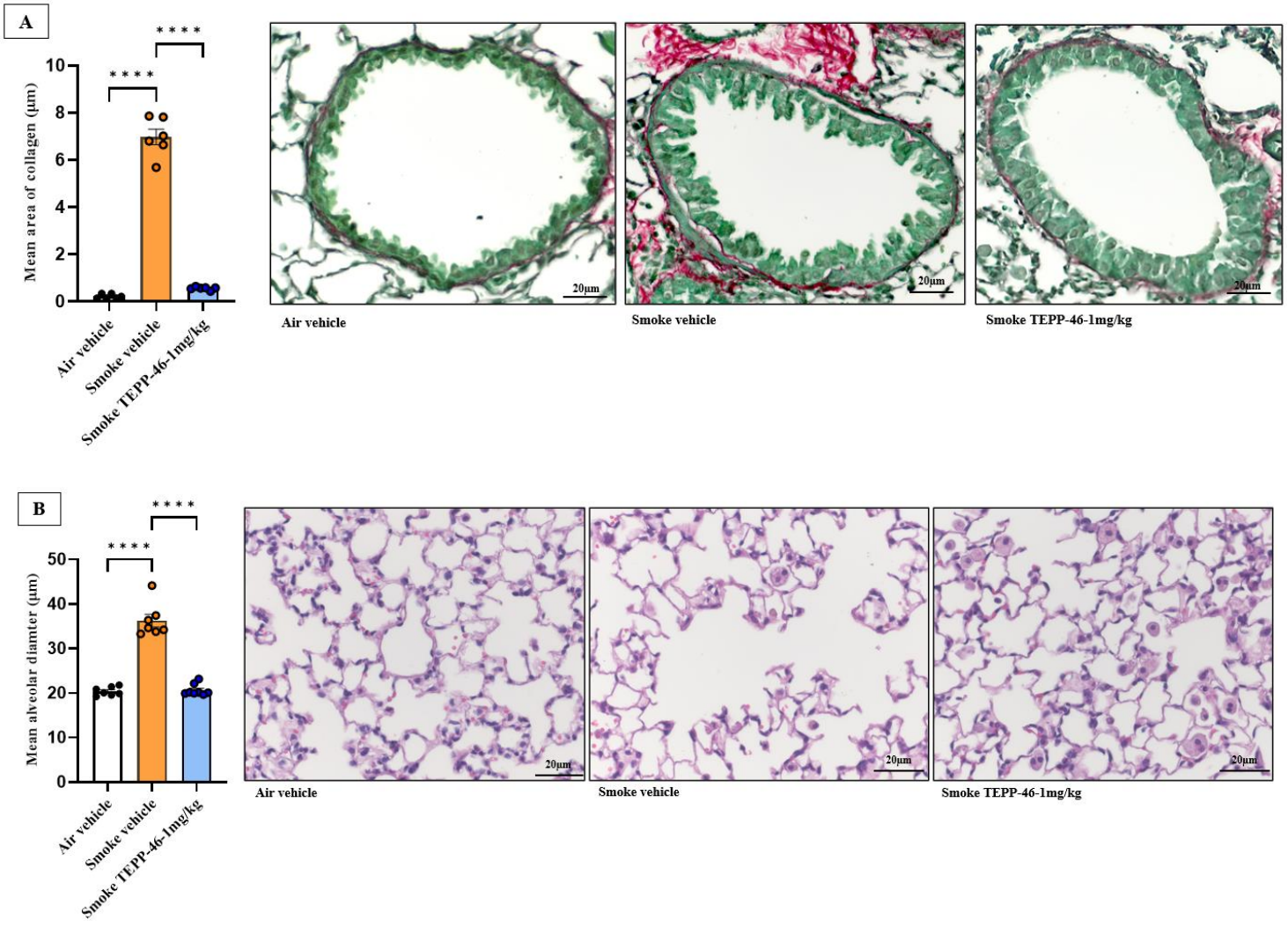
A
Mean area of collagen (µm)
10
8
6
4
2
0
****
****
Air vehicle
Smoke vehicle
Smoke TEPP-46-1mg/kg
20µm
Air vehicle
Smoke vehicle
Smoke TEPP-46-1mg/kg
B
Mean alveolar diamter (µm)
50
40
30
20
10
0
****
****
Air vehicle
Smoke vehicle
Smoke TEPP-46-1mg/kg
20µm
Air vehicle
Smoke vehicle
Smoke TEPP-46-1mg/kg

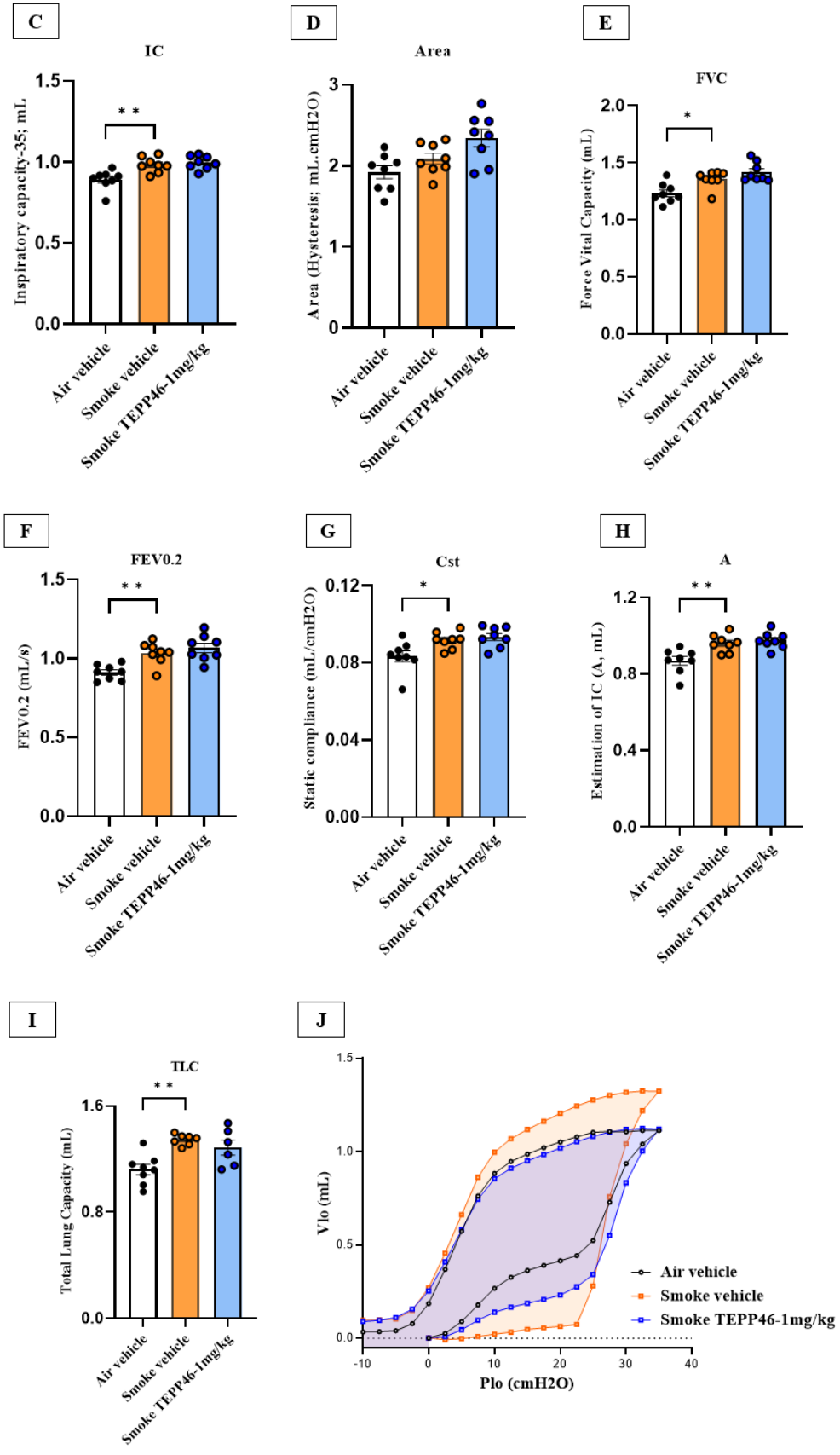

Figure 6.9: Administration of TEPP46 protected from COPD features:

*TEPP46 treatment in COPD (A) reduced collagen deposition around airways, (B) reduced MLI in the lung parenchyma, increased (C) IC, (D) Area, (E) FVC, (F) FEV, (G) Cst, (H) A, (I) TLC, and (J) reduced lung compliance curves. Data represented are means ± SEM of 6-8 mice/group, * P<0.05, ** P<0.01, *** P<0.001, **** P<0.0001.*

6.3.9 Administration of TEPP46 promoted tetramerisation of PKM2 in experimental COPD model

A decrease in PK activity levels was observed in the smoke vehicle group with respect to the air vehicle group (P<0.0001) which was increased in the treatment group of smoke TEPP46-1 mg/kg group (P<0.0001) as represented below in Figure 6.10A.

Further, the gene expression levels of PKM2 were increased in the smoke vehicle as compared to the air vehicle group (P<0.01) and remained unchanged in the smoke TEPP46 group (Figure 6.10B). Protein levels of PKM2 were analysed using immunofluorescence staining, which identified decreased PKM2 levels in the smoke vehicle group as compared to both the air vehicle and TEPP46 smoke groups (P<0.05) (Figure 6.10C).

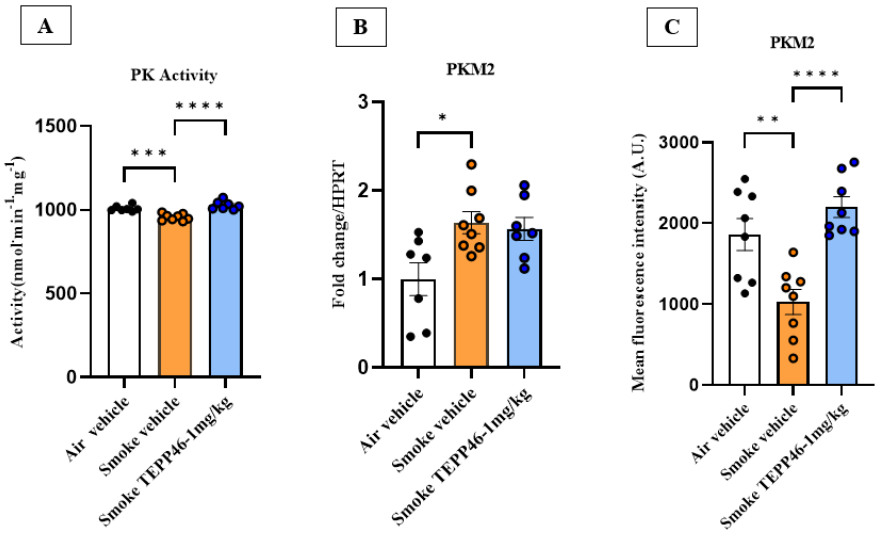

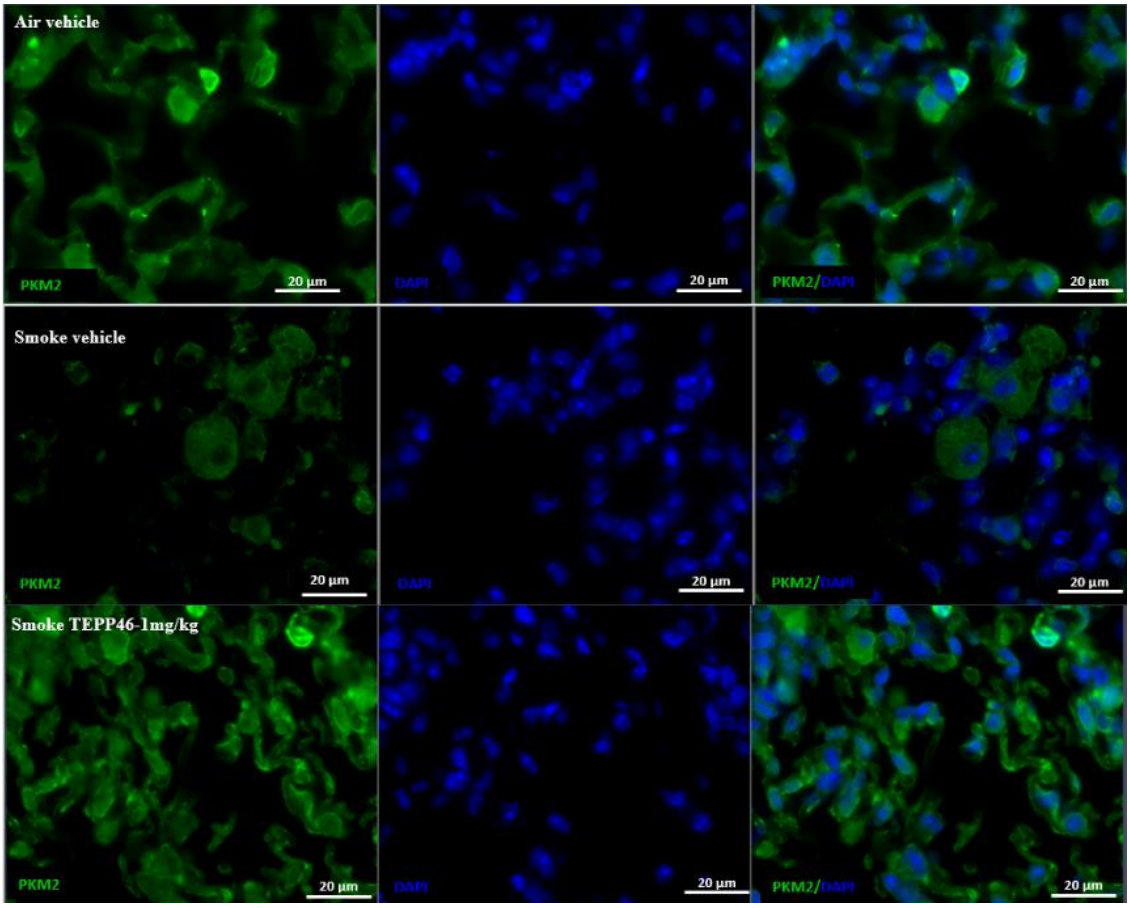

Figure 6.10: TEPP46 promoted tetramerisation of PKM2:

*TEPP46 treatment increased (A) PK activity (B) Gene expression of PKM2 and (C) Protein level of PKM2. Data represented are means ± SEM of 6-8 mice/group, * P<0.05, ** P<0.01, *** P<0.001, **** P<0.0001.*

6.3.10 Administration of TEPP46 promoted the metabolic role of PKM2 in experimental COPD study

There was a significant reduction in the PDH activity levels in the smoke vehicle group as compared to both the air vehicle and smoke TEPP46-1 mg/kg group (P<0.05) (Figure 6.11A).

The gene expression of HIF1α was determined to be unchanged across all the groups (Figure 6.11B). Further, the protein levels analysed using immunofluorescence showed a

reduced MFI of HIF1α in the smoke vehicle group in comparison to the air vehicle and TEPP46 smoke groups (P<0.05) (Figure 6.11C).

The gene expression of metabolic markers such as PDK1 was reduced in the smoke vehicle group however this was not significantly different to the air vehicle group (Figure 6.11D). PGC1α levels were reduced significantly in the smoke vehicle with respect to the air group (P<0.05) but remained unchanged in the smoke TEPP46-1 mg/kg group (Figure 6.11E). The gene expression of PKM1 (Figure 6.11G) and NFκB (Figure 6.11H) remained unchanged in all the groups in this study.

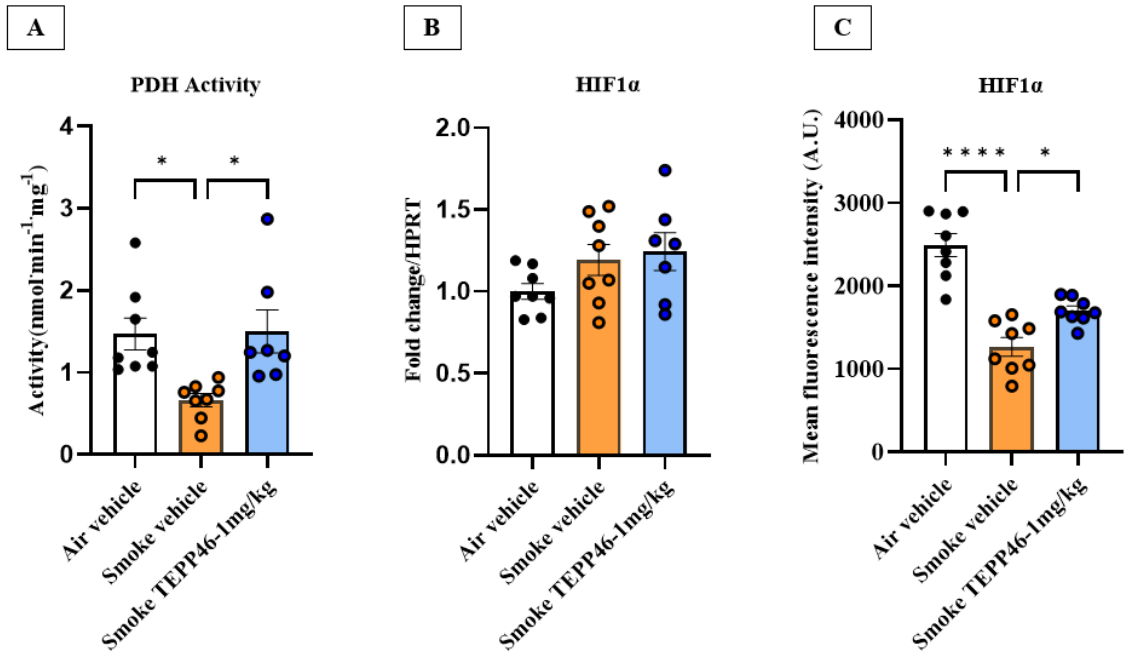

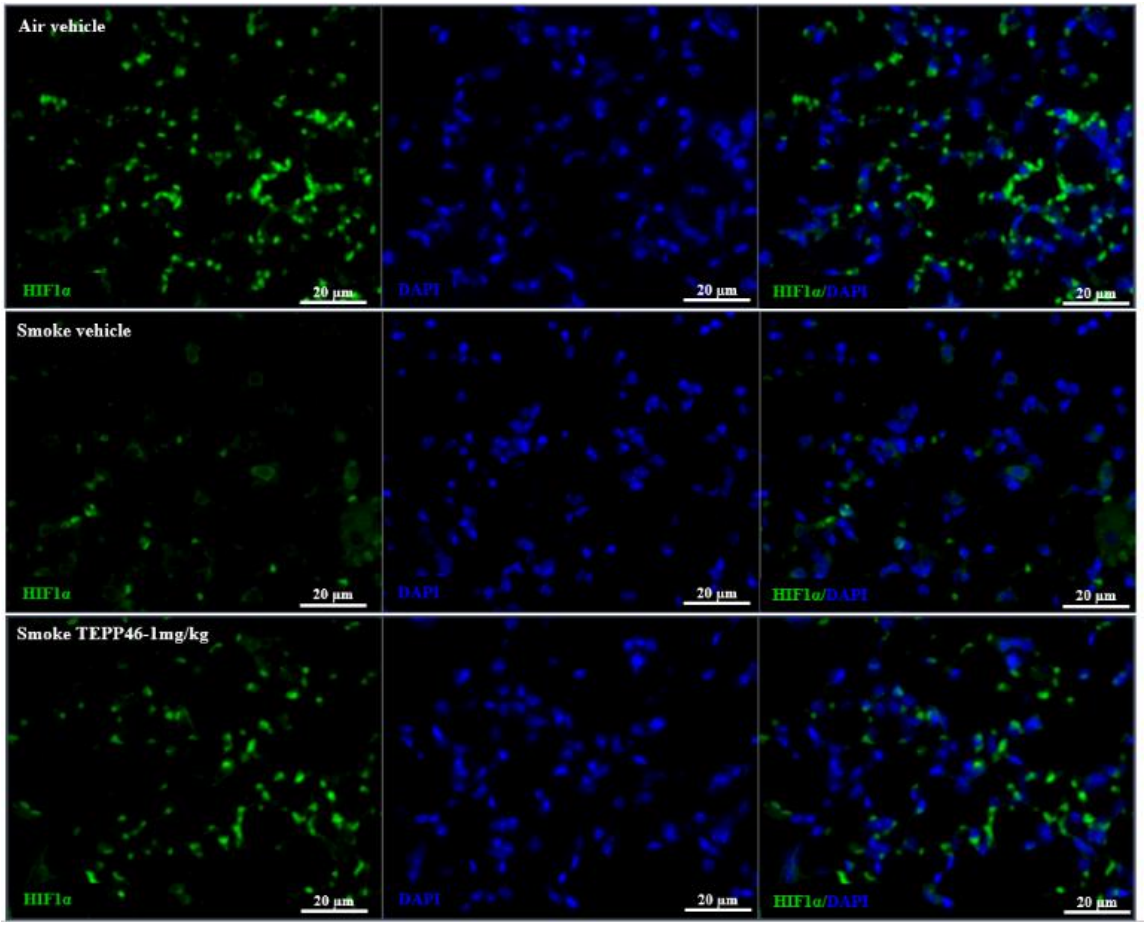
Air vehicle
HIF1α
20 μm
DAPI
20 μm
HIF1α/DAPI
20 μm
Smoke vehicle
HIF1α
20 μm
DAPI
20 μm
HIF1α/DAPI
20 μm
Smoke TEPP46-1mg/kg
HIF1α
20 μm
DAPI
20 μm
HIF1α/DAPI
20 μm

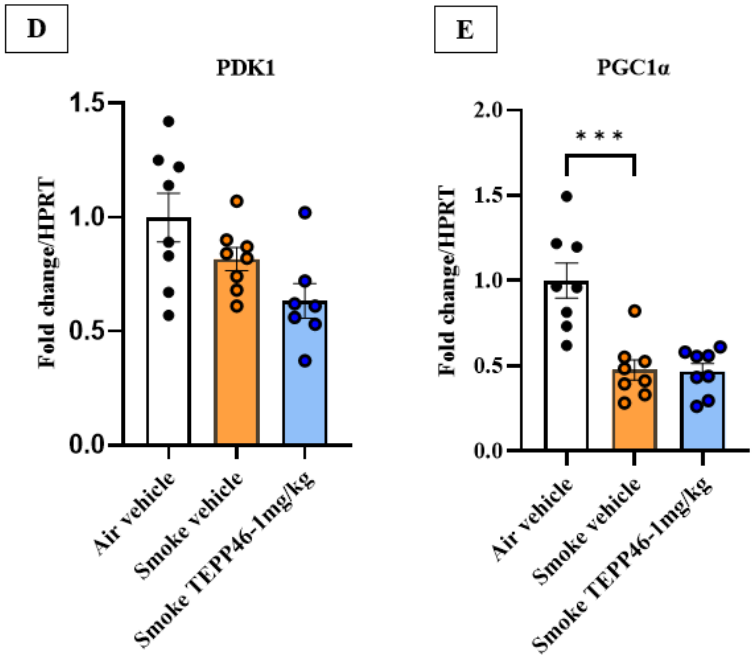
D
PDK1
Fold change/HPRT
1.5
1.0
0.5
0.0
Air vehicle
Smoke vehicle
Smoke TEPP46-1mg/kg
E
PGC1α
Fold change/HPRT
2.0
1.5
1.0
0.5
0.0
* * *
Air vehicle
Smoke vehicle
Smoke TEPP46-1mg/kg

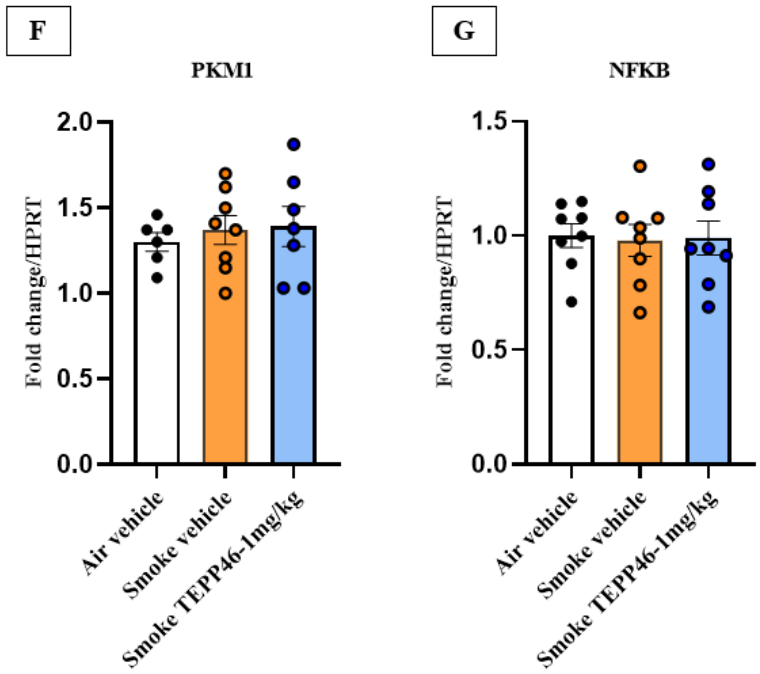

Figure 6.11: TEPP46 promoted the metabolic role of PKM2:

*TEPP46 administration in COPD showed (A) increased PDH activity, (B) unchanged gene expression of HIF1α and (C) increased protein expression of HIF1α, (D) reduced expression of PDK1, (E) PGC1α, and no change in (F) PKM1, and (G) NFκB. Data represented are means ± SEM of 6-8 mice/group, * P<0.05,** P<0.01, *** P<0.001, **** P<0.0001.*

6.3.11 Administration of TEPP46 improved NAD^+ metabolism in the experimental COPD model

The total NAD^+ levels in the smoke vehicle group were lower than that of the air vehicle group (P<0.05) and were increased in the smoke TEPP46-1 mg/kg group in comparison to the smoke vehicle group (P<0.01) (Figure 6.12A). In contrast, we did not observe any difference in the total NADH levels across all the experimental groups (Figure 6.12B). However, there was a significant reduction in the ratio of total NAD^+/NADH in the smoke vehicle group in comparison to the air vehicle group (P<0.05) which was again increased

in the smoke TEPP46-1 mg/kg group with respect to the smoke vehicle group (P<0.01) (Figure 6.12C).

In addition, we also measured the gene expression of NAD^+ consumers such as PARP1 and SIRT1-7, where we observed an increase in PARP1 expression in the smoke vehicle group in comparison to the air vehicle group (P<0.0001) and was reduced in the smoke TEPP46-1 mg/kg group with respect to the smoke vehicle group (P<0.0001) (Figure 6.12D). We observed a reduction in the gene expression of SIRT3 (Figure 6.12G), SIRT4 (Figure 6.12H), SIRT6 (Figure 6.12J) and SIRT7 (Figure 6.12K) in the smoke vehicle group in comparison to the air vehicle group (P<0.05), however, there was no significant difference in the smoke TEPP46-1 mg/kg group. Further, the gene expression levels of SIRT1 (Figure 6.12E), SIRT2 (Figure 6.12F) and SIRT5 (Figure 6.12I) did not change across any experimental groups in this study.

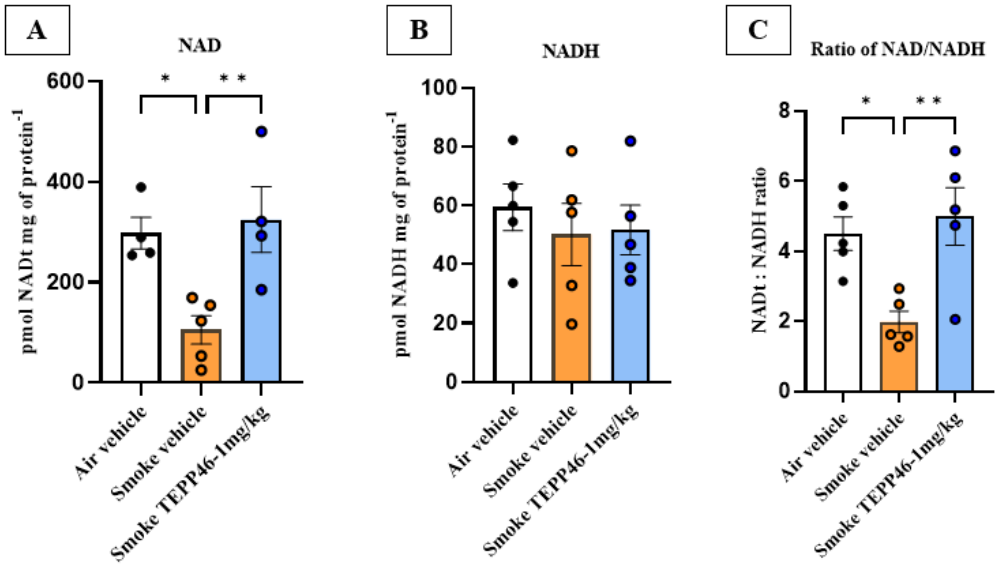

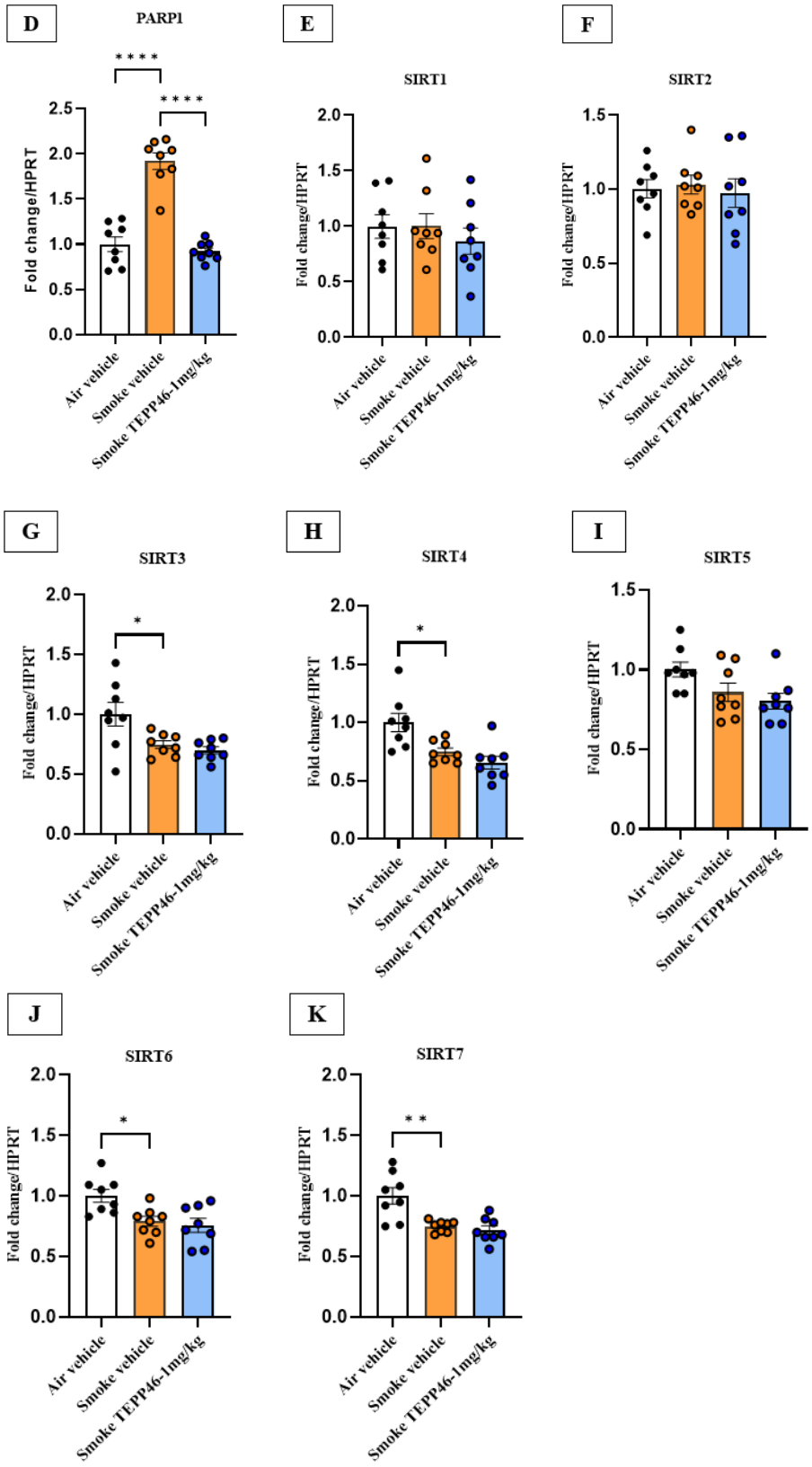

Figure 6.12: TEPP46 improved NAD$^+$ metabolism in experimental COPD:

*TEPP46 administration in COPD showed (A) increased NAD levels, (B) unchanged NADH levels and (C) increased ratio of NAD/NADH, Gene expression levels for (D) PARP1, (E) SIRT1, (F) SIRT2, (G) SIRT3, (H) SIRT4, (I) SIRT5, (J) SIRT6, (K) SIRT7. Data represented are means ± SEM of 6-8 mice/group, * P<0.05, ** P<0.01, *** P<0.001, **** P<0.0001.*

6.3.12 Administration of TEPP46 protected from oxidative stress in experimental COPD model

The gene expression of oxidative stress markers NOX2 and HO1 were examined, whereby the expression of NOX2 was significantly increased in the smoke vehicle in comparison to the air vehicle group (P<0.0001). There was a significant reduction in NOX2 expression in the smoke TEPP46-1 mg/kg group as compared to the smoke vehicle group (P<0.0001) (Figure 6.13A). There was no change in HO1 expression levels in the smoke vehicle group with respect to the air vehicle group, however, the TEPP46 smoke group showed reduced HO1 in comparison to the smoke vehicle group (P<0.001) (Figure 6.13B).

Further, lung sections from all the groups were stained with 4HNE (green) and F4/80 (red) to localise the oxidative stress response to macrophages within the lung due to lipid peroxidation. An increase in the intensity of 4HNE in the smoke vehicle group was observed with respect to the air vehicle group (P<0.0001). There was a significant reduction in the MFI of 4HNE in the smoke TEPP46-1 mg/kg group as compared to the smoke vehicle group (P<0.0001) (Figure 6.13C).

Moreover, lung sections were also stained with 3-NT (red) and LY6G (green) to localise oxidative stress response to the neutrophils in the lung due to nitration. An increase in the MFI of 3-NT was observed in the smoke vehicle group as compared to the air vehicle

group (P<0.0001) which was significantly reduced in the smoke TEPP46-1 mg/kg group as compared to the smoke vehicle group (P<0.0001) as shown below in the Figure 6.13D.

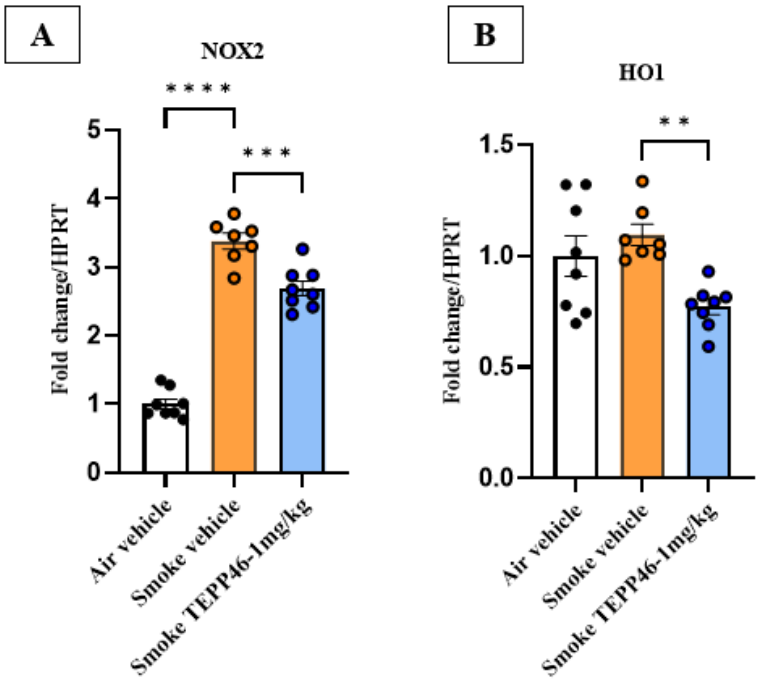

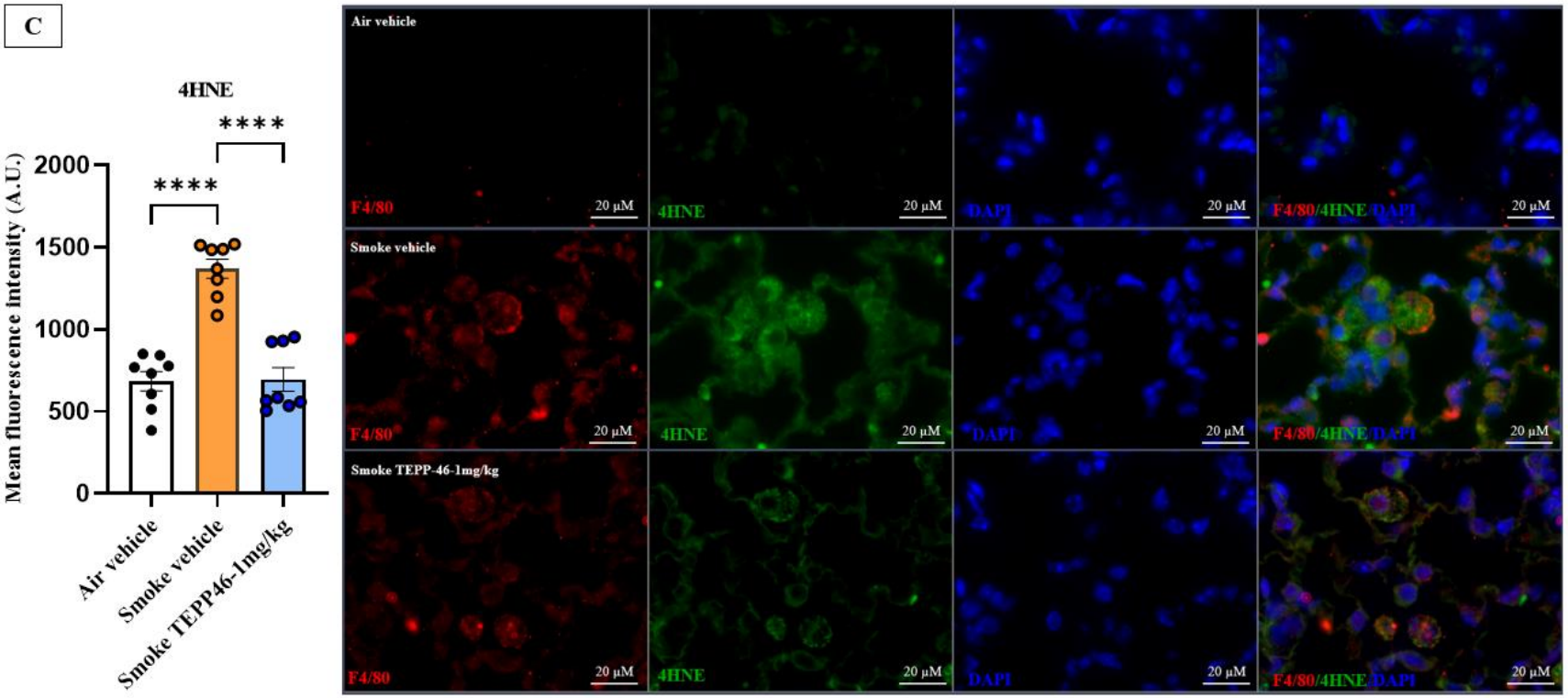
C
4HNE
****
****
Mean fluorescence intensity (A.U.)
2000
1500
1000
500
0
Air vehicle
Smoke vehicle
Smoke TEPP46-1mg/kg
Air vehicle
Smoke vehicle
Smoke TEPP-46-1mg/kg
F4/80
4HNE
DAPI
F4/80/4HNE/DAPI
20 µM

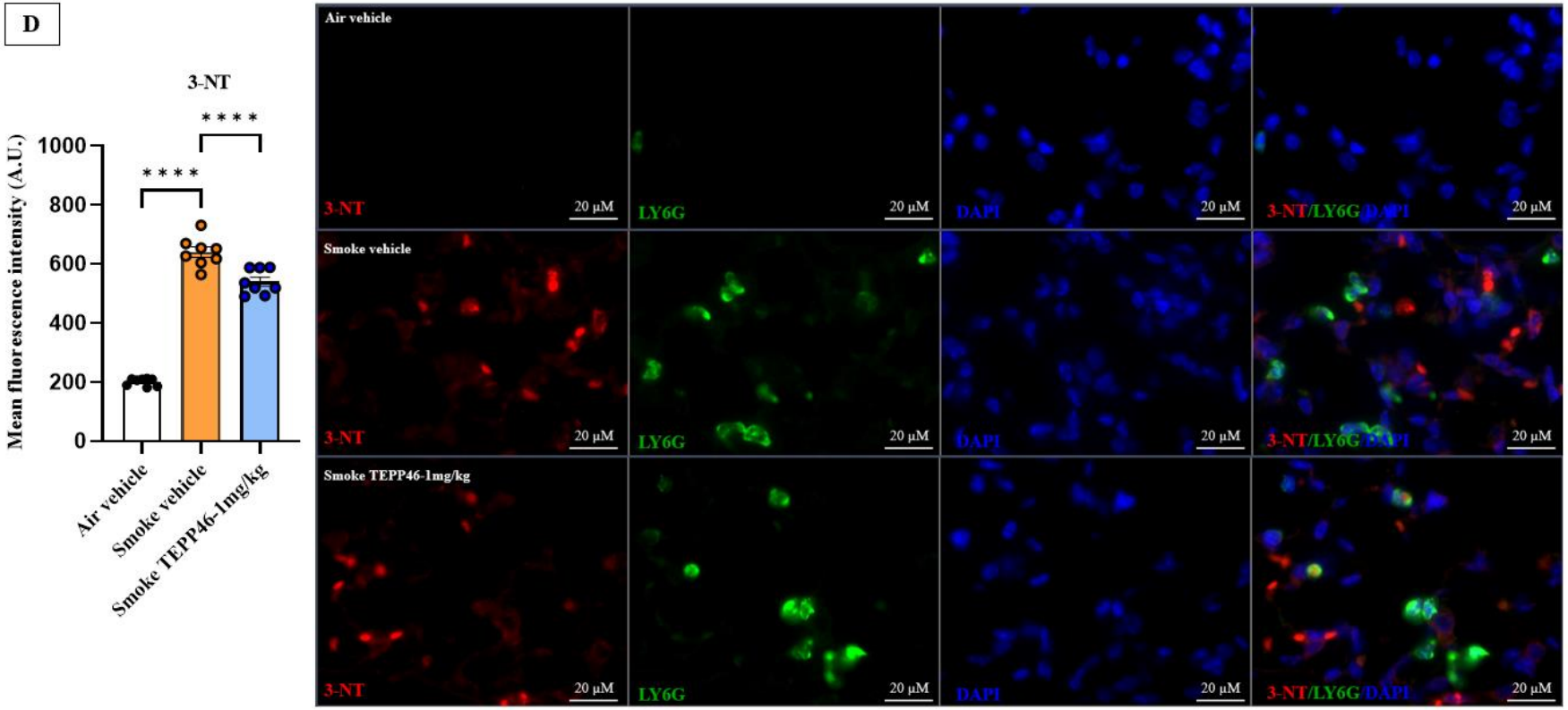

Figure 6.13: TEPP46 protects from oxidative stress in COPD:

*TEPP46 treatment in COPD reduced the (A) gene expression of NOX2, (B) HO1, and the MFI in both (C) 4HNE and (D) 3-NT. Data represented are means ± SEM of 6-8 mice/group, * P<0.05, ** P<0.01, *** P<0.001, **** P<0.0001.*

6.3.13 Administration of TEPP46 preserved mitochondrial ultra-structure in experimental COPD

Lung samples from the 8-week CS-induced COPD study were processed to determine mitochondrial morphology with TEM as mentioned previously. Chronic exposure to CS in our 8-week COPD model demonstrated an increase in mitochondrial density in the smoke vehicle group in comparison to the air vehicle group (P<0.05) (Figure 6.14A). However, the smoke TEPP46-1mg/kg group did not show any significant change in the mitochondrial density with respect to both the smoke vehicle group and air vehicle group (Figure 6.14A).

We also observed damaged mitochondrial ultra-structures with an increase in mitochondrial area in the smoke vehicle group with respect to the air vehicle group (P<0.001) (Figure 6.14B) Importantly, the smoke TEPP46-1mg/kg group displayed a reduction in damaged mitochondria via reduced mitochondrial area in comparison to the smoke vehicle group (P<0.05) (Figure 6.14B).

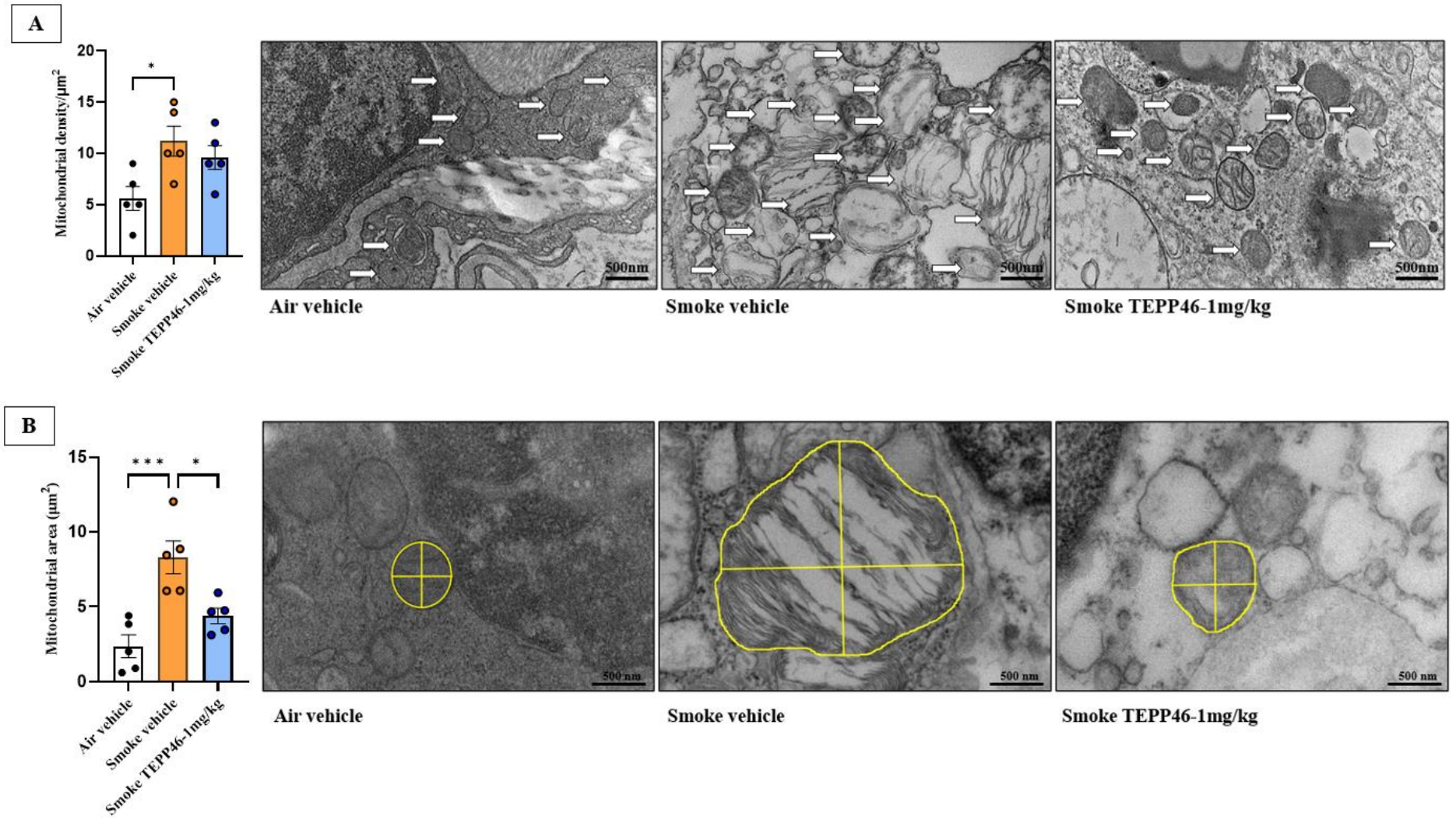

Figure 6.14: Administration of TEPP46 protected mitochondrial ultra-structure in experimental COPD:

*(A) Increase in mitochondrial density in the smoke vehicle group does not change with TEPP46 administration; (B) Reduced mitochondrial area in air vehicle and smoke TEPP46-1 mg/kg in comparison to the smoke vehicle group. Data represented are means ± SEM of 5 mice/group, * P<0.05, ** P<0.01, *** P<0.001, **** P<0.0001.*

6.3.14 Administration of TEPP46 promoted oxidative phosphorylation and ΔΨm in experimental COPD

To perform a quantitative analysis of oxidative phosphorylation, we also measured the protein abundance of complex I-NDUFB8 (Figure 6.15A), complex II-SDHB (Figure 6.15B), complex III-UQCRC2 (Figure 6.15C), complex IV-MTCO1 (Figure 6.15D), and complex V-ATP5A (Figure 6.15E). A significant increase in the protein levels of complex I, III, IV and V were observed in the smoke TEPP46-1 mg/kg in comparison to the smoke vehicle group (P<0.05). In comparison, there was no change in the protein abundance of complex II in all experimental groups. However, the protein levels of all the complexes remain unchanged between the air vehicle and smoke vehicle groups.

Furthermore, the determination of ΔΨm was performed using JC1 staining on lung histology sections and the ratio of J-aggregates in comparison to J-monomers was measured for all the groups. J-aggregates were reduced in the smoke vehicle group as compared to the air vehicle and smoke TEPP46-1 mg/kg group (P<0.05) (Figure 6.15F). J-monomers were significantly increased in the smoke vehicle group as compared to the air vehicle and smoke TEPP46-1 mg/kg group (P<0.0001) (Figure 6.15G). Further, the ΔΨm representing the ratio of J-aggregates to J-monomers was reduced in the smoke vehicle group as compared to the air vehicle and smoke TEPP46-1 mg/kg group (P<0.0001) (Figure 6.15H).

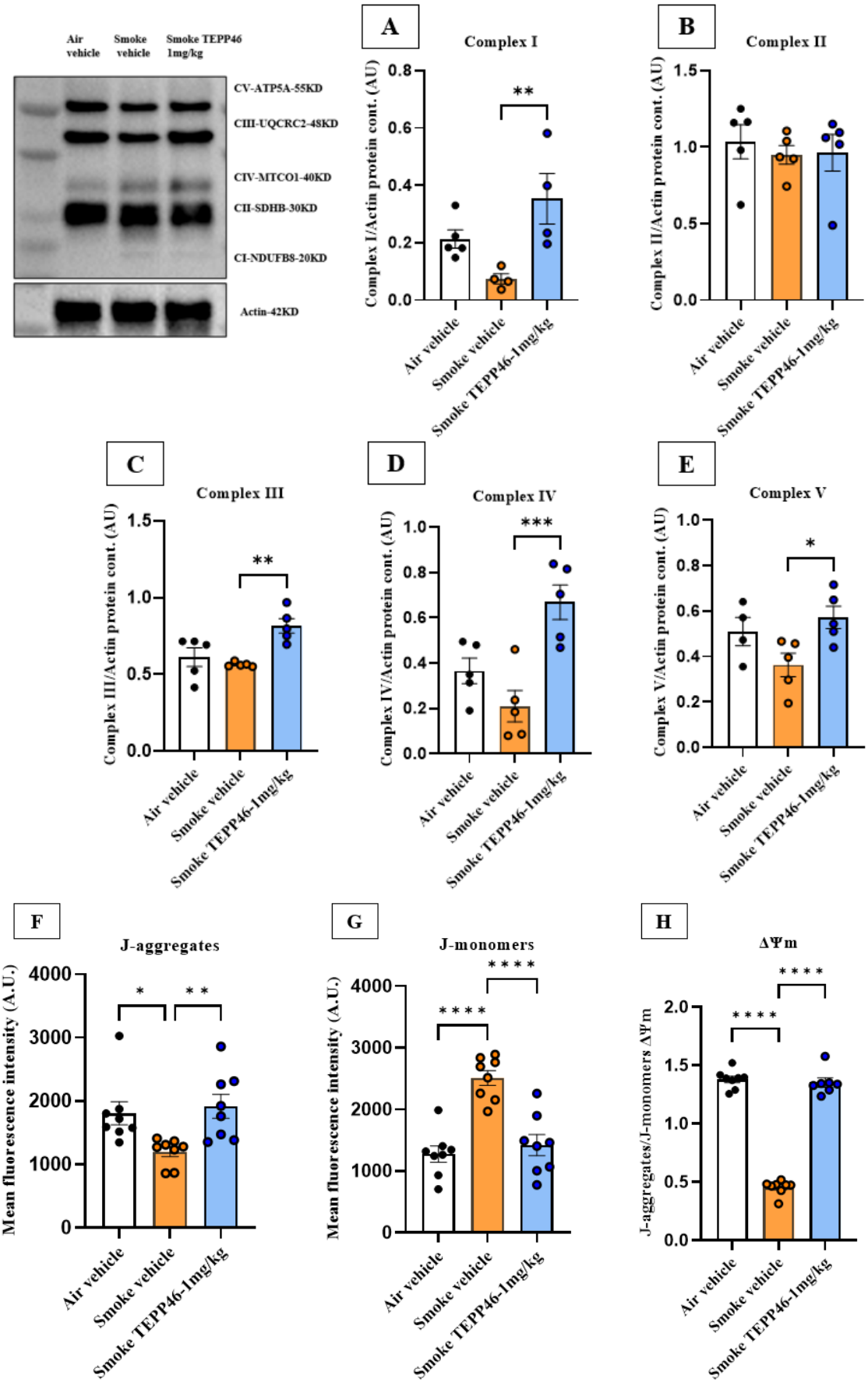
Air vehicle
Smoke vehicle
Smoke TEPP46 1mg/kg
CV-ATP5A-55KD
CIII-UQCRC2-48KD
CIV-MTCO1-40KD
CII-SDHB-30KD
CI-NDUFB8-20KD
Actin-42KD
A
Complex I
Complex I/Actin protein cont. (AU)
B
Complex II
Complex II/Actin protein cont. (AU)
C
Complex III
Complex III/Actin protein cont. (AU)
D
Complex IV
Complex IV/Actin protein cont. (AU)
E
Complex V
Complex V/Actin protein cont. (AU)
F
J-aggregates
Mean fluorescence intensity (A.U.)
G
J-monomers
Mean fluorescence intensity (A.U.)
H
ΔΨm
J-aggregates/J-monomers ΔΨm
Air vehicle
Smoke vehicle
Smoke TEPP46-1mg/kg

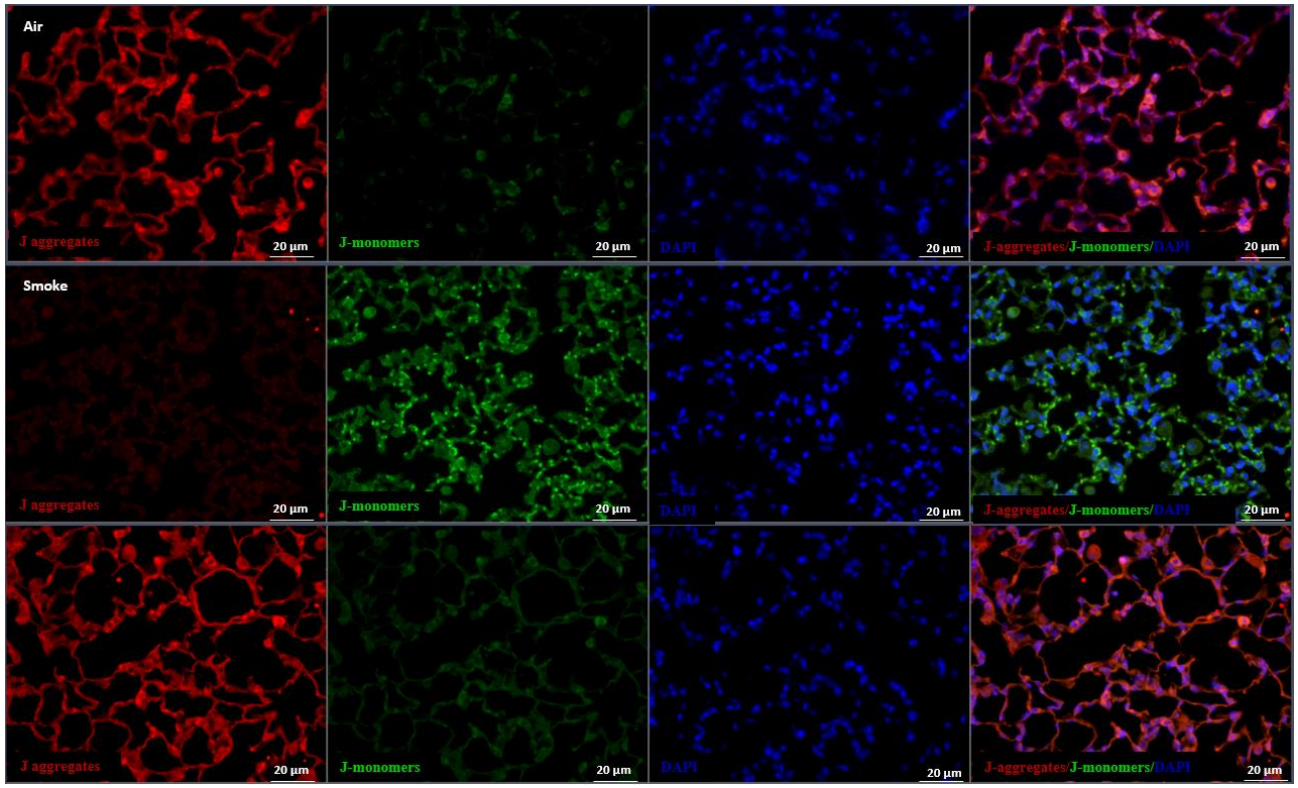

Figure 6.15: Administration of TEPP46 promoted mitochondrial function in experimental COPD:

*Graphical representation of the increase in protein levels of (A) Complex I-NDUFB8, (B) Complex II-SDHB, (C) Complex III-UQCRC2, (D) Complex IV-MTCO1, (E) Complex V-ATP5A in the smoke TEPP46-1 mg/kg group; TEPP46 also (F) increased J-aggregates, (G) reduced J-monomers and (H) increased ΔΨm. Data represented are means ± SEM of 6-8 mice/group, * P<0.05,** P<0.01, *** P<0.001, **** P<0.0001.*

6.4 Discussion

The objective of this study was to delineate the role of immunometabolism in the development and progression of COPD and to decipher the therapeutic effects of TEPP46 in our CS-induced experimental COPD mouse model. In our study, we used our well-established murine model to mimic the hallmark features of COPD that include increased cellular infiltration in the lung, airway remodelling and alveolar destruction leading to reduced lung function (117, 146). COPD is a progressive disorder and is driven by multiple other factors even after cessation of smoking such as oxidative stress due to chronic inflammation, as well as mitochondrial and metabolic dysfunction (297). Immune cells rely heavily on oxidative phosphorylation in the resting state however, during inflammation these cells undergo a metabolic shift and depend on glycolysis for instant ATP production (271). PKM2 plays an important role in catalysing the last step of glycolysis along with regulating cellular metabolism (274). This leads to a shift from the normal respiratory chain to glucose metabolism and lactate production (160). PKM2 exists in a highly active tetramer or low-activity dimer form and can switch between both in healthy cells (480). During inflammation, the shift in PKM2 oligomer is impaired leading to metabolic dysfunction which results in reduced cellular metabolism and oxidative stress (163). Studies have demonstrated the role of PKM2 in tumorigenesis and cancer metabolism but to date, there is limited knowledge about the exact mechanisms of impaired immunometabolism in driving COPD (163).

The findings from our study showed an increase in 4HNE; a marker of oxidative stress produced as a by-product of lipid peroxidation upon CS exposure for 8 weeks (Figure 6.2A). This was further confirmed by an increase in the transcripts that encode for HO1 (Figure 6.2B) and NOX2 (Figure 6.2C). Oxidative stress in COPD is an inherent outcome of mitochondrial dysfunction, and therefore to elucidate the mitochondrial activity we

measured mitochondrial membrane potential using JC1 cationic dye. Healthy energised mitochondria are negatively charged and lead to the accumulation of JC1 forming J-aggregates and exhibiting excitation in the red spectrum at 590nm (481). Whereas, in stressed or apoptotic cells, JC1 is unable to form aggregates resulting in the formation of J-monomers due to the reduced negative charge in the mitochondria, increased membrane permeability and consequent loss of electrochemical potential (307). J-monomers exhibit excitation in the green spectrum at 526nm. The ratio of the J-aggregates/J-monomers in the mitochondria is considered a state of mitochondrial polarisation or highly charged membrane to exhibit full membrane potential (481). We observed a significant reduction in J-aggregates (Figure 6.2D) and an increase in the J-monomers (Figure 6.2E) in our COPD model in the smoke vehicle group, resulting in reduced mitochondrial membrane potential (Figure 6.2F). This reflects the impaired process of the ETC and oxphos resulting in depletion of ATP and therefore acting as a potential driver of chronic inflammation in COPD. This was further validated with an increase in the transcripts encoding TNFα (Figure 6.2G), CXCL1 (Figure 6.2H), YM1 (Figure 6.2I) and PARP1 (Figure 6.2J) after 8 weeks of smoke exposure which confirmed the heightened inflammation in our murine COPD model. Further, we also observed a reduction in the transcripts encoding iNOS (Figure 6.2K), PGC1α (Figure 6.2L), PKM1 (Figure 6.2M), PKM2 (Figure 6.2N), and HIF1α (Figure 6.2O), suggestive of impaired cellular metabolism in our 8-week CS-induced COPD murine model. Taken together, these findings demonstrate that impaired immunometabolism drives inflammation in COPD.

Further, we investigated the therapeutic efficacy of immunomodulator TEPP46 in COPD. TEPP46 is known to activate PKM2 by promoting the formation of PKM2 tetramers (271). A 2-week CS-induced acute inflammatory murine model was performed to optimise the dosage for intranasal administration of TEPP46 and elucidate its anti-

inflammatory effects. The 2-week study showed an increase in total leukocyte infiltration in the BAL of the smoke vehicle group compared to the air vehicle group, which was significantly reduced in all three doses of TEPP46 examined in this acute model (Figure 6.3). However, TEPP46 smoke groups treated with either 4 mg/kg or 2 mg/kg lost up to 10-12% of their body weight (Figure 6.3D). Mice in the smoke TEPP46-1 mg/kg group were observed to be healthy, with normal fur and regular posture and behaviour as also noted in the smoke vehicle and air vehicle groups. Based on these observations in the 2-week acute model, it was concluded that these TEPP46 dosages were likely to negatively impact animal welfare in an 8-week COPD model and thus, they were excluded from further analyses. Based on these data, 1 mg/kg was selected as an optimum dosage for long-term 8-week studies. An increase in the gene expression of TNFα (Figure 6.3E), CXCL1 (Figure 6.3F), IL-1β (Figure 6.3G) and YM1 (Figure 6.3H) upon smoke exposure, and the subsequent reduction upon treatment with TEPP46 further validate the anti-inflammatory properties of TEPP46 in our 2-week murine studies. We observed reduced gene expression of iNOS (Figure 6.3I) which is indicative of inflammation upon smoke exposure and remains unchanged in the TEPP46 treatment group potentially due to the constant CS exposure in the 2-week model.

Irreversible changes to the lung structure are one of the hallmark features of COPD (326). While acute CS exposure in a 2-week model does not typically induce permanent structural changes, we wanted to determine whether TEPP46 caused structural changes to the lung architecture as this was an intranasally administered drug. In our model, we observed alveolar damage upon CS exposure and TEPP46 treatment exhibited protection from alveolar damage, providing a strong rationale to extend these studies further into an 8-week model (Figure 6.4).

Previous studies have demonstrated the role of TEPP46 in the tetramerisation of PKM2 and in promoting the metabolic functions of PKM2 in tumorigenesis (160). Our findings display the tetramerisation of PKM2 in the acute CS-exposed murine model following TEPP46 treatment. We observed an increase in the PK activity level and the PKM2 protein level via immunofluorescence in the TEPP46 treatment group, suggesting the presence of a highly active PKM2 tetramer as expected (Figure 6.5). High PK activity is indicative of increased catalysis of the phosphate group from PEP to ADP (164), yielding pyruvate and ATP. Reduced or abolished pyruvate kinase levels can lead to dampening in the rate of glycolysis resulting in impaired mitochondrial and metabolic function (274). Pyruvate derived from glycolysis is converted to acetyl-CoA by PDH, which enters the TCA cycle and leads to ATP production (482). We observed an increase in PDH activity upon TEPP46 treatment which was reduced upon smoke exposure (Figure 6.6A). PDH deficiency reduces mitochondrial function and is linked to chronic neurological diseases affecting the central nervous system (483). Recent studies have shown that PDH is a target of oncogene-induced senescence (484); activation of PDH enhances pyruvate utilization and increases respiration and redox stress (485). PDH activity is controlled by PDKs (486). The gene expression of PDK1 (Figure 6.6D) didn't change in our acute study along with PARP1 (Figure 6.6F) and PKM1 (Figure 6.6G). However, the expression of PGC1α (Figure 6.6E) was reduced upon smoking and was protected upon TEPP46 treatment. PGC1α is a mitochondrial biogenesis marker (331), an increase in mitochondrial biogenesis results in an increase in the metabolic enzymes for glycolysis and oxphos (487). Recent studies have highlighted the importance of PKM2 as a coactivator of HIF1α and its role in the metabolic reprogramming of inflammatory cells in promoting the transcription of glycolytic genes (166, 488). We observed an increase in gene expression of HIF1α upon smoke exposure, which was reduced in the TEPP46 treatment group

(Figure 6.6B), contradictory to the protein levels of HIF1α which was reduced upon exposure to smoke and upregulated in the TEPP46 treatment group (Figure 6.6C). PKM2 and HIF1α are regulated in a positive feedback loop (273), where HIF1α regulates PKM2 gene expression, however, PKM2 then interacts with HIF1α in a loop and promotes the transactivation of HIF1 targeted glycolytic genes.

We further measured ΔΨm in our 2-week model and observed an increase in the TEPP46 treatment in comparison to the smoke group (Figure 6.7). Interestingly, an increase in ΔΨm resulted in reduced oxidative stress as observed with a decrease in the gene expression of NOX2 and HO1 with the TEPP46 treatment (Figure 6.7).

In conclusion, this study has demonstrated that TEPP46 exhibited a versatile therapeutic role in acute CS inflammation study by reducing inflammation, promoting metabolic activity and increase in mitochondrial activity leading to reduced oxidative stress. Further, we investigated the efficacy of TEPP46 in an experimental COPD murine model. Inflammation is a major driver of COPD pathogenesis (139), as in our 8-week model we observed an increase in cellular infiltration in BAL of smoke vehicle mice which was significantly reduced upon the administration of TEPP46 (Figure 6.8). Furthermore, validation of the anti-inflammatory role of TEPP46 in COPD was confirmed with the reduction in the transcripts encoding TNFα, CXCL1, YM1, and iNOS as compared to the smoke vehicle group (Figure 6.8). Further, we observed a significant reduction of body weight in the smoke vehicle group in comparison to the air vehicle group which is a feature of the CS-induced experimental COPD model, however, treatment with TEPP46 did not show any improvements in the overall body weight in comparison to the smoke vehicle group. This could be due to various systemic factors which play important role in the disease progression and further studies will be required to understand the underlying mechanisms for the restoration of body weight.

Emphysema and chronic bronchitis are two important disease features of COPD (489). The mechanisms that drive these features remain unclear and have led to a delay in the development of effective therapies for COPD (490). Nevertheless, high doses of corticosteroids are widely employed through inhalation, but their efficacy is limited to reducing exacerbation frequency or, combined with bronchodilators to improve COPD (491). In the current study, chronic exposure to CS leads to damage in air sacs resulting in emphysema, airway remodelling, and deposition of collagen around the airways when compared to the air vehicle group. Importantly, these measurements were significantly reduced by the administration of TEPP46 relative to the smoke vehicle group (Figure 6.9 A&B). These changes reflected the protective therapeutic role of TEPP46 in preventing or impairing the development of chronic bronchitis and emphysema in our murine model. The structural changes in the lung often lead to impaired lung function which is a clinically-relevant measurement in COPD patients often intrinsically linked to COPD severity (492). The progressive airflow limitation is associated with morbidity and mortality in COPD hence a major goal of recent studies has been to delay or prevent the reduction of lung function (493). Our study showed impaired lung function due to chronic exposure to CS leading to an increase in IC, area (hysteresis), FVC, FEV, Cst, A, and TLC in comparison to the air vehicle group. However, there were no improvements in lung function parameters with TEPP46 treatment (Figure 6.9). This is unsurprising given that until recently, the only known effective intervention to restore lung function capacity in COPD patients was smoke cessation (364). Moreover, lung compliance curves are representative of emphysema, and we observed an increase in the area of the curve in the smoke vehicle group which was reduced with the administration of TEPP46 back to baseline level, suggesting that TEPP46 treatment might potentially restore or delay lung function changes in COPD upon cessation of smoke. Collectively, these results suggest

that intranasal administration of TEPP46 protects lung structure from the damage induced by CS in COPD and might potentially restore function upon cessation of smoke exposure. Further studies will be required to confirm the efficacy of TEPP46 in the restoration of lung function upon cessation of smoke exposure.

To unravel the therapeutic benefits of TEPP46 in COPD, we confirmed our previous findings in a 2-week model of TEPP46 administration in enhanced tetramerisation of PKM2 in our 8-week COPD model. We observed an increase in the PK activity level (Figure 6.10A), the gene expression of PKM2 (Figure 6.10B), and the protein level of PKM2 (Figure 6.10C) in the smoke TEPP46-1 mg/kg group, suggesting the presence of the highly active tetramer form of PKM2 following TEPP46 treatment in smoke-exposed mice and might potentially lead to an increase in glycolysis. Studies have shown that the rate of glycolysis increases in COPD leading to an imbalance in pyruvate produced from glycolysis and oxidation of pyruvate via the TCA cycle which leads to the production of lactate (494, 495).

We further observed an increase in PDH activity upon TEPP46 treatment in COPD (Figure 6.11A). The gene expression of PDK1 is reduced upon the TEPP46 treatment (Figure 6.11D), along with the expression of PGC1α (Figure 6.11E). We did not observe any change in the gene expression of PKM1 (Figure 6.11F), NFκB (Figure 6.11G), and HIF1α (Figure 6.11B), however, the protein levels of HIF1α were reduced upon exposure to smoke and upregulated in the TEPP46 treatment group (Figure 6.11C). Collectively, these results suggest that the administration of TEPP46 promoted the tetramerisation of PKM2 which further increases the metabolic role of PKM2 in COPD.

Chronic exposure to CS in the smoke vehicle group resulted in NAD^+ depletion and a reduction in the ratio of NAD^+ to NADH ratio in comparison to the air vehicle group and was increased in the smoke TEPP46-1 mg/kg group, suggesting that the administration

of TEPP46 improved NAD^+ metabolism in COPD (Figure 6.12A). In contrast, we did not observe any change in total NADH levels across all experimental groups (Figure 6.12B), however, there was a reduction in the ratio of total NAD^+/NADH in the smoke vehicle group in comparison to the air vehicle group which increased with the administration of TEPP46 in the smoke TEPP46-1 mg/kg group as compared to the smoke vehicle group (Figure 6.12C). These results exhibit an imbalance of NAD^+ in COPD, which was protected with the administration of TEPP46. Furthermore, increases in the gene expression of PARP1 (Figure 6.12D) in the smoke vehicle group suggest that hyperactivity of PARP1 is a potential contributing factor for NAD^+ depletion in COPD. In support of this, the administration of TEPP46 reduced PARP1 expression which is in line with our previous findings demonstrating increased NAD^+ levels following TEPP46 treatment. In contrast, we observed reduced gene expression of SIRT3-4, 6-7 (Figure 6.12E-K) in the smoke vehicle group, likely due to reduced NAD^+ levels. However, the TEPP46 treatment did not show any changes in the expression of SIRT1-7, potentially due to the prophylactic administration of the treatment along with the CS exposure in this study and might improve with the therapeutic administration of TEPP46. In conclusion, these results demonstrate that the administration of TEPP46 improved NAD^+ metabolism in experimental COPD.

Oxstress and mitochondrial damage are potential drivers of inflammation in COPD (496). COPD patients show increased oxidative stress in the lungs induced by airway inflammatory and structural cells (316). These changes lead to a reduction in antioxidant defence with the inactivation of several transcription factors and antioxidant enzymes (313). The current study shows increased levels of NOX2 (Figure 6.13A) in the smoke vehicle group in comparison to the air group which was reduced in the smoke TEPP46-1 mg/kg group. This was further confirmed with 4HNE (Figure 6.13C) and 3-NT (Figure

6.13D) levels. However, we did not see any change in gene expression of HO1 between the air vehicle and smoke vehicle groups, but smoke TEPP46-1 mg/kg reduced HO1 expression levels (Figure 6.13B). Taken together, these results suggested that the administration of TEPP46 reduced oxidative stress in COPD.

Previous studies have shown that oxidative stress leads to changes in mitochondrial structure and membrane permeability (317). Mitochondrial ultra-structural changes have revealed novel pathologies in chronic diseases in numerous different studies (497, 498) but there has been no evidence of mitochondrial ultrastructural changes in COPD. In our study, we observed an increase in the number of mitochondria as well as an increase in the mitochondrial area upon chronic exposure to CS indicating damage in mitochondrial ultra-structure (Figure 6.14A & B). TEPP46 treatment in our experimental COPD model protected mitochondrial density and area, preserving mitochondrial structure in COPD (Figure 6.14A & B).

Recent studies have shown that PKM2 tetramer exhibit high catalytic activity which increases pyruvate production and promotes the glucose flux to increase oxidative phosphorylation (499), which is one of the crucial mitochondrial functions to synthesise ATP via the electron transport chain. We observed an increase in the protein levels of complex I, III, IV and V in the smoke TEPP46-1 mg/kg group (Figure 6.15A-E) suggesting that TEPP46 increased oxidative phosphorylation in COPD via increased tetramerisation of PKM2. However, we did not see a change in complex II in any experimental group in this study which isn't surprising as there is no evidence of PKM2 regulating succinate dehydrogenase which helps in promoting the Krebs cycle.

Moreover, an increase in $\Delta\Psi m$ was observed in the TEPP46 treatment group (Figure 6.15F), with increased accumulation of J-aggregates (Figure 6.15G) and reduction in J-monomers (Figure 6.15H). Collectively, these results suggested that the administration of

TEPP46 preserved the mitochondrial structure and function via increased oxidative phosphorylation and mitochondria membrane potential.

In conclusion, our study has demonstrated that chronic exposure to CS leads to impaired immunometabolism driving oxidative stress and inflammation in COPD leading to important pathophysiological features of COPD. We have investigated the therapeutic efficacy of TEPP46 in an acute CS exposure and chronic experimental COPD murine model whereby administration of TEPP46 not only showed improvements in lung inflammation and structure but also promotes metabolic function, resulting in reduced oxidative stress and protection of mitochondrial structure and function. Further studies will be required to decipher the implications of TEPP46 in reversing or delaying the progression of COPD.

Chapter 7. General Discussion

7.1 Introduction

COPD is the 3rd leading cause of chronic morbidity and mortality worldwide (500, 501). Chronic inhalation of CS is notably the major known risk factor for COPD (501, 502). COPD is characterised by the limitation of airflow in the lungs (1) and is largely driven by alveolar destruction (emphysema) (503), chronic bronchitis (504) and impaired lung function (505). These events lead to physiological and pathological changes in the lung which are further associated with increased airway inflammation in COPD (506). The mechanisms that drive the inception and progression of chronic inflammation in COPD are not well understood, and this has hampered the development of effective treatments for the disease (277, 507). Current therapeutic approaches are limited and largely manage symptoms and reduce exacerbations (277, 508). Thus, due to the incomplete understanding of COPD pathogenesis, there are no available treatments that inhibit the progression or reverse the disease features.

Recent studies have highlighted that altered metabolism in immune cells leads to oxidative stress resulting in sustained inflammation in COPD (282, 509), accompanied by impaired metabolism (283, 510), mitochondrial dysfunction (96, 279), decreased mitochondrial density and biogenesis (92, 280), and impaired mitochondrial activity and apoptosis (92, 281). NAD^+ is responsible for carrying out essential biochemical reactions responsible for ATP production in mitochondria which provides the ultimate source of energy in a cell (318, 401). Currently, there is no evidence of the contribution of NAD^+ in impaired immunometabolism driving COPD (238, 511). The objective of the current study was to understand the role of NAD^+ in impaired immunometabolism involved in the induction, progression, and development of COPD. The thesis investigates the role of

NR, PT and TEPP46 as therapeutic interventions in COPD in a clinically relevant CS-induced experimental COPD murine model.

7.2 Experimental findings

7.2.1 Imbalance in NAD^+ homeostasis

NAD^+ is a central redox cofactor that participates in energy metabolism pathways (512, 513) such as glycolysis (514), β-oxidation (515), and oxidative phosphorylation (516, 517). Additionally, it is required for post-translational modifications (324) such as deacetylation (518, 519) and ADP-ribosylation (520) by SIRTs (521, 522) and PARPs (523). NAD^+ is involved in DNA damage repair (524), and oxidative stress responses (525). Impaired NAD^+ metabolism is a causative factor in numerous metabolic disorders such as diabetes (526, 527) and fatty liver disease (528, 529). In addition, NAD^+ levels decrease with aging and obesity (530, 531) suggesting declining NAD^+ levels are associated with reduced metabolism. Primary deficiencies in NAD^+ homeostasis are caused by impaired NAD^+ biosynthesis (532, 533), while secondary deficiencies result from increased NAD^+ consumption driven by PARPs, SIRTs and CD38 (478, 534). Activation of PARPs (379, 535) and reduced histone deacetylation (248, 536) in COPD pathogenesis highlight the potential involvement of NAD+, as both PARPs and SIRTs, are dependent on NAD^+ as a co-factor (537). To date, there is limited knowledge about the imbalances of NAD^+ depletion in the induction and the progression of the disease and if restoration of NAD^+ can potentially exert therapeutic benefits in COPD. Therefore, we investigated the role of NAD^+ during the pathogenesis of the disease and therapeutically targeted NAD^+ imbalances using different dietary modulators in COPD.

We have demonstrated in chapter 3 that there is a significant reduction in the total NAD^+ levels in our CS-induced experimental COPD mouse model and that these NAD^+ levels are consistently reduced from as early as 2 weeks and remain changed throughout the 12-week smoke exposure period. Additionally, we observed an increase in NADH levels upon CS exposure across all these time points. Consequently, the ratio of total NAD+ to NADH levels was reduced, indicative of imbalances of NAD^+/NADH ratios during the development and progression of COPD. Previous studies have shown a decline in NAD^+ levels is associated with aging (538), and metabolic disorders like diabetes (539) and fatty liver disease (540) are linked to worsened outcomes and poor clinical prognosis which is largely driven by imbalances in NAD^+ synthesis and consumption pathways (541, 542). Therefore, it is plausible that imbalances in NAD^+ homeostasis may be a potential contributing factor driving COPD progression. Moreover, therapeutics that are able to modulate NAD^+ metabolism represent attractive interventions to prevent or reduce COPD development or progression.

7.2.2 Targeting impaired NAD^+ homeostasis using NR and PT in COPD

Recent advances in immunometabolism have highlighted NAD^+ as a vital co-factor that can activate SIRTs (543, 544) and maintain mitochondrial fitness via mitochondrial unfolded protein responses (UPRmt) (545, 546) required to maintain cellular functions (547). To therapeutically target impaired NAD^+ biosynthesis and consumption in COPD, we used dietary interventions of NR and PT in this study. NR is a precursor molecule of NAD^+ (548), therefore might potentially increase NAD^+ synthesis in COPD. On the other hand, PT is known to activate SIRT1 (549), which is one of the major NAD^+ consumers (550), therefore might potentially increase NAD^+ consumption in COPD.

Chronic oxidative stress in COPD leads to significant DNA damage during the progression of the disease causing rapid activation of PARP1 to repair DNA lesions (329). In our study, we have demonstrated an increase in the activity of PARPs in COPD which is potentially activated in order to repair DNA damage caused via chronic exposure to CS. Additionally, we have shown a reduction in the total NAD^+ levels in COPD leading to an imbalance in NAD^+/NADH ratios. PARPs rely on NAD^+ to modulate chromatin structure in order to repair DNA damage (551), this suggests that the overactivation of PARPs might result in NAD^+ depletion in COPD. Recent studies have shown that DNA-damage-dependent PARP overactivation contributes to increased inflammation and oxidative stress. in COPD (329, 552). Studies have also shown that reduced deacetylation in COPD patients accounts for amplified inflammation leading to COPD exacerbations (553, 554). Therefore, reduction or inhibition of the overactivation of PARPs is crucial to stop the damage or delay the progression of COPD.

The therapeutic interventions, NR and PT in the CS-induced COPD model reduced inflammatory cell infiltration in the BAL, leading to improvements in lung structure and function as listed below in table 7.1. This was an important finding given that currently there are no known dietary interventions that protect from COPD features. In addition, studies have shown that NRPT reduced hepatic inflammation in non-alcoholic fatty liver disease (NAFLD) patients via increasing NAD^+ in the blood (555). Similarly, the administration of NR and PT increased the total NAD^+ levels and reduced NADH levels in our COPD mouse model. Critically, the administration of NR and PT improved the ratio of NAD^+/NADH, consequently reducing the overactivation of PARPs and leading to an increase in SIRTs. These events potentially lead to a reduction of inflammation subsequently leading to protection from damage to lung structure and function in COPD. Moreover, NR and PT further improved the structure and function of mitochondria via

increased oxphos proteins and increased mitochondria membrane potential. These events subsequently lead to reduced oxidative stress in COPD which further reduced inflammation and COPD exacerbations. In conclusion, our findings from chapter 3 indicate that NR and PT have significant potential as therapeutics for COPD.

Table 7.1: Benefits of NR and/or PT in COPD

NAD^+ modulators	NR	PT	NRPT
COPD features			
Airway inflammation	Reduced	Reduced	Reduced
Airway remodelling	Reduced	Reduced	Reduced
Emphysema	Reduced	Reduced	Reduced
Impaired lung function	Reduced IC, Area, and TLC	Reduced IC and Area	Reduced IC, Area, and TLC
NAD^+ biosynthesis and consumption			
Total NAD^+ levels	Increased	Increased	Increased
Total NADH levels	Reduced	Reduced	Reduced
Ratio of NAD^+/NADH levels	Increased	Increased	Increased
PARP activity	Reduced	Reduced	Reduced
Mitochondrial structure and function			
Mitochondrial structure			
Mitochondrial density	Reduced	No change	Reduced
Mitochondrial area (swelling)	Reduced	Reduced	Reduced
Cristae density	Increased	Increased	Increased
Cristae volume	Increased	Increased	Increased
Cristae area	Increased	Increased	Increased
Mitochondria membrane potential	Increased	Increased	Increased
Relative protein levels for ETC complexes:			
Complex I-NDUFB8	Increased	Increased	Increased
Complex II-SDHB	No change	No change	Increased
Complex III-UQCRC2	Increased	No change	Increased
Complex IV-MTCO1	Increased	Increased	Increased
Complex V-ATP5A	Increased	Increased	Increased
Oxidative stress	Reduced	Reduced	Reduced

7.2.3 Implications of NR and PT in advanced COPD stages

Modulation of NAD^+ levels with NR and PT proved to be beneficial in reducing COPD features as mentioned in chapter 3. As such, we next wanted to explore the therapeutic potential of NR and PT in delaying the progression of COPD as well as reversing the damage in the advanced stages of COPD. Using our 12-week therapeutic COPD model with NR and PT with or without cessation of smoke, we have demonstrated that administration of NR and PT during the COPD progression phase between 8-12 weeks of smoke exposure resulted in suppressed cellular infiltration in the BAL and reduced airway inflammation. Furthermore, administration of NR and PT during the COPD progression phase improved lung structure by reducing airway remodelling and emphysema and restored impaired lung function as listed below in table 7.2. We have also demonstrated that the administration of NR and PT increased total NAD^+ levels and exhibited numerous benefits in restoring mitochondrial impairment as listed below in table 7.2. In addition, we observed a reduction in PARP activity levels and an increase in SIRTs which contributed to reduced oxidative stress and improvement in mitochondrial structure and function.

Further, using our 12-week prophylactic COPD study with NR and PT, we have highlighted the benefits of reducing airway inflammation, and improving the severity of airway remodelling and emphysema as listed below in table 7.2. Interestingly, we observed stark differences in the efficacy of NR and PT to prevent the development and progression of COPD, relative to the length of treatment administration. While we identified that NR and PT were able to improve COPD progression and increase NAD^+ levels during the 8-week model, we found that administration of NR and PT throughout a 12-week model led to no improvements in COPD hallmark features or increases in

NAD^+ levels/PARP consumer activity. Studies have demonstrated that excess NAD^+ can potentially contribute to senescence-associated secretory phenotype (SASP) (556, 557), which drives chronic inflammation and DNA damage in COPD-derived fibroblasts (558, 559). This supports our evidence of no change in PARP activity suggesting DNA damage, however, future studies will be required to validate DNA damage and its effect on PARylation in COPD. Mitochondrial dysfunction in COPD patients is characterised by reduced enzyme activities (172, 395), resulting in loss of oxidative capacity (560, 561), and increased T-cell apoptosis caused due to abnormalities in mitochondrial morphology (562, 563) such as swelling (564, 565). These events further lead to increased exacerbations in COPD patients (566, 567). Additionally, we have shown a reduction in oxidative stress in the 12-week prophylactic COPD study with NR and PT which potentially improved the mitochondrial structure. As a consequence, we observed an increase in mitochondria membrane potential and increased expression of oxphos proteins.

Additionally, we have also shown that cessation of smoke was able to reduce airway inflammation and oxidative stress as well as increase citrate synthase activity and mitochondria membrane potential. However, damage to the lung structure and impaired lung function persisted with the cessation of smoke as listed below in table 7.2. This was to be expected given that CS exposure instigates the constant release of pro-inflammatory cytokines (155, 568) which leads to increased cellular infiltration in the lung (569, 570). Therefore, upon cessation of smoking, we observed a reduction in airway inflammation. CS is a form of exogenous ROS (571, 572) which leads to oxidative stress and the generation of mtROS (170, 571, 573). Henceforth, cessation of smoke was capable of reducing oxidative stress. Additionally, an increase in citrate synthase could potentially be due to an increase in mitochondrial swelling as citrate synthase is a mitochondrial

matrix protein that increases due to chronic exposure to CS in COPD (574, 575). Previous studies have shown the cessation of smoking not only delayed the progression of COPD but also reduced the risk of hospitalisation and mortality (576-578). Furthermore, the damage caused due to CS exposure in COPD is capable of inducing mitochondrial abnormalities leading to mitophagy which is an irreversible process (579-581). This supports our findings of minimal improvement in the mitochondrial structure and function with cessation of smoke, suggesting that additional treatments are required upon smoke cessation to reverse the damage in COPD.

Table 7.2: Therapeutic implications of NR and PT in advanced stages of COPD

Therapeutic implications of NR and PT in COPD				
Experimental groups	8wks smoke + 4wks rest	8wks smoke + 4wks rest+ 4wks NRPT	12wks smoke+ 12wks NRPT	12wks smoke+ 4wks NRPT
COPD features				
Airway inflammation	Reduced	Reduced	Reduced	Reduced
Airway remodelling	No change	Reduced	Reduced	Reduced
Emphysema	No change	Reduced	Reduced	Reduced
Impaired lung function	No change	Reduced IC and Area	No change	Reduced IC and TLC
NAD^+ biosynthesis and consumption				
Total NAD^+ levels	Increased	Increased	No change	Increased
Total NADH levels	Reduced	Reduced	Reduced	Reduced
Ratio of NAD^+/NADH levels	No change	Increased	No change	Increased
PARP activity	Reduced	Reduced	No change	Reduced
Mitochondrial structure and function				
Mitochondrial structure				
Mitochondrial density	Reduced	Reduced	Reduced	Reduced
Mitochondrial area (swelling)	No change	No change	Reduced	Reduced
Cristae density	No change	Increased	Increased	Increased
Cristae volume	No change	No change	Increased	Increased
Cristae area	No change	No change	No change	No change

Mitochondria membrane potential	Increased	Increased	Increased	Increased
Relative protein levels for ETC complexes:				
Complex I-NDUFB8	No change	Increased	Increased	Increased
Complex II-SDHB	No change	Increased	Increased	No change
Complex III-UQCRC2	No change	Increased	No change	Increased
Complex IV-MTCO1	No change	Increased	Increased	Increased
Complex V-ATP5A	No change	Increased	Increased	Increased
Oxidative stress	No change	Reduced	Reduced	Reduced

7.2.4 Therapeutic targeting of NAD^+ compartmentalisation in COPD

Intracellular NAD^+ levels depend on a diverse range of physiological stimuli such as energy stressors (582, 583), glucose deprivation (584, 585), and fluctuations in the circadian cycle (586). The presence of three different isomers of NMNATs (224, 587) including NMNAT1 in the nucleus (415, 588), NMNAT2 in the cytosol (417, 418) and NMNAT3 in the mitochondria (458, 589), are involved in salvaging NAD^+ from NMN (411, 590). NAD^+ degrading enzymes such as PARPs and SIRTs are also present in these compartments (591, 592), which suggests that NAD^+ salvage is tailored according to compartment-specific needs (593, 594). Recent studies have highlighted the importance of targeting NMNATs in modulating NAD^+ homeostasis in research areas of cancer (264), diabetes (225), aging (400, 519) and COPD (595). NMNATs have been shown to modulate the deacetylation activity of SIRT1 in COPD (536, 595). However, as NAD^+ metabolism is a novel research avenue for therapeutic interventions in COPD, the role of NMNATs in COPD remains unexplored. Therefore, we investigated the role of NMNATs in COPD by utilising overexpressing NMNAT1 and NMNAT3 transgenic mice.

Our findings in chapter 3 demonstrated that an imbalance in NAD^+ homeostasis is a potential contributing factor driving the progression of COPD. Moreover, upon therapeutic targeting of NAD^+ homeostasis with NR and PT, we observed benefits in

COPD features as listed above in tables 7.1 and 7.2. Additionally, we identified increased gene expression of NMNAT1, NMNAT2 and NMNAT3 upon administration of NR and PT in our COPD study. Henceforth, we sought to decipher the role of NMNATs in COPD progression by using transgenic overexpressing NMNAT1 and NMNAT3 mice to further unravel the mechanisms of restoration of NAD^+ balance in COPD.

We demonstrated in chapter 5 that overexpression of NMNAT1 and NMNAT3 in COPD reduced cellular infiltrates in the BAL, thereby exhibiting reduced airway inflammation. Additionally, NMNAT1 and NMNAT3 overexpression protected lung structure in COPD via protecting against airway remodelling and emphysema as mentioned below in table 7.3. Furthermore, we observed partial protection from impaired lung function. In addition, we have also demonstrated that overexpression of NMNAT1 and NMNAT3 exhibited a reduction in PARP hyperactivity and regulation of SIRTs, therefore reducing oxidative stress and increasing mitochondria membrane potential in COPD. Studies have shown that NMNAT1 modulates mitochondrial oxstress by inhibiting caspase-3 signalling in Alzheimer's disease (476). It has also been highlighted that NMNAT3 improves mitochondrial function by reducing oxstress by improving NAD^+ levels and promoting SIRT3 expression (467). Therefore, it is possible that NMNAT1 and NMNAT3 overexpression was protective against mitochondrial dysfunction in COPD, which further reduced oxidative stress, increased $\Delta\Psi m$ and reduced subsequent damage during the disease pathogenesis exhibiting protection against the disease features.

The overexpression of NMNAT1 did not increase total NAD^+ but reduced NADH levels in COPD. However, we did not observe a change in the ratio of total NAD^+/NADH with NMNAT1 overexpression. This was intriguing as it is well known that NMNAT1 is crucial for maintaining nuclear NAD^+ levels (596) however, NMNAT1 does not change NAD^+ biosynthesis but protects from SARM1-mediated NAD^+ depletion in axon

degeneration (597). Henceforth, it is plausible that the overexpression of NMNAT1 in COPD did not increase NAD^+ biosynthesis but prevented NAD^+ depletion by regulating its consumption. In contrast, the overexpression of NMNAT3 showed an increase in the total NAD^+ levels as well as a reduction in the NADH level in COPD. This suggests that overexpression of mitochondrial NMNAT3 might directly contribute to NAD^+ biosynthesis in COPD, which further promotes an increase in mitochondrial respiration and reduction in mtROS as previously stated in aging studies (598).

Table 7.3: Elucidating the role of overexpressed NMNAT1 and NMNAT3 in COPD

Experimental groups	**NMNAT1**	**NMNAT3**
COPD features		
Airway inflammation	Reduced	Reduced
Airway remodelling	Reduced	Reduced
Emphysema	Reduced	Reduced
Impaired lung function	Reduced RV	Reduced FRC and VC
NAD^+ biosynthesis and consumption		
Total NAD^+ levels	No change	Increased
Total NADH levels	Reduced	No change
Ratio of NAD^+/NADH levels	No change	No change
PARP activity	Reduced	Reduced
Mitochondrial membrane potential and Oxstress		
Mitochondria membrane potential	Increased	Increased
Oxidative stress	Reduced	Reduced

7.2.5 Implications of NR and PT in transgenically overexpressed NMNAT1 and NMNAT3 in COPD

We have demonstrated in chapter 5 that NMNATs are functionally involved in increasing NAD^+ levels upon the treatment of NR and PT in COPD. Henceforth, to understand if the

administration of NR and PT in overexpressed NMNAT1 and NMNAT3 mice can further boost NAD^+ levels and if that can provide additional benefits in COPD. The overexpression of NMNAT1 and NMNAT3 has exhibited protection against airway inflammation, airway remodelling and emphysema in COPD. Additionally, we also observed partial protection against impaired lung function. Transgenically overexpressed NMNAT1 and NMNAT3 mice are known to have increased NAD^+ levels (435), and as such administration of NR and PT to these mice enabled us to induce an additional boost to the NAD^+ levels. This was to further decipher whether the benefits previously observed with overexpression of NMNAT1 and NMNAT3 are solely due to the restoration of NAD^+ or due to off-target effects.

Our findings in chapter 5 demonstrated that administration of NR and PT to the overexpressed NMNAT1 and NMNAT3 mice exhibited numerous benefits in COPD such as reducing inflammation, protection from airway remodelling and emphysema as listed below in table 7.4. Additionally, we observed a reduction in PARP hyperactivity and oxidative stress upon administration of NR and PT in NMNAT1 and NMNAT3 overexpressed mice in COPD which was previously observed with the overexpression on its own. These findings indicated that NR and PT treatment in NMNAT1 and NMNAT3 overexpression had no additional benefit in COPD.

Future studies will be conducted to understand the underlying mechanisms as currently there is limited knowledge on the effects of NR and PT in NMNAT1 and NMNAT3 overexpression.

We have demonstrated that NR and PT treatment in overexpressing NMNAT1 and NMNAT3 mice worsened impaired lung function parameters. These findings suggested possible negative effects of elevated NAD+ synthesising enzymes. Studies have

suggested that high levels of NAM have shown adverse effects on multiple scenarios such as inhibition of PARPs and compromising genome integrity (225). Additionally, NAM alters cellular methyl metabolism and further affects DNA methylation (599), followed by alterations in the cellular transcriptome (600) and proteomes (601) which contribute to the development and progression of chronic diseases. In this context, these findings are in line with the literature and suggest a mechanism by which NR and PT treatment worsened lung function parameters in NMNAT1 and NMNAT3 overexpressing mice.

Table 7.4: Implications of NR and PT on overexpressed NMNAT1 and NMNAT3 mice in COPD

Experimental groups	NMNAT1+NRPT	NMNAT3+NRPT
COPD features		
Airway inflammation	Reduced	Reduced
Airway remodelling	Reduced	Reduced
Emphysema	Reduced	Reduced
Impaired lung function	Increased IC, A, FVC, VC, FRC	Increased Rn, Rrs
NAD^+ biosynthesis and consumption		
Total NAD^+ levels	Reduced	No change
Total NADH levels	No change	Reduced
Ratio of NAD^+/NADH levels	Reduced	Increased
PARP activity	Reduced	Reduced
Mitochondrial membrane potential and Oxstress		
Mitochondria membrane potential	Increased	Increased
Oxidative stress	Reduced	Reduced

7.2.6 Impairment of PKM2 in COPD

Recent studies have highlighted that cellular bioenergetic pathways play an important role in maintaining cellular function which involves metabolic homeostasis (602), metabolic reprogramming (603) and immune cell activation (604). All of these cellular processes are known to contribute to the pathogenesis of COPD (605), however, the role of metabolic reprogramming and its underlying mechanisms are not fully understood. Studies have shown metabolic marker PKM2 plays an important role in catalysing the last step in the glycolysis pathway which subsequently leads to the production of ATP (606). However, in COPD patients increased glucose production has been noted with faster glucose metabolism via glycolysis suggesting the shift in metabolism may be a contributing factor in COPD pathogenesis (607, 608). In chapter 6, we investigated the role of PKM2 in contributing to impaired metabolism during the progression of COPD. The findings from our study have demonstrated that chronic exposure to CS leads to reduced PKM2 levels which drive impaired immunometabolism in COPD leading to important pathophysiological features of COPD. Studies have shown that PKM2 regulated CS-induced airway inflammation via modulating mitophagy (609), therefore, metabolic dysregulation driven by PKM2 has been a recent focus to develop novel therapeutics for COPD (610). Our study showed a reduction of mitochondria membrane potential and mitochondrial biogenesis further reflecting the impaired process of the ETC and oxphos resulting in depletion of ATP in COPD. This is not surprising as mitochondrial abnormalities have been previously exhibited in COPD patients (172, 611, 612). In addition, it is also known that PKM2 coordinates glycolysis along with mitochondrial fusion which further promotes oxidative phosphorylation (613). Interestingly, our findings have validated the involvement of PKM2 in the pathogenesis

of COPD for the very first time. Therefore, targeting PKM2 in COPD might potentially show benefits from COPD features.

7.2.7 Targeting impaired PKM2 using TEPP46 in COPD

Currently, it is unclear if pharmacologically modulating glucose metabolism would be beneficial in COPD. The first human trial studies of mitochondria-targeted immunomodulator dichloroacetate improved pulmonary arterial hypertension in genetically susceptible patients by inhibiting pyruvate dehydrogenase kinase (614, 615). In addition, enhanced fatty acid oxidation is beneficial in patients with asthma and bronchopulmonary dysplasia (BPD) (616, 617). In our study, we demonstrated a reduction in PKM2 resulted in the reduction of PK and PDH activity as well as HIF1α in COPD indicating reduced metabolism. Furthermore, low levels of PKM2 also contributed to increased oxidative stress and inflammation in COPD causing subsequent damage to the lung structure and function during the pathogenesis of the disease. Therefore, therapeutic targeting of metabolic enzymes like PK via PKM2 has the potential to reduce metabolic abnormalities in chronic lung diseases (612, 618, 619).

We sought to target PKM2 in COPD using TEPP46; a pharmacologically derived small molecule activator (480). TEPP46 has previously been shown to suppress kidney fibrosis (271) and attenuate thoracic aortic aneurysms (167). Similarly, we have shown that administration of TEPP46 exhibited improvements in airway inflammation, airway remodelling and emphysema in COPD as listed below in table 7.5. Although we did not observe a difference in most lung function parameters with TEPP46 treatment, there was a shift in the lung compliance curve indicating improved expandability of the lung. This evidence suggested that TEPP46 treatment protected from damage to the lung structure

and partially protected from impaired lung function in COPD. Furthermore, TEPP46 increased the tetramerisation of PKM2 as measured by increased PK activity, and also increased PKM2 and HIF1α expression in COPD. This is not surprising as TEPP46 has been previously shown to promote tetramerisation of PKM2 in tumour cells (620) which then regulates HIF1α (172, 621). Interestingly, we observed a similar result in COPD with TEPP46 treatment. However, since it is known that mitochondrial dysfunction drives oxidative stress and inflammation leading to COPD exacerbations (622), TEPP46 treatment increases PKM2 levels in COPD and thereby protects against mitochondrial dysfunction and subsequent damage. These findings will be further investigated to elucidate the therapeutic implications of TEPP46 in reversing or delaying the progression of the COPD in advanced stages of the disease.

Table 7.5: Therapeutic potential of immunomodulator TEPP46 in COPD

Immunomodulator	TEPP46
COPD features	
Airway inflammation	Reduced
Airway remodelling	Reduced
Emphysema	Reduced
Impaired lung function	No change
Metabolism in immune cells	
PK activity	Increased
PDH activity	Increased
PKM2 **HIF1α**	Increased Increased
NAD^+ biosynthesis	
Total NAD^+ levels	Increased
Total NADH levels	No change
Ratio of NAD^+/NADH levels	Increased
Mitochondrial structure and function	
Mitochondrial structure	
Mitochondrial density **Mitochondrial area (swelling)**	No change Reduced

Mitochondria membrane potential	Increased
Relative protein levels for ETC complexes:	
Complex I-NDUFB8	Increased
Complex II-SDHB	No change
Complex III-UQCRC2	Increased
Complex IV-MTCO1	Increased
Complex V-ATP5A	Increased
Oxidative stress	Reduced

7.3 Conclusion

Chronic exposure to CS in COPD leads to the activation of immune cells (623) via induction of pro-inflammatory cytokines such as TNFα and IL-1β (624) leading to an accumulation of inflammatory cells in the lungs (625) (Figure 7.1). Activation of immune cells is followed by several functional changes such as cytokine production, proliferation and chemotaxis during the progression of COPD, which are known contributing factors driving COPD pathogenesis (39, 626). These functional changes demand metabolic adaptions to maintain adequate ATP levels for host defence mechanisms (626, 627). The energy demands are met by interconnected metabolic pathways of mitochondria which includes glycolysis (628), Krebs cycle (629) and oxphos (630). Recent evidence has shown that cellular metabolism directly regulates immune cell functions (630, 631). Thus, immune cells upon activation undergo a shift from maintaining a basal metabolic state to an accelerated metabolic state which promotes key effector functions such as glycolysis (632, 633). An increase in glycolysis results in an increased NADH level (634) which is then decomposed to NAD^+ during the Krebs cycle (635). However, the shift in immune cell metabolism inhibits the Krebs cycle and reduces oxphos leading to ATP depletion (636, 637) (Figure 7.1). Increased accumulation of NADH in the cell leads to an imbalance in the redox reaction further contributing to oxstress (541, 638) and increased inflammation leading to impaired activity of SIRTs (541, 639). SIRTs are known to play

an important role during the pathogenesis of COPD and are majorly involved in reducing inflammation, apoptosis, mitochondrial oxidative stress, anti-oxidant response etc (248, 640). SIRTs are solely dependent on NAD^+ as a co-factor for their function, while depletion of NAD^+ leads to impaired sirtuin activity causing enhanced DNA damage in COPD (641, 642). This is further followed by the activation of PARPs to repair DNA damage in COPD (643, 644). All of these events contribute to the burden of endogenous oxidative stress causing accelerated COPD exacerbations (174, 309, 645) (Figure 7.1).

To summarise the findings of this thesis, we have highlighted that impaired NAD^+ metabolism potentially drives a metabolic shift in immune cells during the development and progression of COPD. We have further demonstrated that targeting impaired NAD^+ levels not only protected from pulmonary damage induced by CS but also restored lung structure and function in COPD. We have highlighted that the overactivation of PARPs consumes NAD^+ levels in COPD leading to the imbalance in NAD^+/NADH levels. The imbalance in NAD^+ pools reduced SIRTs levels further leading to sustained inflammation during the induction and progression of the disease. We have demonstrated that targeting the redox imbalance of NAD^+/NADH with NR and PT has therapeutic benefits in COPD. The administration of NR and PT protected from airway inflammation, airway remodelling, emphysema and impaired lung function in COPD. Additionally, the administration of NR and PT increased the ratios of NAD^+/NADH in COPD, further reducing the overactivation of PARPs and increasing SIRTs (Figure 7.1). NR and PT also protected mitochondrial structure and function resulting in the reduction of oxidative stress which further contributed to delayed progression and reversing the damage in COPD (Figure 7.1). We determined that chronic exposure to CS reduced PKM2 protein levels, which further lead to a reduction in PK activity and HIF1α protein expression. This indicated reduced metabolism in the lungs in COPD. Based on these findings, we

further identified that targeting PKM2, with TEPP46 to restore impaired metabolism had therapeutic benefits in COPD. We have demonstrated that administration of TEPP46 reduced airway inflammation leading to a reduction in airway remodelling and emphysema. In addition, TEPP46 administration also displayed partial protection from impaired lung function in COPD. Critically, TEPP46 promoted tetramerisation of PKM2 which further increased oxphos and reduced oxidative stress, exhibiting protective features on mitochondrial structure and function in COPD (Figure 7.1).

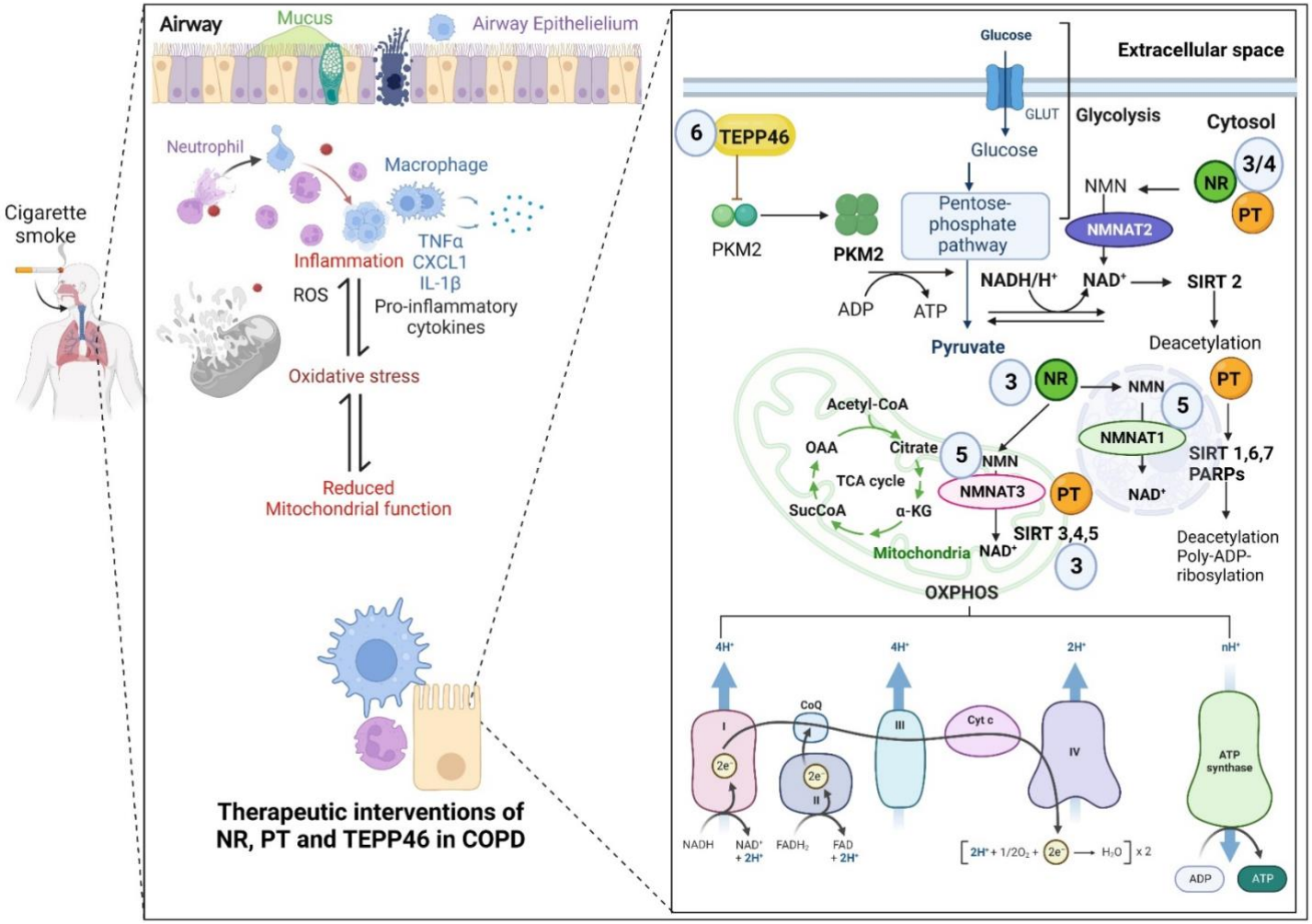

Figure 7.1: Therapeutic intervention of NR, PT and TEPP46 in COPD:

Chronic exposure to CS is a form of exogenous ROS in COPD and can initiate oxidative stress which induces airway inflammation. As a consequence, leads to the release of endogenous ROS from inflammatory cells such as macrophages and neutrophils as well as mtROS via disruption in ETC during oxphos. This further leads to altered cellular metabolism and cell death via apoptosis causing increased COPD exacerbations. Chapters 3, 4, and 5- NR is a precursor of NAD^+ and can synthesise NAD^+ via the salvage pathway i.e. by NMNATs thereby increasing NAD^+ synthesis. Whereas PT activates SIRTs for enhanced consumption of NAD^+ and this further regulates the NAD^+ pool which is essential for maintaining cellular energy, homeostasis, survival, and proliferation. Chapter 6- Additionally, TEPP46 binds to PKM2 dimers inducing the formation of PKM2 tetramer and promoting the rate-limiting step of glycolysis and pyruvate production. Pyruvate enters the TCA cycle and stimulates the oxphos leading to a reduction in ROS production further reducing inflammation and COPD features.

7.4 Future directions

This thesis has focused on targeting various pathways of NAD^+ biosynthesis and glucose metabolism pathways which lead to mitochondrial dysfunction causing impaired immunometabolism in COPD. The use of NR, PT and TEPP46 in our CS-induced experimental COPD mouse model has been shown in this thesis to modulate NAD^+ levels and PKM2 levels to further improve mitochondrial structure and function, therefore reducing COPD features.

Importantly, further studies will be required for the identification of specific alterations of NAD^+ modulators like NMN and NAM, as well as NAD^+ consumers like PARPs, SIRTs and CD38 in COPD. Additional investigation will be required to validate if the

administration of NR and PT can protect or inhibit alterations of NAD^+ modulators and consumers in COPD. These findings would help to understand the modulation of NAD^+ metabolism in COPD and will lead to a further understanding of disease pathogenesis.

Simultaneously, our study has also demonstrated that inhibition of the overactivation of PARPs in COPD could be a potential therapeutic target. Future studies will be conducted using Olaparib, a commercially available PARP inhibitor (379, 646-648), in our clinically relevant CS-induced COPD mouse model. We have previously demonstrated that NR and PT reduced the overactivation of PARPs in COPD, and therefore we will evaluate the therapeutic benefits of NR and PT in combination with Olaparib in COPD. This is to validate if NR and PT are capable of inhibiting the overactivation of PARPs in COPD in order to exert benefits in the disease features.

Further, we have demonstrated the benefits of TEPP46 using a prophylactic COPD model. Therefore it is important to study the implications of TEPP46 in a therapeutic COPD model to further elucidate if TEPP46 can halt the progression or reverse the disease features in advanced stages of COPD when delivered during the late stages of disease progression, or upon smoke cessation.

Finally, studies will be conducted to investigate the pre-clinical potential of NR, PT and TEPP46 using human COPD clinical specimens such as bronchial epithelial cells obtained via bronchoscopy and macrophages obtained via BAL of COPD patients. This will ultimately demonstrate the clinical translation of NAD^+-modulating drugs for the treatment of COPD in human patients.

7.5 References

1. Hogg JC. Pathophysiology of airflow limitation in chronic obstructive pulmonary disease. The Lancet. 2004;364(9435):709-21.
2. Petty TL, Silvers GW, Stanford RE. Mild emphysema is associated with reduced elastic recoil and increased lung size but not with air-flow limitation. Am Rev Respir Dis. 1987;136(4):867-71.
3. Hasegawa M, Nasuhara Y, Onodera Y, Makita H, Nagai K, Fuke S, et al. Airflow limitation and airway dimensions in chronic obstructive pulmonary disease. American journal of respiratory and critical care medicine. 2006;173(12):1309-15.
4. Miravitlles M, Ribera A. Understanding the impact of symptoms on the burden of COPD. Respiratory research. 2017;18(1):1-11.
5. Pauwels RA, Rabe KF. Burden and clinical features of chronic obstructive pulmonary disease (COPD). The Lancet. 2004;364(9434):613-20.
6. Sasaki M, Chubachi S, Kameyama N, Sato M, Haraguchi M, Miyazaki M, et al. Effects of long-term cigarette smoke exposure on bone metabolism, structure, and quality in a mouse model of emphysema. PLoS One. 2018;13(1):e0191611.
7. Schikowski T, Mills IC, Anderson HR, Cohen A, Hansell A, Kauffmann F, et al. Ambient air pollution: a cause of COPD? European Respiratory Journal. 2014;43(1):250-63.
8. Boschetto P, Quintavalle S, Miotto D, Lo Cascio N, Zeni E, Mapp CE. Chronic obstructive pulmonary disease (COPD) and occupational exposures. Journal of Occupational Medicine and Toxicology. 2006;1(1):1-6.
9. Girod CE, King Jr TE. COPD: a dust-induced disease? Chest. 2005;128(4):3055-64.
10. Bergdahl I, Toren K, Eriksson K, Hedlund U, Nilsson T, Flodin R, et al. Increased mortality in COPD among construction workers exposed to inorganic dust. European Respiratory Journal. 2004;23(3):402-6.
11. Yamamoto C, Yoneda T, Yoshikawa M, Fu A, Tokayama T, Tsukaguchi K, et al. Airway inflammation in copd assessed by sputum levels of lnterleukin-8. Chest. 1997;112(2):505-10.
12. Kim V, Criner GJ. The chronic bronchitis phenotype in COPD: features and implications. Current opinion in pulmonary medicine. 2015;21(2):133.
13. Santos S, Peinado VI, Ramirez J, Melgosa T, Roca J, Rodriguez-Roisin R, et al. Characterization of pulmonary vascular remodelling in smokers and patients with mild COPD. European Respiratory Journal. 2002;19(4):632-8.
14. Chilosi M, Carloni A, Rossi A, Poletti V. Premature lung aging and cellular senescence in the pathogenesis of idiopathic pulmonary fibrosis and COPD/emphysema. Translational Research. 2013;162(3):156-73.
15. Cerveri I, Brusasco V. Revisited role for mucus hypersecretion in the pathogenesis of COPD. European Respiratory Review. 2010;19(116):109-12.
16. Hirota N, Martin JG. Mechanisms of airway remodeling. Chest. 2013;144(3):1026-32.
17. Voelkel NF, Gomez-Arroyo J, Mizuno S. COPD/emphysema: the vascular story. Pulmonary circulation. 2011;1(3):320-6.
18. André S, Conde B, Fragoso E, Boléo-Tomé J, Areias V, Cardoso J. COPD and cardiovascular disease. Pulmonology. 2019;25(3):168-76.
19. Brooke M. COPD and its management in Australia. Journal of the Australasian Rehabilitation Nurses Association. 2013;16(2):8-12.

20. Donohue JF. Therapeutic responses in asthma and COPD: bronchodilators. Chest. 2004;126(2):125S-37S.
21. Branson RD. Oxygen therapy in COPD. Respiratory care. 2018;63(6):734-48.
22. Cassivi SD, Meyers BF, Battafarano RJ, Guthrie TJ, Trulock EP, Lynch JP, et al. Thirteen-year experience in lung transplantation for emphysema. The Annals of thoracic surgery. 2002;74(5):1663-70.
23. Berry CE, Wise RA. Mortality in COPD: causes, risk factors, and prevention. COPD: Journal of Chronic Obstructive Pulmonary Disease. 2010;7(5):375-82.
24. Marchetti N, Criner GJ, editors. Surgical approaches to treating emphysema: lung volume reduction surgery, bullectomy, and lung transplantation. Seminars in respiratory and critical care medicine; 2015: Thieme Medical Publishers.
25. Motz GT, Eppert BL, Wortham BW, Amos-Kroohs RM, Flury JL, Wesselkamper SC, et al. Chronic cigarette smoke exposure primes NK cell activation in a mouse model of chronic obstructive pulmonary disease. The Journal of Immunology. 2010;184(8):4460-9.
26. Roth M. Pathogenesis of COPD. Part III. Inflammation in COPD [State of the Art Series. Chronic obstructive pulmonary disease in high-and low-income countries. Edited by G. Marks and M. Chan-Yeung. Number 3 in the series]. The International Journal of Tuberculosis and Lung Disease. 2008;12(4):375-80.
27. Çolak Y, Afzal S, Nordestgaard BG, Vestbo J, Lange P. Prognosis of asymptomatic and symptomatic, undiagnosed COPD in the general population in Denmark: a prospective cohort study. The Lancet Respiratory Medicine. 2017;5(5):426-34.
28. Calverley PM. The GOLD classification has advanced understanding of COPD. American journal of respiratory and critical care medicine. 2004;170(3):211-2.
29. Huijsmans RJ, de Haan A, ten Hacken NN, Straver RV, van't Hul AJ. The clinical utility of the GOLD classification of COPD disease severity in pulmonary rehabilitation. Respiratory medicine. 2008;102(1):162-71.
30. Mittal R, Chhabra SK. GOLD classification of COPD: discordance in criteria for symptoms and exacerbation risk assessment. COPD: Journal of Chronic Obstructive Pulmonary Disease. 2017;14(1):1-6.
31. Casanova C, Marin JM, Martinez-Gonzalez C, de Lucas-Ramos P, Mir-Viladrich I, Cosio B, et al. New GOLD classification: longitudinal data on group assignment. Respiratory research. 2014;15(1):1-9.
32. Golpe R, Figueira-GonÇalves JM, Amado CA, Martín-Audera P, Esteban C, García-Talavera I, et al. A new, three-dimensional approach to the GOLD COPD assessment tool. Respiratory Medicine and Research. 2022;81:100879.
33. Köhler D, Fischer J, Raschke F, Schönhofer B. Usefulness of GOLD classification of COPD severity. Thorax. 2003;58(9):825-.
34. Arkhipov V, Arkhipova D, Miravitlles M, Lazarev A, Stukalina E. Characteristics of COPD patients according to GOLD classification and clinical phenotypes in the Russian Federation: the SUPPORT trial. International journal of chronic obstructive pulmonary disease. 2017;12:3255.
35. Sohn K-H. Asthma-COPD Overlap in Two Comprehensive Cohorts in Korea: Time to Move to Treatable Traits. Journal of Korean Medical Science. 2022;37(30).
36. Takasugi JE, Godwin JD. Radiology of chronic obstructive pulmonary disease. Radiologic Clinics of North America. 1998;36(1):29-55.
37. Jarhyan P, Hutchinson A, Khaw D, Prabhakaran D, Mohan S. Prevalence of chronic obstructive pulmonary disease and chronic bronchitis in eight countries: a

systematic review and meta-analysis. Bulletin of the World Health Organization. 2022;100(3):216.
38. Mitzner W. Emphysema: a disease of small airways or lung parenchyma? The New England journal of medicine. 2011;365(17):1637.
39. Cosio MG, Majo J, Cosio MG. Inflammation of the airways and lung parenchyma in COPD: role of T cells. Chest. 2002;121(5):160S-5S.
40. Ingenito EP, Tsai LW, Majumdar A, Suki B. On the role of surface tension in the pathophysiology of emphysema. American journal of respiratory and critical care medicine. 2005;171(4):300-4.
41. Mostaço-Guidolin L, Rosin NL, Hackett T-L. Imaging collagen in scar tissue: developments in second harmonic generation microscopy for biomedical applications. International journal of molecular sciences. 2017;18(8):1772.
42. Martín Mosquero C, Peces-Barba G, Rubio M, Ortega M, Rodriguez-Nieto M, Martinez Galan L, et al. Increased collagen deposition correlated with lung destruction in human emphysema. Histology and histopathology. 2006.
43. Rogers DF, editor Mucus hypersecretion in chronic obstructive pulmonary disease. Chronic Obstructive Pulmonary Disease: Pathogenesis to Treatment: Novartis Foundation Symposium 234; 2000: Wiley Online Library.
44. Gladysheva ES, Malhotra A, Owens RL. Influencing the decline of lung function in COPD: use of pharmacotherapy. International journal of chronic obstructive pulmonary disease. 2010;5:153.
45. Ferguson GT. Why does the lung hyperinflate? Proceedings of the American Thoracic Society. 2006;3(2):176-9.
46. Pellegrino R, Sterk P, Sont J, Brusasco V. Assessing the effect of deep inhalation on airway calibre: a novel approach to lung function in bronchial asthma and COPD. European Respiratory Journal. 1998;12(5):1219-27.
47. Bui DS, Perret JL, Walters EH, Lodge CJ, Bowatte G, Hamilton GS, et al. Association between very to moderate preterm births, lung function deficits, and COPD at age 53 years: analysis of a prospective cohort study. The Lancet Respiratory Medicine. 2022;10(5):478-84.
48. Parekh TM, Helgeson ES, Connett J, Voelker H, Ling SX, Lazarus SC, et al. Lung Function and the Risk of Exacerbation in the BLOCK COPD Trial. Annals of the American Thoracic Society. 2022(ja).
49. Rennard SI. Inflammation and repair processes in chronic obstructive pulmonary disease. American journal of respiratory and critical care medicine. 1999;160(supplement_1):S12-S6.
50. Xu F, Vasilescu DM, Kinose D, Tanabe N, Ng KW, Coxson HO, et al. The molecular and cellular mechanisms associated with the destruction of terminal bronchioles in COPD. European Respiratory Journal. 2022;59(5).
51. Dey S, Eapen MS, Chia C, Gaikwad AV, Wark PA, Sohal SS. Pathogenesis, clinical features of asthma COPD overlap, and therapeutic modalities. American Journal of Physiology-Lung Cellular and Molecular Physiology. 2022;322(1):L64-L83.
52. Rajabi H, Konyalilar N, Erkan S, Mortazavi D, Korkunc SK, Kayalar O, et al. Emerging role of exosomes in the pathology of chronic obstructive pulmonary diseases; destructive and therapeutic properties. Stem Cell Research & Therapy. 2022;13(1):1-16.
53. Dima E, Koltsida O, Katsaounou P, Vakali S, Koutsoukou A, Koulouris NG, et al. Implication of Interleukin (IL)-18 in the pathogenesis of chronic obstructive pulmonary disease (COPD). Cytokine. 2015;74(2):313-7.

54. Churg A, Wang RD, Tai H, Wang X, Xie C, Wright JL. Tumor necrosis factor-α drives 70% of cigarette smoke–induced emphysema in the mouse. American journal of respiratory and critical care medicine. 2004;170(5):492-8.
55. Profita M, Chiappara G, Mirabella F, Di Giorgi R, Chimenti L, Costanzo G, et al. Effect of cilomilast (Ariflo) on TNF-α, IL-8, and GM-CSF release by airway cells of patients with COPD. Thorax. 2003;58(7):573-9.
56. Jeffery PK. Structural and inflammatory changes in COPD: a comparison with asthma. Thorax. 1998;53(2):129.
57. Saetta M, Turato G, Maestrelli P, Mapp CE, Fabbri LM. Cellular and structural bases of chronic obstructive pulmonary disease. American journal of respiratory and critical care medicine. 2001;163(6):1304-9.
58. Bhat TA, Panzica L, Kalathil SG, Thanavala Y. Immune dysfunction in patients with chronic obstructive pulmonary disease. Annals of the American Thoracic Society. 2015;12(Supplement 2):S169-S75.
59. Aoshiba K, Tsuji T, Yamaguchi K, Itoh M, Nakamura H. The danger signal plus DNA damage two-hit hypothesis for chronic inflammation in COPD. European Respiratory Journal. 2013;42(6):1689-95.
60. Hirano T, Yamagata T, Gohda M, Yamagata Y, Ichikawa T, Yanagisawa S, et al. Inhibition of reactive nitrogen species production in COPD airways: comparison of inhaled corticosteroid and oral theophylline. Thorax. 2006;61(9):761-6.
61. Sadowska AM, Van Overveld F, Gorecka D, Zdral A, Filewska M, Demkow U, et al. The interrelationship between markers of inflammation and oxidative stress in chronic obstructive pulmonary disease: modulation by inhaled steroids and antioxidant. Respiratory medicine. 2005;99(2):241-9.
62. Adeloye D, Song P, Zhu Y, Campbell H, Sheikh A, Rudan I, et al. Global, regional, and national prevalence of, and risk factors for, chronic obstructive pulmonary disease (COPD) in 2019: a systematic review and modelling analysis. The Lancet Respiratory Medicine. 2022.
63. Yang IA, Jenkins CR, Salvi SS. Chronic obstructive pulmonary disease in never-smokers: risk factors, pathogenesis, and implications for prevention and treatment. The Lancet Respiratory Medicine. 2022.
64. Salvi S. Tobacco smoking and environmental risk factors for chronic obstructive pulmonary disease. Clinics in chest medicine. 2014;35(1):17-27.
65. Mannino DM, Buist AS. Global burden of COPD: risk factors, prevalence, and future trends. The Lancet. 2007;370(9589):765-73.
66. Pathak U, Gupta NC, Suri JC. Risk of COPD due to indoor air pollution from biomass cooking fuel: a systematic review and meta-analysis. International journal of environmental health research. 2020;30(1):75-88.
67. Cohen BH, BALL JR WC, Brashears S, Diamond EL, Kreiss P, Levy DA, et al. Risk factors in chronic obstructive pulmonary disease (COPD). American journal of epidemiology. 1977;105(3):223-32.
68. Holm KE, Borson S, Sandhaus RA, Ford DW, Strange C, Bowler RP, et al. Differences in adjustment between individuals with alpha-1 antitrypsin deficiency (AATD)-associated COPD and non-AATD COPD. COPD: Journal of Chronic Obstructive Pulmonary Disease. 2013;10(2):226-34.
69. Craig TJ, Henao MP. Advances in managing COPD related to α1-antitrypsin deficiency: An under-recognized genetic disorder. Allergy. 2018;73(11):2110-21.
70. DeMeo D, Silverman E. α1-Antitrypsin deficiency· 2: Genetic aspects of α1-antitrypsin deficiency: phenotypes and genetic modifiers of emphysema risk. Thorax. 2004;59(3):259-64.

71. Dhami R, Zay K, Gilks B, Porter S, Wright J, Churg A. Pulmonary epithelial expression of human α1-antitrypsin in transgenic mice results in delivery of α1-antitrypsin protein to the interstitium. Journal of molecular medicine. 1999;77(4):377-85.
72. Guo S, Booten SL, Watt A, Alvarado L, Freier SM, Teckman JH, et al. Using antisense technology to develop a novel therapy for α-1 antitrypsin deficient (AATD) liver disease and to model AATD lung disease. Rare Diseases. 2014;2(1):251-61.
73. Silva GE, Sherrill DL, Guerra S, Barbee RA. Asthma as a risk factor for COPD in a longitudinal study. Chest. 2004;126(1):59-65.
74. Scannapieco FA, Bush RB, Paju S. Associations between periodontal disease and risk for nosocomial bacterial pneumonia and chronic obstructive pulmonary disease. A systematic review. Annals of periodontology. 2003;8(1):54-69.
75. Maclay JD, MacNee W. Cardiovascular disease in COPD: mechanisms. Chest. 2013;143(3):798-807.
76. Shin S, King CS, Brown AW, Albano MC, Atkins M, Sheridan MJ, et al. Pulmonary artery size as a predictor of pulmonary hypertension and outcomes in patients with chronic obstructive pulmonary disease. Respiratory medicine. 2014;108(11):1626-32.
77. Wedzicha JA, Seemungal TA. COPD exacerbations: defining their cause and prevention. The lancet. 2007;370(9589):786-96.
78. Patil SP, Krishnan JA, Lechtzin N, Diette GB. In-hospital mortality following acute exacerbations of chronic obstructive pulmonary disease. Archives of internal medicine. 2003;163(10):1180-6.
79. Wedzicha JA, Donaldson GC. Exacerbations of chronic obstructive pulmonary disease. Respiratory care. 2003;48(12):1204-15.
80. Chin M, De Zoysa M, Slinger R, Gaudet E, Vandemheen KL, Chan F, et al. Acute effects of viral respiratory tract infections on sputum bacterial density during CF pulmonary exacerbations. Journal of Cystic Fibrosis. 2015;14(4):482-9.
81. Bouquet J, Tabor DE, Silver JS, Nair V, Tovchigrechko A, Griffin MP, et al. Microbial burden and viral exacerbations in a longitudinal multicenter COPD cohort. Respiratory research. 2020;21(1):1-13.
82. Sharif-Askari NS, Sharif-Askari FS, Alabed M, Temsah M-H, Al Heialy S, Hamid Q, et al. Airways expression of SARS-CoV-2 receptor, ACE2, and TMPRSS2 is lower in children than adults and increases with smoking and COPD. Molecular Therapy-Methods & Clinical Development. 2020;18:1-6.
83. Pinto-Plata VM, Müllerova H, Toso JF, Feudjo-Tepie M, Soriano JB, Vessey RS, et al. C-reactive protein in patients with COPD, control smokers and non-smokers. Thorax. 2006;61(1):23-8.
84. Shaykhiev R, Crystal RG. Innate immunity and chronic obstructive pulmonary disease: a mini-review. Gerontology. 2013;59(6):481-9.
85. Whitsett JA, Alenghat T. Respiratory epithelial cells orchestrate pulmonary innate immunity. Nature immunology. 2015;16(1):27-35.
86. Araya J, Cambier S, Markovics JA, Wolters P, Jablons D, Hill A, et al. Squamous metaplasia amplifies pathologic epithelial-mesenchymal interactions in COPD patients. The Journal of clinical investigation. 2007;117(11):3551-62.
87. Garmendia J, Morey P, Bengoechea JA. Impact of cigarette smoke exposure on host–bacterial pathogen interactions. European Respiratory Journal. 2012;39(2):467-77.
88. Johansen MD, Mahbub RM, Idrees S, Nguyen DH, Miemczyk S, Pathinayake P, et al. Increased SARS-CoV-2 Infection, Protease, and Inflammatory Responses in Chronic Obstructive Pulmonary Disease Primary Bronchial Epithelial Cells Defined with Single-Cell RNA Sequencing. Am J Respir Crit Care Med. 2022:712-29.

89. Woods JA, Wheeler JS, Finch CK, Pinner NA. Corticosteroids in the treatment of acute exacerbations of chronic obstructive pulmonary disease. International journal of chronic obstructive pulmonary disease. 2014;9:421.
90. Celli B, Barnes P. Exacerbations of chronic obstructive pulmonary disease. European Respiratory Journal. 2007;29(6):1224-38.
91. Kagoshima M, Ito K, Cosio B, Adcock I. Glucocorticoid suppression of nuclear factor-κB: a role for histone modifications. Biochemical Society Transactions. 2003;31(1):60-5.
92. Rahman I, Adcock I. Oxidative stress and redox regulation of lung inflammation in COPD. European respiratory journal. 2006;28(1):219-42.
93. Miravitlles M, Anzueto A. Chronic respiratory infection in patients with chronic obstructive pulmonary disease: what is the role of antibiotics? International journal of molecular sciences. 2017;18(7):1344.
94. Miravitlles M, Anzueto A. Antibiotics for acute and chronic respiratory infection in patients with chronic obstructive pulmonary disease. American journal of respiratory and critical care medicine. 2013;188(9):1052-7.
95. Levack WM, Watson J, Hay-Smith EJC, Davies C, Ingham T, Jones B, et al. Factors influencing referral to and uptake and attendance of pulmonary rehabilitation for chronic obstructive pulmonary disease: a qualitative evidence synthesis of the experiences of service users, their families, and healthcare providers. The Cochrane Database of Systematic Reviews. 2018;2018(11).
96. Zuo L, He F, Sergakis GG, Koozehchian MS, Stimpfl JN, Rong Y, et al. Interrelated role of cigarette smoking, oxidative stress, and immune response in COPD and corresponding treatments. American Journal of Physiology-Lung Cellular and Molecular Physiology. 2014;307(3):L205-L18.
97. Beeh KM, Beier J. The short, the long and the "ultra-long": why duration of bronchodilator action matters in chronic obstructive pulmonary disease. Advances in therapy. 2010;27(3):150-9.
98. Beeh KM, Burgel P-R, Franssen FM, Lopez-Campos JL, Loukides S, Hurst JR, et al. How do dual long-acting bronchodilators prevent exacerbations of chronic obstructive pulmonary disease? American journal of respiratory and critical care medicine. 2017;196(2):139-49.
99. Tashkin DP, Cooper CB. The role of long-acting bronchodilators in the management of stable COPD. Chest. 2004;125(1):249-59.
100. Truitt T, Witko J, Halpern M. Levalbuterol compared to racemic albuterol: efficacy and outcomes in patients hospitalized with COPD or asthma. Chest. 2003;123(1):128-35.
101. Datta D, Lahiri B, ZuWallack R. A randomized, double-blinded, placebo-controlled study comparing single doses of nebulized levalbuterol, albuterol and combined ipratropium-albuterol in stable COPD.(COPD: therapeutics and management: 12: 30pm-2: 00pm). Chest. 2002;122(4):44S-S.
102. Lal C, Strange C. Aclidinium bromide plus formoterol for the treatment of chronic obstructive pulmonary disease. Expert Opinion on Pharmacotherapy. 2015;16(3):427-34.
103. Dhungana S, Criner GJ. Spotlight on glycopyrronium/formoterol fumarate inhalation aerosol in the management of COPD: design, development, and place in therapy. International Journal of Chronic Obstructive Pulmonary Disease. 2017;12:2307.
104. Antus B. Pharmacotherapy of chronic obstructive pulmonary disease: a clinical review. International Scholarly Research Notices. 2013;2013.

105. Crim C, Calverley P, Anderson J, Celli B, Ferguson G, Jenkins C, et al. Pneumonia risk in COPD patients receiving inhaled corticosteroids alone or in combination: TORCH study results. European Respiratory Journal. 2009;34(3):641-7.
106. Rossi A, Guerriero M, Corrado A. Withdrawal of inhaled corticosteroids can be safe in COPD patients at low risk of exacerbation: a real-life study on the appropriateness of treatment in moderate COPD patients (OPTIMO). Respiratory research. 2014;15(1):1-12.
107. NIELSEN LP, DAHL R. Therapeutic ratio of inhaled corticosteroids in adult asthma: a dose–range comparison between fluticasone propionate and budesonide, measuring their effect on bronchial hyperresponsiveness and adrenal cortex function. American journal of respiratory and critical care medicine. 2000;162(6):2053-7.
108. Lipson DA, Crim C, Criner GJ, Day NC, Dransfield MT, Halpin DM, et al. Reduction in all-cause mortality with fluticasone furoate/umeclidinium/vilanterol in patients with chronic obstructive pulmonary disease. American journal of respiratory and critical care medicine. 2020;201(12):1508-16.
109. Hatzelmann A, Morcillo EJ, Lungarella G, Adnot S, Sanjar S, Beume R, et al. The preclinical pharmacology of roflumilast–a selective, oral phosphodiesterase 4 inhibitor in development for chronic obstructive pulmonary disease. Pulmonary pharmacology & therapeutics. 2010;23(4):235-56.
110. Kroegel C, Foerster M. Phosphodiesterase-4 inhibitors as a novel approach for the treatment of respiratory disease: cilomilast. Expert opinion on investigational drugs. 2007;16(1):109-24.
111. Windisch W, Magnet FS. Long-term oxygen therapy in COPD: what is the evidence? The Lancet Respiratory Medicine. 2022.
112. Michaelchuk W, Oliveira A, Marzolini S, Nonoyama M, Maybank A, Goldstein R, et al. Design and delivery of home-based telehealth pulmonary rehabilitation programs in COPD: A systematic review and meta-analysis. International journal of medical informatics. 2022:104754.
113. Jiang W, Song Y. Internet of things-based home noninvasive ventilation in COPD patients with hypercapnic chronic respiratory failure: study protocol for a randomized controlled trial. Trials. 2022;23(1):1-10.
114. Cohen E. Lung Volume Reduction Surgery. Cohen's Comprehensive Thoracic Anesthesia: Elsevier; 2022. p. 410-22.
115. Meyers B, Patterson G. Chronic obstructive pulmonary disease• 10: Bullectomy, lung volume reduction surgery, and transplantation for patients with chronic obstructive pulmonary disease. Thorax. 2003;58(7):634-8.
116. Jones B, Donovan C, Liu G, Gomez HM, Chimankar V, Harrison CL, et al. Animal models of COPD: W hat do they tell us? Respirology. 2017;22(1):21-32.
117. Fricker M, Deane A, Hansbro PM. Animal models of chronic obstructive pulmonary disease. Expert opinion on drug discovery. 2014;9(6):629-45.
118. Mannino DM. COPD: epidemiology, prevalence, morbidity and mortality, and disease heterogeneity. Chest. 2002;121(5):121S-6S.
119. Agusti A, Calverley P, Celli B, Coxson HO, Edwards LD, Lomas DA, et al. Characterisation of COPD heterogeneity in the ECLIPSE cohort. Respiratory research. 2010;11(1):1-14.
120. Kodavanti UP, Costa DL. Rodent models of susceptibility: what is their place in inhalation toxicology? Respiration physiology. 2001;128(1):57-70.
121. Canning BJ, Chou Y. Using guinea pigs in studies relevant to asthma and COPD. Pulmonary pharmacology & therapeutics. 2008;21(5):702-20.

122. Abraham WM. Modeling of asthma, COPD and cystic fibrosis in sheep. Pulmonary pharmacology & therapeutics. 2008;21(5):743-54.
123. Chapman RW. Canine models of asthma and COPD. Pulmonary pharmacology & therapeutics. 2008;21(5):731-42.
124. Plopper CG, Hyde DM. The non-human primate as a model for studying COPD and asthma. Pulmonary pharmacology & therapeutics. 2008;21(5):755-66.
125. Wright JL, Cosio M, Churg A. Animal models of chronic obstructive pulmonary disease. american journal of physiology-lung cellular and molecular physiology. 2008;295(1):L1-L15.
126. Shapiro SD. Animal models for COPD. Chest. 2000;117(5):223S-7S.
127. Antunes MA, Rocco PR. Elastase-induced pulmonary emphysema: insights from experimental models. Anais da Academia Brasileira de Ciencias. 2011;83:1385-96.
128. Baron RM, Choi AJ, Owen CA, Choi AM. Genetically manipulated mouse models of lung disease: potential and pitfalls. American Journal of Physiology-Lung Cellular and Molecular Physiology. 2012;302(6):L485-L97.
129. Zheng H, Liu Y, Huang T, Fang Z, Li G, He S. Development and characterization of a rat model of chronic obstructive pulmonary disease (COPD) induced by sidestream cigarette smoke. Toxicology Letters. 2009;189(3):225-34.
130. Williamson JD, Sadofsky LR, Hart SP. The pathogenesis of bleomycin-induced lung injury in animals and its applicability to human idiopathic pulmonary fibrosis. Experimental lung research. 2015;41(2):57-73.
131. Pelgrim CE, Wang L, Peralta Marzal LN, Korver S, van Ark I, Leusink-Muis T, et al. Increased exploration and hyperlocomotion in a cigarette smoke and LPS-induced murine model of COPD: linking pulmonary and systemic inflammation with the brain. American Journal of Physiology-Lung Cellular and Molecular Physiology. 2022;323(3):L251-L65.
132. Rydell-Törmänen K, Johnson JR. The applicability of mouse models to the study of human disease. Mouse Cell Culture: Springer; 2019. p. 3-22.
133. Rushton L. Chronic obstructive pulmonary disease and occupational exposure to silica. Reviews on environmental health. 2007;22(4):255-72.
134. Suki B, Bartolák-Suki E, Rocco PR. Elastase-induced lung emphysema models in mice. Alpha-1 Antitrypsin Deficiency: Springer; 2017. p. 67-75.
135. Kononov S, Brewer K, Sakai H, Cavalcante FS, Sabayanagam CR, Ingenito EP, et al. Roles of mechanical forces and collagen failure in the development of elastase-induced emphysema. American journal of respiratory and critical care medicine. 2001;164(10):1920-6.
136. Ghorani V, Boskabady MH, Khazdair MR, Kianmeher M. Experimental animal models for COPD: a methodological review. Tobacco induced diseases. 2017;15(1):1-13.
137. Shibata S, Miyake K, Tateishi T, Yoshikawa S, Yamanishi Y, Miyazaki Y, et al. Basophils trigger emphysema development in a murine model of COPD through IL-4–mediated generation of MMP-12–producing macrophages. Proceedings of the National Academy of Sciences. 2018;115(51):13057-62.
138. Pan Z, Yu H, Liao J-L. Probing cellular and molecular mechanisms of cigarette smoke-induced immune response in the progression of chronic obstructive pulmonary disease using multiscale network modeling. PLoS One. 2016;11(9):e0163192.
139. Churg A, Cosio M, Wright JL. Mechanisms of cigarette smoke-induced COPD: insights from animal models. American Journal of Physiology-Lung Cellular and Molecular Physiology. 2008;294(4):L612-L31.

140. Leberl M, Kratzer A, Taraseviciene-Stewart L. Tobacco smoke induced COPD/emphysema in the animal model—are we all on the same page? Frontiers in physiology. 2013;4:91.
141. Shu J, Li D, Ouyang H, Huang J, Long Z, Liang Z, et al. Comparison and evaluation of two different methods to establish the cigarette smoke exposure mouse model of COPD. Scientific Reports. 2017;7(1):1-11.
142. Rinaldi M, Maes K, De Vleeschauwer S, Thomas D, Verbeken EK, Decramer M, et al. Long-term nose-only cigarette smoke exposure induces emphysema and mild skeletal muscle dysfunction in mice. Disease models & mechanisms. 2012;5(3):333-41.
143. Walters DM, Kleeberger SR. Mouse models of bleomycin-induced pulmonary fibrosis. Current protocols in pharmacology. 2008;40(1):5.46. 1-5.. 17.
144. Izbicki G, Segel M, Christensen T, Conner M, Breuer R. Time course of bleomycin-induced lung fibrosis. International journal of experimental pathology. 2002;83(3):111-9.
145. Hnizdo E, Vallyathan V. Chronic obstructive pulmonary disease due to occupational exposure to silica dust: a review of epidemiological and pathological evidence. Occupational and environmental medicine. 2003;60(4):237-43.
146. Hansbro P, Beckett E, Stevens R, Jarnicki A, Wark P, Foster P. A short-term model of COPD identifies a role for mast cell tryptase. Eur Respiratory Soc; 2013.
147. Wang Y, Xu J, Meng Y, Adcock IM, Yao X. Role of inflammatory cells in airway remodeling in COPD. International journal of chronic obstructive pulmonary disease. 2018;13:3341.
148. Moldoveanu B, Otmishi P, Jani P, Walker J, Sarmiento X, Guardiola J, et al. Inflammatory mechanisms in the lung. Journal of inflammation research. 2009;2:1.
149. Cornwell WD, Kim V, Song C, Rogers TJ, editors. Pathogenesis of inflammation and repair in advanced COPD. Seminars in respiratory and critical care medicine; 2010: © Thieme Medical Publishers.
150. Serhan CN, Brain SD, Buckley CD, Gilroy DW, Haslett C, O'Neill LA, et al. Resolution of inflammation: state of the art, definitions and terms. FASEB journal: official publication of the Federation of American Societies for Experimental Biology. 2007;21(2):325.
151. Rittirsch D, Flierl MA, Ward PA. Harmful molecular mechanisms in sepsis. Nature Reviews Immunology. 2008;8(10):776-87.
152. Brannon ER, Guevara MV, Pacifici NJ, Lee JK, Lewis JS, Eniola-Adefeso O. Polymeric particle-based therapies for acute inflammatory diseases. Nature Reviews Materials. 2022:1-18.
153. Lugg ST, Scott A, Parekh D, Naidu B, Thickett DR. Cigarette smoke exposure and alveolar macrophages: Mechanisms for lung disease. Thorax. 2022;77(1):94-101.
154. Smith PD, Ochsenbauer-Jambor C, Smythies LE. Intestinal macrophages: unique effector cells of the innate immune system. Immunological reviews. 2005;206(1):149-59.
155. Gao W, Li L, Wang Y, Zhang S, Adcock IM, Barnes PJ, et al. Bronchial epithelial cells: the key effector cells in the pathogenesis of chronic obstructive pulmonary disease? Respirology. 2015;20(5):722-9.
156. Barnes PJ. Mediators of chronic obstructive pulmonary disease. Pharmacological reviews. 2004;56(4):515-48.
157. Zheng J. Energy metabolism of cancer: Glycolysis versus oxidative phosphorylation. Oncology letters. 2012;4(6):1151-7.
158. Palsson-McDermott EM, O'neill LA. The Warburg effect then and now: from cancer to inflammatory diseases. Bioessays. 2013;35(11):965-73.

159. Icard P, Lincet H, Wu Z, Coquerel A, Forgez P, Alifano M, et al. The key role of Warburg effect in SARS-CoV-2 replication and associated inflammatory response. Biochimie. 2021;180:169-77.
160. Zahra K, Dey T, Mishra SP, Pandey U. Pyruvate kinase M2 and cancer: the role of PKM2 in promoting tumorigenesis. Frontiers in oncology. 2020;10:159.
161. Puckett DL, Alquraishi M, Chowanadisai W, Bettaieb A. The role of PKM2 in metabolic reprogramming: insights into the regulatory roles of non-coding RNAs. International Journal of Molecular Sciences. 2021;22(3):1171.
162. Anastasiou D, Yu Y, Israelsen WJ, Jiang J-K, Boxer MB, Hong BS, et al. Pyruvate kinase M2 activators promote tetramer formation and suppress tumorigenesis. Nature chemical biology. 2012;8(10):839-47.
163. Wu S, Le H. Dual roles of PKM2 in cancer metabolism. Acta Biochim Biophys Sin. 2013;45(1):27-35.
164. Zhang Z, Deng X, Liu Y, Liu Y, Sun L, Chen F. PKM2, function and expression and regulation. Cell & bioscience. 2019;9(1):1-25.
165. Corcoran SE, O'Neill LA. HIF1α and metabolic reprogramming in inflammation. The Journal of clinical investigation. 2016;126(10):3699-707.
166. Zhao T, Zhu Y, Morinibu A, Kobayashi M, Shinomiya K, Itasaka S, et al. HIF-1-mediated metabolic reprogramming reduces ROS levels and facilitates the metastatic colonization of cancers in lungs. Scientific reports. 2014;4(1):1-7.
167. Le S, Zhang H, Huang X, Chen S, Wu J, Chen S, et al. PKM2 activator TEPP-46 attenuates thoracic aortic aneurysm and dissection by inhibiting NLRP3 inflammasome-mediated IL-1β secretion. Journal of Cardiovascular Pharmacology and Therapeutics. 2020;25(4):364-76.
168. Domej W, Oettl K, Renner W. Oxidative stress and free radicals in COPD–implications and relevance for treatment. International journal of chronic obstructive pulmonary disease. 2014;9:1207.
169. Tirichen H, Yaigoub H, Xu W, Wu C, Li R, Li Y. Mitochondrial reactive oxygen species and their contribution in chronic kidney disease progression through oxidative stress. Frontiers in Physiology. 2021;12:398.
170. Jiang Y, Wang X, Hu D. Mitochondrial alterations during oxidative stress in chronic obstructive pulmonary disease. International journal of chronic obstructive pulmonary disease. 2017;12:1153.
171. MacNee W. Oxidative stress and chronic obstructive pulmonary disease. European Respiratory Monograph. 2006;38:100.
172. Rabinovich RA, Bastos R, Ardite E, Llinàs L, Orozco-Levi M, Gea J, et al. Mitochondrial dysfunction in COPD patients with low body mass index. European Respiratory Journal. 2007;29(4):643-50.
173. Aghapour M, Remels AH, Pouwels SD, Bruder D, Hiemstra PS, Cloonan SM, et al. Mitochondria: at the crossroads of regulating lung epithelial cell function in chronic obstructive pulmonary disease. American Journal of Physiology-Lung Cellular and Molecular Physiology. 2020;318(1):L149-L64.
174. Antunes MA, Lopes-Pacheco M, Rocco PR. Oxidative stress-derived mitochondrial dysfunction in chronic obstructive pulmonary disease: A concise review. Oxidative Medicine and Cellular Longevity. 2021;2021.
175. Repine JE, Bast A, Lankhorst I, Group OSS. Oxidative stress in chronic obstructive pulmonary disease. American journal of respiratory and critical care medicine. 1997;156(2):341-57.

176. Wiegman CH, Li F, Ryffel B, Togbe D, Chung KF. Oxidative stress in ozone-induced chronic lung inflammation and emphysema: a facet of chronic obstructive pulmonary disease. Frontiers in Immunology. 2020:1957.
177. Barnes PJ. Oxidative Stress in Chronic Obstructive Pulmonary Disease. Antioxidants. 2022;11(5):965.
178. Colarusso C, Terlizzi M, Molino A, Pinto A, Sorrentino R. Role of the inflammasome in chronic obstructive pulmonary disease (COPD). Oncotarget. 2017;8(47):81813.
179. Barnes PJ. The cytokine network in chronic obstructive pulmonary disease. American journal of respiratory cell and molecular biology. 2009;41(6):631-8.
180. McGuinness AJA, Sapey E. Oxidative stress in COPD: sources, markers, and potential mechanisms. Journal of clinical medicine. 2017;6(2):21.
181. Malaviya R, Laskin JD, Laskin DL. Anti-TNFα therapy in inflammatory lung diseases. Pharmacology & therapeutics. 2017;180:90-8.
182. Bal SM, Bernink JH, Nagasawa M, Groot J, Shikhagaie MM, Golebski K, et al. IL-1β, IL-4 and IL-12 control the fate of group 2 innate lymphoid cells in human airway inflammation in the lungs. Nature immunology. 2016;17(6):636-45.
183. Tavilani H, Nadi E, Karimi J, Goodarzi MT. Oxidative stress in COPD patients, smokers, and non-smokers. Respiratory Care. 2012;57(12):2090-4.
184. MARGINEAN C, Popescu M, Vladaia M, TUDORASCU D, Pirvu D, Petrescu F. Involvement of oxidative stress in COPD. Current health sciences journal. 2018;44(1):48.
185. Carvalho VF, Barreto E, Victoni T, Lagente V. The Role of Oxidative Imbalance on Pulmonary Diseases. 2022.
186. Frias V, Carvalho B, Emiliano V, Tatiana L. The Role of Oxidative Imbalance on Pulmonary Diseases. Oxidative Medicine and Cellular Longevity. 2022.
187. Prosad R, Chandel NS. Beyond ATP, new roles of mitochondria.
188. Giacomello M, Pyakurel A, Glytsou C, Scorrano L. The cell biology of mitochondrial membrane dynamics. Nature reviews Molecular cell biology. 2020;21(4):204-24.
189. Deshpande OA, Mohiuddin SS. Biochemistry, Oxidative Phosphorylation. StatPearls [Internet]: StatPearls Publishing; 2021.
190. Nolfi-Donegan D, Braganza A, Shiva S. Mitochondrial electron transport chain: Oxidative phosphorylation, oxidant production, and methods of measurement. Redox biology. 2020;37:101674.
191. Ogawa S, Lee TM. The relation between the internal phosphorylation potential and the proton motive force in mitochondria during ATP synthesis and hydrolysis. Journal of Biological Chemistry. 1984;259(16):10004-11.
192. Ripple MO, Kim N, Springett R. Mammalian complex I pumps 4 protons per 2 electrons at high and physiological proton motive force in living cells. Journal of Biological Chemistry. 2013;288(8):5374-80.
193. Popov V, Medvedev NI, Davies HA, Stewart MG. Mitochondria form a filamentous reticular network in hippocampal dendrites but are present as discrete bodies in axons: A three-dimensional ultrastructural study. Journal of Comparative Neurology. 2005;492(1):50-65.
194. Mannella CA. The relevance of mitochondrial membrane topology to mitochondrial function. Biochimica et Biophysica Acta (BBA)-Molecular Basis of Disease. 2006;1762(2):140-7.
195. Kadenbach B, Ramzan R, Vogt S. Degenerative diseases, oxidative stress and cytochrome c oxidase function. Trends in molecular medicine. 2009;15(4):139-47.

196. Zhao Y, Yang Y. Profiling metabolic states with genetically encoded fluorescent biosensors for NADH. Current Opinion in Biotechnology. 2015;31:86-92.
197. Vander Heiden MG, Cantley LC, Thompson CB. Understanding the Warburg effect: the metabolic requirements of cell proliferation. science. 2009;324(5930):1029-33.
198. Selivanov VA, Votyakova TV, Pivtoraiko VN, Zeak J, Sukhomlin T, Trucco M, et al. Reactive oxygen species production by forward and reverse electron fluxes in the mitochondrial respiratory chain. PLoS computational biology. 2011;7(3):e1001115.
199. Nicolson GL. Mitochondrial dysfunction and chronic disease: treatment with natural supplements. Integrative Medicine: A Clinician's Journal. 2014;13(4):35.
200. Hertz L, Peng L, Dienel GA. Energy metabolism in astrocytes: high rate of oxidative metabolism and spatiotemporal dependence on glycolysis/glycogenolysis. Journal of Cerebral Blood Flow & Metabolism. 2007;27(2):219-49.
201. Chaudhry R, Varacallo M. Biochemistry, glycolysis. 2018.
202. Rosenthal MD, Glew RH. Medical biochemistry: human metabolism in health and disease: John Wiley & Sons; 2011.
203. Meurant G. Cellular energy metabolism and its regulation: Elsevier; 2012.
204. Winkler BS. Glycolytic and oxidative metabolism in relation to retinal function. The Journal of general physiology. 1981;77(6):667-92.
205. He C. Balancing nutrient and energy demand and supply via autophagy. Current Biology. 2022;32(12):R684-R96.
206. Arnold PK, Jackson BT, Paras KI, Brunner JS, Hart ML, Newsom OJ, et al. A non-canonical tricarboxylic acid cycle underlies cellular identity. Nature. 2022;603(7901):477-81.
207. Ryan DG, O'Neill LA. Krebs cycle rewired for macrophage and dendritic cell effector functions. FEBS letters. 2017;591(19):2992-3006.
208. Gupta R, Gupta N. Tricarboxylic Acid Cycle. Fundamentals of Bacterial Physiology and Metabolism: Springer; 2021. p. 327-46.
209. Sugden MC, Holness MJ. The pyruvate carboxylase-pyruvate dehydrogenase axis in islet pyruvate metabolism: Going round in circles? Islets. 2011;3(6):302-19.
210. Courtnay R, Ngo DC, Malik N, Ververis K, Tortorella SM, Karagiannis TC. Cancer metabolism and the Warburg effect: the role of HIF-1 and PI3K. Molecular biology reports. 2015;42(4):841-51.
211. Martínez-Reyes I, Chandel NS. Mitochondrial TCA cycle metabolites control physiology and disease. Nature communications. 2020;11(1):1-11.
212. Smeitink J, van den Heuvel L, DiMauro S. The genetics and pathology of oxidative phosphorylation. Nature Reviews Genetics. 2001;2(5):342-52.
213. Wilden L, Karthein R. Import of radiation phenomena of electrons and therapeutic low-level laser in regard to the mitochondrial energy transfer. Journal of clinical laser medicine & surgery. 1998;16(3):159-65.
214. Peña FJ, Ortiz-Rodríguez JM, Gaitskell-Phillips GL, Gil MC, Ortega-Ferrusola C, Martín-Cano FE. An integrated overview on the regulation of sperm metabolism (glycolysis-Krebs cycle-oxidative phosphorylation). Animal Reproduction Science. 2021:106805.
215. Wang Y, Mohsen A-W, Mihalik SJ, Goetzman ES, Vockley J. Evidence for physical association of mitochondrial fatty acid oxidation and oxidative phosphorylation complexes. Journal of Biological Chemistry. 2010;285(39):29834-41.
216. Haas RH, Nasirian F, Nakano K, Ward D, Pay M, Hill R, et al. Low platelet mitochondrial complex I and complex II/III activity in early untreated Parkinson's

disease. Annals of Neurology: Official Journal of the American Neurological Association and the Child Neurology Society. 1995;37(6):714-22.
217. Rodgers AJ, Wilce MC. Structure of the γ–ε complex of ATP synthase. Nature structural biology. 2000;7(11):1051-4.
218. Ashton TM, McKenna WG, Kunz-Schughart LA, Higgins GS. Oxidative phosphorylation as an emerging target in cancer therapy. Clinical Cancer Research. 2018;24(11):2482-90.
219. Cantó C, Menzies KJ, Auwerx J. NAD+ metabolism and the control of energy homeostasis: a balancing act between mitochondria and the nucleus. Cell metabolism. 2015;22(1):31-53.
220. Yoshino J, Baur JA, Imai S-i. NAD+ intermediates: the biology and therapeutic potential of NMN and NR. Cell metabolism. 2018;27(3):513-28.
221. Verdin E. NAD+ in aging, metabolism, and neurodegeneration. Science. 2015;350(6265):1208-13.
222. Ying W. Roles of NAD+, PARP-1, and sirtuins in cell death, ischemic brain injury, and synchrotron radiation X-ray-induced tissue injury. Scientifica. 2013;2013.
223. Revollo JR, Grimm AA, Imai S-i. The NAD biosynthesis pathway mediated by nicotinamide phosphoribosyltransferase regulates Sir2 activity in mammalian cells. Journal of Biological Chemistry. 2004;279(49):50754-63.
224. Badawy AA. Kynurenine pathway of tryptophan metabolism: regulatory and functional aspects. International Journal of Tryptophan Research. 2017;10:1178646917691938.
225. Katsyuba E, Romani M, Hofer D, Auwerx J. NAD+ homeostasis in health and disease. Nature metabolism. 2020;2(1):9-31.
226. Magni G, Orsomando G, Raffelli N, Ruggieri S. Enzymology of mammalian NAD metabolism in health and disease. Frontiers in Bioscience-Landmark. 2008;13(16):6135-54.
227. Krishnakumar R, Kraus WL. The PARP side of the nucleus: molecular actions, physiological outcomes, and clinical targets. Molecular cell. 2010;39(1):8-24.
228. Aksoy P, White TA, Thompson M, Chini EN. Regulation of intracellular levels of NAD: a novel role for CD38. Biochemical and biophysical research communications. 2006;345(4):1386-92.
229. Nakagawa T, Guarente L. Sirtuins at a glance. Journal of cell science. 2011;124(6):833-8.
230. Cohen MS. Interplay between compartmentalized NAD+ synthesis and consumption: a focus on the PARP family. Genes & development. 2020;34(5-6):254-62.
231. Hurtado-Bagès S, Knobloch G, Ladurner AG, Buschbeck M. The taming of PARP1 and its impact on NAD+ metabolism. Molecular metabolism. 2020;38:100950.
232. Franco L, Guida L, Bruzzone S, Zocchi E, Usai C, De Flora A. The transmembrane glycoprotein CD38 is a catalytically active transporter responsible for generation and influx of the second messenger cyclic ADP-ribose across membranes. The FASEB journal. 1998;12(14):1507-20.
233. Ghose J, Viola D, Terrazas C, Caserta E, Troadec E, Khalife J, et al. Daratumumab induces CD38 internalization and impairs myeloma cell adhesion. Oncoimmunology. 2018;7(10):e1486948.
234. Ben Baruch B, Mantsur E, Franco-Barraza J, Blacher E, Cukierman E, Stein R. CD38 in cancer-associated fibroblasts promotes pro-tumoral activity. Laboratory Investigation. 2020;100(12):1517-31.

235. Lund FE, Cockayne DA, Randall TD, Solvason N, Schuber F, Howard MC. CD38: a new paradigm in lymphocyte activation and signal transduction. Immunological reviews. 1998;161(1):79-93.
236. Amici SA, Young NA, Narvaez-Miranda J, Jablonski KA, Arcos J, Rosas L, et al. CD38 is robustly induced in human macrophages and monocytes in inflammatory conditions. Frontiers in immunology. 2018;9:1593.
237. Lam JH, Ng HHM, Lim CJ, Sim XN, Malavasi F, Li H, et al. Expression of CD38 on macrophages predicts improved prognosis in hepatocellular carcinoma. Frontiers in immunology. 2019:2093.
238. Canto C, Menzies KJ, Auwerx J. NAD+ metabolism and the control of energy homeostasis: a balancing act between mitochondria and the nucleus. Cell metabolism. 2015;22(1):31-53.
239. Iqbal J, Zaidi M. TNF regulates cellular NAD+ metabolism in primary macrophages. Biochemical and biophysical research communications. 2006;342(4):1312-8.
240. Preyat N, Rossi M, Kers J, Chen L, Bertin J, Gough PJ, et al. Intracellular nicotinamide adenine dinucleotide promotes TNF-induced necroptosis in a sirtuin-dependent manner. Cell Death & Differentiation. 2016;23(1):29-40.
241. Nakagawa T, Guarente L. SnapShot: sirtuins, NAD, and aging. Cell metabolism. 2014;20(1):192-. e1.
242. Grabowska W, Sikora E, Bielak-Zmijewska A. Sirtuins, a promising target in slowing down the ageing process. Biogerontology. 2017;18(4):447-76.
243. Chalkiadaki A, Guarente L. The multifaceted functions of sirtuins in cancer. Nature Reviews Cancer. 2015;15(10):608-24.
244. Winnik S, Auwerx J, Sinclair DA, Matter CM. Protective effects of sirtuins in cardiovascular diseases: from bench to bedside. European heart journal. 2015;36(48):3404-12.
245. Zhang F, Wang S, Gan L, Vosler PS, Gao Y, Zigmond MJ, et al. Protective effects and mechanisms of sirtuins in the nervous system. Progress in neurobiology. 2011;95(3):373-95.
246. Li Q, Cheng JCy, Jiang Q, Lee WYw. Role of sirtuins in bone biology: Potential implications for novel therapeutic strategies for osteoporosis. Aging Cell. 2021;20(2):e13301.
247. Corbi G, Bianco A, Turchiarelli V, Cellurale M, Fatica F, Daniele A, et al. Potential mechanisms linking atherosclerosis and increased cardiovascular risk in COPD: focus on sirtuins. International Journal of Molecular Sciences. 2013;14(6):12696-713.
248. Chun P. Role of sirtuins in chronic obstructive pulmonary disease. Archives of pharmacal research. 2015;38(1):1-10.
249. Barbosa MTP, Soares SM, Novak CM, Sinclair D, Levine JA, Aksoy P, et al. The enzyme CD38 (a NAD glycohydrolase, EC 3.2. 2.5) is necessary for the development of diet-induced obesity. The FASEB Journal. 2007;21(13):3629-39.
250. Tamsett TJ, Picchione KE, Bhattacharjee A. NAD+ activates KNa channels in dorsal root ganglion neurons. Journal of Neuroscience. 2009;29(16):5127-34.
251. Yang T, Sauve AA. NAD metabolism and sirtuins: metabolic regulation of protein deacetylation in stress and toxicity. The AAPS journal. 2006;8(4):E632-E43.
252. Braidy N, Berg J, Clement J, Khorshidi F, Poljak A, Jayasena T, et al. Role of nicotinamide adenine dinucleotide and related precursors as therapeutic targets for age-related degenerative diseases: rationale, biochemistry, pharmacokinetics, and outcomes. Antioxidants & redox signaling. 2019;30(2):251-94.

253. Lee HJ, Yang SJ. Supplementation with nicotinamide riboside reduces brain inflammation and improves cognitive function in diabetic mice. International journal of molecular sciences. 2019;20(17):4196.
254. Leung CKS, Ren ST, Chan PPM, Wan KHN, Kam AKW, Lai GWK, et al. Nicotinamide riboside as a neuroprotective therapy for glaucoma: study protocol for a randomized, double-blind, placebo-control trial. Trials. 2022;23(1):1-10.
255. Brown KD, Maqsood S, Huang J-Y, Pan Y, Harkcom W, Li W, et al. Activation of SIRT3 by the NAD+ precursor nicotinamide riboside protects from noise-induced hearing loss. Cell metabolism. 2014;20(6):1059-68.
256. Custodero C, Saini SK, Shin MJ, Jeon YK, Christou DD, McDermott MM, et al. Nicotinamide riboside—a missing piece in the puzzle of exercise therapy for older adults? Experimental gerontology. 2020;137:110972.
257. Murray MF. Nicotinamide: an oral antimicrobial agent with activity against both Mycobacterium tuberculosis and human immunodeficiency virus. Clinical infectious diseases. 2003;36(4):453-60.
258. Tannous C, Booz GW, Altara R, Muhieddine DH, Mericskay M, Refaat MM, et al. Nicotinamide adenine dinucleotide: Biosynthesis, consumption and therapeutic role in cardiac diseases. Acta Physiologica. 2021;231(3):e13551.
259. Gariani K, Menzies KJ, Ryu D, Wegner CJ, Wang X, Ropelle ER, et al. Eliciting the mitochondrial unfolded protein response by nicotinamide adenine dinucleotide repletion reverses fatty liver disease in mice. Hepatology. 2016;63(4):1190-204.
260. Salic K, Gart E, Seidel F, Verschuren L, Caspers M, van Duyvenvoorde W, et al. Combined treatment with L-carnitine and nicotinamide riboside improves hepatic metabolism and attenuates obesity and liver steatosis. International journal of molecular sciences. 2019;20(18):4359.
261. Hashimoto S, Kankanam Gamage U, Morimoto Y. P-200 An addition of nicotinamide adenine dinucleotide (NAD+) precursor to oocyte maturation medium improves the developmental competence of bovine oocytes after IVF. Human Reproduction. 2022;37(Supplement_1):deac107. 93.
262. Faivre A, Katsyuba E, Verissimo T, Lindenmeyer M, Rajaram RD, Naesens M, et al. Differential role of nicotinamide adenine dinucleotide deficiency in acute and chronic kidney disease. Nephrology Dialysis Transplantation. 2021;36(1):60-8.
263. Cantó C, Houtkooper RH, Pirinen E, Youn DY, Oosterveer MH, Cen Y, et al. The NAD+ precursor nicotinamide riboside enhances oxidative metabolism and protects against high-fat diet-induced obesity. Cell metabolism. 2012;15(6):838-47.
264. Griffiths H, Williams C, King SJ, Allison SJ. Nicotinamide adenine dinucleotide (NAD+): essential redox metabolite, co-substrate and an anti-cancer and anti-ageing therapeutic target. Biochemical Society Transactions. 2020;48(3):733-44.
265. Waltz TB, Fivenson EM, Morevati M, Li C, Becker KG, Bohr VA, et al. Sarcopenia, aging and prospective interventional strategies. Current medicinal chemistry. 2018;25(40):5588-96.
266. Martens CR, Denman BA, Mazzo MR, Armstrong ML, Reisdorph N, McQueen MB, et al. Chronic nicotinamide riboside supplementation is well-tolerated and elevates NAD+ in healthy middle-aged and older adults. Nature communications. 2018;9(1):1-11.
267. Lange KW, Li S. Resveratrol, pterostilbene, and dementia. BioFactors. 2018;44(1):83-90.
268. Kala R, Tollefsbol TO. A novel combinatorial epigenetic therapy using resveratrol and pterostilbene for restoring estrogen receptor-α (ERα) expression in ERα-negative breast cancer cells. PLoS One. 2016;11(5):e0155057.

269. Acharya JD, Ghaskadbi SS. Protective effect of Pterostilbene against free radical mediated oxidative damage. BMC complementary and alternative medicine. 2013;13(1):238.
270. Dellinger RW, Santos SR, Morris M, Evans M, Alminana D, Guarente L, et al. Repeat dose NRPT (nicotinamide riboside and pterostilbene) increases NAD+ levels in humans safely and sustainably: a randomized, double-blind, placebo-controlled study. npj Aging and Mechanisms of Disease. 2017;3(1):1-9.
271. Liu H, Takagaki Y, Kumagai A, Kanasaki K, Koya D. The PKM2 activator TEPP-46 suppresses kidney fibrosis via inhibition of the EMT program and aberrant glycolysis associated with suppression of HIF-1α accumulation. Journal of Diabetes Investigation. 2021;12(5):697-709.
272. Yamada M, Ichinose M. The cholinergic pathways in inflammation: a potential pharmacotherapeutic target for COPD. Frontiers in pharmacology. 2018;9:1426.
273. Palsson-McDermott EM, Curtis AM, Goel G, Lauterbach MA, Sheedy FJ, Gleeson LE, et al. Pyruvate kinase M2 regulates Hif-1α activity and IL-1β induction and is a critical determinant of the warburg effect in LPS-activated macrophages. Cell metabolism. 2015;21(1):65-80.
274. Liu Z, Le Y, Chen H, Zhu J, Lu D. Role of PKM2-Mediated Immunometabolic Reprogramming on Development of Cytokine Storm. Frontiers in Immunology. 2021:4480.
275. Angiari S, Runtsch MC, Sutton CE, Palsson-McDermott EM, Kelly B, Rana N, et al. Pharmacological activation of pyruvate kinase M2 inhibits CD4+ T cell pathogenicity and suppresses autoimmunity. Cell metabolism. 2020;31(2):391-405. e8.
276. Miravitlles M, Soler-Cataluña JJ, Calle M, Molina J, Almagro P, Quintano JA, et al. Spanish COPD Guidelines (GesEPOC): pharmacological treatment of stable COPD. Archivos de Bronconeumología (English Edition). 2012;48(7):247-57.
277. Spurzem JR, Rennard SI, editors. Pathogenesis of COPD. Seminars in respiratory and critical care medicine; 2005: Published by Thieme Medical Publishers, Inc., 333 Seventh Avenue, New York ….
278. Mannino DM, Kiri VA. Changing the burden of COPD mortality. International journal of chronic obstructive pulmonary disease. 2006;1(3):219.
279. Ghesquière B, Wong BW, Kuchnio A, Carmeliet P. Metabolism of stromal and immune cells in health and disease. Nature. 2014;511(7508):167-76.
280. Almalki WH. The sepsis induced defective aggravation of immune cells: a translational science underling chemico-biological interactions from altered bioenergetics and/or cellular metabolism to organ dysfunction. Molecular and Cellular Biochemistry. 2021;476(6):2337-44.
281. van Horssen J, van Schaik P, Witte M. Inflammation and mitochondrial dysfunction: A vicious circle in neurodegenerative disorders? Neuroscience letters. 2019;710:132931.
282. Sohrabi Y, Godfrey R, Findeisen HM. Altered cellular metabolism drives trained immunity. Trends in Endocrinology & Metabolism. 2018;29(9):602-5.
283. MacIver NJ, Jacobs SR, Wieman HL, Wofford JA, Coloff JL, Rathmell JC. Glucose metabolism in lymphocytes is a regulated process with significant effects on immune cell function and survival. Journal of leukocyte biology. 2008;84(4):949-57.
284. Kang M-J, Shadel GS. A mitochondrial perspective of chronic obstructive pulmonary disease pathogenesis. Tuberculosis and respiratory diseases. 2016;79(4):207-13.
285. Meyer KC, editor Bronchoalveolar lavage as a diagnostic tool. Seminars in respiratory and critical care medicine; 2007: © Thieme Medical Publishers.

286. Piaton E, Fabre M, Goubin-Versini I, Bretz-Grenier M-F, Courtade-Saidi M, Vincent S, et al., editors. Technical recommendations and best practice guidelines for May-Grünwald-Giemsa staining: literature review and insights from the quality assurance. Annales de pathologie; 2015.
287. Ma C, Ma Z, Fu Q, Ma S. Curcumin attenuates allergic airway inflammation by regulation of CD4+ CD25+ regulatory T cells (Tregs)/Th17 balance in ovalbumin-sensitized mice. Fitoterapia. 2013;87:57-64.
288. Morton J, Snider TA. Guidelines for collection and processing of lungs from aged mice for histological studies. Pathobiology of Aging & Age-related Diseases. 2017;7(1):1313676.
289. Zhou X, Moore BB. Lung section staining and microscopy. Bio-protocol. 2017;7(10).
290. Segnani C, Ippolito C, Antonioli L, Pellegrini C, Blandizzi C, Dolfi A, et al. Histochemical detection of collagen fibers by sirius red/fast green is more sensitive than van gieson or sirius red alone in normal and inflamed rat colon. PloS one. 2015;10(12):e0144630.
291. Bonnardel E, Prevel R, Campagnac M, Dubreuil M, Marthan R, Berger P, et al. Determination of reliable lung function parameters in intubated mice. Respiratory research. 2019;20(1):1-14.
292. McGovern TK, Robichaud A, Fereydoonzad L, Schuessler TF, Martin JG. Evaluation of respiratory system mechanics in mice using the forced oscillation technique. JoVE (Journal of Visualized Experiments). 2013(75):e50172.
293. Lorch SA, Foust R, Gow A, Arkovitz M, Salzman AL, Szabo C, et al. Immunohistochemical localization of protein 3-nitrotyrosine and S-nitrosocysteine in a murine model of inhaled nitric oxide therapy. Pediatric research. 2000;47(6):798-805.
294. Hatasa K, Nakamura T. Electron microscopic observations of lung alveolar epithelial cells of normal young mice, with special reference to formation and secretion of osmiophilic lamellar bodies. Zeitschrift für Zellforschung und Mikroskopische Anatomie. 1965;68(2):266-77.
295. Aitken EH, Negri EM, Barboza R, Lima MR, Álvarez JM, Marinho CR, et al. Ultrastructure of the lung in a murine model of malaria-associated acute lung injury/acute respiratory distress syndrome. Malaria journal. 2014;13(1):1-10.
296. Muyal JP, Muyal V, Kaistha BP, Seifart C, Fehrenbach H. Systematic comparison of RNA extraction techniques from frozen and fresh lung tissues: checkpoint towards gene expression studies. Diagnostic pathology. 2009;4(1):1-8.
297. Beckett EL, Stevens RL, Jarnicki AG, Kim RY, Hanish I, Hansbro NG, et al. A new short-term mouse model of chronic obstructive pulmonary disease identifies a role for mast cell tryptase in pathogenesis. Journal of Allergy and Clinical Immunology. 2013;131(3):752-62. e7.
298. Finch DK, Stolberg VR, Ferguson J, Alikaj H, Kady MR, Richmond BW, et al. Lung dendritic cells drive natural killer cytotoxicity in chronic obstructive pulmonary disease via IL-15Rα. American Journal of Respiratory and Critical Care Medicine. 2018;198(9):1140-50.
299. Wu M, Stockley PG, Martin WJ. An improved western blotting technique effectively reduces background. Electrophoresis. 2002;23(15):2373-6.
300. Taylor SC, Posch A. The design of a quantitative western blot experiment. BioMed research international. 2014;2014.
301. Gilda JE, Gomes AV. Stain-Free total protein staining is a superior loading control to β-actin for Western blots. Analytical biochemistry. 2013;440(2):186-8.

302. Park S-H, Ozden O, Liu G, Song HY, Zhu Y, Yan Y, et al. SIRT2-mediated deacetylation and tetramerization of pyruvate kinase directs glycolysis and tumor growth. Cancer research. 2016;76(13):3802-12.
303. Liu X, Pervez H, Andersen LW, Uber A, Montissol S, Patel P, et al. Immunocapture and microplate-based activity and quantity measurement of pyruvate dehydrogenase in human peripheral blood mononuclear cells. Bioanalysis. 2015;7(5):583-92.
304. Tran T, Pencina KM, Schultz MB, Li Z, Ghattas C, Lau J, et al. Reduced levels of NAD in skeletal muscle and increased physiologic frailty are associated with viral coinfection in asymptomatic middle-aged adults. JAIDS Journal of Acquired Immune Deficiency Syndromes. 2022;89(1):S15-S22.
305. Curtin NJ. PARP inhibitors for cancer therapy. Expert reviews in molecular medicine. 2005;7(4):1-20.
306. Wibom R, Hagenfeldt L, von Döbeln U. Measurement of ATP production and respiratory chain enzyme activities in mitochondria isolated from small muscle biopsy samples. Analytical biochemistry. 2002;311(2):139-51.
307. Sivandzade F, Bhalerao A, Cucullo L. Analysis of the mitochondrial membrane potential using the cationic JC-1 dye as a sensitive fluorescent probe. Bio-protocol. 2019;9(1):e3128-e.
308. Drost Ea, Skwarski K, Sauleda J, Soler N, Roca J, Agusti A, et al. Oxidative stress and airway inflammation in severe exacerbations of COPD. Thorax. 2005;60(4):293-300.
309. Kirkham PA, Barnes PJ. Oxidative stress in COPD. Chest. 2013;144(1):266-73.
310. van der Vliet A, Janssen-Heininger YM, Anathy V. Oxidative stress in chronic lung disease: from mitochondrial dysfunction to dysregulated redox signaling. Molecular aspects of medicine. 2018;63:59-69.
311. Van Eeden SF, Sin DD. Oxidative stress in chronic obstructive pulmonary disease: a lung and systemic process. Hindawi; 2013. p. 27-9.
312. Wiegman CH, Michaeloudes C, Haji G, Narang P, Clarke CJ, Russell KE, et al. Oxidative stress–induced mitochondrial dysfunction drives inflammation and airway smooth muscle remodeling in patients with chronic obstructive pulmonary disease. Journal of Allergy and Clinical Immunology. 2015;136(3):769-80.
313. Zinellu E, Zinellu A, Fois AG, Pau MC, Scano V, Piras B, et al. Oxidative Stress Biomarkers in Chronic Obstructive Pulmonary Disease Exacerbations: A Systematic Review. Antioxidants. 2021;10(5):710.
314. Santus P, Corsico A, Solidoro P, Braido F, Di Marco F, Scichilone N. Oxidative stress and respiratory system: pharmacological and clinical reappraisal of N-acetylcysteine. COPD: Journal of Chronic Obstructive Pulmonary Disease. 2014;11(6):705-17.
315. Aman Y, Qiu Y, Tao J, Fang EF. Therapeutic potential of boosting NAD+ in aging and age-related diseases. Translational Medicine of Aging. 2018;2:30-7.
316. Paudel KR, Panth N, Manandhar B, Singh SK, Gupta G, Wich PR, et al. Attenuation of Cigarette-Smoke-Induced Oxidative Stress, Senescence, and Inflammation by Berberine-Loaded Liquid Crystalline Nanoparticles: In Vitro Study in 16HBE and RAW264. 7 Cells. Antioxidants. 2022;11(5):873.
317. Cipollina C, Bruno A, Fasola S, Cristaldi M, Patella B, Inguanta R, et al. Cellular and Molecular Signatures of Oxidative Stress in Bronchial Epithelial Cell Models Injured by Cigarette Smoke Extract. International Journal of Molecular Sciences. 2022;23(3):1770.
318. Rajman L, Chwalek K, Sinclair DA. Therapeutic potential of NAD-boosting molecules: the in vivo evidence. Cell metabolism. 2018;27(3):529-47.

319. Chung K, Adcock I. Multifaceted mechanisms in COPD: inflammation, immunity, and tissue repair and destruction. European Respiratory Journal. 2008;31(6):1334-56.
320. Agustí A, Edwards LD, Rennard SI, MacNee W, Tal-Singer R, Miller BE, et al. Persistent systemic inflammation is associated with poor clinical outcomes in COPD: a novel phenotype. PloS one. 2012;7(5):e37483.
321. Mittal M, Siddiqui MR, Tran K, Reddy SP, Malik AB. Reactive oxygen species in inflammation and tissue injury. Antioxidants & redox signaling. 2014;20(7):1126-67.
322. King PT. Inflammation in chronic obstructive pulmonary disease and its role in cardiovascular disease and lung cancer. Clinical and translational medicine. 2015;4(1):1-13.
323. Yarbro JR, Emmons RS, Pence BD. Macrophage immunometabolism and inflammaging: roles of mitochondrial dysfunction, cellular senescence, CD38, and NAD. Immunometabolism. 2020;2(3).
324. Dölle C, Rack JG, Ziegler M. NAD and ADP-ribose metabolism in mitochondria. The FEBS journal. 2013;280(15):3530-41.
325. Koh Y-C, Yang G, Lai C-S, Weerawatanakorn M, Pan M-H. Chemopreventive effects of phytochemicals and medicines on M1/M2 polarized macrophage role in inflammation-related diseases. International Journal of Molecular Sciences. 2018;19(8):2208.
326. Fernández-Blanco JA, Arike L, Ermund A, Fakih D, Rodríguez-Piñeiro AM, Martínez-Abad B, et al. COPD lungs show an attached stratified mucus layer resembling the protective colonic mucus. bioRxiv. 2017:205948.
327. Viegi G, Pistelli F, Sherrill D, Maio S, Baldacci S, Carrozzi L. Definition, epidemiology and natural history of COPD. European Respiratory Journal. 2007;30(5):993-1013.
328. Copot D, De Keyser R, Derom E, Ionescu C. Structural changes in the COPD lung and related heterogeneity. PloS one. 2017;12(5):e0177969.
329. Tang J, Curull V, Wang X, Ampurdanés C, Duran X, Pijuan L, et al. Increased PARP Activity and DNA Damage in NSCLC Patients: The Influence of COPD. Cancers. 2020;12(11):3333.
330. Verdin E. The many faces of sirtuins: coupling of NAD metabolism, sirtuins and lifespan. Nature medicine. 2014;20(1):25-7.
331. Brenmoehl J, Hoeflich A. Dual control of mitochondrial biogenesis by sirtuin 1 and sirtuin 3. Mitochondrion. 2013;13(6):755-61.
332. Cloonan SM, Choi AM. Mitochondria in lung disease. The Journal of clinical investigation. 2016;126(3):809-20.
333. Zhang L, Wang W, Zhu B, Wang X. Epithelial mitochondrial dysfunction in lung disease. Mitochondrial DNA and Diseases. 2017:201-17.
334. Mabalirajan U, Dinda AK, Kumar S, Roshan R, Gupta P, Sharma SK, et al. Mitochondrial structural changes and dysfunction are associated with experimental allergic asthma. The Journal of Immunology. 2008;181(5):3540-8.
335. Hara H, Kuwano K, Araya J. Mitochondrial quality control in COPD and IPF. Cells. 2018;7(8):86.
336. Puente-Maestu L, Pérez-Parra J, Godoy R, Moreno N, Tejedor A, González-Aragoneses F, et al. Abnormal mitochondrial function in locomotor and respiratory muscles of COPD patients. European Respiratory Journal. 2009;33(5):1045-52.
337. Rhoads DM, Umbach AL, Subbaiah CC, Siedow JN. Mitochondrial reactive oxygen species. Contribution to oxidative stress and interorganellar signaling. Plant physiology. 2006;141(2):357-66.

338. Patel B, Priefer R. Impact of chronic obstructive pulmonary disease, lung infection, and/or inhaled corticosteroids use on potential risk of lung cancer. Life Sciences. 2022:120374.
339. Fu Y-S, Kang N, Yu Y, Mi Y, Guo J, Wu J, et al. Polyphenols, flavonoids and inflammasomes: the role of cigarette smoke in COPD. European Respiratory Review. 2022;31(164).
340. Tønnesen P. Smoking cessation and COPD. European respiratory review. 2013;22(127):37-43.
341. Lapperre TS, Postma DS, Gosman MM, Snoeck-Stroband JB, ten Hacken NH, Hiemstra PS, et al. Relation between duration of smoking cessation and bronchial inflammation in COPD. Thorax. 2006;61(2):115-21.
342. Figueiredo RG, Araujo LF, de Bessa Junior J. The Role of Dual Bronchodilation and the Conscientious Use of Inhaled Corticosteroid in COPD. Sinusitis. 2022;6(2):32-5.
343. Cazzola M, Page C, Rogliani P, Calzetta L, Matera MG. Dual bronchodilation for the treatment of COPD-From bench to bedside. British Journal of Clinical Pharmacology. 2022.
344. BORGES IV, ROCHA PA, PALERMO KR, SFORSIN AP, PINTO VB, STELMACH R. Management of pharmacological treatment in patients with COPD and the direct cost of long-term anticholinergic therapy: real-word experience. Revista Brasileira de Farmácia Hospitalar e Serviços de Saúde. 2022;13(1):716-.
345. Altawalbeh SM, Almomani BA, Alefan Q, Mohammad Momany S, Al-Share QY. The influence of adverse drug effects on health-related quality of life in chronic obstructive pulmonary disease patients. International Journal of Pharmacy Practice. 2022.
346. Karal A, Celik H. Drugs and Natural Products Used in COPD. International Journal of Innovative Research and Reviews. 2022;6(1):51-8.
347. Barnes PJ, Baker J, Donnelly LE. Autophagy in asthma and chronic obstructive pulmonary disease. Clinical Science. 2022;136(10):733-46.
348. Barnes PJ. New treatments for COPD. Nature reviews Drug discovery. 2002;1(6):437-46.
349. Singh S, Loke YK. Risk of pneumonia associated with long-term use of inhaled corticosteroids in COPD: A critical review and update. Current opinion in pulmonary medicine. 2010;16(2):118.
350. Suissa S, Patenaude V, Lapi F, Ernst P. Inhaled corticosteroids in COPD and the risk of serious pneumonia. Thorax. 2013;68(11):1029-36.
351. Tan BH, Fearon KC. Cachexia: prevalence and impact in medicine. Current Opinion in Clinical Nutrition & Metabolic Care. 2008;11(4):400-7.
352. Sabit R, Thomas P, Shale DJ, Collins P, Linnane SJ. The effects of hypoxia on markers of coagulation and systemic inflammation in patients with COPD. Chest. 2010;138(1):47-51.
353. Stoller JK, Panos RJ, Krachman S, Doherty DE, Make B, Group L-tOTTR. Oxygen therapy for patients with COPD: current evidence and the long-term oxygen treatment trial. Chest. 2010;138(1):179-87.
354. Lane CR, Tonelli AR. Lung transplantation in chronic obstructive pulmonary disease: patient selection and special considerations. International journal of chronic obstructive pulmonary disease. 2015;10:2137.
355. van Ranst D, Otten H, Meijer JW, van't Hul AJ. Outcome of pulmonary rehabilitation in COPD patients with severely impaired health status. International Journal of Chronic Obstructive Pulmonary Disease. 2011;6:647.

356. Bairapareddy KC, Chandrasekaran B, Agarwal U. Telerehabilitation for chronic obstructive pulmonary disease patients: an underrecognized management in tertiary care. Indian journal of palliative care. 2018;24(4):529.
357. Alwakeel AJ, Sicondolfo A, Robitaille C, Bourbeau J, Saad N. The accessibility, feasibility, and safety of a standardized community-based tele-pulmonary rehab program for chronic obstructive pulmonary disease: a 3-year real-world prospective study. Annals of the American Thoracic Society. 2022;19(1):39-47.
358. Yawn B. Strategies to Improve Outcomes in COPD. The Journal of family practice. 2022;71(6 Suppl):S52-S7.
359. De Coster DA, Jones M. Tailoring of corticosteroids in COPD management. Current respiratory care reports. 2014;3(3):121-32.
360. Sutherland E, Allmers H, Ayas N, Venn A, Martin R. Inhaled corticosteroids reduce the progression of airflow limitation in chronic obstructive pulmonary disease: a meta-analysis. Thorax. 2003;58(11):937-41.
361. Agusti A, Fabbri LM, Singh D, Vestbo J, Celli B, Franssen FM, et al. Inhaled corticosteroids in COPD: friend or foe? European Respiratory Journal. 2018;52(6).
362. PAPI A, ROMAGNOLI M, BARALDO S, BRACCIONI F, GUZZINATI I, SAETTA M, et al. Partial reversibility of airflow limitation and increased exhaled NO and sputum eosinophilia in chronic obstructive pulmonary disease. American journal of respiratory and critical care medicine. 2000;162(5):1773-7.
363. Obrador E, Salvador R, Marchio P, López-Blanch R, Jihad-Jebbar A, Rivera P, et al. Nicotinamide riboside and pterostilbene cooperatively delay motor neuron failure in ALS SOD1G93A mice. Molecular Neurobiology. 2021;58(4):1345-71.
364. Willemse BW, Postma DS, Timens W, ten Hacken NH. The impact of smoking cessation on respiratory symptoms, lung function, airway hyperresponsiveness and inflammation. European Respiratory Journal. 2004;23(3):464-76.
365. Laniado-Laborín R. Smoking and chronic obstructive pulmonary disease (COPD). Parallel epidemics of the 21st century. International journal of environmental research and public health. 2009;6(1):209-24.
366. Zhang Y-Y, Tang W-T, Zhang H, Wang J, Bai X-X, Liao Y-H, et al. Barriers and Facilitators for Smoking Cessation in Chinese Smokers with Chronic Obstructive Pulmonary Disease: A Qualitative Study. International journal of chronic obstructive pulmonary disease. 2022;17:1107.
367. Godtfredsen NS, Prescott E. Benefits of smoking cessation with focus on cardiovascular and respiratory comorbidities. The clinical respiratory journal. 2011;5(4):187-94.
368. Godtfredsen NS, Lam TH, Hansel TT, Leon M, Gray N, Dresler C, et al. COPD-related morbidity and mortality after smoking cessation: status of the evidence. European Respiratory Journal. 2008;32(4):844-53.
369. Morris JF, Temple W. Spirometric “lung age” estimation for motivating smoking cessation. Preventive medicine. 1985;14(5):655-62.
370. Chaudhuri R, Livingston E, McMahon AD, Lafferty J, Fraser I, Spears M, et al. Effects of smoking cessation on lung function and airway inflammation in smokers with asthma. American journal of respiratory and critical care medicine. 2006;174(2):127-33.
371. Scanlon PD, Connett JE, Waller LA, Altose MD, Bailey WC, Sonia Buist A, et al. Smoking cessation and lung function in mild-to-moderate chronic obstructive pulmonary disease: the Lung Health Study. American journal of respiratory and critical care medicine. 2000;161(2):381-90.
372. Moores LK. Smoking and postoperative pulmonary complications: An evidence-based review of the recent literature. Clinics in chest medicine. 2000;21(1):139-46.

373. Gooneratne NS, Patel NP, Corcoran A. Chronic obstructive pulmonary disease diagnosis and management in older adults. Journal of the American Geriatrics Society. 2010;58(6):1153-62.
374. Rosado MM, Bennici E, Novelli F, Pioli C. Beyond DNA repair, the immunological role of PARP-1 and its siblings. Immunology. 2013;139(4):428-37.
375. Kunze FA, Hottiger MO. Regulating immunity via ADP-ribosylation: therapeutic implications and beyond. Trends in immunology. 2019;40(2):159-73.
376. Barnes PJ. Reduced histone deacetylase in COPD: clinical implications. Chest. 2006;129(1):151-5.
377. Ito K, Ito M, Elliott WM, Cosio B, Caramori G, Kon OM, et al. Decreased histone deacetylase activity in chronic obstructive pulmonary disease. New England Journal of Medicine. 2005;352(19):1967-76.
378. Barnes PJ. Histone deacetylase-2 and airway disease. Therapeutic advances in respiratory disease. 2009;3(5):235-43.
379. Dharwal V, Naura AS. PARP-1 inhibition ameliorates elastase induced lung inflammation and emphysema in mice. Biochemical pharmacology. 2018;150:24-34.
380. Li W, Li Y, Jin X, Liao Q, Chen Z, Peng H, et al. CD38: A significant regulator of macrophage function. Frontiers in Oncology. 2022;12.
381. Künzi L, Holt GE. Cigarette smoke activates the parthanatos pathway of cell death in human bronchial epithelial cells. Cell death discovery. 2019;5(1):1-8.
382. Chen G, Huang P, Hu C. The role of SIRT2 in cancer: A novel therapeutic target. International Journal of Cancer. 2020;147(12):3297-304.
383. Sidorova-Darmos E, Wither RG, Shulyakova N, Fisher C, Ratnam M, Aarts M, et al. Differential expression of sirtuin family members in the developing, adult, and aged rat brain. Frontiers in aging neuroscience. 2014;6:333.
384. Newman JC, He W, Verdin E. Mitochondrial protein acylation and intermediary metabolism: regulation by sirtuins and implications for metabolic disease. Journal of Biological Chemistry. 2012;287(51):42436-43.
385. Huang J-Y, Hirschey MD, Shimazu T, Ho L, Verdin E. Mitochondrial sirtuins. Biochimica et Biophysica Acta (BBA)-Proteins and Proteomics. 2010;1804(8):1645-51.
386. He W, Newman JC, Wang MZ, Ho L, Verdin E. Mitochondrial sirtuins: regulators of protein acylation and metabolism. Trends in Endocrinology & Metabolism. 2012;23(9):467-76.
387. Osborne B, Bentley NL, Montgomery MK, Turner N. The role of mitochondrial sirtuins in health and disease. Free radical biology and medicine. 2016;100:164-74.
388. Saunders RM, Biddle M, Amrani Y, Brightling CE. Stressed out-The role of oxidative stress in airway smooth muscle dysfunction in asthma and COPD. Free Radical Biology and Medicine. 2022.
389. Russo C, Valle MS, Casabona A, Spicuzza L, Sambataro G, Malaguarnera L. Vitamin D Impacts on Skeletal Muscle Dysfunction in Patients with COPD Promoting Mitochondrial Health. Biomedicines. 2022;10(4):898.
390. Wang X, Murugesan P, Zhang P, Xu S, Peng L, Wang C, et al. NADPH Oxidase Isoforms in COPD Patients and Acute Cigarette Smoke-Exposed Mice: Induction of Oxidative Stress and Lung Inflammation. Antioxidants. 2022;11(8):1539.
391. Carinci M, Palumbo L, Pellielo G, Agyapong ED, Morciano G, Patergnani S, et al. The Multifaceted Roles of Autophagy in Infectious, Obstructive, and Malignant Airway Diseases. Biomedicines. 2022;10(8):1944.
392. Liu C, Li P, Zheng J, Wang Y, Wu W, Liu X. Role of necroptosis in airflow limitation in chronic obstructive pulmonary disease: focus on small-airway disease and emphysema. Cell Death Discovery. 2022;8(1):1-8.

393. Demedts IK, Demoor T, Bracke KR, Joos GF, Brusselle GG. Role of apoptosis in the pathogenesis of COPD and pulmonary emphysema. Respiratory research. 2006;7(1):1-10.
394. Naimi AI, Bourbeau J, Perrault H, Baril J, Wright-Paradis C, Rossi A, et al. Altered mitochondrial regulation in quadriceps muscles of patients with COPD. Clinical physiology and functional imaging. 2011;31(2):124-31.
395. Gosker H, Hesselink M, Duimel H, Ward K, Schols A. Reduced mitochondrial density in the vastus lateralis muscle of patients with COPD. European Respiratory Journal. 2007;30(1):73-9.
396. Suárez-Rivero JM, Pastor-Maldonado CJ, Romero-González A, Gómez-Fernandez D, Povea-Cabello S, Álvarez-Córdoba M, et al. Pterostilbene in Combination With Mitochondrial Cofactors Improve Mitochondrial Function in Cellular Models of Mitochondrial Diseases. Frontiers in pharmacology. 2022;13:862085.
397. de Groot LE, van der Veen TA, Martinez FO, Hamann J, Lutter R, Melgert BN. Oxidative stress and macrophages: driving forces behind exacerbations of asthma and chronic obstructive pulmonary disease? American journal of physiology-lung cellular and molecular physiology. 2019;316(2):L369-L84.
398. Austin V, Crack PJ, Bozinovski S, Miller AA, Vlahos R. COPD and stroke: are systemic inflammation and oxidative stress the missing links? Clinical Science. 2016;130(13):1039-50.
399. Chu X, Raju RP. Regulation of NAD+ metabolism in aging and disease. Metabolism. 2022;126:154923.
400. Covarrubias AJ, Perrone R, Grozio A, Verdin E. NAD+ metabolism and its roles in cellular processes during ageing. Nature Reviews Molecular Cell Biology. 2021;22(2):119-41.
401. Stein LR, Imai S-i. The dynamic regulation of NAD metabolism in mitochondria. Trends in Endocrinology & Metabolism. 2012;23(9):420-8.
402. Zapata-Pérez R, Tammaro A, Schomakers BV, Scantlebery AM, Denis S, Elfrink HL, et al. Reduced nicotinamide mononucleotide is a new and potent NAD+ precursor in mammalian cells and mice. The FASEB Journal. 2021;35(4):e21456.
403. Amjad S, Nisar S, Bhat AA, Frenneaux MP, Fakhro K, Haris M, et al. Role of NAD+ in regulating cellular and metabolic signaling pathways. Molecular Metabolism. 2021;49:101195.
404. Navarro MN, Gomez de las Heras MM, Mittelbrunn M. Nicotinamide adenine dinucleotide metabolism in the immune response, autoimmunity and inflammageing. British Journal of Pharmacology. 2022;179(9):1839-56.
405. Ding Y, Li X, Horsman GP, Li P, Wang M, Li J, et al. Construction of an alternative NAD+ de novo biosynthesis pathway. Advanced Science. 2021;8(9):2004632.
406. Badawy AA-B. Kynurenine pathway and human systems. Experimental Gerontology. 2020;129:110770.
407. Liu G, Foster J, Manlapaz-Ramos P, Olivera BM. Nucleoside salvage pathway for NAD biosynthesis in Salmonella typhimurium. Journal of Bacteriology. 1982;152(3):1111-6.
408. Chiarugi A, Dölle C, Felici R, Ziegler M. The NAD metabolome—a key determinant of cancer cell biology. Nature Reviews Cancer. 2012;12(11):741-52.
409. Petrelli R, Felczak K, Cappellacci L. NMN/NaMN adenylyltransferase (NMNAT) and NAD kinase (NADK) inhibitors: chemistry and potential therapeutic applications. Current medicinal chemistry. 2011;18(13):1973-92.

410. Berger F, Lau C, Dahlmann M, Ziegler M. Subcellular compartmentation and differential catalytic properties of the three human nicotinamide mononucleotide adenylyltransferase isoforms. Journal of Biological Chemistry. 2005;280(43):36334-41.
411. N Jayaram H, Kusumanchi P, A Yalowitz J. NMNAT expression and its relation to NAD metabolism. Current medicinal chemistry. 2011;18(13):1962-72.
412. Srivastava S. Emerging therapeutic roles for NAD+ metabolism in mitochondrial and age-related disorders. Clinical and translational medicine. 2016;5(1):1-11.
413. Kulkarni CA, Brookes PS. Cellular compartmentation and the redox/nonredox functions of NAD+. Antioxidants & redox signaling. 2019;31(9):623-42.
414. Mesquita I, Varela P, Belinha A, Gaifem J, Laforge M, Vergnes B, et al. Exploring NAD+ metabolism in host–pathogen interactions. Cellular and molecular life sciences. 2016;73(6):1225-36.
415. Sasaki Y, Vohra BP, Baloh RH, Milbrandt J. Transgenic mice expressing the Nmnat1 protein manifest robust delay in axonal degeneration in vivo. Journal of Neuroscience. 2009;29(20):6526-34.
416. Avery MA, Sheehan AE, Kerr KS, Wang J, Freeman MR. WldS requires Nmnat1 enzymatic activity and N16–VCP interactions to suppress Wallerian degeneration. Journal of Cell Biology. 2009;184(4):501-13.
417. Challa S, Khulpateea BR, Nandu T, Camacho CV, Ryu KW, Chen H, et al. Ribosome ADP-ribosylation inhibits translation and maintains proteostasis in cancers. Cell. 2021;184(17):4531-46. e26.
418. Milde S, Gilley J, Coleman MP. Subcellular localization determines the stability and axon protective capacity of axon survival factor Nmnat2. PLoS biology. 2013;11(4):e1001539.
419. Felici R, Lapucci A, Ramazzotti M, Chiarugi A. Insight into molecular and functional properties of NMNAT3 reveals new hints of NAD homeostasis within human mitochondria. PloS one. 2013;8(10):e76938.
420. Nikiforov A, Dölle C, Niere M, Ziegler M. Pathways and subcellular compartmentation of NAD biosynthesis in human cells: from entry of extracellular precursors to mitochondrial NAD generation. Journal of Biological Chemistry. 2011;286(24):21767-78.
421. Ruszkiewicz JA, Bürkle A, Mangerich A. Fueling genome maintenance: On the versatile roles of NAD+ in preserving DNA integrity. Journal of Biological Chemistry. 2022:102037.
422. Sara A, Nisar S, Bhat AA, Shah AR, Frenneaux MP, Fakhro K, et al. Role of NAD+ in regulating cellular and metabolic signaling pathways. 2021.
423. Lautrup S, Sinclair DA, Mattson MP, Fang EF. NAD+ in brain aging and neurodegenerative disorders. Cell metabolism. 2019;30(4):630-55.
424. Harlan BA, Killoy KM, Pehar M, Liu L, Auwerx J, Vargas MR. Evaluation of the NAD+ biosynthetic pathway in ALS patients and effect of modulating NAD+ levels in hSOD1-linked ALS mouse models. Experimental neurology. 2020;327:113219.
425. Cui C-P, Zhang Y, Wang C, Yuan F, Li H, Yao Y, et al. Dynamic ubiquitylation of Sox2 regulates proteostasis and governs neural progenitor cell differentiation. Nature communications. 2018;9(1):1-15.
426. Zhou Q, Zhu L, Qiu W, Liu Y, Yang F, Chen W, et al. Nicotinamide Riboside Enhances Mitochondrial Proteostasis and Adult Neurogenesis through Activation of Mitochondrial Unfolded Protein Response Signaling in the Brain of ALS SOD1G93A Mice. International Journal of Biological Sciences. 2020;16(2):284-97.

427. Fang X, Huang Z, Zhai K, Huang Q, Tao W, Kim L, et al. Inhibiting DNA-PK induces glioma stem cell differentiation and sensitizes glioblastoma to radiation in mice. Science Translational Medicine. 2021;13(600):eabc7275.
428. Conforti L, Janeckova L, Wagner D, Mazzola F, Cialabrini L, Di Stefano M, et al. Reducing expression of NAD+ synthesizing enzyme NMNAT1 does not affect the rate of Wallerian degeneration. The FEBS journal. 2011;278(15):2666-79.
429. Fakouri NB, Hou Y, Demarest TG, Christiansen LS, Okur MN, Mohanty JG, et al. Toward understanding genomic instability, mitochondrial dysfunction and aging. The FEBS Journal. 2019;286(6):1058-73.
430. Jokinen R, Pirnes-Karhu S, Pietiläinen KH, Pirinen E. Adipose tissue NAD+-homeostasis, sirtuins and poly (ADP-ribose) polymerases-important players in mitochondrial metabolism and metabolic health. Redox biology. 2017;12:246-63.
431. Orsomando G, Cialabrini L, Amici A, Mazzola F, Ruggieri S, Conforti L, et al. Simultaneous single-sample determination of NMNAT isozyme activities in mouse tissues. PloS one. 2012;7(12):e53271.
432. Brazill JM, Li C, Zhu Y, Zhai RG. NMNAT: It's an NAD+ synthase… It'sa chaperone… It'sa neuroprotector. Current Opinion in Genetics & Development. 2017;44:156-62.
433. Zochodne D, Ramji N, Toth C. Neuronal targeting in diabetes mellitus: a story of sensory neurons and motor neurons. The Neuroscientist. 2008;14(4):311-8.
434. Liu X, Liu M, Tang C, Xiang Z, Li Q, Ruan X, et al. Overexpression of Nmnat improves the adaption of health span in aging Drosophila. Experimental Gerontology. 2018;108:276-83.
435. Yahata N, Yuasa S, Araki T. Nicotinamide mononucleotide adenylyltransferase expression in mitochondrial matrix delays Wallerian degeneration. Journal of Neuroscience. 2009;29(19):6276-84.
436. Singhal A, Cheng CY. Host NAD+ metabolism and infections: therapeutic implications. International Immunology. 2019;31(2):59-67.
437. Li X, Fang P, Mai J, Choi ET, Wang H, Yang X-f. Targeting mitochondrial reactive oxygen species as novel therapy for inflammatory diseases and cancers. Journal of hematology & oncology. 2013;6(1):1-19.
438. Mills E, O'Neill LA. Succinate: a metabolic signal in inflammation. Trends in cell biology. 2014;24(5):313-20.
439. Wang J, Zhai Q, Chen Y, Lin E, Gu W, McBurney MW, et al. A local mechanism mediates NAD-dependent protection of axon degeneration. The Journal of cell biology. 2005;170(3):349-55.
440. Galindo R, Banks Greenberg M, Araki T, Sasaki Y, Mehta N, Milbrandt J, et al. NMNAT3 is protective against the effects of neonatal cerebral hypoxia-ischemia. Annals of Clinical and Translational Neurology. 2017;4(10):722-38.
441. Kitaoka Y, Munemasa Y, Kojima K, Hirano A, Ueno S, Takagi H. Axonal protection by Nmnat3 overexpression with involvement of autophagy in optic nerve degeneration. Cell death & disease. 2013;4(10):e860-e.
442. Hwang ES, Song SB. Possible adverse effects of high-dose nicotinamide: mechanisms and safety assessment. Biomolecules. 2020;10(5):687.
443. Sasaki Y, Vohra BP, Lund FE, Milbrandt J. Nicotinamide mononucleotide adenylyl transferase-mediated axonal protection requires enzymatic activity but not increased levels of neuronal nicotinamide adenine dinucleotide. Journal of Neuroscience. 2009;29(17):5525-35.
444. Yang H, Yang T, Baur JA, Perez E, Matsui T, Carmona JJ, et al. Nutrient-sensitive mitochondrial NAD+ levels dictate cell survival. Cell. 2007;130(6):1095-107.

445. Son MJ, Kwon Y, Son T, Cho YS. Restoration of mitochondrial NAD+ levels delays stem cell senescence and facilitates reprogramming of aged somatic cells. Stem Cells. 2016;34(12):2840-51.
446. Clark AJ, Saade MC, Parikh SM, editors. The Significance of NAD+ Biosynthesis Alterations in Acute Kidney Injury. Seminars in Nephrology; 2022: Elsevier.
447. Dai Y, Lin J, Ren J, Zhu B, Wu C, Yu L. NAD+ metabolism in peripheral neuropathic pain. Neurochemistry International. 2022:105435.
448. Narne P, Phanithi PB. Role of NAD+ and FAD in Ischemic Stroke Pathophysiology: An Epigenetic Nexus and Expanding Therapeutic Repertoire. Cellular and Molecular Neurobiology. 2022:1-50.
449. Samsudeen A. Investigating the Effect of NMNAT1 Overexpression on Skeletal Muscle Physiology and Metabolism: UNSW Sydney; 2022.
450. Cercillieux A, Ciarlo E, Canto C. Balancing NAD+ deficits with nicotinamide riboside: therapeutic possibilities and limitations. Cellular and Molecular Life Sciences. 2022;79(8):1-28.
451. Fortunato C, Mazzola F, Raffaelli N. The key role of the NAD biosynthetic enzyme nicotinamide mononucleotide adenylyltransferase in regulating cell functions. IUBMB life. 2022;74(7):562-72.
452. Jones A, Kraus WL. Multiomics analysis of the NAD+–PARP1 axis reveals a role for site-specific ADP-ribosylation in splicing in embryonic stem cells. Genes & Development. 2022;36(9-10):601-17.
453. Zhang T, Berrocal JG, Yao J, DuMond ME, Krishnakumar R, Ruhl DD, et al. Regulation of poly (ADP-ribose) polymerase-1-dependent gene expression through promoter-directed recruitment of a nuclear NAD+ synthase. Journal of Biological Chemistry. 2012;287(15):12405-16.
454. Kraus WL. Transcriptional control by PARP-1: chromatin modulation, enhancer-binding, coregulation, and insulation. Current opinion in cell biology. 2008;20(3):294-302.
455. Berger F, Lau C, Ziegler M. Regulation of poly (ADP-ribose) polymerase 1 activity by the phosphorylation state of the nuclear NAD biosynthetic enzyme NMN adenylyl transferase 1. Proceedings of the National Academy of Sciences. 2007;104(10):3765-70.
456. Huang D, Kraus WL. The expanding universe of PARP1-mediated molecular and therapeutic mechanisms. Molecular Cell. 2022.
457. Henderson DJ, Miranda JL, Emerson BM. The β-NAD+ salvage pathway and PKC-mediated signaling influence localized PARP-1 activity and CTCF Poly (ADP) ribosylation. Oncotarget. 2017;8(39):64698.
458. Yamamoto M, Hikosaka K, Mahmood A, Tobe K, Shojaku H, Inohara H, et al. Nmnat3 is dispensable in mitochondrial NAD level maintenance in vivo. PloS one. 2016;11(1):e0147037.
459. Yu A, Zhou R, Xia B, Dang W, Yang Z, Chen X. NAMPT maintains mitochondria content via NRF2-PPARα/AMPKα pathway to promote cell survival under oxidative stress. Cellular Signalling. 2020;66:109496.
460. Ziegler M, Monné M, Nikiforov A, Agrimi G, Heiland I, Palmieri F. Welcome to the family: Identification of the NAD+ transporter of animal mitochondria as member of the solute carrier family SLC25. Biomolecules. 2021;11(6):880.
461. Van de Ven RA, Santos D, Haigis MC. Mitochondrial sirtuins and molecular mechanisms of aging. Trends in molecular medicine. 2017;23(4):320-31.
462. Chang H-C, Guarente L. SIRT1 and other sirtuins in metabolism. Trends in Endocrinology & Metabolism. 2014;25(3):138-45.

463. Zhu Y, Yan Y, Principe DR, Zou X, Vassilopoulos A, Gius D. SIRT3 and SIRT4 are mitochondrial tumor suppressor proteins that connect mitochondrial metabolism and carcinogenesis. Cancer & metabolism. 2014;2(1):1-11.
464. Sack MN. Emerging characterization of the role of SIRT3-mediated mitochondrial protein deacetylation in the heart. American Journal of Physiology-Heart and Circulatory Physiology. 2011;301(6):H2191-H7.
465. Ahuja N, Schwer B, Carobbio S, Waltregny D, North BJ, Castronovo V, et al. Regulation of insulin secretion by SIRT4, a mitochondrial ADP-ribosyltransferase. Journal of Biological Chemistry. 2007;282(46):33583-92.
466. Wu S, Liu H. Sirtuins—Novel Regulators of Epigenetic Alterations in Airway Inflammation. Frontiers in Genetics. 2022;13.
467. Wang T, Peng W, Zhang F, Wang L, Zhang J, Dong W, et al. NMNAT3 improves mitochondrial function and enhances BMSCs anti-oxidative stress through the NAD+-Sirt3 pathway. 2020.
468. Wang T, Zhang F, Peng W, Wang L, Zhang J, Dong W, et al. Overexpression of NMNAT3 improves mitochondrial function and enhances anti-oxidative stress of bone marrow mesenchymal stem cells via the NAD+-Sirt3 pathway. Bioscience Reports. 2022.
469. Wang T, Zhang F, Peng W, Wang L, Zhang J, Dong W, et al. Overexpression of NMNAT3 improves mitochondrial function and enhances antioxidative stress capacity of bone marrow mesenchymal stem cells via the NAD+-Sirt3 pathway. Bioscience reports. 2022;42(1):BSR20211005.
470. Majeed Y, Halabi N, Madani AY, Engelke R, Bhagwat AM, Abdesselem H, et al. SIRT1 promotes lipid metabolism and mitochondrial biogenesis in adipocytes and coordinates adipogenesis by targeting key enzymatic pathways. Scientific reports. 2021;11(1):1-19.
471. Kiss A, Ráduly AP, Regdon Z, Polgár Z, Tarapcsák S, Sturniolo I, et al. Targeting nuclear NAD+ synthesis inhibits DNA repair, impairs metabolic adaptation and increases chemosensitivity of U-2OS osteosarcoma cells. Cancers. 2020;12(5):1180.
472. Valacchi G, Pecorelli A, Cervellati C, Hayek J. 4-hydroxynonenal protein adducts: key mediator in Rett syndrome oxinflammation. Free Radical Biology and Medicine. 2017;111:270-80.
473. Pillon NJ, Croze ML, Vella RE, Soulère L, Lagarde M, Soulage CO. The lipid peroxidation by-product 4-hydroxy-2-nonenal (4-HNE) induces insulin resistance in skeletal muscle through both carbonyl and oxidative stress. Endocrinology. 2012;153(5):2099-111.
474. Rahman I, van Schadewijk AA, Crowther AJ, Hiemstra PS, Stolk J, MacNee W, et al. 4-Hydroxy-2-nonenal, a specific lipid peroxidation product, is elevated in lungs of patients with chronic obstructive pulmonary disease. American journal of respiratory and critical care medicine. 2002;166(4):490-5.
475. Liu H, Xu J. The role of 4-hydroxynonenal in assessment of chronic obstructive pulmonary disease severity. Zhonghua jie he he hu xi za zhi= Zhonghua Jiehe he Huxi Zazhi= Chinese Journal of Tuberculosis and Respiratory Diseases. 2012;35(10):758-61.
476. Jiang H, Wan Z, Ding Y, Yao Z. Nmnat1 modulates mitochondrial oxidative stress by inhibiting caspase-3 signaling in Alzheimer's disease. Journal of molecular neuroscience. 2021;71(7):1467-72.
477. Verghese PB, Sasaki Y, Yang D, Stewart F, Sabar F, Finn MB, et al. Nicotinamide mononucleotide adenylyl transferase 1 protects against acute neurodegeneration in developing CNS by inhibiting excitotoxic-necrotic cell death. Proceedings of the National Academy of Sciences. 2011;108(47):19054-9.

478. Houtkooper RH, Cantó C, Wanders RJ, Auwerx J. The secret life of NAD+: an old metabolite controlling new metabolic signaling pathways. Endocrine reviews. 2010;31(2):194-223.
479. Magnifico S, Saias L, Deleglise B, Duplus E, Kilinc D, Miquel MC, et al. NAD+ acts on mitochondrial SirT3 to prevent axonal caspase activation and axonal degeneration. The FASEB Journal. 2013;27(12):4712-22.
480. Jiang S. Tetrameric PKM2 Activation Curbs CD4+ T Cell Overactivation. Trends in Endocrinology & Metabolism. 2020;31(6):393-5.
481. Reers M, Smiley ST, Mottola-Hartshorn C, Chen A, Lin M, Chen LB. [29] Mitochondrial membrane potential monitored by JC-1 dye. Methods in enzymology. 260: Elsevier; 1995. p. 406-17.
482. López-Armada MJ, Riveiro-Naveira RR, Vaamonde-García C, Valcárcel-Ares MN. Mitochondrial dysfunction and the inflammatory response. Mitochondrion. 2013;13(2):106-18.
483. Brown G, Otero L, LeGris M, Brown R. Pyruvate dehydrogenase deficiency. Journal of Medical Genetics. 1994;31(11):875.
484. Kaplon J, Zheng L, Meissl K, Chaneton B, Selivanov VA, Mackay G, et al. A key role for mitochondrial gatekeeper pyruvate dehydrogenase in oncogene-induced senescence. Nature. 2013;498(7452):109-12.
485. Zhu H, Blake S, Kusuma FK, Pearson RB, Kang J, Chan KT. Oncogene-induced senescence: From biology to therapy. Mechanisms of ageing and development. 2020;187:111229.
486. Woolbright BL, Rajendran G, Harris RA, Taylor JA. Metabolic flexibility in cancer: targeting the pyruvate dehydrogenase kinase: pyruvate dehydrogenase axis. Molecular cancer therapeutics. 2019;18(10):1673-81.
487. LeBleu VS, O'Connell JT, Gonzalez Herrera KN, Wikman H, Pantel K, Haigis MC, et al. PGC-1α mediates mitochondrial biogenesis and oxidative phosphorylation in cancer cells to promote metastasis. Nature cell biology. 2014;16(10):992-1003.
488. Yang L, Xie M, Yang M, Yu Y, Zhu S, Hou W, et al. PKM2 regulates the Warburg effect and promotes HMGB1 release in sepsis. Nature communications. 2014;5(1):1-9.
489. Higham A, Quinn AM, Cançado JED, Singh D. The pathology of small airways disease in COPD: historical aspects and future directions. Respiratory research. 2019;20(1):1-11.
490. Vogelmeier CF, Román-Rodríguez M, Singh D, Han MK, Rodríguez-Roisin R, Ferguson GT. Goals of COPD treatment: focus on symptoms and exacerbations. Respiratory medicine. 2020;166:105938.
491. Mei D, Tan WSD, Wong WSF. Pharmacological strategies to regain steroid sensitivity in severe asthma and COPD. Current opinion in pharmacology. 2019;46:73-81.
492. Hunninghake GM, Cho MH, Tesfaigzi Y, Soto-Quiros ME, Avila L, Lasky-Su J, et al. MMP12, lung function, and COPD in high-risk populations. New England Journal of Medicine. 2009;361(27):2599-608.
493. Celli BR, Thomas NE, Anderson JA, Ferguson GT, Jenkins CR, Jones PW, et al. Effect of pharmacotherapy on rate of decline of lung function in chronic obstructive pulmonary disease: results from the TORCH study. American journal of respiratory and critical care medicine. 2008;178(4):332-8.
494. Yun J, Ghosh A, Hobbs B, Saferali A, Chase R, Xu Z, et al. Lung Tissue Gene Expression Profile of Eosinophilic Chronic Obstructive Pulmonary Disease. B101 VARIED OMICS TECHNIQUES APPLIED TO ALLERGIC AND RESPIRATORY TRAITS: American Thoracic Society; 2022. p. A3485-A.

495. Meng H, Chang J, Wang B, Geng B, He R, Hao B, et al. Single-Cell RNA Sequencing Reveals the Tissue-Specific Immune Signatures of Lung Cancer with COPD. Available at SSRN 4104282.
496. Finicelli M, Digilio FA, Galderisi U, Peluso G. The Emerging Role of Macrophages in Chronic Obstructive Pulmonary Disease: The Potential Impact of Oxidative Stress and Extracellular Vesicle on Macrophage Polarization and Function. Antioxidants. 2022;11(3):464.
497. Li S-J, Lin Y-H, Chiang C-H, Wang P-Y, Chen C-Y. Early-onset dietary restriction maintains mitochondrial health, autophagy and ER function in the left ventricle during aging. The Journal of Nutritional Biochemistry. 2022:108944.
498. Amorim JA, Coppotelli G, Rolo AP, Palmeira CM, Ross JM, Sinclair DA. Mitochondrial and metabolic dysfunction in ageing and age-related diseases. Nature Reviews Endocrinology. 2022;18(4):243-58.
499. Gao J, Zhao Y, Li T, Gan X, Yu H. The Role of PKM2 in the Regulation of Mitochondrial Function: Focus on Mitochondrial Metabolism, Oxidative Stress, Dynamic, and Apoptosis. PKM2 in Mitochondrial Function. Oxidative Medicine and Cellular Longevity. 2022;2022.
500. Dritsas E, Alexiou S, Moustakas K, editors. Copd severity prediction in elderly with ml techniques. Proceedings of the 15th International Conference on PErvasive Technologies Related to Assistive Environments; 2022.
501. Alqahtani JS. Prevalence, incidence, morbidity and mortality rates of COPD in Saudi Arabia: Trends in burden of COPD from 1990 to 2019. Plos one. 2022;17(5):e0268772.
502. O'Toole RF, Shukla SD, Walters EH. TB meets COPD: An emerging global co-morbidity in human lung disease. Tuberculosis. 2015;95(6):659-63.
503. Brandsma CA, Van den Berge M, Hackett TL, Brusselle G, Timens W. Recent advances in chronic obstructive pulmonary disease pathogenesis: from disease mechanisms to precision medicine. The Journal of pathology. 2020;250(5):624-35.
504. Postma DS, Bush A, van den Berge M. Risk factors and early origins of chronic obstructive pulmonary disease. The Lancet. 2015;385(9971):899-909.
505. Usmani OS, Barnes PJ. Assessing and treating small airways disease in asthma and chronic obstructive pulmonary disease. Annals of medicine. 2012;44(2):146-56.
506. Siafakas N, Vermeire P, Pride Na, Paoletti P, Gibson J, Howard P, et al. Optimal assessment and management of chronic obstructive pulmonary disease (COPD). The European Respiratory Society Task Force. European Respiratory Journal. 1995;8(8):1398-420.
507. Edwards MR, Saglani S, Schwarze J, Skevaki C, Smith JA, Ainsworth B, et al. Addressing unmet needs in understanding asthma mechanisms: From the European Asthma Research and Innovation Partnership (EARIP) Work Package (WP) 2 collaborators. European Respiratory Journal. 2017;49(5).
508. Stolz D, Mkorombindo T, Schumann DM, Agusti A, Ash SY, Bafadhel M, et al. Towards the elimination of chronic obstructive pulmonary disease: a Lancet Commission. The Lancet. 2022;400(10356):921-72.
509. Dong T, Chen X, Xu H, Song Y, Wang H, Gao Y, et al. Mitochondrial metabolism mediated macrophage polarization in chronic lung diseases. Pharmacology & Therapeutics. 2022:108208.
510. Rahman I. Oxidative stress, chromatin remodeling and gene transcription in inflammation and chronic lung diseases. BMB Reports. 2003;36(1):95-109.

511. Sica A, Colombo MP, Trama A, Horn L, Garassino MC, Torri V. Immunometabolic status of COVID-19 cancer patients. Physiological Reviews. 2020;100(4):1839-50.
512. Depeint F, Bruce WR, Shangari N, Mehta R, O'Brien PJ. Mitochondrial function and toxicity: role of the B vitamin family on mitochondrial energy metabolism. Chemico-biological interactions. 2006;163(1-2):94-112.
513. Cheng S-C, Joosten LA, Netea MG. The interplay between central metabolism and innate immune responses. Cytokine & growth factor reviews. 2014;25(6):707-13.
514. Li B, Shi Y, Liu M, Wu F, Hu X, Yu F, et al. Attenuates of NAD+ impair BMSC osteogenesis and fracture repair through OXPHOS. Stem cell research & therapy. 2022;13(1):1-16.
515. Nsiah-Sefaa A, McKenzie M. Combined defects in oxidative phosphorylation and fatty acid β-oxidation in mitochondrial disease. Bioscience reports. 2016;36(2).
516. Yaku K, Okabe K, Gulshan M, Takatsu K, Okamoto H, Nakagawa T. Metabolism and biochemical properties of nicotinamide adenine dinucleotide (NAD) analogs, nicotinamide guanine dinucleotide (NGD) and nicotinamide hypoxanthine dinucleotide (NHD). Scientific reports. 2019;9(1):1-12.
517. Ryu WI, Shen M, Lee Y, Healy RA, Bormann MK, Cohen BM, et al. Nicotinamide riboside and caffeine partially restore diminished NAD availability but not altered energy metabolism in Alzheimer's disease. Aging Cell. 2022;21(7):e13658.
518. Poltronieri P, Miwa M, Masutani M. ADP-Ribosylation as Post-Translational Modification of Proteins: Use of Inhibitors in Cancer Control. International Journal of Molecular Sciences. 2021;22(19):10829.
519. Goody MF, Henry CA. A need for NAD+ in muscle development, homeostasis, and aging. Skeletal Muscle. 2018;8(1):1-14.
520. Xie N, Zhang L, Gao W, Huang C, Huber PE, Zhou X, et al. NAD+ metabolism: pathophysiologic mechanisms and therapeutic potential. Signal transduction and targeted therapy. 2020;5(1):1-37.
521. Okabe K, Yaku K, Tobe K, Nakagawa T. Implications of altered NAD metabolism in metabolic disorders. Journal of biomedical science. 2019;26(1):1-13.
522. Kruszewski M, Szumiel I. Sirtuins (histone deacetylases III) in the cellular response to DNA damage—facts and hypotheses. DNA repair. 2005;4(11):1306-13.
523. Wang H, Yang L, Liu M, Luo J. Protein post-translational modifications in the regulation of cancer hallmarks. Cancer Gene Therapy. 2022:1-19.
524. Hou Y, Lautrup S, Cordonnier S, Wang Y, Croteau DL, Zavala E, et al. NAD+ supplementation normalizes key Alzheimer's features and DNA damage responses in a new AD mouse model with introduced DNA repair deficiency. Proceedings of the National Academy of Sciences. 2018;115(8):E1876-E85.
525. Zhang T, Kraus WL. SIRT1-dependent regulation of chromatin and transcription: linking NAD+ metabolism and signaling to the control of cellular functions. Biochimica et Biophysica Acta (BBA)-Proteins and Proteomics. 2010;1804(8):1666-75.
526. Jung UJ, Choi M-S. Obesity and its metabolic complications: the role of adipokines and the relationship between obesity, inflammation, insulin resistance, dyslipidemia and nonalcoholic fatty liver disease. International journal of molecular sciences. 2014;15(4):6184-223.
527. Blüher M. Adipose tissue dysfunction contributes to obesity related metabolic diseases. Best practice & research Clinical endocrinology & metabolism. 2013;27(2):163-77.
528. Choudhury M, Jonscher KR, Friedman JE. Reduced mitochondrial function in obesity-associated fatty liver: SIRT3 takes on the fat. Aging (Albany NY). 2011;3(2):175.

529. Cho E-H. SIRT3 as a regulator of non-alcoholic fatty liver disease. Journal of lifestyle medicine. 2014;4(2):80.
530. Fang EF, Lautrup S, Hou Y, Demarest TG, Croteau DL, Mattson MP, et al. NAD+ in aging: molecular mechanisms and translational implications. Trends in molecular medicine. 2017;23(10):899-916.
531. Abdellatif M, Sedej S, Kroemer G. NAD+ metabolism in cardiac health, aging, and disease. Circulation. 2021;144(22):1795-817.
532. Frederick DW, Loro E, Liu L, Davila Jr A, Chellappa K, Silverman IM, et al. Loss of NAD homeostasis leads to progressive and reversible degeneration of skeletal muscle. Cell metabolism. 2016;24(2):269-82.
533. Revollo JR, Körner A, Mills KF, Satoh A, Wang T, Garten A, et al. Nampt/PBEF/visfatin regulates insulin secretion in β cells as a systemic NAD biosynthetic enzyme. Cell metabolism. 2007;6(5):363-75.
534. Pirinen E, Auranen M, Khan NA, Brilhante V, Urho N, Pessia A, et al. Niacin cures systemic NAD+ deficiency and improves muscle performance in adult-onset mitochondrial myopathy. Cell Metabolism. 2020;31(6):1078-90. e5.
535. Sethi GS, Dharwal V, Naura AS. Poly (ADP-ribose) polymerase-1 in lung inflammatory disorders: a review. Frontiers in immunology. 2017;8:1172.
536. Hwang J-w, Yao H, Caito S, Sundar IK, Rahman I. Redox regulation of SIRT1 in inflammation and cellular senescence. Free Radical Biology and Medicine. 2013;61:95-110.
537. Di Stefano M, Conforti L. Diversification of NAD biological role: the importance of location. The FEBS journal. 2013;280(19):4711-28.
538. Chini CC, Tarragó MG, Chini EN. NAD and the aging process: Role in life, death and everything in between. Molecular and cellular endocrinology. 2017;455:62-74.
539. Kincaid JW, Berger NA. NAD metabolism in aging and cancer. Experimental Biology and Medicine. 2020;245(17):1594-614.
540. Yaku K, Okabe K, Nakagawa T. NAD metabolism: Implications in aging and longevity. Ageing research reviews. 2018;47:1-17.
541. Yan Lj. Redox imbalance stress in diabetes mellitus: Role of the polyol pathway. Animal models and experimental medicine. 2018;1(1):7-13.
542. Navarro CD, Figueira TR, Francisco A, Dal'Bó GA, Ronchi JA, Rovani JC, et al. Redox imbalance due to the loss of mitochondrial NAD (P)-transhydrogenase markedly aggravates high fat diet-induced fatty liver disease in mice. Free Radical Biology and Medicine. 2017;113:190-202.
543. Aggarwal S, Trehanpati N, Nagarajan P, Ramakrishna G. The Clock-NAD+-Sirtuin connection in nonalcoholic fatty liver disease. Journal of Cellular Physiology. 2022;237(8):3164-80.
544. Wu Q, Gao Z-J, Yu X, Wang P. Dietary regulation in health and disease. Signal Transduction and Targeted Therapy. 2022;7(1):1-29.
545. Suárez-Rivero JM, Pastor-Maldonado CJ, Povea-Cabello S, Álvarez-Córdoba M, Villalón-García I, Talaverón-Rey M, et al. Activation of the Mitochondrial Unfolded Protein Response: A New Therapeutic Target? Biomedicines. 2022;10(7):1611.
546. Zhou Z, Fan Y, Zong R, Tan K. The mitochondrial unfolded protein response: A multitasking giant in the fight against human diseases. Ageing Research Reviews. 2022:101702.
547. Shpilka T, Haynes CM. The mitochondrial UPR: mechanisms, physiological functions and implications in ageing. Nature reviews Molecular cell biology. 2018;19(2):109-20.

548. Trammell SA, Yu L, Redpath P, Migaud ME, Brenner C. Nicotinamide riboside is a major NAD+ precursor vitamin in cow milk. The Journal of nutrition. 2016;146(5):957-63.
549. Cheng Y, Di S, Fan C, Cai L, Gao C, Jiang P, et al. SIRT1 activation by pterostilbene attenuates the skeletal muscle oxidative stress injury and mitochondrial dysfunction induced by ischemia reperfusion injury. Apoptosis. 2016;21(8):905-16.
550. Wang S, Yang X, Lin Y, Qiu X, Li H, Zhao X, et al. Cellular NAD depletion and decline of SIRT1 activity play critical roles in PARP-1-mediated acute epileptic neuronal death in vitro. Brain research. 2013;1535:14-23.
551. Kim MY, Mauro S, Gévry N, Lis JT, Kraus WL. NAD+-dependent modulation of chromatin structure and transcription by nucleosome binding properties of PARP-1. Cell. 2004;119(6):803-14.
552. Oit-Wiscombe I, Virag L, Soomets U, Altraja A. Increased DNA damage in progression of COPD: a response by poly (ADP-ribose) polymerase-1. PLoS One. 2013;8(7):e70333.
553. Barnes P, Adcock I, Ito K. Histone acetylation and deacetylation: importance in inflammatory lung diseases. European Respiratory Journal. 2005;25(3):552-63.
554. Mroz R, Noparlik J, Chyczewska E, Braszko J, Holownia A. Molecular basis of chronic inflammation in lung diseases: new therapeutic approach. Journal of Physiology and Pharmacology. 2007;58(5):453-60.
555. Dellinger RW, Holmes HE, Hu-Seliger T, Butt RW, Harrison SA, Mozaffarian D, et al. NRPT reduces markers of hepatic inflammation in non-alcoholic fatty liver disease: a double-blind, placebo-controlled clinical trial. Hepatology. 2022.
556. Cuollo L, Antonangeli F, Santoni A, Soriani A. The senescence-associated secretory phenotype (SASP) in the challenging future of cancer therapy and age-related diseases. Biology. 2020;9(12):485.
557. Han X, Lei Q, Xie J, Liu H, Li J, Zhang X, et al. Potential Regulators of the Senescence-Associated Secretory Phenotype During Senescence and Aging. The Journals of Gerontology: Series A. 2022;77(11):2207-18.
558. Wrench CL. Regulation of cellular senescence in COPD small airway fibroblasts. 2020.
559. Burgoyne RA, Fisher AJ, Borthwick LA. The role of epithelial damage in the pulmonary immune response. Cells. 2021;10(10):2763.
560. Adami A, Corvino RB, Calmelat RA, Porszasz J, Casaburi R, Rossiter HB. Muscle oxidative capacity is reduced in both upper and lower limbs in COPD. Medicine and science in sports and exercise. 2020;52(10):2061.
561. Haji G, Wiegman CH, Michaeloudes C, Patel MS, Curtis K, Bhavsar P, et al. Mitochondrial dysfunction in airways and quadriceps muscle of patients with chronic obstructive pulmonary disease. Respiratory Research. 2020;21(1):1-11.
562. Hodge S, Hodge G, Holmes M, Reynolds P. Increased airway epithelial and T-cell apoptosis in COPD remains despite smoking cessation. European Respiratory Journal. 2005;25(3):447-54.
563. Thompson EA, Cascino K, Ordonez AA, Zhou W, Vaghasia A, Hamacher-Brady A, et al. Mitochondrial induced T cell apoptosis and aberrant myeloid metabolic programs define distinct immune cell subsets during acute and recovered SARS-CoV-2 infection. MedRxiv. 2020.
564. Bhatia D, Capili A, Choi ME. Mitochondrial dysfunction in kidney injury, inflammation, and disease: Potential therapeutic approaches. Kidney research and clinical practice. 2020;39(3):244.

565. van der Toorn M, Slebos D-J, de Bruin HG, Leuvenink HG, Bakker SJ, Gans RO, et al. Cigarette smoke-induced blockade of the mitochondrial respiratory chain switches lung epithelial cell apoptosis into necrosis. American Journal of Physiology-Lung Cellular and Molecular Physiology. 2007;292(5):L1211-L8.
566. Gayan-Ramirez G, Decramer M. Mechanisms of striated muscle dysfunction during acute exacerbations of COPD. Journal of Applied Physiology. 2013;114(9):1291-9.
567. Eapen MS, Sharma P, Sohal SS. Mitochondrial dysfunction in macrophages: a key to defective bacterial phagocytosis in COPD. Eur Respiratory Soc; 2019.
568. Mei D, Tan WD, Liao W, Heng CM, Wong WF. Activation of angiotensin II type-2 receptor protects against cigarette smoke-induced COPD. Pharmacological research. 2020;161:105223.
569. Arunachalam G, Sundar IK, Hwang J-w, Yao H, Rahman I. Emphysema is associated with increased inflammation in lungs of atherosclerosis-prone mice by cigarette smoke: implications in comorbidities of COPD. Journal of Inflammation. 2010;7(1):1-10.
570. Zong D, Liu X, Li J, Ouyang R, Chen P. The role of cigarette smoke-induced epigenetic alterations in inflammation. Epigenetics & Chromatin. 2019;12(1):1-25.
571. Boukhenouna S, Wilson MA, Bahmed K, Kosmider B. Reactive oxygen species in chronic obstructive pulmonary disease. Oxidative medicine and cellular longevity. 2018;2018.
572. James AM, Cochemé HM, Smith RA, Murphy MP. Interactions of Mitochondria-targeted and Untargeted Ubiquinones with the Mitochondrial Respiratory Chain and Reactive Oxygen Species: IMPLICATIONS FOR THE USE OF EXOGENOUS UBIQUINONES AS THERAPIES AND EXPERIMENTAL TOOLS*♦. Journal of Biological Chemistry. 2005;280(22):21295-312.
573. Mumby S, Adcock IM. Recent evidence from omic analysis for redox signalling and mitochondrial oxidative stress in COPD. Journal of Inflammation. 2022;19(1):1-15.
574. Michaeloudes C, Bhavsar PK, Mumby S, Chung KF, Adcock IM. Dealing with stress: defective metabolic adaptation in chronic obstructive pulmonary disease pathogenesis. Annals of the American Thoracic Society. 2017;14(Supplement 5):S374-S82.
575. Gosker HR, Schrauwen P, Broekhuizen R, Hesselink MK, Moonen-Kornips E, Ward KA, et al. Exercise training restores uncoupling protein-3 content in limb muscles of patients with chronic obstructive pulmonary disease. American Journal of Physiology-Endocrinology and Metabolism. 2006;290(5):E976-E81.
576. Young RP, Hopkins R, Eaton TE. Forced expiratory volume in one second: not just a lung function test but a marker of premature death from all causes. European Respiratory Journal. 2007;30(4):616-22.
577. May SM, Li JT, editors. Burden of chronic obstructive pulmonary disease: healthcare costs and beyond. Allergy and asthma proceedings; 2015: OceanSide Publications.
578. Dabscheck E, George J, Hermann K, McDonald CF, McDonald VM, McNamara R, et al. COPD-X Australian guidelines for the diagnosis and management of chronic obstructive pulmonary disease: 2022 update. Medical Journal of Australia. 2022;217(8):415-23.
579. Ahmad T, Sundar IK, Lerner CA, Gerloff J, Tormos AM, Yao H, et al. Impaired mitophagy leads to cigarette smoke stress-induced cellular senescence: implications for chronic obstructive pulmonary disease. The FASEB Journal. 2015;29(7):2912-29.

580. Ito S, Araya J, Kurita Y, Kobayashi K, Takasaka N, Yoshida M, et al. PARK2-mediated mitophagy is involved in regulation of HBEC senescence in COPD pathogenesis. Autophagy. 2015;11(3):547-59.
581. Tsubouchi K, Araya J, Kuwano K. PINK1-PARK2-mediated mitophagy in COPD and IPF pathogeneses. Inflammation and regeneration. 2018;38(1):1-9.
582. Garten A, Schuster S, Penke M, Gorski T, De Giorgis T, Kiess W. Physiological and pathophysiological roles of NAMPT and NAD metabolism. Nature Reviews Endocrinology. 2015;11(9):535-46.
583. Imai S-i, Yoshino J. The importance of NAMPT/NAD/SIRT1 in the systemic regulation of metabolism and ageing. Diabetes, Obesity and Metabolism. 2013;15(s3):26-33.
584. Wang Q, Liang B, Shirwany NA, Zou M-H. 2-Deoxy-D-glucose treatment of endothelial cells induces autophagy by reactive oxygen species-mediated activation of the AMP-activated protein kinase. PloS one. 2011;6(2):e17234.
585. Zhuo L, Fu B, Bai X, Zhang B, Wu L, Cui J, et al. NAD blocks high glucose induced mesangial hypertrophy via activation of the sirtuins-AMPK-mTOR pathway. Cellular Physiology and Biochemistry. 2011;27(6):681-90.
586. Eckel-Mahan K, Sassone-Corsi P. Metabolism control by the circadian clock and vice versa. Nature structural & molecular biology. 2009;16(5):462-7.
587. Shen Q, Zhang S-J, Xue Y-Z, Peng F, Cheng D-Y, Xue Y-P, et al. Biological synthesis of nicotinamide mononucleotide. Biotechnology Letters. 2021;43(12):2199-208.
588. Shi X, Jiang Y, Kitano A, Hu T, Murdaugh RL, Li Y, et al. Nuclear NAD+ homeostasis governed by NMNAT1 prevents apoptosis of acute myeloid leukemia stem cells. Science advances. 2021;7(30):eabf3895.
589. VanLinden MR, Dölle C, Pettersen IK, Kulikova VA, Niere M, Agrimi G, et al. Subcellular distribution of NAD+ between cytosol and mitochondria determines the metabolic profile of human cells. Journal of Biological Chemistry. 2015;290(46):27644-59.
590. Lau C, Niere M, Ziegler M. The NMN/NaMN adenylyltransferase (NMNAT) protein family. Frontiers in Bioscience-Landmark. 2009;14(2):410-31.
591. Niere M, Kernstock S, Koch-Nolte F, Ziegler M. Functional localization of two poly (ADP-ribose)-degrading enzymes to the mitochondrial matrix. Molecular and cellular biology. 2008;28(2):814-24.
592. Dölle C, Hvidsten Skoge R, R VanLinden M, Ziegler M. NAD biosynthesis in humans-enzymes, metabolites and therapeutic aspects. Current topics in medicinal chemistry. 2013;13(23):2907-17.
593. VanLinden MR, Niere M, Nikiforov AA, Ziegler M, Dölle C. Compartment-specific poly-ADP-ribose formation as a biosensor for subcellular NAD pools. Poly (ADP-ribose) polymerase: Springer; 2017. p. 45-56.
594. Lim EW, Parker SJ, Metallo CM. Deuterium tracing to interrogate compartment-specific NAD (P) H metabolism in cultured mammalian cells. Metabolic Flux Analysis in Eukaryotic Cells: Springer; 2020. p. 51-71.
595. Maiese K. SIRT1 and stem cells: In the forefront with cardiovascular disease, neurodegeneration and cancer. World journal of stem cells. 2015;7(2):235.
596. Iqbal T, Nawaz A, Karim M, Yaku K, Hikosaka K, Matsumoto M, et al. Loss of hepatic Nmnat1 has no impact on diet-induced fatty liver disease. Biochemical and Biophysical Research Communications. 2022;636:89-95.
597. Sasaki Y, Nakagawa T, Mao X, DiAntonio A, Milbrandt J. NMNAT1 inhibits axon degeneration via blockade of SARM1-mediated NAD+ depletion. elife. 2016;5.

598. Gulshan M, Yaku K, Okabe K, Mahmood A, Sasaki T, Yamamoto M, et al. Overexpression of Nmnat3 efficiently increases NAD and NGD levels and ameliorates age-associated insulin resistance. Aging Cell. 2018;17(4):e12798.
599. Pissios P. Nicotinamide N-methyltransferase: more than a vitamin B3 clearance enzyme. Trends in Endocrinology & Metabolism. 2017;28(5):340-53.
600. Li Y, Zhang Z, Jiang S, Xu F, Tulum L, Li K, et al. Using transcriptomics, proteomics and phosphoproteomics as new approach methodology (NAM) to define biological responses for chemical safety assessment. Chemosphere. 2022:137359.
601. McQuattie-Pimentel AC, Ren Z, Joshi N, Watanabe S, Stoeger T, Chi M, et al. The lung microenvironment shapes a dysfunctional response of alveolar macrophages in aging. The Journal of clinical investigation. 2021;131(4).
602. Wilson DF. Regulation of cellular metabolism: programming and maintaining metabolic homeostasis. Journal of applied physiology. 2013;115(11):1583-8.
603. Guo L. Mitochondria and the permeability transition pore in cancer metabolic reprogramming. Biochemical Pharmacology. 2021;188:114537.
604. Bu T, Wang LF, Yin YQ. How do innate immune cells contribute to airway remodeling in copd progression? International Journal of Chronic Obstructive Pulmonary Disease. 2020;15:107.
605. Tuder RM, Yoshida T, Arap W, Pasqualini R, Petrache I. State of the art. Cellular and molecular mechanisms of alveolar destruction in emphysema: an evolutionary perspective. Proceedings of the American Thoracic Society. 2006;3(6):503-10.
606. Pålsson-McDermott EM, O'Neill LA. Targeting immunometabolism as an anti-inflammatory strategy. Cell research. 2020;30(4):300-14.
607. Sauerwein H, Schols A. Glucose metabolism in chronic lung disease. Clinical Nutrition. 2002;21(5):367-71.
608. Kao CC, Hsu JW-C, Bandi V, Hanania NA, Kheradmand F, Jahoor F. Glucose and pyruvate metabolism in severe chronic obstructive pulmonary disease. Journal of Applied Physiology. 2012;112(1):42-7.
609. Li D, Shen C, Liu L, Hu J, Qin J, Dai L, et al. PKM2 regulates cigarette smoke-induced airway inflammation and epithelial-to-mesenchymal transition via modulating PINK1/Parkin-mediated mitophagy. Toxicology. 2022;477:153251.
610. Zhao H, Dennery PA, Yao H. Metabolic reprogramming in the pathogenesis of chronic lung diseases, including BPD, COPD, and pulmonary fibrosis. American Journal of Physiology-Lung Cellular and Molecular Physiology. 2018;314(4):L544-L54.
611. Kosmider B, Lin C-R, Karim L, Tomar D, Vlasenko L, Marchetti N, et al. Mitochondrial dysfunction in human primary alveolar type II cells in emphysema. EBioMedicine. 2019;46:305-16.
612. Slebos D, Van der Toorn M, Bakker S, Kauffman H. Mitochondrial dysfunction in COPD patients with low body mass index. European Respiratory Journal. 2007;30(3):600-.
613. Li T, Han J, Jia L, Hu X, Chen L, Wang Y. PKM2 coordinates glycolysis with mitochondrial fusion and oxidative phosphorylation. Protein & cell. 2019;10(8):583-94.
614. Michaeloudes C, Bhavsar PK, Mumby S, Xu B, Hui CKM, Chung KF, et al. Role of metabolic reprogramming in pulmonary innate immunity and its impact on lung diseases. Journal of Innate Immunity. 2020;12(1):31-46.
615. Erlich JR, To EE, Liong S, Brooks R, Vlahos R, O'Leary JJ, et al. Targeting evolutionary conserved oxidative stress and immunometabolic pathways for the treatment of respiratory infectious diseases. Antioxidants & Redox Signaling. 2020;32(13):993-1013.

616. Ghelfi E, Karaaslan C, Berkelhamer S, Akar S, Kozakewich H, Cataltepe S. Fatty acid–binding proteins and Peribronchial angiogenesis in Bronchopulmonary dysplasia. American journal of respiratory cell and molecular biology. 2011;45(3):550-6.
617. Piersigilli F, Bhandari V. Metabolomics of bronchopulmonary dysplasia. Clinica chimica acta. 2020;500:109-14.
618. Kotlyarov S, Bulgakov A. Lipid metabolism disorders in the comorbid course of nonalcoholic fatty liver disease and chronic obstructive pulmonary disease. Cells. 2021;10(11):2978.
619. Hamanaka RB, Mutlu GM. Metabolic requirements of pulmonary fibrosis: role of fibroblast metabolism. The FEBS Journal. 2021;288(22):6331-52.
620. Wong N, Ojo D, Yan J, Tang D. PKM2 contributes to cancer metabolism. Cancer letters. 2015;356(2):184-91.
621. Wang JZ, Zhu W, Han J, Yang X, Zhou R, Lu HC, et al. The Role of the HIF-1α/ALYREF/PKM2 axis in Glycolysis and Tumorigenesis of Bladder Cancer. Cancer Communications. 2021;41(7):560-75.
622. Meyer A, Zoll J, Charles AL, Charloux A, de Blay F, Diemunsch P, et al. Skeletal muscle mitochondrial dysfunction during chronic obstructive pulmonary disease: central actor and therapeutic target. Experimental physiology. 2013;98(6):1063-78.
623. John-Schuster G, Günter S, Hager K, Conlon TM, Eickelberg O, Yildirim AÖ. Inflammaging increases susceptibility to cigarette smoke-induced COPD. Oncotarget. 2016;7(21):30068.
624. Motz GT, Eppert BL, Wesselkamper SC, Flury JL, Borchers MT. Chronic cigarette smoke exposure generates pathogenic T cells capable of driving COPD-like disease in Rag2−/− mice. American journal of respiratory and critical care medicine. 2010;181(11):1223-33.
625. Singla E, Dharwal V, Naura AS. Gallic acid protects against the COPD-linked lung inflammation and emphysema in mice. Inflammation Research. 2020;69(4):423-34.
626. Chung KF. The role of airway smooth muscle in the pathogenesis of airway wall remodeling in chronic obstructive pulmonary disease. Proceedings of the American Thoracic Society. 2005;2(4):347-54.
627. Cairns RA, Harris IS, Mak TW. Regulation of cancer cell metabolism. Nature Reviews Cancer. 2011;11(2):85-95.
628. Al-Khami AA, Rodriguez PC, Ochoa AC. Energy metabolic pathways control the fate and function of myeloid immune cells. Journal of leukocyte biology. 2017;102(2):369-80.
629. Sciacovelli M, Frezza C. Metabolic reprogramming and epithelial-to-mesenchymal transition in cancer. The FEBS journal. 2017;284(19):3132-44.
630. Van den Bossche J, O'Neill LA, Menon D. Macrophage immunometabolism: where are we (going)? Trends in immunology. 2017;38(6):395-406.
631. Palmer CS, Ostrowski M, Balderson B, Christian N, Crowe SM. Glucose metabolism regulates T cell activation, differentiation, and functions. Frontiers in immunology. 2015;6:1.
632. Zhang X, Zink F, Hezel F, Vogt J, Wachter U, Wepler M, et al. Metabolic substrate utilization in stress-induced immune cells. Intensive Care Medicine Experimental. 2020;8(1):1-14.
633. Cai W-w, Yu Y, Zong S-y, Wei F. Metabolic reprogramming as a key regulator in the pathogenesis of rheumatoid arthritis. Inflammation Research. 2020;69(11):1087-101.
634. Rose IA, Warms JV. Control of glycolysis in the human red blood cell. Journal of Biological Chemistry. 1966;241(21):4848-54.

635. Gaude E, Schmidt C, Gammage PA, Dugourd A, Blacker T, Chew SP, et al. NADH shuttling couples cytosolic reductive carboxylation of glutamine with glycolysis in cells with mitochondrial dysfunction. Molecular cell. 2018;69(4):581-93. e7.
636. Williams NC, O'Neill LA. A role for the Krebs cycle intermediate citrate in metabolic reprogramming in innate immunity and inflammation. Frontiers in immunology. 2018;9:141.
637. Angajala A, Lim S, Phillips JB, Kim J-H, Yates C, You Z, et al. Diverse roles of mitochondria in immune responses: novel insights into immuno-metabolism. Frontiers in immunology. 2018:1605.
638. Wu J, Jin Z, Zheng H, Yan L-J. Sources and implications of NADH/NAD+ redox imbalance in diabetes and its complications. Diabetes, metabolic syndrome and obesity: targets and therapy. 2016;9:145.
639. Hershberger KA, Martin AS, Hirschey MD. Role of NAD+ and mitochondrial sirtuins in cardiac and renal diseases. Nature Reviews Nephrology. 2017;13(4):213-25.
640. Zhang M, Zhang Y, Roth M, Zhang L, Shi R, Yang X, et al. Sirtuin 3 inhibits airway epithelial mitochondrial oxidative stress in cigarette smoke-induced COPD. Oxidative Medicine and Cellular Longevity. 2020;2020.
641. Gu C, Li Y, Xu W-L, Yan J-P, Xia Y-j, Ma Y-Y, et al. Sirtuin 1 activator SRT1720 protects against lung injury via reduction of type II alveolar epithelial cells apoptosis in emphysema. COPD: Journal of Chronic Obstructive Pulmonary Disease. 2015;12(4):444-52.
642. Beauharnois JM, Bolívar BE, Welch JT. Sirtuin 6: a review of biological effects and potential therapeutic properties. Molecular BioSystems. 2013;9(7):1789-806.
643. Gallí M, Van Gool F, Leo O. Sirtuins and inflammation: friends or foes? Biochemical pharmacology. 2011;81(5):569-76.
644. Nelson BC, Dizdaroglu M. Implications of DNA damage and DNA repair on human diseases. Mutagenesis. 2020;35(1):1-3.
645. Dekhuijzen P. Antioxidant properties of N-acetylcysteine: their relevance in relation to chronic obstructive pulmonary disease. European Respiratory Journal. 2004;23(4):629-36.
646. Dharwal V, Sandhir R, Naura AS. PARP-1 inhibition provides protection against elastase-induced emphysema by mitigating the expression of matrix metalloproteinases. Molecular and Cellular Biochemistry. 2019;457(1):41-9.
647. Sethi GS, Sharma S, Naura AS. PARP inhibition by olaparib alleviates chronic asthma-associated remodeling features via modulating inflammasome signaling in mice. Iubmb Life. 2019;71(7):1003-13.
648. Naura A, Dharwal V. Pharmacological Inhibition of Poly ADP-Ribose Polymerase Ameliorates Elastase Induced Inflammation and Emphysema in Mice. D53 OFF THE BEATEN PATH: NEW APPROACHES TO COPD PATHOGENESIS: American Thoracic Society; 2018. p. A7151-A.